NASA SPACE ENGINEERING RESEARCH CENTER

for utilization of local planetary resources

P. 285

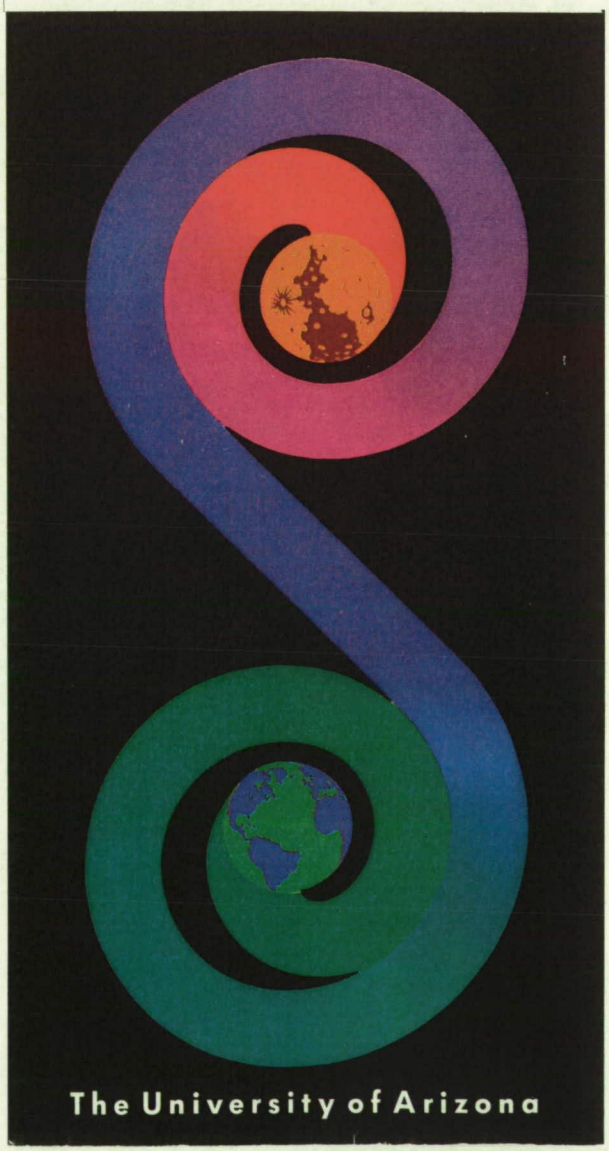

The University of Arizona

NASA Space Engineering Research Center
for Utilization of Local Planetary Resources

Annual
Progress Report
1989-90

Director: T. Triffet Principal Investigators: K. Ramohalli, J. Lewis

THE UNIVERSITY OF ARIZONA
4717 E. Ft. Lowell Rd./AML
Tucson AZ 85712
TEL (602) 322-2304 FAX (602) 326-0938

TABLE OF CONTENTS

EXECUTIVE SUMMARY

OMIT TO P. 1-1

EXECUTIVE SUMMARY

The University of Arizona and NASA have joined to form the UA/NASA Space Engineering Research Center. In its second year, the Center has successfully brought together leaders in the engineering fields and many space sciences to assemble the knowledge and develop the systems necessary for man to find a home in space.

The purpose of the Center is sharply focused: To discover, characterize, extract, process, and fabricate useful products from the extraterrestrial resources available in the Inner Solar System (the Moon, the Mars system, and nearby asteroids). During this reporting period, important progress has been made on the evolution of the "big picture" through a quantitative interdependent matrix that enables a visual display of the overall space mission when the components are specified. This development enables not only quick evaluations of the various candidates, but also provides quick guidance for promising avenues of research in order to reap the maximum benefit. For the first time, we now have a quantitative tool for evaluating the overall "Figure of Merit" of emerging technologies.

Early emphasis has been placed on minerals and the methods for processing them to provide propellants and life-support volatiles. At the same time, investigations into using the direct coproducts from these processes, such as metals and refractories, are underway. Manufacturing propellants near to where they will be used saves a significant percentage of the cost of space travel; local production of life-support volatiles saves in transportation costs and also lends greater flexibility to missions. The goal is to become self-sufficient for both these classes of materials.

Later projects must serve the long-range goal of investigating all potential low-technology, high-demand products for use in space, including not only propellants and life-support materials, but also construction materials (such as anhydrous "cements," metals, etc.), and refractory materials for furnaces and aerobrake construction.

Following this summary, individual progress reports covering each of these areas are included as updates on each group's work. They represent the current status of the field of space resources. The summary here includes highlights of our activities in the past year.

In an engineering sense, the first step in developing extraterrestrial sources of propellants is acquiring a firm understanding of the tradeoffs involved in making and using propellants under specific, realistic conditions compatible with foreseeable national plans in space. Dr. Kumar Ramohalli is leading this effort. Mario Rascon in Dr. Ramohalli's group has carried out a broad assessment of the performance characteristics of a wide range of fuel-oxidizer combinations using both frozen-kinetic and equilibrium models of the combustion process. This work provides a valuable reference point for a very wide range of future scenarios for use of non-terrestrial propellants.

Underlying these efforts are certain essential scientific investigations. Proceeding sequentially with the results of these, Dr. Tom Gehrels, from the Lunar and Planetary Laboratory at the University of Arizona, and his Spacewatch group have greatly improved their ability to find comets and asteroids through the permanent installation of a 2048 × 2048 CCD. During an early test of the equipment, team member Dr. David Rabinowitz visually discovered a new, fast-moving asteroid, 1989UP. Dr. Gehrels is

also working with SERC and ASPERA on the production of a book on space resources in the highly regarded University of Arizona Press Space Sciences Series.

Dr. Robert Singer's group, also from the Lunar and Planetary Laboratory, has been observing the full Moon using a Tucson-based telescope and lunar CCD-image processing to estimate concentrations of TiO_2 on the lunar surface. Areas of high concentration may make good landing sites; for example, high titanium dioxide concentration should be a good indicator of high abundances of lunar ilmenite, potentially a rich source of oxygen on the Moon.

Dr. Larry Lebofsky and Dr. Marcia L. Nelson at LPL have made spectral studies of several asteroids to determine their composition. They have also studied Mars' smaller moon Deimos, the asteroid Vesta, and the Moon to determine whether the Hapke reflectance theory can be applied to compositional analysis using these well-known bodies. Early results look promising.

Once useful bodies are found and characterized, propellants and volatiles can be derived from them. The first step is the actual mining and extraction of useful materials. Dr. Charles Glass is working with GPR (ground-penetrating radar) to see if it might prove useful in finding water on the Moon and Mars. GPR has a greater depth of penetration than do other radar techniques.

The next important step is production. Several techniques are being investigated for oxygen production, including several schemes for reduction of lunar ilmenite. The most widely discussed scheme for manufacture of oxygen on the Moon, hydrogen reduction of ilmenite, and several other related processes, such as carbothermal ilmenite reduction, are under broad study within SERC. The first challenge, to characterize lunar ilmenite and find or develop satisfactory simulants for it, is being addressed by Melinda Hutson in Dr. John S. Lewis' research group. After a lengthy search, she has found and purchased a large quantity of material from a basaltic achondrite meteorite, very similar to lunar basalt, that contains abundant ilmenite. These samples are the basis of experimentation on ilmenite beneficiation by Dr. Ruiz.

Dr. Joaquin Ruiz in the Geosciences Department is developing techniques for extracting the ilmenite. Some of these techniques are only for use in the laboratory for separation of ilmenite simulant used in the experiments conducted by Dr. Farhang Shadman's group. Dr. Ruiz is also working on both magnetic (ineffectual) and electrostatic (promising) separation techniques for beneficiation of ilmenite from crushed lunar (and meteoritic) basalts. The great difficulty of extracting pure (and FeS-free) ilmenite from the agglutinate-rich lunar regolith has led Dr. Ruiz into a more serious examination of the extraction of ilmenite from basaltic lithic fragments rather than directly from regolith fines.

Dr. Shadman's laboratory in the Chemical Engineering Department has refined the techniques for measuring the rate of reduction of ilmenite, both synthetic and natural meteoritic simulants, in preparation for the use of small samples of actual lunar ilmenite to verify the validity of the simulant behavior. They have successfully built and operated two reactor systems for these studies, and have already gained some insight into the kinetic factors limiting the reduction rate. Hydrogen, carbon monoxide, methane, mixtures of these gases, or carbon can be used as reducing agents.

Dr. Larry Haskin, of the Center for Earth and Planetary Sciences at Washington University in St. Louis, has made considerable progress on refining the conditions necessary to optimize production of oxygen through electrolysis of a molten sample of lunar regolith. Some interesting and complex chemistry seems to be occurring at the

anode and cathode; nonetheless, early results seem promising; for example, the energy cost per ton of oxygen produced by electrolysis now appears similar to that for reduction of ilmenite.

Dr. Jibamitra Ganguly of the Geosciences Department is developing the computational tools for modeling the equilibrium chemistry and kinetic behavior of heated carbonaceous chondrite material. These calculations are supported by experimental work on the dehydration kinetics of relevant OH-silicate phases. A goal is to develop a computational model that reproduces experimental results on volatile release from carbonaceous meteorites and their component minerals. Such a model can then be used for preliminary process design for the extraction of volatiles from carbonaceous asteroids and the Martian moons Phobos and Deimos.

Dr. David C. Lynch in the Department of Materials Science and Engineering is investigating another innovative process for extraction of oxygen from ilmenite by plasma-enhanced chlorination. An apparatus has been built and experiments have been conducted that clearly demonstrate benefits of chlorination of ilmenite. Similar reduction of ilmenite by a hydrogen plasma is also under study.

A promising scheme for the production of an atomic chlorine plasma by absorption of highly concentrated sunlight is also under study by Dr. Lynch, Donald E. Osborn, and Dr. Rocco Fazzolari of the Solar Energy Research Facility of the Department of Nuclear and Energy Engineering. Their experimental apparatus has been designed and built, and will be ready for use in the immediate future.

In a final project concerning lunar volatiles, Dr. Timothy Swindle of LPL and Dr. Charles Glass are carrying out a study of the distribution and extraction of Helium-3 from the lunar regolith. This is contract work not supported by NASA, but indicates an important interest and potential future direction for SERC research.

Dr. P. E. Nikravesh has developed a numerical model for mixing the components of propellants in rockets. In a closely related study, Dr. T. L. Vincent's group has also studied the automatic control of temperature during propellant processing for the purpose of making propellant processing hardware more amenable to automation.

Investigations concerning structural materials are also progressing well. A team at SAIC (San Diego) has studied the feasibility of producing large solar reflectors from endogenous lunar materials.

Dr. C. S. Desai, from the Department of Civil Engineering at the University of Arizona, is in the process of determining if concrete-like materials can be made without water from lunar-type soils. Applications of various vacuums and cyclic loading are being used to find if particles of these materials can combine in such a way as to yield a material with adequate strength and deformation properties.

Dr. Tom Meek, from the Department of Materials Science and Engineering at the University of Tennessee, has also been working with simulated lunar material. He is carefully trying to reproduce as many properties as possible of actual lunar material from the Apollo program in order to have a supply of material with which to test a microwave-sintering process he has developed. The sintered material may be useful for construction.

Dr. Henry Freiser, from the University of Arizona's Department of Chemistry and the Strategic Metals Recovery Facility, is working on the recovery in space of precious metals in the platinum group. He is currently using Earth-derived materials to refine his

methods; he has also established a data base on solvent extraction methods of metals separation. Eventually, his work could be used for extracting precious-metal byproducts from oxygen production on asteroids and the Moon.

Another major pursuit might best be called "major enabling technology." Each of these individual processes must be optimized within the overall constraints of the location and its resources, the energy cost of transportation, and the properties of the processing equipment and support systems. As mentioned, a Figure-of-Merit scheme dedicated to the assessment of the relative overall merits of different competing schemes for using those resources to make propellants is developed. In some cases, low-performance propellants have sufficiently modest equipment demands (such as no need for refrigeration of liquid hydrogen) that they are, overall, preferable to schemes that make higher performance propellants at the same site.

Dr. Rocco Fazzolari and Belinda Wong-Swanson have investigated a particular scheme for lunar oxygen production (hydrogen reduction of ilmenite) for the purpose of developing the tools for analyzing energy use and flow and total energy demand for the process. This is an essential prelude to the specification of energy sources for industrial use at the lunar base.

Finally, SERC is working on several fronts to develop data bases on the scientific data on space resources and the technology for processing them. Leo Masursky in Dr. Lewis' group, Dr. Andrew H. Cutler of SERC, the Planetary Sciences Institute, and Dr. David Criswell of the California Space Institute are all working on different aspects of the development of these data bases.

On the educational front, SERC has recently passed a significant education milestone with the award of its first Master of Science degrees. The Center actively participated, through an invited paper, at the 40th Congress of the International Astronautical Federation. A "first" in education has been achieved through the development of a senior/graduate-level course in *space technologies*, as was promised in the original proposal. This course has proved to be extremely popular and has the largest enrollment (51) of any elective course in the department. The structure is given in Appendix A.

This summary illustrates the intimate interrelatedness of the functions of SERC, spanning activities from the discovery of new space resources through development of new principles for the assessment of resource-related technologies.

I. PROPELLANTS AND VOLATILES

Performance of Unconventional Propellants*

Mario Rascon
Department of Aerospace and Mechanical Engineering
The University of Arizona

This research involves the theoretical calculations of rocket performance of "exotic" propellants at various operating conditions, such as chamber pressure, pressure ratios, and oxidizer-to-fuel ratios. By "exotic" propellants, we mean using materials that may not normally be used as propellants here on Earth due to their low performance characteristics or other factors. The majority of the work was done using the Gordon and McBride CET 86 program in both a mainframe version and personal computer versions. In addition, the Lockheed/Air Force Solid Propellant Theoretical Performance program for the IBM PS/2, which handles condensed product species better, was also used.

Background

With the high cost of putting payloads into orbit, the ability to reduce the size and weight of the payload is highly beneficial. Since the largest part of any space vehicle consists of propellant, it is hoped that the overall size and weight of the vehicle can be reduced by finding near-Earth-orbit materials suitable for use as fuels.

To this end, this work seeks to find propellants that will give acceptable performance, yet be producible or readily available in near-Earth orbit. Another possibility for fuels is the use of materials, such as nylon and rubbers, that would be taken for other purposes. Also considered is the need for the propellant to be easily stored over long periods of time while, ideally, avoiding the use of heavy refrigeration systems.

Although extensive research has been done on Earth-transported propellants that give high performance characteristics, very little work is available on propellants that give less than ideal performance. In addition to studying such overlooked propellants, low chamber pressures need to be considered to help reduce weight and high-pressure ratios, which can be achieved in atmospheres such as that of Mars. Some propellants considered unacceptable for use on Earth could be ideal for use since tradeoffs of performance for availability, storability, and cost are acceptable within the scope of this research.

*This work is independently funded by NASA Code XEU.

Approach

We identified propellants that might be suitable for our purposes. These propellants have been divided into three areas: low-Earth orbit, the Moon, and Mars. The propellants were divided this way due to the availability of materials in these areas, such as CO_2 in the Martian atmosphere. A range of chamber pressures was also determined for each of the above areas, along with a range of expansion ratios.

The CET 86 program was first set up on a mainframe so that the two personal computer versions could be compared for accuracy. One version was obtained from the University of Minnesota, and the second was obtained from AVCO. Both proved to give results identical to those of the mainframe version.

Results to Date

Personal computer versions of the Gordon and McBride CET 86 program were obtained from the University of Minneosta and AVCO and set up on an IBM PS/2 Model 80. These two versions were compared to the mainframe version and were found to give identical results.

The Lockheed/Air Force Solid Propellant Theoretical Performance program was obtained and set up on an IBM PS/2. Since no mainframe version of this program was available for comparison, the CET 86 program was used to test the accuracy of the program. The Lockheed/Air Force program also proved to give accurate results.

Computer programs were written to help organize the data obtained from the CET 86 and Lockheed/Air Force programs into more useful forms. A commercially available plotting program, GRAPHER, was obtained for this purpose.

Twenty-one propellant combinations were analyzed using the CET 86 and Lockheed/Air Force programs. This generated over 1000 sets of data. Graphs were made of I_{sp} versus oxidizer-to-fuel ratio for various pressure ratios for each of the propellants. The data were organized into presentable formats. Some samples are shown in Appendix B.

Summary

This work involves analyzing propellants at various operating conditions and determining which give acceptable performance, yet can be easily stored for long periods of time and are readily available in near-Earth orbit. We have found that a number of the propellants studied would give acceptable performance for space missions. Another graduate student is using the data obtained in this work to develop a method for identifying the propellants and operating conditions that are best for a

particular space mission. So far, conditions in excess of 30,000 separate sets have been calculated.

Participants

Jennifer Kares and Yamel Caquias, both undergraduate students, helped in analyzing the propellants. Jeff Kahl, also an undergraduate student, assisted in developing the various computer programs needed to process the data.

"Cold" Plasma Processing of Local Planetary Ores for Oxygen and Metallurgically Important Metals

D. C. Lynch, D. Bullard, and R. Ortega
Department of Materials Science and Engineering
The University of Arizona

Abstract

In the previous progress report for 1988-89, the utilization of a "cold" plasma in chlorination processing was described. This report is a continuation of that discussion, but is focused on the progress that has been achieved in the past 12 months. During that period, essential equipment and instruments were received, the experimental apparatus assembled and tested, and preliminary experiments conducted. The results of the latter lend support to the original hypothesis, namely, that a "cold" plasma can both significantly enhance and bias chemical reactions.

In two separate experiments, a "cold" plasma was used to reduce $TiCl_4$ vapor and chlorinate ilmenite. The latter, reacted in an argon-chlorine plasma, yielded oxygen. The former experiment reveals that chlorine can be recovered as HCl vapor from metal chlorides in a hydrogen plasma. Furthermore, the success of the hydrogen experiments has lead to an analysis of the feasibility of direct hydrogen reduction of metal oxides in a "cold" plasma. That process would produce water vapor and numerous metal by-products.

Introduction

Those who read last year's report will note a change in title. This change reflects an expansion of the investigation as a result of supplementary funding (received October 1, 1989) from the U.S. Bureau of Mines. A focal point of that investigation involves hydrogen reduction of refractory oxides in a "cold" plasma. The results of that work are significant from both a terrestrial and extraterrestrial viewpoint and, thus, the results from the Bureau study are included in this report and will be included in all future reports.

The advantages associated with a "cold" plasma were discussed in the previous progress report. That material, although focused on chlorination processing, is applicable to hydrogen reduction. While there is no intention to repeat that material here, this report offers an opportunity to at least identify both the advantages and disadvantages associated with "cold" plasma hydrogen reduction in an extraterrestrial environment.

That discussion is followed by a description of the activities during the past year. The discussion includes a description of building activities, as well as a review of

preliminary experimental results. The progress report is concluded by a review of activities planned for the coming year.

Hydrogen Reduction With a "Cold" Plasma

A "cold" plasma can generate a substantial concentration of monatomic hydrogen at low molecular temperatures. With conventional heating, the same effect can only be achieved at temperatures approaching 3000°K (see 1988-89 progress report). The reduction of rutile with H_2 is, for practical purposes, impossible, as the following thermodynamic data indicate:

$$TiO_2(s) + 2H_2(g) = Ti(s) + 2H_2O(g)\ , \qquad \Delta G°(1100°C) = 83{,}962\ \text{cal.}$$

For all reasonable values for the partial pressures of H_2 and H_2O, the reaction involves an increase in the chemical potential of the system. In a "cold" plasma, monatomic hydrogen can react with rutile according to the reaction,

$$TiO_2(s) + 4H(g) = Ti(s) + 2H_2O(g)\ , \qquad \Delta G°(1100°C) = -53{,}750\ \text{cal.}$$

The large negative standard Gibbs' energy for this reaction favors reduction of the metal oxide. Similar conditions exist for other lunar oxides.

The evolved water vapor leaves the reactor with the bulk gas, which is continually passed through the reactor. Removal of the water vapor prevents any back reaction. The water vapor can be condensed and purified for human consumption or electrolysis can be used to recover O_2 and H_2. The advantages and problems associated with the process are summarized in Table 1.1.

Table 1.1 Hydrogen reduction in a "cold" plasma.

Advantages
• Highly reactive environment Near 100% theoretically efficient use of H_2
• No beneficiation of ore required
• Minimal equipment Plasma reactor, condenser, and electrolytic cell
• Continous operation
• Numerous metal by-products
Disadvantages
• Plasma reduction process unproven technology
• Electrical energy utilized
• Problems in handling and storage of hydrogen

Results to Date

Experimental Apparatus. Construction of the experimental apparatus was completed during the past year. The apparatus, shown in Figure 1.1, consists of a microwave source; an applicator, where the plasma is generated, as shown in Figure 1.2; a gas delivery system; a mass spectrometer for monitoring the extent of reaction; an optical pyrometer for recording the temperature of the solid specimen in the plasma; a specimen holder that both rotates and allows for vertical translation of the solid specimen; and a vacuum system. The microwave unit, mass spectrometer, optical pyrometer, and vacuum system have been tested. As a result of testing, modifications have been incorporated in the system design and faulty equipment was returned to the manufacturer for repair.

Experimental Results. Equipment problems, unfortunately, delayed the experimental program. Some experimental results have been obtained, even with the delay. These results, although preliminary, lend support to the general hypothesis that a "cold" plasma can be used to enhance reactions and bias thermodynamics such that products can be formed from reactants that otherwise would not react.

Ilmenite heated in a plasma releases oxygen. Ilmenite was heated in both an inert and argon-chlorine plasma.* The results of those experiments are compared in Table 1.2, where the intensity of signal for O_2 is tabulated as a function of power absorbed by the plasma. The results indicate that oxygen is evolved upon heating of the mineral in a plasma, but that significantly more oxygen is evolved with the chlorine present.

At an absorbed power level of 1 kw, rapid chlorination took place. At this power level, the reaction chamber was rapidly coated with metal chlorides. The results in Table 1.3 indicate that the chlorine was readily consumed.

These results are very encouraging, but preliminary. We are developing both proficiency and experience in operating the mass spectrometer and in evaluating the resulting data. In future reports, we expect to give all results in more meaningful terms, either as normalized intensities or mole fractions.

In another experiment, hydrogen was used to reduce $TiCl_4(g)$ for reaction with Al(l) in a "cold" plasma. The reaction involved formation of titanium aluminides and HCl(g). Thermodynamically, the reaction is impossible unless monatomic hydrogen is the reducing agent. These experiments revealed that radicals generated in a plasma can be used to bias a reaction and that ungrounded metal pieces can be placed in a

*All future experiments will be conducted with either N_2, Cl_2, or a mixture of these gases. Nitrogen produces a more stable plasma than can be achieved with Ar.

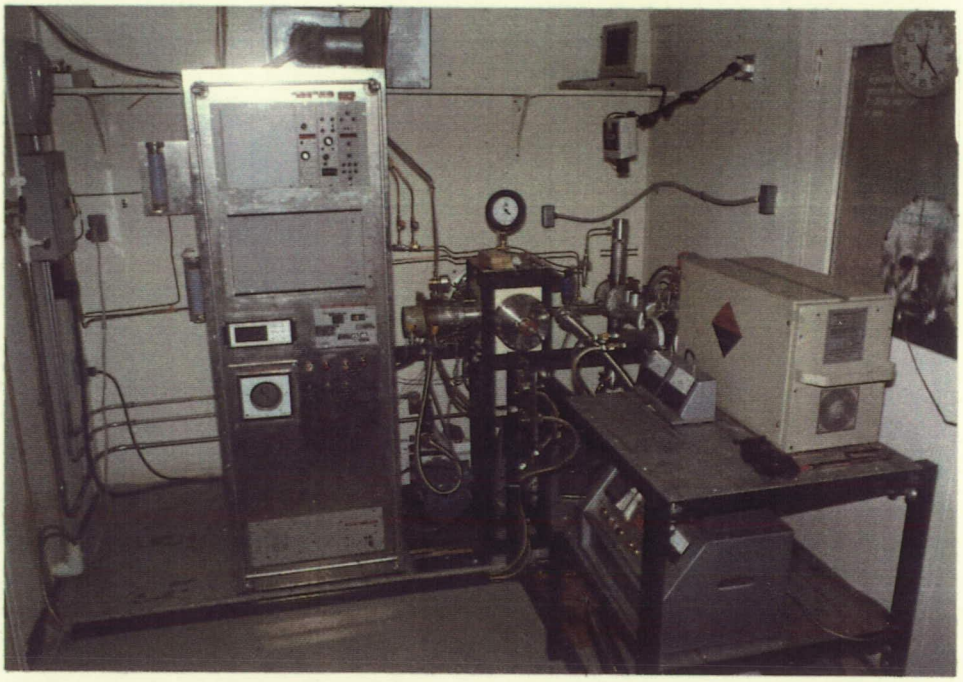

Figure 1.1 Experimental apparatus.

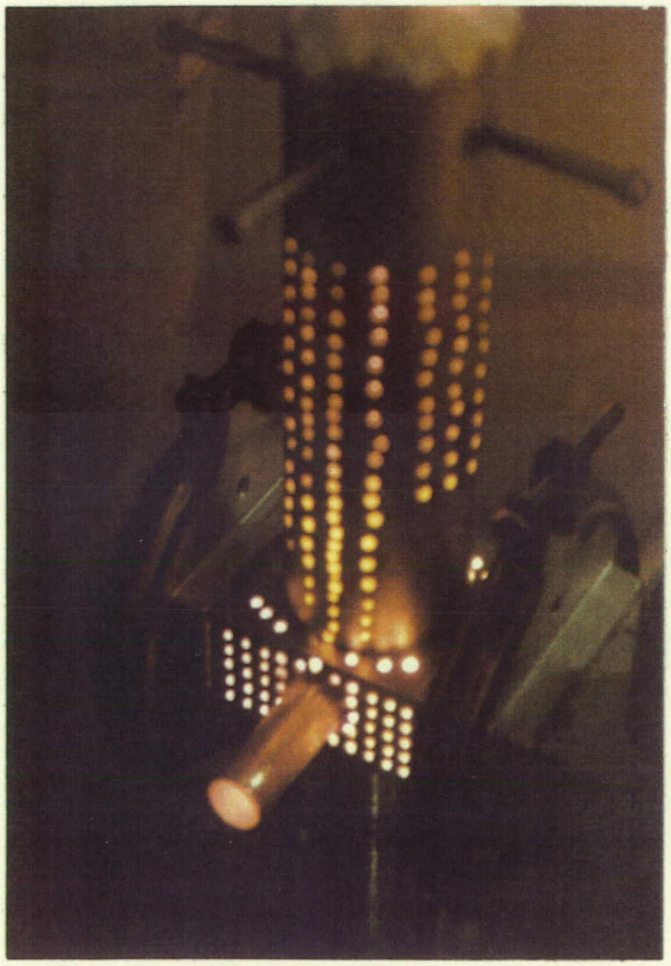

(a) With Plasma

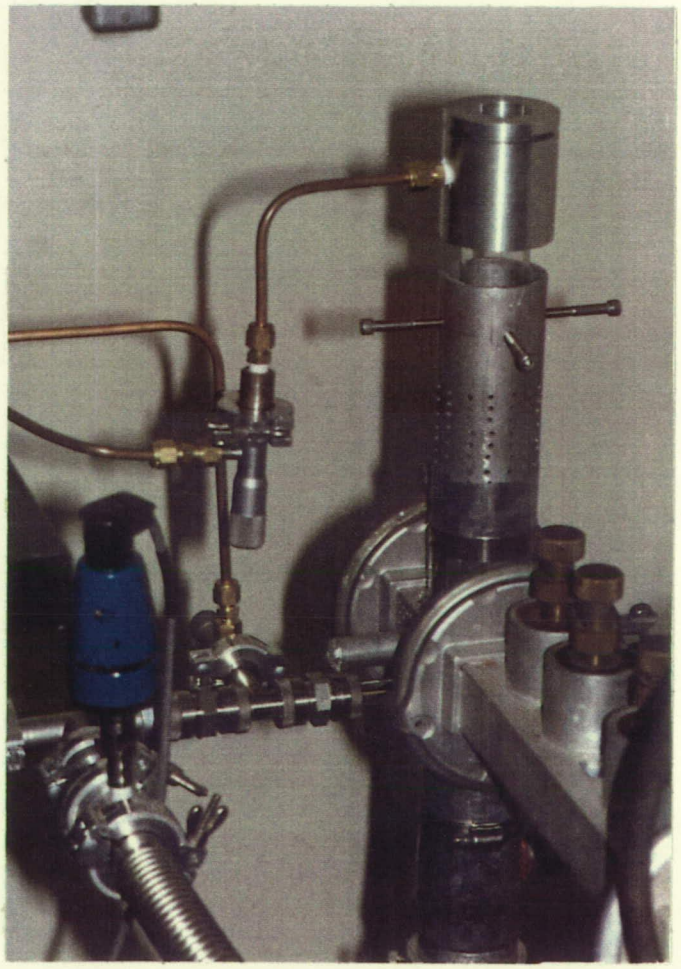

(b) Connected to Mass Spectrometer

Figure 1.2 Applicator where plasma is generated.

Table 1.2 Experimental results for ilmenite: oxygen generation.

Power (kw)	Signal Intensity[a] O_2 (Arbitrary Units)			
	Nitrogen Plasma		Argon-Chlorine[b] Plasma	
	O_2	O	O_2	O
0	0	0	0	0
0.2	1	0	60	7
0.4	0	0	--	--
0.6	0	0	53	6
0.8	3	0	--	--
1.0	24	0	1384	4900
1.4	25	0	--	--
1.6	29	0	--	--

[a] Signal intensity is time averaged and corrected for background O_2 signal.
[b] 10% Cl_2.

Table 1.3 Experimental results for ilmenite: chlorine consumption.

Power (kw)	Signal Intensity[a] O_2 (Arbitrary Units) Argon-Chlorine[b] Plasma	
	Cl	Cl_2
0	1045	585
0.2	603	329
0.6	276	79
1.0	--	--

[a] Signal intensity is time averaged and corrected for background O_2 signal.
[b] 10% Cl_2.

microwave-induced plasma without charge buildup. It was feared that charge buildup would lead to electrical discharge and damage to the reactor vessel. As a result of the success of this work, the program was expanded to include the hydrogen reduction of lunar oxides.

Future Work

Kinetic studies of plasma-enhanced reactions involving both chlorination and hydrogen reduction of lunar ores will continue throughout the coming year. The purpose of this work is to both demonstrate the feasibility of oxygen recovery using a "cold" plasma and to refine our understanding of the role plasma power and plasma

density play in mass transfer, heat transfer, and chemically controlled processes in gas-solid reactions.

Coupled with the experimental program during the coming year will be an analysis of the applicability of plasma processing of lunar ores. That analysis will draw heavily on the experimental information developed throughout the investigation. Scaling up of "cold" plasmas to the size required for a lunar base will be examined. Finally, the cost of the process will be estimated to determine the applicability of the experimental work in establishing a lunar base.

Student Participation

Mr. Daniel Bullard and Mr. Robert Ortega, both U.S. citizens, are working on this project. Daniel has generally been responsible for the construction of the experimental apparatus. He is currently in our M.S. degree program, but plans to petition the department to have his standing changed to the Ph.D. program in January. Dan is doing an excellent job, both academically and in his research.

Robert Ortega joined our research group in July. He has assisted Mr. Bullard and is now engaged in setting up a second plasma unit. Robert is seeking an M.S. degree.

Autonomous Production of Propellants

K. Ramohalli and P. Schallhorn
Department of Aerospace and Mechanical Engineering
The University of Arizona

Abstract

This research work deals with the autonomous production of propellants. Because, typically, 80% to 90% of a spacecraft's mass is propellants, it is advantageous to produce propellants in strategic locations en route to, and at, the desired mission destination. This will then reduce the weight of the spacecraft and the cost of each mission. Since one of the primary goals of the space program is safety, a totally automated propellant production system is therefore desirable. This system would thereby remove, from hostile, high-risk extraterrestrial environments, the constant human intervention currently required in the production of many propellants. This enables the exploration of space to be more than the search for and production of fuel. As a proof-of-concept demonstration, one specific case was chosen for this study, that of composite propellant processor; the principle is more important than the application, and the specific processor used saved SERC the considerable cost of acquiring a new liquid propellant processor that would also have required similar automation.

Background

Currently, most space propellant production is done with constant human intervention. Using a control room, man has total control over all aspects of the propellant production. This is fine on Earth, but it is too costly in space. Thus, the need for automated composite propellant production exists.

Approach

During the last year, we have completed testing on a heating system, which was designed by a graduate student (Paul Schallhorn), for the 1-pint mixer that is to be used for this project. Because propellant production requires mixing the ingredients at two constant temperatures (160 and 140°F), a self-contained water heating system is required for space-based operation. This system provides the required temperatures and only needs an electric power source to drive the pump motor and to heat the water in the heaters. This is not unrealistic, considering that electricity is also required for the mixer and controlling computer.

One approach, therefore, is to use a personal computer to control the introduction and mixing of the composite propellant ingredients (making sure that temperature is

constant on the walls of the bowl, detecting local "hot spots" within the mixture, and taking in-situ measurements of the viscosity of the mixture to check if it is within an acceptable range) in the mixer. Then, the mixture is pumped, via a computer program, into a cast, which will be placed into an oven for curing and then stored for future use.

Results to Date

The major results for 1989 are as follows:

1. During the spring of the year, the heating system for the propellant mixer was thoroughly tested for its ability to achieve the design requirements. The system not only achieved, but greatly exceeded these requirements. The system was able to maintain a negligible temperature drop across the bowl of the mixer (the 1°F temperature drop for which the system was designed had easily been reached). The temperature of the system was easily changed from 160°F to the required 140°F in a short amount of time, even without the aid of the computer. The automatic control work performed by Richard Wilson has allowed the system to easily maintain the required temperature within a ±2°F tolerance, with this tolerance continually decreasing.
2. An IBM PS/2 Model 80 was purchased for use on this project. This model has an Intel 80386 microprocessor operating at 20 MHz, a 115-megabyte hard disk drive, 4 megabytes of RAM, and a 1.44-megabyte 3.5-inch internal floppy disk drive. The computer was ordered with the following peripherals: a 14-inch VGA monitor, an 80387 math coprocessor, a 1200-baud internal modem, two 5.25-inch external diskette drives (360 Kb and 1.2 Mb), a mouse, and a Hewlett Packard Laserjet II printer. The computer arrived in January, and the peripherals arrived in early February. The computer system was operational by the middle of February. This computer system is also being used on various other SERC projects.
3. An Inframetrics infrared camera, Model 600L, has been purchased for this project. It will be used for direct surface temperature measurement of the propellant slurry. It will be mounted (not permanently) at the entrance of one of the mixer's view ports. It will eventually be integrated into the computer system for aiding the temperature control process of the automation.
4. A prototype hopper is currently being built for the injection of the propellant ingredients. This work is being done by undergraduate students under the supervision of Paul Schallhorn. This portion of the project has a projected completion date of May 1990. The hopper consists of a series of chambers containing the required ingredients, a means of weighing the solid ingredients, an

injection system for the liquid ingredients, a thermal jacket to preheat the ingredients, and a port to inject the ingredients.

5. An in-situ viscometer is being designed for placement within the mixing bowl. This would give more accurate viscosity measurements of the slurry at any point in time, and it is the only way in which an automated system could check for viscosity problems.

Summary

In summary, this task has shown that there is a need for automatic space-based production of propellants. We have also shown that there is no current system to produce composite propellants without human intervention. Work has begun on achieving this task. The heating system (previously designed) for a 1-pint vertical propellant mixer has been thoroughly tested. The result is that the heating system meets or exceeds the design criteria. A prototype hopper is being built for the injection of the required ingredients. It consists of a measuring system (for solid particles), a liquid injection system, a series of containers for the solid particles, a thermal jacket, and a delivery system. An IBM personal computer has been acquired. An Inframetrics infrared camera has been procured for temperature measurements of the propellant slurry. An in-situ measuring device is being developed for future integration in the system.

Participants

We would like to take this opportunity to thank Gary Hopkins and Milton Schick for their help in assembling and maintaining the entire system. We would also like to acknowledge Richard Wilson, who is doing the automatic controls portion of the heating system.

Extraction of Volatile and Metals From Extraterrestrial Materials

J. S. Lewis
Lunar and Planetary Laboratory
The University of Arizona

Abstract

Since 1 March 1989, we have concentrated our attention on the extraction of ilmenite from extraterrestrial materials and on the planning and development of laboratory facilities for carbonyl extraction of ferrous metal alloys. Work under three subcontracts was administered by this project: electrolytic production of oxygen from molten lunar materials (L. Haskin, Washington University), microwave processing of lunar materials (T. Meek, University of Tennessee), and production of a resource-oriented space science data base (D. Davis, Planetary Sciences Institute).

Introduction

As the first principal target of SERC's research, the production of propellants from nonterrestrial materials, especially those found on the lunar surface, has necessarily been the focal point of much of our research activity. Since the large majority of the mass of an H/O propellant (89%) is liquid oxygen, and since programmatic considerations seem to favor relatively early operations on the Moon, the focus of efforts within this program has been the production of oxygen on the Moon. Our research group has participated in this program in two very different ways. First, we have studied the prospects for extracting reactive FeO-bearing minerals suitable for oxygen production from the lunar regolith, concentrating on the properties and extraction physics of ilmenite and the preparation of suitable stimulants for lunar-derived ilmenite. Second, we have searched for simple ways to coproduce other products along with oxygen, so as to maximize the total yield of useful products per unit energy expended. This latter search has exposed ferrous metals and refractory oxides as the most likely products to accompany lunar oxygen production. We have chosen to begin this effort with an experimental investigation of the use of the gaseous carbonyl process for recovery of ferrous metals in conjunction with the ilmenite reduction and melt electrolysis schemes for lunar oxygen production.

Lunar Ilmenite and Simulants

As the result of a continuing literature search, several major concerns regarding proposed schemes for oxygen production from lunar ilmenite have been identified. These are the effects of other minerals on oxygen production, the chemical nature of simulants of lunar ilmenite, procedures for beneficiation of ilmenite from lunar regolith

feedstocks, and the merits of using lunar fines versus lithic fragments as the source of ilmenite.

Effects of Other Minerals. Hydrogen reduction experiments by Williams (1985), using terrestrial ilmenite simulants containing trace amounts of iron sulfides, has demonstrated that small amounts of sulfur have dramatic effects on the ilmenite reduction process. During hydrogen reduction of the simulant, hydrogen sulfide formed along with water vapor in such quantity as to force the termination of the experiment. When such a mixture is electrolytically decomposed to regenerate hydrogen and oxygen, sulfur is oxidized to sulfur trioxide and forms sulfuric acid, which is highly corrosive. Since lunar soils typically contain approximately 0.5 wt% of the sulfide mineral troilite (stoichiometric FeS) (Vaniman et al. 1989), some method of removing sulfides from the feedstock must be devised. Because both troilite and lunar ilmenite are nonmagnetic (*stoichiometric* FeS is antiferromagnetic whereas familiar terrestrial pyrrhotite is ferrimagnetic), and since both minerals have nearly the same density, devising an adequate separation scheme is not trivial. Pre-oxidation of the sulfide by roasting to release sulfur dioxide is a possibility, but this necessitates more complexities: either (a) the SO_2 must be discarded, which wastes oxygen, or (b) it must be further reacted to make sulfuric acid *for process use*, which apparently requires the demonstration of a whole new family of processes in which some practical and profitable use can be made of the sulfuric acid, and in which the sulfuric acid can be recycled. This introduces a wholly unwanted set of complications into what was intended to be a simple, early processing scheme to make oxygen.

Simulants. Lunar ilmenite is almost stoichiometric $FeTiO_3$ and, hence, contains no ferric iron. Therefore, terrestrial ilmenite, which is a solid solution of Fe_2O_3 in $FeTiO_3$, is not a good thermodynamic or kinetic analogue of lunar ilmenite. Synthetic ilmenites are useful for determining the effects of minor substitution of other (lunar) constitutents of the kinetics of ilmenite reduction. The most abundant solute in lunar ilmenite is $MgTiO_3$, which is never the dominant impurity in terrestrial ilmenites. Synthetic ilmenites, although useful for kinetic studies, do not suffice either for beneficiation experiments or for determining the effects of other native lunar minerals on the reduction process.

In the search for a better, more relevant analogue of lunar ilmenite, we have considered in some detail the use of many different types of meteorites. The closest analogue is found in the eucritic (basaltic) meteorites, ilmenite-bearing rocks with overall chemistry and oxidation state similar to lunar basalts. Indeed, with respect to oxidation state, the eucrites are known to be formed under conditions strikingly similar

(but not identical) to those under which lunar basalts formed, at far lower oxygen fugacities than terrestrial basalts. Table 1.4 compares the composition of lunar and eucritic ilmenite.

Table 1.4 Composition of natural lunar and eucritic ilmenites.[a]

	Lunar		Eucritic	
Moiety	Mean	Range (wt%)	Mean	Range (wt%)
FeO	43.3	35.20 - 47.70	44.20	42.80 - 45.00
TiO_2	52.7	49.90 - 55.50	52.80	52.50 - 53.00
Al_2O_3	--	0.10 - 0.30	0.06	0.03 - 0.11
Cr_2O_3	0.64	0.50 - 2.12	0.09	0.03 - 0.27
MgO	2.23	0.00 - 9.50	1.05	0.46 - 2.35
MnO	0.42	0.00 - 0.95	0.88	0.82 - 0.93
CaO	--	0.00 - 0.30	0.10	0.03 - 0.16

[a] Lunar data from a compilation of 133 ilmenites from high-Ti basalts (Vaniman et al. 1989), except for Al_2O_3 and CaO, which are Apollo 11 ilmenites (Masan and Nelson 1970). Ilmenite data for eight eucrites are from Bunch and Keil (1971).

Beneficiation. Due to its lack of ferric iron, lunar ilmenite has a low magnetic susceptibility, similar to that of the coexisting silicate phases. Attempts to beneficiate eucritic ilmenites (which also lack ferric iron) magnetically were unsuccessful. It appears that electrostatic separation is the most viable presently conceived technique for use with lunar feedstocks. The amount of recoverable ilmenite in the lunar soils (about 1-2% ilmenite) is far lower than in high-titanium basaltic rocks (8-16%) (Vaniman, personal communication). Moreover, experiments by William Agosto have shown that electrostatic separation experiments on terrestrial soil simulants *lacking agglutinates* (shock-fused glass and rock fragments) produced fairly satisfactory enrichments of ilmenite. This suggests that lithic fragments from high-titanium basalts may be a much better ilmenite source than soils.

Unfortunately, the use of rocks as a feedstock requires a crushing step before beneficiation, and crushing may not, by itself, efficiently liberate single ilmenite grains. During a recent attempt to separate ilmenite from a crushed eucrite, the rock did not disaggregate cleanly along grain boundaries and most of the ilmenite remained trapped in composite grains. In addition, a serious "static cling" problem was observed, in which individual mineral and composite grain-sized lithic fragments were coated with a fine adherent dust produced during crushing. This coating introduced a large amount

of contamination, including FeS, into even the "ilmenite grain" fraction. This problem is traditionally combated by passing moist air over the material, a solution most inappropriate for use on the Moon. Further, static (and van der Waals) adhesion of particles is likely to be much more severe in the lunar environment than in our laboratory, since lunar grains lack adsorbed multilayer coatings of "sticky" (high-dipole-moment, easily condensed, or highly polarizable) gases that, on Earth, inhibit the "welding" of these grains to each other at their points of contact. At the very least, study of a variety of methods of disaggregating strong rocks is needed.

Ferrous Metal Extraction

Extraction and use of nonterrestrial ferrous metals is very attractive for several reasons that are quite unrelated to the terrestrial mining experience. First, the iron-group elements are extremely abundant in the solar system. The terrestrial planets, their moons, and the asteroids are generally about 30% iron and nickel by mass. Further, these elements are often found as native metals, instead of being tied up in thermodynamically stable oxides and sulfides as they are in Earth-surface ore deposits. Indeed, some belt asteroids, and even one near-Earth asteroid, have reflection spectra characteristic of pure native metal. The amounts of ferrous native metals available in nearby space are not trivial; one of the metallic (M-type) asteroids in the belt, 16 Psyche, has a diameter of 250 km. If the surface composition is representative of its interior, Psyche contains about 6×10^{16} tonnes of ferrous native metals, equivalent to 200,000,000 years of global iron and steel production at present rates.

On a more modest scale, several opportunities for acquiring ferrous native metals for early use in space present themselves. First, there are native metals found in the lunar regolith, both tiny fragments of asteroidal metal from the explosion of impactors and nearly pure elemental iron made by reduction of lunar FeO-bearing minerals by solar wind-implanted hydrogen. These forms of native metals make up about 1000 ppm of the regolith, most of which is readily extractable by a magnetic rake. Second, the ilmenite reduction process leaves an intimate, partly sintered mixture of metallic iron and the titanium oxide rutile (TiO_2). Each ton of oxygen extracted leaves behind 4.5 tons of metallic iron, 5.7 tons of rutile, and an unknown amount of unreacted ilmenite and dross. Third, electrolysis of molten silicates produces a cathode deposit of metals, dominantly iron during the early stages of electrochemical reduction. The mixed metals in the cathode deposit also include nickel, cobalt, chromium, and manganese, all of which form gaseous carbonyls. Further electrolysis produces abundant silicon, leaving a refractory oxide melt rich in calcium, magnesium, titanium, and aluminum.

Beyond the Moon, asteroids are abundant, rich sources of ferrous native metals. Concentrations of 10 to 30% by weight of native metals are typically present in undifferentiated (chondritic) meteorites, and many asteroids in the inner part of the belt have metallic (M-type) reflection spectra. There is even a near-Earth asteroid that has an M-type spectrum. These bodies may be up to 99% native ferrous metal alloy. The concentration of free metals in the **average** meteorite is about 20%, some 200 times as high as in the lunar regolith.

In order to extract and purify these metals with minimal energy consumption, it is highly desirable to avoid forming intermediate compounds that are strongly bonded. Attractive schemes include physical separation by magnetic beneficiation and volatilization by the gaseous carbonyl process. Efficient magnetic separation, even in the case of the lunar regolith, requires crushing to a fine enough size to liberate particles of metal. Both native metal minerals, kamacite (alpha iron; 4 to 7% Ni content) and taenite (gamma iron; 20 to 60% Ni), are ferromagnetic, as are the widespread trace minerals schreibersite, $(Fe,Ni)_3P$, and cohenite, $(Fe,Ni)_3C$. The sulfide mineral troilite, FeS, is antiferromagnetic and, hence, follows free metals during magnetic extraction only because of the common textural association of FeS with metal in intergrowths. In carbonaceous chondrites, the metals are progressively oxidized, culminating in zero free metal and abundant magnetite in the highly oxidized, carbon- and volatile-rich Ci chondrites. Magnetite is ferrimagnetic and, hence, it is almost as easily extracted as free metal. Strong heating of CI chondrites leads to extensive autoreduction, with release of carbon oxides and water and the formation of metallic iron.

Gaseous carbonyl extraction is appealing for several reasons (Lewis et al. 1988): The only reagent necessary is carbon monoxide, which is released upon heating every known class of meteorite. The compounds formed, principally iron pentacarbonyl and nickel tetracarbonyl, are weakly bonded, can be readily separated from each other by distillation, and can also be readily separated into their component elements by gentle thermal decomposition (or by isothermal pressure reduction). Separation of ferrous metals is not practical in any operation involving melting of a metal mixture. It is indeed remarkable that the low-energy route to ironmaking also gives a natural and highly effective route to making pure metal separates. This is very desirable, because it permits the formulation of a wide variety of alloy compositions.

We have surveyed the literature on the thermodynamics and kinetics of gaseous carbonyl formation and developed several designs for extraction systems. We have acquired several of the crucial components and will be assembling them in the near

future, so we can resume the experimentation we originally began in 1982. The ideal materials for the system construction are brass and aluminum, which are completely invulnerable to carbonyl attack. The initial experiments will be aimed at validating the safety and functional design of the system. Safety is paramount in handling carbonyls, because they are highly toxic. The next step will be the volatilization of pure samples of iron and nickel (and possibly cobalt, if we are confident in the reliability of the system at the high pressures necessary for cobalt carbonyl formation). We may then move directly to volatilization of meteoritic iron. Iron meteorite samples are available in large quantities and at low prices, and nothing is to be gained by lengthly and expensive excursions into simulant production and validation. Indeed, magnetic separates from chondritic meteorite powders are themselves very good first-order stimulants of lunar regolith native free metals and will permit us to prepare for requesting lunar samples for similar study.

We will then use native iron produced in ilmenite reduction experiments and mixed-metal cathode deposits from Haskin's electrolysis project as feedstock for the carbonyl extraction. Analytic services will be provided by Boynton (neutron activation) and by Ruiz (inductively coupled plasma mass spectrometer). Platinum-group metal extraction from the carbonyl volatilization residues will be carried out by Freiser's group (Strategic Metals Recovery Research Facility).

We are not presently planning extensive experimentation on fabrication of metal products in our laboratory. However, we have already begun discussions with Vaporform Products regarding collaborative research on codeposition of Fe/Ni alloys. They have the greatest body of expertise in the world on fabrication of nickel products by chemical vapor deposition (CVD) from gaseous nickel carbonyl, but have no experience with the effects of admixtures of iron carbonyl as an "extender." It is, however, well established that pure nickel tetracarbonyl produces nickel deposits ("castings") of excellent quality, whereas pure iron pentacarbonyl produces only a fine black powder of ultra-high-purity iron. The intermediate compositional regime is ripe for exploration. The facilities required for large-scale experimentation with mixed-carbonyl CVD are available only at their facility in Pennsylvania.

References

Bunch, T. E. and Keil, K., 1971, "Chromite and ilmenite in nonchondritic meteorites," *Amer. Mineral.* 56, 146-157.

Lewis, J. S., Jones, T. D., and Farrand, W., 1988, "Carbonyl Extraction of Lunar and Asteroidal Metals," pages 111-122 in *Space 88*, AIAA, New York.*

Mason, B. and Nelson, W. G., 1970, *The Lunar Rocks*, J. Wiley and Sons, N. Y.

Vaniman, D., Heiken, G., and Muhich, T., 1989, "Lunar Ilmenite," preprint.

Williams, R. J., 1985, "Oxygen Extraction From Lunar Materials: An Experimental Test of an Ilmenite Reduction Process," in *Lunar Bases and Space Activities of the 21st Century*, LPI, Houston.

*See Appendix C.

Ilmenite Beneficiation and High-Precision Analyses of Extraterrestrial Material

J. Ruiz
Department of Geosciences
The University of Arizona

During the past year, our group has worked on characterizing lunar material that has the potential of becoming ilmenite lunar ore. The important aspects of any such material are that it has abundant ilmenite and that the ilmenite be easily separated. The final result sought is a pure (greater than 99% ilmenite) concentrate that will be used as feed for the ilmenite reduction process.

There are two types of starting material available on the Moon. Solid rock (basalt or anorthosite) and regolith. We have not done any ilmenite separation experiments on either of these materials, but have done extensive literature reviews and have separated simulants (meteorites). We have tentatively concluded that, because of the large amounts of agglomerates, regolith may not be the best starting material for ilmenite beneficiation and either basalts or anorthosites may be better. This is because no matter how finely the regolith is ground, it would not be possible to efficiently separate all the ilmenite. This hypothesis, however, needs to be tested with lunar material. We propose, for the next year, to obtain some lunar regolith, which will be used to separate the ilmenite. Since our separation process will be nondestructive, we will be able to return all the regolith to NASA.

We separated meteoritic ilmenite so that Professor Shadman had extraterrestrial simulant for his reduction experiments. Ms. Melinda Hutson and I ground the sample, sieved it, and used conventional separation techniques to separate the ilmenite. It was found that extraterrestrial ilmenite cannot be separated by electromagnetic separators, because of the complete absence of ferric iron in the ilmenite. We used heavy liquid separation procedures to obtain a reasonably pure separate (about 70% ilmenite). Final purification needs to be done by hand picking. The final concentrate will be analyzed by Hutson using XRD before turning the sample over to Shadman. The possible impurities in the concentrate are pyroxens and sulfides. Our work with the meteorite samples clearly shows that magnetic separators will not work with lunar material and that the most likely separation technique that will work on these samples is electrostatic. We will build an electrostatic separator that can be subjected to high vacuum, and we start performing realistic separations on simulants next year. After we have successfully installed the electrostatic separator and have performed some separations with extraterrestrial simulants, we will need to ask NASA for lunar material.

In addition to the separation experiments, we have obtained all the isotopic spikes to make isotope dilution spikes for analyses of trace elements in extraterrestrial material using an induced coupled plasma quadropole mass spectrometer. Our aim is to very accurately analyze elements that might be commerically recoverable from extraterrestrial material and then be brought back to Earth. The elements of interest are mostly platinoids, and the necessary analytical techniques have been developed to analyze small amounts (ppb levels) of these elements. We have already made some of the spikes and plan on finishing the calibration of all spikes and standards next year. Our lab will be among the best laboratories in the country actively analyzing extraterrestrial material for a large number of trace elements at very low abundances. Already, other planetary scientists are interested in analyzing a variety of types of meteorites in this lab.

Production of Oxygen From Lunar Ilmenite

Y. Zhao and F. Shadman
Department of Chemical Engineering
The University of Arizona

Oxygen is a consumable material that needs to be produced continuously in most space missions. Its use for propulsion, as well as life support, makes oxygen one of the largest volume chemicals to be produced in space. Production of oxygen from lunar materials is of particular interest and is a very attractive possibility.

Among the proposed processes, the hydrogen and carbothermal reductions of ilmenite appear very promising. Hydrogen reduction has a relatively simple process configuration; the individual steps are relatively well studied. However, the major problem is the large heating and cooling loads required to condense the water and then heat the hydrogen to its reaction temperature. Handling and storage of large amounts of hydrogen are also a problem. Hydrogen reduction of lunar ilmenite has been studied by several investigators. Carbothermal reduction of terrestrial ilmenite has also been extensively studied, but its application to lunar ilmenite is still an open area for investigation.

The overall objectives of this study can be described as follows:

- Study of the mechanism and kinetics of carbothermal reduction of simulated lunar ilmenite using carbon and, particularly, CO as reducing agents; determination of the rate-limiting steps; investigation of the effect of impurities, particularly magnesium; search for catalysts suitable for enhancement of the rate-limiting step.
- Comparison of the kinetics of carbothermal reduction with those of hydrogen reduction; study the combined use of CO and hydrogen as products of gasification of carbonaceous solids.
- Development of new reduction methods that are based on the use of waste carbonaceous compounds for the process; development of a novel carbothermal reaction path that utilizes gasification of carbonaceous solids to reducing gaseous species (hydrocarbons and carbon monoxide) to facilitate the reduction reaction kinetics and make the process more flexible in using various forms of carbonaceous feeds.
- Development of advanced gas separation techniques, including the use of high-temperature ceramic membranes.
- Development of an optimum process flow sheet for carbothermal reduction, and comparison of this process with the hydrogen reduction scheme, as well as a general comparison with other leading oxygen production schemes; use of new and advanced material processing and separation techniques.

Experimental Method

Two reactor systems have been designed, fabricated, and put into operation: A small fluidized bed reactor for quick response times and a thermo-gravimetric reactor system with an electronic microbalance for the continuous measurement of the rate and the sample conversion. A unique method is developed for preparation of two types of ilmenite samples used in the experiments. The first type was pure synthetic ilmenite with impurity less than 0.1%. The second was synthetic ilmenite in which known and controllable amounts of impurities are introduced to simulate actual impurities found in lunar samples. A series of tests, including X-ray diffraction experiments and Mossbauer spectroscopy, were performed on synthetic ilmenite to ensure that the iron in these samples was Fe^{++}.

In each experiment, a known amount of ilmenite was exposed to the reducing gas, and the rate of conversion was monitored using both gravimetric response and continuous monitoring of the gases produced. The starting samples were fully characterized by particle size, porosity, surface area, and composition. The important reaction parameters are temperature, reducing gas composition, and flow rate.

Results and Conclusions

A typical temporal profile of conversion is shown in Figure 1.3. The results indicate the presence of three stages:

- Induction stage during which reaction is very slow. Detailed microprobe analysis of samples quenched during this stage indicate that the formation of iron nuclei is the rate-controlling step. The presence of small amounts of impurities can affect this stage.
- Acceleration stage during which rate increases progressively. The reaction rate during this stage is influenced by diffusion of reducing gas into the particles and diffusion of iron away from the reaction front.
- Deceleration stage which is primarily due to depletion of ilmenite.

The effect of temperature on the rate and the activation energies at different levels of conversion are shown in Figure 1.4. The effect of CO concentration on the rate is shown in Figure 1.5. Partially converted samples were probed using high-resolution energy dispersive X-ray analysis; the micrographs and concentration maps show the importance of iron nuclei formation and growth in controlling the rate. Sample results are shown in Figures 1.6 and 1.7.

An important finding during this phase of the project has been the determination of the rate-limiting step and the mechanism of impurities action. These results are

important in developing reaction conditions and selecting catalysts to enhance the rate and lower the reaction temperature. The experimental work on the effect of magnesium, an important impurity, on kinetics is currently in progress. The reactor system is being prepared for experimental runs with hydrogen and mixtures of hydrogen and carbon monoxide as reducing gases.

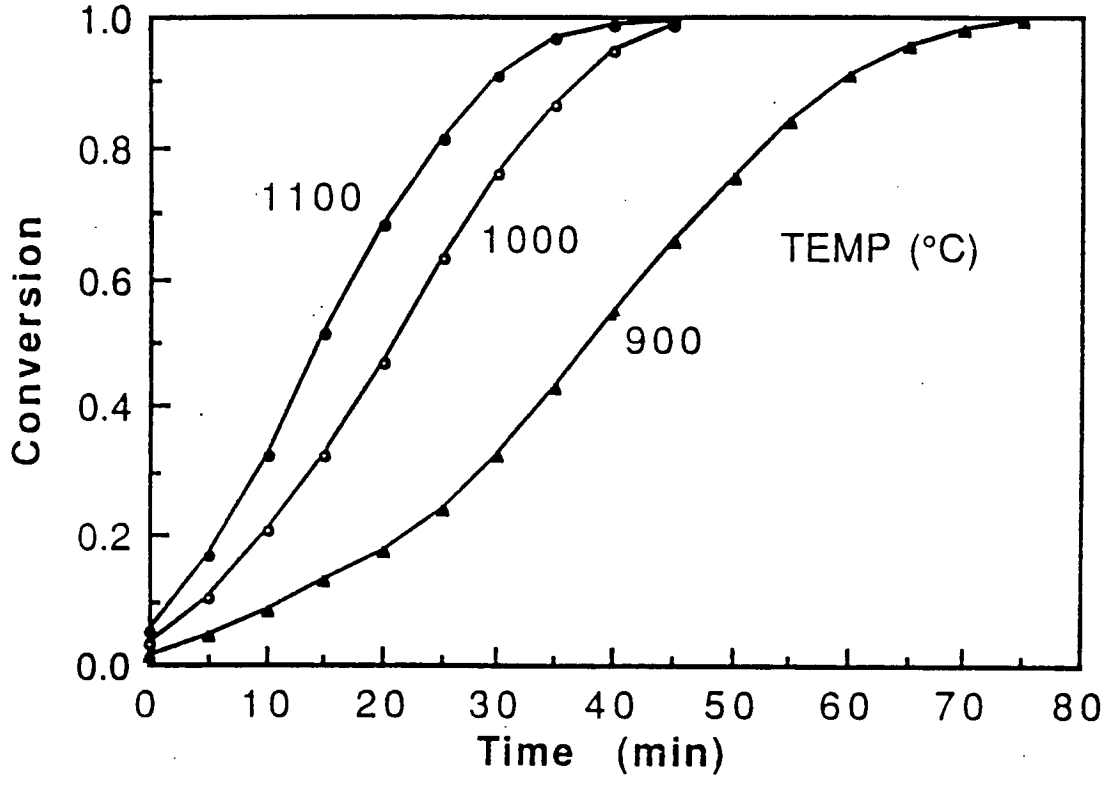

Figure 1.3 Temporal profile of synthetic ilmenite reduction by carbon monoxide.

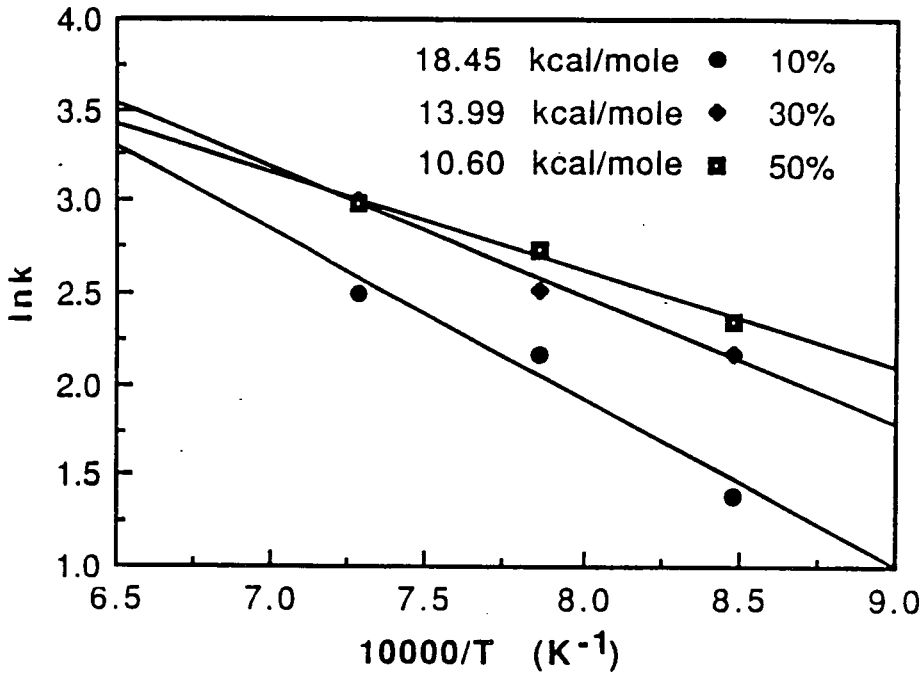

Figure 1.4 Apparent activation energy at 10, 30, and 50% conversions.

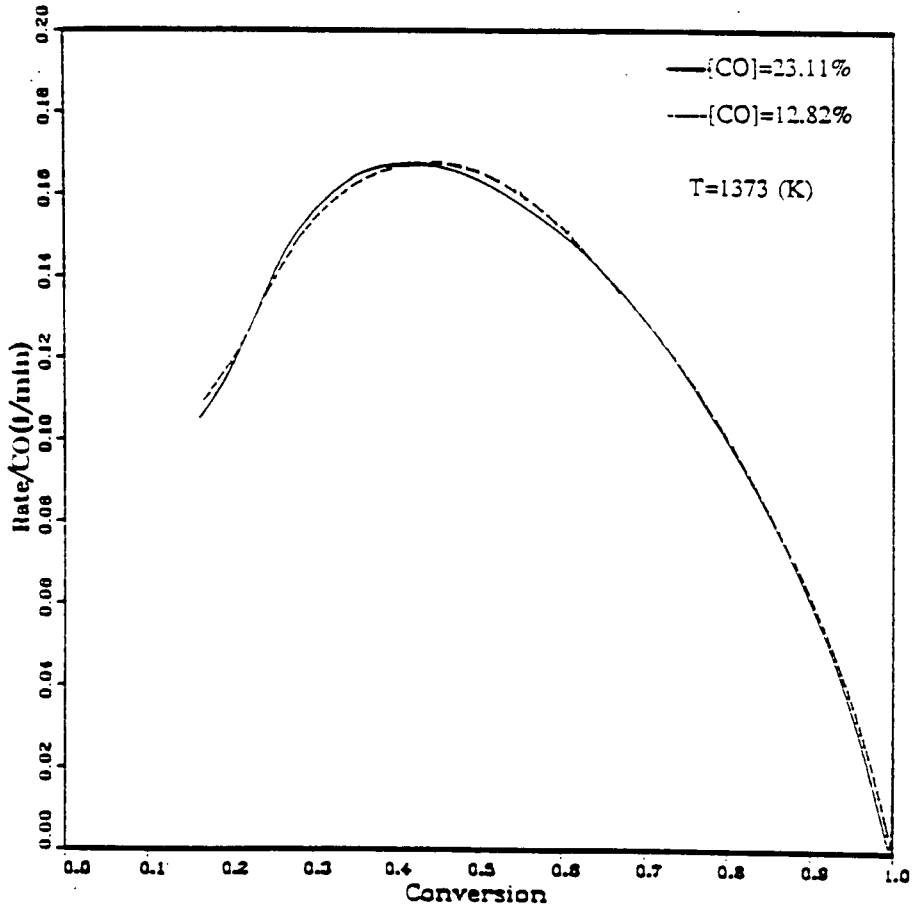

Figure 1.5 Effect of CO concentration on the rate of reduction.

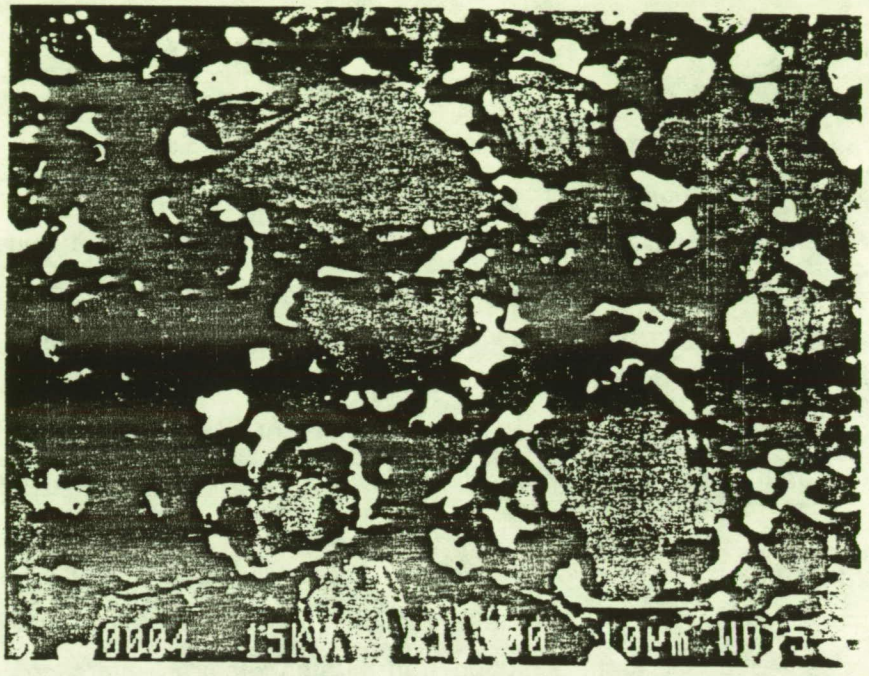

Figure 1.6 SEM backscattered electron micrograph of the polished cross section of a synthetic ilmenite flake after partial reduction at 1000° C.

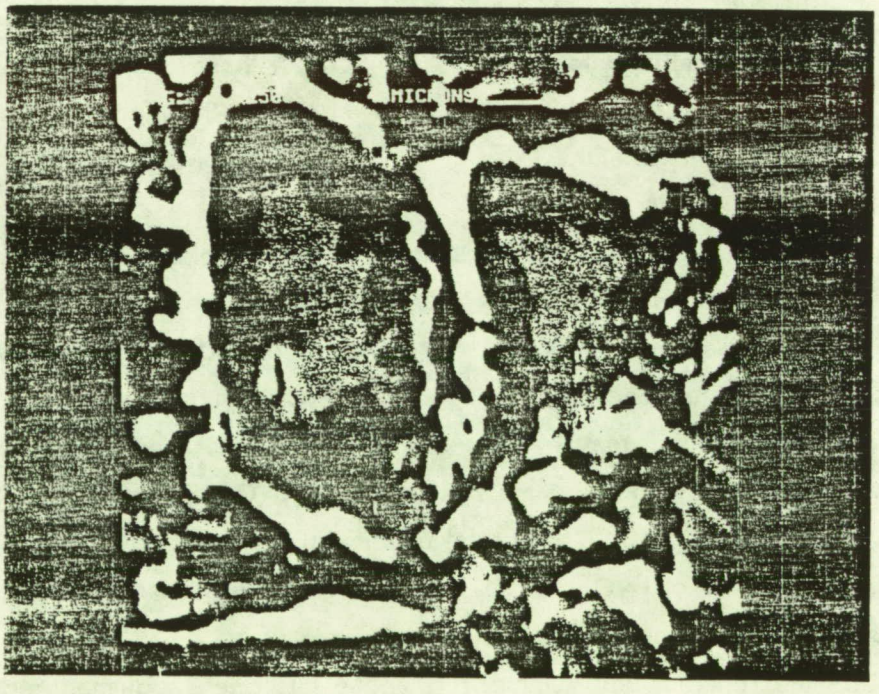

Figure 1.7 SEM secondary electron micrograph of two grains of the sample shown in Figure 1.6.

Volatile-Bearing Phases in Carbonaceous Chondrites: Compositions, Modal Abundances, and Reaction Kinetics

J. Ganguly
Department of Geosciences
The University of Arizona

The spectral and density characteristics strongly suggest that the Phobos and Deimos (the two small natural satellites of Mars) and a significant fraction of the near-Earth asteroids are made of carbonaceous chondrites, which are quite rich in volatile components and, thus, could serve as potential resources for propellants and life-supporting systems in future planetary missions. However, in order to develop energy efficient engineering designs for the extraction of volatiles, we must have a good knowledge of the nature and modal abundances of the minerals in which the volatiles are structurally bound and appropriate kinetic data on the rates of the devolatilization reactions.

The grain size of the volatile-bearing phases in carbonaceous chondrites are often too small (100 to 1000 A) to permit identification under optical microscopes and are best observed under high-resolution transmission electron microscopy (HRTEM). We have, therefore, carried out theoretical calculations to predict the modal abundances and compositions of the *major* volatile-bearing and other mineral phases that could develop in the bulk compositions of C1 and C2 classes as functions of pressure and temperature. These are the most volatile-rich classes among carbonaceous chondrites. The results suggest that **talc** and **antigorite ± magnesite** are the major volatile-bearing phases and are stable below ~400°C at 1 bar in these chondritic compositions. The phyllosilicates are fairly iron rich, with about 25-30 mol% of Fe^{2+}- end-member components in solid solution.

Simulated *equilibrium* heating of a kilogram of C2 chondrite at fixed bulk composition between 400 and 800°C at 1 bar yields about 135 gm of volatile, which is made primarily of H_2O, H_2, CH_4, CO_2, and CO. The relative abundances of these volatile species change as functions of temperature and, on a molar basis, H_2 becomes the most dominant species above 550°C. Hydrogen is a very good propellant and reducing agent, which may be preferentially extracted, according to the above results, by heating the C2 chondritic material to T > 550°C. In contrast to the C2 chondrite, the volatiles given off by C1 material under equilibrium conditions at 1 bar, T > 400°C, consist essentially of H_2O and CO_2. Per kilogram of material, the total yield of volatile is about 306 grams, of which nearly 60 wt% is H_2O.

The theoretical study summarized above has been published recently in a paper entitled "Theoretical Predictions of Volatile Bearing Phases and Volatile Abundances in

Carbonaceous Chondrites" (pages 97-105 in *Space Manufacturing 7*, American Institute of Aeronautics and Astronautics, 1989). A copy is included as Appendix D.

Having identified the most likely mineralogical source of volatiles in the carbonaceous chondrites, we have begun a program of systematic kinetic study of devolatilization reactions. The results will provide the framework for optimal engineering designs for the extraction of volatiles from the mineral phases. These will also help resolve the problems concerning the process and condition of formation of the volatile-bearing phases, especially the phyllosilicates, in the carbonaceous chondrites, which are of fundamental importance to our understanding of the planetary processes.

We have determined the rates of dehydration of talc at 585, 600, 637, and 670°C, P(total) = 1 bar, according to the reaction

$$\text{Talc} = 3\ \text{Enstatite} + \text{Quartz} + H_2O\ .$$

The dehydration kinetics was studied before by Greenwood (1963) at P_{H_2O} = 2 Kb. However, the available data were inadequate to permit reliable extrapolation to lower pressure. The "process condition" for the extraction of volatiles is likely to be set at a pressure of the order of 1 bar.

The starting material talc is nearly pure Mg-end member. The weight loss of a known quantity of material was determined continuously as a function of time at the above temperatures by the thermogravimetric (TG) method. The results are illustrated in Figure 1.8 in terms of fractional weight of talc remaining versus time. The sample was suspended within the reactor in open platinum containers shaped from Pt-foils. The TG setup used in this study has the drawback that it does not permit introduction of the sample within a reactor that has been preheated to the desired run temperature. Thus, corrections have to be made for the weight loss through the induction period to the run temperature. The corrections, however, are quite straightforward. Another drawback of this particular TG setup is that the change of weight as a function of time is recorded in a strip-chart recorder, but it is not available in the form of a digitized output. Thus, the curves in the strip-chart recorder have to be visually read to compute fractional weight loss, which has led to the irregularities seen in the curves in Figure 1.8. The raw data show a very smooth relation of weight of talc versus time. We are in the process of developing a TG setup that would permit direct introduction of the sample into a preheated reactor and also provide digitized output of the data.

We have not yet carried out detailed analyses of the experimental data to obtain the kinetic parameters and to understand the mechanism of reaction. These analyses

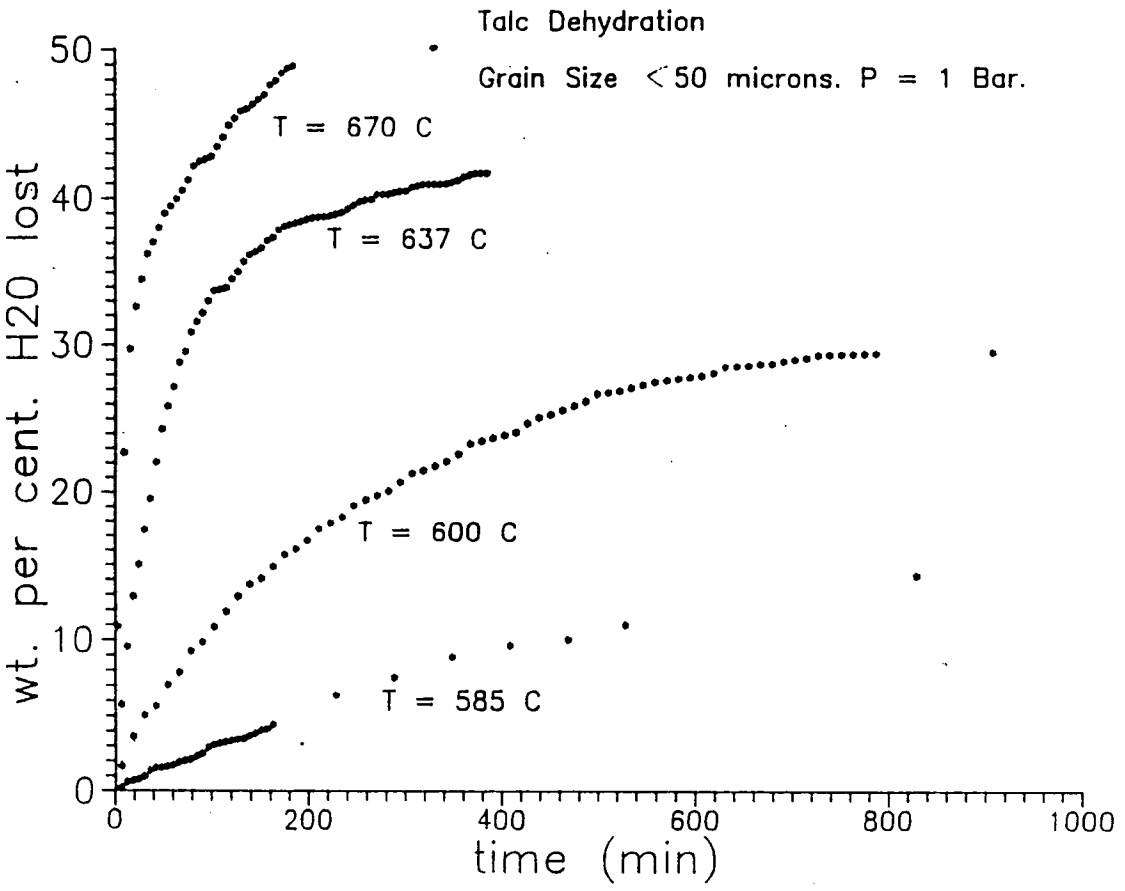

Figure 1.8 Weight fraction of talc remaining as a function of time at different temperatures. Reaction: talc → 3 enstatite + quartz + H_2O (Talc: $Mg_3Si_4O_{10}(OH)_2$; Enstatite: $MgSiO_3$; Quartz: SiO_2)

will eventually be carried out after we gather a larger body of experimental data and refine the experimental techniques. However, we find that the dehydration reaction does not seem to follow the first-order mechanism, which is in contrast to the high-pressure results of Greenwood (1963).

It is important for the kinetic study, especially for understanding the mechanism of reaction, to be able to determine the modal abundance of phases at various stages of reactions. In the only work of this nature to date involving phyllosilicates, Greenwood (1963) determined the abundances of the various phases in the run products by the extremely laborious technique of petrographic modal analysis, i.e., by "point counting" the amount of phases under an optical microscope. We have conducted a scanning electron microscopic (SEM) study to see if the relative abundance of phases can be determined on the basis of the spectral identification and X-ray mapping. On standard samples made up of known amounts of talc, anthophyllite, and quartz, X-ray mapping

and software processing of the data resulted in the determination of quartz to talc-plus-anthophyllite combined, but the latter two could not be distinguished separately. However, once the amount of quartz is known, the proportions of talc and anthophyllite can be estimated by mass balance, assuming that no other phase is present. The latter can be checked by microprobe and X-ray analysis. In the analysis of the standard samples, we have, however, systematically overestimated the amount of talc by about 6%. With further work, we hope to be able to refine the method to yield better estimates of phases in a standard mixture.

Reference

Greenwood, H. J., 1963, "The Synthesis and Stability of Anthophyllite," *Journal of Petrology*, Vol. 4, pp. 317-351.

Quantitative Computer Representation of Propellant Processing

M. D. Hicks and P. E. Nikravesh
Department of Aerospace and Mechanical Engineering
The University of Arizona

With the technology currently available for the manufacture of propellants, it is possible to control the variance of the total specific impulse obtained from the rocket boosters to within approximately 5%. Though at first inspection this may appear to be a reasonable amount of control, when we consider that any uncertainty in the total kinetic energy delivered to the spacecraft translates into a design with less total usable payload, even this degree of uncertainty becomes unacceptable. There is strong motivation to control the variance in the specific impulse of the shuttle's solid boosters. Any small gains in the predictability and reliability of the boosters would lead to a very substantial payoff in Earth-to-orbit payload. The purpose of this study is to examine one aspect of the manufacture of solid propellants, namely, the mixing process. We attempt to introduce a unique methodology to enable understanding of this process.

The traditional approach of computational fluid mechanics is notoriously complex and time consuming. We wish to make certain simplifications, yet be able to investigate certain fundamental aspects of the mixing process as a whole. It is possible to consider a mixing process in a mathematical sense as an operator, F, which maps a domain back upon itself (Figure 1.9). An operator which demonstrates good mixing should be able to spread any subset of the domain completely and evenly throughout the whole domain by successive applications of the mixing operator, F.

A two-dimensional model was first developed using this approach. The differential equations of motion were designed to satisfy conditions of continuity and incompressibility for two-dimensional flow in a unit circle. These equations of motion were designed by Arthur Maser and are given as:

$$\dot{x} = [1 + \sin(t)] \left\{ \frac{2y[4x - 2 + [(2 - x)^2 - 3(1 - x^2 - y^2)]^{1/2}]}{3[(2 - x)^2 - 3(1 - x^2 - y^2)]^{1/2}} + 2y \right\}$$

$$+ [1 - \sin(t)] \left\{ \frac{2y[4x + 2 - [(2 + x)^2 - 3(1 - x^2 - y^2)]^{1/2}]}{3[(2 + x)^2 - 3(1 - x^2 - y^2)]^{1/2}} + 2y \right\} \quad (1)$$

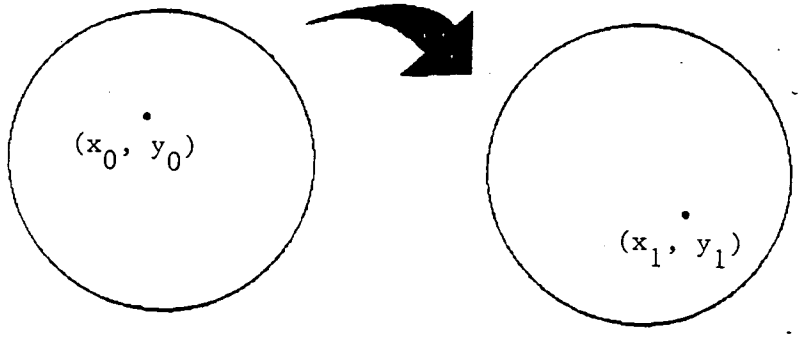

Figure 1.9 Application of mixing operator in a two-dimensional domain.

$$\dot{y} = [1 + \sin(t)]\left\{\frac{2}{9}\left[2x - 2 - [(2 - x)^2 - 3(1 - x^2 - y^2)]^{1/2}\right] \times \left[2 + \frac{4x - 2}{[(2 - x)^2 - 3(1 - x^2 - y^2)]^{1/2}}\right]\right\}$$

$$+ [1 - \sin(t)]\left\{\frac{2}{9}\left[2x - 2 + [(2 + x)^2 - 3(1 - x^2 - y^2)]^{1/2}\right] \times \left[4 + \frac{4x - 2}{[(2 + x)^2 - 3(1 - x^2 - y^2)]^{1/2}}\right]\right\}. \quad (2)$$

If we examine the streamlines generated by this velocity function, we can see that the flow consists of two superimposed eccentric vortices, rotating in opposite directions. The two vortices lie along the x-axis at $x \pm 0.5$. The two components of the flow are modulated by sinusoidal forcing functions that are 180° out of phase. It is the periodic forcing function that gives rise to the chaotic behavior of the flow by perturbing the regular flow field set up by the nested eccentric vortices. Equation (1) is therefore an attempt to design a mapping that will give random mixing from completely nonrandom functions.

Numerical methods were employed to investigate these equations in order to determine if they can give rise to mixing. The computational process and the animation of the results were conducted on a Silicone Graphics IRIS workstation. One objective was to determine if any small region within the domain can spread itself more or less evenly throughout the whole domain given sufficient applications of the mixing operator. To demonstrate this, we defined small clusters of points within the

domain and integrated the equations of motion with the initial conditions being the starting locations of each of these particles. The path of each individual particle could then be followed across successive iterations of the mixing cycle. The period of the mixing cycle is defined as the period of the sinusoidal forcing functions. This approach mimics a traditional approach for studying flow fields.

In laboratory experiments, highly localized amounts of tracer dyes are introduced, via injection, into the fluid, and the position and the distribution of these dyes can be followed as the flow develops. In the numerical experiment, each group or species of particles is branded with its own particular color so that the species can be followed throughout the experiment and its interaction with other species can be studied visually. To be consistent with the mapping approach, the position of each of the particles was updated after each completion of a mixing cycle. In several simulations of the mixing process, five sets of particles, initially very tightly spaced together, were considered. Each block of particles represents a 30-by-30 set of particles, and we ran the simulations across 20 iterations of the mixing cycle. Figure 1.10 documents the graphical animation derived for these simulations. Each successive frame in the sequence represents the application of one or more mapping operations onto the previous frame and, thus, we are able to study how the flow field evolves through time. We can see how very quickly all apparent structure to the species distribution becomes lost, and we state that our original mapping can give rise to good mixing of the domain within a few iterations of the mixing cycle. We recall a theorem in set theory that states that for any two-dimensional mapping of a domain back upon itself, there must be at least one invariant set or, in terms of the mixing process, at least one dead zone. We therefore seek to find this invariant set. If we animate the same data set such that each successive mapping of the species is superimposed on top of the previous ones, then any region of the domain that remains unmixed should become apparent. We find that when we graph the data with this approach, one dead zone can be found in the lower right-hand corner (Figure 1.11).

Another test of mixing can be outlined as follows. We partition the domain into many elements of equal area. We begin with a particle in some initial position within the domain and follow the particle as it takes many cycles through the mixing operator. A measure can be defined as the number of times the particle falls within an element divided by the total number of iterations. A necessary but not sufficient condition for perfect mixing is that this measure must go to a mean value for each partition as the number of iterations becomes very large. When we apply this test to our operator, we can see that the invariant set becomes apparent as a trough in the plot of the density function (Figure 1.12).

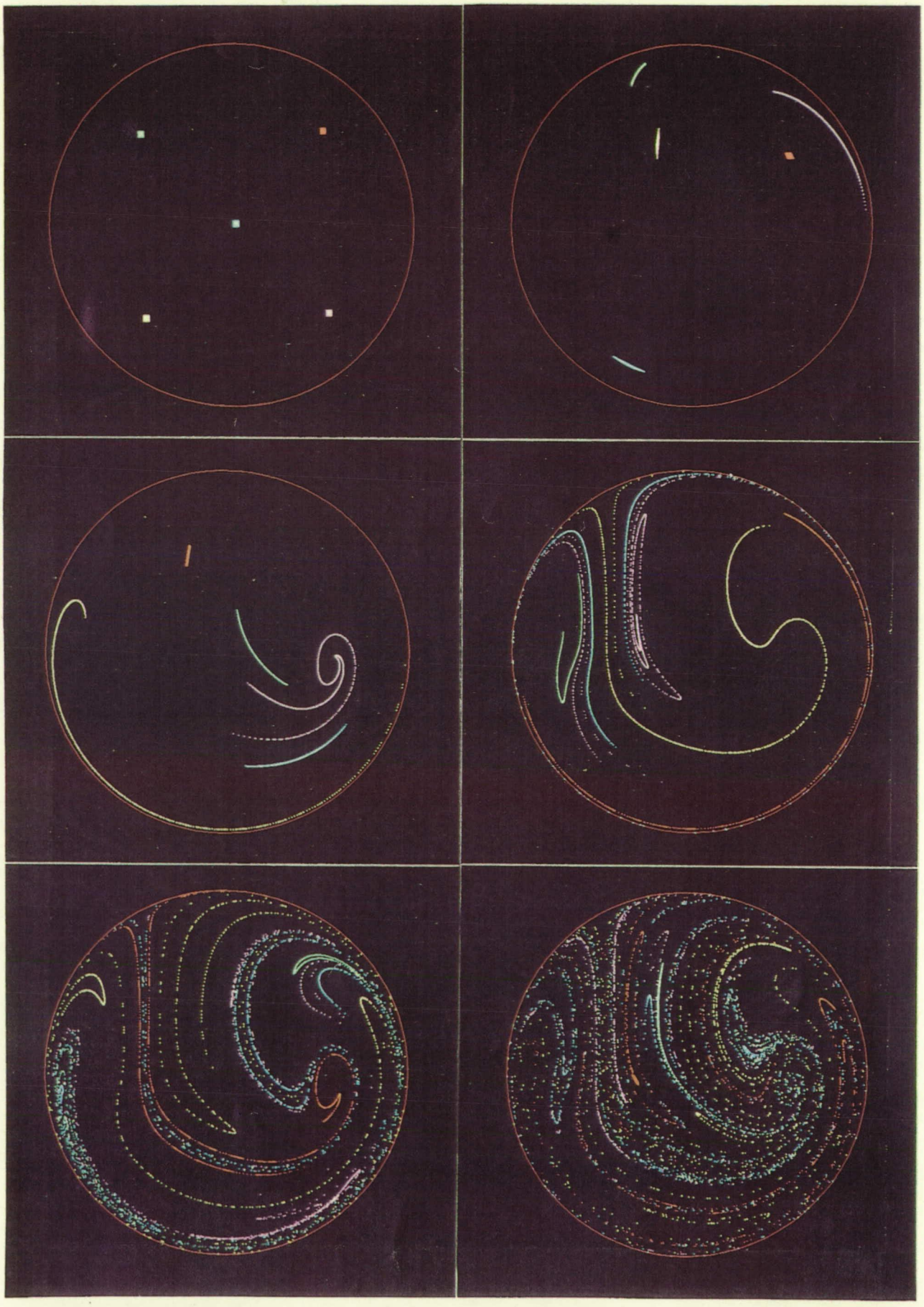

Figure 1.10 Graphical visualization of a two-dimensional mixing process.

Figure 1.10 (Continued).

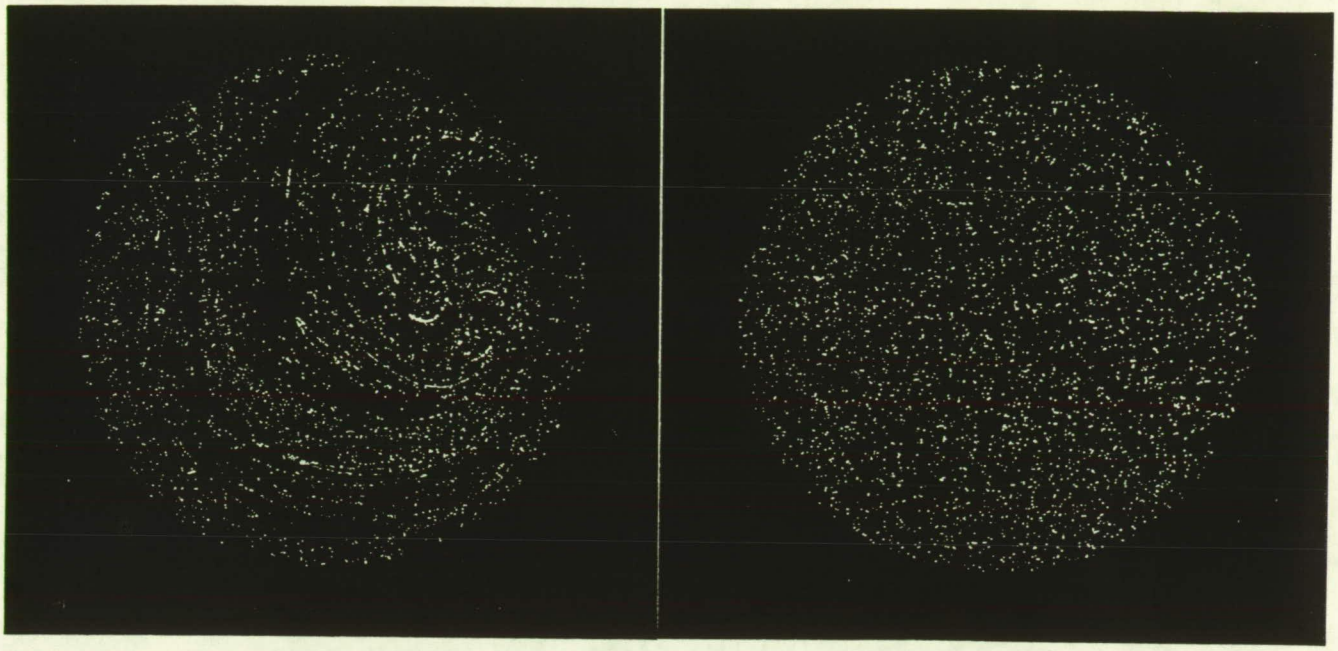

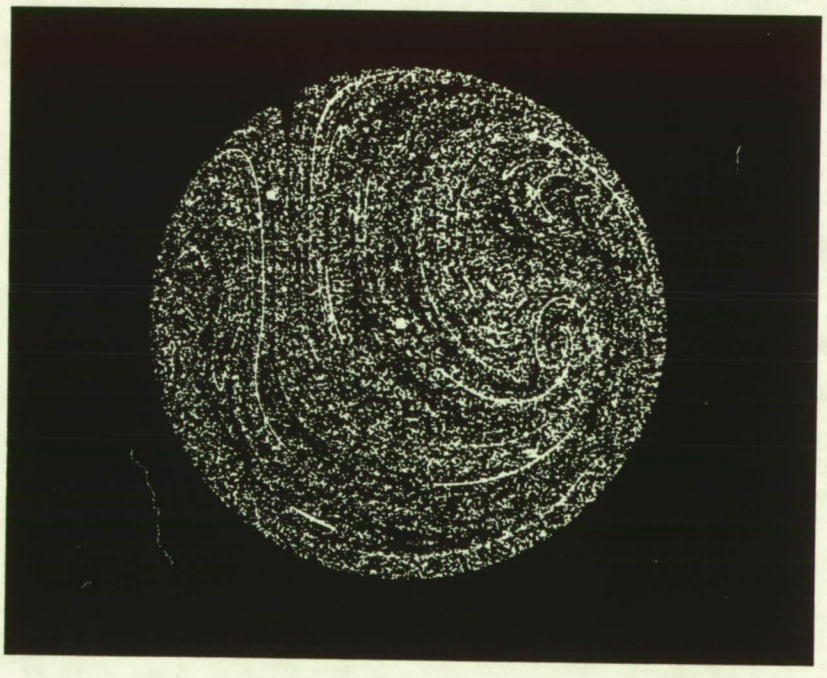

Figure 1.11 Two-dimensional model after 20 iterations.

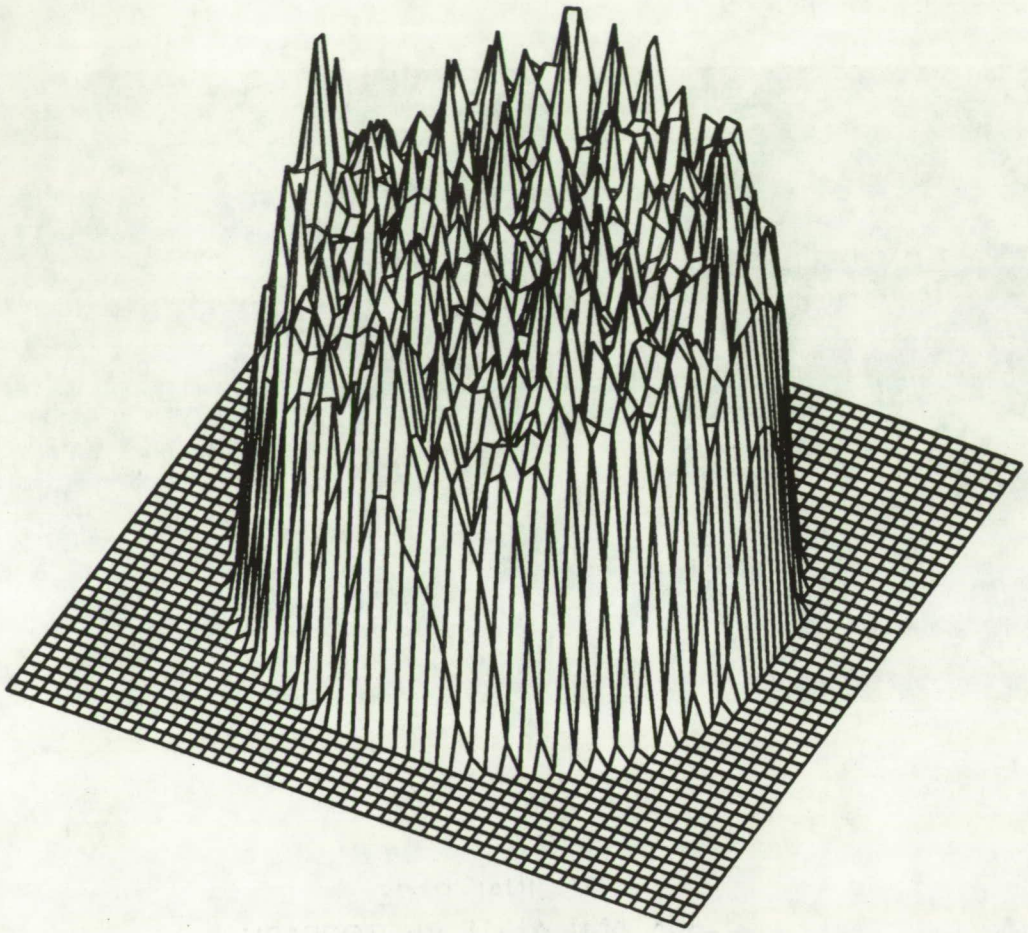

Figure 1.12 Probability density function for two-dimensional mapping.

Later work expanded this approach to investigate mixing in three dimensions. Here, the domain was a torus that was cut and mapped to a unit cube. Particles would flow across the domain and, upon impinging upon the boundary, would be mapped to a point on the opposite face. The mapping function chosen for this experiment was the well-known Baker's transformation. This transformation is an example of a discontinuous mapping that can be used to investigate mixing due to its action of stretching and folding a domain back upon itself (Figure 1.13). We are guaranteed ergodicity through successive iterations of the mapping due to its discontinuity. Real mixers can be designed to mimic this action of splitting, stretching, and refolding the flow without the traditional use of paddles. As in the two-dimensional case, an initially small, very tightly spaced group of particles was carried along by the flow field and the graphical visualization of the results showed the presence of mixing (Figure 1.14). In the three-dimensional case, it was also observed that pseudorandom behavior can be induced from completely nonrandom functions.

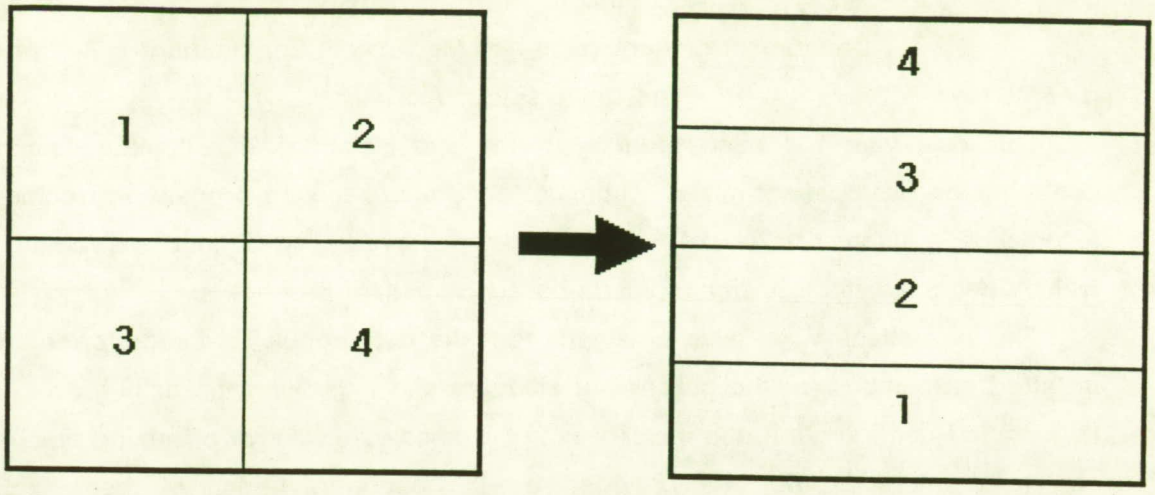

Figure 1.13 Baker's transformation in base two.

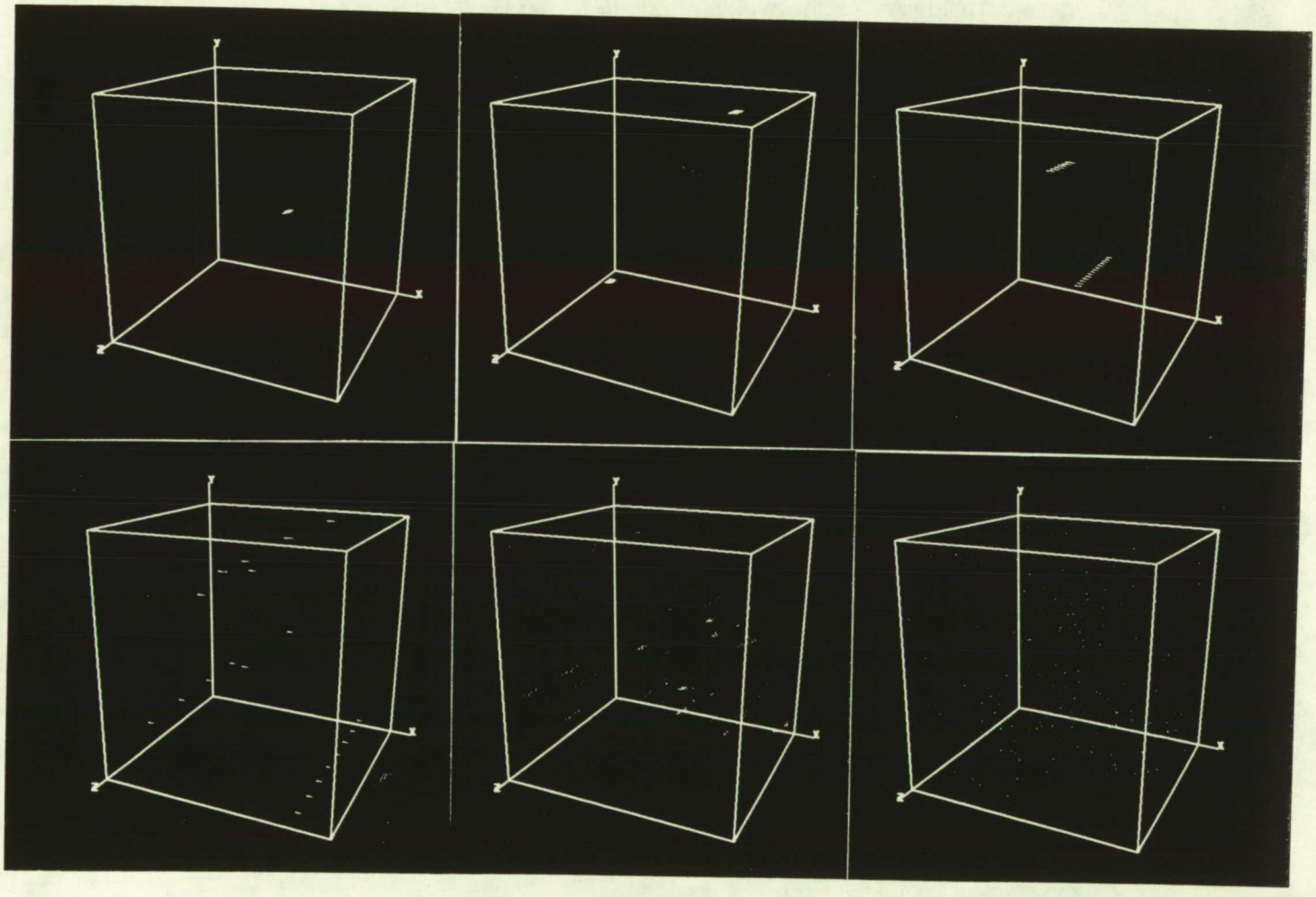

Figure 1.14 Graphical visualization of three-dimensional mixing process.

Temperature Automation for a Propellant Mixer

T. L. Vincent and R. G. Wilson
Department of Aerospace and Mechanical Engineering
The University of Arizona

This past year has been spent analyzing and installing an automatic temperature controller on a propellant mixer. Ultimately, the entire mixing process will come under automation. Automation is not only important for producing a uniform product, but it will be necessary for envisioned space-based propellant production.

The propellant mixer was obtained from the Jet Propulsion Laboratories. It was installed on campus for the purpose of studying and improving the mixing process. In its installed configuration, the mixer was not automated. Control of mixing time, speed, and temperature profile was provided by the operator. Each of these factors is important in providing a reliable and predictable product. Since precise adherence to the temperature profile is very difficult to sustain manually, this was the first component to be automated.

Figure 1.15 illustrates the water circulation system for the installed system. It was a closed system in which water could be drawn from one of two hot water tanks that were set at 140°F and 160°F. The water was circulated around the system by means of a pump. The storage tank provided for fluctuations in the flow. The actual mixing bowl is surrounded by a jacket through which the water flows. By operating valves at the outlet of the hot water tanks, the operator is able to vary the water temperature in the jacket and thus influence the temperature of the components in the mixing bowl. The temperature profile desired during the mixing process is one in which the components are held at 160°F (for the first 35 minutes) and then at 140°F (for an additional 165 minutes). The manual operation involved simply drawing water from the 160°F tank for the first 35 minutes and then drawing water from the 140°F tank for the remaining time. However, this procedure did not provide an accurate profile, as illustrated in Figure 1.16. This figure illustrates (for the first 65 minutes) the desired temperture profile, the water temperature in the jacket, and the temperature at the inside of the jacket in contact with the materials being mixed. This latter temperature (jacket temperature) is taken to be representative of the temperature of the components.

In order to improve the jacket temperature profile, as well as to automate the process, a control system (Figure 1.17) was designed and implemented. The system uses the same water circulation system as before, except now water is drawn from the two tanks by means of a control valve. Rather than having the tanks at the two set-point

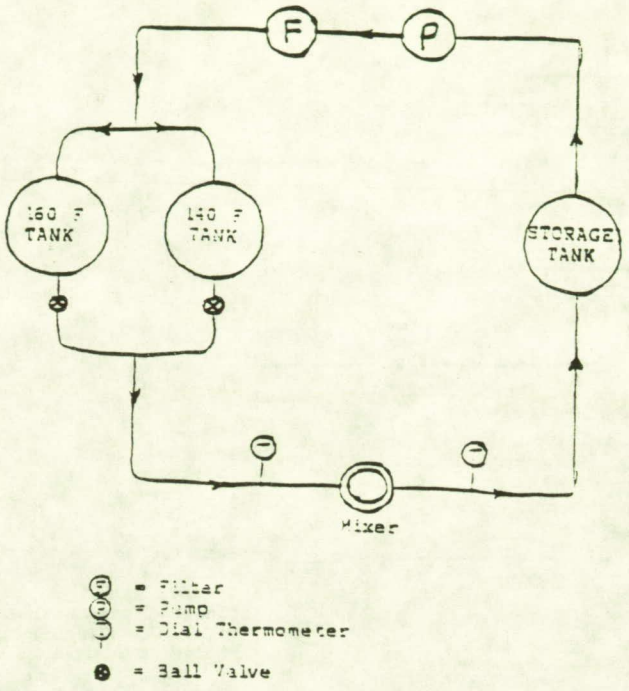

Figure 1.15 Original water circulation system.

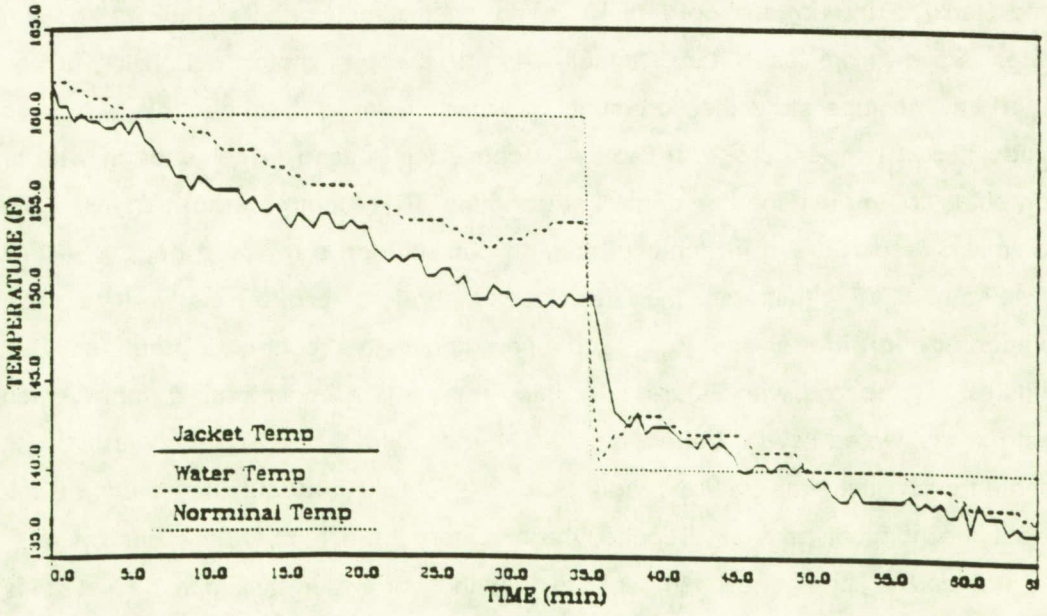

Figure 1.16 Temperature profile for the manual control system.

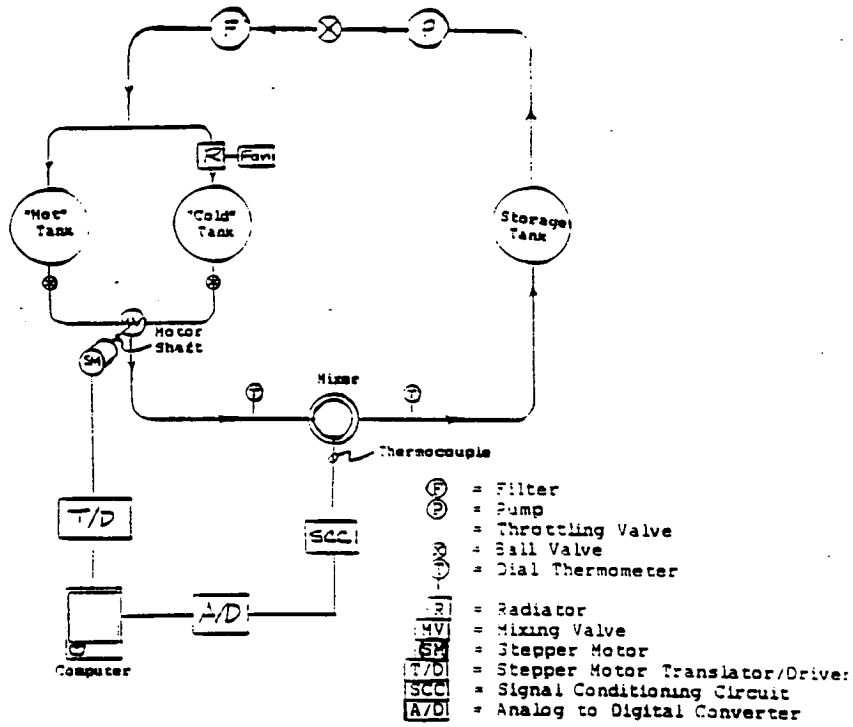

Figure 1.17 Automatic control system.

temperatures, one tank (hot tank) is set for a temperature greater than 160°F and the other tank is turned off (cold tank). The control valve that regulates the amount of water drawn from each tank is set using a stepper motor according to a control algorithm. Temperature measurements are made using a thermocouple, which scans the inside jacket temperature. An 8-bit A/D converter is used in conjunction with an Apple computer to implement the control algorithm. The control algorithm uses open-loop command feed-forward in conjunction with closed-loop error feed-back.

Figure 1.18 illustrates the desired temperature profile, as well as the actual temperature profile of the jacket obtained under this control system for the first 65 minutes. Compared with Figure 1.16, this represents a considerable improvement. Two factors prevented even better results. First, the 8-bit A/D converter limited the resolution of the temperature readings to 0.4°F. This is about the extent of the chatter about the nominal profile. Second, there is very little temperature control available at the hot end. The highest temperature that the hot water tank can be set to is 170°F. This is very close to the higher command temperature. As water is circulated through the system, the heat loss is greater than the heating element in the hot water tank can

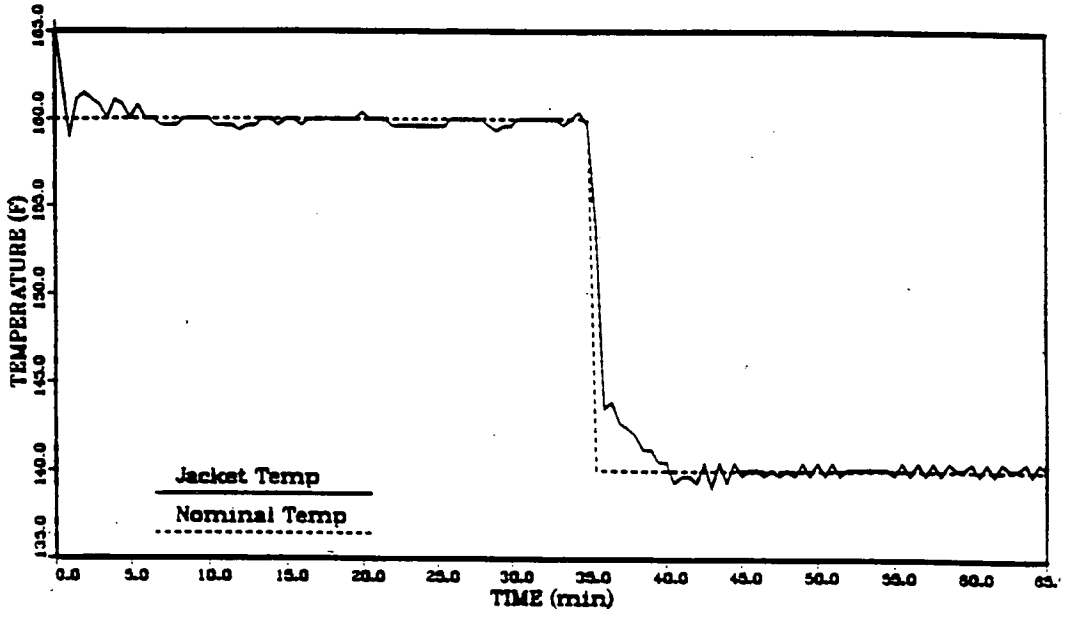

Figure 1.18 Temperature profile using automatic control.

replace, hence, the system is started hot (165°F) to give enough reserve to last the first 35 minutes. At the jump point in command temperature, the temperature of the cold water tank is not known with sufficient accuracy to allow for a proper setting of the control valve. This accounts for the discrepancy in jacket temperature for about the first 5 minutes after the jump. This problem can be eliminated by installing a thermocouple in the tanks so that these temperatures can be used in the control algorithm.

This first design was implemented with minimal change to the existing system and with some older equipment (Apple computer, A/D converter) in order to demonstrate the feasibility of the procedure. Our intent now is to replace this older equipment and to modify the water circulation system. With these changes, it should be possible to precisely maintain any desired temperature profile. The new design will also consider minimizing the energy required to heat the water.

A complete description of this project is contained in a Master's report submitted by R. G. Wilson to the Department of Aerospace and Mechanical Engineering, dated November 20, 1989.

Innovative Techniques for the Production of Energetic Radicals for Lunar Materials Processing Including Photogeneration Via Concentrated Solar Energy

D. E. Osborn, D. C. Lynch, and R. Fazzolari
Department of Materials Science and Engineering
and
Solar and Energy Research Facility, Department of Nuclear and Energy Engineering
The University of Arizona

Introduction

The Department of Materials Science and Engineering (MSE), with funding from the NASA Space Engineering Research Center (SERC) for Utilization of Local Planetary Resources, is investigating use of monatomic chlorine produced in a "cold" plasma to recover oxygen and metallurgically significant metals from lunar materials (Lynch 1989). Development of techniques for the production of the chlorine radical (and other energetic radicals for these processes) using local planetary resources is a key step for a successful approach.

It has been demonstrated terrestrially that the use of UV light to energize the photogeneration of OH* radicals from ozone or hydrogen peroxide in aqueous solutions can lead to rapid reaction rates for the breakdown of toxic organic compounds in water (Osborn et al. 1988). A key question is how to use the expanded solar resource at the lunar surface to generate process-useful radicals. This project is aimed at investigating that question as a joint effort of MSE and the Solar and Energy Research Facility (SERF) of the Department of Nuclear and Energy Engineering (NEE). It is being conducted by Donald E. Osborn under the supervision of Dr. David Lynch.

Approach

Sunlight provides useful energy for processing in the forms of both thermal and quantum energy. While the use of thermal energy is well accepted, the use of quantum energy of the solar photons (photonic processes) for chemical reactions presents new and exciting possibilities.

Photonic Processing. Sunlight is electromagnetic radiation that is normally divided into three major bands: Ultraviolet (UV) ranges from about 180 nm to 380 nm, visible ranges from 380 nm to 780 nm, and infrared (IR) ranges from 780 nm to about 10,000 nm. The energy of a photon varies inversely with wavelength as follows:

$$E = \frac{hc}{\lambda} = h\nu .$$

where E is energy, h is Planck's constant, λ is wavelength, and v is frequency. If one considers a gram-mole (gmol) of photons, the energy associated with a given wavelength is

$$E = \frac{28591}{\lambda} \text{ kcal/gmol} .$$

The shorter wavelengths are the most energetic.

Light can affect material in two basic ways: thermally or through photonic processes. The absorption of light can lead to an increase in the vibrational, rotational, and translational energy of the atoms of the material. Macroscopically, this shows up as an increase in temperature and, once absorbed, the effectiveness of the energy is not dependent on the wavelength of the light. Photonic processes are wavelength dependent and are characterized by a threshold wavelength that is specific for each process and material.

If light is absorbed by a molecule and if it has sufficient energy (i.e., short enough wavelength), it can cause a transition of electrons from one orbital to another. If the electron belongs to a chemical bond, the bond may be broken by this transition. UV and near UV, as the most energetic wavelengths, can break a wide variety of bonds, as seen in Table 1.5. While it may not be possible with the wavelengths available to break the bonds of the material of interest directly, a photocatalytic process may be used, or energetic free radicals that can break the bonds can be photogenerated. Some of the photochemical reactions that can lead to such free radicals are shown in Table 1.6.

It has been demonstrated that the combination of ozone and UV photons produces rapid reactions in the form of photochemical oxidation of halogenated organic compounds (Fletcher 1987). Ozone and hydrogen peroxide decomposition to free radicals is accelerated by absorption of UV light. Free radicals, having a considerably higher oxidation potential than molecular ozone, produce the favorable reaction rates. Experiments by Osborn et al. (1988) demonstrate the increased reaction rate for the decomposition of a red organic dye using UV from natural sunlight in combination with H_2O_2 or TiO_2. The process produces free radicals that lead to bond breaking and reduction of the color of the dye solution (Figure 1.19). Further experiments at a concentration of 6 suns show greatly enhanced reaction rates over the 1-sun case.

The concentrated solar irradiation could be used in materials processes by using the UV and near-UV photons to form free radicals desired for "cold" plama processing (Lynch 1989). These radicals could include monatomic Cl, F, O, H, and OH* for reduction and oxidation.

Table 1.5 Dissociation energies for chemical bonds (Legan 1982).

Bond	D (Kcal/mol)	λp (nm)
Cl-Cl	58	490
C-Cl	81	353
C-F	116	247
C-H	99	290
C-O	86	334
C-C	83	346
C=C	146	196
C≡C	200	143
H-H	104	274
O-O	119	240
O-H	118	243
H-Cl	103	279
F-F	37	780

Table 1.6 Photochemical reactions leading to free radicals.

Reaction	λp (nm)	Resultant Radicals
$H_2O + hv = H^* + OH^*$	185	Atomic hydrogen and hydroxy
$H_2O_2 + hv = 2OH^*$	254	Hydroxy
$O_2 + hv = O_3$	254	Ozone
$Fe^{+2} + hv = Fe^{+3}$	254	Ferrous ion to ferric ion
$O_3 + hv = O_2 + O^*$	310	Atomic oxygen (Note: $O^* + H_2O = 2OH^*$)
$Cl_2 + hv = 2CL^*$	490	Atomic chlorine

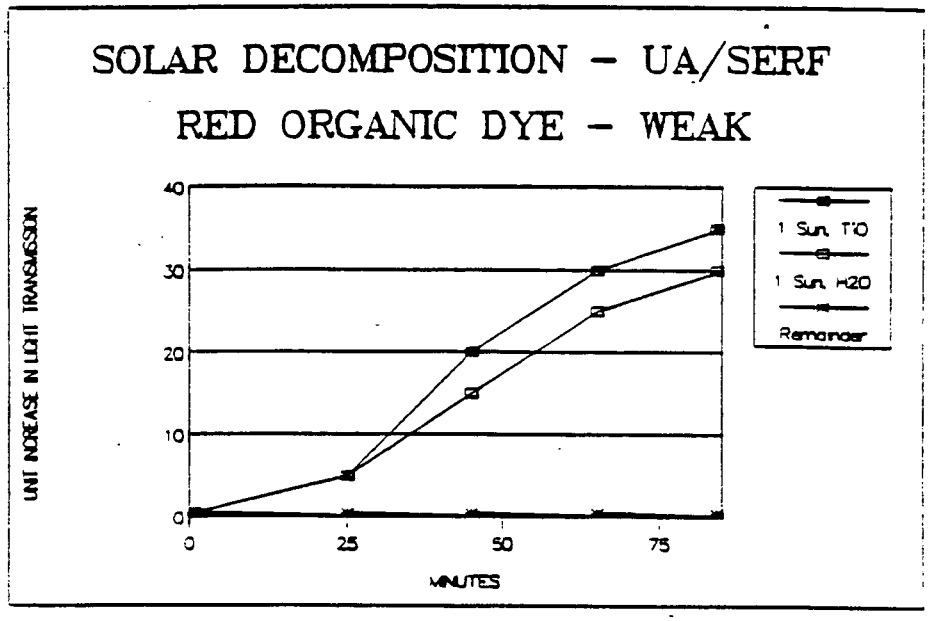

Figure 1.19 Effect of solar light on red dye.

Extraterrestrial Radiation. While the UV content of the solar spectrum at the Earth's surface is very limited in quantity and decreases rapidly with decreasing wavelength, sunlight at the Moon's surface or in Earth orbit contains both greatly increased levels of total UV and the shorter wavelengths. For Earth-based systems, we have little UV below 320-340 nm. Extraterrestrial solar radiation, however, extends below 240 nm, with significantly higher levels throughout the UV band (see Table 1.7). The use of Al reflectors would permit the concentration of this energy, with good reflectance throughout the solar UV band. Appropriate spectrally selective filters could remove excess energy at unwanted wavelengths if excess thermal energy is a problem (Osborn 1986).

Table 1.7 UV content in sunlight for AM0, AM1, and AM4 (W/m^2).

	AM0	AM1	AM4
< 400 nm	118.1	88.4	11.1
< 310 nm	22.5	0.5	0.0

Chlorination Kinetics

Extensive studies of chlorination kinetics of several materials were undertaken by the Bureau of Mines (Landsberg and Block 1965). The experiment being conducted under this project extends the Bureau of Mines' work and seeks to determine the effect of concentrated solar energy on the chlorination kinetics of iron and molybdenum. Those metals were chosen because the rate of chlorination of Mo is known to be limited by the dissociation of Cl_2, while that for Fe is not. Furthermore, the rate constants for reactions are well established. In addition, the reaction products are volatile at reasonable temperatures (250-450°C). Simulated solar light should lead to the dissociation of Cl_2 and thereby enhance the rate of chlorination of Mo. The increase should, initially, be linear with the intensity of the simulated solar energy. The solar energy should have no effect on the chlorination rate of Fe, unless a new reaction path is created with the presence of monatomic chlorine.

The objective of these experiments is to test the hypothesis that solar energy can be used to produce reactive radicals. If the experiments are successful, an attempt will be made to use solar energy in the chlorination of metal oxides and thereby the liberation of O_2.

Experimental Setup. The experimental apparatus is shown in Figure 1.20. The sample to be chlorinated will be suspended by a fiber resistant to the chlorine environment. The fiber is attached to one arm of the Cahn R-100 electrobalance. A tare weight is suspended from the other arm. The balance is enclosed by a bell jar and base plate. The balance will be flushed with argon gas to protect it from the corrosive environment. A 1-inch fused silica tube extends from the balance into a resistance wound furnace. The tube is U-shaped so that an argon-chlorine gas mixture is preheated in the electric furnace before it contacts the metallic specimen. The specimen will be positioned just above the electric furnace, where the simulated solar light can be absorbed by the specimen and gas mixture near the specimen. A solar reflector will be used to concentrate the light around the specimen. During an experiment, the region of the silica tube above the furnace will be insulated with ceramic wool to minimize heat loss.

A thermocouple will be extended down the tube to a position near or in contact with the specimen to record its temperature during an experiment. The thermocouple will be placed in contact with the specimen when it is necessary to determine how much addtional heating the simulated solar energy provides.

The chlorine-argon gas mixture is supplied from a pressure-regulated cylinder with a needle valve. If deemed necessary, the gas mixture can be scrubbed in concentrated sulfuric acid and passed over calcium chloride pellets before being metered by a

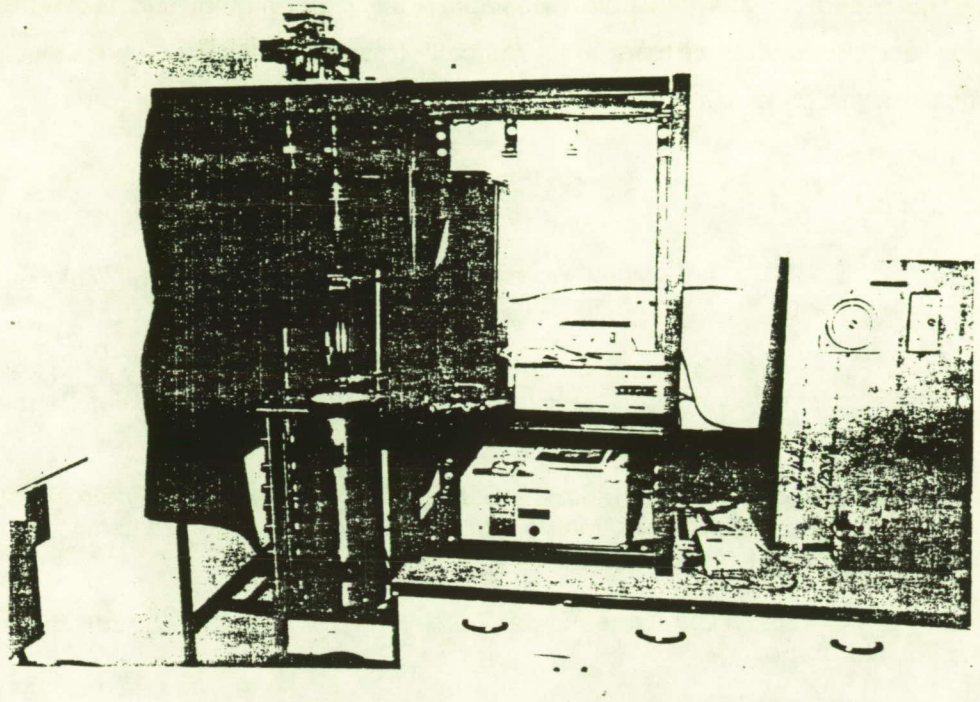

Figure 1.20 Experimental apparatus.

calibrated orifice-manometer. An accuracy of ±2% is desired for gas flow rates. A total gas flow rate of 500 cc/minute or greater will be used with chlorine concentrations ranging from 0 to 12%.

The metal specimens will be both annealed and cold rolled. They will be rubbed with abrasive powder and rinsed with acetone to remove scale and thereby provide a uniform surface. The surface area should be about 4-5 cm^2.

Results to Date. The primary effort in the past 5 months has involved design and construction of the experimental apparatus. A photograph of the nearly completed unit is shown in Figure 1.20. The system includes a Cahn microbalance, resistance wound furnace, solar simulator, gas delivery system, reaction chamber, furnace control unit, and associated electronics. The apparatus is undergoing initial testing at this time.

Future Work

Three major experimental tests will be performed. The first seeks to confirm the Bureau of Mines' results and to determine the chlorination rates without UV light. The second set of experiments will determine the reaction rates under the same conditions, but with UV light. The third stage of the experimental program will extend those tests to lower reaction temperatures and varying concentrations of light. Chlorine levels will vary from 0% to 12%, and the reaction temperature between 300° and 450°C.

These experiments will help to establish the experimental and theoretical basis for the direct production of energetic radicals from solar energy and the use of those radicals in the processing of lunar materials.

References

Fletcher, D. B., 1987, "UV/Ozone Process Treats Toxics," *Water World News*, Vol. 3, No. 3, pp. 25-27.

Glaze, W. H., Kang, J. W., and Chapin, D. H., 1987, "The Chemistry of Water Treatment Processes Involving Ozone, Hydrogen Peroxide and Ultra Violet Ratiation," *Ozone Science and Engineering*, Vol. 9, pp. 335-352.

Landsberg, A. and Block, F., 1965, "A Study of the Chlorination Kinetics of Germanium, Silicon, Iron, Tungsten, Molybdenum, Columbium, and Tantalum," Report 6649, U.S. Bureau of Mines.

Legan, R. W., 1982, "Ultraviolet Light Takes on CPI Role," *Chemical Engineering*, Vol. 89, No. 2, pp. 95-100.

Lynch, D. C., 1989, "Chlorination Processing of Local Planetary Ores for Oxygen and Metallurgically Important Metals," Annual Progress Report 1989-99, NASA Space Engineering Research Center, University of Arizona, pp. I-25-35.

Osborn, D. E., 1986, "Spectrally Selective Beam Splitters Designed to Decouple Quantum and Thermal Solar Energy Conversion in Hybrid Concentrating Systems," Final Report, SERI Contract XK-4-04070-01 and Sandia Contract 04-5348, University of Arizona.

Osborn, D. E., Sierka, R., and Karpiscak, M., 1988, "Solar Thermal Water Reclamation and Toxic Waste Destruction," Final Report SERI Contract XX-7-07199-1, University of Arizona.

Oxygen Production by Electrolysis of Molten Lunar Regolith

L. A. Haskin
Department of Earth and Planetary Sciences
Washington University

Introduction

Previous work has shown that FeO and O_2 can be derived by electrolysis from silicate melt of a composition typical of lunar soils (Oppenheim 1968, Lindstrom and Haskin 1979). In the present study, we attempt to further refine the conditions necessary to optimize production and to determine efficiencies of production (how much product is derived for a given current) and purity of products.

Our goal in this study has been threefold. First, we want to define the theoretical energy requirements of the process. This includes studies of the relevant oxidation-reduction reactions in the melt, their kinetics and energies of reaction, and experimental determination of production efficiencies and melt resistivities as functions of melt composition and applied potential.

Second, we want to characterize the product(s) of silicate electrolysis. This includes evaluating the phase relationships in the systems SiO_2-TiO_2-Al_2O_3-MgO-FeO-CaO and Fe-Si; estimating the compositions of the metal products as a function of applied potential and feedstock composition based on phase equilibria in the Fe-Si system and free energy values for SiO_2 and FeO reported in the literature; definition of compositions of products in actual experiments; and definition of the form the product takes, whether phases separate or remain fixed, whether crystals settle or float in the remaining melt, and how large crystals form.

Third, we want to identify materials that can serve as electrodes and container materials for these highly corrosive high-temperature silicate melts. This includes identifying materials that may be either inert or thermodynamically stable in these melts, and experimental testing of the materials to confirm that they do not deteriorate. The ensuing report discusses our results within this framework.

Theory

We now understand in some detail the chemistry of the oxidation-reduction reactions involved in the electrolysis of silicate melts. This includes identifying the reactions involved and studying their kinetics, evaluating the dependence of oxygen production efficiency on melt composition, and determining the resistivities of melts as a function of composition. Much of this work is currently in final revision before publication (Haskin et al. 1990).

We have identified the cathode reactions that produce melt as the following:

$$Fe^{2+} + 2e^- = Fe^o \quad (1)$$

$$Si(IV) + 4e^- = Si^o \; . \quad (2)$$

Based on comparison with reductions of other cations such as Ni, Co, and Zn, these reactions are fast and will present no kinetics problems at current-densities needed to produce oxygen at a sufficiently high rate. Competing reactions at the cathode include the reductions of trace and minor melts, such as Cr, Ti, Mn, and Ni, and the reduction of oxygen dissolved in the silicate melt.

At the anode, the principal reaction is

$$4(SiO^-) = 2(Si\text{-}O\text{-}Si) + O^{2-} + 4e^- \; . \quad (3)$$

The kinetics of this reaction are also fast.

A serious competing reaction at the anode in melts with high iron concentrations is oxidation of Fe^{2+}

$$Fe^{2+} = Fe^{3+} + e^- \; . \quad (4)$$

Other competing reactions at the anode include oxidation of other multivalent cations such as Ti and Cr.

We identify the variables important in calculating the energy required by the electrolysis process as follows: Power to drive the electrolysis equals E*I, where I is the current required to get oxygen at the desired rate and is proportional to oxygen production rate/oxygen production efficiency. This demonstrates the dependence of power requirements on oxygen production efficiency. E is the potential required to drive the electrolysis and is equal to $E_c - E_a - \eta_c - \eta_a - I(R_{cell})$, where $E_c - E_a$ is the potential required to drive the reaction(s) and is a function of the cation reduced ($|E_c - E_a|$ increases in the order Fe < Si,Ti < Mg,Al < Ca) and the concentrations of the cations in the melt. The quantity $-\eta_c - \eta_a$ is the overpotential required because of slow reaction kinetics or, as we use it in this paper, because of cation mobility problems (inability of cations to migrate to the cathode fast enough to yield the desired production rate). R_{cell} is the resistance of the electrolysis cell and is equal to $L/\kappa A$, where L is the distance between electrodes, A is the electrode surfac area, and κ is the melt conductivity. This expression illustrates the dependence of power on both cell configuration and resistivity of the molten feedstock. Not unexpectedly, κ is found to increase as the average ionic mobility of the melt increases. That is, κ increases systematically as mobile cations such as Fe, Mg, and Ca increase relative to Si and Al in the melt.

We have now determined values for most of the variables identified in the discussion above. Because reaction (4) is the primary competing reaction at the anode, the efficiency of oxygen production (defined as moles O_2 produced/4 moles electrons passed through the melt) depends primarily on the concentration of Fe^{2+} cations. The dependence of oxygen production efficiency on Fe^{2+} concentration can be expressed as $\%O_2/(100 - \%O_2) \cong 0.049/X_{FeO}$, where $\%O_2$ is the oxygen production efficiency as a percentage and X_{FeO} is molar fraction FeO in the melt (see Figure 1.21). This has the consequence that electrolysis to produce oxygen as a main product is most efficiently carried out in melts with relatively low iron concentrations (<2%).

We have reported conductivities of molten silicates with compositions similar to those of molten lunar rocks and soils in the temperature range 1420-1550° (Haskin et al. 1990). The values lie in the range 0.08-40 $ohms^{-1}\,cm^{-1}$. These values appear adequate for robust cell design. A systematic variation in conductivity with composition is observed. The theoretically expected variation of conductivity with composition at

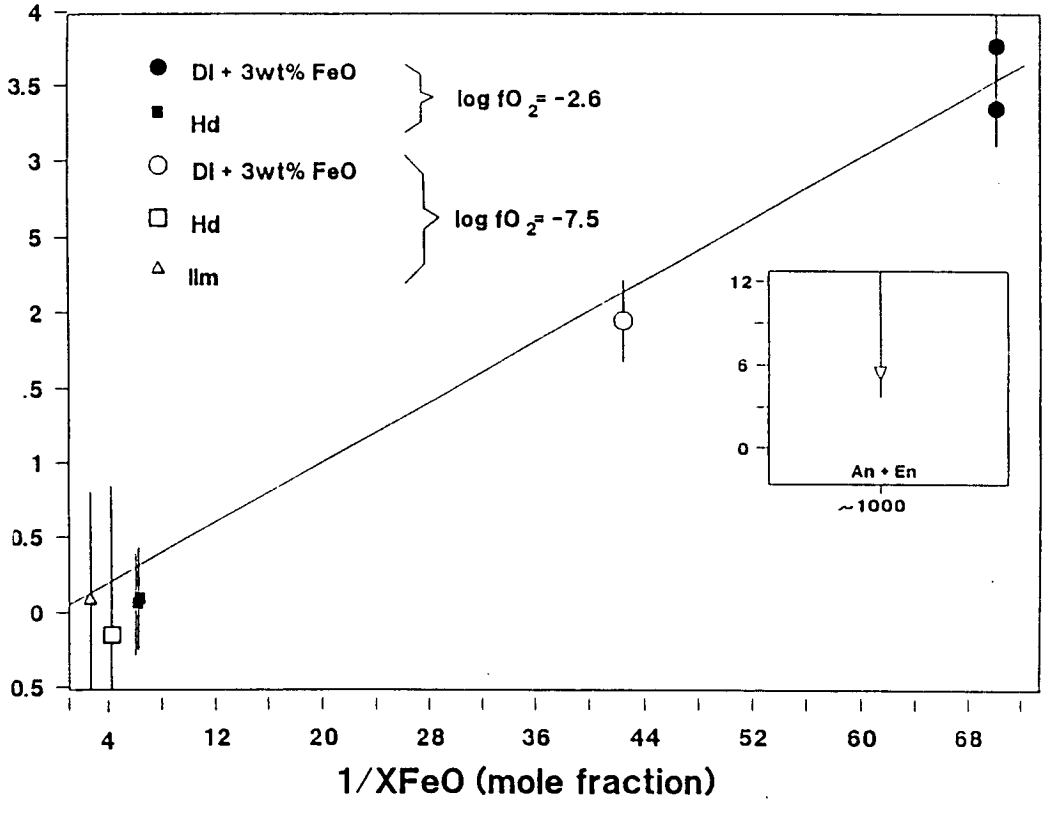

Figure 1.21 Diagram from Haskin et al. (1990) showing the dependence of oxygen production efficiency (defined in text) on concentration of ferrous iron in the melt.

constant temperature can be expressed by

$$\text{Conductivity} \propto \Sigma X_i D_i Z_i^2 ,$$

where X_i is the molar concentration of i, D_i is diffusivity of i, and Z_i is the charge of i (Reiger 1987, p. 160). This expression is similar to the relationship we observe between composition and conductivity, permitting conductivity to be predicted for any given composition.

We have found no kinetic problems associated with either anodic or cathodic reactions (both reactions being fast at the expected current-densities) and therefore expect low overpotentials arising from kinetic problems. We are now studying dynamic problems in the electrolysis and how they relate to overpotentials needed to drive reductions in the melt. We are studying whether material flow and thermal convection in a cell can keep fresh material at the electrodes or whether active mixing will be necessary.

New experiments are currently underway that will extend some of these results to compositions more typical of lunar soils. These experiments include a study of redox reactions for various cations in silicate melts of basaltic composition (similar to Apollo 12 soil) and compositions along the join Diopside ($Mg_2Si_2O_6$)-Anorthite ($CaAl_2Si_2O_8$). These studies will demonstrate how the potential required to reduce various species changes as a function of composition [extending the results of Semkow and Haskin (1985) to more realtistic soil compositions], as well as confirm that there are no kinetic problems with the reactions in these more realistic melts. Figure 1.22 shows preliminary results of these experiments illustrating the shift in Ni reduction potential as a function of silicate melt polymerization.

Characterization of Products

Based on known phase equilibria in basaltic systems; on phase equilibria in the system Fe-Si; on thermodynamic data for the reduction of the cations of Fe, Si, Al, Ti, Mg, and Ca; and on our experiments already reported (Lindstrom and Haskin 1979, Semkow and Haskin 1985, Colson and Haskin 1990a,b), we expect the products of silicate electrolysis to be as follows (at a temperature of, for example, 1350°C and at a reduction potential of about -1.5 volts):

> *Predictions From Theory*: Two or three metal phases form at the cathode (depending on the Si/Fe ratio of the bulk metal). These metal phases will contain varying amounts of Si, Fe, Cr, Mn, and Ti (and small amounts of trace constituents such as Ni), with the Si/Fe ratio of each phase

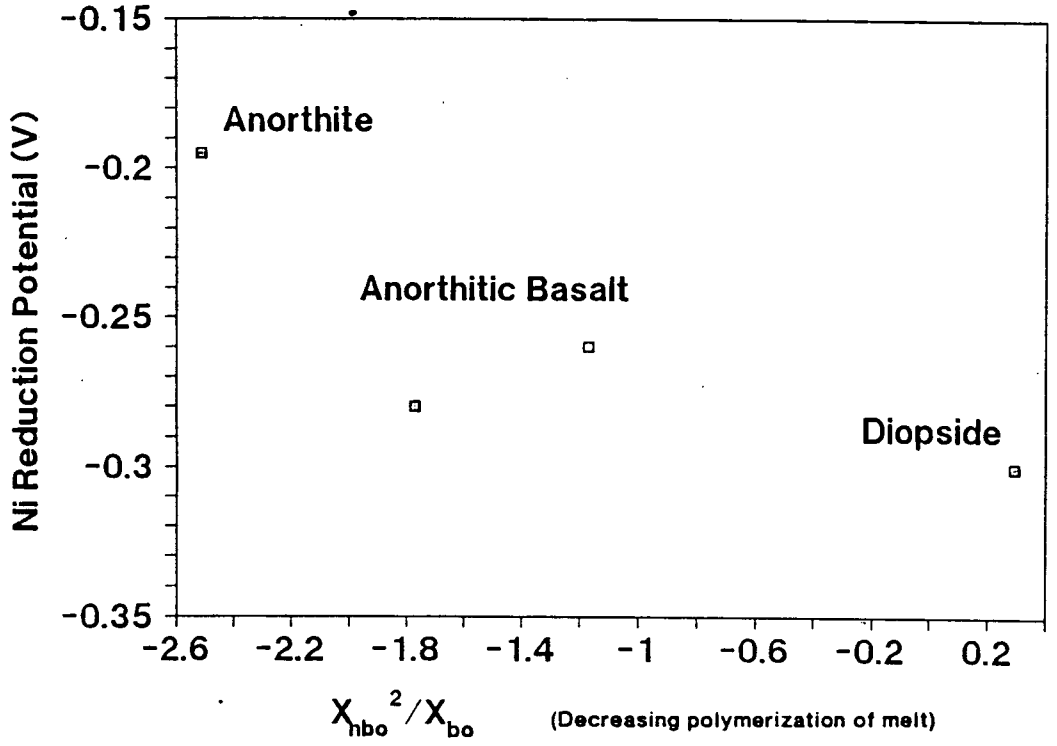

Figure 1.22 Diagram showing the dependence of Ni reduction potential on polymerization of the melt. X_{nbo} and X_{bo} are fraction non-bridging (Si-O) and bridging (Si-O-Si) oxygens, respectively. Trend is opposite of that expected and that reported by Semkow and Haskin (1985).

roughly defined by the Si-Fe phase diagram. Oxygen is liberated at the anode. Depending on the temperature and extent of SiO_2 removal, spinel $(Mg,Fe)(Al,Cr)_2O_4$ is expected to precipitate from the residual melt.

We have now begun a new set of experiments designed to test these predictions. These experiments are designed so that current and cell resistance can be measured and potential controlled simultaneously. This permits results to be interpreted in light of a known value for $E_c - E_a$. All measurements are made and instruments controlled by an AT-type personal computer attached to the instruments by an IEEE-488 bus. A diagram of the experimental circuitry is shown in Figure 1.23.

Results of these experiments should define product compositions as a function of feedstock, applied potential, and extent of electrolysis, thereby testing theory. They should give a qualitative idea of how cell resistance changes with extent of electrolysis, again testing theory. They should give a semi-quantitative estimate of the overpotentials required to drive the electrolysis and how the required overpotentials

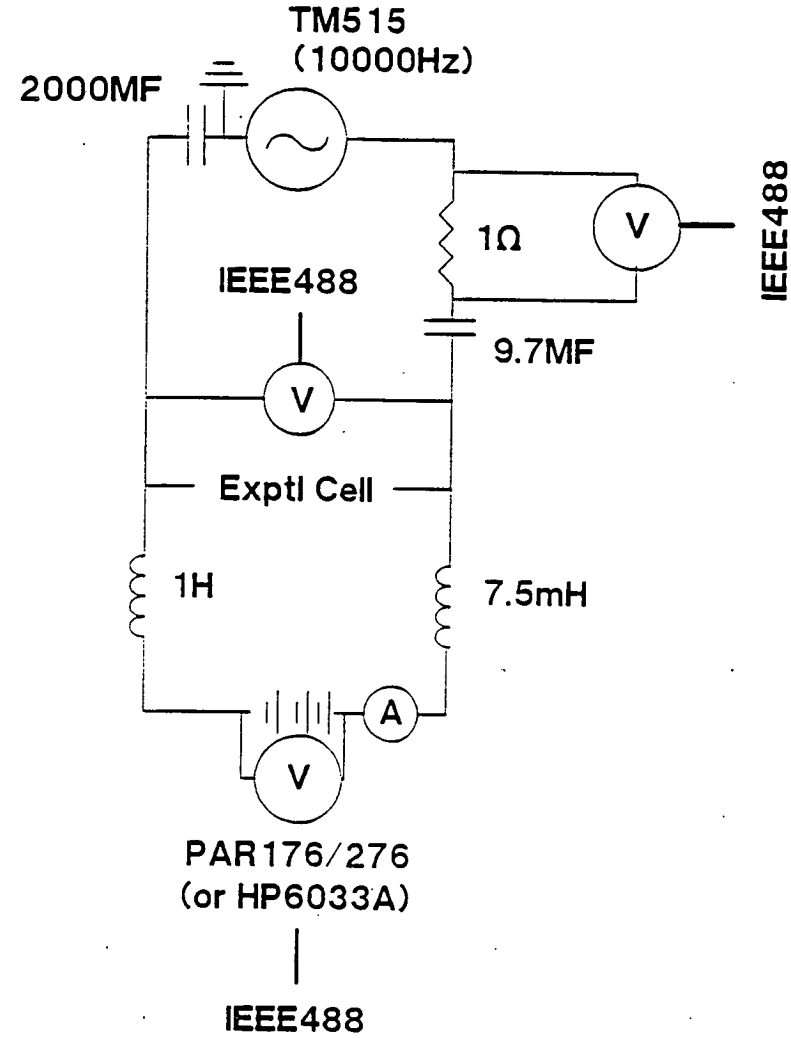

Figure 1.23 Diagram of circuit designed to measure cell resistance (via the 10000-Hz waveform generator and voltmeters) and control the DC potential (via the PAR 176/276 for current <1A, or the HP6033A for higher currents). IEEE-488 bus lines go to an AT-type computer that controls the experiment.

affect product composition. They should define the behavior of the products, whether the products float or sink, whether they separate or mix with other products, and what size of crystals or crystal aggregates are formed. As discussed below, these experiments also give a handle on the durability of the chosen electrode materials.

Preliminary experiments (each sample about 80 mg, mounted on a small Pt wire loop with temperature, atmosphere, and electrode potential controlled) show that the phase equilibria and metal phase compositions vary in a manner similar to that predicted from theoretical calculations, with Si/Fe ratio in the product melt increasing

with increasing potential and spinel crystallizing as SiO_2 removed from the melt (at 1350°C). The metal has a somewhat lower Si/Fe ratio than expected, possibly reflecting the lower mobility of Si in the melt relative to Fe.

Microprobe analyses of products from two experiments are reported in Table 1.8, illustrating the effects of applied potential and initial magma composition on metal composition, oxygen production efficiency, and spinel composition. The difference in composition between the two is that the second is like the first, with Si and Fe removed in the proportions expected to be removed by the electrolysis. Therefore, to some degree, these two illustrate how compositions change with extent of electrolysis.

Experiment A12_1, an electrolysis of an Apollo 12-soil-like composition, contains Fe-Cr-rich spinel and nearly pure Fe metal, and has a low oxygen production efficiency (28%). Experiment A12_1cb, which was at a higher potential with lower Si and Fe in the initial melt, contains Mg-Al-rich spinel, three distinct Fe-Si phases that contain significant amounts of Ti and Cr (the presence of Ir is due to use of Ir as the cathode material in these experiments), and somewhat higher oxygen production efficiency (45%). A backscattered electron image of the three metal phases is shown in Figure 1.24.

Testing of Electrode and Container Materials

We have suggested that Si may make a suitable cathode material (Haskin et al. 1990). We have made several efforts to test Si experimentally, but have run into difficulty mounting the Si as a cathode in our experiments. The Si cannot be mounted to Pt because of the low Si-Pt eutectic. We have tried welding the Si to Ir but, so far, the Si has either broken away from the weld-joint or has reacted with C in the reducing acetylene flame. We have tried mounting the Si to tungsten, but the tungsten oxidizes under our experimental conditions.

We have suggested the use of Pt as anode material (Haskin et al. 1990). There are also some experimental difficulties with testing the Pt as an anode, linked primarily to the small scale of our experiments. Even if the Pt lost from the anode was 10% of the amount of oxygen generated, it would not necessarily be apparent from looking at the electrode after the experiment that any Pt was lost, because the total Pt mass is large compared to the mass of oxygen generated. However, we have taken an alternative approach to estimating the Pt lost from the anode. We note that any Pt lost would be dissolved in the silicate melt and ultimately reduced to metal at the cathode. We have analyzed for Pt in the silicate glass and metal product of our electrolysis experiments (by electron microprobe) and have detected a Pt peak (Figure 1.25), suggesting that

Table 1.8 Microprobe analyses of metals and glasses in two experiments in Apollo 12-like melts.[a]

a. Metal Phase(s).

	A12_1		A12_1cb	
Si	0.024	2.471	6.999	7.389
Ti	0.040	0.142	0.464	0.581
Cr	-0.007	0.567	0.370	0.356
Mn	-0.037	0.231	0.041	0.037
Fe	92.13	33.12	29.28	30.06
Ir	0.000	56.40	56.50	56.40
Pt	-0.021	--	--	--

b. Glass and Spinel+Glass (S+G).

	A12_1		A12_1cb	
	Glass	S+G	Glass	S+G
SiO_2	49.48	0.13	49.21	48.07
TiO_2	2.34	1.16	2.76	2.78
Al_2O_3	10.78	9.10	18.92	19.31
FeO	13.23	42.37	0.69	0.41
MgO	10.09	12.63	14.23	14.69
CaO	9.96	0.31	12.48	11.99
Na_2O	1.12	-0.01	0.82	0.70
K_2O	0.10	0.00	0.08	0.08

[a] A12_1cb has lower initial Fe and Si and a higher applied potential than A12_1. Metal in A12_1 is nearly pure Fe (the low totals <100% is likely due to oxidation of the Fe during quenching of the experiment). Metal in A12_1cb contains significant Si, Ti, Cr, and possibly Mn. The presence of Ir in metals of A12_1cb is due to use of Ir as the cathode material. Otherwise, the compositions correspond to the phases γ-Fe, α-Fe, and melt in the system Fe-Si. Spinel grains were too small to analyze and, therefore, the analyses of spinel include glass as well. In the case of A12_1cb, the glass constitues the major portion of the analysis. Spinel in A12_1 is Fe-Cr rich; spinel in A12_1cb is apparently Mg-Al rich.

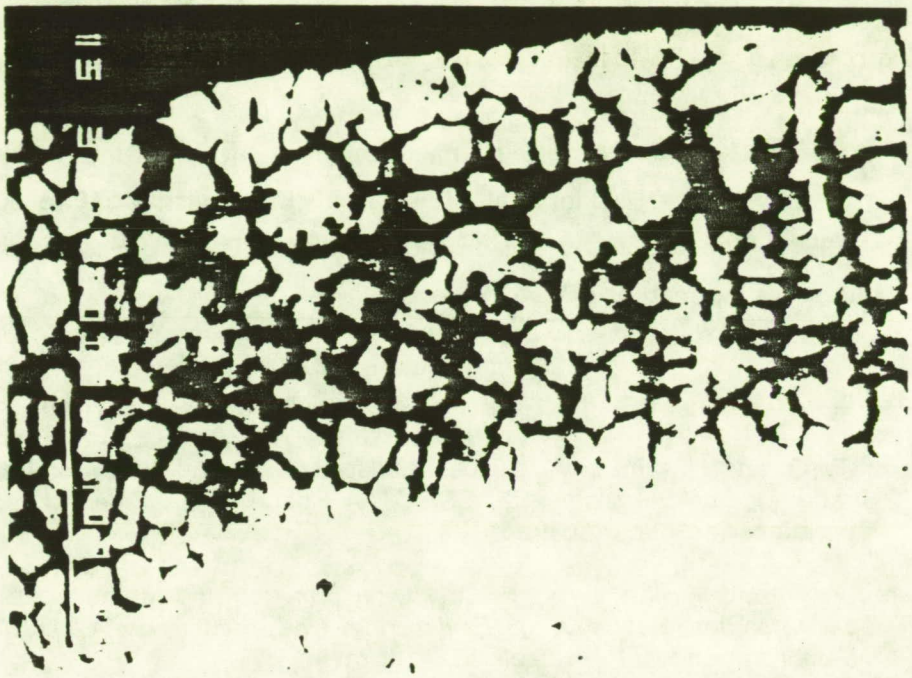

Figure 1.24 Backscattered electron image of the three metal phases in A12_1cb showing differences in density (white is more iron-rich, black is more Si-rich) and the mixed nature of the phases.

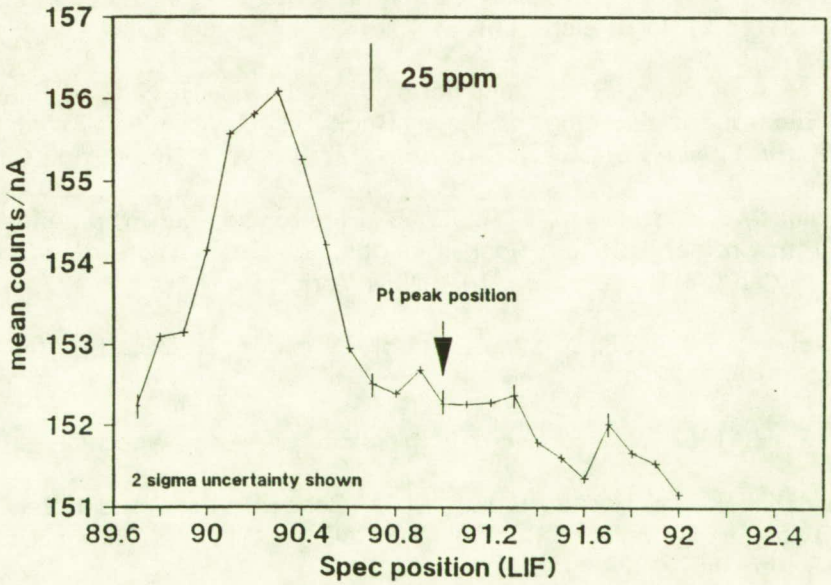

Figure 1.25 Microprobe profile across the Pt L-alpha peak illustrating the absence of Pt in the glass of experiment A12_1, suggesting significant Pt does not erode from the anodes during electrolysis. The peak observed at the left of the profile is a higher order Zn peak (although Zn was not added to these experiments, it exists as a contaminant in the reagents used to make the synthetic composition).

significant Pt is not lost from the anode. Shown as a function of oxygen generated, this is expressed as: Pt lost (mass)/oxygen produced (mass) $< 1.8 \times 10^{-3}$ (2 sigma uncertainty).

Papers and abstracts describing many of these results in more detail are given in the list of references. Haskin et al. (1990) is in final revision before publication, as is Haskin (1990). The papers by Colson and Haskin (1990b) and Haskin and Colson (1990) are included as Appendices D and E, respectively.

References

Colson, R. O. and Haskin, L. A., 1990a, "Lunar Oxygen and Metal for Use in Near-Earth Space: Magma Electrolysis," ASCE/AIAA Space 90 Engineering, Construction, and Operations in Space (abstract).

Colson, R. O. and Haskin, L. A., 1990b, "Lunar Oxygen and Metal for Use in Near-Earth Space: Magma Electrolysis," *Engineering, Construction, and Operations in Space* (S. W. Johnson and J. P. Wetzel, eds.) (in review).*

Haskin, L. A., 1990, "Water and Cheese From the Lunar Desert: Abundances and Accessibility of H, N, and C on the Moon," *Lunar Bases and Space Activities of the 21st Century (II)* (W. W. Mendell, ed.) (in press).

Haskin, L. A. and Colson, R. O., 1990, "Lunar Resources: Toward Living Off the Lunar Land," *Proceedings of the First Annual Invitational Symposium of the UA/NASA Space Engineering Research Center for Utilization of Local Planetary Resources* (T. Triffet, ed.) (in preparation).**

Haskin, L. A., Colson, R. O., Lindstorm, D. J., Lewis, R. H., and Semkow, K. W., 1990, "Electrolytic Smelting of Lunar Rock for Oxygen and Iron," *Lunar Bases and Space Activities of the 21st Century (II)* (W. W. Mendell, ed.) (in press).

Lindstrom, D. J. and Haskin, L. A., 1979, "Electrochemical Preparation of Useful Material From Ordinary Silicate Rocks," pages 129-134 in *Space Manufacturing Facilities* J. Grey and C. Drop, eds.), AIAA, New York.

Oppenheim, M. J., 1968, "On the Electrolysis of Molten Basalt," *Mineral. Mag.*, Vol. 36, pp. 1104-1122.

Reiger, P. H., 1987, *Electrochemistry*, Prentice-Hall, Englewood Cliffs, N.J.

Semkow, K. W. and Haskin, L. A., 1985, "Concentrations and Behavior of Oxygen and Oxide Ion in Melts of Composition $CaO{\cdot}Mg{\cdot}xSiO_2$," *Geochim. Cosmochim. Acta*, Vol. 49, pp. 1897-1908.

*See Appendix E.

**See Appendix F.

Helium-3 in the Lunar Regolith*

T. Swindle
Lunar and Planetary Laboratory
The University of Arizona

We have completed a preliminary assessment of ^{3}He distribution in lunar soils, including variations with soil location, depth, composition, grain size, and other parameters that might be useful in developing mining scenarios. One of the primary tools is a compilation of available analyses of ^{3}He in lunar samples. The compilation includes analyses of more than 250 numbered samples (plus duplicates and subsamples in many cases) from the American and Russian lunar programs, reported in nearly 100 publications. In addition, we have computed average abundances for soils from each of the Apollo landing sites. These have been coupled with models and measurements of other pertinent parameters.

The distributions of ^{3}He within grains, and hence variations of ^{3}He concentration with grain size, are well-understood. Solar-wind-implanted gases, including ^{3}He, are concentrated near the surfaces of grains, in a region less than 10^{-7} m thick. Therefore, smaller grains, which have a larger ratio of surface to volume, contain more ^{3}He per gram than larger grains. Whether the enhancement is sufficient to warrant grain-size separation before extraction is less certain, particularly when losses during separation are considered.

Variations with soil composition are also well-understood. For grains with comparable exposure histories, ^{3}He concentration correlates with Ti concentration. This is because Ti is primarily found in the mineral ilmenite, which is far more resistant to He loss than any other common mineral. In this case, it is clear that beneficiation is not economical, since only a small fraction of the ilmenite can be readily separated.

Regional variations in ^{3}He concentration depend both on Ti concentration and exposure history. They can be estimated, though with some uncertainty, by using remote sensing techniques. Estimates based on presently available remote-sensing data suggest that the areas richest in Ti, and hence in ^{3}He, are likely to be the nearside maria, with Mare Tranquillitatis probably the most promising site. It might be possible to refine these estimates, but it would require work (in particular, improving techniques for remote determinations of soil "maturity" or bombardment history) beyond the scope of this project.

By far the largest uncertainty stems from our lack of knowledge of variations with depth in the structure and ^{3}He content of the regolith. Only three drill cores with depths of more than 1 m have been returned from the Moon, and the deepest of these sampled less than 3 m. Furthermore, the depth to which the regolith extends is largely

unknown, although there are experimental techniques (based on seismic data and analyses of the morphology of photographed craters) and models that address the question. Since the range of reasonable assumptions gives total lunar ^{3}He abundances that vary by a factor of about 10, our estimates are based on the extreme values of reasonable assumptions. We calculate total lunar ^{3}He contents ranging from about 4 × 105 metric tons to 4 × 106 metric tons. Even from the few drill cores available, it is clear that the ^{3}He distribution with depth is variable from one location to another, a factor that has to be considered in designing the mining system.

II. STRUCTURAL MATERIALS

The Feasibility of Solar Reflector Production From Lunar Materials for Solar Power in Space

SAIC Corporation, San Diego

Summary

Science Applications International Corporation (SAIC) has investigated the feasibility of producing solar reflectors from indigenous lunar materials for solar power production on the Moon. First, lunar construction materials and production processes were reviewed, and candidate materials for reflector production were identified. At the same time, lunar environmental conditions were reviewed for their effect on production of concentrators. Next, conceptual designs and fabrication methods were proposed and studied for production of dish concentrators and heliostats. Finally, fabrication testing was performed on small-scale models using Earth analogues of lunar materials. Findings from this initial investigation indicate that production of concentrators from lunar materials may be an attractive approach for solar energy production on the Moon. Further design and testing are required to determine the best techniques and approaches to optimize this concept.

Four materials were identified as having high potential for solar reflector manufacture. These baseline materials were foamed glass, concrete with glass-fiber reinforcement, a glass-fiber/glass-melt composite, and an iron-glass sintered material. Lunar-produced metals were generally expected to be too costly and their production too energy intensive for large-scale use in solar reflector fabrication. Two exceptions to this conclusion are the use of very thin foils for heliostat membranes (like terrestrial membrane heliostats) and the use of aluminum for reflective surfaces. Vacuum-sputtering of aluminum onto the front surface of concentrators was selected as the best approach for production of all reflective surfaces.

Molding of dish reflectors on male molds was chosen as the preferred method of fabrication over free-forming techniques using membrane technology or spin molding. The main advantage of molding is reduced risk. Techniques for focusing heliostat concentrators using static electricity were identified. A passive tracker drive for dish concentrators was also proposed.

Testing of fabrication techniques is being carried out for the four baseline materials. Small-scale models of lunar dishes are being fabricated. The foam glass material is being simulated by polyester resin containing glass microspheres. This allows testing to be conducted at room temperature. Lunar concrete is being simulated with high-alumina cement and ground terrestrial anorthite aggregate, and chopped glass fibers are being used for reinforcement. Fabrication tests with the glass-glass composite and iron-glass sintered material are being conducting using high-lead glass,

with a low melting temperature for the molten glass portion, in order to reduce temperature requirements for the tests.

Introduction

Dependence upon the Earth for materials and power makes a space colony very vulnerable to supply problems. Also, the cost of transport of materials out of the Earth's gravitational potential well is very high. Finally, the most available form of long-term power is solar energy. Therefore, production of a solar collection system in which large portions of the system are constructed of indigenous materials has promise for increasing the autonomy and security of such colonies. Lunar colonies are of particular interest at present, due to the Moon's proximity and its likelihood as a starting point for colonization and as a debarkation point for extended excursions into space.

In this project, Science Applications Interational Corporation (SAIC) has studied the feasibility of using materials produced from lunar soil to form reflectors for distributed or central concentrating solar power systems for lunar settlements. These systems may employ photovoltaic or solar thermal receivers to produce electric power or provide high-temperature thermal energy for the needs of the lunar colony.

Lunar Materials Evaluation

The lunar surface is unique in comparison to terrestrial soils. One effect of meteorite impacts is to mix and homogenize surface constituents through great depths of soil. This fact, together with the lack of a hydraulic cycle on the Moon, means that no ore deposits or mineral concentrations due to evaporation are to be found. Another effect of meteorite impacts is the lithification of various components of the soil into lunar rocks called breccias. Thermal cycling and micrometeorite impacts contribute to the comminution of surface materials into a very fine dust, which forms the "lunar soil," or regolith. The lack of life-forms eliminates the presence of organic compounds, and many common terrestrial constituents such as C, Na, and Cl are also rare. Finally, the lunar surface environment, consisting of a high vacuum, means that the only gases present in the surface materials are those captured from the solar wind.

The lunar surface may be broadly divided into mare and highland regions. Mare regions are characterized by being low-lying areas consisting mainly of basalts that were ejected from the Moon's core. The highlands are, physically, about a kilometer above the maria and consist mainly of feldspar-rich plutonic material, with minor amounts of aluminum and trace-element-rich basaltic minerals. Table 2.1 (taken from

Table 2.1 Chemical compositions (Wt. %) for the major minerals.

a. High-Titanium Basalts

	Modal Abundance (Volume %)			
	Pyroxene 42-60%	Olivine 0-10%	Plagioglase 15-33%	Opaques (Mostly Ilmenite) 10-34%
Al_2O_3	0.6- 6.0	--	28.9- 34.5	0.0- 2.0
TiO_2	0.7- 6.0	--	--	52.1- 74.0
Cr_2O_3	0.0- 0.7	0.1- 0.2	--	0.4- 2.2
FeO	8.1- 45.8	25.4- 28.8	0.3- 1.4	14.9- 45.7
MnO	0.0- 0.7	0.2- 0.3	--	<1.0
MgO	1.7- 22.8	33.5- 36.5	0.0- 0.3	0.7- 8.6
CaO	3.7- 20.7	0.2- 0.3	14.3- 18.6	<1.0
Na_2O	0.0- 0.2	--	0.7- 2.7	--
K_2O	--	--	0.0- 0.4	--

b. Low-Titanium Basalts

	Modal Abundance (Volume %)			
	Pyroxene 42-60%	Olivine 0-36%	Plagioglase 17-33%	Opaques (Mostly Ilmenite) 1-11%
SiO_2	41.2- 54.0	33.5- 38.1	44.4- 48.2	<1.0
Al_2O_3	0.6- 11.9	--	32.0- 35.2	0.1- 1.2
TiO_2	0.2- 3.0	--	--	50.7- 53.9
Cr_2O_3	0.0- 1.5	0.3- 0.7	--	0.2- 0.8
FeO	13.1- 45.5	21.2- 47.2	0.4- 2.6	44.1- 46.8
MnO	0.0- 0.6	0.1- 0.4	--	0.3- 0.5
MgO	0.3- 26.3	18.5- 39.2	0.1- 1.2	0.1- 2.3
CaO	2.0- 16.9	0.0- 0.3	16.9- 19.2	<1.0
Na_2O	0.0- 0.1	--	0.4- 1.3	--
K_2O	--	--	0.0- 0.3	--

c. Highlands Rocks

	Modal Abundance (Volume %)			
	Pyroxene 5-35%	Olivine 0-35%	Plagioglase 45-95%	Opaques (Mostly Ilmenite) 0-5%
SiO_2	51.1- 55.4	37.7- 39.9	44.0- 48.0	0.0- 0.1
Al_2O_3	1.0- 2.5	0.0- 0.1	32.0- 36.0	0.8- 65.0
TiO_2	0.45- 1.3	0.0- 0.1	0.02- 0.03	0.4- 53.0
Cr_2O_3	0.3- 0.7	0.0- 0.1	0.0- 0.02	0.4- 4.0
FeO	8.2- 24.0	13.4- 27.3	0.18- 0.34	11.6- 36.0
MgO	16.7- 30.9	33.4- 45.5	0.0- 0.18	7.7- 20.0
CaO	1.9- 16.7	0.2- 0.3	19.0- 20.0	0.0- 0.6
Na_2O	--	--	0.2- 0.6	--
K_2O	--	--	0.03- 0.15	--

Waldron et al. 1979) summarizes the ranges of chemical compositions for the major minerals that are found in these regions.

The metal-bearing silicates, pyroxene, anorthite, and olivine are the primary minerals available from the lunar surface. The oxide ilmenite is also present to a lesser extent. These mineral groups contain oxygen, silica, and the metals iron, magnesium, titanium, and aluminum. The lunar regolith also contains a high concentration of glass from micrometeorite bombardment. To exploit these natural resources, the raw material must be heated to allow certain chemical reactions to occur. The amount of thermal energy required to process these minerals depends largely on the specific heats and melting points of the minerals. These data are shown in Table 2.2 (taken from SAIC 1989).

Table 2.2 Thermal properties of various lunar materials.

Mineral	C_p (kJ/kg/K)	C_p (kWh/kg/K)	Melting Point (°K)[a]
Ilmenite ($FeTiO_3$)	0.687	0.000190	1640
Anorthite ($CaAl_2Si_2O_8$)	0.755	0.000209	1823
Olivine [$(Mg_2,Fe_2)SiO_4$]	0.790	0.000219	1478-2163
Pyroxene [(Mg, CA, Fe)SiO_3]	0.766	0.000213	1813-1830

[a] From Williams and Jadwick (1980).

Many useful products can be generated from lunar minerals via various chemical and physical processes. Some of the processes being considered are hydrogen reduction, carbothermal reduction, carbochlorination, hydrofluoric acid leaching, magma electrolysis, and vapor phase reduction. These processes extract oxygen, metals, and silicates from the lunar regolith. For the purposes of this study, the materials of particular interest are structural materials for solar reflector support structures and surfaces and materials that can be used for coatings (particularly aluminum for reflective surfaces). Table 2.3 shows that high-strength metals, glasses, ceramic materials, and concrete-like materials form the basic possibilities for lunar structural materials. The production, abundance, and characteristics of each of these types of materials are discussed in the following subsections.

Metals. Metals found on the Moon in significant quantities include iron, aluminum, magnesium, and titanium. Processes to extract these elements from lunar soil have been

Table 2.3 Possible useful products from lunar sources.

Structural Materials
Metals: Steels, aluminum, magnesium, titanium
Reinforced Metals: Aluminum, magnesium reinforced with silica, steel, or alumina
Glasses, fused silica
Ceramics, alumina, magnesia, silica, compounds
Hydraulic cements (need water
Thermal Materials
Refractories plus chromia, titania, titanium silicide
Same as ceramics above, plus castables, ramming cements, insulation, fiberglass, fibrous or powdered ceramics
Electrical Materials
Conductors: Aluminum, iron, resistance alloys (FeCrAl)
Electrodes: Graphite, Fe_3O_4
Magnetic materials, iron alloys, magnetic ceramics
Insulation, glass, ceramics
Fibrous Materials
Glass, silica (for apparel, paper, filters, etc.)
Plastics, Elastomers, and Sealants
Soluble silicates, silicone resins (contain some C)
Adhesives and Coatings
Anodized aluminum, magnesium, titanium electroplating (Cr)
Sputtered coatings, etc.
Lubricants, Heat-Transfer Fluids
Sulfides, SO_2, He
Industrial Chemicals
Detergents, cleansers, solvents, acids, bases, H_2SO_4, H_3PO_4, CaO, NaOH
Biosupport
Oxygen (breathing), 16/18 of water by mass
SiO_2: Soil component (includes many trace nutrients)
Constituent Elements of Life-Forms: O, Ca, C, Fe, Mg, K, P, N, Na, H, and others

developed (Waldron et al. 1979, AIAA 1988) and their use as structural elements needs no explanation. However, there are constraints in both their absolute quantities in lunar soils and in other materials needed to utilize these materials effectively. For instance, some important alloying materials for the production of steel, such as C, Ni, Mo, W, V, and Nb, are not readily available on the Moon. Likewise, production of high-strength alloys of aluminum, magnesium, and titanium require elements (particularly Zn and Mo) not found in abundance on the Moon. Thus, although many commercial alloys can be

made solely from lunar materials, importation of small amounts of some materials from Earth is almost certain.

Metals are not found in large concentrations in lunar materials, although elemental iron is found in the form of small particles in some lunar materials. In any case, significant processing must be done to obtain useful structural alloys. Therefore, in comparison to some of the other structural materials available, such as glass, it may require more effort to produce the large quantities of metallic materials needed for large solar reflectors from lunar materials. Also, metallic materials have many uses for which other materials cannot easily be substituted, such as electrical conductors. Thus, their use may be, to a large extent, dictated by other needs of the lunar colony. For these reasons, metals are expected to be less attractive than other lunar materials for use in solar reflectors. One probable use for metals in solar reflectors is vacuum-deposited aluminum to produce highly reflective surfaces. This is expected to be attractive because the process uses very little material, it requires a vacuum environment anyway, and it produces high-quality reflective surfaces.

Glasses. All lunar materials form glasses easily upon being melted. In fact, the presence of small glass spheres is common in lunar samples (although they constitute only a tiny percentage of the total mass) due to vitrification from meteorite impacts. Lunar mare materials consist of a material very similar to terrestrial basalt. Here on Earth, cast basalt is already used for chemical process components, including pipes, tees, Y-sections, and cyclones. Thus, the technology for processing this material is already developed. Although normal lunar glass is brown due to impurities, glass produced from anorthite can be made colorless by the removal of iron contamination.

In earlier studies (NASA n.d., Lunar and Planetary Institute 1980), glass from lunar materials was proposed as the structural material from which most of a space power system could be constructed. The proposed process, shown in Figure 2.1 (from Lunar and Planetary Institute 1980), takes normal lunar soil, removes metallic iron particles magnetically, and then melts the remainder to form a glass melt from which fiberglass and glass sheet are produced. In addition, it was proposed to electrolyze oxygen from the melt for the production of foamed glass. Other studies performed at Los Alamos National Laboratory proposed that lunar soil could be melted in-place by an electrically heated molybdenum or tungsten mandrill to form a glass-like material that would form the walls and ceilings of a lunar habitat (Rowley and Neudecker 1980).

Another factor in favor of the use of glass over metals is the amount of energy required to produce it. Table 2.4 (from Friedlander and Cole 1989) summarizes the energy and power requirements for lunar glass and metals processing. Glass products

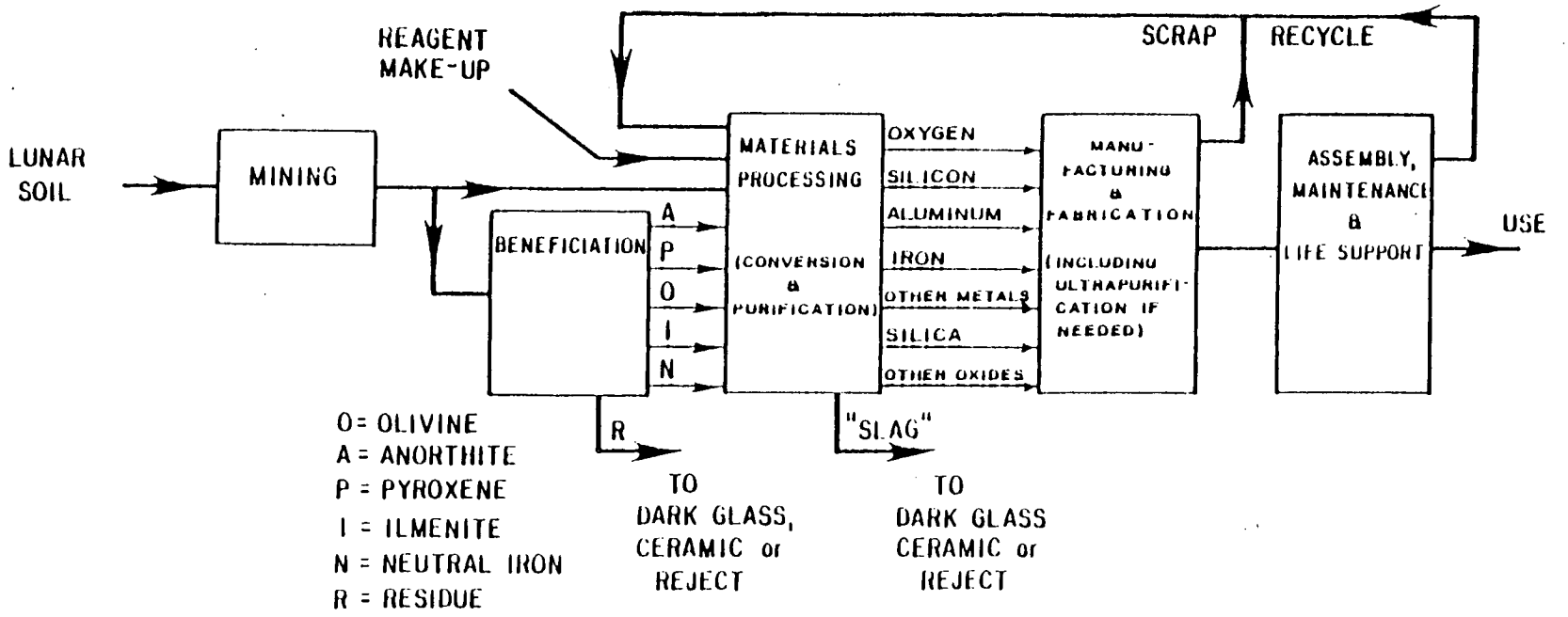

Figure 2.1 Schematic process for production of lunar glass products.

Table 2.4 Energy and power requirements for lunar glass and metal production.

	Product				
	Fiberglass	SilicaGlass	Aluminum	Titanium/Iron	Iron
Beneficiated Feedstock	Anorthite	Bulk soil slag, CoO	Anorthite	Ilmenite	Ilmenite
Process Technique	Meltdown	Meltdown	-------Carbochlorination-------		Carbothermal
Process Energy (kWh/ton)					
Thermal	878	534	9890	2080/4910	3500
Electric			9000		
Throughput (tons/yr)	10,000	10,000	1000	860/1000	1000
Total Power (kW)					
Thermal	1000	610	1129	765	400
Electrical	55	17	1049	25	41

require far less energy to produce than any of the metals listed. In addition, they are amenable to far larger production volumes.

Since glass can be easily produced from lunar materials in large quantities, it appears a very promising material for solar reflectors. Glass has many desirable characteristics for production of solar reflectors, including high strength, low chemical activity, excellent surface finish, and ease of forming. Clear glasses could also have applications as lenses or cover glasses for optical components.

Ceramic Materials. Along with components that form glasses, lunar materials contain a high fraction of ceramic materials and ceramic pre-cursors. In particular, alumina (Al_2O_3), silica (SiO_2), and magnesia are all present, or can be produced in significant quantities. It is possible to produce a glass-ceramic product from lunar materials that has a tensile strength greater than 345 MPa (50,000 psi) (MacKenzie and Claridge 1979). Ceramics may be useful in the production of glass (e.g., melt tanks can be made of silica), and they can be used as refractory components of solar collectors (e.g., thermal receivers). Finally, pure silicon produced from lunar materials can be used to make photovoltaic cells.

Cementitious Materials. Little consideration has been given to cement-like lunar materials until very recently, when the Construction Technology Laboratory (CTL) associated with the Portland Cement Institute began to study the production and use of concrete from lunar materials (Lin 1987a, 1987b). These studies have shown that lunar soils can serve as aggregate and that the residue from a simple high-temperature

evaporation process performed on lunar basalt materials may serve as a high-alumina cement. A small block of concrete was, in fact, produced by CTL using Apollo 16 lunar sample materials as aggregate. This concrete sample was tested at CTL to determine its properties, which are summarized in Table 2.5.

Table 2.5 Physical properties of concrete with lunar aggregate.

Compressive Strength: 75.7 MPa
Modulus of Rupture: 8.3 MPa
Modulus of Elasticity: 21,400 MPa
Thermal Expansion Coefficient: 5.4×10^{-6} cm/cm/°C

Normal concrete has a flow flexural strength (about 10% of its compressive strength). Reinforcement of lunar concrete with glass or steel fibers can greatly increase its flexural strength, strain energy capacity, and ductility. For instance, reinforcement with 4% steel fibers by weight nearly doubles the flexural strength. Both glass and steel can be produced from lunar materials for use as fiber reinforcements.

Lunar concrete has many good characteristics as a construction material. Concrete strength is retained at temperatures as low as -150°C; in fact, its strength actually increases at low temperatures if the humidity is high. Similarly, strength is nearly constant to temperatures of 250°C or more, and concrete is thermally stable to 600°C or more. Another useful characteristic of concrete is its high resistance to abrasion, which protects against micrometeorite damage. Finally, concrete is resistant to radiation damage and is stabile in a vacuum environment.

One possible complication in the use of lunar concrete is that water is required for the formation of concrete (about 4% by mass). Since water is essentially non-existent on the Moon, it would probably need to be imported from Earth. The impact of this can be reduced by shipping only hydrogen, which saves 16/18 in the mass that needs to be transported. The hydrogen would be combined with oxygen produced from the lunar soil to form the needed water. Using this approach, the material that would need to be transported from Earth is 0.4% of the final concrete mass.

Lunar Conditions and Constraints

In considering the production of solar reflectors on the Moon, consideration of the characteristics of the lunar environment is essential. The lunar environment affects the design, the fabrication, and the operation of any solar reflectors that are produced.

Salient characteristics of the lunar environment are listed in Table 2.6. These include both atmospheric and geologic factors.

Table 2.6 Characteristics of the lunar environment.

Atmosphere	
Pressure:	$<10^{-14}$ torr
Surface Temperatures:	Daytime up to 110°C
	Night down to -170°C
Solar Insolation:	1350 W/m^2 ± 3% due to orbital eccentricity
Solar Wind:	Charged particles of H, O, and other species
Length of Lunar Day:	708 hours
Inclination of Axis to Ecliptic:	1/2°
Geology	
Gravitational Constant:	1.62 m/s^2 + perturbations in maria
Magnetic Field:	$<4.4 \times 10^9$ tesla/cm^3
Moonquakes--Frequency:	Several thousand per year
Energy Release:	$<3.6 \times 10^5$ MW
Average Severity:	< 2 on Richter Scale
Maximum Severity:	4 on Richter Scale
Surface Heat Flux:	0.02 W/m^2

In the present study, the most important characteristics related to the production and operation of solar reflectors are micrometeorite impacts, temperature variations, gravity, and atmospheric pressure on the lunar surface. Of secondary importance are the solar wind components and the effects of moonquakes. Finally, magnetic field and heat flux effects are expected to be negligible.

Summary of Lunar Concentrator Meeting of 21 November

Materials. Several additional potential structural materials were identified in the course of the meeting:

- Relatively low-temperature (1000°C) sintering of iron-enriched (i.e., magnetically separated) lunar soil to produce a structural material. This would be a simpler process than either glass or concrete production from lunar soil.
- Use of foamed glass in the same way as concrete to form structural shapes. This would have the additional advantage that the front surface could be made to form a smooth skin for application of the reflective coating. Also, compared to a thin sheet of glass, a foam would be more resistant to fracturing from micrometeorite impacts.

- A glass-glass composite consisting of high-temperature glass fibers in a low-temperature glass "cement" matrix. This would give a composite with good tensile, as well as compressive, strength for dishes, etc.
- Lamination of glass layers to achieve improved strength.

Vacuum-deposited aluminum as a reflective surface was adopted as a baseline. Because of the difficulty in obtaining an optically smooth surface on concrete, it will require a surface coat of glass or some other substance. This adds another step to the fabrication process.

One possible disadvantage identified for glass collectors is their susceptibility to fracture once cracked (for instance, by micrometeorite impact). Thermal cycling causes stresses that would tend to propagate cracks through a sheet of glass. Some approaches to mitigate this problem are to use foamed glass instead of sheet glass, to design the collector as a faceted dish so that failure of one facet would not put the entire dish out of commission, and to attach the glass surface to another material that would support it (e.g., concrete).

Fabrication Techniques. Several techniques and conceptual design approaches were presented for producing concentrators from lunar materials (see Figure 2.2). A consensus was that molding techniques were preferred to free-forming techniques to reduce the risks in the production process. Several methods, including blow molding, spin molding, injection molding, stamping, and gravity sagging of a sheet into a mold, were determined to be applicable to glass production. Gravity sagging has the disadvantage of requiring production of glass sheet first. Spray-up on a male mold is the preferred technique for concrete collector production. Spin molding of concrete is not likely to be successful, because the concrete will have minimum water and will therefore be quite stiff. Material to be sintered could be placed onto a male mold, then pressed and sintered in place.

Use of solar energy as a heat source is attractive because of its availability and ability to be directed where desired by simple reflectors. The vacuum atmosphere makes heat loss reduction simple, since only radiative heat transfer is possible and, therefore, layers of thin foils will work as excellent thermal insulation.

Conceptual Designs. As mentioned above, free-forming of concentrators was felt to be more risky, so molded methods were preferred. Based upon the designs that were discussed at the meeting, the following are proposed as baseline designs to be examined initially:

- Foam glass over male mold. The approach is to form a glass foam that can be poured/draped over a mold. As the front surface contacts the mold, the foam will coalesce to form a solid glass surface on which the reflective aluminum

Parabolic Dishes

Blow-mold glass sheet into a spherical shape like a soap bubble; gravity sagging at the bottom would make it more nearly parabolic; extrude glass beams for the edge support ring.

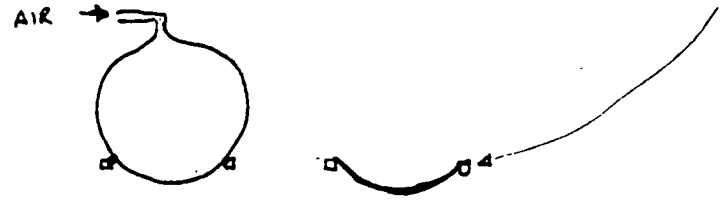

Blow-mold glass sheet into parabolic mold.

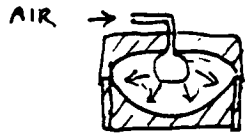

Gravity-sag glass sheet into mold.

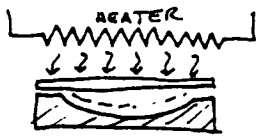

Spin molding: rotating mold in which a thin layer of glass is melted as it rotates. When the glass cools, it takes on a perfect parabolic shape.

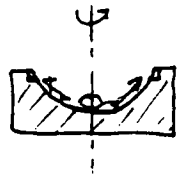

Concrete sprayed over parabolic mold, with glass fiber or iron fiber reinforcement; excess water removed by vacuum pumping and condensation; front surface coated with thin glass and aluminum to form reflective surface.

Squirt liquid glass into the air; the liquid will follow a parabolic path, solidifying as it goes, to form parabolic shapes. A single nozzle could produce parabolic ribs, a slotted distributor could make parabolic trough shapes, or a central distributor (like a sprinkler head) could produce a parabolic dish shape.

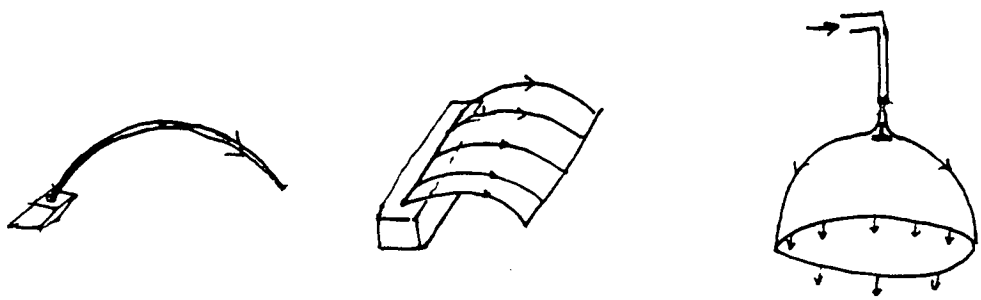

Figure 2.2 Solar collector manufacturing processes.

Figure 2.2 (Continued).

Heliostats

Concrete poured into mold or sprayed over forms to make a ring; iron or steel foil, or very thin glass, for membrane. These heliostats would have to be unfocused, which would mean small sizes, or else the membranes would have to be self-supporting.

Support Structures

Glass beams, with glass foam core for compressive loads and glass fibers for tensile loads.

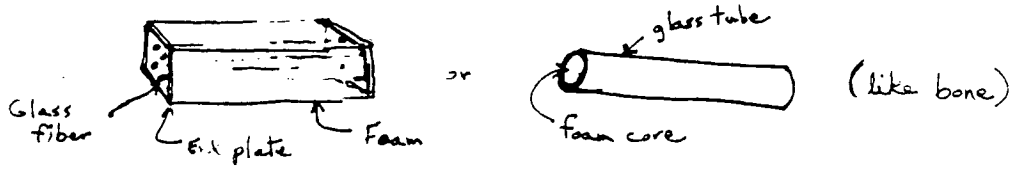

Zomeworks-type passive trackers, based upon liquid-vapor balance system. This requires the system be supported very near the CG, and that an appropriate liquid be chosen.

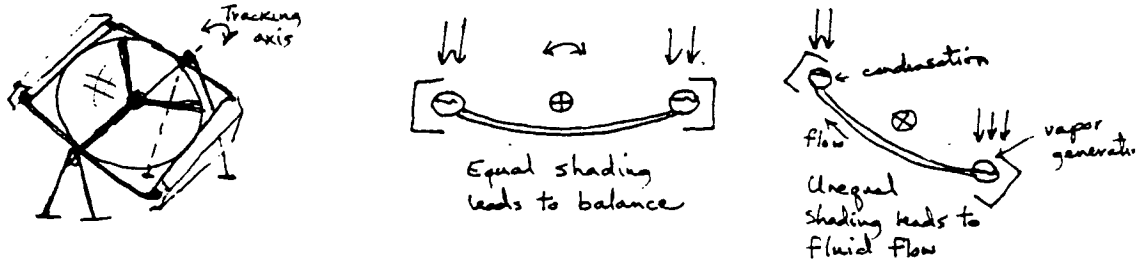

Miscellaneous

Sputtered aluminum first-surface mirror surface on glass substrates. The aluminum will oxidize slightly on the surface due to impingement of oxygen ions from the solar wind. This oxide layer will eliminate the dip in reflectance at about 880 nm that is present for a pure aluminum reflective surface, yielding an excellent reflector.

C-2

layer can be deposited. The back of the dish will remain foam, for structural support and for protection against micrometeorites.

- Concrete applied over male mold. After molding, the concrete shell will be inverted and a thin glass layer applied, possibly by spin-molding. Finally, a reflective layer of aluminum will be applied to the glass surface.
- Iron-ore concentrator formed on male mold by sintering.
- Glass-glass composite. High-temperature fibers will be laid out on a mold, and low-temperature binder glass will be melted and forced to flow onto the mold to bind the fibers together, and form a composite.
- Heliostat ring of concrete, glass-glass composite, or foam glass-cored glass tube, with thin metal or microsheet glass membranes. Focusing via electrostatic forces (see below).
- Multi-faceted dish structure with foam-glass/glass beam construction to support mirror facets.

More designs can be added along the way if we come up with improvements.

Miscellaneous. Use of static electricity to focus heliostats was proposed. By placing opposite charges on the front and rear membranes, the attractive force between them will cause the membranes to deform to a shape approximating a parabola. This approach has been used in some satellite systems. An advantage over pressure-focusing is that pinholes due to micrometeorites will not affect the focusing system.

Due to the lack of wind loads, a very simple tracking device for parabolic dishes may be possible. A design similar to the passive tracker sold by Zomeworks for terrestrial photovoltaic systems might be appropriate. This tracker relies on a mechanical balance between two partially shaded accumulators that are partially filled with liquid. If the collector gets off-track, one of the accumulators becomes more exposed to the sun, increasing the vapor pressure in the accumulator and forcing more fluid to the other accumulator. The shift in the system's center of gravity causes the collector to rotate back to its proper tracking position. Since the lunar rotation axis is very close to perpendicular to the ecliptic, no seasonal adjustment for declination would be necessary, and a very simple polar mount would be sufficient.

Testing. It may be possible to simulate foam glass fabrication techniuqes at room temperature, using a standard polyurethane foam or an adhesive/glass microsphere mixture. As soon as we identify materials that duplicate as well as possible the lunar materials, we can begin some fabrication tests.

References

American Institute of Aeronautics and Astronautics, 1988, *Commercial Opportunities in Space--Progress in Astronautics and Aeronautics*, Vol. 110, AIAA.

Friedlander, A. and Cole, K., 1989, "Power Requirements for Lunar and Mars Exploration Scenarios," Report No. SAIC-89/1000, SAIC, San Diego.

Lin, T. D., 1987a, "Concrete for Lunar Base Construction," *Commercial Opportunities in Space--Progress in Astronautics and Aeronautics*, Vol. 110, AIAA.

Lin, T. D., 1987b, "Physical Properties of Concrete Made With Apollo 16 Lunar Soil Sample," *Commercial Opportunities in Space--Progress in Astronautics and Aeronautics*, Vol. 110, AIAA.

Lunar and Planetary Institute, 1980, *Extraterrestrial Materials Processing and Construction: Final Report*, Lunar & Planetary Institute.

MacKenzie, J. D. and Claridge, R. C., 1979, "Glass and Ceramics From Lunar Materials, *Commercial Opportunities in Space--Progress in Astronautics and Aeronautics*, Vol. 110, AIAA.

NASA, n.d., Publication SP-482.

Rowley, J. C. and Neudecker, J. W., 1980, "Melted In-Place Lunar Soil for Construction of Primary Lunar Surface Structures," *Extraterrestrial Materials Processing and Construction: Final Report*, Lunar & Planetary Institute.

Science Applications International Corporation, 1989, "Use of Thermal Energy From Nuclear Power Systems for Lunar Materials Processing," Report No. SAIC-89/1001, SAIC, San Diego.

Waldron, R. D., Erstfeld, T. E., and Criswell, D. R., 1979, "The Role of Chemical Engineering in Space Manufacturing," *Chemical Engineering*, February, pp. 80-94.

Williams, R. J. and Jadwick, J. J. (Eds.), 1980, *Handbook of Lunar Materials*, NASA Reference Publication 1057.

Investigation of Mechanical and Thermal Properties of Microwave-Sintered Lunar Simulant Material Using 2.45 GHz Radiation

T. T. Meek
Department of Materials Science and Engineering
University of Tennessee

During the past year, the focus of our research was in two areas. While they may appear to be different, they are closely related. One project investigated the mechanical and thermal properties of lunar simulant material. The current status of this research is given in the following. An alternative method of examining thermal shock in microwave-sintered lunar samples is being researched. At present, a computer code has been developed that models how the fracture toughness of a thermally shocked lunar simulant sample is related to the sample hardness as measured by a micro-hardness indentor apparatus. This technique will enable much data to be gathered from a few samples. To date, several samples have been sintered at different temperatures and for different times at temperature. During the past year, a technical presentation was made on this work and a paper submitted for publication (Nehls et al. 1989). During this investigation, photomicrographs of microwave-heated samples showed what appear to be glassy regions in between grains (Figures 2.4 and 2.5). Currently, these samples are being examined using TEM techniques to determine if, indeed, the intergranular regions are amorphous. If they are, then this may help explain the apparently enhanced thermal shock resistance of microwave-sintered lunar simulant materials. Figures 2.4 and 2.5 show the fractured surface of simulant material, which is compositionally the same as Apollo 11 lunar material. Note the apparently melted intergranular regions. This phenomenon was first observed by Meek et al. (1986) in earlier microwave sintering of conventional ceramics. Earlier work on the diffusion of various metal cations in pyrex also revealed unusual nucleation characteristics when the system was heated and cooled in a microwave field (Meek et al. 1988).

It was decided to investigate (along with the above work) the melting and recrystallization characteristics of a well-studied binary system to see if the thermodynamic barrier for the nucleation of a crystalline phase may be affected by the presence of a microwave field. The system chosen was the albite (sodium alumino silicate)-anorthite system (calcium alumino silicate). Table 2.7 shows the design of the experiment. Mixtures of albite and anorthite were melted at 1400°C and then cooled to 1200°C and held for specific lengths of time in both a conventional furnace and a microwave furnace (frequency 2.45 GHz). Heating duration varied from 1 hour to 128 hours, and thermally processed samples were investigated using X-ray, microprobe, and optical polarized light techniques to determine if differences resulted from the two

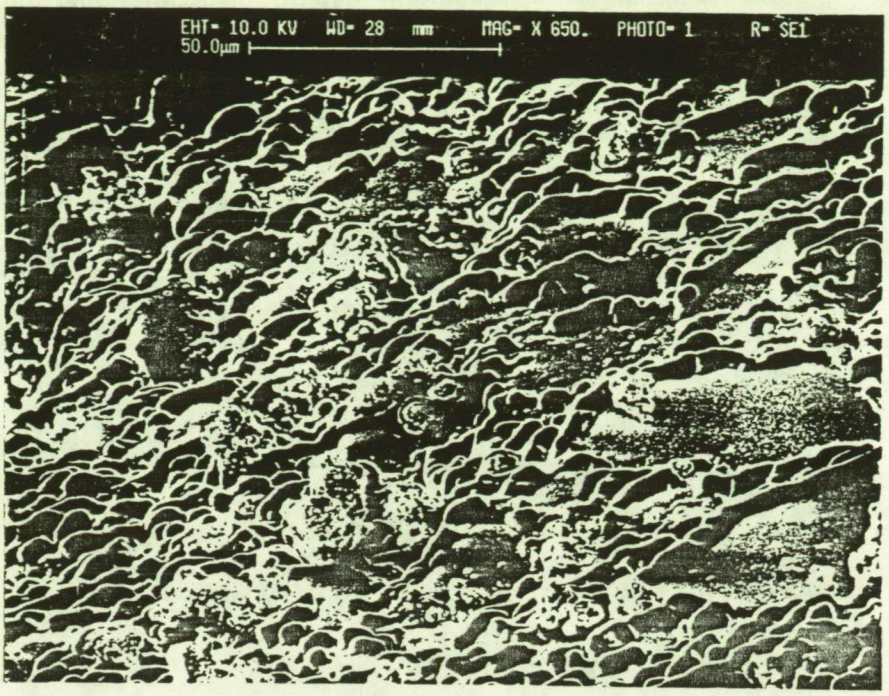

Figures 2.3 SEM photomicrograph of 2A11XLB sample heated at 56,070°C per hour using 2.45 GHz radiation. Note the apparent melt regions located in between grains. Magnification 650X.

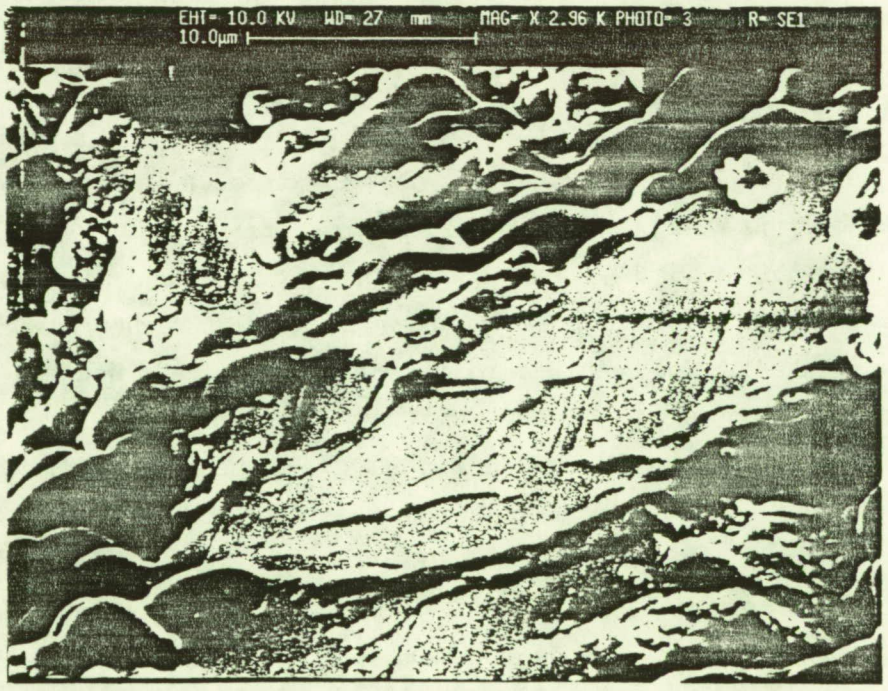

Figure 2.4 Same as Figure 2.3, but with magnification 2960X.

Table 2.7 Sample compositions and duration time at constant holding temperature in a microwave field.

Sample Composition	Holding Temperature (Degrees C)	Duration Time (Hours)
90 wt% Ab-10 wt% An	1200	1
90 wt% Ab-10 wt% An	1200	2
90 wt% Ab-10 wt% An	1200	4
90 wt% Ab-10 wt% An	1200	8
90 wt% Ab-10 wt% An	1200	16
90 wt% Ab-10 wt% An	1200	32
90 wt% Ab-10 wt% An	1200	64
90 wt% Ab-10 wt% An	1200	128
81 wt% Ab-19 wt% An	1200	1
81 wt% Ab-19 wt% An	1200	2
81 wt% Ab-19 wt% An	1200	4
81 wt% Ab-19 wt% An	1200	8
81 wt% Ab-19 wt% An	1200	16
81 wt% Ab-19 wt% An	1200	32
81 wt% Ab-19 wt% An	1200	64
81 wt% Ab-19 wt% An	1200	128
72 wt% Ab-28 wt% An	1200	1
72 wt% Ab-28 wt% An	1200	2
72 wt% Ab-28 wt% An	1200	4
72 wt% Ab-28 wt% An	1200	8
72 wt% Ab-28 wt% An	1200	16
72 wt% Ab-28 wt% An	1200	32
72 wt% Ab-28 wt% An	1200	64
72 wt% Ab-28 wt% An	1200	128

heating techniques. Figure 2.5 shows the portion of the albite-anorthite system investigated in this work.

All three conventionally heated compositions of albite and anorthite showed the presence of the crystalline α phase as shown by X-ray diffraction analysis in Figures 2.6-2.8. For the samples heated in a 2.45-GHz electromagnetic field, all compositions heated for 64 hours and the 90 wt% Ab-10 wt% An heated for 128 hours showed no trace of crystalline phase (Figures 2.9 and 2.10). For the 128-hour runs heated in the microwave field, only the 81 wt% Ab-19 wt% An and the 72 wt% Ab-28 wt% An showed a trace of crystallinity (Figures 2.11 and 2.12).

The above results show that a 2.45-GHz field affects the nucleation of the plagioclase phase in the albite-anorthite system. This effect results from the different dielectric constants of the crystalline phase and the liquid phase, respectively.

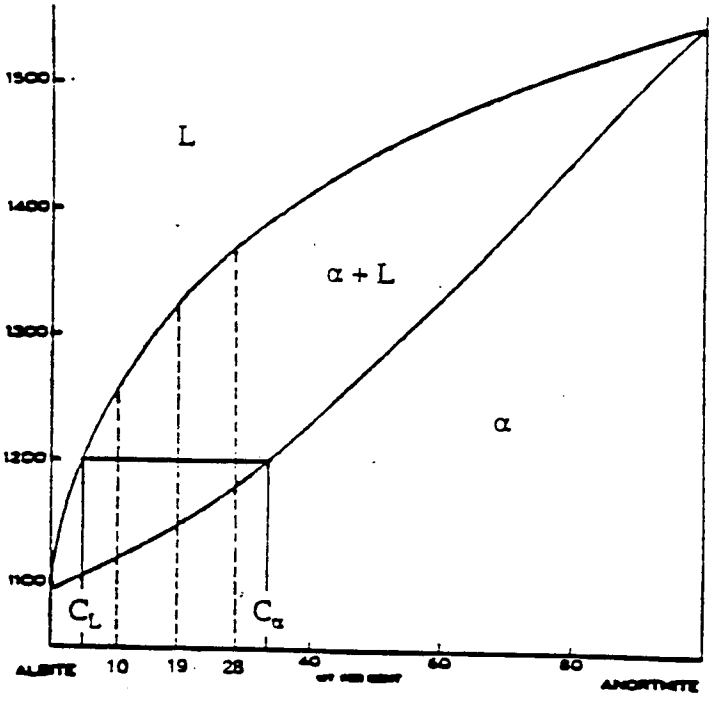

Figure 2.5 Albite-anorthite phase diagram.

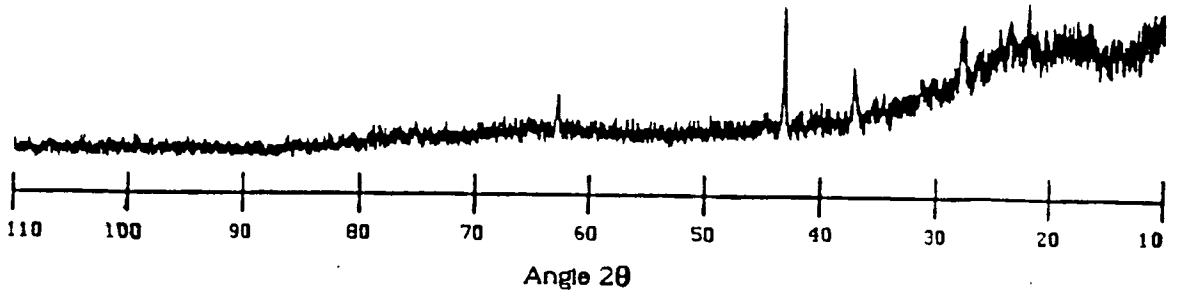

Figure 2.6 X-ray diffraction pattern of the 90 wt% Ab-10 wt% An heated in a conventional furnace at 1200°C for 128 hours.

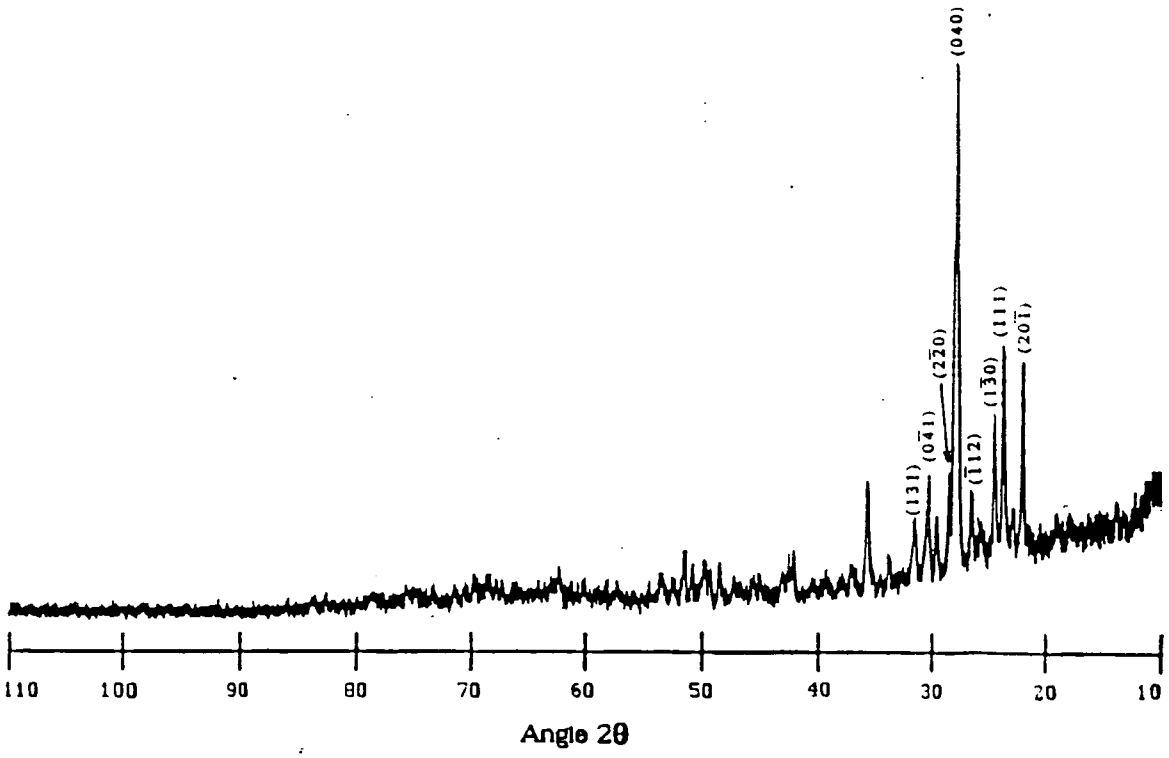

Figure 2.7 X-ray diffraction pattern of the 81 wt% Ab-19 wt% An heated in a conventional furnace at 1200°C for 128 hours.

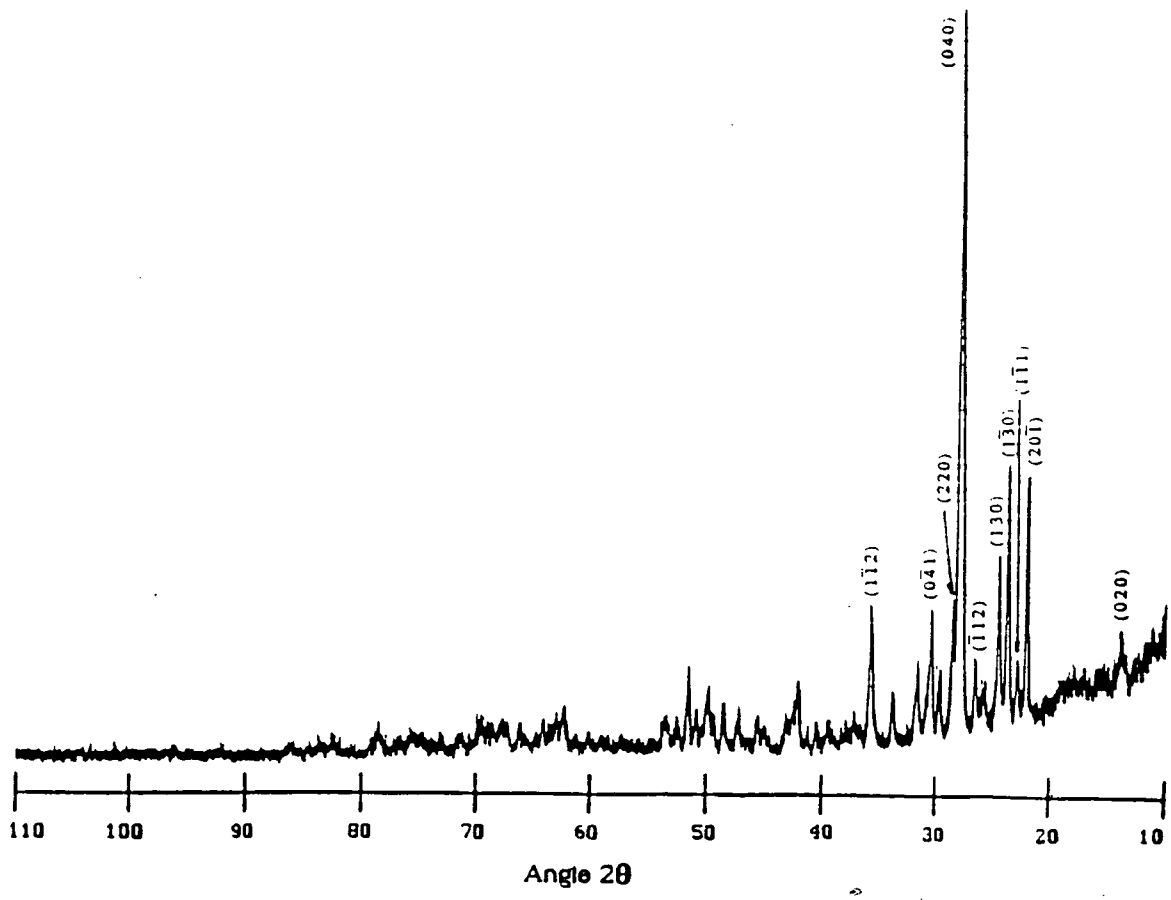

Figure 2.8 X-ray diffraction pattern of the 72 wt% Ab-28 wt% An heated in a conventional furnace at 1200°C for 128 hours.

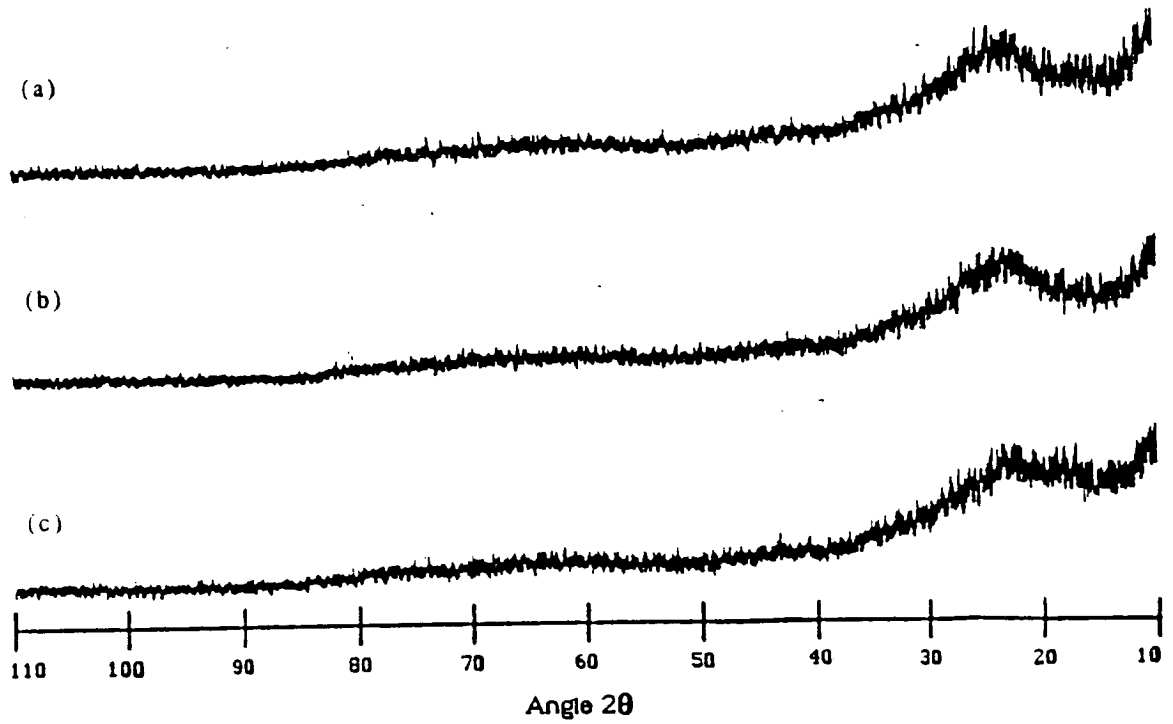

Figure 2.9 X-ray diffraction patterns of the (a) 90 wt% Ab-10 wt% An, (b) 81 wt% Ab-19 wt% An, and (c) 72 wt% Ab-28 wt% An heated in a microwave overn at 1200°C for 64 hours.

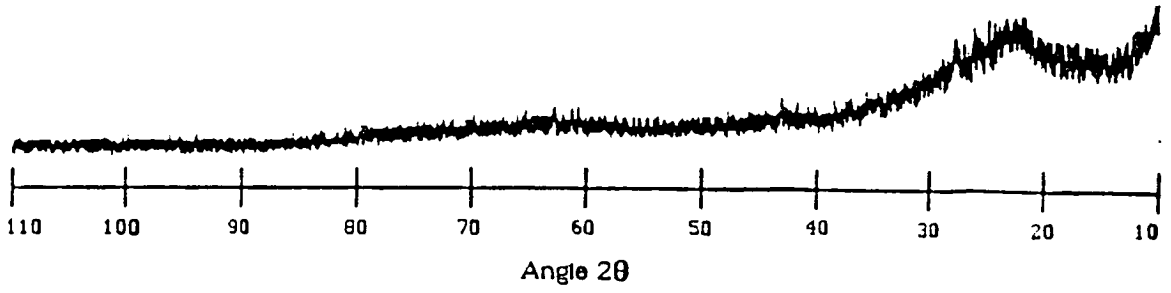

Figure 2.10 X-ray diffraction pattern of the 90 wt% Ab-10 wt% An heated in a microwave oven at 1200°C for 128 hours.

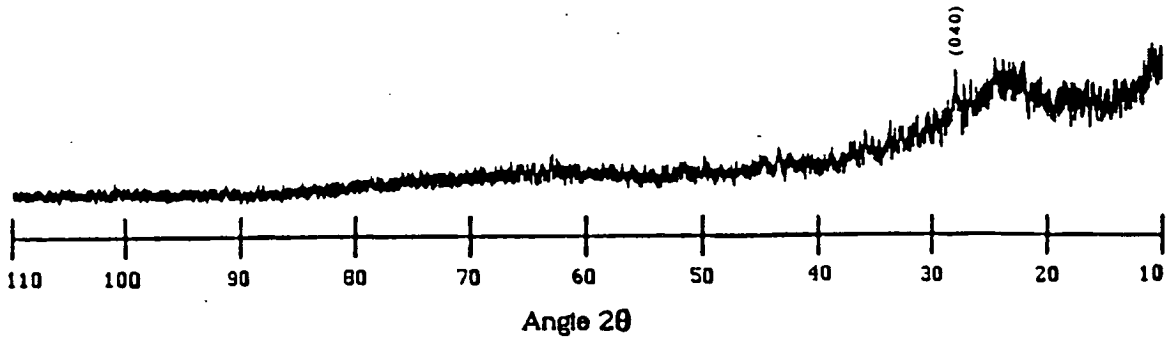

Figure 2.11 X-ray diffraction pattern of the 81 wt% Ab-19 wt% An heated in a microwave oven at 1200°C for 128 hours.

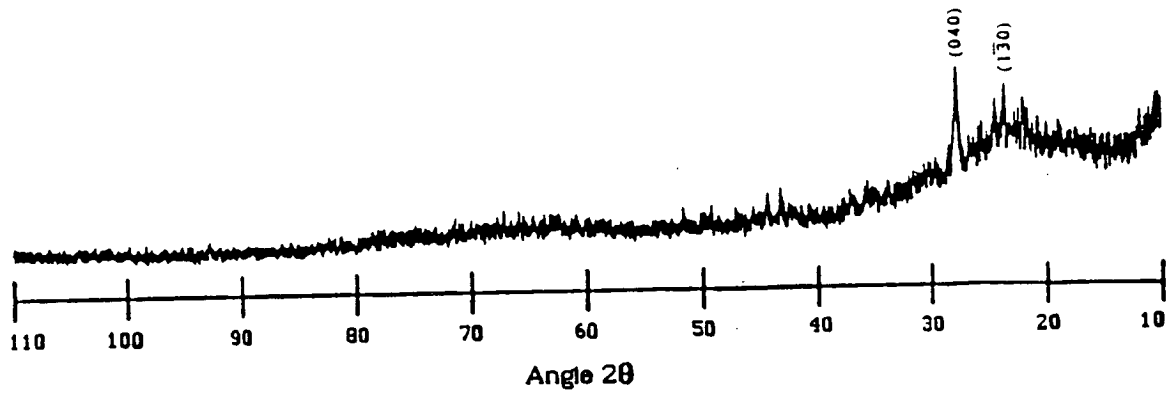

Figure 2.12 X-ray diffraction pattern of the 72 wt% Ab-28 wt% An heated in a microwave oven at 1200°C for 128 hours.

Electromagnetic field theory predicts that more power will be deposited into the lower dielectric constant region (crystalline phase) than into the higher dielectric constant region (liquid phase). This phenomenon results in the inhibition of the nucleation of the crystalline phase in the crystal-liquid two-phase region in the albite-anorthite system.

The results of this investigation suggest that all oxide-phase systems may be different when heated in a microwave field. Thus, we may expect that processing extraterrestrial materials using microwave radiation will possibly result in some different microstructures that exhibit different mechanical and thermal properties from those that are processed using conventional heating techniques.

References

Meek, T. T., Brooks, M. H., Blake, R. D., Petrovic, J. J., Jory, H., and Milewski, J. V., 1986, "Microwave Processing of Ceramics," *Journal of Microwave Power and Electro Magnetic Energy*, Vol. 21, pp. 193-194.

Meek, T. T., Blake, R. D., Katz, J. D., Bradberry, J. R., and Brooks, M. H., 1988, "Cation Diffusion in Glass Heated Using 2.45 GHz Radiation," *Journal of Materials Science Letters*, Vol. 7, pp. 928-931.

Nehls, M. K., Park, S. S., and Meek, T. T., 1989, "Processing Lunar Simulant Materials Using 2.45 GHz Radiation," *Proceedings of the Ninth Princeton/AIAA/SSI Conference*, May 10-13, pp. 94-96.

Development and Mechanical Properties of Construction Materials From Lunar Simulants

C. S. Desai
Department of Civil Engineering and Engineering Mechanics
The University of Arizona

Abstract

The development of construction materials such as "concrete" from lunar soils without the use of water requires a different methodology than that used for conventional terrestrial concrete. At this time, this research project involves two aspects: (1) liquefaction of lunar simulants with various additives in a furnace so as to produce a construction material like an intermediate ceramic, and (2) cyclic loading of simulant with different initial vacuums and densities in a specially designed new device leading to a compacted material with different final densities with respect to the theoretical maximum densities (TMD). In both cases, bending, triaxial compression, extension, and hydrostatic tests will be performed to define the /stress-strain-strength response of the resulting materials. In the case of the intermediate ceramic, bending and available multiaxial test devices will be used, while for the compacted case, tests will be performed directly in the new device. The tests will be performed by simulating in situ confining conditions. A preliminary review of high-purity metal is also conducted.

Introduction

Significant progress has been made in the area of space exploration in the past three decades. However, little has been done for development of construction materials for long-term shelters, work stations, pavements, excavation, and shielding materials for man on the Moon and other planets. For large-scale productivity on other planets, buildings and other structures are indispensable. Because of payload limitations on spacecrafts and the high cost of transportation, a prudent and efficient approach to construction on other planets requires that every effort be made to utilize the materials available on the planets themselves. The technique that is being developed in the Department of Civil Engineering and Engineering Mechanics is intended to utilize extraterrestrial "soils" to develop construction materials for building safe and serviceable structures and other systems.

The Lunar Soil Simulant

The simulant used in this study was crushed basalt rock from the Pomona Flow near Hanford, Washington. The chemical composition of the simulant and that of some

returned lunar soils are quite similar. Although the composition of the simulant did not exactly match that of lunar soil, the differences were not deemed significant enough to affect this investigation.

Every attempt was made to accurately simulate the grain size distribution of returned lunar soil. The crushed basalt rock was shaken through a stack of U.S. Standard sieves to separate the constituents by size. By re-combining the different-sized particles in the correct proportions, a satisfactory lunar soil simulant has been produced.

Progress to Date

The new test device for compression testing is ready. Two photographs showing the device are given in Figure 2.13.

The new furnace has been acquired. Preliminary molds made of tungsten are prepared for bending tests.

A draft report on high-quality purity metal is almost ready.

Planned Research

A series of laboratory tests will be performed in the new compression testing device with different initial vacuums and densities. Then, stress-strain behavior of each specimen will be obtained with different confining pressures.

The furnace will be used to obtain a number of specimens for bending and multiaxial tests.

The literature review of high-purity metals will be finalized.

Approach and Test Procedure

The locally developed lunar simulant with additives will be placed in molds of different sizes for bending and multiaxial tests and will be liquefied in a furnace with Argonne environment around a temperature of about 1100°C. A number of combinations of simulant and additives will be tried, and the resulting specimens will be tested for their stress-strain-strength properties.

For the cyclic loading in the new test device (Figure 2.13), specimens (under different initial vacuums and densities) of about 3" diameter and 6" height will be subjected to cycles of loading until an equilibrium compaction is achieved. The resulting density will be compared with the TMD. Then, a specially designed sleeve will be extracted and the specimen will receive a rubber membrane around it. A confining pressure will be applied, and the specimen will be subjected to increasing shear stress until failure.

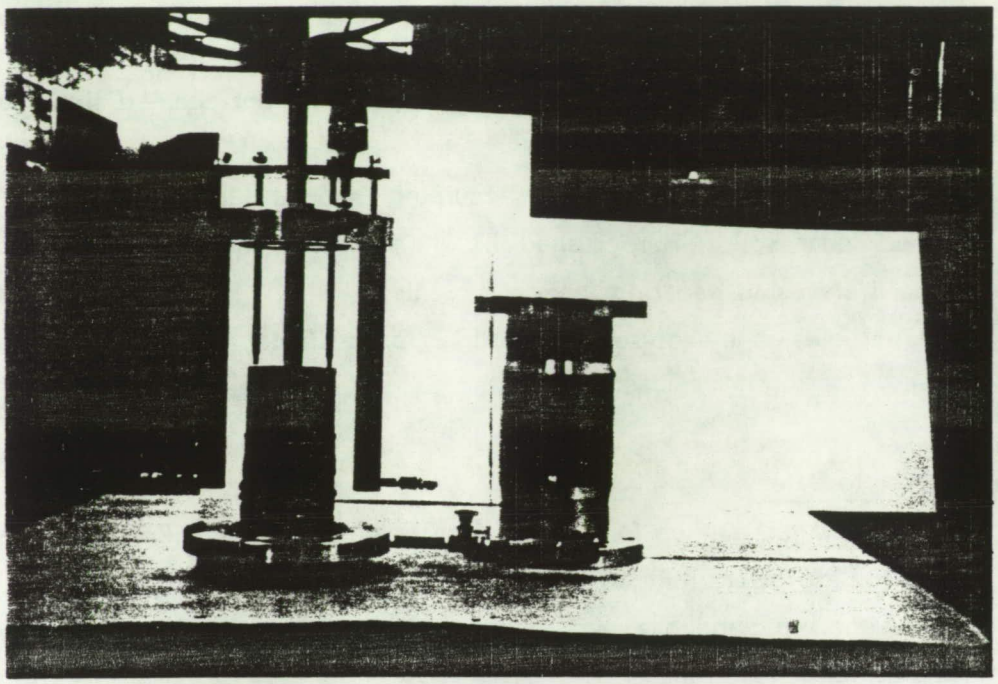

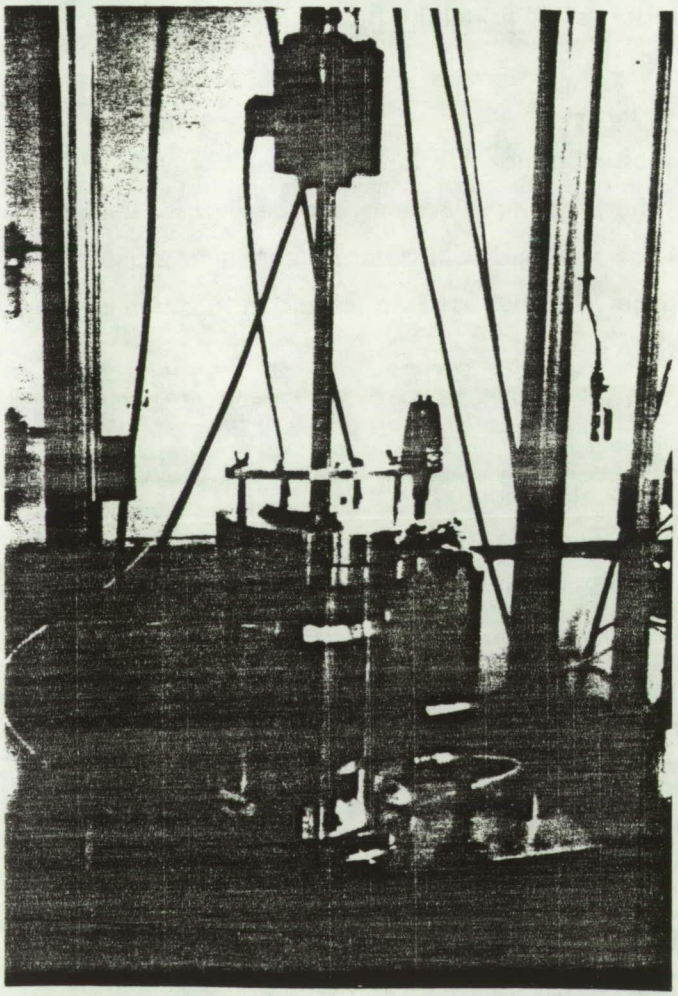

Figure 2.13 New device for cyclic compression testing with initial vacuums, densities, and confining pressures.

Expected Results

In both cases, the test results will lead to stress-strain-strength response including pre-failure, failure, and ultimate response. These results will be used to evaluate deformation parameters such as modulus of elasticity, Poisson's ratio, cohesive and frictional constants, and other plasticity constants. These constitutive constants will permit evaluation of the applicability and use of the resulting materials for construction such as shielding, structures, pavements, and excavation systems.

Participants

C. S. Desai, Regents' Professor and Head
H. Saadatmanesh, Assistant Professor
G. Frantziskonis, Assistant Professor
T. Allen, Graduate Student
K. Girdner, Graduate Student

Recovery of Precious Metals in Space

H. Freiser
Department of Chemistry and
Strategic Metals Recovery Research Facility
The University of Arizona

This program is proceeding along the lines compatible with the objective of developing feasible separation and recovery processes for precious metals in a space environment. We are exploring efficient, compact, solvent extraction systems, both single- and multistage, capable of high selectivity and rapid equilibration, based on chelate and ion pair complexes. During the current reporting period, two research projects were undertaken: (a) study of the time-dependent aspects of the formation of Pd(II) extractable chelate complexes, and (b) development of a multistage countercurrent distribution process for the separation and recovery of Pd(II) and Pt(II) ions.

Kinetics of Chelate Formation of Pd(II) Ions

Using the stopped-flow kinetics system, the rate of formation of the 8-quinolinol (HOx) chelate of Pd ($PdOx_2$) from the extractant and a solution of PdI_4^{2-} was found to be first order in both Pd and HOx, but independent of pH in the range 5-7. We are now investigating the effect of surfactants of varying charge type, in order to explore the possibility of significantly increasing the rate of chelate formation, which is desirable to enhance separation efficiency.

Countercurrent Distribution Separation of Pd and Pt

We have obtained a 2400-stage centrifugal partition "chromatograph (CPC) and tested a number of solvent extraction systems for their suitability to separate precious metals efficiently. We found that the neutral phosphorus extractant tri-n-octylphosphine oxide dissolved in heptane provided sufficient selectively to accomplish total separation of Pt and Pd by extraction from hydrochloric acid. We are planning to extend this system to the other precious metal ions and, with the acquisition of higher capacity CPC modules, developed scaled-up separation processes.

Finally, a data base system is being developed that will make the vast literature on metals separation of solvent extraction processes more accessible to the research group working on this project. The work to date has proven to be of great utility in the location and selection of the extraction systems employed above.

III. RESOURCE DISCOVERY AND CHARACTERIZATION

Search for Near-Earth Asteroids With the Spacewatch Camera

T. Gehrels
Lunar and Planetary Laboratory
The University of Arizona

The Spacewatch program began as an engineering development for the discovery of near-Earth asteroids and comets, with the first observations starting in 1983 using an RCA CCD that has 320 × 512 pixels. We wrote extensive software to scan the sky and learned how to do astrometry for precise orbits of newly discovered objects. The merit of the concept was proven, with many observations reported in the *Minor Planet Circulars* and recovery of comets in the *Circulars of the International Astronomical Union*. We improved the precision of astrometric observations for comets and asteroids (T. Gehrels, B. G. Marsden, R. S. McMillan, and J. V. Scotti, "Astrometry With a Scanning CCD," *Astron. J.*, Vol. 91, pp. 1242-1243, 1986). For efficient scanning and discovery of new objects, however, one needs a larger CCD, for which we have obtained a Tektronix 2048 × 2048 CCD.

This type of pioneering work has not been done before with such a large CCD in the scanning mode. We have defined most of the problems: For instance, what is the best scanning routine to find near-Earth asteroids and comets? Which are the best scan regions for this goal? In addition to the automatic detection that we have done before with the computer system in Tucson, it may be possible to inspect the data already on the mountain in order to recognize fast-moving objects with the new computer equipment. How to recognize fast-moving objects on the screen already at the telescope? How to interpret the data on that screen, and next on the tapes for further analysis with our computer on the campus in Tucson? Should the data be partially pre-processed or compressed before being sent to Tucson, or should we attempt to concentrate all the data-reduction capability at one site?

Since 1981, we have obtained some of the answers to these questions through various exercises that usually resulted in the accomplishment of useful research on various objects, with publication of the results. This is all summarized in a paper entitled "Various Modes of Using Charge-Coupled Devices" that Gehrels, McMillan, Scotti, Perry, and Rabinowitz have submitted to the *Astrophysical Journal*. Its abstract reads:

> This paper describes a new discipline in astrophysics, "scannerscopy," of scanning the sky with charge-coupled detectors (CCD) and computerized reduction. Usually we turn the drive off, and the scanning motion of the sky is precisely followed by slaving the charge-transfer of the CCD to the sidereal drift rate. The CCD is read out during the observing, and flat-fielding corrections are not needed. In this paper, a comparison is made with photographic surveying of Schmidt telescopes,

showing that the CCD-scanning is to be preferred, especially for the detection of fast-moving objects. With the "Spacewatch Telescope" of the Steward Observatory of The University of Arizona on Kitt Peak, we have developed new modes of using the CCD for searches of gamma-ray bursters, space debris, satellites, comets, cometesimals, the tenth planet, and various types of asteroids. Routine astrometry is done for moving objects, with a precision of ±0.6 arcsecs. We are presently using a Tektronix 2048 × 2048 CCD, which appears to be successful also in the discovery of near-Earth asteroids. The goal is to study magnitude-frequency relations of asteroids, comets, and satellites, as well as to develop new techniques for surveying; the need for a 1.8-m CCD-scanning reflector, and for surveying with CCD cameras on spacecraft that pass through the asteroid belt, is apparent.

The 2048 × 2048 CCD is now permanently on the Spacewatch Telescope. A Solbourne computer has arrived and is being programmed by Dr. David Rabinowitz, who joined us for postdoctoral study in September. It will take at least half a year to complete these programs, but every month we test the next step in this work with observations at the telescope. During one of these tests, Rabinowitz discovered the trail of a fast-moving asteroid, 1989 UP. Its perihelion distance is near 0.9 AU, which seems to indicate that it is dynmaically under the influence of the Earth and will eventually impact it. The aphelion distance is in the asteroid belt, which seems to indicate that it is a fragment of collisions there. A lightcurve obtained by Dr. Wieslaw Wisniewski yielded an amplitude near 1 magnitude, and this seems to confirm that it is an elongated fragment.

We have taken the first organizational steps towards a text and source book on Space Resources in the Space Science Series of The University of Arizona Press. The book will be based on an international conference to be held in Tucson in January 1991. The leading scientific editor is P. Lewis.

Determination of Lunar Ilmenite Abundances From Remotely Sensed Data

J. R. Johnson, S. M. Larson, and R. B. Singer
Department of Geosciences/Lunar and Planetary Laboratory
The University of Arizona

Abstract

The mapping of ilmenite on the surface of the Moon is a necessary precursor to the investigation of prospective lunar base sites. Telescopic observations of the Moon using a variety of narrow bandpass optical interference filters are being performed as a preliminary means of achieving this goal. Specifically, ratios of images obtained using filters centered at 0.40 μm and 0.56 μm provide quantitative estimates of TiO_2 abundances. Analysis of preliminary distribution maps of TiO_2 concentrations allows identification of specific high-Ti areas. Investigations of these areas using slit spectra in the range 0.30-0.85 μm are underway to search for discrete spectral signatures attributable to ilmenite.

Introduction and Background

An important criterion during selection of lunar base sites will be the availability of ilmenite ($FeTiO_3$) for use as a local resource. The distribution of ilmenite across the surface of the Moon must therefore be well known. Earth-based telescopic remote sensing of the lunar surface in combination with laboratory spectral reflectance measurements of returned lunar samples has proven to be a valuable tool, both in discerning relative differences between lunar material and in establishing more quantitative estimates of surface compositions (e.g., Head et al. 1978).

Lunar ilmenites most often contain greater than 50 wt% titanium dioxide (TiO_2), making ilmenite the dominant titanium-bearing mineral on the surface of the Moon. Surface distribution maps of TiO_2 abundances are consequently valuable in determining regions of probable high-ilmenite concentrations.

Charette et al. (1974) measured TiO_2 contents of sampled bulk lunar soils and compared their spectral reflectivities in the laboratory. An empirical relation between weight percent TiO_2 and the reflectance slope between 0.40 μm and 0.56 μm was established (Figure 3.1). The slope of the lunar reflectance spectrum in this region is primarily affected by the absorptions due to Fe and Ti in the lunar soil, i.e., the agglutinates and glasses. The relation is therefore more accurate for mature soils (those that have been extensively reworked by micrometeorite impacts), particularly in the lunar maria. Charette et al. also found the relation to hold for telescopic spectra of lunar landing sites (Figure 3.2).

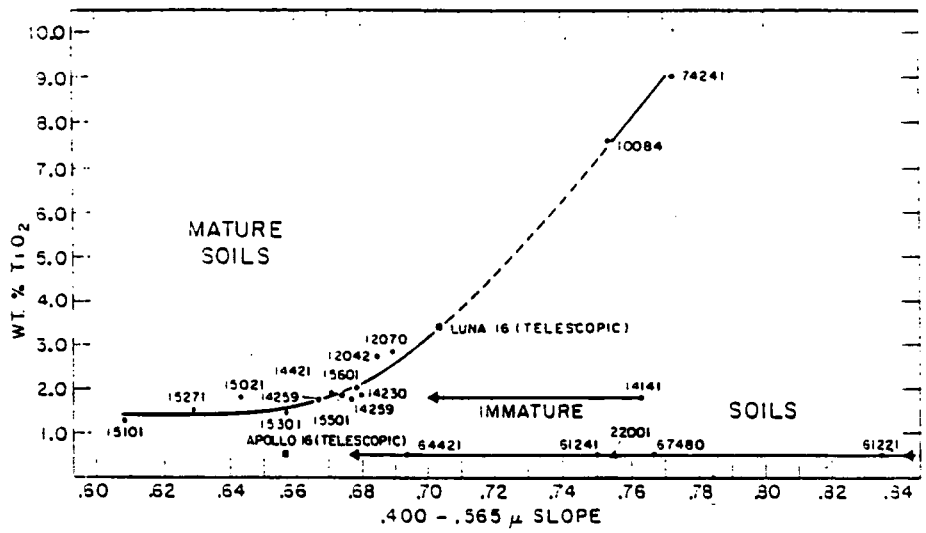

Figure 3.1 Plot of TiO_2 percentage of the bulk lunar soils as a function of 0.40 μm to 0.56 μm slope. (From Charette et al. 1974.)

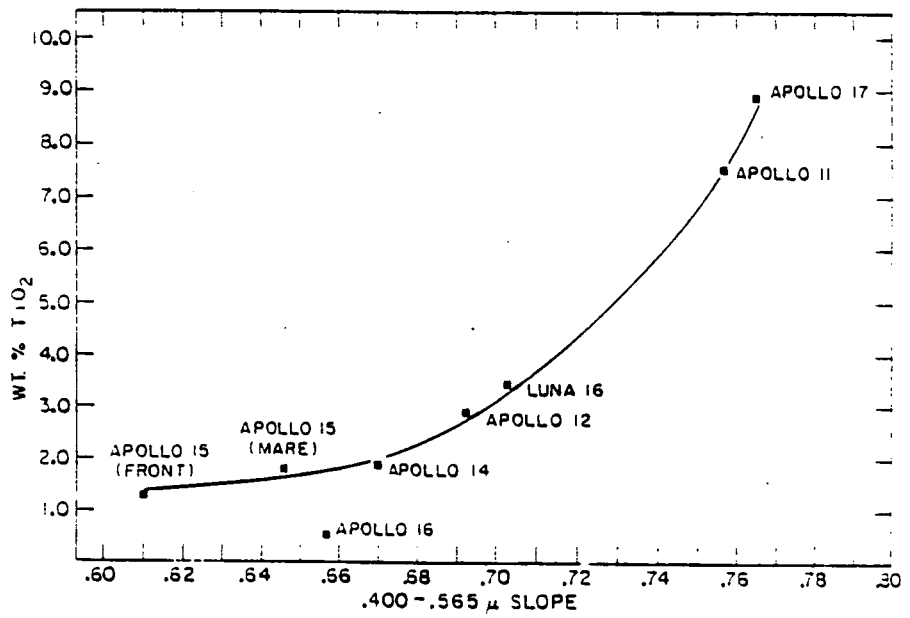

Figure 3.2 Plot of TiO_2 percentage versus 0.40 μm to 0.56 μm slope for telescopic spectra. The TiO_2 contents of telescopic areas are averages of sampled soils used in Figure 3.1. (From Charette et al. 1974.)

Johnson et al. (1977) used a silicon vidicon imaging system to obtain multispectral images of the Moon through narrow bandpass interference filters centered at 0.38 μm and 0.56 μm. An abundance map of TiO_2 for the northern maria was produced by converting the 0.38/0.56 μm ratio (normalized to a standard area in Mare Serenitatis named MS-2) to weight percent TiO_2 (Figure 3.3).

Figure 3.4 shows the most recent version of the relation between the 0.40/0.56 μm ratio and weight percent TiO_2 (Pieters 1978). At values of TiO_2 less than about 4 wt%, the absorbing effects of the Ti-Fe opaque phases can be obscured by the effects of other contaminants such as Fe-metal, plagioclase, and non-opaque (homogeneous) glass compositions in the soil. Thus, a ratio value of 1.00 may correspond to a range of 0-2.5 wt% TiO_2.

Multispectral Image Acquisition and Results

Previous efforts to obtain multispectral images of the Moon used television-type silicon vidicon tubes (e.g., McCord et al. 1976, 1979). These images possessed spatial resolutions of about 2 km per picture element (pixel) but covered relatively small areas on the lunar surface. Mosaicking of photographs taken of the individual vidicon images was necessary to achieve greater areal perspective. Contrast differences between the mosaic frames suffer from some uncertainties, which discourage comparison of apparently similar gray-level intensities between frames not contiguous.

Newer imaging technologies use charge-coupled device (CCD) systems that provide better stability and higher photometric precision. For our project, an RCA 320 × 512-pixel CCD chip has been used at The University of Arizona Tumamoc Hill Station 0.5-m telescope. In October 1989, multispectral images of the Moon were obtained at the f/4 Newtonian focus using a variety of narrowband interference filters (Table 3.1). In addition to the 0.40 μm and 0.56 μm filters, ultraviolet filters were used to discern reflectance differences in that interesting but seldom-imaged portion of the lunar spectrum. The near-infrared filters can be used to investigate additional surface properties; for example, the 0.95/0.56 μm ratio can be used as a relative indicator of surface maturity (McCord et al. 1976).

Five images are necessary to cover the full Moon (Figure 3.5). The spatial resolution of the images is about 5.3 km per pixel on the Moon. Figure 3.6 shows four of the image ratios obtained by dividing the 0.40 μm images by the 0.56 μm images in which the brighter areas correspond to higher ratio values. Full-size versions of the 0.40 μm image and 0.40/0.56 μm ratio for the eastern section of the Moon are shown in Figures 3.7 and 3.8. Using an average of the plot in Figure 3.4 (dotted line) to calibrate

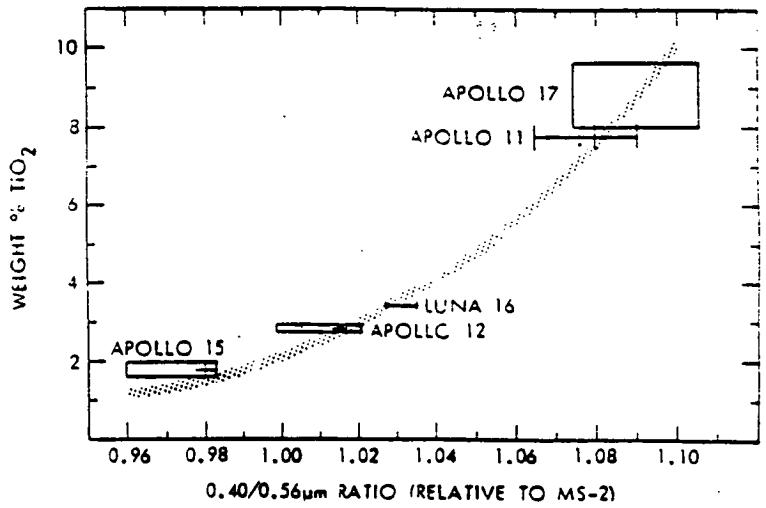

Figure 3.3 Weight percent TiO_2 versus 0.40/0.56 μm ratio (relative to MS-2). (From Pieters and McCord 1976.)

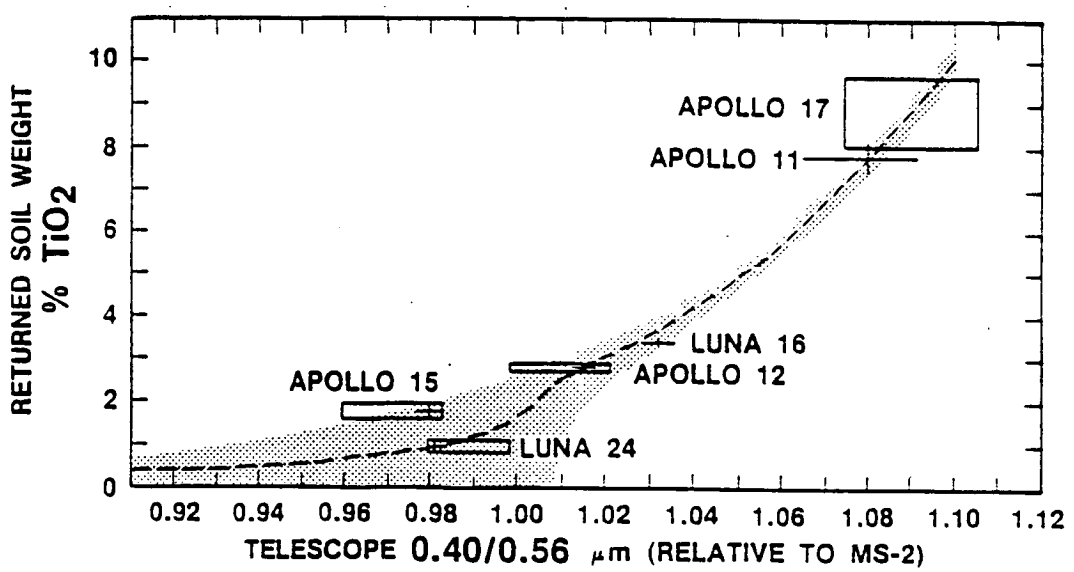

Figure 3.4 Relationship between weight percent TiO_2 in lunar mare soils and the the 0.40/0.56 μm ratio for telescopic spectra relative to MS-2. The stippled area is the estimated range of TiO_2 that can be derived from a 0.40/0.56 μm ratio measurement of mature mare regions. Dotted curve approximates the curve used for calibration of ratio values to wt% TiO_2 in present study. (After Pieters, 1978.)

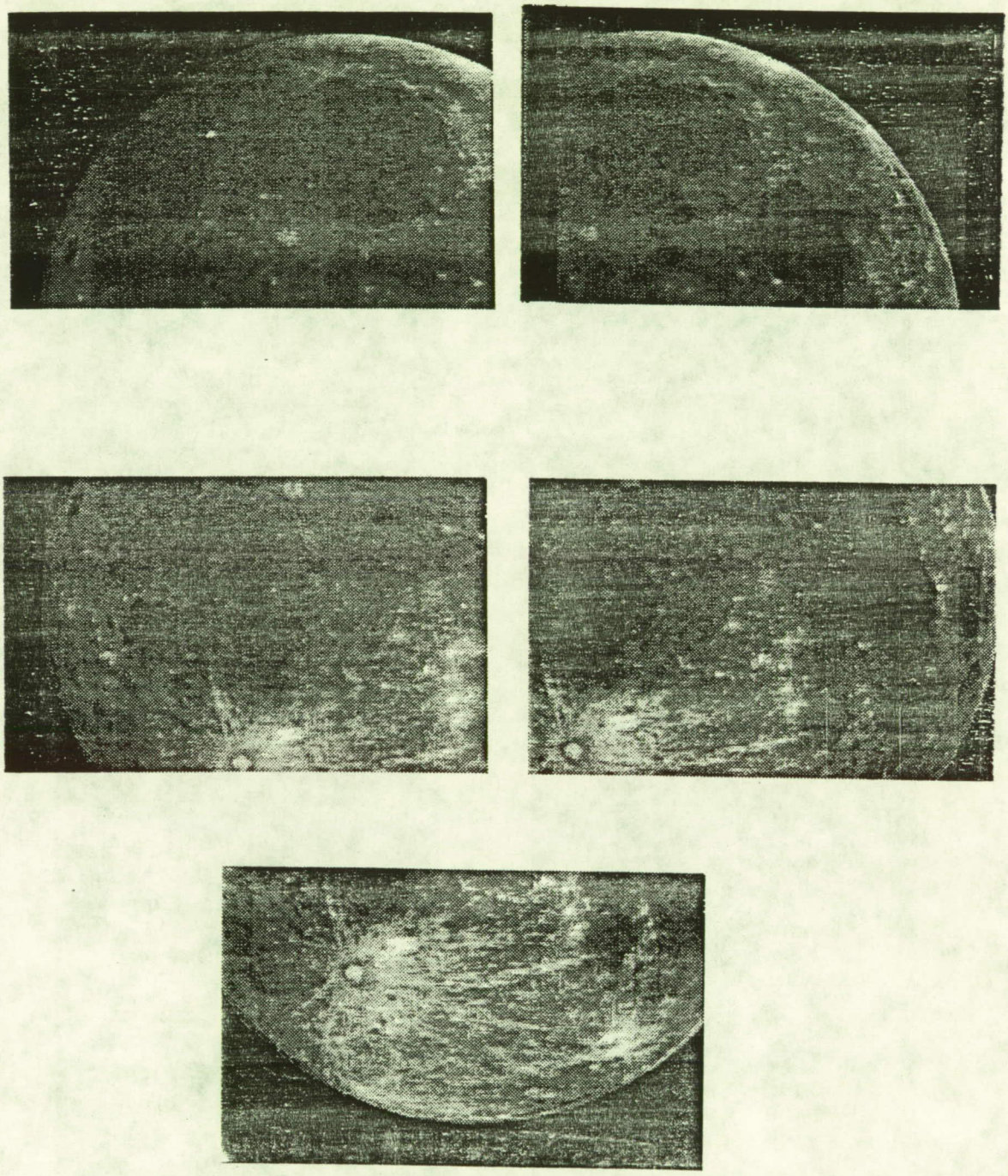

Figure 3.5 Images of the Moon obtained with bandpass interference filter centered at 0.40 μm. (Reduced-size postscript laser printer copies.)

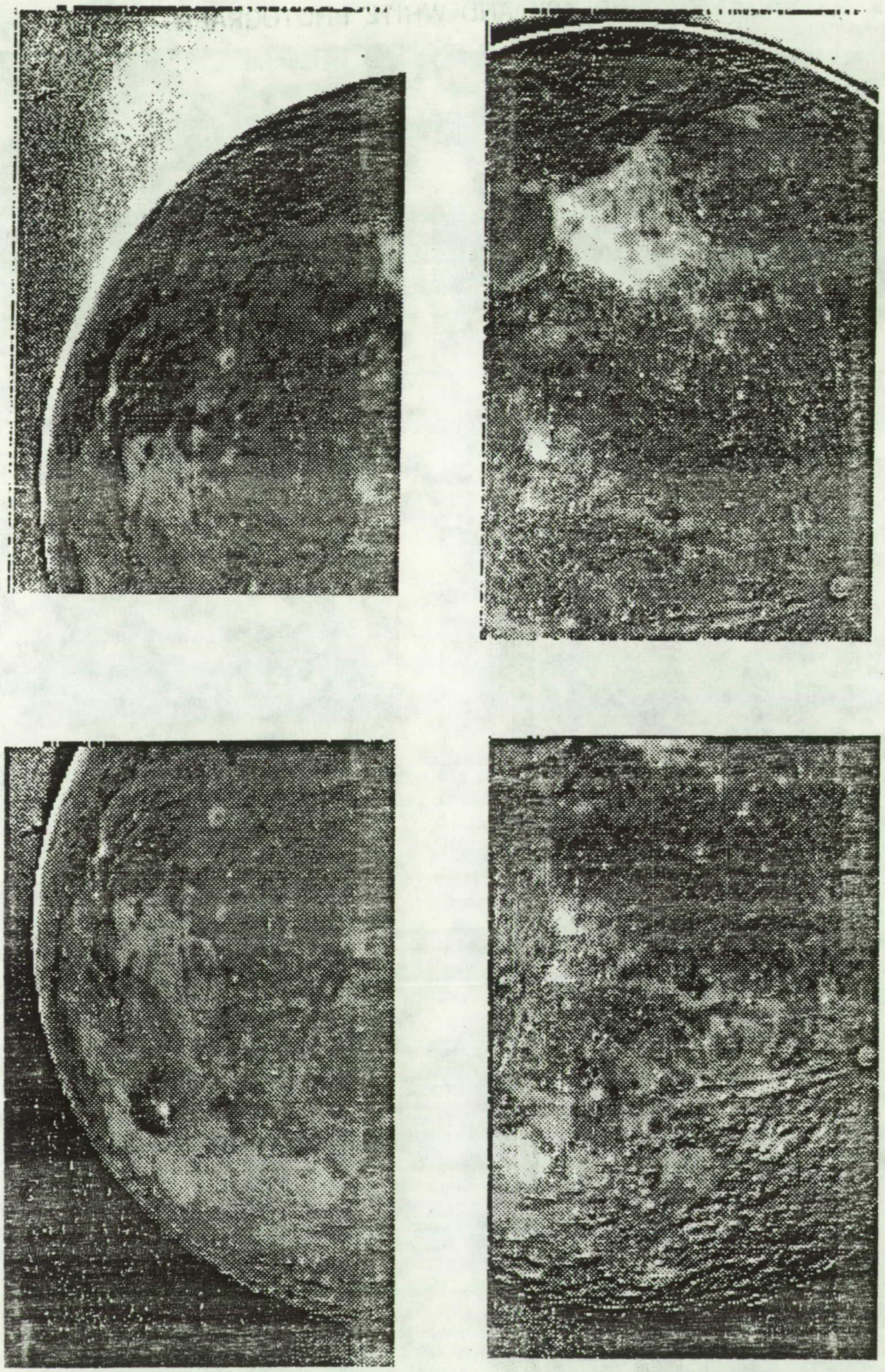

Figure 3.6 Preliminary 0.40/0.56 μm ratio images of the moon. (Reduced-size postscript laser printer copies.)

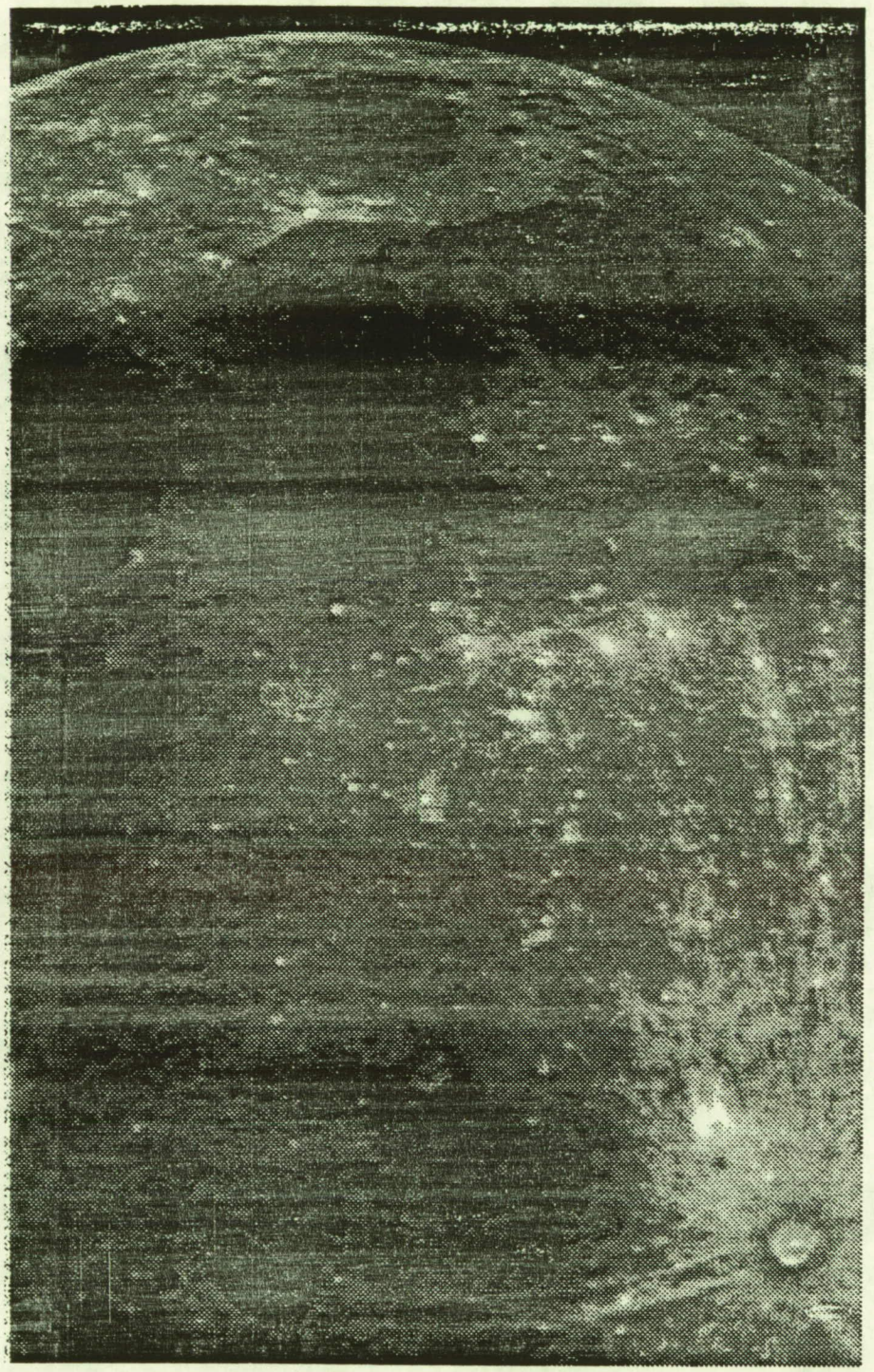

Figure 3.7 Image of eastern section of Moon taken through 0.40 μm filter. (Full-sized postscript laser printer copy).

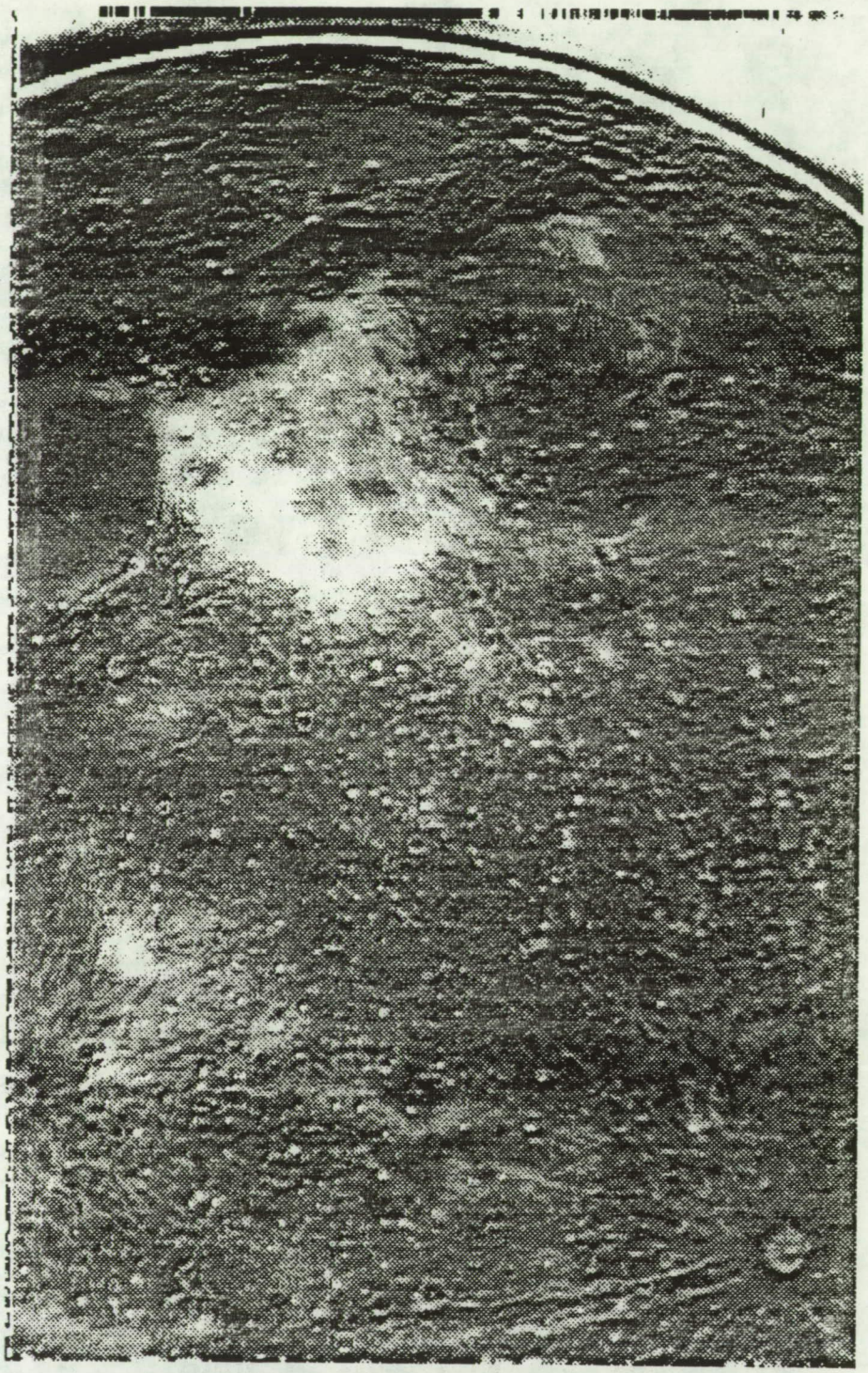

Figure 3.8 Preliminary 0.40/0.56 μm ratio image of the eastern section of the moon. (Full-sized postscript laser printer copy.)

Table 3.1 Bandpass interference filters.

Center Wavelength (nm)	Bandwidth [FWHM] (Å)
309	75
319	102
338	106
365	80
389	48
400	95
427	80
560	95
729	128
902	289
948	184

images, a TiO_2 wt% abundance map can be constructed (Figure 3.9). The value for MS-2 was taken from the eastern ratioed image section in Figure 3.8.

Variability in observed TiO_2 concentrations in some overlapping areas between adjacent image ratio sections rarely exceeds 2 wt% but is nevertheless problematic. Investigations are underway to calibrate the MS-2 standard to areas common to the overlapping portions of individual images in order to provide a standard ("tied" to MS-2) for those images in which MS-2 is not in view.

Spectroscopic Studies

Those areas highest in TiO_2 content (as determined from analysis of the preliminary maps of TiO_2 concentration) are being studied spectroscopically as well. Initial attempts were made in November 1989 (again at Tumamoc Hill) to obtain slit spectra for several regions of interest using the CCD spectrograph/camera designed by one of us (S.M.L.). It includes two blue-blazed gratings, one giving a spectral range from 0.30 μm to about 0.88 μm with 11 Å per pixel and the other providing spectra from 0.30 μm to about 0.56 μm at 5 Å per pixel. The 6 × 0.2 mm slit used corresponded to 130.0 × 4.3 km on the Moon. In December 1989, further spectra were obtained using a 20 × 0.25 mm slit with the spectrograph, corresponding to 442.3 × 5.5 km on the Moon. For the December run, a new reflecting slit allowed the image of the spectrographic slit on the Moon to be simultaneously videotaped for all lunar spectra so that the precise region being analyzed could be recorded accurately.

For both the November and December observations, each spectral observation was followed immediately by acquisition of spectra for the MS-2 area. In this way, relative reflectance spectra (ratioed to MS-2) free from instrumental and atmospheric effects were collected.

Figure 3.9 TiO_2 abundance map of the eastern section of the Moon based on 0.40/0.56 μm ratio image. Dark gray areas correspond to <5 wt %. Light gray areas correspond to 5-8 wt%. Brightest areas correspond to >8 wt%.

Figure 3.10 shows relative reflectance plots obtained in December with the lower resolution grating for four lunar areas. The spectra have been normalized to unity at 5600 Å. The Tranquillitatis and Iridium mare regions show a characteristic upturn in slope toward the near-UV and a noticeable upturn in the near-IR (longward of about 7800 Å). From preliminary maps, Tranquillitatis was shown to have larger TiO_2 concentrations than Iridium. The relative reflectance spectra are consistent with this comparison, as the slope of the spectrum for Tranquillitatis is steeper than that for Iridium, i.e., Tranquillitatis has a greater 0.40/0.56 μm ratio and a corresponding higher TiO_2 value (Figure 3.4). For comparison with mature mare areas, the craters Tycho (located in the southern highlands) and Aristarchus (located in northern Oceanus Procellarum) show a more constant relative reflectance in the near-UV and a steady decrease toward the near-IR. These two spectra also exhibit an abrupt downturn in relative reflectance at about 4800 Å

The relative reflectance spectra can be more readily compared to laboratory spectral reflectance measurements of lunar soils by calibrating them to absolute reflectance. In order to accomplish this, further spectra were obtained at The University of Arizona Catalina Observatory 1.54-m telescope in January 1990. Spectra were recorded for a solar analog star (i.e., one with spectral characteristics indistinguishable from the Sun) and then ratioed to spectra of the MS-2 region for the same air mass in order to provide an absolute spectrum for MS-2. This can be applied to the December relative reflectance ratios in order to provide absolute reflectance spectra for specific lunar areas. Reduction of the spectra to this form is presently underway.

Conclusions

The multispectral image data set taken in October 1989 is of sufficient quality to be used for analysis of both TiO_2 variations in the lunar maria and relative maturity differences of the lunar surface. Initial results from the October images show most of western Mare Tranquillitatis to be a region of high TiO_2 concentrations (>8 wt%) (Figure 3.10); this region is being investigated more fully with high-resolution spectra. Other smaller areas that show high concentrations, such as the "dark spots" east of the crater Copernicus and in the region of Sinus Aestuum (south of Mare Imbrium), are also under spectral scrutiny.

The 0.95/0.56 μm maturity index may be of interest to other SERC investigators when used in conjunction with the TiO_2 abundance map. M. Hutson, J. Ruiz, and J. Lewis conclude that high-Ti soils with low agglutinate content (immature soils) are best for processing and separation of ilmenite grains. T. Swindle and C. Glass note that the

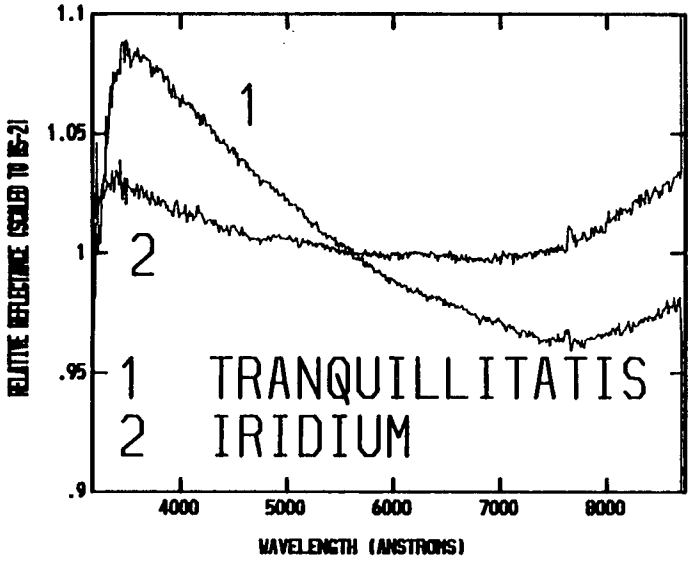

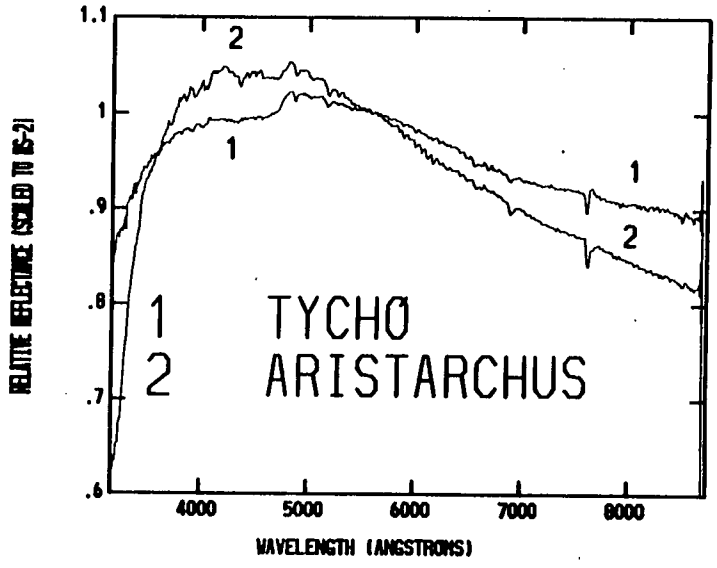

Figure 3.10 Relative reflectance spectra scaled to MS-2 and normalized to unity at 5600 Å The relative reflectance for Iridium (a large flooded crater in northern Mare Imbrium) shows a shallower slope in the 4000-5600 Å region than does the spectrum for western Mare Tranquillitatis. The craters Tycho (in the highlands) and Aristarchus (in Oceanus Procellarum) are shown for comparison.

highest Ti soils are apparently the best sites for ^{3}He implantation. Since ^{3}He will be more abundant in soils that have been long exposed to the solar wind, they prefer high-Ti soils with abundant agglutinates (mature soils).

Final products of this project will be TiO_2 abundance maps of the entire lunar near-side maria. Other ratio images [including the relative maturity index (0.95/0.56 μm)] may be of enough interest in comparison with each other to warrant additional analysis. Qualitative analysis of relative and/or spectral reflectance measurements of several areas will provide further details regarding the mineralogical and chemical makeup of high-Ti regions. The Apollo 15 and 16 orbital gamma-ray data set for titanium is also being used as an additional resource. Comparisons of the two methods' estimates of Ti concentrations will give further insight to the precision of the spectral studies.

References

Charette, M. P., McCord, T. B., Pieters, C., and Adams, J. B., 1974, "Application of Remote Spectral Reflectance Measurements to Lunar Geology Classification and Determination of Titanium Content of Lunar Soils," *J. Geophys Res.*, Vol. 79, p. 1605.

Head, J. W., Pieters, C., McCord, T., Adams, J., and Zisk, S., 1978, "Definition and Detailed Characterization of Lunar Surface Units Using Remote Observations," *Icarus*, Vol. 33, pp. 145-172.

Johnson, T. V., Saunders, R. S., Matson, D. L., and Mosher, J. A., 1977, "A TiO_2 Abundance Map for the Northern Maria," *Proc. Lunar Sci. Conf. 8th*, pp. 1029-1036.

McCord, T. B., Pieters, C., and Feierberg, M. A., 1976, "Multispectral Mapping of the Lunar Surface Using Groundbased Telescopes," *Icarus*, Vol. 29, pp. 1-34.

McCord, T. B., Grabow, M., Feierberg, M., Maclaskey, O, and Pieters, C., 1979, "Lunar Multispectral Maps: Part II of the Lunar Nearside," *Icarus*, Vol. 37, pp. 1-28.

Pieters, C. and McCord, T. B., 1976, "Characterization of Lunar Mare Basalt-Types: Luna 24 Landing Areas as Derived From Remote Observations," *Geophys. Res. Lett.*, Vol. 3, pp. 697-700.

Pieters, C., 1978, "Mare Basalt Types on the Front Side of the Moon: A Summary of Spectral Reflectance Data," *Proc. Lunar Planet. Sci. Conf. 9th*, pp. 2825-2849.

Compositions of Near-Earth Asteroids

L. A. Lebofsky and M. L. Nelson
Lunar and Planetary Laboratory
The University of Arizona

This year we have continued observational studies of near-Earth asteroids and development of techniques for determining their compositions. The analysis techniques have been applied to the spectra of several bodies in preparation for their application to near-Earth asteroids.

In mid-November 1989, we made near-IR observations of three near-Earth asteroids: 1865 Cerberus, 1989 VA, and 1989 VB. We were able to observe these asteroids in 6 broad-band visual and near-IR filters (0.4 to 2.5 μm). We were also able to obtain a few narrow-band measurements in the IR, but the asteroids were too faint to measure beyond 2.5 μm. Simultaneous, high-resolution visual CCD spectra were measured for these objects, but the data have not yet been reduced to determine their quality.

In collaboration with Jeff Bell at the University of Hawaii, we have obtained narrow-band spectra of the Martian satellite Deimos in the 1- to 3-μm spectral region. Both satellites of Mars have spectra similar to C-class asteroids; therefore, this was an opportunity to test the models developed for main-belt asteroids on an object closer to the Sun. Our preliminary analysis indicates that there is little or no water present in the surface silicates. We hope to obtain spectra of Phobos from the infrared spectrometer on the Soviet Phobos mission to analyze next year.

Simultaneous with the observing project, we are also continuing our laboratory studies (funded by NASA) of meteorites and meteorite analogs which are used in spectral analysis of our telescopic data. These spectra will also be used in compositional modeling of some of the asteroid spectra, using Hapke reflectance theory.

Extensive work has been done developing applications of Hapke reflectance theory to compositional analysis. Hapke theory is an adaptation of radiative transfer theory to particulate surfaces. The surface is assumed to be composed of irregularly shaped, randomly oriented particles that are large compared with the wavelength of the light. The particles are in contact, but coherent effects are assumed to average out due to the random orientation and irregularity of the particles. Diffraction is also not included in the derivation because the light diffracted by one particle in the surface encounters another particle before it has dispersed sufficiently to be distinguished from the incident light. By definition, all of the light striking a particle is either scattered or absorbed; therefore, the maximum extinction efficiency of a particle in a surface is one.

In the derivation, the light reflected from the surface is separated into singly and multiply scattered components. The term for the singly scattered component includes all the geometric information, and the multiply scattered component is approximated by the isotropic solution.

The principal equation is an expression for the bidirectional reflectance:

$$r = \frac{w}{4\pi} \frac{\mu_0}{\mu_0 + \mu} \left\{ \left[1 + B(g) \right] P(g) + H(mu_0) H(mu) - 1 \right\},$$

where

w = the single scattering albedo,

μ_0 = the cosine of the incidence angle,

μ = the cosine of the emission angle,

g = the phase angle,

B(g) = the backscatter function,

P(g) = the phase function, and

H(•) = the Chandrasekhar H-function for isotropic multiple scattering.

The single scattering albedo is the percentage of total light encountering a grain that is scattered out of the grain. The backscatter function describes the magnitude and extent of the opposition effect observed at low phase angles. The phase function describes the average angular scattering behavior of the grains in the surface. This basic equation can be manipulated to calculate other quantities, such as the radiance coefficient, the directional hemispherical reflectance, and the normal albedo.

The reflectance of an intimate mineral mixture can be calculated from this equation by substituting average quantities for the single scattering albedo and phase function. The average single scattering albedo is an average of the single scattering albedos of the components, weighted by their relative cross-sectional areas. The average phase function is weighted both by cross-sectional area and single scattering albedo because bright grains contribute a higher portion of the light that strikes them to the total surface reflectance. These equations can be used to determine the relative abundances of minerals in a mixture if the end members are known or can be inferred.

Two applications of relevance to near-Earth asteroids were initiated by Marcia Nelson in her graduate work at the University of Hawaii. The composition of Vesta was determined by fitting a mixture equation to telescopic spectra of Vesta and, in collaboration with Paul Lucey at the University of Hawaii, the theory was used to calculate many lunar analogue spectra to aid in the interpretation of lunar telescopic spectra.

High-resolution, visible, and near-infrared spectra of Vesta have been available for many years. The spectra have been interpreted repeatedly, and a consensus has emerged that the majority of Vesta's surface is very similar, if not identical, to the eucrite meteorites. The eucrites are basalts, which are composed of plagioclase and pyroxene, with little to no olivine or metal. Hapke's equations can be fit to a spectrum to determine the relative abundances of the components, given spectra of the end members. The theory has matched laboratory spectra well, so Vesta was chosen for the first unconstrained test because its spectrum is already so well analyzed.

Spectra of actual eucrite mineral separates are not available, so spectra of the most chemically similar pyroxene, plagioclase, and olivine available were chosen as end members. The single scattering albedos of the end members were determined by fitting the directional hemispherical reflectance equation to the end-member spectra. Then, the abundances of the end members were determined by fitting the normal albedo of a mixture equation to the spectrum of Vesta using the single scattering albedos of the end members as input. The abundances determined were 65% plagioclase/35% pyroxene, which is essentially eucritic. This is an extremely good result, considering the large uncertainties and known approximations in the inputs. Efforts will be made to improve the inputs and the fitting techniques this year so they can be used to analyze other asteroids.

A different approach was used in applying Hapke theory to the analysis of lunar spectra. Instead of analyzing individual telescopic spectra, the theory was used to calculate synthetic mixture spectra from which spectral trends were determined. The eventual goal of the project is to construct actual calibration plots using parameters derived from the synthetic spectra. It was sidetracked this year when it was discovered what a powerful tool this is for investigating the systematics of spectra of intimate mineral mixtures. It is possible to calculate any mixture that can be defined, containing as many components as desired, providing spectra of the end members are avaiable. It is also possible to quickly calculate mixture series, holding components fixed, or varying them as desired. The mixture series calculated to date have explored orthopyroxene, clinopyroxene, olivine, and plagioclase mixtures, and have begun to explore the spectral effects of ilmenite and agglutinates. The effect of shocked plagioclase has yet to be included.

This has proven to be an important, general-purpose tool for quickly investigating the spectra of mineral mixtures. It will be particularly useful in testing the validity of the end members chosen before more time-consuming fits are run to determine absolute abundance. It is also an excellent tool for directing laboratory investigations,

aiding in testing end members, and determining the relevant mixtures to actually create. It will undoubtedly be used regularly in work on near-Earth asteroids next year.

Presentations

The following papers were presented at the American Astronomical Society Division of Planetary Sciences meeting, October 31-November 3, 1989:

J. F. Bell, P. G. Lucey, J. C. Gradie, J. C. Granahan, D. J. Tholen, J. R. Piscitelli, and L. A. Lebofsky, "Reflection Spectroscopy of Phobos and Deimos."

L. A. Lebofsky and T. D. Jones, "The Nature of Low Albedo Asteroids From 3-μm Multi-Color Photometry and Spectrophotometry."

M. L. Nelson and J. F. Bell, "Modal Mineralogy of Vesta From Hapke Theory."

Continuous Monitoring of the Lunar or Martian Subsurface Using On-Board Pattern Recognition and Neural Processing of Rover Geophysical Data

J. W. McGill, C. E. Glass, and B. K. Sternberg
Department of Mining and Geological Engineering
The University of Arizona

A proposal submitted by the Laboratory for Advanced Subsurface Imaging (LASI) to the Center for Utilization of Local Planetary Resources entitled "Continuous Monitoring of the Lunar or Martian Subsurface Using On-Board Pattern Recognition and Neural Processing of Rover Geophysical Data" includes research using the ground-penetrating radar (GPR) and seismic systems. The ultimate goal of this research is to create an extraterrestrial unmanned system for subsurface mapping and exploration. Neural networks are to be used to recognize anomalies in the profiles that correspond to potentially exploitable subsurface features.

The GPR signal patterns are analogous to seismic patterns, and the preprocessing techniques are likewise identical. Hence, our preliminary research focus on GPR systems will be directly applicable to seismic systems once such systems can be designed for continuous operation. The original GPR profile may be very complex due to electrical behavior of the background, targets, and antennas, much as the seismic record is made complex by multiple reflections, ghosting, and ringing. Because the format of the GPR data is similar to the format of seismic data, seismic processing software may be applied to GPR data to help enhance the data. A neural network may then be trained to more accurately identify anomalies from the processed record than from the original record.

Advantages to Designing a GPR System

Earth-based radar has been used to determine statistical descriptions of the surface and near-subsurface properties of the Moon and the near planets since the development of radar during World War II (Evans et al. 1968). The deductions of the lunar surface and subsurface from Earth-based radar were verified by experiments carried out by the Apollo missions. Therefore, it is believed that radar measurements of the planets should give reliable estimates for planetary electrical properties. The data from these measurements can be used in designing the proper parameters for an extraterrestrial radar survey system.

GPR is sensitive to the water content of the soils being surveyed. Although water creates good radar reflectors, it also attenuates the transmitted and reflected signals, seriously limiting the depth of investigation of the system. Lunar samples have shown

that the soils have the electrical properties of very good dielectric insulators and have an absence of water. The mean atmospheric pressure and temperature of Mars is far below the triple point of water. Venus has surface temperatures and pressures that are far above the critical point of water. Therefore, water will most likely not contribute to the dielectric properties of these planets (Strangway and Olhoeft 1977). It may be expected that GPR will have an excellent depth of penetration, as well as excellent responses to changes between the dielectric constants of subsurface anomalies and the dielectric constants of the surrounding regolith.

Past Lunar Experiments

Lunar profiles were collected by the Apollo 17 astronauts during the surface electrical properties (SEP) experiment in December 1972. SEP was designed to perform the same functions through interferometry that LASI is trying to perform with GPR, i.e., to detect electrical layering, discrete scattering bodies, and the possible presence of water.

A single model to fit all of the SEP data was not found. Resolution was not great enough to detect near-surface anomalies (Strangway et al. 1975). High-frequency GPR has excellent resolution, and GPR's use of pulses instead of continuous waves facilitates interpretation as long as the profiles are not saturated with noise. Conclusions and results from the SEP experiment should be utilized in the planning and construction of a new extraterrestrial electrical experiment. LASI is presently corresponding with Dr. Peter Annan, who was a co-scientist of the SEP experiment and is a developer of digital GPR systems, for insight into developing the extraterrestrial GPR system.

Potential Earth Test Sites

The closest terrestrial approximations of the lunar and near-planet surface conditions are the Sahara Desert and the Poles, where there is either very little water present in the wind-blown sands or the water is frozen and therefore not detrimental to the radar wave. The space shuttle Columbia performed shuttle imaging radar (SIR-A) experiments over the Eastern Sahara in November 1981. Although very high frequencies were used, calculated depths of penetration of dry sand based on laboratory experiments were greater than 5 m, while field studies have verified depths greater than 2 m (McCauley et al. 1982). The University of Munster and the Free University of Berlin have worked together with the General Petroleum Company of Egypt in using GPR to survey the groundwater system of Southern Egypt. Frequencies of 20 and 50 MHz were used to survey depths up to 45 m (Blindow et al. 1987). The extremely dry sands are similar to conditions that will be found on lunar and Martian

surfaces. Comparisons between shuttle radar and surface radar over the Sahara sites should help in the design of GPR systems that will work on the surface of planets that already have high-frequency radar data.

Processing Radar Data

Current research at LASI includes using commercial seismic data-processing software to enhance the radar returns. MIRA, from the Oklahoma Seismic Corporation, is the software being used presently. The following figures demonstrate what may be done with the data to make anomalies more easily recognizable for neural networks.

Figure 3.11 is the standard printout from the profile recorder purchased as part of a commercial GPR system from Geophysical Survey Systems, Inc. This profile was taken over a pipe buried at The University of Arizona School Mine GPR test site. The pipe is buried at a known depth of 38 cm. The sweep rate of the recorder was set at 16 scans per second and the 500 MHz antenna was pulled over the pipe at a slow walking pace. Marks on the record were made at meter intervals along the profile line.

After recording the analog signals, another traverse was made with a Tektronix scope digitizing the analog signal, the results of which are shown in Figure 3.12. Traces were recorded every 10 cm along the profile line. Trace 1 on the digital record corresponds to the first mark on the left of Figure 3.11, trace 10 corresponds to the second, trace 20 to the third, and so on. By having the antenna fixed in one position during a sampling, a real-time stacking may be performed by the Tektronix scope in order for coherent signals to add and incoherent noise to cancel, thereby increasing the signal-to-noise ratio.

Because the traces have been digitized, computer algorithms may be applied to the traces to enhance the returns. All trace-attribute data of Figures 3.13 to 3.19 are the same data presented as profile traces in Figure 3.12. The basic assumption of MIRA is that any periodic function, such as a GPR trace s(t) can be considered as the real part of a complex function S(t), which has both a real part and an imaginary part:

$$S(t) = s(t) + is^*(t) .$$

$s^*(t)$ can be calculated from the trace s(t) with a Hilbert Transform. Any complex number can also be written as

$$S(t) = A(t)e^{i\theta(t)}$$

so that

$$A(t)e^{i\theta(t)} = s(t) + is^*(t) ,$$

where A(t) is called the instantaneous amplitude and

$\theta(t)$ is called the instantaneous phase.

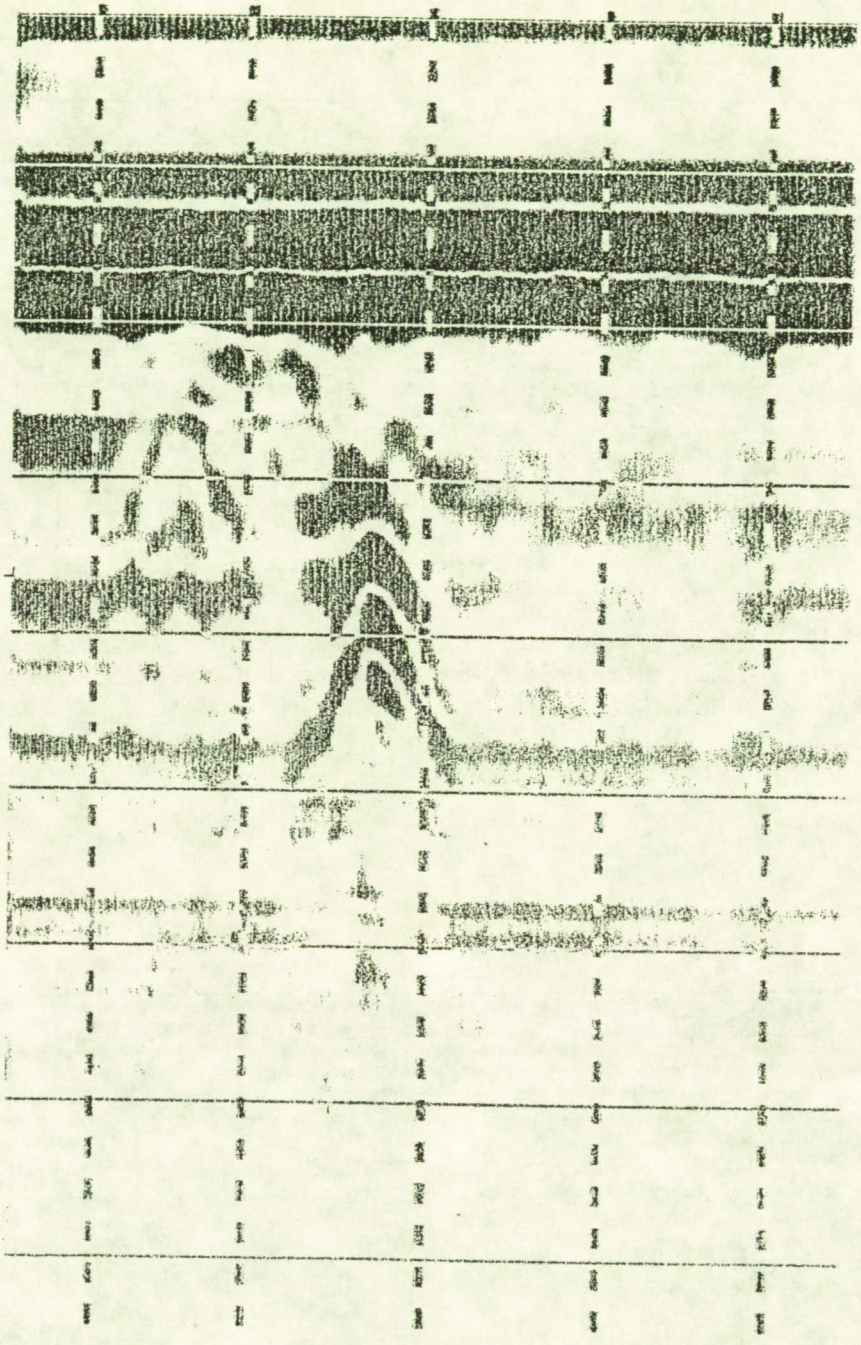

Figure 3.11 Output of analog profile over pipe buried 38 cm deep. Vertical axis is time (2.5 nsecs/div.); horizontal axis is distance (1 m/div.).

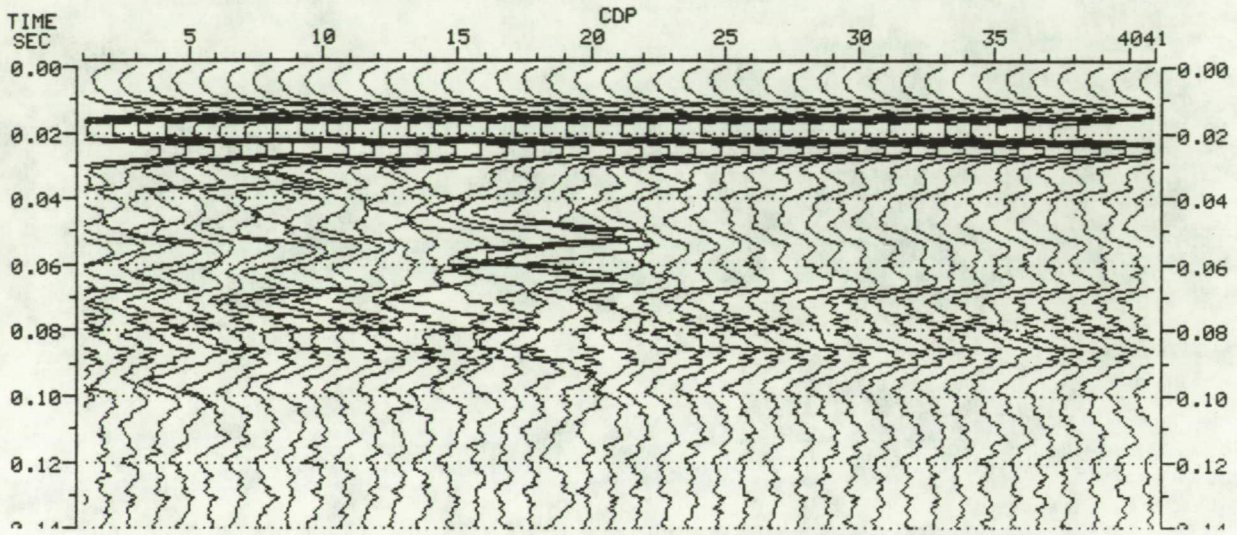

Figure 3.12 Output of digitized profile of same target as that of Figure 3.11. Each CDP represents a 10-cm shift such that 10 CDP's equal a 1-m horizontal shift.

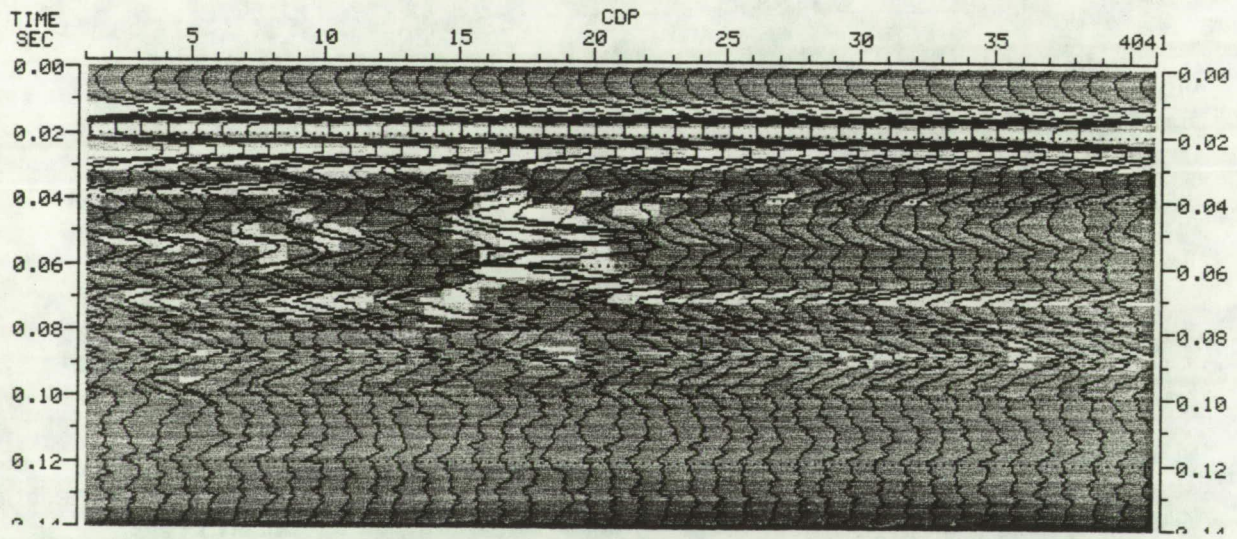

Figure 3.13 Instantaneous amplitude from digitized traces of Figure 3.12. Traces were left on the plot for reference.

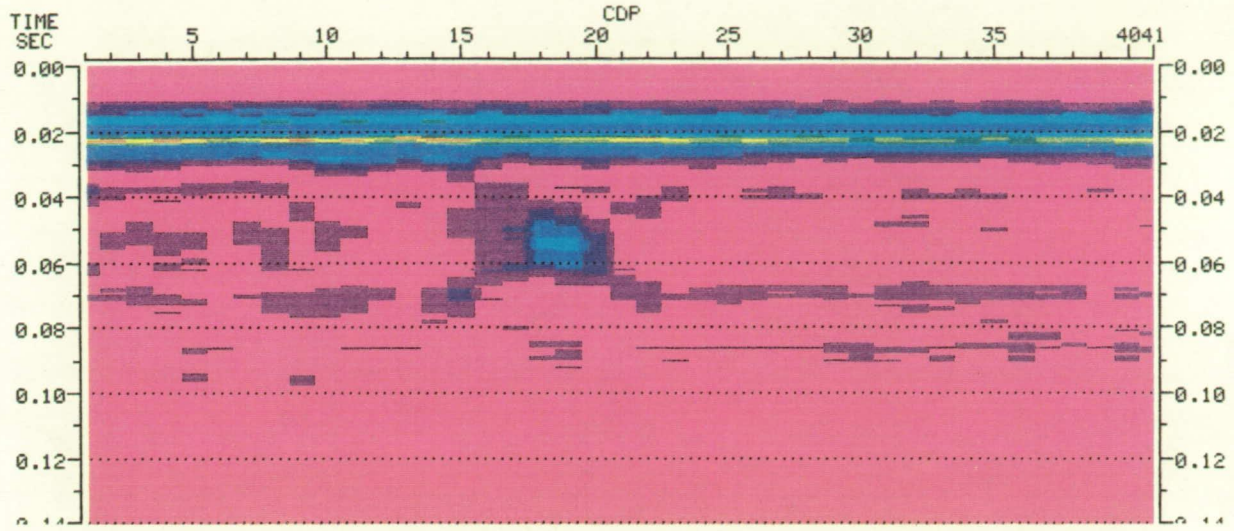

Figure 3.14 Instantaneous power from digitized traces of Figure 3.12.

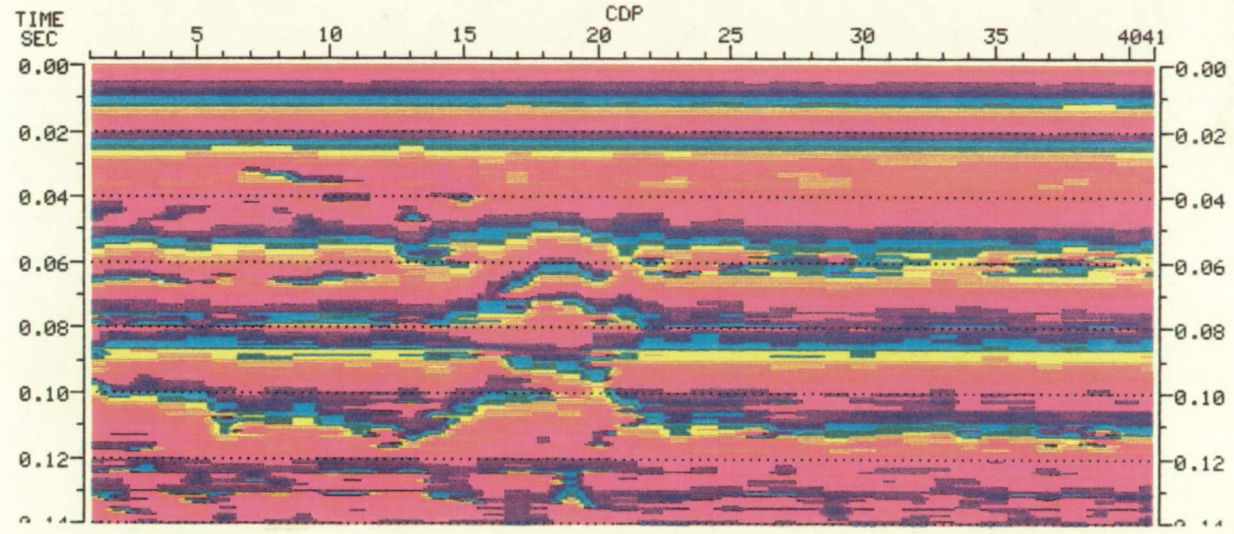

Figure 3.15 Instantaneous phase from digitized traces of Figure 3.12.

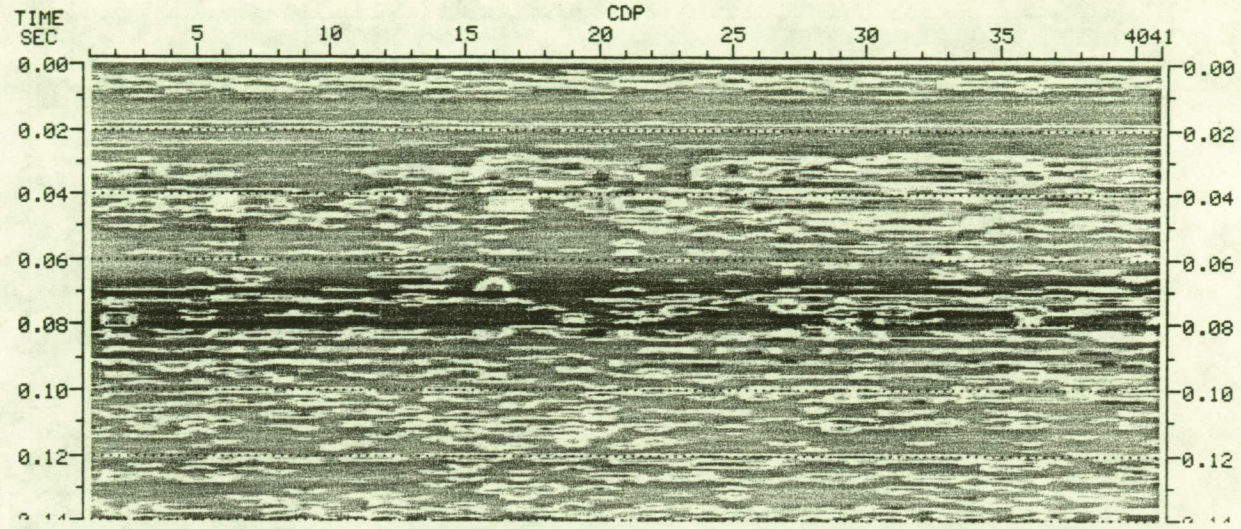

Figure 3.16 Instantaneous frequency from digitized traces of Figure 3.12.

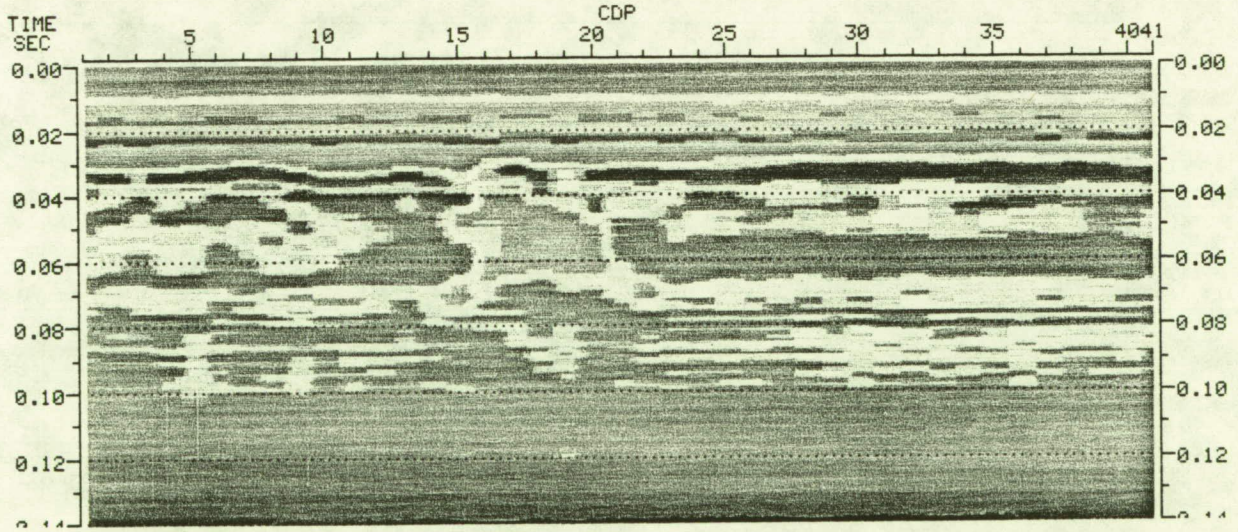

Figure 3.17 Reflection strength from digitized traces of Figure 3.12.

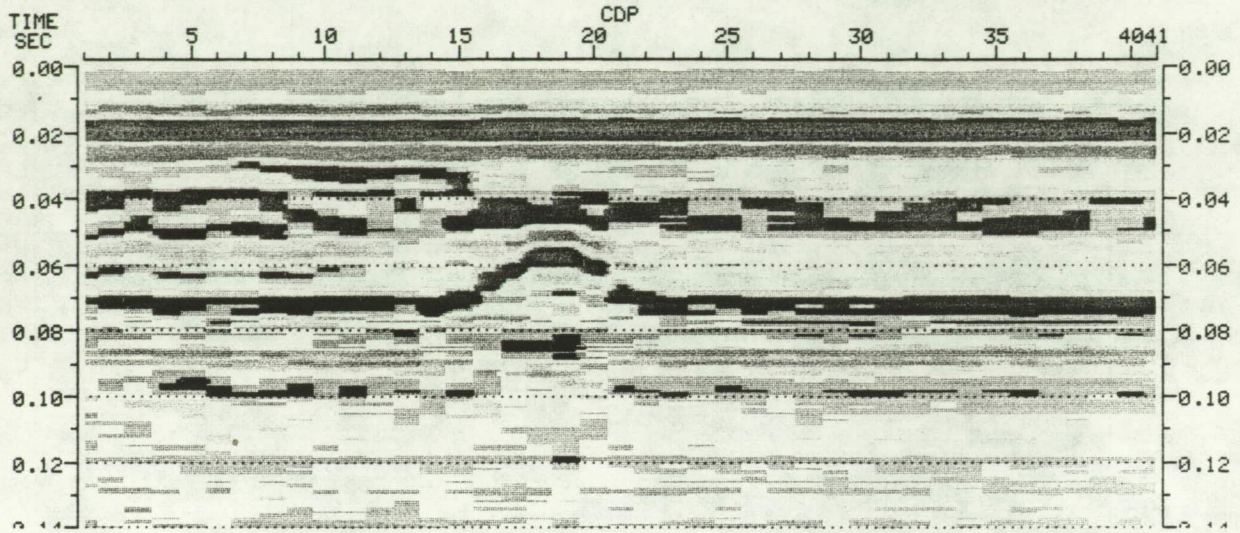

Figure 3.18 Real polarity from digitized traces of Figure 3.12.

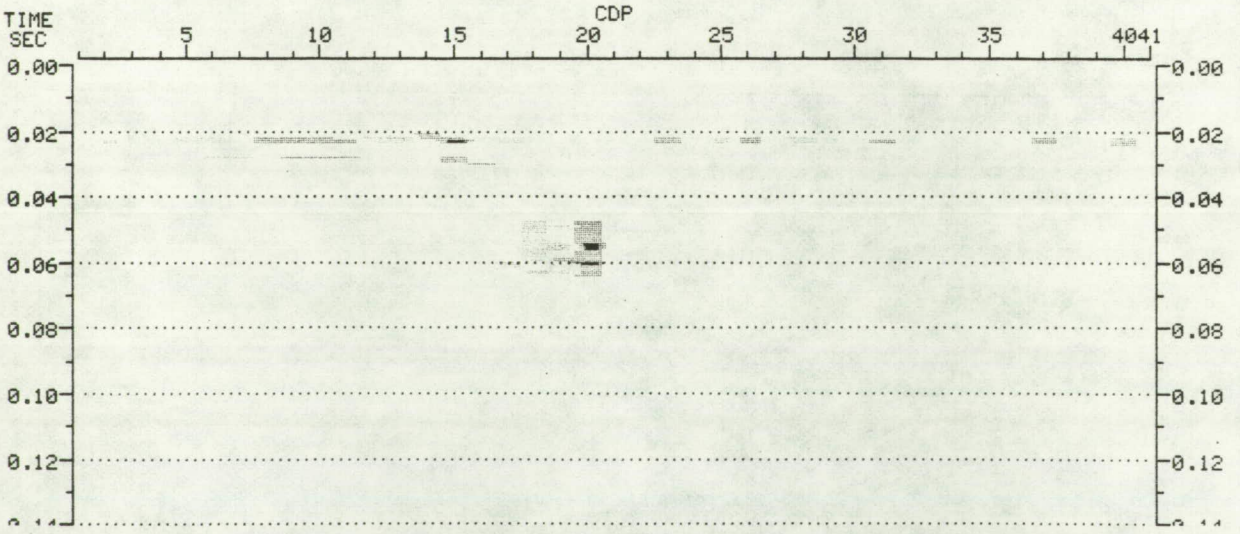

Figure 3.19 Amplitude-weighted imaginary part of the phase difference of adjacent traces of Figure 3.12.

MIRA uses the instantaneous amplitude and the instantaneous phase to calculate all other attributes. The individual traces are plotted in MIRA by a color spectrum, with low values represented by violet and high values represented by red. Instantaneous amplitude is plotted in Figure 3.13, and instantaneous phase in Figure 3.15.

A few examples of some other attributes calculated by MIRA are given in Figures 3.14 to 3.19. Figure 3.14 is the instantaneous power display that is computed by squaring the instantaneous amplitude. Power displays tend to accentuate high-amplitude events. Figure 3.16 is the instantaneous frequency, which is calculated by taking the time derivative of the instantaneous phase attribute. Figure 3.17 is the reflection strength, or decibel display, which is a normalized logarithmic display of the instantaneous amplitude. This function tends to equalize the low- and high-amplitude events. Figure 3.18 is the real polarity, which is simply a color-coded display of the real seismic trace weighted by its amplitude. Figure 3.19 is an amplitude-sine-phase difference plot created by taking two adjacent traces, calculating the phase difference between them, and then weighting the resulting imaginary part of the phase difference by the instantaneous amplitude.

From these examples, it may be seen that MIRA can be very useful, enhancing the returns from a subsurface feature. However, most features are found with a much lower signal-to-noise ratio that the example shown. The algorithms used by MIRA are not powerful enough to increase the signal-to-noise ratio significantly for many of these features. For this reason, LASI is reformatting the GPR data for a more powerful data-processing package. Routines such as deconvolution, various filters, and migration will be applied to these data to determine which sequence of operations will best increase the signal-to-noise ratio, so that subsurface anomalies will be more distinct from the surrounding background.

Once signal patterns are considered optimal, neural network pattern recognition will be applied to permit rapid recall of pattern associations. Our research on neural network pattern recognition of other EM geophysical patterns has demonstrated, for the first time (see, for example, Poulton et al. 1989), that our pattern recognizers can not only recall known patterns accurately, but can generalize and form abstractions when faced with patterns that are not part of the training suite.

Selected Bibliography

Annan, A. P. and Davis, J. L., 1977, "Radar Range Analysis for Geological Material: Report of Activities," *Geol. Surv. Can. Paper 77-1B*, pp. 117-124.

Blindow, N., Ergenzinger, P., Pahls, H., Scholz, H., and Thyssen, F., 1987, "Continuous Profiling of Subsurface Structures and Groundwater Surface by EMR Methods in Southern Egypt, Subproject B11," pages 575-627 in *Research in Egypt and Sudan, Results of the Special Research Project Arid Areas Period 1984-1987* (E. Klitzsch and E. Schrank, eds.), Verlag von Dietrich Reimer, Berlin.

Daniels, J. J., 1988, "Fundamentals of Ground Penetrating Radar," Department of Geology and Mineralogy, Ohio State University, Columbus.

Elachi, C., Brown, W. E., Cimino, J. B., Dixon, T., Evans, D. L., Ford, J. P. Saunders, R. S., Breed, C., Masursky, H., McCauley, J. F., Schaber, G., Dellwig, L., England, A., MacDonald, H., Martin-Kaye, P., and Sabins, F., 1982, "Shuttle Imaging Radar Experiment," *Science*, Vol. 218, pp. 996-1003.

Evans, J. V. and Hagfors, T., 1968, *Radar Astronomy*, McGraw-Hill Book Company, New York.

McCauley, J. F., Schaber, G. G., Breed, C. S., Grolier, M. J., Haynes, C. V., Issawi, B., Elachi, C., and Blom, R., 1982, "Subsurface Valleys and Geoarchaeology of the Eastern Sahara Revealed by Shuttle Radar," *Science*, Vol. 218, pp. 1004-1020.

McDonald, H. C., 1980, "Techniques and Applications of Imaging Radars," pages 297-336 in *Remote Sensing in Geology* (B. S. Seigal and A. R. Gillespie, eds.), John Wiley and Sons, New York.

McGill, J. W., Sternberg, B. K., and Glass, C. E., 1989, "Applications of Ground Penetrating Radar in Southern Arizona," LASI-89-2, The University of Arizona, Tucson.

Poulton, M. M., Glass, C. E., and Sternberg, B. K., 1989, "Recognizing EM Elipticity Patterns With Neural Networks," *SEG 59th Annual Meeting, Expanded Abstracts*, Vol. 1, EM38, pp. 208-212.

Strangway, D. W., Annan, A. P., Redman, J. D., Rossiter, J. R., and Watts, R. D., 1975, "Electrical Structure at Taurus-Littrow," NASA Techical Publications N-75-16308.

Strangway, D. W. and Olhoeft, G. R., 1977, "Electrical Properties of Planetary Surfaces," *Phil. Trans. Roy. Soc. Lond. A*, Vol. 285, pp. 441-450.

IV. SYSTEMS OPTIMIZATION

A "Figure-of-Merit" Approach to Extraterrestrial Resource Utilization

K. Ramohalli and T. Kirsch
Department of Aerospace and Mechanical Engineering
The University of Arizona

Abstract

A concept is developed for interrelated optimizations in space missions that utilize extraterrestrial resources. It is shown that isolated (component) optimizations may not result in the best mission. Overall economics in the broadest sense must include the "costs" of transportation, storage, continuous monitoring, and corrective actions in situ. When all of these needs are quantitatively considered, it is shown that substantial benefits can be had through less-than-the-best propellants, propellant combinations, propulsion hardware, and, actually, some waste in the traditional sense. One ready example is the possibility of discarding hydrogen produced extraterrestrially by water splitting and using only the oxygen to burn storable fuels. The gains in refrigeration and leak-proof equipment mass (elimination) outweigh the loss in specific impulse.

After a brief discussion of this concept, the synthesis of the four major components of any future space mission is developed. The four components are: **orbital mechanics** of the transportation; **performance** of the rocket motors; **support** systems that include power, thermal and process controls, and instruments; and **in-situ resource utilization** plant equipment. State-of-the-art numbers are used for the components' performances; each is studied in depth elsewhere, but those studies are beyond the scope of this paper, whose main aim is the development of the concept of a figure-of-merit for the mission. One specific example is used to illustrate the new concept; this is the Mars Sample Return mission. At this time, a popular spreadsheet is used to quantitatively indicate the interdependent nature of the mission optimization. Future prospects are outlined that promise great economy through extraterrestrial resource utilization and a technique for quickly evaluating the same.

Introduction

The remarkable potential for cost reduction in space missions that use extraterrestrial resources, as contrasted with more traditional missions that depend exclusively on all-Earth-transported resources, has been amply discussed elsewhere (Ash and Cuda 1984; Ash et al. 1978, 1982; Carroll 1983; French et al. 1985; Frisbee and Jones 1983; Ramohalli et al. 1987a, 1987b, 1989; (Presidential) National Commission on Space 1986). Every pound, or kilogram, that can be saved in the initial liftoff mass from Earth can pay back several pounds, or kilograms, because of the leverage effect

of the mass ratio equation. In this regard, it is obvious that we should specifically target those fractions of the liftoff mass that have the maximum impact on the mission. Even a cursory glance at the state-of-the-art spacecraft indicates that a very large fraction of the overall mass is the **propellant** mass. Thus begun the studies that explored the possibilities of manufacturing propellants in situ on extraterrestrial bodies to "refuel" out there, instead of from Earth-transported precious propellants. These ISPP studies concluded that it is definitely advantageous to manufacture propellants extraterrestrially. The pioneering paper by Ash et al. (1978) showed the first technical aspects of such an ISPP mission. More recent studies (Ramohalli et al. 1987a, 1987b, 1989) not only looked at specific missions, but also explored the general class of extra-terrestrial resources instead of just resources to be used as propellants. These results were sufficiently promising for NASA to establish a Center devoted to utilization of extraterrestrial resources. In addition to the all-important propellants, structural materials, shield materials, and other useful materials are being seriously considered. The fundamental goal is to render large-scale space operations economically feasible without depending upon a fleet of dedicated heavy-lift launch vehicles and upon Earth-transported repair, relief, and support supplies. It is also of utmost importance to evolve a long-range ecologically acceptable plan to minimize contamination, and subsequent cleanup, of space.

After this recognition of the significant merits of extraterrestrial resource utilization, some of the more traditional thoughts on space missions may have to be re-examined. For example, many of the components and systems that are used almost routinely for their superior performance may **not** be the best ones in light of the overall mission impact. Simple examples will illustrate the point. Oxygen-hydrogen rockets have been used almost exclusively because of their excellent specific impulse, years of accumulated design experience, contingency margins, and reliability. In fact, use of the LOX-H_2 system for primary, and even secondary, propulsion seems beyond question for future space missions. And yet when one considers the cryogenics, refrigeration, leaks, long-term material compatibility, power needs in simple storage, and safety of remote operations, several important questions arise. It is necessary to consider the full support equipment, too, in space missions. When one adds these support masses to the primary LOX-H_2 propulsion system, the desirability picture changes. It may be better to utilize a propellant system that is far less demanding in terms of refrigeration, leaks, and other related aspects, even if the specific impulse performance is inferior. The point is that what we lose in specific impulse can be more than made up in the Earth-transported mass. Some of the storable propellant combinations are seen to offer several advantages.

Expanding on these simple thoughts, we next consider several other aspects, such as long-term reliability, repairability, ease of resupply, and multiple use of components (e.g., Can an empty propellant tank become the chamber for the next-stage rocket? Can the TVC injector for the first stage become the main propellant injector for the third stage?). Also, what are the implications of using some of the unconventional propellants in rocket hardware? Will injector nozzle buildup and blockage become a serious problem? Will some of the highly solids-laden flow cause excessive erosion of the nozzle throats? With the less energetic propellants, can we use a simple nozzle and not worry about replacing critical nozzle throats? What is the overall gain to the mission?

By now, it is obvious that future space missions, especially those designed to utilize extraterrestrial resources, will have to be designed from an overall mission advantage point of view rather than in a simple component-optimized fashion. This may seem simple enough, but we must evolve a **quantitative engineering design methodology** that reflects this new design philosophy. We term this the **figure-of-merit (FoM)** approach. Although it may seem like an over-simplification, one number may be useful, purely for the purposes of initial screening of a myriad of concepts, in characterizing the overall merits of a space mission The figure-of-merit considers the specific impulse, mass ratio, reliability, inverse risk, repairability, ease of autonomous controls, scalability, and adaptability. We recognize that this is only the first step; more involved considerations will be added later. Here, the idea is to introduce a new methodology that is quantitative and considers the known engineering facts and technologies for future space missions.

The next section gives a brief overview of the components of the space missions of interest. These missions are largely the recommendations of the Sally Ride report and the Space Commission report. To render some of these thoughts more concrete, it is important to consider some specific missions. We have chosen one of the most popular missions of the next century, namely, Mars Sample Return (MSR). An advantage of this mission is that it has been extensively studied both in the USA and the USSR, including some joint-effort possibilities. Thus, it is easy to see the advantages of the FoM approach over the conventional approach. The basic mission "ground rules" are mentioned in order to provide a meaningful basis for comparisons. Whenever hard numbers are not readily available, the best estimate has been used based upon conversations with experts; it is an easy matter to change these numbers as they become more exact.

The heart of this paper considers the **development** of a quantitative, interrelated, color-coded program that enables the FoM to be readily examined for all mission

variations. This was first accomplished through the use of simple manual entry into one of the popular spreadsheets (Lotus 1-2-3). After checking for consistency and simple verifications, the program is now being upgraded to use one of the expert systems. While other researchers may have taken similar approaches to this interrelated "spreadsheet" development, our main contribution has been the **detailed quantitative considerations** of the ISPP itself. Since the ISPP modules represent the most critically important components of the entire mission, it is very important to treat them in detail. The results indicate the definite advantages of this FoM approach.

It is concluded that the FoM approach may provide a powerful and yet easy and simple tool to design future space missions that can introduce great economy (and ecology) through the utilization of local planetary (extraterrestrial) resources.

The Concept of "Figure-of-Merit"

It is very important to have a clear understanding of what is meant by the figure-of-merit. The FoM could be different for different missions and **should** be different for different priorities. The simplest definition appears to be simply the payload ratio as the most easily understood form of FoM. In some circles, the specific impulse (I_{sp}) is good enough as the FoM. In the context of the more complex missions that we need in order to utilize extraterrestrial resources, several possible definitions are indicated in Table 4.1.

Table 4.1. Possible definitions of a figure-of-merit.

1.	$\frac{m_{pl}}{m_{launch}} = \frac{m_{payload}}{m_{launch}}$
2.	$\frac{\text{A Standard "Cost"}}{\text{Total Life-Cycle Cost of This Mission}}$
3.	$\frac{\text{State-of-the-Art Launch Cost of This Payload}}{\text{Launch Cost of the Payload in This Mission}}$
4.	$\frac{\text{Mass of the Sample Returned to LEO}}{\text{Mass of the Craft Launched From LEO}}$
5.	$\frac{\text{Total Useful Mass}}{\text{Mass at Launch}}$
6.	Any of the above, modified by factors for Reliability (R_{el}), Repairability (R_{ep}), Inverse Risk (1/Risk), . . .

Note: Definition 1 will not consider the shuttle external tank in the numerator, but Definition 5 may include the ET in the numerator if it can be usefully employed in the space operation, such as ISRU.

For the purposes of introducing the concept of the FoM approach in extraterrestrial resource utilization and for the purposes of this paper, we have chosen definition number four (4), modified by factors for reliability, repairability, and inverse risk (Table 4.2); also, a factor of 10^4 is used as a multiplier for reasons of convenience. We recognize the limitations of the above definition. For example, it gives no indication of the relative ease, or difficulty, of getting to LEO in the first place. It also gives no indication of the ease, or difficulty, of assembling the spacecraft in LEO to be launched towards its destination. If the main intention of the mission is an extended duration settlement on Mars, the *return* of a small sample to LEO is no indication of the FoM. The main point is to start with an FoM that is easily modified subsequently while retaining the meaning and spirit of the quantitative interpretation and the flexibility to accommodate the modifications. Our present choice of the FoM definition possesses that capability. Thus, for the purposes of this initial introduction,

$$\text{FoM} = \frac{m_{\text{pl.returned}}}{m_{\text{launch.LEO}}} R_{el} \cdot R_{epr} \cdot (1/\text{Risk}) \cdot 10^4 \ .$$

In this specific example of MSR, the assembled spacecraft is launched from LEO on a Hohmann ellipse. The craft is made to enter a circular Mars parking orbit (MPO) approximately 200 km above the Martian surface. The orbiting craft is decelerated by aerobreaking (through the thin atmosphere of CO_2). Soft landing is achieved through retrorockets. The craft spends several months on Mars, until the time is right for a minimum energy transfer and travel to Earth. The Mars ascent vehicle (MAV) is propelled to the MPO, from which the vehicle is sent on a Hohmann ellipse towards Earth. Upon approaching Earth, the craft is captured in a highly elliptic orbit around Earth, instead of the more energy-consuming circular LEO. The design, configuration, and operation of the MAV is critical, and the entire mission FoM is extremely sensitive to changes in the MAV design. The energy requirement calculations (Δv's) are straightforward and, after verification with two reliable sources (Irving and Blum 1959, Bursard and deLauer 1965), we used the numbers given in Table 4.3.

Table 4.2. The modifier factors.[a]

	Cases				
	1	2a	2b	3	4
Risk/Inverse Risk and Reliability & Repairability	0.9	0.7	0.7	0.6	0.2

[a] These numbers represent the total effects of all the factors. They have not been reviewed individually as yet.

Table 4.3. The Δv's for the Mars Sample Return mission.

Physical Constants
Radial distance from body to Sun, Earth-Sun ref: Earth = 1.00000E+00 Mars = 1.52400E+00
Radial distance from body to Sun [m]: Earth = 1.49600E+11 Mars = 2.27990E+11
GZERO [m/s] = 9.81000E+00
Propulsive Velocity Requirements [m/s]
LEO to Hohmann towards Mars (Stage I) = 1.90000E+03
LEO to Hohmann towards Mars (Stage II) = 1.90000E+03
Hohmann to Mars parking orbit (MPO), 200 km (Stage I includes 0.5 km/s midcourse correction) = 1.85000E+03
Hohmann to Mars parking orbit, 200 km (Stage I) = 1.35000E+03
MPO to Mars soft landing = 1.00000E+03
Mars ascent vehicle to MPO (Stage I) = 1.75000E+03
Mars ascent vehicle to MPO (Stage II) = 1.75000E+03
MPO to Hohmann towards Earth (Stage I) = 1.35000E+03
MPO to Hohmann towards Earth (Stage II) = 1.35000E+03
Hohmann to highly eccentric Earth orbit (includes 0.5 km/s midcourse correction) = 1.50000E+03

Four different scenarios, to accomplish an identical MSR, are considered in detail. The first is the base line (case 1) and involves state-of-the-art, Earth-transported resources; LOX/H_2 propulsion; and the associated cryogenic storage both en route and on Mars. Variation 1 (case 2) considers Earth-transported resources, but employs storable propellants in order to clearly reveal the influence of refrigeration as distinct from the influences of in-situ resource utilization (ISRU); here, a fairly routine oxidizer (N_2O_4) and a slightly unconventional oxidizer in space missions (H_2O_2) are considered as cases 2a and 2b. Variation 2 (case 3) considers Earth-transported fuel (hydrocarbon) and the production of the oxidizer from the Martian atmosphere; the ISRU equipment to produce oxygen on Mars is Earth-transported. Variation 3 (case 4) considers only ISRU propellants; oxygen is manufactured on Mars through Earth-transported equipment. In variations 2 and 3, the Earth-transported ISRU equipment is left behind on Mars and is not part of the MAV. In variation 3, the fuel is a hydrocarbon derived from the spent case of the Mars lander vehicle (Kevlar or Nylon). The specific impulse of the MAV is highest in the base line case and lowest in variation 3. The specific cases considered

in this paper are shown in Table 4.4. It is a simple matter to consider various other combinations of fuel/oxidizer, chamber pressures, nozzle expansion ratios, rocket chamber and propellant container cases, and all related equipment.

Table 4.4. Comparative study.

Base Line (case 1)	All Earth-transported resources, LOX/H_2 propulsion, cryogenic storage
Variation 1 (case 2a;b)	All Earth-transported resources, storable propellants (CH_4/N_2O_4; CH_4/H_2O_2)
Variation 2 (case 3)	Earth-transported fuel (HC), in-situ resource utilization (ISRU) of LOX from atmosphere (CH_4/LOX)
Variation 3 (case 4)	All ISRU propellants (fuel is the spent case; Nylon/LOX)

A Brief Description of Components

The overall system to accomplish the mission depends upon the performance of the individual components. It is important to understand the nature of the components that comprise the integrated system. Such an understanding also enables us to change the components, almost in a *modular* fashion, to see the influences of variations and the sensitivity to changes, and to incorporate advances in technology. It is the specific intention of this FoM approach to retain the flexibility to incorporate any change in any component in a clearly understandable manner. Thus, this approach is distinctly different from complex programs and software "packages" that frequently fail to reveal the component influences individually. The fundamental essence of this FoM approach is shown in Figure 4.1. The components are fairly straightforward and have been discussed in the literature. For the purposes of this paper, we give only a brief description of the components that make up the FoM system.

The Mission. As was stated earlier, the mission we chose as a case study is the Mars Sample Return. The high-thrust propulsion technique is employed. The incremental velocities needed are broken up into different stages, as shown in Table 4.3. Some midcourse corrections, Δv's needed to account for the noncircular nature of orbits of the Earth and Mars (around the Sun) and the non-coplanar nature of the two orbits, are all taken as incidentals and amount to a total of approximately 1 to 2 km/s. The return journey is on a Hohmann ellipse, but the Earth capture is in an energy-efficient, highly elliptical orbit rather than a circular orbit. The main variations are not so much in the value of the Δv's necessary, but in the way one could choose to split

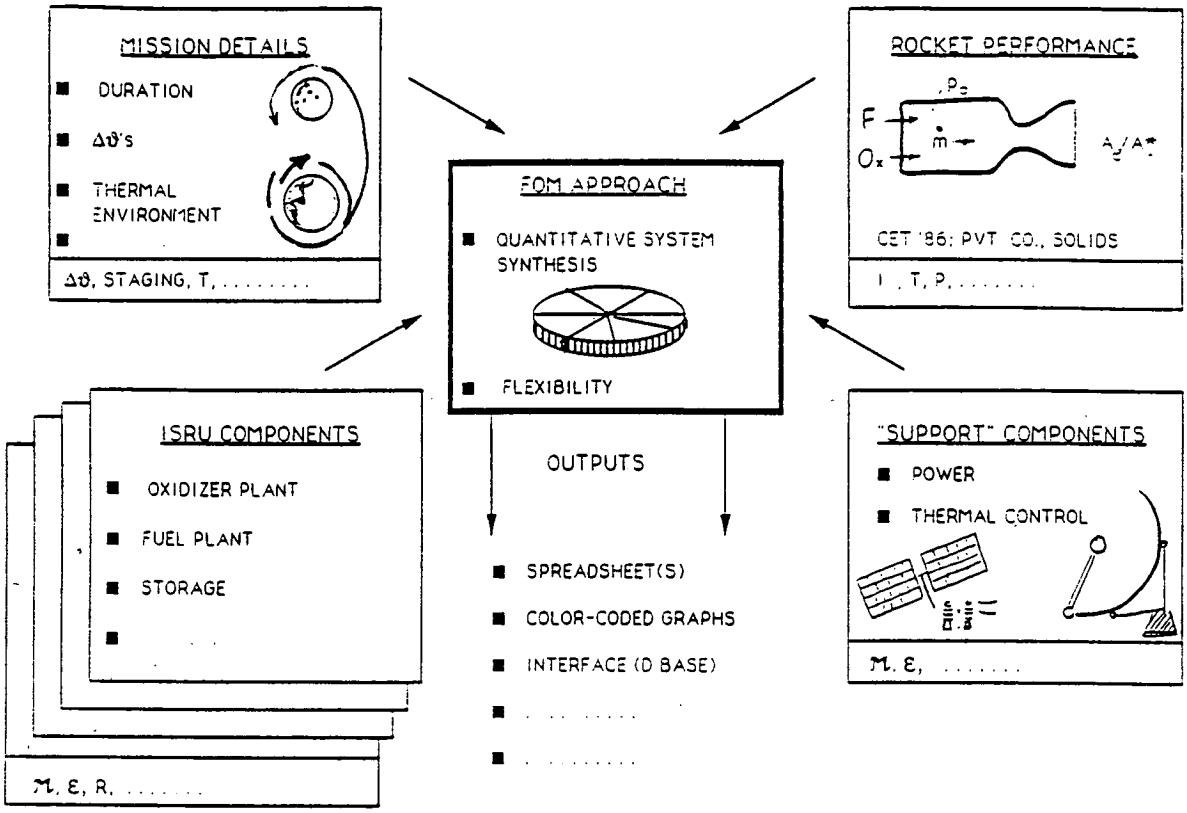

Figure 4.1 The essence of the figure-of-merit concept.

the stages. Our choice is by no means the best, but is consistently used, so the comparisons are meaningful.

Rocket Performance. The performance of the rocket(s) at various stages of the mission are needed in order to calculate the mass ratios. The main program used here is CET86, which is an improvement over the highly popular CEC72 program, from NASA Lewis Research Center. The PC version of this program was obtained from the University of Minnesota, and the results were verified with the mainframe version of the program at the University of Arizona. Another version of this program was obtained from a private company. This version has the specific capability of handling large fractions of charged species, or plasmas. Yet another program has been independently developed by a private company in California for the specific purpose of handling large fractions of solid particles in the products. This program is also installed on a PC (with a 386 board) at the University of Arizona. Thus, two versions of the NASA Lewis program, a variation with plasma capability enchancement, and an independent thermochemical program were used. After satisfactory verifications, the CET86 output was used as the input in this FoM study. More than 30,000 data sets were generated and covered various fuels, oxidizers, fuel/oxidizer ratios, chamber pressures, and

expansion ratios in the nozzle. Both equilibrium and frozen cases were run, and usually the mean was taken as the reliable number. The output includes the usual matrix of specific impulse, temperatures, and species concentrations, along with a myriad of parameters. Unconventional propellants and combinations were specifically studied, as were the more conventional ones. LOX/H_2 formed the standard basis for comparisons. Its performance is illustrated in Figure 4.2. Some of the unconventional combinations involved highly fuel-rich and highly oxidizer-rich cases; some unconventional fuels included Nylon and Kevlar burned with oxygen; some unconventional oxidizers included hydrogen peroxide. These unconventional propellant studies are intrinsically important, and are important to space missions, but the details are beyond the scope of this paper. They are the subject of a Master's thesis (Rascon 1989), the extensive calculations of which will be published shortly.

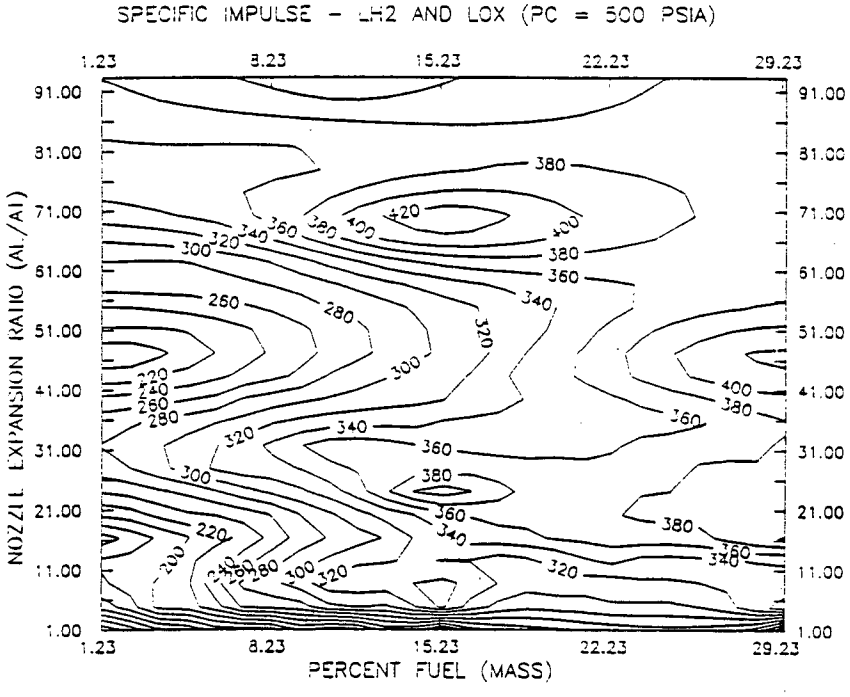

Figure 4.2 Typical performance contour for LH_2/LOX.

The "Support" Components. These include the power, thermal control, radiation shield, pumping, storage, and monitoring equipment. Again, these are very important to the FoM calculations, but do not form the mainstream of our discussions here. We have used the state-of-the-art numbers for nuclear, radioisotopic, solar photovoltaic, solar dynamic, and solar thermal power sources. The sources of these are shown in Table

4.5. These "support" components are likely to undergo rapid advances in the next few years and will ultimately translate into lower masses and costs.

Table 4.5. The "support" energy data.

RTG	333 kg/kW_e
Nuclear	340 kg/kW_e
Solar PV	300 kg/kW_e
Solar Dynamic	100 kg/kW_e

The In-Situ Resource Utilization Components. The in-situ resource utilization (ISRU) components represent the very core of the present study to the extent that the ISRU influences upon space missions are brought out by this FoM approach. The NASA Center at the University of Arizona is devoted to the development of ISRU. Various schemes are being considered for the manufacture of propellants and other useful materials from extraterrestrial resources. Associated with these are innovative concepts for energy utilization, separation of species in microgravity, reactor designs, and storage. The details, as of early 1989, are available in the University of Arizona, NASA Space Enginering Research Center "Annual Progress Report 1988-89." The idea of ISRU is relatively new, and the available studies have taken a somewhat traditional(!) approach. This statement is not as paradoxical as it may seem at first glance. The advantages of ISRU have been well recognized indeed; the approaches toward ISRU have involved ideas of transporting terrestrially used processing plants to extraterrestrial sites in order to manufacture useful substances "out there." Some innovation, a little high technology, some reductions in mass, and smaller safety margins have been the recipe of such proposed ISRU missions. At the NASA SERC of the University of Arizona, a fundamentally different approach is being taken. Here, the aim is to design the ISRU systems as one would design them from local resources, using the **information bank** from terrestrial and previous space missions. The details used in this paper are shown in Table 4.6. The numbers and technologies will certainly change and will be incorporated in future calculations.

Table 4.6. The ISRU plant data for LOX production on Mars.

70 kg (Zr cells)
10 kg/day
425 kg support mass

The Development of the Interdependent Matrix

The purpose of this section is to develop the fundamentals of the interdependent matrix that can evaluate the influences of various components upon the overall system. Mathematically, the problem can be formulated as an optimization problem with constraints. The use of Lagrange multipliers may seem natural. When one considers that there are at least twenty constraints at a time and that the nature of the mass equation is highly nonlinear (exponential), the use of analytical methods may not be straightforward. There are many modern techniques that could be used for such a problem. At the present time, we have used a popular spreadsheet (Lotus 1-2-3) to represent the interdependent matrix. The actual technique of quantitatively interrelating the variables and calculating the optimum is not critically important for the purposes of this paper, although the evolution of the optimum **technique** could be as important as the evolution of the optimum itself in terms of the economy of arriving at the solution. The use of this spreadsheet has the advantages of simplicity, popularity and ease of use at various locations, ready color graphing capability, and the ease of interfacing with other software. There is certainly room for improvement, and that is the subject of the graduate thesis of the junior author.

The Evolution of the Spreadsheet

The spreadsheet was used to build the relationship between the initial mass and final mass in a single-stage rocket. The usual approach is to select a propellant and make an estimate of the structural mass. In this study, the structural mass was separated into different system masses, starting with the most general case. The different options included the aeroshell, nozzle, guidance and control, fuel tankage, oxidizer tankage, and a structural mass (pumps, valves, lines, etc.). The refrigeration needs of the propellant were then addressed. An interesting problem arose in the evaluation of the refrigeration needs. The propellant and the refrigeration masses are dependent upon each other. In transit, the dominant effect was assumed to be the solar radiation introducing a heat flux. The spreadsheet was used to solve the equations without attempting to linearize the highly nonlinear expression. The result is the solution of a cubic. Each stage then served as input for the previous stage. The masses for each category were then summed and the FoM was calculated for each case.

Sample Results

These are shown in Table 4.7 and Figures 4.3 and 4.4. The liquid oxygen needs refrigeration on Mars. The heat transfer is taken to be a combination of natural

Table 4.7. Summary of masses from low Earth orbit (kg) and figures of merit.

Masses	Case 1	Case 2a	Case 2b	Case 3	Case 4
Aeroshell	2.48E+04	5.86E+01	6.16E+01	2.56E+01	1.01E+03
Fuel	4.74E+05	4.72E+03	9.44E+03	1.52E+03	1.62E+04
Fuel leaked	2.12E+04	--	--	--	--
Fuel tanks	6.63E+04	7.73E+01	1.57E+02	2.39E+01	2.76E+02
Guidance and control	6.63E+05	4.04E+03	4.37E+03	1.06E+03	1.17E+04
Nozzle	6.63E+05	4.04E+03	4.37E+03	1.06E+03	1.17E+04
Nylon factory	--	--	--	--	1.42E+02
Oxidizer	3.79E+06	2.30E+04	2.01E+04	6.04E+03	6.50E+04
LOX refinery	--	--	--	1.84E+01	3.59E+01
Oxidizer leaked	1.69E+05	--	--	2.30E+02	2.49E+03
Oxidizer tanks	2.65E+05	2.42E+03	2.62E+03	4.26E+02	4.66E+03
Refrigeration (fuel)	4.20E+05	--	--	--	--
Rover	1.50E+02	1.50E+02	1.50E+02	1.50E+02	1.50E+02
Refrigeration (oxidizer)	4.42E+04	--	--	--	--
Structural	2.65E+05	2.02E+03	2.62E+03	4.26E+02	4.66E+03
Sample	1.00E+00	1.00E+00	1.00E+00	1.00E+00	1.00E+00
Sample support	1.00E+00	1.00E+00	1.00E+00	1.00E+00	1.00E+00
Total	6.86E+06	4.05E+04	4.39E+04	1.10E+04	1.18E+05
Modification factor (R_{el}, R_{ep}, inverse risk, ...)	9.00E-01	7.00E-01	8.00E-01	5.90E-01	1.94E-03
Figure-of-merit (FoM)	2.62E-03	3.46E-01	3.65E-01	1.07E+00	3.28E-02

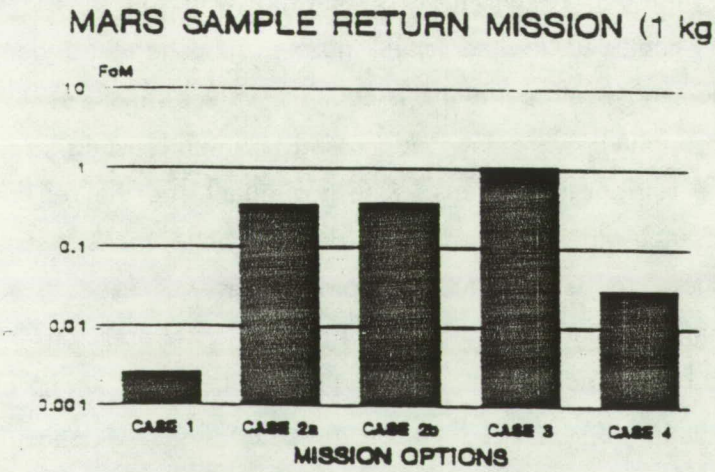

Figure 4.3 Figure-of-merit results.

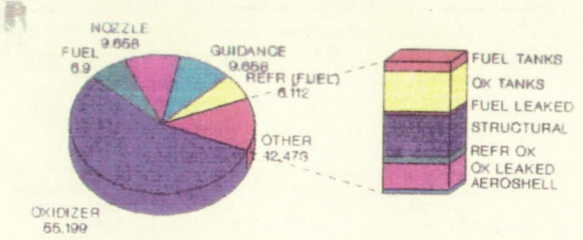

Case 1. All-earth-carried LOX/H_2
(Mass at LEO = 6860 tonnes)

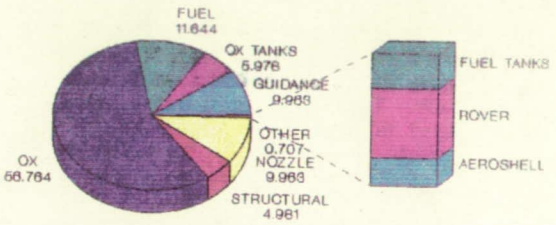

Case 2a. All-earth-carried CH_4/N_2O_4
(Mass at LEO = 40.5 tonnes)

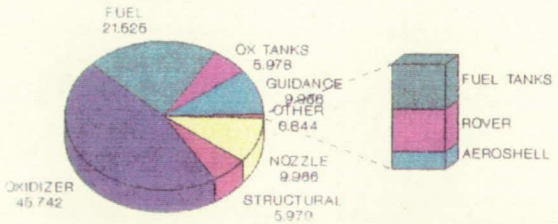

Case 2b. All-earth-carried CH_4/H_2O_2
(Mass at LEO = 43.9 tonnes)

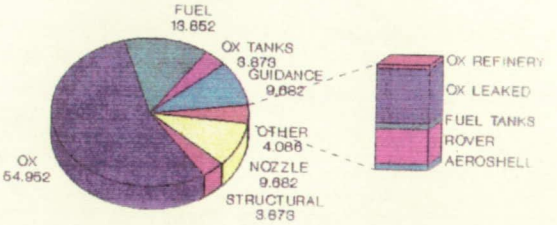

Case 3. Earth-carried CH_4/LOX (ISRU)
(Mass at LEO = 11.0 tonnes)

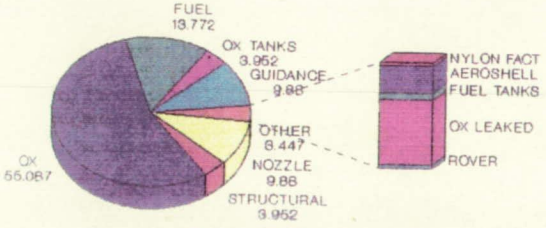

Case 4. ISRU Nylon/LOX
(Mass at LEO = 118 tonnes)

Figure 4.4 Mission mass summaries.

convection and solar radiation. The LH_2 needs refrigeration always. During space travel, it is assumed that the infinite heat sink (space) can be used to keep the LOX cool and that no active refrigeration is used. Further innovations may alter some of these numbers. The rest of the results are straightforward solutions to the governing equations.

Preliminary Findings

As was expected (Ramohalli et al. 1987a, 1987b), the LOX/H_2 case is not the best for this mission. In order of merit, the options should be:

1. ISRU LOX/Earth-transported CH_4 [BEST]
2. All-Earth-transported H_2O_2/CH_4
3. All-Earth-transported N_2O_4/CH_4
4. Spent case as fuel/ISRU LOX
5. All-Earth-transported LOX/H_2 [WORST]

Discussion

The preliminary results of these studies indicate two important facts. One is that it *is* feasible to attempt a figure-of-merit approach to space missions that utilize extra-terrestrial resources. The other is that the ISRU plant (hardware, equipment, controls, . . .) per se is not very taxing in terms of mass penalties, but the **refrigeration needs** of the liquid oxidizer (LOX) produced extraterrestrially can impose a very heavy penalty on the entire mission. Nevertheless, the decisive advantages of the ISRU mission are brought out, once again, in relation to all-Earth-transported resources. However, the demands of refrigeration prompts one to seriously consider the prospects for **non-cryogenically** storing the valuable oxidizer produced extraterrestrially. The production itself is quite simple, if not easy, through the use of modern high-tech zirconia oxygen cells. The necessary duration of 9-12 months on Mars, dictated by the orbital mechanics of minimum energy transfers of interplanetary travel, provides us with the important opportunity of carrying a small oxidizer plant that has a small output per hour, but produces a large quantity over the 9-12 months. The main issue is to find a means of economically storing the oxidizer for that length of time.

In this regard, one scheme that may seem very radical is to think of storing the oxidizer as a **solid**. Many powerful oxidizers are solids, and many of these possess a fairly low (negative) enthalpy of formation, Δh_f^0. A ready example is ammonium perchlorate that has been extensively used as an oxidizer in rocket propellant over a wide temperature range. While we are not suggesting making AP on Mars, the concept of a solid oxidizer, such as ammonium nitrate, may be worth some consideration. Nitrogen is found in the Martian atmosphere, and there are indications that the polar regions of Mars may have as much as 10-14% nitrogen in the atmosphere because of some differential diffusional effects [Source: Prof. John Lewis, University of Arizona]. The point to note is that some innovation in storing and end-use of the extraterrestrially produced oxidizer may make ISRU schemes orders-of-magnitude better than they are now through the elimination of refrigeration. On other planets and moons, where very low-temperature (< melting point of oxygen) regions are present, the concept of oxygen bricks has been suggested by James Burke. Some work on these schemes is proceeding at the UA NASA Space Engineering Research Center at the University of Arizona.

Future Work

Further study will include variations in the overall mission and additional testing of the propellant options. The MSR mission needs testing for an orbiting craft left in MPO, where the sample could be transferred from the MAV and propelled on towards LEO.

Other options would be to investigate how ISRU could be used to enhance missions to Phobos and Deimos. Other possibilities include long-term refueling stations. Propellant selection will prove vital to future analyses. Refrigeration requirements have proved to be a dominant factor in the analysis. In this light, the use of solids must also be evaluated. The mission requirements and propellant selection will determine the role of ISRU.

Summary

The approach to extraterrestrial resource utilization through the concept of an overall mission **figure-of-merit** leads to more realistic designs than through individual component performance maximizations. Simple examples show that the much studied LOX/H_2 propulsion system may be capable of specific impulses in the 460 to 462 sec range, but the necessary refrigeration systems, leak-proofing, extended storage, cryogenic handling, pumping, and safety hazards all translate into excessive mass. This mass increase can easily exceed the mass ratio advantage gained through the superb specific impulse. Generalizing these thoughts, several variations were considered. It was shown that some of the less spectacular components can add up to a better system, overall. Conservative assumptions were made where specific numbers were not available. The actual numbers, although critically important for the final mission, are not critical for the purpose of this paper, ***which is advancing a new concept of extraterrestrial resource utilization rather than precise delineation of mission design numbers.*** A popular spreadsheet was used to demonstrate quantitatively the interrelationships among the various parameters. The approach is flexible. A specific MSR mission was considered to illustrate the approach at this time. It is easy to consider more involved Mars missions, such as those described by Nock and Friedlander (1987), as the mission component, instead of the very simple mission mechanics we have considered here to develop the FoM concept. Some of the unconventional propellant combinations were compared with the all-Earth-transported LOX/H_2 system. In summary, this new approach using a figure-of-merit may be more revealing, helpful, and meaningful than the conventional approaches of individual optimizations. An FoM approach may well become the key to economical utilizations of extraterrestrial resources to the benefit of all mankind.

Acknowledgments

The authors are grateful to Steve Hartman for support and the Advisory Committee of the Center for constructive criticisms on an earlier version of this study.

References

Ash, R. L., et al., 1978, "Feasibility of Rocket Propellant Production on Mars," *Acta Astronautica*, Vol. 5, pp. 705-734.

Ash, R. L., et al., 1982, "Autonomous Oxygen Production for a Mars Return Vehicle," IAF (Paris) Paper 82-210.

Ash, R. L. and Cuda, V., Jr., 1984, "Technology Status Report for In Situ Propellant Production," Report to Jet Propulsion Lab., Pasadena, California.

Bursard, R. W. and deLauer, R. D., 1965, *Fundamentals of Nuclear Flight*, 2nd Ed., McGraw Hill, New York, pp. 40-44.

Carroll, W. F. (Ed.), 1983, "Research on the Use of Space Resources, JPL Publication 83-86.

French, J. R., et al., 1985, "Mars Sample Return Options," *Aerospace America*, Vol. 23, pp. 50-53.

Frisbee, R. H. and Jones, R. M., 1983, "An Analysis of Propulsion Options for Transport of Lunar Materials to Earth Orbit," AIAA Paper 83-1344.

Irving, J. H. and Blum, E. K., 1959, "Comparative Performance of Ballistic and Low-Thrust Vehicles for Flight to Mars," pages 191-218 in *Vistas in Astronautics*, Vol. II (Alperin and Gregory, eds.), Pergamon Press, New York.

Nock, K. T. and Friedlander, A. L., 1987, "Elements of a Mars Transportation System," *Acta Astronautica*, Vol. 15, pp. 505-522.

(Presidential) National Commission on Space, *Pioneering the Space Frontier*, Bantam Books, New York, 1986.

Ramohalli, K. N., et al., 1987a, "Novel Extraterrestrial Processing for Space Propulsion, *Acta Astronautica*, Vol. 15, pp. 259-273.

Ramohalli, K. N., et al., 1987b, "Some Aspects of Space Propulsion With Extraterrestrial Processing," *AIAA J. Spacecraft & Rockets*, Vol. 24, pp. 236-244.

Ramohalli, K. N., et al., 1989, "Recent Concepts in Missions to Mars--Extraterrestrial Processing," *AIAA J. Propulsion & Power*, Vol. 5, pp. 181-187.

Rascon, M., 1989, "Performance Calculations for Unconventional Propellants and Combinations," M.S. Thesis, University of Arizona, Tucson.

Energy Management Analysis of Lunar Oxygen Production

R. Fazzolari and B. Wong-Swanson
Department of Nuclear and Energy Engineering
The University of Arizona

Abstract

Energy load models in the process of hydrogen reduction of ilmenite for lunar oxygen production are being developed. The load models will be used as a first step to ultimately determine the optimal energy system needed to supply the power requirements for the process.

Introduction

The goal of this project this year is to determine the energy requirements in the process of hydrogen reduction of ilmenite to produce oxygen. The general approach is shown schematically in Figure 4.5. Our objectives are to determine the energy loads of the processes in the system. Subsequent energy management studies will be made to minimize the system losses (irreversibilities) and to design optimal energy system power requirements.

A number of processes are being proposed as possible candidates for lunar application as outlined in the recent study by Eagle Engineering (1988). Some detailed experimental efforts are being conducted within this project at The University of Arizona. Our priorities are directed toward developing the energy models for each of the proposed processes being considered. Our immediate goals are to identify the variables that would impact energy requirements and energy sources of supply.

Objective

The objective of this study is to develop a preliminary comprehensive energy load model of the lunar oxygen production plant processes. The model, when refined, will be used to help identify energy management opportunities and optimal energy supply source(s).

Research Status

Figure 4.6 is a block diagram of the five component processes in a lunar oxygen production plant that is based on the hydrogen reduction of ilmenite. The subprocesses are: mining, mineral processing, ilmenite reduction, water decomposition, and oxygen liquefaction. Those identified with an asterisk are items for which preliminary models have been developed. Beneath each process block in the diagram are listed the probable energy users associated with each process. The following is a

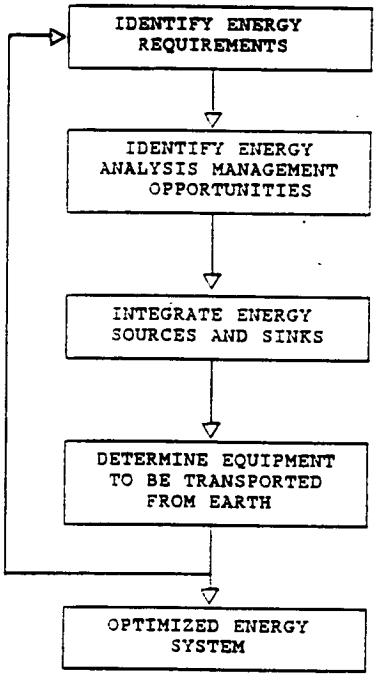

Figure 4.5 Study flow diagram.

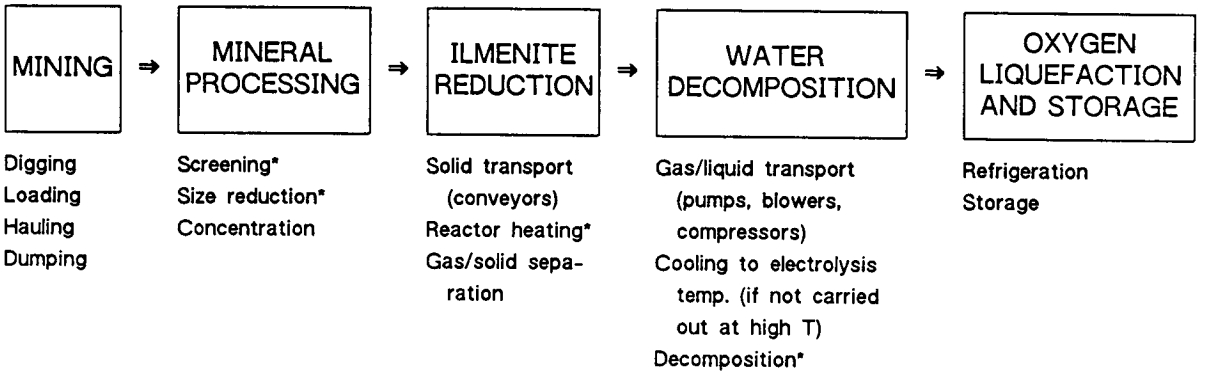

*Preliminary energy models developed.

Figure 4.6 Energy consumers in lunar oxygen production.

summary of these models and their associated variables that impact energy supply and demand.

- *Energy Isuses Related to Mining.* Lunar mining devices will probably be electrically powered to operate in a vacuum. Thus, power requirements of terrestrial mining devices, which are mostly powered by internal combustion engines, could not be used to extrapolate power requirements on the Moon.

  The choice of an energy source will depend on the power demands of the mining devices, which depend on the grade of the haul path, the shear strength of the regolith being cut, the size (boulders vs. gravels vs. fines) of the regolith being excavated, and the depth.

  Use of modified terrestrial mining technology vs. specialized lunar mining technology, e.g., lunar rovers that mine and process the ores on location and haul only concentrated ilmenite to the oxygen production plant, needs to be studied. This would affect energy loads and distribution.

- *Energy Issues Related to Mineral Processing.* The particle size of the mined regolith will affect the type of mineral processing equipment (for sorting and size reduction) needed to reduce the ilmenite to specified size. For example, the energy demand of revolving screens is represented by

$$E = DL \text{ (kw)}$$

  where D is the trommel diameter in meters and L is the trommel length in meters. The energy demand of plane screens is given by

$$E = kF \text{ (kw)}$$

  where k (in KW/M^2) equals 1.5 for a screen-surface area F of 1 to 2 M^2 and k equals 1.2 for F of 2 to 7 M^2.

  Energy consumption in size-reduction machines is related to the hardness of the particles, the initial size, and the reduction achieved. A general model for the work required for size reduction is

$$dE = - c \frac{dx}{x\eta}$$

  where x is the particle size, $\eta = 1$ for crushing and fine impact pulverizing (coarse particles), $\eta = 2$ for fine grinding and ball milling (fine particles), $\eta = 1.5$ for rough milling of in-between-sized particles, and c is a constant that depends on material strength and brittleness.

- *Energy Requirement for Hydrogen Reduction of Ilmenite.*

$$FeTiO_3(s) + H_2(g) = Fe(s) + TiO_2(s) + H_2O(g)$$

q_{in}	=	$\Sigma(h_o - h_i)$	-	Δh_r	+	q_{loss}
Energy supplied to reactor to sustain the reaction at required T.P.		Sensible heat change of the flow streams due to difference in inlet and outlet Ts		Internal energy (heat of reaction)		Energy loss from reactor

$$\Sigma(h_o - h_i) = h_{Fe}(T_0) + h_{TiO_2}(T_0) + h_{H_2O}(T_0) - h_{FeTiO_3}(T_{i1}) - h_{H_2}(T_{i2}) ,$$

where

T_{i1} = temperature of ilmenite entering the reactor

T_{i2} = temperature of hydrogen entering the reactor

T_0 = temperature of the streams leaving the reactor

$$\Delta_{h_r} = \Delta h_f(TiO_2) + \Delta h_f(H_2O) - \Delta h_f(FeTiO_3)$$

where h_f are the enthalpy of formation for the substances at temperature T.

$q_{loss} = \epsilon A \sigma T^4$ (radiation loss from the reactor to the environment)

where

ϵ = reactor emissivity

A = exterior surface area of reactor

σ = Stefan-Boltzmann constant

T = exterior surface temperature of reactor

- *Energy Requirement for Water Decomposition.*

$$H_2O \Rightarrow H_2 + \frac{1}{2} O_2$$

For the reversible process at constant temperature and pressure, the useful work required is

$$W = \Delta G = \Delta H - T\Delta S .$$

The heat (thermal energy) required is $q = T\Delta S$. ΔG, ΔH, and ΔS are changes in the Gibbs free energy, the enthalpy, and the entropy for the reaction. ΔG is the minimum amount of electrical energy for the process to take place endothermally, with an additional amount of heat $T\Delta S$ being added. When the energy supplied to the process is greater than ΔH, the process takes place exothermally and excess

heat is given off. Therefore, ΔH is the amount of energy required by the process. This energy can be supplied electrically or thermally. Assuming an efficiency η for the energy source, the total energy required is $E = \Delta H/\eta$.

- *Energy Issues Related to Water Decomposition.* It has been suggested that high-temperature thermal decomposition should be used to decompose water to minimize heating of the recycled hydrogen to the reactor. An energy load model for both electrolysis and thermal decomposition will be developed to evaluate the merits of each.

Problems Encountered

A major uncertainty in lunar oxygen production modeling efforts is the applicability of terrestrial mining techniques to the lunar surface. Power and energy estimates based on terrestrial mining devices must be used at this time, but they may not be appropriate for lunar applications. The lunar mining mechanisms need to be refined in order to develop an appropriate energy load model. The ongoing efforts in lunar mining studies at The University of Arizona and the Colorado School of Mines should be able to provide more insight into the problem.

Future Work

The goal of the upcoming year is to complete the energy load models for the last three process blocks shown in Figure 4.6: ilmenite reduction, water reduction, and oxygen liquefaction. A secondary goal is to develop energy load models for mining and mineral processing.

References

Casper, M. S. (Ed.), 1978, "Hydrogen Manufacture by Electrolysis, Thermal Decomposition and Unusual Techniques," Noyes Data Corporation,

Eagle Engineering, Inc., "Conceptual Design of a Lunar Oxygen Pilot Plant, Lunar Base Systems Study (LBSS), Task 4.2," EEI Report 88-182, NASA Contract No. NAS9-17878, Houston, Texas, 1988.

Engineering, Construction, and Operations in Space, Proceedings of Space 88, American Society of Civil Engineers, 1988.

Justi, E. W., 1987, *A Solar-Hydrogen Energy System*, Plenum Press.

Lynch, A. J., 1977, *Mineral Crushing and Grinding Circuits*, Elksevier Scientific Publishing Company.

Magerowski, A. J., 1984, "Energy Utilization in a Comminution Circuit," paper presented at the International Conference on Mineral Processing and Extractive Metallurgy.

Perry, J. H., *Chemical Engineer's Handbook*,

Trajan, G., 1981, *Mineral Processing*, Vol. 1, *Fundamentals, Comminution, Sizing and Classification*, Akademiai Kiado, Budapest.

Turkdogan, E. T., 1980, *Physical Chemistry of High Temperature Technology*, Academic Press,

V. DATA BASE DEVELOPMENT

538674 S3-90 147710

N91-25246

P. 2

AX852975

Data Base on Physical Observations of Near-Earth Asteroids and Establishment of a Network to Coordinate Observations of Newly Discovered Near-Earth Asteroids

D. R. Davis, C. R. Chapman, and H. Campins
Planetary Sciences Institute
The University of Arizona

This programs consists of two tasks: (1) development of a data base of physical observations of near-Earth asteroids and establishment of a network to coordinate observations of newly discovered Earth-approaching asteroids and (2) a simulation of the surfaces of low-activity comets. Significant progress was made on Task 1, and Task 2 was completed during the period covered by this progress report.

Task 1: Astromical Data Bank on Local Space Resources

(D. R. Davis and C. R. Chapman)

In the past six months, work continued on the development of the data base of near-Earth asteroids. Specific items accomplished in this period were:

- Completion of the initial data base as an ASCII file containing data from: (i) Russian ephemeris on orbit elements, (ii) McFadden review paper for the forthcoming *Asteroids II* book on physical observations of near-Earth asteriods, and (iii) IRAS data files. A printout of the ASCII file is given in Appendix G.
- Installation and familiarization with dBase IV at PSI. The ASCII data base described above was tranferred into a dBase IV file for evaluation of the dBase software for scientific use. A major defect in dBase is the inability to produce plots in any convenient fashion. Generally, one has to create an ASCII file containing the data to be plotted, exit dBase, and go to a separate plotting program in order to generate graphical output.
- We started work to extend the data base to include reference to the scientific literature for all entries. This subtask will be completed by the end of the current contract period (February 1, 1990).
- All entries in the data base were verified against original sources.

The second part of the Astronomical Data Bank task is to establish and operate a coordination/communication network to inform astronomical observers worldwide of newly discovered asteroids and to encourage them to make physical observations of such bodies. In the past six months, we sent a participation request form to 87 individual astronomers and 24 observatories (Appendix H). The individuals and observatories were selected based on their having done asteroid work previously. To date, we have received 20 positive responses from individuals (23%) and 8 responses

from observatories (30%), with 1 refusal of participation from an observatory. Only 3 individual responses and 1 observatory response came from outside the United States. Further effort will be made to expand the global availability of participating observers.

Following the relocation of PSI to our new quarters at 2421 East 6th Street in early October, we prepared a master schedule of observers that we can consult immediately upon receiving word of newly discovered asteroids. We have re-established the electronic IAU circular service and will notify teams searching for near-Earth asteroids (Shoemakers, Helin, Spacewatch, etc.) in the next few weeks requesting that they alert us as soon as new objects are found. The network is anticipated to be operational by the end of the year. A telephone-answering machine will be installed so that messages can be left regarding discoveries and observations outside of normal business hours.

Task 2: Modeling of the Surface Properties of Cometary Nuclei

H. Campins

This task was aimed at characterizing the surface and subsurface properties of cometary nuclei, particularly to characterize regoliths and reveal indications of surface ice and water of hydration. Such studies are vital in order to plan how to utilize asteroidal resources. An analysis of the surface characteristics of the nuclei of periodic Comets Arend-Rigaux and Tempel 2 has been completed. We have used extensive visible and infrared observations of the nuclei of these two Earth-approaching comets to constrain a nonspherical thermal model developed by Dr. R. H. Brown (1985, *Icarus*, Vol. 64, p. 53). Our results indicate that the albedo and emissivity (at 10 μm) of the nuclear surface of both comets is constant within the uncertainties. We interpret such constancy as due to a uniform mantle of dust that covers the surface of each nucleus. It appears that the source of volatiles is buried sufficiently deep that it does not significantly affect the surface temperature. We estimated how deep inside the nucleus the ice must be to be consistent with our results.

Meanwhile, we are preparing to publish our results. A paper by A'Hearn et al. describing our preliminary analysis of nuclear properties of Comet Tempel 2 has been accepted for publication in the *Astrophysical Journal* (Appendix I).

APPENDICES

omit to Appendix C p. 64

APPENDIX A

AME 464/564 COURSE DESCRIPTION

AN INTRODUCTION TO SPACE TECHNOLOGIES (AME 464/564)

Instructor: Dr. Kumar Ramohalli (office in Aero Bldg room 200A)

Teaching Assistant: Paul Schallhorn

a senior/graduate credit course: Spring, 1990; M.W.F. 11:00 a.m. Social Sciences 206

OFFICE HOURS: M.W.F. 9:00 a.m.

AIM The principal aim of this course is to familiarize interested students with the mutli-faceted disciplines that constitute space missions. Missions to/in Low Earth Orbit (LEO), Geosynchronos Orbit (GEO), the Moon, Mars, Phobos, Deimos, Asteroids, or the outer planets, all have many common features. These include the initial launch, the space environment, best use of trajectories, best use of available resources, and the maximum "returns" for our investment in the mission; these returns could include scientific data, weather/climate patterns, earth resource maps, colonization, platforms for further missions, to name only a few possibilities. It is also the specific aim to introduce students to the synthesis/design of space missions from these component technologies, results from a study of the individual disciplines will have to be combined in an efficient manner in order to tailer-fit the missions. This synthesis has frequently evolved into an art; however, the students will be introduced to some modern tools that are attempting to introduce scientific methodology to evolve the "best" design. The course will also indicate important terrestrial applications of the modern space technologies.

Throughout the course the emphasis is on synthesis of technologies for engineering space missions (rather than the details of component disciplines; i.e., orbital mechanics or advanced propulsion will be covered to the extent that they provide useful information on space technologies, but will not be covered in-depth, since such in-depth treatments are available in separate courses).

CONTENTS

1. The Space Environment: the "atmosphere" out there, the chemical composition of the available species, plasma belts, solar and other radiation, microgravity, meteorites, space debris, levels of "vacuum",....

2. A Little Orbital Mechanics: Newton's law of gravitation, the two-body problem, simple Δv calculations, orbit, escape, capture, mid-course corrections, some practical considerations,...

3. Elements of Rocketry and Space Flight: the high-thrust and low-thrust options, typical state-of-the-art and projected specific impulses, thrust-to-weight ratios, available vehicles, ELV's, STS, Buran, Hermes, and the NASP,....

4. Introduction to Planetary Sciences: composition of inner planets, surface features, atmospheres, simple theories of evolution, characterization of resources,....

5. Control, Command and Communications: the typical time lag, introduction to system analyses, telescience possibilities, stability of control systems,....

6. Materials and Structures: space-age materials, metals, plastics, ceramics, composites, strength-to-weight ratios, thermal behavior, long-term space exposure, effects of space environment on performance of materials, innovative space structures,....

7. Robotics and Man-Machine Systems: introduction to theory of robotics, degrees of freedom, available hardware, projections,....

8. The Thermal Design Issue: introduction to heat transfer, conduction, radiation, microgravity-convection, simulations under 1g conditions, thermal cycling in orbit, the thermal lag and equilibration,....

9. System Synthesis: design of a complete mission (possibilities include earth-watch satellites, ozone-monitoring satellites, return-to-the-Moon, Mars Sample Return, Asteroidal Missions,....)

EVALUATION AND FEEDBACK

Homework assignments: 1 each on the first 8 chapters..... 80 points
1 on the 9th chapter, synthesis.....20 points

Tests: (50 minutes each)

#1 on February 16.....100 points
#2 on the third week on March (TBA).....100 points
#3 on April 13.....100 points

Final Examination.....200 points

Grades will be determined by the distribution of cummulative points.

REQUIRED READING IN THE FIRST TWO WEEKS

1. Paine, Dr. Thomas O., "The Next 40 Years in Space", Plenary Paper given at the 40th Congress of the International Astronautical Federation, Malaga, Spain, October, 1989 (copy on file at the UA NASA Space Engineering Research Center). Also, Dr. Paine, who was the NASA Administrator during its heyday, will visit the AME Department and give a seminar on this topic on February 22. You are strongly urged to attend.

2. Ride, Dr. Sally K., "Leadership and America's Future in Space", NASA, August, 1987 (copy on file at the UA NASA SERC).

In addition, "Report of the 90-Day Study on Human Exploration of the Moon and Mars", November, 1989, will be a useful reference throughout the course.

OPEN FORUM/QUESTIONS AND ANSWERS

On Monday, January 29, the class will be conducted in an open forum format with questions and answers.

A NOTE ON THE LOGISTICS OF THE COURSE

January 10: Distribution of course structure material; student survey; video
January 12: The STS and project Moon-base (two videos)
January 15: NO CLASSES.

January 17 and 19: Chapter 8: Thermal Design Issues in Space; introduction to heat transfer, conduction, radiation, convection, microgravity influences in convection, simple problems (guest professor, Dr. K.R. Sridhar).

APPENDIX B

THEORETICAL ROCKET PERFORMANCE DATA

THEORETICAL ROCKET PERFORMANCE ASSUMING EQUILIBRIUM COMPOSITION DURING EXPANSION

PC = 1000.0 PSIA

	CHEMICAL FORMULA	WT FRACTION (SEE NOTE)	ENERGY CAL/MOL	STATE	TEMP DEG K
FUEL	H 2.00000	1.000000	-2154.000	L	298.15
OXIDANT	H 2.00000 O 2.00000	1.000000	-44880.000	L	298.15

O/F= 17.0000 PERCENT FUEL= 5.5556 EQUIVALENCE RATIO= 0.9963 PHI= 0.9926

	CHAMBER	THROAT	EXIT	EXIT	EXIT	EXIT	EXIT	EXIT	EXIT	EXIT	EXIT
PC/P	1.0000	1.7345	2.0000	5.0000	10.000	20.000	50.000	100.00	200.00	500.00	1000.00
P, ATM	68.046	39.230	34.023	13.609	6.8046	3.4023	1.3609	0.68046	0.34023	0.13609	0.06805
T, DEG K	2989.7	2817.3	2773.5	2496.5	2290.0	2084.5	1816.2	1620.5	1436.2	1213.8	1061.7
RHO, G/CC	4.8514-3	2.9901-3	2.6388-3	1.1841-3	6.4894-4	3.5774-4	1.6462-4	9.2306-5	5.2083-5	2.4651-5	1.4092-5
H, CAL/G	-1305.50	-1486.47	-1531.33	-1801.72	-1986.13	-2153.92	-2351.06	-2482.24	-2598.86	-2732.38	-2819.15
U, CAL/G	-1645.17	-1804.20	-1843.56	-2080.04	-2240.07	-2384.24	-2551.26	-2660.77	-2757.05	-2866.07	-2936.10
G, CAL/G	-11508.2	-11101.0	-10996.4	-10321.5	-9801.08	-9267.48	-8549.08	-8012.41	-7500.05	-6874.62	-6442.31
S, CAL/(G)(K)	3.4127	3.4127	3.4127	3.4127	3.4127	3.4127	3.4127	3.4127	3.4127	3.4127	3.4127
M, MOL WT	17.490	17.621	17.652	17.825	17.920	17.985	18.028	18.038	18.041	18.041	18.041
(DLV/DLP)T	1.01126	-1.00856	-1.00792	-1.00440	1.00248	-1.00120	-1.00031	-1.00007	-1.00001	-1.00000	-1.00000
(DLV/DLT)P	1.2398	1.1935	1.1818	1.1121	1.0687	1.0363	1.0109	1.0028	1.0005	1.0000	1.0000
CP, CAL/(G)(K)	1.3249	1.2290	1.2033	1.0348	0.9133	0.8073	0.7018	0.6508	0.6179	0.5831	0.5576
GAMMA (S)	1.1371	1.1392	1.1399	1.1479	1.1577	1.1707	1.1907	1.2050	1.2172	1.2329	1.2462
SON VEL,M/SEC	1271.2	1230.6	1220.3	1156.2	1109.1	1062.1	998.7	948.7	897.6	830.5	780.9
MACH NUMBER	0.000	1.000	1.126	1.762	2.152	2.509	2.962	3.308	3.665	4.161	4.558

PERFORMANCE PARAMETERS

AE/AT	1.0000	1.0144	1.5250	2.3759	3.8603	7.5566	12.703	21.475	43.198	73.371
CSTAR, FT/SEC	6147	6147	6147	6147	6147	6147	6147	6147	6147	6147
CF	0.657	0.734	1.088	1.274	1.422	1.579	1.675	1.756	1.844	1.899
IVAC,LB-SEC/LB	235.6	237.1	266.1	288.8	308.6	330.5	344.3	356.0	368.9	376.9
ISP, LB-SEC/LB	125.5	140.2	207.8	243.4	271.7	301.6	320.0	335.5	352.4	362.9

MOLE FRACTIONS

H	0.00368	0.00244	0.00217	0.00087	0.00035	0.00010	0.00001	0.00000	0.00000	0.00000
HO2	0.00008	0.00004	0.00004	0.00001	0.00000	0.00000	0.00000	0.00000	0.00000	0.00000
H2	0.03976	0.03136	0.02929	0.01718	0.00993	0.00475	0.00112	0.00023	0.00003	0.00000	0.00000
H2O	0.91179	0.93165	0.93644	0.96336	0.97856	0.98893	0.99590	0.99763	0.99805	0.99814	0.99814
H2O2	0.00001	0.00001	0.00001	0.00000	0.00000	0.00000	0.00000	0.00000	0.00000	0.00000	0.00000
O	0.00159	0.00102	0.00090	0.00034	0.00013	0.00004	0.00001	0.00000	0.00000	0.00000	0.00000
OH	0.02847	0.02122	0.01951	0.01035	0.00559	0.00259	0.00073	0.00023	0.00006	0.00001	0.00000
O2	0.01462	0.01225	0.01164	0.00788	0.00543	0.00358	0.00223	0.00191	0.00186	0.00186	0.00186

THEORETICAL ROCKET PERFORMANCE ASSUMING EQUILIBRIUM COMPOSITION DURING EXPANSION

PC = 1000.0 PSIA

	CHEMICAL FORMULA	WT FRACTION (SEE NOTE)	ENERGY CAL/MOL	STATE	TEMP DEG K
FUEL	H 2.00000	1.000000	-2154.000	L	298.15
OXIDANT	H 2.00000 O 2.00000	1.000000	-44880.000	L	298.15

O/F= 25.5000 PERCENT FUEL= 3.7736 EQUIVALENCE RATIO= 0.8309 PHI= 0.6617

	CHAMBER	THROAT	EXIT	EXIT	EXIT	EXIT	EXIT	EXIT	EXIT	EXIT	EXIT
PC/P	1.0000	1.7498	2.0000	5.0000	10.000	20.000	50.000	100.00	200.00	500.00	1000.00
P, ATM	68.046	38.889	34.023	13.609	6.8046	3.4023	1.3609	0.68046	0.34023	0.13609	0.06805
T, DEG K	2706.3	2514.4	2469.1	2163.8	1941.9	1731.3	1474.4	1297.6	1135.8	943.8	814.7
RHO, G/CC	5.8613-3	3.6181-3	3.2257-3	1.4771-3	8.2387-4	4.6227-4	2.1717-4	1.2338-4	7.0481-5	3.3928-5	1.9651-5
H, CAL/G	-1309.97	-1461.39	-1495.86	-1714.96	-1861.54	-1992.55	-2143.53	-2242.33	-2329.04	-2426.91	-2489.56
U, CAL/G	-1591.11	-1721.69	-1751.29	-1938.09	-2061.56	-2170.79	-2295.29	-2375.89	-2445.95	-2524.05	-2573.41
G, CAL/G	9700.17	-9256.79	-9150.65	-8423.41	7881.98	-7360.05	-6714.64	-6265.32	5850.29	-5352.89	-5015.41
S, CAL/(G)(K)	3.1003	3.1003	3.1003	3.1003	3.1003	3.1003	3.1003	3.1003	3.1003	3.1003	3.1003
M, MOL WT	19.129	19.196	19.209	19.271	19.293	19.303	19.306	19.307	19.307	19.307	19.307
(DLV/DLP)T	-1.00335	-1.00201	-1.00175	-1.00059	1.00022	-1.00007	-1.00001	-1.00000	-1.00000	-1.00000	-1.00000
(DLV/DLT)P	1.0830	1.0543	1.0484	1.0193	1.0080	1.0028	1.0005	1.0001	1.0000	1.0000	1.0000
CP, CAL/(G)(K)	0.8801	0.8072	0.7909	0.6961	0.6446	0.6074	0.5708	0.5471	0.5243	0.4950	0.4759
GAMMA (S)	1.1562	1.1635	1.1655	1.1811	1.1935	1.2054	1.2203	1.2318	1.2443	1.2625	1.2760
SON VEL,M/SEC	1166.2	1125.7	1116.1	1050.1	999.4	948.1	880.3	829.7	780.1	716.3	669.1
MACH NUMBER	0.000	1.000	1.118	1.753	2.150	2.521	3.000	3.367	3.743	4.268	4.696

PERFORMANCE PARAMETERS

AE/AT	1.0000	1.0123	1.4978	2.3010	3.6864	7.1009	11.818	19.788	39.265	65.966
CSTAR, FT/SEC	5554	5554	5554	5554	5554	5554	5554	5554	5554	5554
CF	0.665	0.737	1.087	1.269	1.412	1.560	1.650	1.725	1.806	1.856
IVAC,LB SEC/LB	213.4	214.6	239.4	258.8	275.5	293.8	305.2	314.9	325.3	331.8
ISP, LB-SEC/LB	114.8	127.2	187.7	219.1	243.7	269.3	284.8	297.8	311.7	320.4

MOLE FRACTIONS

H	0.00052	0.00024	0.00019	0.00003	0.00001	0.00000	0.00000	0.00000	0.00000	0.00000
HO2	0.00017	0.00010	0.00008	0.00003	0.00001	0.00000	0.00000	0.00000	0.00000	0.00000
H2	0.00541	0.00305	0.00261	0.00073	0.00021	0.00004	0.00000	0.00000	0.00000	0.00000
H2O	0.88237	0.89174	0.89358	0.90239	0.90557	0.90695	0.90751	0.90760	0.90762	0.90762
H2O2	0.00002	0.00001	0.00001	0.00000	0.00000	0.00000	0.00000	0.00000	0.00000	0.00000
O	0.00133	0.00074	0.00063	0.00017	0.00005	0.00001	0.00000	0.00000	0.00000	0.00000
OH	0.02218	0.01486	0.01334	0.00555	0.00236	0.00083	0.00015	0.00003	0.00000	0.00000
O2	0.08801	0.08927	0.08954	0.09109	0.09180	0.09217	0.09234	0.09237	0.09238	0.09238

THEORETICAL ROCKET PERFORMANCE ASSUMING EQUILIBRIUM COMPOSITION DURING EXPANSION

PC = 1000.0 PSIA

	CHEMICAL FORMULA				WT FRACTION (SEE NOTE)	ENERGY CAL/MOL	STATE	TEMP DEG K
FUEL	N	2.00000	H	2.00000	1.000000	12100.000	L	298.15
OXIDANT	N	2.00000	O	4.00000	1.000000	-4680.000	L	298.15

O/F= 1.0066 PERCENT FUEL= 49.8355 EQUIVALENCE RATIO= 0.7610 PHI= 0.7610

	CHAMBER	THROAT	EXIT	EXIT	EXIT	EXIT	EXIT	EXIT	EXIT	EXIT	EXIT
PC/P	1.0000	1.7624	2.0000	5.0000	10.000	20.000	50.000	100.00	200.00	500.00	1000.00
P, ATM	68.046	38.610	34.023	13.609	6.8046	3.4023	1.3609	0.68046	0.34023	0.13609	0.06805
T, DEG K	2980.7	2749.0	2697.7	2331.5	2064.2	1811.4	1507.7	1303.1	1119.9	908.3	769.9
RHO, G/CC	6.6568-3	4.1167-3	3.7000-3	1.7204-3	9.7310-4	5.5476-4	2.6667-4	1.5427-4	8.9757-5	4.4265-5	2.6113-5
H, CAL/G	175.29	40.843	12.396	-177.25	-302.27	-412.34	-536.77	-616.52	-685.25	-761.21	-808.80
U, CAL/G	-72.257	-186.29	-210.29	-368.83	-471.61	-560.86	-660.36	-723.34	-777.05	-835.67	-871.91
G, CAL/G	-7209.17	-6769.43	-6670.89	-5953.38	-5416.02	-4900.01	-4271.91	-3844.84	-3459.63	-3011.46	-2716.07
S, CAL/(G)(K)	2.4774	2.4774	2.4774	2.4774	2.4774	2.4774	2.4774	2.4774	2.4774	2.4774	2.4774
M, MOL WT	23.928	24.051	24.073	24.185	24.222	24.237	24.242	24.243	24.243	24.243	24.243
(DLV/DLP)T	-1.00521	-1.00304	-1.00266	-1.00083	-1.00027	-1.00007	-1.00001	-1.00000	-1.00000	-1.00000	-1.00000
(DLV/DLT)P	1.1131	1.0726	1.0649	1.0240	1.0091	1.0028	1.0004	1.0001	1.0000	1.0000	1.0000
CP, CAL/(G)(K)	0.6678	0.6002	0.5860	0.4988	0.4538	0.4238	0.3977	0.3822	0.3679	0.3499	0.3376
GAMMA (S)	1.1749	1.1839	1.1863	1.2076	1.2252	1.2414	1.2599	1.2731	1.2867	1.3059	1.3207
SON VEL,M/SEC	1103.1	1060.7	1051.4	983.9	931.7	878.3	807.2	754.3	703.0	637.8	590.5
MACH NUMBER	0.000	1.000	1.111	1.746	2.146	2.525	3.024	3.413	3.817	4.389	4.860

PERFORMANCE PARAMETERS

AE/AT	1.0000	1.0108	1.4778	2.2447	3.5495	6.7081	10.996	18.129	35.238	58.272
CSTAR, FT/SEC	5180	5180	5180	5180	5180	5180	5180	5180	5180	5180
CF	0.672	0.739	1.088	1.266	1.404	1.546	1.630	1.700	1.773	1.817
IVAC,LB-SEC/LB	199.5	200.4	222.7	240.0	254.7	270.5	280.2	288.2	296.8	302.0
ISP, LB-SEC/LB	108.2	119.1	175.1	203.8	226.1	248.9	262.5	273.6	285.5	292.6

MOLE FRACTIONS

H	0.00166	0.00076	0.00062	0.00010	0.00002	0.00000	0.00000	0.00000	0.00000	0.00000
HNO	0.00001	0.00000	0.00000	0.00000	0.00000	0.00000	0.00000	0.00000	0.00000	0.00000
HNO2	0.00001	0.00000	0.00000	0.00000	0.00000	0.00000	0.00000	0.00000	0.00000	0.00000
HO2	0.00012	0.00007	0.00006	0.00002	0.00001	0.00000	0.00000	0.00000	0.00000	0.00000
H2	0.00858	0.00480	0.00414	0.00110	0.00029	0.00005	0.00000	0.00000	0.00000	0.00000
H2O	0.37542	0.38559	0.38747	0.39705	0.40040	0.40176	0.40225	0.40231	0.40232	0.40232
H2O2	0.00001	0.00001	0.00001	0.00000	0.00000	0.00000	0.00000	0.00000	0.00000	0.00000
NO	0.01850	0.01404	0.01311	0.00723	0.00401	0.00193	0.00057	0.00018	0.00005	0.00000
NO2	0.00004	0.00003	0.00003	0.00002	0.00001	0.00000	0.00000	0.00000	0.00000	0.00000
N2	0.51826	0.52322	0.52419	0.52960	0.53203	0.53340	0.53419	0.53440	0.53447	0.53449
N2O	0.00001	0.00000	0.00000	0.00000	0.00000	0.00000	0.00000	0.00000	0.00000	0.00000
O	0.00286	0.00163	0.00141	0.00039	0.00010	0.00002	0.00000	0.00000	0.00000	0.00000
OH	0.02438	0.01666	0.01511	0.00630	0.00257	0.00082	0.00012	0.00002	0.00000	0.00000
O2	0.05014	0.05317	0.05384	0.05819	0.06056	0.06200	0.06286	0.06308	0.06316	0.06318

THEORETICAL ROCKET PERFORMANCE ASSUMING FROZEN COMPOSITION DURING EXPANSION

PC = 1000.0 PSIA

	CHEMICAL FORMULA				WT FRACTION (SEE NOTE)	ENERGY CAL/MOL	STATE	TEMP DEG K
FUEL	H	2.00000	H	2.00000	1.000000	12100.000	L	298.15
OXIDANT	N	2.00000	O	4.00000	1.000000	-4680.000	L	298.15

O/F= 1.0066 PERCENT FUEL= 49.8355 EQUIVALENCE RATIO= 0.7610 PHI= 0.7610

	CHAMBER	THROAT	EXIT	EXIT	EXIT	EXIT	EXIT	EXIT	EXIT	EXIT	EXIT
PC/P	1.0000	1.7938	2.0000	5.0000	10.000	20.000	50.000	100.00	200.00	500.00	1000.00
P, ATM	68.046	37.933	34.023	13.609	6.8046	3.4023	1.3609	0.68046	0.34023	0.13609	0.06805
T, DEG K	2980.7	2667.9	2613.0	2167.6	1906.0	1654.8	1363.9	1171.7	1001.0	805.6	678.9
RHO, G/CC	6.6568-3	4.1460-3	3.7969-3	1.8141-3	1.0410-3	5.9955-4	2.9097-4	1.6935-4	9.9114-5	4.9263-5	2.9226-5
H, CAL/G	175.29	38.349	14.495	-167.75	-285.42	-387.77	-502.35	-575.22	-637.65	-706.18	-748.82
U, CAL/G	-72.257	-183.22	-202.51	-349.43	-443.71	-525.20	-615.61	-672.52	-720.78	-773.08	-805.21
G, CAL/G	7209.17	-6571.11	-6458.85	-5587.25	5007.29	-4487.25	-3881.20	-3477.86	3117.47	-2701.88	-2430.77
S, CAL/(G)(K)	2.4774	2.4774	2.4774	2.4774	2.4774	2.4774	2.4774	2.4774	2.4774	2.4774	2.4774
M, MOL WT	23.928	23.928	23.928	23.928	23.928	23.928	23.928	23.928	23.928	23.928	23.928
CP, CAL/(G)(K)	0.4405	0.4348	0.4336	0.4226	0.4127	0.4017	0.3855	0.3724	0.3589	0.3422	0.3312
GAMMA (S)	1.2323	1.2361	1.2369	1.2446	1.2519	1.2607	1.2746	1.2870	1.3010	1.3204	1.3346
SON VEL,M/SEC	1129.8	1070.5	1059.7	972.7	910.6	851.4	777.2	723.9	672.7	608.0	561.1
MACH NUMBER	0.000	1.000	1.095	1.742	2.156	2.550	3.004	3.402	3.877	4.467	4.956

PERFORMANCE PARAMETERS

AE/AT	1.0000	1.0077	1.4440	2.1713	3.4104	6.4056	10.458	17.169	33.173	54.610
CSTAR, FT/SEC	5097	5097	5097	5097	5097	5097	5097	5097	5097	5097
CF	0.689	0.747	1.091	1.264	1.397	1.533	1.613	1.679	1.748	1.790
IVAC, LB-SEC/LB	197.5	198.1	218.5	234.6	248.4	263.1	272.1	279.6	287.5	292.2
ISP, LB-SEC/LB	109.2	118.3	172.8	200.2	221.3	242.8	255.5	266.0	276.9	283.6

MOLE FRACTIONS

H	0.00166	HNO	0.00001	HNO2	0.00001	HO2	0.00012
H2	0.00858	H2O	0.37542	H2O2	0.00001	NO	0.01850
NO2	0.00004	N2	0.51826	N2O	0.00001	O	0.00286
OH	0.02438	O2	0.06014				

THEORETICAL ROCKET PERFORMANCE ASSUMING EQUILIBRIUM COMPOSITION DURING EXPANSION

PC = 1000.0 PSIA

	CHEMICAL FORMULA				WT FRACTION (SEE NOTE)	ENERGY CAL/MOL	STATE	TEMP DEG K
FUEL	N	2.00000	H	2.00000	1.000000	12100.000	L	298.15
OXIDANT	N	2.00000	O	4.00000	1.000000	-4680.000	L	298.15

O/F= 1.4380 PERCENT FUEL= 41.0172 EQUIVALENCE RATIO= 0.5327 PHI= 0.5327

	CHAMBER	THROAT	EXIT	EXIT	EXIT	EXIT	EXIT	EXIT	EXIT	EXIT	EXIT
PC/P	1.0000	1.7747	2.0000	5.0000	10.000	20.000	50.000	100.00	200.00	500.00	1000.00
P, ATM	68.046	38.343	34.023	13.609	6.8046	3.4023	1.3609	0.68046	0.34023	0.13609	0.06805
T, DEG K	2701.9	2464.2	2415.6	2054.5	1799.7	1565.0	1288.8	1105.3	942.5	756.6	636.6
RHO, G/CC	7.6847-3	4.7600-3	4.3105-3	2.0310-3	1.1598-3	6.6697-4	3.2399-4	1.8889-4	1.1076-4	5.5185-5	3.2795-5
H, CAL/G	135.27	17.865	-5.2186	-166.96	-272.36	-364.31	-467.28	-532.67	-588.59	-649.84	-687.88
U, CAL/G	-79.161	-177.21	-196.37	-329.24	-414.44	-487.85	-569.00	-619.91	-662.98	-709.57	-738.13
G, CAL/G	-6202.68	-5762.63	-5671.55	-4986.35	-4494.01	-4035.49	-3490.39	-3125.36	-2799.40	-2424.74	-2181.22
S, CAL/(G)(K)	2.3458	2.3458	2.3458	2.3458	2.3458	2.3458	2.3458	2.3458	2.3458	2.3458	2.3458
M, MOL WT	25.039	25.103	25.112	25.159	25.171	25.175	25.176	25.176	25.176	25.176	25.176
(DLV/DLP)T	-1.00192	-1.00098	-1.00084	-1.00021	-1.00006	-1.00001	-1.00000	-1.00000	-1.00000	-1.00000	-1.00000
(DLV/DLT)P	1.0474	1.0271	1.0237	1.0072	1.0023	1.0006	1.0001	1.0000	1.0000	1.0000	1.0000
CP, CAL/(G)(K)	0.5347	0.4905	0.4822	0.4296	0.4025	0.3829	0.3629	0.3497	0.3372	0.3219	0.3119
GAMMA (S)	1.1917	1.2037	1.2065	1.2289	1.2453	1.2601	1.2780	1.2915	1.3057	1.3248	1.3388
SON VEL,M/SEC	1034.0	991.2	982.3	913.5	860.4	807.0	737.5	686.6	637.5	575.4	530.5
MACH NUMBER	0.000	1.000	1.104	1.741	2.147	2.534	3.045	3.443	3.861	4.455	4.947

PERFORMANCE PARAMETERS

AE/AT	1.0000	1.0095	1.4608	2.2026	3.4597	6.4852	10.565	17.308	33.356	54.817
CSTAR, FT/SEC	4794	4794	4794	4794	4794	4794	4794	4794	4794	4794
CF	0.678	0.742	1.088	1.264	1.399	1.537	1.618	1.684	1.754	1.796
IVAC,LB-SEC/LB	185.0	185.8	205.7	221.2	234.3	248.3	256.8	263.9	271.3	275.8
ISP, LB-SEC/LB	101.1	110.6	162.2	188.3	208.5	229.0	241.1	251.0	261.4	267.6

MOLE FRACTIONS

H	0.00028	0.00009	0.00007	0.00001	0.00000	0.00000	0.00000	0.00000	0.00000	0.00000
HNO2	0.00001	0.00001	0.00000	0.00000	0.00000	0.00000	0.00000	0.00000	0.00000	0.00000
HO2	0.00014	0.00007	0.00006	0.00002	0.00001	0.00000	0.00000	0.00000	0.00000	0.00000
H2	0.00161	0.00072	0.00060	0.00010	0.00002	0.00000	0.00000	0.00000	0.00000	0.00000
H2O	0.33266	0.33767	0.33847	0.34234	0.34343	0.34378	0.34388	0.34389	0.34389	0.34389
H2O2	0.00001	0.00000	0.00000	0.00000	0.00000	0.00000	0.00000	0.00000	0.00000	0.00000
NO	0.02032	0.01405	0.01290	0.00593	0.00280	0.00112	0.00025	0.00006	0.00001	0.00000
NO2	0.00010	0.00007	0.00006	0.00003	0.00002	0.00001	0.00000	0.00000	0.00000	0.00000
N2	0.49229	0.49673	0.49751	0.50195	0.50377	0.50469	0.50515	0.50525	0.50527	0.50528
N2O	0.00001	0.00000	0.00000	0.00000	0.00000	0.00000	0.00000	0.00000	0.00000	0.00000
O	0.00162	0.00073	0.00060	0.00010	0.00002	0.00000	0.00000	0.00000	0.00000	0.00000
OH	0.01501	0.00878	0.00774	0.00238	0.00074	0.00017	0.00001	0.00000	0.00000	0.00000
O2	0.13594	0.14106	0.14197	0.14713	0.14920	0.15022	0.15071	0.15081	0.15083	0.15084

THEORETICAL ROCKET PERFORMANCE ASSUMING FROZEN COMPOSITION DURING EXPANSION

PC = 1000.0 PSIA

	CHEMICAL FORMULA				WT FRACTION (SEE NOTE)	ENERGY CAL/MOL	STATE	TEMP DEG K
FUEL	N	2.00000	H	2.00000	1.000000	12100.000	L	298.15
OXIDANT	N	2.00000	O	4.00000	1.000000	-4680.000	L	298.15

O/F= 1.4380 PERCENT FUEL= 41.0172 EQUIVALENCE RATIO= 0.5327 PHI= 0.5327

	CHAMBER	THROAT	EXIT	EXIT	EXIT	EXIT	EXIT	EXIT	EXIT	EXIT	EXIT
PC/P	1.0000	1.7984	2.0000	5.0000	10.000	20.000	50.000	100.00	200.00	500.00	1000.00
P, ATM	68.046	37.837	34.023	13.609	6.8046	3.4023	1.3609	0.68046	0.34023	0.13609	0.06805
T, DEG K	2701.9	2410.6	2360.9	1967.1	1707.0	1475.4	1208.4	1032.8	877.8	701.8	588.7
RHO, G/CC	7.6847-3	4.7894-3	4.3973-3	2.1110-3	1.2164-3	7.0364-4	3.4365-4	2.0103-4	1.1827-4	5.9173-5	3.5267-5
H, CAL/G	135.27	16.319	-3.7992	-160.80	-261.72	-349.13	-446.46	-508.01	-560.48	-617.72	-653.14
U, CAL/G	-79.161	-175.00	-191.17	-316.92	-397.20	-466.23	-542.37	-589.98	-630.14	-673.42	-699.87
G, CAL/G	-6202.68	-5638.43	-5541.93	-4775.19	-4265.83	-3810.12	-3281.04	2930.75	-2619.60	-2263.93	-2034.18
S, CAL/(G)(K)	2.3458	2.3458	2.3458	2.3458	2.3458	2.3458	2.3458	2.3458	2.3458	2.3458	2.3458
M, MOL WT	25.039	25.039	25.039	25.039	25.039	25.039	25.039	25.039	25.039	25.039	25.039
CP, CAL/(G)(K)	0.4114	0.4053	0.4041	0.3927	0.3828	0.3719	0.3565	0.3444	0.3324	0.3179	0.3088
GAMMA (S)	1.2391	1.2435	1.2444	1.2533	1.2616	1.2713	1.2864	1.2995	1.3137	1.3327	1.3459
SON VEL,M/SEC	1054.4	997.7	987.7	904.8	845.6	789.2	718.5	667.6	618.8	557.3	513.0
MACH NUMBER	0.000	1.000	1.092	1.740	2.155	2.551	3.071	3.475	3.899	4.504	5.007

PERFORMANCE PARAMETERS

AE/AT	1.0000	1.0073	1.4381	2.1553	3.3730	6.3022	10.245	16.745	32.170	52.750
CSTAR, FT/SEC	4734	4734	4734	4734	4734	4734	4734	4734	4734	4734
CF	0.691	0.748	1.091	1.263	1.395	1.529	1.608	1.672	1.740	1.780
IVAC,LB-SEC/LB	183.6	184.1	202.8	217.6	230.1	243.5	251.7	258.4	265.4	269.7
ISP, LB-SEC/LB	101.7	110.0	160.5	185.9	205.3	225.0	236.6	246.0	256.0	261.9

MOLE FRACTIONS

H	0.00028	HNO2	0.00001	HO2	0.00014	H2	0.00161
H2O	0.33266	H2O2	0.00001	NO	0.02032	NO2	0.00010
N2	0.49229	N2O	0.00001	O	0.00162	OH	0.01501
O2	0.13594						

THEORETICAL ROCKET PERFORMANCE ASSUMING EQUILIBRIUM COMPOSITION DURING EXPANSION

PC = 1000.0 PSIA

CHEMICAL FORMULA		WT FRACTION (SEE NOTE)	ENERGY CAL/MOL	STATE	TEMP DEG K
FUEL H 2.00000		1.000000	-2154.000	L	20.27
OXIDANT O 2.00000		1.000000	-3102.000	L	90.18

O/F= 8.0000 PERCENT FUEL= 11.1111 EQUIVALENCE RATIO= 0.9921 PHI= 0.9921

	CHAMBER	THROAT	EXIT	EXIT	EXIT	EXIT	EXIT	EXIT	EXIT	EXIT	EXIT
PC/P	1.0000	1.7269	2.0000	5.0000	10.000	20.000	50.000	100.00	200.00	500.00	1000.00
P, ATM	68.046	39.402	34.023	13.609	6.8046	3.4023	1.3609	0.68046	0.34023	0.13609	0.06805
T, DEG K	3599.6	3427.4	3383.0	3121.3	2937.8	2763.5	2541.9	2376.9	2210.3	1981.9	1800.6
RHO, G/CC	3.7096-3	2.2863-3	2.0071-3	8.8867-4	4.7915-4	2.5821-4	1.1412-4	6.1666-5	3.3445-5	1.5041-5	8.3059-6
H, CAL/G	-204.90	-440.16	-500.92	-858.52	-1106.11	-1335.78	-1614.09	-1806.74	-1984.71	-2197.96	-2342.67
U, CAL/G	-649.12	-857.52	-911.43	-1229.38	-1450.03	-1654.88	-1902.88	-2073.97	-2231.07	-2417.08	-2541.07
G, CAL/G	13658.2	-13249.6	-13144.5	-12524.0	-12085.9	-11664.0	-11114.3	-10690.3	-10245.5	-9605.05	-9072.34
S, CAL/(G)(K)	3.7374	3.7374	3.7374	3.7374	3.7374	3.7374	3.7374	3.7374	3.7374	3.7374	3.7374
M, MOL WT	16.103	16.319	16.376	16.725	16.975	17.210	17.491	17.676	17.829	17.973	18.035
(DLV/DLP)T	-1.04338	-1.03855	-1.03726	-1.02944	-1.02383	-1.01859	-1.01239	-1.00841	-1.00516	-1.00214	-1.00081
(DLV/DLT)P	1.7526	1.7029	1.6885	1.5902	1.5080	1.4215	1.3058	1.2221	1.1466	1.0676	1.0283
CP, CAL/(G)(K)	2.3871	2.3302	2.3115	2.1625	2.0151	1.8414	1.5806	1.3702	1.1613	0.9130	0.7667
GAMMA (S)	1.1305	1.1274	1.1266	1.1230	1.1214	1.1212	1.1238	1.1288	1.1377	1.1573	1.1781
SON VEL,M/SEC	1449.5	1403.1	1391.1	1320.0	1270.3	1223.5	1165.3	1123.4	1082.9	1030.0	988.9
MACH NUMBER	0.000	1.000	1.131	1.772	2.162	2.514	2.947	3.259	3.564	3.965	4.277

PERFORMANCE PARAMETERS

AE/AT	1.0000	1.0155	1.5435	2.4380	4.0385	8.1856	14.209	24.854	52.225	91.315
CSTAR, FT/SEC	7051	7051	7051	7051	7051	7051	7051	7051	7051	7051
CF	0.653	0.732	1.088	1.278	1.431	1.598	1.703	1.796	1.900	1.968
IVAC,LB-SEC/LB	270.0	271.8	306.1	333.5	357.9	386.0	404.5	420.8	439.3	451.3
ISP, LB-SEC/LB	143.1	160.5	208.5	280.0	313.7	350.2	373.3	393.5	416.4	431.3

MOLE FRACTIONS

H	0.02964	0.02529	0.02417	0.01758	0.01317	0.00933	0.00523	0.00295	0.00140	0.00035	0.00007
HO2	0.00031	0.00021	0.00019	0.00010	0.00006	0.00003	0.00001	0.00001	0.00000	0.00000	0.00000
H2	0.11186	0.10239	0.09981	0.08340	0.07074	0.05803	0.04150	0.02967	0.01902	0.00799	0.00290
H2O	0.71339	0.74261	0.75041	0.79824	0.83316	0.86652	0.90728	0.93463	0.95788	0.98044	0.99032
H2O2	0.00004	0.00002	0.00002	0.00001	0.00001	0.00000	0.00000	0.00000	0.00000	0.00000	0.00000
O	0.01436	0.01196	0.01135	0.00789	0.00569	0.00387	0.00206	0.00112	0.00051	0.00013	0.00003
OH	0.09462	0.08342	0.08047	0.06273	0.05025	0.03877	0.02542	0.01698	0.01024	0.00419	0.00171
O2	0.03578	0.03408	0.03358	0.03005	0.02692	0.02345	0.01849	0.01463	0.01094	0.00690	0.00497

THEORETICAL ROCKET PERFORMANCE ASSUMING FROZEN COMPOSITION DURING EXPANSION

PC = 1000.0 PSIA

	CHEMICAL FORMULA	WT FRACTION (SEE NOTE)	ENERGY CAL/MOL	STATE	TEMP DEG K
FUEL	H 2.00000	1.000000	2154.000	L	20.27
OXIDANT	O 2.00000	1.000000	-3102.000	L	90.18

O/F= 8.0000 PERCENT FUEL= 11.1111 EQUIVALENCE RATIO= 0.9921 PHI= 0.9921

	CHAMBER	THROAT	EXIT	EXIT	EXIT	EXIT	EXIT	EXIT	EXIT	EXIT	EXIT
PC/P	1.0000	1.7701	2.0000	5.0000	10.000	20.000	50.000	100.00	200.00	500.00	1000.00
P, ATM	68.046	38.441	34.023	13.609	6.8046	3.4023	1.3609	0.68046	0.34023	0.13609	0.06805
T, DEG K	3599.6	3278.3	3212.9	2756.3	2447.7	2167.3	1835.4	1610.8	1407.0	1167.0	1005.9
RHO, G/CC	3.7086-3	2.3010-3	2.0780-3	9.6890-4	5.4554-4	3.0806-4	1.4551-4	8.2896-5	4.7451-5	2.2885-5	1.3275-5
H, CAL/G	-204.90	-447.10	-498.00	-832.95	-1055.31	-1252.50	-1478.41	-1625.65	-1754.58	-1899.81	-1992.62
U, CAL/G	-649.12	-851.67	-892.51	-1173.10	-1357.38	-1519.96	-1704.91	-1824.44	-1928.22	-2043.83	-2116.76
G, CAL/G	13658.2	12699.6	12504.1	-11134.5	10203.3	-9352.44	-8337.97	-7645.97	-7013.31	-6261.25	-5751.98
S, CAL/(G)(K)	3.7374	3.7374	3.7374	3.7374	3.7374	3.7374	3.7374	3.7374	3.7374	3.7374	3.7374
M, MOL WT	16.103	16.103	16.103	16.103	16.103	16.103	16.103	16.103	16.103	16.103	16.103
CP, CAL/(G)(K)	0.7585	0.7489	0.7467	0.7283	0.7120	0.6937	0.6666	0.6442	0.6207	0.5883	0.5635
GAMMA (S)	1.1943	1.1973	1.1980	1.2040	1.2097	1.2164	1.2272	1.2369	1.2482	1.2655	1.2804
SON VEL,M/SEC	1489.9	1423.6	1409.8	1309.0	1236.5	1166.7	1078.4	1014.3	952.3	873.2	815.5
MACH NUMBER	0.000	1.000	1.107	1.751	2.157	2.538	3.027	3.309	3.782	4.313	4.743

PERFORMANCE PARAMETERS

AE/AT	1.0000	1.0100	1.0748	2.2510	3.5915	6.8964	11.461	19.171	38.009	63.800
CSTAR, FT/SEC	6905	6905	6905	6905	6905	6905	6905	6905	6905	6905
CF	0.676	0.742	1.009	1.267	1.407	1.551	1.638	1.711	1.789	1.838
IVAC,LB SEC/LB	266.4	267.5	297.1	320.3	340.5	362.5	376.2	387.8	400.3	408.1
ISP, LB SEC/LB	145.2	159.2	233.8	272.0	301.9	332.9	351.6	367.2	384.0	394.4

MOLE FRACTIONS

H	0.02964	HO2	0.00031	H2	0.11186	H2O	0.71939
H2O2	0.00004	O	0.01436	OH	0.09462	O2	0.03578

THEORETICAL ROCKET PERFORMANCE ASSUMING EQUILIBRIUM COMPOSITION DURING EXPANSION

PC = 1000.0 PSIA

	CHEMICAL FORMULA	WT FRACTION (SEE NOTE)	ENERGY CAL/MOL	STATE	TEMP DEG K
FUEL	H 2.00000	1.000000	-2154.000	L	20.27
OXIDANT	O 2.00000	1.000000	-3102.000	L	90.18

O/F= 12.0000 PERCENT FUEL= 7.6923 EQUIVALENCE RATIO= 0.6614 PHI= 0.6614

	CHAMBER	THROAT	EXIT	EXIT	EXIT	EXIT	EXIT	EXIT	EXIT	EXIT	EXIT
PC/P	1.0000	1.7314	2.0000	5.0000	10.000	20.000	50.000	100.00	200.00	500.00	1000.00
P, ATM	68.046	39.301	34.023	13.609	6.8046	3.4023	1.3609	0.68046	0.34023	0.13609	0.06805
T, DEG K	3415.5	3234.5	3188.3	2904.8	2697.1	2490.7	2213.9	2001.3	1790.4	1525.1	1340.5
RHO, G/CC	4.7740-3	2.9431-3	2.5917-3	1.1559-3	6.2869-4	3.4312-4	1.5551-4	8.6272-5	4.8286-5	2.2687-5	1.2907-5
H, CAL/G	-171.68	-355.11	-401.35	-677.38	-866.96	-1040.98	-1248.04	-1387.66	-1512.96	-1657.53	-1752.04
U, CAL/G	-516.86	-678.50	-719.26	-962.50	-1129.08	-1281.11	-1459.97	-1578.67	-1683.60	-1802.80	-1879.71
G, CAL/G	10877.1	-10493.3	-10394.9	-9782.07	-9320.88	-8847.72	-8187.29	-7660.43	-7124.66	-6437.87	-5953.84
S, CAL/(G)(K)	3.1344	3.1344	3.1344	3.1344	3.1344	3.1344	3.1344	3.1344	3.1344	3.1344	3.1344
M, MOL WT	19.663	19.876	19.930	20.245	20.448	20.611	20.759	20.820	20.850	20.862	20.864
(DLV/DLP)T	-1.02372	-1.01929	-1.01817	-1.01169	-1.00762	-1.00444	-1.00172	-1.00068	-1.00021	-1.00003	-1.00001
(DLV/DLT)P	1.4448	1.3841	1.3677	1.2627	1.1867	1.1197	1.0537	1.0239	1.0087	1.0017	1.0004
CP, CAL/(G)(K)	1.4754	1.3902	1.3655	1.1905	1.0448	0.8995	0.7312	0.6370	0.5741	0.5250	0.5006
GAMMA (S)	1.1354	1.1344	1.1343	1.1361	1.1407	1.1493	1.1677	1.1854	1.2030	1.2225	1.2351
SON VEL,M/SEC	1280.5	1238.9	1228.3	1164.1	1118.5	1074.6	1017.6	973.3	926.7	862.0	812.3
MACH NUMBER	0.000	1.000	1.129	1.767	2.157	2.510	2.949	3.277	3.615	4.091	4.477

PERFORMANCE PARAMETERS

AE/AT	1.0000	1.0148	1.5334	2.4045	3.9401	7.8126	13.250	22.540	45.580	77.687
CSTAR, FT/SEC	6204	6204	6204	6204	6204	6204	6204	6204	6204	6204
CF	0.655	0.733	1.088	1.276	1.426	1.587	1.687	1.772	1.865	1.923
IVAC,LB-SEC/LB	237.7	239.2	268.9	292.3	313.0	336.2	350.8	363.4	377.1	385.8
ISP, LB-SEC/LB	126.3	141.4	209.8	246.0	275.0	306.0	325.3	341.6	359.6	370.8

MOLE FRACTIONS

H	0.01012	0.00763	0.00703	0.00382	0.00208	0.00095	0.00022	0.00005	0.00001	0.00000	0.00000
HO2	0.00077	0.00054	0.00049	0.00026	0.00015	0.00008	0.00003	0.00001	0.00000	0.00000	0.00000
H2	0.02993	0.02440	0.02299	0.01473	0.00947	0.00534	0.00186	0.00062	0.00015	0.00001	0.00000
H2O	0.66420	0.68663	0.69233	0.72611	0.74818	0.76637	0.78331	0.79064	0.79426	0.79587	0.79614
H2O2	0.00006	0.00004	0.00004	0.00002	0.00001	0.00000	0.00000	0.00000	0.00000	0.00000	0.00000
O	0.01991	0.01599	0.01501	0.00940	0.00594	0.00330	0.00112	0.00037	0.00009	0.00001	0.00000
OH	0.10137	0.08660	0.08278	0.05934	0.04303	0.02860	0.01373	0.00644	0.00243	0.00046	0.00009
O2	0.17364	0.17816	0.17932	0.18632	0.19113	0.19536	0.19972	0.20188	0.20306	0.20365	0.20376

THEORETICAL ROCKET PERFORMANCE ASSUMING FROZEN COMPOSITION DURING EXPANSION

PC = 1000.0 PSIA

	CHEMICAL FORMULA	WT FRACTION (SEE NOTE)	ENERGY CAL/MOL	STATE	TEMP DEG K
FUEL	H 2.00000	1.000000	-2154.000	L	20.27
OXIDANT	O 2.00000	1.000000	-3102.000	L	90.18

O/F= 12.0000 PERCENT FUEL= 7.6923 EQUIVALENCE RATIO= 0.6614 PHI= 0.6614

	CHAMBER	THROAT	EXIT	EXIT	EXIT	EXIT	EXIT	EXIT	EXIT	EXIT	EXIT
PC/P	1.0000	1.7722	2.0000	5.0000	10.000	20.000	50.000	100.00	200.00	500.00	1000.00
P, AIM	68.046	38.396	34.023	13.609	6.8046	3.4023	1.3609	0.68046	0.34023	0.13609	0.06805
T, DEG K	3415.5	3105.9	3043.7	2605.0	2308.9	2040.1	1722.7	1508.5	1314.6	1086.9	934.9
RHO, G/CC	4.7740-3	2.9622-3	2.6786-3	1.2518-3	7.0620-4	3.9961-4	1.8930-4	1.0809-4	6.2018-5	3.0002-5	1.7441-5
H, CAL/G	-171.68	-360.13	-397.71	-658.82	-830.76	-982.94	-1156.85	-1269.91	-1368.67	-1479.62	-1550.34
U, CAL/G	-516.86	-674.03	-705.31	-922.09	-1064.11	-1189.13	-1330.96	-1422.36	-1501.53	-1589.47	-1644.82
G, CAL/G	10877.1	10095.3	-9937.79	-8824.08	-8067.73	-7377.56	-6556.52	-5998.06	-5489.04	-4886.51	-4480.59
S, CAL/(G)(K)	3.1344	3.1344	3.1344	3.1344	3.1344	3.1344	3.1344	3.1344	3.1344	3.1344	3.1344
M, MOL WT	19.663	19.663	19.663	19.663	19.663	19.663	19.663	19.663	19.663	19.663	19.663
CP, CAL/(G)(K)	0.6128	0.6045	0.6027	0.5871	0.5736	0.5585	0.5364	0.5185	0.4998	0.4744	0.4557
GAMMA (S)	1.1975	1.2007	1.2015	1.2079	1.2139	1.2210	1.2321	1.2421	1.2535	1.2707	1.2850
SON VEL,M/SEC	1315.1	1255.8	1243.5	1151.5	1088.6	1026.3	947.4	890.1	834.7	764.2	712.7
MACH NUMBER	0.000	1.000	1.106	1.750	2.157	2.539	3.031	3.406	3.792	4.329	4.766

PERFORMANCE PARAMETERS

AE/AT	1.0000	1.0098	1.4718	2.2430	3.5728	6.8441	11.852	18.952	37.478	62.794
CSTAR, FT/SEC	6081	6081	6081	6081	6081	6081	6081	6081	6081	6081
CF	0.678	0.742	1.089	1.267	1.406	1.549	1.636	1.708	1.785	1.833
IVAC,LB SEC/LB	234.7	245.7	261.5	281.9	299.4	318.7	340.6	340.6	351.5	358.2
ISP, LB SEC/LB	128.1	140.2	205.9	239.5	265.7	292.8	309.1	322.7	337.4	346.4

MOLE FRACTIONS

H	0.01012	HO2	0.00077	H2	0.02998	H2O	0.66420
H2O2	0.00006	O	0.01991	OH	0.10137	O2	0.17364

THEORETICAL ROCKET PERFORMANCE ASSUMING EQUILIBRIUM COMPOSITION DURING EXPANSION

PC = 100.0 PSIA

	CHEMICAL FORMULA				WT FRACTION (SEE NOTE)	ENERGY CAL/MOL	STATE	TEMP DEG K
FUEL	C	1.00000	H	4.00000	1.000000	-21390.000	L	111.66
OXIDANT	H	2.00000	O	2.00000	1.000000	-44880.000	L	298.15

O/F= 8.5000 PERCENT FUEL= 10.5263 EQUIVALENCE RATIO= 0.9989 PHI= 0.9978

	CHAMBER	THROAT	EXIT	EXIT	EXIT	EXIT	EXIT	EXIT	EXIT	EXIT	EXIT
PC/P	1.0000	1.7239	2.0000	5.0000	10.000	20.000	50.000	100.00	200.00	500.00	1000.00
P, ATM	6.8046	3.9472	3.4023	1.3609	0.68046	0.34023	0.13609	0.06805	0.03402	0.01361	0.00680
T, DEG K	2763.0	2629.1	2593.1	2374.7	2209.8	2041.7	1811.5	1633.7	1459.1	1243.1	1094.4
RHO, G/CC	6.2205-4	3.8278-4	3.3531-4	1.4844-4	8.0415-5	4.3793-5	1.9845-5	1.1021-5	6.1740-6	2.8993-6	1.6466-6
H, CAL/G	-1320.90	-1460.99	-1497.79	-1711.97	-1859.91	-1996.13	-2158.41	-2267.77	-2365.80	-2478.87	-2552.89
U, CAL/G	-1585.81	-1710.72	-1743.51	-1934.00	-2064.83	-2184.27	-2324.49	-2417.29	-2499.26	-2592.55	-2652.96
G, CAL/G	10034.5	-9752.20	-9675.67	-9200.93	8828.89	-8434.85	-7871.16	-7420.08	-6967.45	-6399.07	-6004.12
S, CAL/(G)(K)	3.1537	3.1537	3.1537	3.1537	3.1537	3.1537	3.1537	3.1537	3.1537	3.1537	3.1537
M, MOL WT	20.726	20.920	20.971	21.254	21.429	21.564	21.675	21.713	21.727	21.730	21.731
(DLV/DLP)T	-1.01617	-1.01304	-1.01222	-1.00766	-1.00485	-1.00269	-1.00093	-1.00031	-1.00007	-1.00000	-1.00000
(DLV/DLT)P	1.3760	1.3192	1.3035	1.2083	1.1416	1.0850	1.0330	1.0121	1.0029	1.0002	1.0000
CP, CAL/(G)(K)	1.4598	1.3577	1.3280	1.1318	0.9767	0.8293	0.6714	0.5917	0.5428	0.5077	0.4877
GAMMA (S)	1.1213	1.1220	1.1224	1.1273	1.1349	1.1470	1.1693	1.1878	1.2039	1.2198	1.2308
SON VEL,M/SEC	1114.8	1082.7	1074.2	1023.3	986.5	950.2	901.4	862.0	819.9	761.7	717.9
MACH NUMBER	0.000	1.000	1.133	1.768	2.153	2.502	2.937	3.265	3.606	4.087	4.473

PERFORMANCE PARAMETERS

AE/AT	1.0000	1.0159	1.5434	2.4267	3.9813	7.8890	13.359	22.701	45.921	78.389
CSTAR, FT/SEC	5458	5458	5458	5458	5458	5458	5458	5458	5458	5458
CF	0.651	0.731	1.087	1.277	1.429	1.591	1.692	1.777	1.871	1.930
IVAC,LB-SEC/LB	208.8	210.2	236.8	257.7	276.2	296.7	309.7	320.8	333.0	340.7
ISP, LB SEC/LB	110.4	124.1	184.5	216.6	242.4	270.0	287.0	301.5	317.4	327.4

MOLE FRACTIONS

CO	0.03184	0.02628	0.02478	0.01595	0.01013	0.00551	0.00172	0.00047	0.00007	0.00000	0.00000
CO2	0.10416	0.11099	0.11282	0.12351	0.13048	0.13598	0.14050	0.14200	0.14249	0.14258	0.14258
H	0.00507	0.00366	0.00331	0.00162	0.00079	0.00031	0.00006	0.00001	0.00000	0.00000	0.00000
HO2	0.00004	0.00002	0.00002	0.00001	0.00000	0.00000	0.00000	0.00000	0.00000	0.00000	0.00000
H2	0.03448	0.02867	0.02713	0.01817	0.01220	0.00725	0.00271	0.00091	0.00018	0.00001	0.00000
H2O	0.76449	0.78216	0.78674	0.81242	0.82839	0.84081	0.85123	0.85501	0.85642	0.85676	0.85678
O	0.00287	0.00197	0.00176	0.00077	0.00034	0.00012	0.00002	0.00000	0.00000	0.00000	0.00000
OH	0.03130	0.02433	0.02257	0.01316	0.00779	0.00398	0.00120	0.00037	0.00009	0.00001	0.00000
O2	0.02575	0.02192	0.02086	0.01440	0.00987	0.00603	0.00256	0.00123	0.00074	0.00064	0.00064

THEORETICAL ROCKET PERFORMANCE ASSUMING EQUILIBRIUM COMPOSITION DURING EXPANSION

PC = 100.0 PSIA

	CHEMICAL FORMULA				WT FRACTION (SEE NOTE)	ENERGY CAL/MOL	STATE	TEMP DEG K
FUEL	C	1.00000	H	4.00000	1.000000	-21390.000	L	111.66
OXIDANT	H	2.00000	O	2.00000	1.000000	-44880.000	L	298.15

O/F = 12.7500 PERCENT FUEL= 7.2727 EQUIVALENCE RATIO= 0.8326 PHI= 0.6652

	CHAMBER	THROAT	EXIT	EXIT	EXIT	EXIT	EXIT	EXIT	EXIT	EXIT	EXIT
PC/P	1.0000	1.7404	2.0000	5.0000	10.000	20.000	50.000	100.00	200.00	500.00	1000.00
P, ATM	6.8046	3.9097	3.4023	1.3609	0.68046	0.34023	0.13609	0.06805	0.03402	0.01361	0.00680
T, DEG K	2559.6	2400.3	2360.0	2090.6	1885.6	1686.2	1440.1	1270.4	1115.0	930.7	806.7
RHO, G/CC	7.0274-4	4.3292-4	3.8360-4	1.7413-4	9.6712-5	5.4116-5	2.5351-5	1.4370-5	8.1864-6	3.9229-6	2.2629-6
H, CAL/G	-1320.44	-1445.99	-1476.13	-1661.21	-1785.83	-1897.59	-2026.74	-2111.47	-2186.02	-2270.46	-2324.74
U, CAL/G	-1554.94	-1664.70	-1690.92	-1850.48	-1956.22	-2049.85	-2156.75	-2226.14	-2286.67	-2354.47	-2397.56
G, CAL/G	8974.42	8623.72	8533.39	7912.94	7424.37	6939.76	6333.28	5910.34	5520.21	5053.57	4737.10
S, CAL/(G)(K)	2.9903	2.9903	2.9903	2.9903	2.9903	2.9903	2.9903	2.9903	2.9903	2.9903	2.9903
M, MOL WT	21.691	21.809	21.834	21.950	21.991	22.007	22.013	22.014	22.014	22.014	22.014
(DLV/DLP)T	1.00587	1.00363	1.00316	-1.00104	1.00035	-1.00010	-1.00001	-1.00000	1.00000	-1.00000	-1.00000
(DLV/DLT)P	1.1517	1.1010	1.0898	1.0343	1.0132	1.0042	1.0007	1.0001	1.0000	1.0000	1.0000
CP, CAL/(G)(K)	0.9440	0.8326	0.8062	0.6599	0.5884	0.5447	0.5095	0.4891	0.4702	0.4460	0.4297
GAMMA (S)	1.1401	1.1481	1.1506	1.1706	1.1867	1.2006	1.2157	1.2264	1.2376	1.2538	1.2660
SON VEL,M/SEC	1057.6	1025.0	1016.9	962.8	919.8	874.5	813.2	767.1	721.9	663.9	621.1
MACH NUMBER	0.000	1.000	1.122	1.294	2.146	2.513	2.990	3.354	3.728	4.247	4.668

PERFORMANCE PARAMETERS

AE/AT	1.0000	1.0135	1.5091	2.3250	3.7312	7.1999	12.002	20.141	40.118	67.642
CSTAR, FT/SEC	5098	5098	5098	5098	5098	5098	5098	5098	5098	5098
CF	0.660	0.735	1.087	1.270	1.414	1.565	1.656	1.732	1.815	1.866
IVAC,LB SEC/LB	195.6	196.7	240.0	238.1	253.7	270.7	281.4	290.4	300.2	306.3
ISP, LB SEC/LB	104.5	116.4	172.2	201.2	224.1	247.9	262.4	274.4	287.5	296.6

MOLE FRACTIONS

CO	0.00564	0.00323	0.00275	0.00072	0.00018	0.00003	0.00000	0.00000	0.00000	0.00000
CO2	0.09272	0.09564	0.09623	0.09878	0.09951	0.09974	0.09979	0.09980	0.09980	0.09980
H	0.00106	0.00054	0.00044	0.00009	0.00002	0.00000	0.00000	0.00000	0.00000	0.00000
HO2	0.00007	0.00004	0.00004	0.00001	0.00001	0.00000	0.00000	0.00000	0.00000	0.00000
H2	0.00739	0.00450	0.00390	0.00119	0.00035	0.00007	0.00001	0.00000	0.00000	0.00000
H2O	0.76750	0.77875	0.78116	0.79271	0.79703	0.79888	0.79960	0.79971	0.79973	0.79973
O	0.00231	0.00137	0.00118	0.00035	0.00010	0.00002	0.00000	0.00000	0.00000	0.00000
OH	0.02503	0.01747	0.01577	0.00689	0.00298	0.00104	0.00018	0.00004	0.00000	0.00000
O2	0.09830	0.09845	0.09852	0.09925	0.09983	0.10022	0.10042	0.10046	0.10047	0.10047

THEORETICAL ROCKET PERFORMANCE ASSUMING EQUILIBRIUM COMPOSITION DURING EXPANSION

PC = 300.0 PSIA

	CHEMICAL FORMULA						WT FRACTION (SEE NOTE)	ENERGY CAL/MOL	STATE	TEMP DEG K
FUEL	C 1.00000	H 3.00000	O 1.00000	H 1.00000			1.000000	-18840.000	L	283.72
OXIDANT	O 2.00000						1.000000	-3102.000	L	90.18

O/F= 1.5000 PERCENT FUEL= 40.0000 EQUIVALENCE RATIO= 0.9990 PHI= 0.9987

	CHAMBER	THROAT	EXIT	EXIT	EXIT	EXIT	EXIT	EXIT	EXIT	EXIT	EXIT
PC/P	1.0000	1.7189	2.0000	5.0000	10.000	20.000	50.000	100.00	200.00	500.00	1000.00
P, ATM	6.8046	3.9587	3.4023	1.3609	0.68046	0.34023	0.13609	0.06805	0.03402	0.01361	0.00680
T, DEG K	3275.9	3142.9	3107.4	2905.5	2765.9	2635.6	2475.0	2360.2	2249.6	2106.8	1998.6
RHO, G/CC	5.6250-4	3.4622-4	3.0220-4	1.3243-4	7.0774-5	3.7759-5	1.6422-5	8.7384-6	4.6481-6	2.0189-6	1.0762-6
H, CAL/G	-293.36	-447.63	-489.25	-727.94	-894.80	-1051.05	-1242.82	-1377.69	-1504.44	-1660.37	-1770.00
U, CAL/G	-586.31	-724.54	-761.90	-976.82	-1127.64	-1269.26	-1443.52	-1566.27	-1681.70	-1823.62	-1923.13
G, CAL/G	10117.1	-9872.67	-9807.63	-9440.89	-9189.16	-8954.75	-8664.77	-8455.54	-8250.56	-7978.17	-7763.36
S, CAL/(G)(K)	2.9988	2.9988	2.9988	2.9988	2.9988	2.9988	2.9988	2.9988	2.9988	2.9988	2.9988
M, MOL WT	22.221	22.555	22.648	23.200	23.606	24.002	24.506	24.871	25.219	25.645	25.937
(DLV/DLP)T	1.05704	-1.05300	-1.05188	-1.04510	1.04004	-1.03504	-1.02859	-1.02386	-1.01932	-1.01369	-1.00984
(DLV/DLT)P	2.0946	2.0628	2.0529	1.9830	1.9194	1.8470	1.7387	1.6483	1.5522	1.4196	1.3187
CP, CAL/(G)(K)	2.4130	2.4097	2.4064	2.3621	2.3007	2.2143	2.0614	1.9167	1.7481	1.4929	1.2813
GAMMA (S)	1.1180	1.1143	1.1133	1.1080	1.1047	1.1019	1.0993	1.0982	1.0980	1.1000	1.1049
SON VEL,M/SEC	1170.6	1136.2	1127.0	1074.1	1037.4	1003.0	960.8	930.9	902.4	866.8	841.0
MACH NUMBER	0.000	1.000	1.136	1.775	2.163	2.510	2.934	3.246	3.528	3.902	4.180

PERFORMANCE PARAMETERS

AE/AT	1.0000	1.0167	1.5577	2.4776	4.1375	8.4984	14.945	26.585	57.612	103.99
CSTAR, FT/SEC	5750	5750	5750	5750	5750	5750	5750	5750	5750	5750
CF	0.648	0.731	1.088	1.280	1.437	1.608	1.719	1.816	1.930	2.006
IVAC,LB-SEC/LB	219.8	221.4	250.1	273.0	293.7	317.8	333.9	348.4	365.5	377.0
ISP, LB-SEC/LB	115.9	130.6	194.5	228.8	256.8	287.4	307.2	324.6	344.9	358.4

MOLE FRACTIONS

CO	0.14758	0.14028	0.13814	0.12438	0.11313	0.10128	0.08494	0.07228	0.05958	0.04314	0.03140
CO2	0.12981	0.14129	0.14458	0.16523	0.18156	0.19835	0.22099	0.23820	0.25525	0.27701	0.29238
H	0.03283	0.02915	0.02816	0.02259	0.01881	0.01537	0.01135	0.00870	0.00638	0.00385	0.00236
HO2	0.00016	0.00011	0.00010	0.00006	0.00004	0.00002	0.00001	0.00001	0.00000	0.00000	0.00000
H2	0.06296	0.05903	0.05793	0.05133	0.04639	0.04148	0.03507	0.03026	0.02551	0.01933	0.01480
H2O	0.42900	0.44763	0.45276	0.48303	0.50501	0.52613	0.55269	0.57168	0.58963	0.61154	0.62649
H2O2	0.00001	0.00000	0.00000	0.00000	0.00000	0.00000	0.00000	0.00000	0.00000	0.00000	0.00000
O	0.02842	0.02461	0.02361	0.01804	0.01440	0.01124	0.00774	0.00558	0.00383	0.00208	0.00116
OH	0.09268	0.08370	0.08125	0.06708	0.05713	0.04790	0.03683	0.02934	0.02263	0.01499	0.01019
O2	0.07654	0.07419	0.07345	0.06826	0.06355	0.05822	0.05038	0.04395	0.03720	0.02806	0.02122

THEORETICAL ROCKET PERFORMANCE ASSUMING EQUILIBRIUM COMPOSITION DURING EXPANSION

PC = 100.0 PSIA

	CHEMICAL FORMULA								WT FRACTION (SEE NOTE)	ENERGY CAL/MOL	STATE	TEMP DEG K
FUEL	C	1.00000	H	3.00000	O	1.00000	H	1.00000	1.000000	-18840.000	L	283.72
OXIDANT	O	2.00000							1.000000	-3102.000	L	90.18

O/F = 2.2500 PERCENT FUEL= 30.7692 EQUIVALENCE RATIO= 0.7265 PHI= 0.6658

	CHAMBER	THROAT	EXIT	EXIT	EXIT	EXIT	EXIT	EXIT	EXIT	EXIT	EXIT
PC/P	1.0000	1.7195	2.0000	5.0000	10.000	20.000	50.000	100.00	200.00	500.00	1000.00
P, ATM	6.8046	3.9572	3.4023	1.3609	0.68046	0.34023	0.13609	0.06805	0.03402	0.01361	0.00680
T, DEG K	3184.8	3051.4	3015.6	2809.6	2663.7	2523.4	2341.3	2200.7	2051.6	1833.0	1654.0
RHO, G/CC	6.4390-4	3.9629-4	3.4607-4	1.5188-4	8.1352-5	4.3558-5	1.9098-5	1.0269-5	5.5540-6	2.5033-6	1.3899-6
H, CAL/G	-248.03	382.88	-419.14	627.43	772.77	-908.48	-1074.12	-1189.54	-1296.58	-1424.94	-1511.66
U, CAL/G	-503.95	-624.70	-657.22	-844.42	-975.33	-1097.64	-1246.69	-1350.01	-1444.93	-1556.60	-1630.22
G, CAL/G	8972.71	8742.13	-8680.36	-8324.22	8069.94	-7821.45	-7488.14	-7218.34	-6916.94	-6446.39	-6042.86
S, CAL/(G)(K)	2.7395	2.7395	2.7395	2.7395	2.7395	2.7395	2.7395	2.7395	2.7395	2.7395	2.7395
M, MOL WT	24.729	25.075	25.170	25.730	26.132	26.510	26.961	27.252	27.481	27.667	27.724
(DLV/DLP)T	1.04377	-1.03931	-1.03806	1.03046	1.02475	-1.01916	-1.01224	1.00765	-1.00399	-1.00111	1.00029
(DLV/DLT)P	1.8762	1.8236	1.8076	1.6973	1.6000	1.4927	1.3416	1.2288	1.1295	1.0414	1.0124
CP, CAL/(G)(K)	1.8916	1.8472	1.8316	1.7064	1.5755	1.4140	1.1600	0.9502	0.7476	0.5432	0.4604
GAMMA (S)	1.1183	1.1153	1.1146	1.1110	1.1097	1.1098	1.1137	1.1214	1.1356	1.1659	1.1895
SON VEL,M/SEC	1094.3	1062.3	1053.7	1004.3	969.8	937.2	896.7	867.7	839.6	801.4	768.1
MACH NUMBER	0.000	1.000	1.136	1.774	2.161	2.508	2.932	3.235	3.528	3.916	4.233

PERFORMANCE PARAMETERS

AE/AT	1.0000	1.0166	1.5556	2.4695	4.1111	8.3837	14.605	25.589	53.587	91.141
CSTAR, FT/SEC	5373	5373	5373	5373	5373	5373	5373	5373	5373	5373
CF	0.649	0.731	1.088	1.279	1.435	1.605	1.714	1.809	1.916	1.985
IVAC,LB-SEC/LB	205.4	206.9	233.7	254.9	274.1	296.1	310.6	323.4	337.9	347.1
ISP, LB SEC/LB	108.3	122.0	181.7	213.7	239.7	268.1	286.2	302.1	320.0	331.6

MOLE FRACTIONS

CO	0.08257	0.07412	0.07173	0.05694	0.04570	0.03476	0.02139	0.01280	0.00623	0.00144	0.00028
CO2	0.15490	0.16666	0.16997	0.19014	0.20523	0.21981	0.23751	0.24889	0.25767	0.26424	0.26594
H	0.01702	0.01445	0.01377	0.00994	0.00741	0.00521	0.00285	0.00152	0.00064	0.00011	0.00002
HO2	0.00027	0.00019	0.00018	0.00010	0.00006	0.00004	0.00002	0.00001	0.00001	0.00000	0.00000
H2	0.02746	0.02459	0.02379	0.01902	0.01549	0.01206	0.00782	0.00497	0.00264	0.00073	0.00018
H2O	0.39151	0.40727	0.41159	0.43695	0.45511	0.47224	0.49293	0.50659	0.51786	0.52772	0.53120
H2O2	0.00001	0.00001	0.00001	0.00000	0.00000	0.00000	0.00000	0.00000	0.00000	0.00000	0.00000
O	0.03479	0.02995	0.02866	0.02144	0.01663	0.01236	0.00755	0.00461	0.00236	0.00063	0.00015
OH	0.09463	0.08477	0.08208	0.06633	0.05508	0.04441	0.03125	0.02211	0.01395	0.00569	0.00214
O2	0.19683	0.19798	0.19823	0.19914	0.19928	0.19910	0.19868	0.19849	0.19865	0.19944	0.20010

THEORETICAL ROCKET PERFORMANCE ASSUMING EQUILIBRIUM COMPOSITION DURING EXPANSION

PC = 100.0 PSIA

	CHEMICAL FORMULA	WT FRACTION (SEE NOTE)	ENERGY CAL/MOL	STATE	TEMP DEG K
FUEL	C 2.00000 H 5.00000 O 1.00000 H 1.00000	1.000000	-66370.000	L	298.15
OXIDANT	O 2.00000	1.000000	-3102.000	L	90.18

O/F= 2.0870 PERCENT FUEL= 32.3939 EQUIVALENCE RATIO= 0.9987 PHI= 0.9984

	CHAMBER	THROAT	EXIT	EXIT	EXIT	EXIT	EXIT	EXIT	EXIT	EXIT	EXIT
PC/P	1.0000	1.7175	2.0000	5.0000	10.000	20.000	50.000	100.00	200.00	500.00	1000.00
P, ATM	6.8046	3.9618	3.4023	1.3609	0.68046	0.34023	0.13609	0.06805	0.03402	0.01361	0.00680
T, DEG K	3172.3	3044.2	3009.7	2813.7	2677.3	2549.1	2389.3	2273.7	2160.5	2010.8	1893.8
RHO, G/CC	6.3518-4	3.9082-4	3.4080-4	1.4914-4	7.9654-5	4.2481-5	1.8479-5	9.8404-6	5.2424-6	2.2858-6	1.2246-6
H, CAL/G	-532.23	-668.73	-705.82	-917.62	-1065.84	-1204.69	-1375.15	-1494.96	-1607.43	-1745.46	-1842.06
U, CAL/G	-791.66	-914.23	-947.59	-1138.60	-1272.72	-1398.65	-1553.50	-1662.42	-1764.60	-1889.64	-1976.62
G, CAL/G	-9380.70	-9159.87	-9100.53	-8765.71	-8533.44	-8314.71	-8039.62	-7836.87	-7633.58	-7354.00	-7124.32
S, CAL/(G)(K)	2.7893	2.7893	2.7893	2.7893	2.7893	2.7893	2.7893	2.7893	2.7893	2.7893	2.7893
M, MOL WT	24.299	24.642	24.738	25.303	25.717	26.117	26.622	26.981	27.317	27.714	27.968
(DLV/DLP)T	-1.04793	-1.04423	-1.04319	-1.03695	-1.03227	-1.02767	-1.02175	-1.01746	-1.01342	-1.00861	-1.00551
(DLV/DLT)P	1.9615	1.9270	1.9162	1.8418	1.7750	1.6998	1.5890	1.4984	1.4043	1.2794	1.1904
CP, CAL/(G)(K)	2.0776	2.0646	2.0586	1.9995	1.9280	1.8331	1.6719	1.5244	1.3576	1.1152	0.9258
GAMMA (S)	1.1155	1.1121	1.1112	1.1066	1.1038	1.1016	1.1001	1.1001	1.1016	1.1070	1.1151
SON VEL,M/SEC	1100.4	1068.8	1060.2	1011.5	977.4	945.5	906.0	878.0	851.1	817.2	792.3
MACH NUMBER	0.000	1.000	1.137	1.775	2.162	2.509	2.931	3.233	3.524	3.899	4.178

PERFORMANCE PARAMETERS

AE/AT	1.0000	1.0169	1.5595	2.4816	4.1450	8.5111	14.955	26.563	57.351	103.02
CSTAR, FT/SEC	5415	5415	5415	5415	5415	5415	5415	5415	5415	5415
CF	0.647	0.730	1.088	1.280	1.437	1.609	1.720	1.817	1.930	2.006
IVAC,LB-SEC/LB	207.0	208.5	235.6	257.2	276.8	299.5	314.6	328.2	344.2	354.9
ISP, LB-SEC/LB	109.0	122.9	183.1	215.5	241.9	270.8	289.4	305.9	324.9	337.6

MOLE FRACTIONS

CO	0.15412	0.14435	0.14152	0.12382	0.10983	0.09552	0.07641	0.06211	0.04825	0.03123	0.01999
CO2	0.18760	0.20220	0.20638	0.23202	0.25183	0.27177	0.29798	0.31733	0.33592	0.35851	0.37332
H	0.02116	0.01852	0.01781	0.01388	0.01124	0.00888	0.00618	0.00446	0.00301	0.00155	0.00079
HO2	0.00013	0.00009	0.00008	0.00005	0.00003	0.00002	0.00001	0.00000	0.00000	0.00000	0.00000
H2	0.04540	0.04220	0.04131	0.03599	0.03203	0.02813	0.02303	0.01924	0.01553	0.01079	0.00746
H2O	0.41882	0.43471	0.43909	0.46470	0.48311	0.50066	0.52246	0.53780	0.55202	0.56879	0.57958
H2O2	0.00001	0.00000	0.00000	0.00000	0.00000	0.00000	0.00000	0.00000	0.00000	0.00000	0.00000
O	0.02088	0.01774	0.01692	0.01244	0.00959	0.00717	0.00459	0.00308	0.00192	0.00087	0.00039
OH	0.07544	0.06721	0.06497	0.05221	0.04343	0.03541	0.02600	0.01979	0.01438	0.00851	0.00508
O2	0.07645	0.07297	0.07192	0.06490	0.05892	0.05245	0.04334	0.03618	0.02898	0.01974	0.01337

THEORETICAL ROCKET PERFORMANCE ASSUMING EQUILIBRIUM COMPOSITION DURING EXPANSION

PC = 100.0 PSIA

	CHEMICAL FORMULA							WT FRACTION (SEE NOTE)	ENERGY CAL/MOL	STATE	TEMP DEG K
FUEL	C	2.00000	H	5.00000	O	1.00000	H 1.00000	1.000000	-66370.000	L	298.15
OXIDANT	O	2.00000						1.000000	-3102.000	L	90.18

O/F= 2.0870 PERCENT FUEL= 32.3939 EQUIVALENCE RATIO= 0.9987 PHI= 0.9984

	CHAMBER	THROAT	EXIT	EXIT	EXIT	EXIT	EXIT	EXIT	EXIT	EXIT	EXIT
PC/P	1.0000	1.7175	2.0000	5.0000	10.000	20.000	50.000	100.00	200.00	500.00	1000.00
P, ATM	6.8046	3.9618	3.4023	1.3609	0.68046	0.34023	0.13609	0.06805	0.03402	0.01361	0.00680
T, DEG K	3172.3	3044.2	3009.7	2813.7	2677.3	2549.1	2389.3	2273.7	2160.5	2010.8	1893.8
RHO, G/CC	6.3518-4	3.9082-4	3.4080-4	1.4914-4	7.9654-5	4.2481-5	1.8479-5	9.8404-6	5.2424-6	2.2858-6	1.2246-6
H, CAL/G	-532.23	-668.73	-705.82	-917.62	-1065.84	-1204.69	-1375.15	-1494.96	-1607.43	-1745.46	-1842.06
U, CAL/G	-791.66	-914.23	-947.59	-1138.60	-1272.72	-1398.65	-1553.50	-1662.42	-1764.60	-1889.64	-1976.62
G, CAL/G	-9380.70	-9159.87	-9100.53	-8765.71	-8533.44	-8314.71	-8039.62	-7836.87	-7633.58	-7354.00	-7124.32
S, CAL/(G)(K)	2.7893	2.7893	2.7893	2.7893	2.7893	2.7893	2.7893	2.7893	2.7893	2.7893	2.7893
M, MOL WT	24.299	24.642	24.738	25.303	25.717	26.117	26.622	26.981	27.317	27.714	27.968
(DLV/DLP)T	-1.04793	-1.04423	-1.04319	-1.03695	-1.03227	-1.02767	-1.02175	-1.01746	-1.01342	-1.00861	-1.00551
(DLV/DLT)P	1.9615	1.9270	1.9162	1.8418	1.7750	1.6998	1.5890	1.4984	1.4043	1.2794	1.1904
CP, CAL/(G)(K)	2.0776	2.0646	2.0586	1.9995	1.9280	1.8331	1.6719	1.5244	1.3576	1.1152	0.9258
GAMMA (S)	1.1155	1.1121	1.1112	1.1066	1.1038	1.1016	1.1001	1.1001	1.1016	1.1070	1.1151
SON VEL,M/SEC	1100.4	1068.8	1060.2	1011.5	977.4	945.5	906.0	878.0	851.1	817.2	792.3
MACH NUMBER	0.000	1.000	1.137	1.775	2.162	2.509	2.931	3.233	3.524	3.899	4.178

PERFORMANCE PARAMETERS

AE/AT	1.0000	1.0169	1.5595	2.4816	4.1450	8.5111	14.955	26.563	57.351	103.02
CSTAR, FT/SEC	5415	5415	5415	5415	5415	5415	5415	5415	5415	5415
CF	0.647	0.730	1.088	1.280	1.437	1.609	1.720	1.817	1.930	2.006
IVAC,LB-SEC/LB	207.0	208.5	235.6	257.2	276.8	299.5	314.6	328.2	344.2	354.9
ISP, LB-SEC/LB	109.0	122.9	183.1	215.5	241.9	270.8	289.4	305.9	324.9	337.6

MOLE FRACTIONS

CO	0.15412	0.14435	0.14152	0.12382	0.10983	0.09552	0.07641	0.06211	0.04825	0.03123	0.01999
CO2	0.18760	0.20220	0.20638	0.23202	0.25183	0.27177	0.29798	0.31733	0.33592	0.35851	0.37332
H	0.02116	0.01852	0.01781	0.01388	0.01124	0.00888	0.00618	0.00446	0.00301	0.00155	0.00079
HO2	0.00013	0.00009	0.00008	0.00005	0.00003	0.00002	0.00001	0.00000	0.00000	0.00000	0.00000
H2	0.04540	0.04220	0.04131	0.03599	0.03203	0.02813	0.02303	0.01924	0.01553	0.01079	0.00746
H2O	0.41882	0.43471	0.43909	0.46470	0.48311	0.50066	0.52246	0.53780	0.55202	0.56879	0.57958
H2O2	0.00001	0.00000	0.00000	0.00000	0.00000	0.00000	0.00000	0.00000	0.00000	0.00000	0.00000
O	0.02088	0.01774	0.01692	0.01244	0.00959	0.00717	0.00459	0.00308	0.00192	0.00087	0.00039
OH	0.07544	0.06721	0.06497	0.05221	0.04343	0.03541	0.02600	0.01979	0.01438	0.00851	0.00508
O2	0.07645	0.07297	0.07192	0.06490	0.05892	0.05245	0.04334	0.03618	0.02898	0.01974	0.01337

THEORETICAL ROCKET PERFORMANCE ASSUMING EQUILIBRIUM COMPOSITION DURING EXPANSION

PC = 100.0 PSIA

CHEMICAL FORMULA					WT FRACTION (SEE NOTE)	ENERGY CAL/MOL	STATE	TEMP DEG K
FUEL	C 1.00000	H 4.00000			1.000000	-21390.000	L	111.66
OXIDANT	O 2.00000				1.000000	-3102.000	L	90.18

O/F= 4.0000 PERCENT FUEL= 20.0000 EQUIVALENCE RATIO= 0.9973 PHI= 0.9973

	CHAMBER	THROAT	EXIT	EXIT	EXIT	EXIT	EXIT	EXIT	EXIT	EXIT	EXIT
PC/P	1.0000	1.7186	2.0000	5.0000	10.000	20.000	50.000	100.00	200.00	500.00	1000.00
P, ATM	6.8046	3.9593	3.4023	1.3609	0.68046	0.34023	0.13609	0.06805	0.03402	0.01361	0.00680
T, DEG K	3254.2	3122.2	3086.8	2885.8	2746.7	2616.6	2455.7	2340.5	2228.9	2084.0	1973.3
RHO, G/CC	5.7062-4	3.5120-4	3.0649-4	1.3428-4	7.1758-5	3.8284-5	1.6653-5	8.8639-6	4.7171-6	2.0510-6	1.0948-6
H, CAL/G	344.22	-496.28	-537.35	-772.73	-937.29	-1091.39	-1280.52	-1413.50	-1538.42	-1692.01	-1799.85
U, CAL/G	-633.01	-769.29	-806.18	-1018.17	-1166.93	-1306.61	-1478.43	-1599.41	-1713.10	-1852.69	-1950.37
G, CAL/G	-10047.3	-9805.52	-9741.05	-9377.33	9126.98	-8893.17	-8602.71	-8391.97	-8184.27	-7905.72	-7683.51
S, CAL/(G)(K)	2.9817	2.9817	2.9817	2.9817	2.9817	2.9817	2.9817	2.9817	2.9817	2.9817	2.9817
M, MOL WT	22.393	22.725	22.817	23.365	23.768	24.160	24.658	25.017	25.358	25.772	26.051
(DLV/DLP)T	1.05488	-1.05088	-1.04976	-1.04305	-1.03804	-1.03310	-1.02673	-1.02209	-1.01764	-1.01219	-1.00851
(DLV/DLT)P	2.0622	2.0290	2.0187	1.9465	1.8812	1.8073	1.6974	1.6063	1.5100	1.3784	1.2798
CP, CAL/(G)(K)	2.3579	2.3508	2.3463	2.2954	2.2290	2.1377	1.9786	1.8297	1.6577	1.4001	1.1895
GAMMA (S)	1.1175	1.1139	1.1130	1.1078	1.1046	1.1020	1.0997	1.0988	1.0991	1.1019	1.1068
SON VEL,M/SEC	1162.0	1128.0	1118.9	1066.6	1030.2	996.2	954.2	924.5	896.2	860.7	834.9
MACH NUMBER	0.000	1.000	1.136	1.775	2.162	2.510	2.933	3.236	3.527	3.902	4.180

PERFORMANCE PARAMETERS

AE/AT	1.0000	1.0167	1.5580	2.4782	4.1383	8.4986	14.941	26.567	57.514	103.68
CSTAR, FT/SEC	5710	5710	5710	5710	5710	5710	5710	5710	5710	5710
CF	0.648	0.730	1.088	1.280	1.437	1.608	1.719	1.816	1.930	2.005
IVAC,LB-SEC/LB	218.3	219.9	248.4	271.1	291.7	315.6	331.5	345.9	362.9	374.3
ISP, LB-SEC/LB	115.0	129.6	193.1	227.2	255.0	285.4	305.0	322.4	342.5	355.9

MOLE FRACTIONS

CO	0.14427	0.13669	0.13448	0.12030	0.10876	0.09668	0.08011	0.06736	0.05464	0.03838	0.02696
CO2	0.13490	0.14662	0.14998	0.17099	0.18755	0.20452	0.22730	0.24453	0.26148	0.28292	0.29781
H	0.03047	0.02695	0.02601	0.02070	0.01711	0.01386	0.01007	0.00759	0.00545	0.00316	0.00184
HO2	0.00015	0.00011	0.00010	0.00005	0.00003	0.00002	0.00001	0.00001	0.00000	0.00000	0.00000
H2	0.06066	0.05673	0.05563	0.04905	0.04412	0.03923	0.03285	0.02808	0.02336	0.01727	0.01283
H2O	0.43749	0.45595	0.46104	0.49099	0.51270	0.53354	0.55967	0.57828	0.59581	0.61706	0.63138
H2O2	0.00001	0.00000	0.00000	0.00000	0.00000	0.00000	0.00000	0.00000	0.00000	0.00000	0.00000
O	0.02655	0.02290	0.02194	0.01662	0.01317	0.01017	0.00689	0.00489	0.00328	0.00171	0.00091
OH	0.08975	0.08081	0.07837	0.06431	0.05448	0.04538	0.03453	0.02722	0.02071	0.01337	0.00883
O2	0.07576	0.07324	0.07245	0.06699	0.06209	0.05660	0.04858	0.04205	0.03525	0.02615	0.01944

THEORETICAL ROCKET PERFORMANCE ASSUMING EQUILIBRIUM COMPOSITION DURING EXPANSION

PC = 100.0 PSIA

	CHEMICAL FORMULA			WT FRACTION (SEE NOTE)	ENERGY CAL/MOL	STATE	TEMP DEG K
FUEL	C 1.00000	H 4.00000		1.000000	-21380.000	L	111.66
OXIDANT	O 2.00000			1.000000	-3102.000	L	90.18

O/F= 6.0000 PERCENT FUEL= 14.2857 EQUIVALENCE RATIO= 0.6649 PHI= 0.6649

	CHAMBER	THROAT	EXIT	EXIT	EXIT	EXIT	EXIT	EXIT	EXIT	EXIT	EXIT
PC/P	1.0000	1.7205	2.0000	5.0000	10.000	20.000	50.000	100.00	200.00	500.00	1000.00
P, ATM	6.8046	3.9550	3.4023	1.3609	0.68046	0.34023	0.13609	0.06805	0.03402	0.01361	0.00680
T, DEG K	3123.7	2989.0	2952.8	2742.1	2590.1	2440.6	2239.1	2076.8	1901.3	1655.3	1472.7
RHO, G/CC	6.7740-4	4.1692-4	3.6434-4	1.6019-4	8.6000-5	4.6215-5	2.0430-5	1.1098-5	6.0901-6	2.8053-6	1.5774-6
H, CAL/G	-273.57	-401.85	-436.16	-633.86	-771.52	-899.68	-1055.23	-1162.62	-1261.00	-1376.80	-1453.68
U, CAL/G	-516.83	-631.58	-662.31	-839.60	-963.13	-1077.96	-1216.56	-1311.11	-1396.29	-1494.28	-1558.15
G, CAL/G	-8589.82	-8359.52	-8297.64	-7934.26	-7667.23	-7397.32	-7016.52	-6691.79	-6322.82	-5783.77	-5374.56
S, CAL/(G)(K)	2.6623	2.6623	2.6623	2.6623	2.6623	2.6623	2.6623	2.6623	2.6623	2.6623	2.6623
M, MOL WT	25.517	25.855	25.947	26.485	26.861	27.203	27.582	27.793	27.926	27.999	28.013
(DLV/DLP)T	-1.03661	-1.03204	-1.03077	-1.02315	-1.01758	-1.01238	-1.00650	-1.00323	-1.00123	-1.00022	-1.00005
(DLV/DLT)P	1.7516	1.6897	1.6712	1.5469	1.4420	1.3323	1.1924	1.1043	1.0442	1.0094	1.0023
CP, CAL/(G)(K)	1.6697	1.6061	1.5853	1.4280	1.2759	1.1002	0.8504	0.6740	0.5381	0.4406	0.4093
GAMMA (S)	1.1192	1.1168	1.1163	1.1143	1.1148	1.1179	1.1286	1.1443	1.1668	1.1960	1.2107
SON VEL,M/SEC	1067.3	1036.1	1027.7	979.4	945.4	913.2	872.8	843.2	812.7	766.7	727.5
MACH NUMBER	0.000	1.000	1.135	1.773	2.159	2.507	2.930	3.235	3.537	3.963	4.320

PERFORMANCE PARAMETERS

AE/AT	1.0000	1.0164	1.5530	2.4606	4.0834	8.2673	14.271	24.675	50.678	87.144
CSTAR, FT/SEC	5237	5237	5237	5237	5237	5237	5237	5237	5237	5237
CF	0.649	0.731	1.088	1.279	1.434	1.602	1.709	1.801	1.904	1.969
IVAC,LB-SEC/LB	200.3	201.7	227.6	248.2	266.6	287.7	301.4	313.2	326.3	334.6
ISP, LB-SEC/LB	105.7	118.9	177.1	208.2	233.4	260.8	278.1	293.1	309.8	320.4

MOLE FRACTIONS

CO	0.06462	0.05628	0.05396	0.03988	0.02966	0.02026	0.00996	0.00453	0.00147	0.00017	0.00002
CO2	0.16260	0.17395	0.17710	0.19596	0.20953	0.22198	0.23565	0.24297	0.24721	0.24916	0.24944
H	0.01237	0.01018	0.00961	0.00643	0.00441	0.00275	0.00118	0.00044	0.00011	0.00001	0.00000
HO2	0.00028	0.00020	0.00018	0.00010	0.00006	0.00004	0.00002	0.00001	0.00000	0.00000	0.00000
H2	0.02037	0.01781	0.01710	0.01290	0.00986	0.00701	0.00375	0.00188	0.00070	0.00011	0.00002
H2O	0.38417	0.39897	0.40298	0.42651	0.44309	0.45835	0.47581	0.48614	0.49321	0.49762	0.49864
H2O2	0.00001	0.00001	0.00001	0.00000	0.00000	0.00000	0.00000	0.00000	0.00000	0.00000	0.00000
O	0.03157	0.02664	0.02534	0.01804	0.01323	0.00906	0.00462	0.00224	0.00081	0.00012	0.00002
OH	0.08714	0.07700	0.07424	0.05802	0.04642	0.03545	0.02215	0.01349	0.00679	0.00186	0.00051
O2	0.23687	0.23897	0.23949	0.24215	0.24373	0.24511	0.24688	0.24831	0.24970	0.25096	0.25136

THEORETICAL ROCKET PERFORMANCE ASSUMING EQUILIBRIUM COMPOSITION DURING EXPANSION

PC = 100.0 PSIA

CHEMICAL FORMULA			WT FRACTION (SEE NOTE)	ENERGY CAL/MOL	STATE	TEMP DEG K
FUEL	N 1.00000	H 3.00000	1.000000	-17090.000	L	239.72
OXIDANT	O 2.00000		1.000000	-3102.000	L	90.18

O/F= 1.6270 PERCENT FUEL= 38.0662 EQUIVALENCE RATIO= 0.8661 PHI= 0.8661

	CHAMBER	THROAT	EXIT	EXIT	EXIT	EXIT	EXIT	EXIT	EXIT	EXIT	EXIT
PC/P	1.0000	1.7325	2.0000	5.0000	10.000	20.000	50.000	100.00	200.00	500.00	1000.00
P, ATM	6.8046	3.9276	3.4023	1.3609	0.68046	0.34023	0.13609	0.06805	0.03402	0.01361	0.00680
T, DEG K	2881.9	2726.3	2685.8	2425.7	2221.9	2010.1	1727.5	1523.3	1334.0	1109.0	957.5
RHO, G/CC	5.8666-4	3.6136-4	3.1847-4	1.4279-4	7.8435-5	4.3509-5	2.0290-5	1.1509-5	6.5718-6	3.1621-6	1.8311-6
H, CAL/G	-442.03	-591.50	-628.98	-853.18	-1005.98	-1144.42	-1305.52	-1411.36	-1504.35	-1609.33	-1676.56
U, CAL/G	-722.92	-854.72	-887.70	-1083.99	-1216.08	-1333.79	-1467.95	-1554.54	-1629.72	-1713.56	-1766.55
G, CAL/G	-9502.97	-9163.04	-9073.34	-8479.74	-7991.77	-7464.33	-6736.82	-6200.77	-5698.43	-5096.03	-4687.15
S, CAL/(G)(K)	3.1441	3.1441	3.1441	3.1441	3.1441	3.1441	3.1441	3.1441	3.1441	3.1441	3.1441
M, MOL WT	20.389	20.582	20.629	20.884	21.016	21.093	21.134	21.142	21.144	21.144	21.144
(DLV/DLP)T	-1.01551	-1.01146	-1.01047	-1.00513	-1.00240	-1.00088	-1.00016	-1.00003	-1.00001	-1.00000	-1.00000
(DLV/DLT)P	1.3407	1.2671	1.2481	1.1360	1.0707	1.0293	1.0063	1.0015	1.0003	1.0000	1.0000
CP, CAL/(G)(K)	1.3192	1.1835	1.1466	0.9094	0.7494	0.6296	0.5392	0.5038	0.4798	0.4533	0.4345
GAMMA (S)	1.1329	1.1357	1.1369	1.1493	1.1658	1.1872	1.2142	1.2302	1.2438	1.2615	1.2760
SON VEL,M/SEC	1153.9	1118.4	1109.3	1053.5	1012.3	969.9	908.4	858.5	807.7	741.7	693.2
MACH NUMBER	0.000	1.000	1.127	1.761	2.146	2.500	2.959	3.318	3.691	4.214	4.637

PERFORMANCE PARAMETERS

AE/AT	1.0000	1.0146	1.5260	2.3719	3.8313	7.4100	12.330	20.626	40.893	68.669
CSTAR, FT/SEC	5597	5597	5597	5597	5597	5597	5597	5597	5597	5597
CF	0.656	0.733	1.087	1.273	1.421	1.576	1.669	1.748	1.832	1.884
IVAC,LB-SEC/LB	214.5	215.8	242.2	262.8	280.5	299.9	311.9	322.0	332.9	339.7
ISP, LB-SEC/LB	114.0	127.5	189.1	221.5	247.2	274.1	290.4	304.0	318.7	327.7

MOLE FRACTIONS

H	0.00734	0.00483	0.00426	0.00157	0.00053	0.00012	0.00001	0.00000	0.00000	0.00000	0.00000
HO2	0.00007	0.00005	0.00004	0.00002	0.00001	0.00000	0.00000	0.00000	0.00000	0.00000	0.00000
H2	0.03169	0.02357	0.02157	0.01054	0.00480	0.00162	0.00022	0.00003	0.00000	0.00000	0.00000
H2O	0.62575	0.64628	0.65131	0.67904	0.69388	0.70284	0.70765	0.70862	0.70886	0.70891	0.70891
H2O2	0.00001	0.00000	0.00000	0.00000	0.00000	0.00000	0.00000	0.00000	0.00000	0.00000	0.00000
NO	0.01074	0.00872	0.00822	0.00538	0.00359	0.00216	0.00089	0.00038	0.00014	0.00003	0.00001
NO2	0.00001	0.00001	0.00001	0.00000	0.00000	0.00000	0.00000	0.00000	0.00000	0.00000	0.00000
N2	0.22248	0.22566	0.22644	0.23071	0.23308	0.23466	0.23574	0.23609	0.23623	0.23629	0.23630
O	0.00637	0.00455	0.00413	0.00192	0.00085	0.00028	0.00004	0.00000	0.00000	0.00000	0.00000
OH	0.04486	0.03558	0.03325	0.01964	0.01132	0.00539	0.00139	0.00036	0.00007	0.00000	0.00000
O2	0.05067	0.05075	0.05077	0.05120	0.05193	0.05292	0.05406	0.05451	0.05470	0.05477	0.05478

THEORETICAL ROCKET PERFORMANCE ASSUMING EQUILIBRIUM COMPOSITION DURING EXPANSION

PC = 100.0 PSIA

CHEMICAL FORMULA				WT FRACTION (SEE NOTE)	ENERGY CAL/MOL	STATE	TEMP DEG K
FUEL	N 1.00000	H 3.00000		1.000000	-17090.000	L	239.72
OXIDANT	O 2.00000			1.000000	-3102.000	L	90.18

O/F= 2.4410 PERCENT FUEL= 29.0613 EQUIVALENCE RATIO= 0.5773 PHI= 0.5773

	CHAMBER	THROAT	EXIT	EXIT	EXIT	EXIT	EXIT	EXIT	EXIT	EXIT	EXIT
PC/P	1.0000	1.7484	2.0000	5.0000	10.000	20.000	50.000	100.00	200.00	500.00	1000.00
P, ATM	6.8046	3.8919	3.4023	1.3609	0.68046	0.34023	0.13609	0.06805	0.03402	0.01361	0.00680
T, DEG K	2660.0	2480.5	2437.1	2138.1	1911.4	1691.0	1420.5	1235.7	1068.7	874.2	745.8
RHO, G/CC	7.0592-4	4.3539-4	3.8783-4	1.7778-4	9.9627-5	5.6348-5	2.6840-5	1.5427-5	8.9186-6	4.3616-6	2.5559-6
H, CAL/G	-360.40	-486.06	-514.90	-697.12	-818.66	-926.60	-1049.66	-1129.15	-1198.10	-1274.85	-1323.30
U, CAL/G	-593.84	-702.54	-727.35	-882.50	-984.06	-1072.82	-1172.45	-1235.97	-1290.48	-1350.41	-1387.78
G, CAL/G	-7903.11	-7519.78	-7425.50	-6760.09	-6238.61	-5721.73	-5077.63	-4633.21	-4228.64	-3753.63	-3438.26
S, CAL/(G)(K)	2.8356	2.8356	2.8356	2.8356	2.8356	2.8356	2.8356	2.8356	2.8356	2.8356	2.8356
M, MOL WT	22.644	22.770	22.796	22.919	22.964	22.981	22.988	22.989	22.989	22.989	22.989
(DLV/DLP)T	-1.00562	-1.00342	-1.00299	-1.00099	-1.00033	-1.00009	-1.00001	1.00000	-1.00000	-1.00000	-1.00000
(DLV/DLT)P	1.1399	1.0928	1.0829	1.0322	1.0125	1.0039	1.0006	1.0001	1.0000	1.0000	1.0000
CP, CAL/(G)(K)	0.8301	0.7335	0.7115	0.5829	0.5164	0.4738	0.4398	0.4212	0.4046	0.3843	0.3709
GAMMA (S)	1.1518	1.1610	1.1637	1.1869	1.2069	1.2252	1.2450	1.2583	1.2717	1.2902	1.3039
SON VEL,M/SEC	1060.6	1025.5	1017.1	959.5	913.9	865.8	799.8	749.9	701.1	638.7	593.1
MACH NUMBER	0.000	1.000	1.118	1.749	2.143	2.514	3.003	3.382	3.776	4.331	4.786

PERFORMANCE PARAMETERS

AE/AT	1.0000	1.0125	1.4961	2.2885	3.6401	6.9265	11.411	18.908	37.005	61.537
CSTAR, FT/SEC	5067	5067	5067	5067	5067	5067	5067	5067	5067	5067
CF	0.664	0.736	1.087	1.268	1.410	1.555	1.642	1.714	1.791	1.838
IVAC,LB-SEC/LB	194.6	195.7	218.3	235.7	250.6	266.7	276.6	284.9	293.7	299.1
ISP, LB-SEC/LB	104.6	115.9	171.2	199.7	222.0	244.9	258.6	270.0	282.1	289.5

MOLE FRACTIONS

H	0.00143	0.00068	0.00056	0.00010	0.00002	0.00000	0.00000	0.00000	0.00000	0.00000
HO2	0.00012	0.00007	0.00006	0.00002	0.00001	0.00000	0.00000	0.00000	0.00000	0.00000
H2	0.00592	0.00345	0.00297	0.00083	0.00022	0.00004	0.00000	0.00000	0.00000	0.00000
H2O	0.55600	0.56738	0.56971	0.58139	0.58578	0.58765	0.58833	0.58842	0.58843	0.58843
H2O2	0.00001	0.00000	0.00000	0.00000	0.00000	0.00000	0.00000	0.00000	0.00000	0.00000
NO	0.01412	0.01069	0.00992	0.00541	0.00297	0.00141	0.00041	0.00013	0.00003	0.00000
NO2	0.00003	0.00002	0.00002	0.00001	0.00001	0.00000	0.00000	0.00000	0.00000	0.00000
N2	0.18612	0.18892	0.18952	0.19284	0.19444	0.19538	0.19593	0.19608	0.19613	0.19614
O	0.00515	0.00298	0.00256	0.00070	0.00018	0.00003	0.00000	0.00000	0.00000	0.00000
OH	0.03380	0.02325	0.02098	0.00876	0.00355	0.00112	0.00016	0.00002	0.00000	0.00000
O2	0.19730	0.20254	0.20368	0.20994	0.21283	0.21437	0.21517	0.21535	0.21541	0.21542

THEORETICAL ROCKET PERFORMANCE ASSUMING EQUILIBRIUM COMPOSITION DURING EXPANSION

PC = 100.0 PSIA

	CHEMICAL FORMULA		WT FRACTION (SEE NOTE)	ENERGY CAL/MOL	STATE	TEMP DEG K
FUEL	N 1.00000	H 3.00000	1.000000	-17090.000	L	239.72
OXIDANT	O 2.00000		1.000000	-3102.000	L	90.18

O/F= 4.0680 PERCENT FUEL= 19.7316 EQUIVALENCE RATIO= 0.3464 PHI= 0.3464

	CHAMBER	THROAT	EXIT	EXIT	EXIT	EXIT	EXIT	EXIT	EXIT	EXIT	EXIT
PC/P	1.0000	1.7803	2.0000	5.0000	10.000	20.000	50.000	100.00	200.00	500.00	1000.00
P, ATM	6.8046	3.8222	3.4023	1.3609	0.68046	0.34023	0.13609	0.06805	0.03402	0.01361	0.00680
T, DEG K	2226.0	2021.4	1980.7	1672.5	1458.7	1264.4	1038.0	888.4	756.2	606.1	509.6
RHO, G/CC	9.3894-4	5.8169-4	5.2852-4	2.5056-4	1.4367-4	8.2875-5	4.0382-5	2.3590-5	1.3857-5	6.9153-6	4.1126-6
H, CAL/G	-275.82	-372.30	-390.63	-522.15	-607.40	-681.51	-764.25	-816.67	-861.41	-910.32	-940.66
U, CAL/G	-451.32	-531.43	-546.52	-653.68	-722.10	-780.93	-845.87	-886.52	-920.87	-957.98	-980.73
G, CAL/G	-5808.45	5396.24	-5313.47	-4679.10	-4232.81	-3824.12	-3344.06	-3024.72	-2740.98	-2416.80	-2207.25
S, CAL/(G)(K)	2.4854	2.4854	2.4854	2.4854	2.4854	2.4854	2.4854	2.4854	2.4854	2.4854	2.4854
M, MOL WT	25.205	25.243	25.248	25.269	25.272	25.273	25.273	25.273	25.273	25.273	25.273
(DLV/DLP)T	1.00085	1.00036	1.00030	1.00005	1.00001	1.00000	1.00000	1.00000	1.00000	1.00000	1.00000
(DLV/DLT)P	1.0268	1.0128	1.0108	1.0023	1.0005	1.0001	1.0000	1.0000	1.0000	1.0000	1.0000
CP, CAL/(G)(K)	0.5033	0.4596	0.4523	0.4097	0.3894	0.3741	0.3566	0.3442	0.3327	0.3188	0.3099
GAMMA (S)	1.1966	1.2126	1.2158	1.2389	1.2533	1.2662	1.2829	1.2961	1.3094	1.3273	1.3400
SON VEL,M/SEC	937.4	898.5	890.5	825.7	775.5	725.7	661.9	615.5	570.8	514.5	474.0
MACH NUMBER	0.000	1.000	1.101	1.749	2.148	2.539	3.054	3.457	3.878	4.479	4.976

PERFORMANCE PARAMETERS

AE/AT	1.0000	1.0089	1.4529	2.1839	3.4228	6.4020	10.414	17.039	32.800	54.880
CSTAR, FT/SEC	4328	4328	4328	4328	4328	4328	4328	4328	4328	4328
CF	0.681	0.743	1.088	1.263	1.397	1.533	1.613	1.678	1.747	1.788
IVAC,LB-SEC/LB	167.2	167.8	185.5	199.2	210.9	223.4	230.9	237.2	243.8	247.8
ISP, LB-SEC/LB	91.6	99.9	146.4	169.9	187.9	206.2	216.9	225.7	235.0	240.5

MOLE FRACTIONS

H	0.00005	0.00001	0.00001	0.00000	0.00000	0.00000	0.00000	0.00000	0.00000	0.00000
HO2	0.00006	0.00003	0.00002	0.00000	0.00000	0.00000	0.00000	0.00000	0.00000	0.00000
H2	0.00035	0.00012	0.00009	0.00001	0.00000	0.00000	0.00000	0.00000	0.00000	0.00000
H2O	0.43836	0.43652	0.43696	0.43878	0.43914	0.43922	0.43923	0.43923	0.43923	0.43923
HO	0.00292	0.00485	0.00435	0.00157	0.00060	0.00019	0.00003	0.00000	0.00000	0.00000
HO2	0.00004	0.00002	0.00002	0.00001	0.00000	0.00000	0.00000	0.00000	0.00000	0.00000
O2	0.14204	0.14380	0.14408	0.14559	0.14610	0.14631	0.14640	0.14641	0.14641	0.14641
O	0.00077	0.00026	0.00020	0.00002	0.00000	0.00000	0.00000	0.00000	0.00000	0.00000
OH	0.00856	0.00409	0.00345	0.00071	0.00015	0.00002	0.00000	0.00000	0.00000	0.00000
O2	0.40686	0.41030	0.41082	0.41330	0.41400	0.41426	0.41435	0.41436	0.41436	0.41436

THEORETICAL ROCKET PERFORMANCE ASSUMING EQUILIBRIUM COMPOSITION DURING EXPANSION

PC = 100.0 PSIA

	CHEMICAL FORMULA	WT FRACTION (SEE NOTE)	ENERGY CAL/MOL	STATE	TEMP DEG K
FUEL	N 2.00000 H 4.00000	1.000000	12100.000	L	298.15
OXIDANT	O 2.00000	1.000000	-3102.000	L	90.18

O/F= 1.0000 PERCENT FUEL= 50.0000 EQUIVALENCE RATIO= 0.9986 PHI= 0.9986

	CHAMBER	THROAT	EXIT	EXIT	EXIT	EXIT	EXIT	EXIT	EXIT	EXIT	EXIT
PC/P	1.0000	1.7262	2.0000	5.0000	10.000	20.000	50.000	100.00	200.00	500.00	1000.00
P, ATM	6.8046	3.9420	3.4023	1.3609	0.68046	0.34023	0.13609	0.06805	0.03402	0.01361	0.00680
T, DEG K	3161.0	3012.7	2973.9	2741.3	2572.0	2404.0	2176.6	1994.5	1801.7	1539.4	1348.2
RHO, G/CC	5.1207-4	3.1545-4	2.7678-4	1.2259-4	6.6243-5	3.5869-5	1.6052-5	8.8186-6	4.9013-6	2.2996-6	1.3133-6
H, CAL/G	140.33	-30.053	-74.246	-333.57	-512.88	-678.66	-877.93	-1013.86	-1136.91	-1279.53	-1372.62
U, CAL/G	-181.48	-332.68	-371.94	-602.41	-761.65	-908.37	-1083.25	-1200.73	-1305.01	-1422.85	-1498.10
G, CAL/G	-10117.5	-9806.73	-9725.06	-9229.56	-8859.31	-8480.09	-7941.22	-7486.44	-6983.83	-6275.10	-5747.81
S, CAL/(G)(K)	3.2451	3.2451	3.2451	3.2451	3.2451	3.2451	3.2451	3.2451	3.2451	3.2451	3.2451
M, MOL WT	19.519	19.783	19.852	20.263	20.546	20.797	21.067	21.211	21.298	21.345	21.352
(DLV/DLP)T	-1.03425	-1.02921	-1.02788	-1.01998	-1.01458	-1.00985	-1.00493	-1.00240	-1.00092	-1.00016	-1.00002
(DLV/DLT)P	1.6740	1.6040	1.5842	1.4553	1.3548	1.2570	1.1423	1.0757	1.0322	1.0063	1.0009
CP, CAL/(G)(K)	1.9332	1.8315	1.8008	1.5823	1.3909	1.1866	0.9192	0.7428	0.6099	0.5087	0.4718
GAMMA (S)	1.1278	1.1260	1.1256	1.1252	1.1275	1.1330	1.1481	1.1676	1.1934	1.2273	1.2463
SON VEL,M/SEC	1232.3	1194.0	1184.1	1125.0	1083.3	1043.5	993.1	955.4	916.2	857.9	808.9
MACH NUMBER	0.000	1.000	1.132	1.770	2.158	2.509	2.939	3.253	3.568	4.018	4.399

PERFORMANCE PARAMETERS

AE/AT	1.0000	1.0156	1.5429	2.4320	4.0112	8.0384	13.744	23.507	47.518	80.605
CSTAR, FT/SEC	6006	6006	6006	6006	6006	6006	6006	6006	6006	6006
CF	0.652	0.732	1.088	1.277	1.430	1.595	1.698	1.786	1.883	1.944
IVAC,LB-SEC/LB	229.9	231.4	260.7	283.8	304.4	327.7	342.6	355.3	369.2	377.9
ISP, LB-SEC/LB	121.8	136.6	203.1	238.4	266.9	297.7	316.9	333.4	351.5	362.8

MOLE FRACTIONS

H	0.02852	0.02299	0.02159	0.01373	0.00889	0.00511	0.00185	0.00061	0.00013	0.00001	0.00000
HO2	0.00006	0.00004	0.00004	0.00002	0.00001	0.00000	0.00000	0.00000	0.00000	0.00000	0.00000
H2	0.08783	0.07825	0.07563	0.05909	0.04651	0.03421	0.01936	0.01033	0.00421	0.00066	0.00007
H2O	0.47728	0.50220	0.50883	0.54898	0.57752	0.60372	0.63296	0.64934	0.65969	0.66532	0.66623
N	0.00001	0.00000	0.00000	0.00000	0.00000	0.00000	0.00000	0.00000	0.00000	0.00000	0.00000
NO	0.01216	0.00999	0.00945	0.00642	0.00453	0.00299	0.00146	0.00071	0.00027	0.00006	0.00002
NO2	0.00001	0.00000	0.00000	0.00000	0.00000	0.00000	0.00000	0.00000	0.00000	0.00000	0.00000
N2	0.29847	0.30367	0.30502	0.31295	0.31831	0.32301	0.32797	0.33060	0.33218	0.33302	0.33315
O	0.01147	0.00900	0.00838	0.00504	0.00310	0.00167	0.00054	0.00016	0.00003	0.00000	0.00000
OH	0.05943	0.05075	0.04845	0.03477	0.02535	0.01704	0.00831	0.00386	0.00135	0.00021	0.00004
O2	0.02476	0.02310	0.02260	0.01900	0.01578	0.01226	0.00753	0.00440	0.00213	0.00073	0.00050

THEORETICAL ROCKET PERFORMANCE ASSUMING EQUILIBRIUM COMPOSITION DURING EXPANSION

PC = 100.0 PSIA

	CHEMICAL FORMULA				WT FRACTION (SEE NOTE)	ENERGY CAL/MOL	STATE	TEMP DEG K
FUEL	N	1.00000	H	3.00000	1.000000	-17090.000	L	239.72
OXIDANT	N	2.00000	O	4.00000	1.000000	-4680.000	L	298.15

O/F= 2.0294 PERCENT FUEL= 33.0098 EQUIVALENCE RATIO= 0.9983 PHI= 0.9983

	CHAMBER	THROAT	EXIT	EXIT	EXIT	EXIT	EXIT	EXIT	EXIT	EXIT	EXIT
PC/P	1.0000	1.7397	2.0000	5.0000	10.000	20.000	50.000	100.00	200.00	500.00	1000.00
P, ATM	6.8046	3.9114	3.4023	1.3609	0.68046	0.34023	0.13609	0.06805	0.03402	0.01361	0.00680
T, DEG K	2766.9	2601.9	2560.5	2285.7	2072.5	1855.8	1575.0	1376.8	1195.9	983.7	842.5
RHO, G/CC	6.3121-4	3.8912-4	3.4462-4	1.5603-4	8.6472-5	4.8420-5	2.2851-5	1.3073-5	7.5256-6	3.6597-6	2.1366-6
H, CAL/G	-365.33	-504.96	-538.61	744.85	-884.09	-1009.09	-1152.99	-1246.58	-1328.11	-1419.32	-1477.18
U, CAL/G	-626.39	-748.39	-777.70	-956.08	-1074.66	-1179.25	-1297.22	-1372.63	-1437.60	-1509.38	-1554.31
G, CAL/G	-8639.02	-8285.24	-8194.91	-7579.56	-7081.36	-6558.39	-5862.64	-5363.50	-4904.07	-4360.66	-3996.27
S, CAL/(G)(K)	2.9902	2.9902	2.9902	2.9902	2.9902	2.9902	2.9902	2.9902	2.9902	2.9902	2.9902
M, MOL WT	21.062	21.240	21.281	21.503	21.612	21.672	21.701	21.705	21.706	21.706	21.706
(DLV/DLP)T	-1.01100	-1.00785	-1.00714	1.00334	-1.00154	-1.00056	-1.00009	-1.00001	-1.00000	-1.00000	-1.00000
(DLV/DLT)P	1.2530	1.1923	1.1776	1.0932	1.0473	1.0192	1.0034	1.0005	1.0000	1.0000	1.0000
CP, CAL/(G)(K)	1.0922	0.9763	0.9468	0.7602	0.6416	0.5549	0.4874	0.4604	0.4413	0.4178	0.4017
GAMMA (S)	1.1424	1.1473	1.1489	1.1654	1.1843	1.2064	1.2332	1.2485	1.2618	1.2807	1.2952
SON VEL,M/SEC	1117.0	1081.0	1072.1	1014.9	971.8	926.8	862.6	811.5	760.3	694.7	646.5
MACH NUMBER	0.000	1.000	1.123	1.756	2.144	2.504	2.976	3.347	3.733	4.275	4.718

PERFORMANCE PARAMETERS

AE/AT	1.0000	1.0136	1.5128	2.3347	3.7428	7.1697	11.848	19.692	38.701	64.542
CSTAR, FT/SEC	5378	5378	5378	5378	5378	5378	5378	5378	5378	5378
CF	0.659	0.735	1.087	1.271	1.416	1.566	1.657	1.732	1.812	1.861
IVAC,LB-SEC/LB	206.3	207.5	232.3	251.5	268.0	285.8	296.7	305.9	315.8	321.8
ISP, LB-SEC/LB	110.2	122.8	181.7	212.5	236.7	261.8	276.9	289.4	302.8	311.0

MOLE FRACTIONS

H	0.00542	0.00331	0.00287	0.00090	0.00026	0.00005	0.00000	0.00000	0.00000	0.00000	0.00000
H02	0.00002	0.00001	0.00001	0.00000	0.00000	0.00000	0.00000	0.00000	0.00000	0.00000	0.00000
H2	0.03819	0.02894	0.02672	0.01386	0.00681	0.00253	0.00033	0.00003	0.00000	0.00000	0.00000
H20	0.56034	0.57910	0.58347	0.60769	0.62003	0.62710	0.63055	0.63102	0.63108	0.63108	0.63108
NO	0.00555	0.00389	0.00353	0.00162	0.00074	0.00028	0.00006	0.00002	0.00001	0.00000	0.00000
N2	0.35468	0.35855	0.35943	0.36414	0.36643	0.36769	0.36829	0.36837	0.36839	0.36839	0.36839
O	0.00196	0.00114	0.00098	0.00028	0.00007	0.00001	0.00000	0.00000	0.00000	0.00000	0.00000
OH	0.02220	0.01570	0.01422	0.00638	0.00276	0.00092	0.00014	0.00003	0.00000	0.00000	0.00000
O2	0.01164	0.00936	0.00878	0.00513	0.00289	0.00142	0.00062	0.00052	0.00052	0.00052	0.00052

THEORETICAL ROCKET PERFORMANCE ASSUMING EQUILIBRIUM COMPOSITION DURING EXPANSION

PC = 100.0 PSIA

	CHEMICAL FORMULA				WT FRACTION (SEE NOTE)	ENERGY CAL/MOL	STATE	TEMP DEG K
FUEL	N	1.00000	H	3.00000	1.000000	-17090.000	L	239.72
OXIDANT	N	2.00000	O	4.00000	1.000000	-4680.000	L	298.15

O/F= 3.0441 PERCENT FUEL= 24.7274 EQUIVALENCE RATIO= 0.6656 PHI= 0.6656

	CHAMBER	THROAT	EXIT	EXIT	EXIT	EXIT	EXIT	EXIT	EXIT	EXIT	EXIT
PC/P	1.0000	1.7623	2.0000	5.0000	10.000	20.000	50.000	100.00	200.00	500.00	1000.00
P, ATM	6.8046	3.8612	3.4023	1.3609	0.68046	0.34023	0.13609	0.06805	0.03402	0.01361	0.00680
T, DEG K	2536.4	2338.8	2294.6	1976.0	1743.6	1526.0	1266.7	1092.7	937.0	757.7	641.0
RHO, G/CC	7.5933-4	4.6908-4	4.2157-4	1.9639-4	1.1137-4	6.3639-5	3.0669-5	1.7777-5	1.0365-5	5.1271-6	3.0302-6
H, CAL/G	-286.43	-404.37	-429.34	-595.68	-705.06	-801.12	-909.45	-978.73	-1038.32	-1104.00	-1145.05
U, CAL/G	-503.44	-603.71	-624.79	-763.50	-853.03	-930.59	-1016.92	-1071.43	-1117.81	-1168.28	-1199.43
G, CAL/G	-7174.98	-6756.27	-6661.09	-5962.14	-5440.49	-4945.55	-4349.57	-3946.28	-3582.99	-3161.82	-2885.96
S, CAL/(G)(K)	2.7159	2.7159	2.7159	2.7159	2.7159	2.7159	2.7159	2.7159	2.7159	2.7159	2.7159
M, MOL WT	23.226	23.315	23.330	23.398	23.416	23.422	23.423	23.424	23.424	23.424	23.424
(DLV/DLP)T	-1.00313	-1.00163	-1.00138	-1.00034	-1.00009	-1.00002	-1.00000	1.00000	-1.00000	-1.00000	-1.00000
(DLV/DLT)P	1.0821	1.0473	1.0411	1.0122	1.0038	1.0009	1.0001	1.0000	1.0000	1.0000	1.0000
CP, CAL/(G)(K)	0.6752	0.5972	0.5818	0.4953	0.4558	0.4303	0.4060	0.3902	0.3751	0.3575	0.3461
GAMMA (S)	1.1699	1.1833	1.1867	1.2126	1.2308	1.2462	1.2642	1.2779	1.2922	1.3111	1.3248
SON VEL,M/SEC	1030.7	993.4	985.1	922.7	872.9	821.6	753.9	704.0	655.6	593.8	549.0
MACH NUMBER	0.000	1.000	1.110	1.743	2.144	2.526	3.029	3.419	3.826	4.405	4.882

PERFORMANCE PARAMETERS

AE/AT	1.0000	1.0108	1.4750	2.2357	3.5284	6.6546	10.891	17.923	34.749	57.373
CSTAR, FT/SEC	4854	4854	4854	4854	4854	4854	4854	4854	4854	4854
CF	0.671	0.739	1.087	1.265	1.403	1.543	1.627	1.695	1.768	1.812
IVAC,LB-SEC/LB	186.9	187.8	208.5	224.6	238.2	252.9	261.9	269.3	277.2	282.0
ISP, LB-SEC/LB	101.3	111.5	164.0	190.9	211.6	232.8	245.4	255.8	266.7	273.3

MOLE FRACTIONS

H	0.00070	0.00026	0.00020	0.00002	0.00000	0.00000	0.00000	0.00000	0.00000	0.00000	0.00000
HO2	0.00006	0.00003	0.00003	0.00001	0.00000	0.00000	0.00000	0.00000	0.00000	0.00000	0.00000
H2	0.00390	0.00188	0.00156	0.00029	0.00005	0.00001	0.00000	0.00000	0.00000	0.00000	0.00000
H2O	0.49180	0.49978	0.50118	0.50759	0.50939	0.50998	0.51014	0.51015	0.51015	0.51015	0.51015
NO	0.01224	0.00866	0.00794	0.00374	0.00180	0.00073	0.00017	0.00004	0.00001	0.00000	0.00000
NO2	0.00002	0.00001	0.00001	0.00001	0.00000	0.00000	0.00000	0.00000	0.00000	0.00000	0.00000
N2	0.35249	0.35566	0.35625	0.35941	0.36066	0.36128	0.36159	0.36165	0.36167	0.36167	0.36168
O	0.00225	0.00109	0.00090	0.00017	0.00003	0.00000	0.00000	0.00000	0.00000	0.00000	0.00000
OH	0.01952	0.01193	0.01051	0.00340	0.00109	0.00026	0.00002	0.00000	0.00000	0.00000	0.00000
O2	0.11702	0.12069	0.12141	0.12537	0.12697	0.12773	0.12808	0.12815	0.12817	0.12817	0.12817

ELEMENTS	GRAM-ATOM/100 GRAMS	INGRED NO.	PROPELLANT INGREDIENTS	PER CENT	DEL HF	SUM IS	1.000
HYDROGEN	1.88417	245	POLYSTYRENE	24.5300	7681.0		
CARBON	1.88417	268	OXYGEN (LIQUID @ 76.5 K)	75.4700	-10166.0		
OXYGEN	4.71688						

DENSITY 1.1193 GM/CC .04044 LB/CU IN

EQUILIBRIUM COMPOSITION

	CHAMBER	THROAT	EXIT	EXIT	EXIT	EXIT	EXIT	EXIT
PRESSURE LB/SQ IN	20.00000	11.16201	14.70069	10.00000	4.00000	2.00000	1.00000	.40000
TEMPERATURE (K)	3191.	3063.	3123.	3041.	2862.	2740.	2627.	2489.
TEMPERATURE (F)	5284.	5054.	5161.	5013.	4691.	4471.	4268.	4021.
ENTHALPY, KCAL/100 GM	-5.79	-19.33	-13.03	-21.79	-41.35	-55.07	-67.97	-83.88
HT CONT, CAL/GRAM	1036.99	987.04	1009.51	977.47	907.02	859.06	814.98	761.81
ENTROPY, CAL/100GM(K)	263.27	263.27	263.27	263.27	263.27	263.27	263.27	263.27
MOL WT P, GM/MOL	26.53	27.01	26.78	27.10	27.83	28.38	28.92	29.62
MOL WT G, GM/MOL	26.53	27.01	26.78	27.10	27.83	28.38	28.92	29.62
MOLES GAS	3.769	3.702	3.734	3.691	3.593	3.524	3.458	3.377
TOTAL MOLES	3.769	3.702	3.734	3.691	3.593	3.524	3.458	3.377
CPP, BTU/(MOL)(R)	10.5020	10.6687	10.5890	10.6983	10.9513	11.1376	11.3190	11.5512
CPG, BTU/(MOL)(R)	10.5020	10.6687	10.5890	10.6983	10.9513	11.1376	11.3190	11.5512
CPP, BTU/(LB)(R)	.3958	.3950	.3954	.3948	.3935	.3925	.3914	.3900
CPG, BTU/(LB)(R)	.3958	.3950	.3954	.3948	.3935	.3925	.3914	.3900
ISP, SEC	.0	108.5	79.4	118.0	175.9	207.1	232.6	260.7
ISP(V), SEC	.0	198.9	206.3	200.2	226.4	247.4	266.4	288.5
CSTAR, FT/SEC	.00	5207.15	5207.15	5207.15	5207.15	5207.15	5207.15	5207.15
CF	.00000	.67059	.49055	.72909	1.08687	1.27951	1.43721	1.61061
CF(V)	.00000	1.22869	1.27490	1.23699	1.39909	1.52849	1.64578	1.78284
EXPANSION COEFFICIENT	.000	1.075	1.076	1.075	1.073	1.071	1.069	1.068
EXIT VELOCITY, FT/SEC	.00	3491.87	2554.36	3796.47	5659.47	6662.59	7483.79	8386.70
GAS DENSITY, LB/CU IN	4.9860E-06	2.9510E-06	3.7805E-06	2.6720E-06	1.1663E-06	6.2119E-07	3.3010E-07	1.4268E-07
AREA, SQ IN	.0000	8.0922	8.6350	8.2201	12.6327	20.1481	33.7543	69.6844
EXPANSION RATIO	.0000	1.0000	1.0671	1.0158	1.5611	2.4898	4.1712	8.6113

MOLES PRODUCTS / 100 GRAMS PROPELLANT

C	4.3460E-10	1.4859E-10	2.4737E-10	1.2175E-10	2.2561E-11	6.2560E-12	1.7167E-12	3.0343E-13
CH	3.3385E-11	1.0170E-11	1.7877E-11	8.1508E-12	1.2574E-12	3.0330E-13	7.2392E-14	1.0645E-14
CHO	4.1307E-06	2.2547E-06	3.0054E-06	2.0127E-06	7.6999E-07	3.6885E-07	1.7509E-07	6.4313E-08
CO	1.1357E+00	1.0765E+00	1.1049E+00	1.0657E+00	9.7229E-01	9.0157E-01	8.3118E-01	7.3914E-01
CO2	7.4843E-01	8.0768E-01	7.7927E-01	8.1851E-01	9.1188E-01	9.8260E-01	1.0530E+00	1.1450E+00
H	1.5716E-01	1.4136E-01	1.4878E-01	1.3871E-01	1.1738E-01	1.0320E-01	9.0428E-02	7.5394E-02
HO	2.9896E-01	2.7094E-01	2.8411E-01	2.6597E-01	2.2595E-01	1.9840E-01	1.7317E-01	1.4323E-01
H2	1.1960E-01	1.1331E-01	1.1632E-01	1.1219E-01	1.0266E-01	9.5672E-02	8.8887E-02	8.0211E-02
H2O	5.9435E-01	6.2258E-01	6.0927E-01	6.2751E-01	6.6773E-01	6.9560E-01	7.2138E-01	7.5255E-01
H2O2	5.7857E-06	3.7572E-06	4.6111E-06	3.4614E-06	1.7301E-06	1.0131E-06	5.8796E-07	2.8243E-07
O	2.3900E-01	2.0855E-01	2.2271E-01	2.0342E-01	1.6344E-01	1.3771E-01	1.1533E-01	9.0181E-02
O2	4.7585E-01	4.6139E-01	4.6857E-01	4.5856E-01	4.3181E-01	4.0917E-01	3.8490E-01	3.5085E-01
HO2	1.2132E-04	8.4424E-05	1.0031E-04	7.8824E-05	4.3916E-05	2.7901E-05	1.7553E-05	9.3632E-06
H2O (L)	0.0000	0.0000	0.0000	0.0000	0.0000	0.0000	0.0000	0.0000
C (S)	0.0000	0.0000	0.0000	0.0000	0.0000	0.0000	0.0000	0.0000

FROZEN COMPOSITION									
PRESSURE LB/SQ IN	20.00000	11.14881	10.70069	10.00000	4.00000	2.00000	1.00000	.50000	
TEMPERATURE (K)	3191.	2856.	3010.	2797.	2343.	2045.	1780.	1474.	
TEMPERATURE (F)	5284.	4680.	4959.	4575.	3757.	3221.	2744.	2194.	
ENTHALPY, KCAL/100 GM	-5.79	19.01	12.94	-21.31	38.91	50.28	60.20	71.34	
HT CONT, CAL/GRAM	1036.99	904.76	965.51	881.74	705.78	592.06	492.90	381.49	
ENTROPY, CAL/100GM(K)	263.27	263.27	263.27	263.27	263.27	263.27	263.27	263.27	
MOL WT P, GM/MOL	26.53	26.53	26.53	26.53	26.53	26.53	26.53	26.53	
MOL WT G, GM/MOL	26.53	26.53	26.53	26.53	26.53	26.53	26.53	26.53	
MOLES GAS	3.769	3.769	3.769	3.769	3.769	3.769	3.769	3.769	
TOTAL MOLES	3.769	3.769	3.769	3.769	3.769	3.769	3.769	3.769	
CPP, BTU/(MOL)(R)	10.5020	10.3949	10.4470	10.3738	10.1798	10.0408	9.8151	9.5036	
CPG, BTU/(MOL)(R)	10.5020	10.3949	10.4470	10.3738	10.1798	10.0408	9.8151	9.5036	
CPP, BTU/(LB)(R)	.3958	.3918	.3938	.3910	.3837	.3785	.3700	.3582	
CPG, BTU/(LB)(R)	.3958	.3918	.3938	.3910	.3837	.3785	.3700	.3582	
ISP, SEC	.0	107.3	78.9	116.2	169.8	196.8	217.6	238.8	
ISP(V), SEC	.0	194.0	203.2	194.6	214.7	230.6	244.2	258.9	
CSTAR, FT/SEC	.00	5006.47	5006.47	5006.47	5006.47	5006.47	5006.47	5006.47	
CF	.00000	.68932	.50682	.74692	1.09098	1.26447	1.39830	1.53479	
CF(V)	.00000	1.24676	1.30604	1.25077	1.37993	1.48209	1.56960	1.66405	
EXPANSION COEFFICIENT	.000	1.234	1.233	1.235	1.238	1.239	1.242	1.246	
EXIT VELOCITY, FT/SEC	.00	3451.05	2537.37	3739.42	5461.93	6330.54	7000.54	7683.90	
GAS DENSITY, LB/CU IN	4.9860E-06	3.1056E-06	3.8847E-06	2.8442E-06	1.3582E-06	7.7797E-07	4.4687E-07	2.1582E-07	
AREA, SQ IN	.0000	7.7803	8.4597	7.8403	11.2410	16.9314	26.6552	50.2823	
EXPANSION RATIO	.0000	1.0000	1.0873	1.0077	1.4448	2.1762	3.4260	6.4628	

ELEMENTS	GRAM-ATOM/100 GRAMS	INGRED NO.	PROPELLANT INGREDIENTS	PER CENT	DEL HF	SUM IS	1.000
HYDROGEN	1.36800	245	POLYSTYRENE	17.8100	7681.0		
CARBON	1.36800	268	OXYGEN (LIQUID @ 76.5 K)	82.1900	-10166.0		
OXYGEN	5.13688						

DENSITY 1.1249 GM/CC .04064 LB/CU IN

EQUILIBRIUM COMPOSITION

	CHAMBER	THROAT	EXIT	EXIT	EXIT	EXIT	EXIT	EXIT
PRESSURE LB/SQ IN	20.00000	11.19354	14.70069	10.00000	4.00000	2.00000	1.00000	.40000
TEMPERATURE (K)	3072.	2948.	3005.	2925.	2748.	2625.	2509.	2363.
TEMPERATURE (F)	5070.	4847.	4950.	4805.	4487.	4265.	4055.	3794.
ENTHALPY, KCAL/100 GM	-6.99	-18.80	-13.34	-21.02	-38.19	-50.23	-61.53	-75.45
HT CONT, CAL/GRAM	930.53	884.62	905.64	876.32	811.06	765.83	723.39	670.48
ENTROPY, CAL/100GM(K)	244.22	244.22	244.22	244.22	244.22	244.22	244.22	244.22
MOL WT P, GM/MOL	29.13	29.62	29.39	29.71	30.45	31.00	31.53	32.20
MOL WT G, GM/MOL	29.13	29.62	29.39	29.71	30.45	31.00	31.53	32.20
MOLES GAS	3.432	3.376	3.402	3.366	3.284	3.226	3.172	3.106
TOTAL MOLES	3.432	3.377	3.403	3.366	3.284	3.226	3.172	3.106
CPP, BTU/(MOL)(R)	10.8155	10.9678	10.8965	10.9975	11.2273	11.3921	11.5476	11.7352
CPG, BTU/(MOL)(R)	10.8155	10.9678	10.8965	10.9975	11.2273	11.3921	11.5476	11.7352
CPP, BTU/(LB)(R)	.3712	.3703	.3708	.3701	.3687	.3675	.3663	.3645
CPG, BTU/(LB)(R)	.3712	.3703	.3708	.3701	.3687	.3675	.3663	.3645
ISP, SEC	.0	101.4	74.3	110.5	164.8	194.0	217.9	244.1
ISP(V), SEC	.0	186.3	193.2	187.5	212.1	231.7	249.4	270.1
CSTAR, FT/SEC	.00	4878.45	4878.45	4878.45	4878.45	4878.45	4878.45	4878.45
CF	.00000	.66874	.49031	.72881	1.08662	1.27923	1.43678	1.60966
CF(V)	.00000	1.22842	1.27443	1.23670	1.39886	1.52809	1.64498	1.78108
EXPANSION COEFFICIENT	.000	1.076	1.077	1.076	1.074	1.073	1.073	1.072
EXIT VELOCITY, FT/SEC	.00	3262.41	2391.94	3555.46	5301.02	6240.67	7009.25	7852.65
GAS DENSITY, LB/CU IN	5.6872E-06	3.3714E-06	4.3105E-06	3.0455E-06	1.3290E-06	7.0823E-07	3.7685E-07	1.6342E-07
AREA, SQ IN	.0000	7.5814	8.0876	7.7010	11.8360	18.8666	31.5686	64.9788
EXPANSION RATIO	.0000	1.0000	1.0668	1.0158	1.5612	2.4886	4.1640	8.5709

MOLES PRODUCTS / 100 GRAMS PROPELLANT

C	4.0875E-11	1.2439E-11	2.1828E-11	9.8230E-12	1.4055E-12	3.0271E-13	6.0409E-14	6.0793E-15
CH	2.3960E-12	6.4498E-13	1.1990E-12	4.9725E-13	5.8438E-14	1.0826E-14	1.8555E-15	1.5237E-16
CHO	1.0185E-06	5.1679E-07	7.1227E-07	4.5163E-07	1.4824E-07	6.1413E-08	2.4368E-08	6.5607E-09
CO	5.5026E-01	4.9797E-01	5.2256E-01	4.8770E-01	4.0652E-01	3.4669E-01	2.8880E-01	2.1616E-01
CO2	8.1774E-01	8.7003E-01	8.4544E-01	8.8030E-01	9.6148E-01	1.0213E+00	1.0792E+00	1.1518E+00
H	6.5191E-02	5.6702E-02	6.0611E-02	5.5101E-02	4.3307E-02	3.5384E-02	2.8242E-02	1.9920E-02
HO	2.4968E-01	2.2433E-01	2.3610E-01	2.1950E-01	1.8274E-01	1.5718E-01	1.3347E-01	1.0474E-01
H2	4.4218E-02	4.0492E-02	4.2247E-02	3.9758E-02	3.3935E-02	2.9593E-02	2.5319E-02	1.9798E-02
H2O	4.8226E-01	5.0293E-01	4.9332E-01	5.0689E-01	5.3701E-01	5.5810E-01	5.7781E-01	6.0186E-01
H2O2	6.0210E-06	3.9112E-06	4.7938E-06	3.5932E-06	1.7911E-06	1.0455E-06	6.0334E-07	2.8561E-07
O	2.2690E-01	1.9650E-01	2.1042E-01	1.9086E-01	1.4987E-01	1.2307E-01	9.9394E-02	7.2273E-02
O2	9.9599E-01	9.8743E-01	9.9166E-01	9.8556E-01	9.6883E-01	9.5457E-01	9.3947E-01	9.1906E-01
HO2	1.5851E-04	1.1080E-04	1.3122E-04	1.0326E-04	5.7768E-05	3.6771E-05	2.3115E-05	1.2212E-05
H2O (L)	0.0000	0.0000	0.0000	0.0000	0.0000	0.0000	0.0000	0.0000
C (S)	0.0000	0.0000	0.0000	0.0000	0.0000	0.0000	0.0000	0.0000

FROZEN COMPOSITION									
PRESSURE LB/SQ IN	20.00000	11.18051	14.70069	10.00000	4.00000	2.00000	1.00000	.40000	
TEMPERATURE (K)	3072.	2759.	2903.	2703.	2276.	1994.	1742.	1451.	
TEMPERATURE (F)	5070.	4507.	4765.	4405.	3636.	3129.	2676.	2152.	
ENTHALPY, KCAL/100 GM	-6.99	-18.54	-13.26	-20.62	-36.14	-46.22	-55.04	-65.06	
HT CONT, CAL/GRAM	930.53	814.97	867.82	794.18	638.96	538.19	450.00	350.45	
ENTROPY, CAL/100GM(K)	244.22	244.22	244.22	244.22	244.22	244.22	244.22	244.22	
MOL WT P, GM/MOL	29.13	29.13	29.13	29.13	29.13	29.13	29.13	29.13	
MOL WT G, GM/MOL	29.13	29.13	29.13	29.13	29.13	29.13	29.13	29.13	
MOLES GAS	3.432	3.432	3.432	3.432	3.432	3.432	3.432	3.432	
TOTAL MOLES	3.432	3.432	3.432	3.432	3.432	3.432	3.432	3.432	
CPP, BTU/(MOL)(R)	10.8155	10.7025	10.7568	10.6798	10.4787	10.3176	10.1051	9.7969	
CPG, BTU/(MOL)(R)	10.8155	10.7025	10.7568	10.6798	10.4787	10.3176	10.1051	9.7969	
CPP, BTU/(LB)(R)	.3712	.3674	.3692	.3666	.3597	.3541	.3468	.3363	
CPG, BTU/(LB)(R)	.3712	.3674	.3692	.3666	.3597	.3541	.3468	.3363	
ISP, SEC	.0	100.3	73.9	108.9	159.3	184.8	204.5	224.7	
ISP(V), SEC	.0	181.9	190.5	182.5	201.7	216.8	229.8	243.8	
CSTAR, FT/SEC	00	4698.80	4698.80	4698.80	4698.80	4698.80	4698.80	4698.80	
CF	.00000	.68661	.50581	.74581	1.09063	1.26515	1.40014	1.53834	
CF(V)	.00000	1.24564	1.30412	1.24990	1.38085	1.48434	1.57321	1.66954	
EXPANSION COEFFICIENT	.000	1.226	1.226	1.227	1.229	1.231	1.234	1.237	
EXIT VELOCITY, FT/SEC	.00	3226.26	2376.72	3504.41	5124.66	5944.69	6578.99	7328.37	
GAS DENSITY, LB/CU IN	5.6872E-06	3.5395E-06	4.4239E-06	3.2322E-06	1.5356E-06	8.7638E-07	5.0146E-07	2.4084E-07	
AREA, SQ IN	.0000	7.3022	7.9307	7.3619	10.5962	16.0059	25.2759	47.8987	
EXPANSION RATIO	.0000	1.0000	1.0861	1.0082	1.4511	2.1919	3.4614	6.5595	

ELEMENTS	GRAM-ATOM/100 GRAMS	INGRED NO.	PROPELLANT INGREDIENTS	PER CENT	DEL HF	SUM IS	1.000
HYDROGEN	3.45160	503	DMPSP (SILICONE)	34.0200	-147000.0		
CARBON	1.15052	268	OXYGEN (LIQUID @ 76.5 K)	65.9800	-10166.0		
OXYGEN	4.41136						
SILICON	.43144						

DENSITY 1.0882 GM/CC .03932 LB/CU IN

EQUILIBRIUM COMPOSITION

	CHAMBER	THROAT	EXIT	EXIT	EXIT	EXIT	EXIT	EXIT
PRESSURE LB/SQ IN	20.00000	11.25797	14.70069	10.00000	4.00000	2.00000	1.00000	.40000
TEMPERATURE (K)	2931.	2842.	2882.	2824.	2694.	2602.	2516.	2409.
TEMPERATURE (F)	4816.	4656.	4728.	4623.	4388.	4224.	4069.	3876.
ENTHALPY, KCAL/100 GM	-56.72	-68.96	-63.35	-71.42	-89.58	-102.46	-114.66	-129.83
HT CONT, CAL/GRAM	1007.02	973.28	991.24	968.19	919.03	881.08	848.23	806.66
ENTROPY, CAL/100GM(K)	265.54	265.54	265.54	265.54	265.54	265.54	265.54	265.54
MOL WT P, GM/MOL	26.54	26.76	26.66	26.80	27.15	27.39	27.63	27.95
MOL WT G, GM/MOL	26.38	26.26	26.31	26.23	26.06	25.94	25.82	25.69
MOLES GAS	3.751	3.683	3.712	3.668	3.566	3.496	3.428	3.343
TOTAL MOLES	3.768	3.737	3.751	3.731	3.684	3.651	3.619	3.578
CPP, BTU/(MOL)(R)	11.4773	11.5984	11.5472	11.6257	11.8086	11.9334	12.0580	12.2124
CPG, BTU/(MOL)(R)	11.4350	11.4661	11.4535	11.4735	11.5214	11.5536	11.5870	11.6291
CPP, BTU/(LB)(R)	.4325	.4335	.4331	.4337	.4350	.4357	.4364	.4370
CPG, BTU/(LB)(R)	.4335	.4366	.4353	.4374	.4422	.4454	.4487	.4527
ISP, SEC	.0	103.2	76.0	113.1	169.1	199.5	224.5	252.2
ISP(V), SEC	.0	190.9	197.7	192.3	218.2	238.9	257.7	279.8
CSTAR, FT/SEC	.00	5009.12	5009.12	5009.12	5009.12	5009.12	5009.12	5009.12
CF	.00000	.66306	.48805	.72640	1.08620	1.28144	1.44221	1.62009
CF(V)	.00000	1.22595	1.26982	1.23490	1.40154	1.53462	1.65544	1.79732
EXPANSION COEFFICIENT	.000	1.057	1.057	1.057	1.055	1.054	1.054	1.053
EXIT VELOCITY, FT/SEC	.00	3321.33	2444.72	3638.61	5440.88	6418.87	7224.21	8115.20
GAS DENSITY, LB/CU IN	5.3972E-06	3.1191E-06	4.0235E-06	2.7854E-06	1.1602E-06	5.9773E-07	3.0775E-07	1.2789E-07
AREA, SQ IN	.0000	7.7844	8.2793	7.9168	12.2738	19.7091	33.1967	68.9844
EXPANSION RATIO	.0000	1.0000	1.0636	1.0170	1.5767	2.5319	4.2645	8.8619

MOLES PRODUCTS / 100 GRAMS PROPELLANT

C	1.7632E-11	8.0404E-12	1.1545E-11	6.8217E-12	1.9368E-12	7.4644E-13	2.8398E-13	7.7927E-14
CO	5.3423E-01	5.2300E-01	5.2810E-01	5.2062E-01	5.0279E-01	4.8950E-01	4.7600E-01	4.5804E-01
CO2	6.1630E-01	6.2752E-01	6.2242E-01	6.2990E-01	6.4773E-01	6.6102E-01	6.7452E-01	6.9248E-01
H	8.7029E-02	8.5335E-02	8.6008E-02	8.4906E-02	8.2136E-02	8.0134E-02	7.7840E-02	7.4546E-02
HO	2.2304E-01	2.0525E-01	2.1311E-01	2.0155E-01	1.7561E-01	1.5793E-01	1.4112E-01	1.2066E-01
H2	1.7144E-01	1.7046E-01	1.7088E-01	1.7025E-01	1.6883E-01	1.6789E-01	1.6695E-01	1.6577E-01
H2O	1.3993E+00	1.4100E+00	1.4054E+00	1.4123E+00	1.4281E+00	1.4389E+00	1.4494E+00	1.4624E+00
O	7.0984E-02	6.5170E-02	6.7666E-02	6.3908E-02	5.5349E-02	4.9540E-02	4.3872E-02	3.6889E-02
OSI	3.8083E-01	3.4838E-01	3.6223E-01	3.4118E-01	2.9244E-01	2.5909E-01	2.2624E-01	1.8585E-01
O2	2.3458E-01	2.1919E-01	2.2582E-01	2.1574E-01	1.9181E-01	1.7485E-01	1.5767E-01	1.3568E-01
O2SI	3.2999E-02	2.8314E-02	3.0331E-02	2.7363E-02	2.1149E-02	1.7313E-02	1.3958E-02	1.0306E-02
SI	3.3608E-06	3.4581E-06	3.4040E-06	3.4705E-06	3.6073E-06	3.7106E-06	3.7765E-06	3.8173E-06
SI2	5.1358E-14	1.6301E-14	2.7605E-14	1.2789E-14	1.9994E-15	4.8761E-16	1.1493E-16	1.6320E-17
H2O (L)	0.0000	0.0000	0.0000	0.0000	0.0000	0.0000	0.0000	0.0000
O2SI [C]	0.0000	0.0000	0.0000	0.0000	0.0000	0.0000	0.0000	0.0000
SI [L]	0.0000	0.0000	0.0000	0.0000	0.0000	0.0000	0.0000	0.0000
SI [C]	0.0000	0.0000	0.0000	0.0000	0.0000	0.0000	0.0000	0.0000
O2SI [L]	1.7587E-02	5.4720E-02	3.8864E-02	6.2874E-02	1.1783E-01	1.5501E-01	1.9122E-01	2.3526E-01
O2SI [C]	0.0000	0.0000	0.0000	0.0000	0.0000	0.0000	0.0000	0.0000
C (S)	0.0000	0.0000	0.0000	0.0000	0.0000	0.0000	0.0000	0.0000

FROZEN COMPOSITION								
PRESSURE LB/SQ IN	20.00000	11.24380	14.70069	10.00000	4.00000	2.00000	1.00000	.40000
TEMPERATURE (K)	2931.	2651.	2778.	2597.	2208.	1948.	1714.	1439.
TEMPERATURE (F)	4816.	4312.	4540.	4215.	3515.	3047.	2625.	2131.
ENTHALPY, KCAL/100 GM	-56.72	-68.69	-63.26	-70.98	-87.36	98.08	107.53	118.28
HT CONT, CAL/GRAM	1007.02	887.33	941.56	864.40	700.61	593.36	498.86	391.40
ENTROPY, CAL/100GM(K)	265.54	265.54	265.54	265.54	265.54	265.54	265.54	265.54
MOL WT P, GM/MOL	26.54	26.54	26.54	26.54	26.54	26.54	26.54	26.54
MOL WT G, GM/MOL	26.38	26.38	26.38	26.38	26.38	26.38	26.38	26.38
MOLES GAS	3.751	3.751	3.751	3.751	3.751	3.751	3.751	3.751
TOTAL MOLES	3.768	3.768	3.768	3.768	3.768	3.768	3.768	3.768
CPP, BTU/(MOL)(R)	11.4773	11.3315	11.4009	11.3001	11.0351	10.8193	10.5639	10.2005
CPG, BTU/(MOL)(R)	11.4350	11.2885	11.3582	11.2570	10.9907	10.7739	10.5173	10.1636
CPP, BTU/(LB)(R)	.4325	.4270	.4296	.4258	.4158	.4077	.3981	.3844
CPG, BTU/(LB)(R)	.4335	.4279	.4306	.4267	.4166	.4084	.3987	.3853
ISP, SEC	.0	102.1	75.5	111.4	163.3	189.7	210.3	231.4
ISP(V), SEC	.0	186.3	194.8	187.0	207.1	223.0	236.7	251.6
CSTAR, FT/SEC	.00	4820.09	4820.09	4820.09	4820.09	4820.09	4820.09	4820.09
CF	.00000	.68120	.50378	.74359	1.08093	1.26639	1.40361	1.54490
CF(V)	.00000	1.24339	1.30026	1.24816	1.38262	1.48864	1.58000	1.67949
EXPANSION COEFFICIENT	.000	1.211	1.211	1.211	1.213	1.216	1.218	1.222
EXIT VELOCITY, FT/SEC	.00	3283.44	2428.27	3584.18	5253.58	6104.14	6765.52	7446.58
GAS DENSITY, LB/CU IN	5.3972E-06	3.3545E-06	4.1860E-06	3.0452E-06	1.4326E-06	8.1190E-07	4.6148E-07	2.1980E-07
AREA, SQ IN	.0000	7.4907	8.1169	7.5592	10.9619	16.6477	26.4255	50.4072
EXPANSION RATIO	.0000	1.0000	1.0836	1.0091	1.4634	2.2225	3.5278	6.7293

ELEMENTS	GRAM ATOM/100 GRAMS	INGRED NO.	PROPELLANT INGREDIENTS	PER CENT	DEL HF	SUM IS 1.000
HYDROGEN	2.59530	503	DMPSP (SILICONE)	25.5800	-147000.0	
CARBON	.86509	268	OXYGEN (LIQUID @ 76.5 K)	74.4200	-10166.0	
OXYGEN	4.86750					
SILICON	.32441					

DENSITY 1.1006 GM/CC .03976 LB/CU IN

EQUILIBRIUM COMPOSITION

	CHAMBER	THROAT	EXIT	EXIT	EXIT	EXIT	EXIT	EXIT
PRESSURE LB/SQ IN	20.00000	11.28580	14.70069	10.00000	4.00000	2.00000	1.00000	.40000
TEMPERATURE (K)	2935.	2844.	2886.	2826.	2691.	2596.	2505.	2392.
TEMPERATURE (F)	4824.	4660.	4735.	4626.	4384.	4213.	4050.	3845.
ENTHALPY, KCAL/100 GM	-45.17	-56.31	-51.23	-58.59	-75.18	-86.93	-98.05	-111.87
HT CONT, CAL/GRAM	951.95	919.65	933.45	911.79	861.57	825.93	792.20	748.02
ENTROPY, CAL/100GM(K)	247.94	247.94	247.94	247.94	247.94	247.94	247.94	247.94
MOL WT P, GM/MOL	28.41	28.66	28.54	28.71	29.10	29.39	29.69	30.07
MOL WT G, GM/MOL	27.49	27.45	27.47	27.44	27.41	27.42	27.44	27.52
MOLES GAS	3.420	3.359	3.388	3.348	3.259	3.196	3.137	3.064
TOTAL MOLES	3.520	3.489	3.504	3.483	3.436	3.402	3.368	3.325
CPP, BTU/(MOL)(R)	11.5392	11.6602	11.6030	11.6827	11.8617	11.9905	12.1140	12.2648
CPG, BTU/(MOL)(R)	11.2779	11.3192	11.2992	11.3268	11.3920	11.4425	11.4946	11.5638
CPP, BTU/(LB)(R)	.4062	.4068	.4065	.4069	.4076	.4079	.4080	.4078
CPG, BTU/(LB)(R)	.4103	.4124	.4114	.4127	.4155	.4174	.4189	.4202
ISP, SEC	.0	98.5	72.6	108.1	161.6	190.6	214.5	240.9
ISP(V), SEC	.0	182.3	189.0	183.7	208.5	228.3	246.2	267.2
CSTAR, FT/SEC	.00	4783.15	4783.15	4783.15	4783.15	4783.15	4783.15	4783.15
CF	.00000	.66224	.48849	.72702	1.08702	1.28228	1.44298	1.62058
CF(V)	.00000	1.22653	1.27124	1.23595	1.40261	1.53536	1.65597	1.79744
EXPANSION COEFFICIENT	.000	1.058	1.058	1.058	1.057	1.056	1.056	1.055
EXIT VELOCITY, FT/SEC	.00	3167.58	2336.53	3477.46	5199.38	6133.34	6901.97	7751.45
GAS DENSITY, LB/CU IN	5.6154E-06	3.2658E-06	4.1951E-06	2.9120E-06	1.2217E-06	6.3332E-07	3.2843E-07	1.3800E-07
AREA, SQ IN	.0000	7.4332	7.9158	7.5660	11.7291	18.8120	31.6648	65.7351
EXPANSION RATIO	.0000	1.0000	1.0649	1.0179	1.5779	2.5308	4.2599	8.8434

MOLES PRODUCTS / 100 GRAMS PROPELLANT

C	5.1135E-12	2.1545E-12	3.2240E-12	1.7977E-12	4.3817E-13	1.4577E-13	4.6610E-14	9.6094E-15
CO	2.7642E-01	2.6280E-01	2.6924E-01	2.6005E-01	2.3784E-01	2.2041E-01	2.0222E-01	1.7715E-01
CO2	5.8866E-01	6.0228E-01	5.9584E-01	6.0503E-01	6.2724E-01	6.4468E-01	6.6286E-01	6.8793E-01
H	5.4221E-02	5.2000E-02	5.3083E-02	5.1582E-02	4.7885E-02	4.4831E-02	4.1474E-02	3.6618E-02
HO	2.5774E-01	2.3954E-01	2.4795E-01	2.3594E-01	2.0892E-01	1.8961E-01	1.7105E-01	1.4773E-01
H2	7.0980E-02	6.8523E-02	6.9703E-02	6.8034E-02	6.3888E-02	6.0479E-02	5.6757E-02	5.1356E-02
H2O	1.0707E+00	1.0834E+00	1.0774E+00	1.0858E+00	1.1054E+00	1.1199E+00	1.1346E+00	1.1541E+00
O	1.2337E-01	1.1527E-01	1.1907E-01	1.1371E-01	1.0148E-01	9.2457E-02	8.3492E-02	7.1839E-02
OSI	1.9355E-01	1.6857E-01	1.8026E-01	1.6392E-01	1.2823E-01	1.0369E-01	8.1294E-02	5.5820E-02
O2	7.5336E-01	7.4088E-01	7.4680E-01	7.3851E-01	7.1942E-01	7.0531E-01	6.9144E-01	6.7391E-01
O2SI	3.1110E-02	2.6237E-02	2.8456E-02	2.5333E-02	1.8925E-02	1.4871E-02	1.1415E-02	7.7248E-03
SI	9.1850E-07	8.7234E-07	8.9657E-07	8.6433E-07	7.7635E-07	6.9535E-07	6.0168E-07	4.6741E-07
SI2	4.3368E-15	1.1593E-15	2.1519E-15	8.8036E-16	9.9401E-17	1.7698E-17	2.8796E-18	2.2247E-19
H2O (L)	0.0000	0.0000	0.0000	0.0000	0.0000	0.0000	0.0000	0.0000
O2SI [C]	0.0000	0.0000	0.0000	0.0000	0.0000	0.0000	0.0000	0.0000
SI [L]	0.0000	0.0000	0.0000	0.0000	0.0000	0.0000	0.0000	0.0000
SI [C]	0.0000	0.0000	0.0000	0.0000	0.0000	0.0000	0.0000	0.0000
O2SI [L]	9.9724E-02	1.2958E-01	1.1567E-01	1.3513E-01	1.7724E-01	2.0583E-01	2.3168E-01	2.6084E-01
O2SI [C]	0.0000	0.0000	0.0000	0.0000	0.0000	0.0000	0.0000	0.0000
C (S)	0.0000	0.0000	0.0000	0.0000	0.0000	0.0000	0.0000	0.0000

FROZEN COMPOSITION								
PRESSURE LB/SQ IN	20.00000	11.27384	14.70069	10.00000	4.00000	2.00000	1.00000	.50000
TEMPERATURE (K)	2935.	2667.	2789.	2613.	2239.	1979.	1749.	1478.
TEMPERATURE (F)	4824.	4340.	4560.	4244.	3568.	3102.	2688.	2201.
ENTHALPY, KCAL/100 GM	-45.17	-56.08	51.16	-58.23	73.29	83.20	91.97	102.00
MT CONT, CAL/GRAM	951.95	842.86	892.06	821.35	670.71	571.60	483.89	383.59
ENTROPY, CAL/100GM(K)	247.94	247.94	247.94	247.94	247.94	247.94	247.94	247.94
MOL WT P, GM/MOL	28.41	28.41	28.41	28.41	28.41	28.41	28.41	28.41
MOL WT G, GM/MOL	27.49	27.49	27.49	27.49	27.49	27.49	27.49	27.49
MOLES GAS	3.420	3.420	3.420	3.420	3.420	3.420	3.420	3.420
TOTAL MOLES	3.520	3.520	3.520	3.520	3.520	3.520	3.520	3.520
CPP, BTU/(MOL)(R)	11.5392	11.4092	11.4712	11.3804	11.1433	10.9490	10.7237	10.3392
CPG, BTU/(MOL)(R)	11.2779	11.1441	11.2079	11.1145	10.8705	10.6706	10.4387	10.1103
CPP, BTU/(LB)(R)	.4062	.4016	.4038	.4006	.3922	.3854	.3775	.3639
CPG, BTU/(LB)(R)	.4103	.4054	.4078	.4044	.3955	.3882	.3798	.3678
ISP, SEC	.0	97.4	72.2	106.6	156.4	181.9	201.8	222.4
ISP(V), SEC	.0	178.3	186.4	179.1	198.6	214.1	227.4	242.0
CSTAR, FT/SEC	.00	4618.87	4618.87	4618.87	4618.87	4618.87	4618.87	4618.87
CF	.00000	.67865	.50284	.74256	1.08969	1.26722	1.40576	1.54909
CF(V)	.00000	1.24234	1.29847	1.24738	1.38369	1.49121	1.58422	1.68598
EXPANSION COEFFICIENT	.000	1.201	1.199	1.201	1.205	1.207	1.209	1.213
EXIT VELOCITY, FT/SEC	.00	3134.60	2322.54	3429.79	5033.12	5854.14	6493.04	7155.05
GAS DENSITY, LB/CU IN	5.6154E-06	3.4840E-06	4.3440E-06	3.1537E-06	1.4760E-06	8.3299E-07	4.7124E-07	2.2299E-07
AREA, SQ IN	.0000	7.1780	7.7698	7.2471	10.5517	16.0779	25.6194	49.1312
EXPANSION RATIO	.0000	1.0000	1.0824	1.0096	1.4700	2.2399	3.5692	6.8447

ELEMENTS	GRAM-ATOM/100 GRAMS	INGRED NO.	PROPELLANT INGREDIENTS	PER CENT	DEL HF	SUM IS	1.000
HYDROGEN	4.00873	303	NYLON	41.2400	-72683.0		
CARBON	2.18659	268	OXYGEN (LIQUID @ 76.5 K)	58.7600	-10166.0		
NITROGEN	.36440						
OXYGEN	4.03690						

DENSITY 1.1232 GM/CC .04058 LB/CU IN

EQUILIBRIUM COMPOSITION

	CHAMBER	THROAT	EXIT	EXIT	EXIT	EXIT	EXIT	EXIT
PRESSURE LB/SQ IN	20.00000	11.16711	14.70069	10.00000	4.00000	2.00000	1.00000	.40000
TEMPERATURE (K)	2986.	2812.	2895.	2778.	2480.	2235.	1990.	1684.
TEMPERATURE (F)	4915.	4601.	4751.	4540.	4003.	3564.	3122.	2572.
ENTHALPY, KCAL/100 GM	35.95	-51.11	-44.09	-53.85	-75.15	-89.44	-102.19	-116.81
HI CONT, CAL/GRAM	1148.30	1063.04	1103.42	1046.60	903.97	790.23	678.26	543.55
ENTROPY, CAL/100GM(K)	302.26	302.26	302.26	302.26	302.26	302.26	302.26	302.26
MOL WT P, GM/MOL	22.01	22.29	22.16	22.34	22.65	22.78	22.84	22.86
MOL WT G, GM/MOL	22.01	22.29	22.16	22.34	22.65	22.78	22.84	22.86
MOLES GAS	4.544	4.486	4.512	4.477	4.415	4.390	4.378	4.374
TOTAL MOLES	4.544	4.486	4.512	4.477	4.415	4.390	4.378	4.374
CPP, BTU/(MOL)(R)	10.5555	10.6116	10.5896	10.6178	10.6005	10.5020	10.3717	10.0722
CPG, BTU/(MOL)(R)	10.5555	10.6116	10.5896	10.6178	10.6005	10.5020	10.3717	10.0722
CPP, BTU/(LB)(R)	.4796	.4761	.4778	.4753	.4680	.4610	.4541	.4406
CPG, BTU/(LB)(R)	.4796	.4761	.4778	.4753	.4680	.4610	.4541	.4406
ISP, SEC	.0	114.8	84.2	124.8	184.7	215.8	240.1	265.3
ISP(V), SEC	.0	209.8	218.3	210.9	235.9	255.1	271.5	289.3
CSTAR, FT/SEC	.00	5471.07	5471.07	5471.07	5471.07	5471.07	5471.07	5471.07
CF	.00000	.67538	.49507	.73405	1.08608	1.26878	1.41190	1.55989
CF(V)	.00000	1.23374	1.28377	1.24052	1.38740	1.49997	1.59637	1.70106
EXPANSION COEFFICIENT	.000	1.115	1.112	1.116	1.131	1.144	1.157	1.171
EXIT VELOCITY, FT/SEC	.00	3695.08	2708.55	4016.03	5942.02	6941.57	7724.61	8534.26
GAS DENSITY, LB/CU IN	4.4202E-06	2.6542E-06	3.3746E-06	2.4109E-06	1.0955E-06	6.1111E-07	3.4415E-07	1.6282E-07
AREA, SQ IN	.0000	8.5023	9.1231	8.6123	12.8097	19.6571	31.3674	60.0120
EXPANSION RATIO	.0000	1.0000	1.0730	1.0129	1.5066	2.3120	3.6893	7.0583

MOLES PRODUCTS / 100 GRAMS PROPELLANT

C	3.4822E-10	7.9308E-11	1.6349E-10	5.8428E-11	2.8776E-12	1.3857E-13	3.1083E-15	5.8146E-18
CO	1.7018E+00	1.6789E+00	1.6892E+00	1.6751E+00	1.6480E+00	1.6250E+00	1.5907E+00	1.5228E+00
CO2	4.8478E-01	5.0767E-01	4.9743E-01	5.1148E-01	5.3858E-01	5.6162E-01	5.9587E-01	6.6375E-01
H	2.1706E-01	1.6346E-01	1.8877E-01	1.5338E-01	7.4945E-02	3.2448E-02	1.0459E-02	1.4468E-03
H2	6.2248E-01	6.2722E-01	6.2373E-01	6.2932E-01	6.6212E-01	7.0039E-01	7.4477E-01	8.1708E-01
H2O	1.2734E+00	1.2954E+00	1.2863E+00	1.2984E+00	1.3048E+00	1.2877E+00	1.2544E+00	1.1866E+00
N	9.7466E-06	3.9144E-06	6.1648E-06	3.2167E-06	4.1241E-07	4.5508E-08	2.6551E-09	2.1788E-11
NO	8.1966E-03	4.7011E-03	6.2351E-03	4.1494E-03	1.0463E-03	2.2417E-04	2.9917E-05	9.5883E-07
NO2	8.2064E-07	2.9136E-07	4.9074E-07	2.3196E-07	2.0144E-08	1.4307E-09	4.8080E-11	1.5864E-13
N2	1.7809E+01	1.7985E+01	1.7908E+01	1.8012E+01	1.8167E+01	1.8209E+01	1.8218E+01	1.8220E+01
O	3.1659E-02	1.5856E-02	2.2597E-02	1.3536E-02	2.2447E-03	2.8154E-04	1.7737E-05	1.4783E-07
O2	2.6160E-02	1.3335E-02	1.8899E-02	1.1390E-02	1.8353E-03	2.1869E-04	1.2917E-05	9.6677E-08
NO3(G)	6.3633E-13	1.0641E-13	2.6023E-13	7.2171E-14	1.2278E-15	1.6406E-17	6.8869E-20	7.4565E-24
H2O (L)	0.0000	0.0000	0.0000	0.0000	0.0000	0.0000	0.0000	0.0000
C (S)	0.0000	0.0000	0.0000	0.0000	0.0000	0.0000	0.0000	0.0000

FROZEN COMPOSITION								
PRESSURE LB/SQ IN	20.00000	11.15667	14.70069	10.00000	4.000000	2.000000	1.000000	.500000
TEMPERATURE (K)	2986.	2673.	2818.	2618.	2193.	1913.	1662.	1371.
TEMPERATURE (F)	4915.	4352.	4612.	4253.	3488.	2983.	2531.	2008.
ENTHALPY, KCAL/100 GM	35.95	-50.86	44.01	-53.46	-73.32	86.15	97.32	109.83
HT CONT, CAL/GRAM	1148.30	999.16	1067.66	973.14	774.61	646.30	534.59	409.45
ENTROPY, CAL/100GM(K)	302.26	302.26	302.26	302.26	302.26	302.26	302.26	302.26
MOL WT P, GM/MOL	22.01	22.01	22.01	22.01	22.01	22.01	22.01	22.01
MOL WT G, GM/MOL	22.01	22.01	22.01	22.01	22.01	22.01	22.01	22.01
MOLES GAS	4.544	4.544	4.544	4.544	4.544	4.544	4.544	4.544
TOTAL MOLES	4.544	4.544	4.544	4.544	4.544	4.544	4.544	4.544
CPP, BTU/(MOL)(R)	10.5555	10.4157	10.4839	10.3879	10.1983	9.9298	9.6579	9.2938
CPG, BTU/(MOL)(R)	10.5555	10.4157	10.4839	10.3879	10.1983	9.9298	9.6579	9.2938
CPP, BTU/(LB)(R)	.4796	.4733	.4764	.4720	.4634	.4512	.4388	.4223
CPG, BTU/(LB)(R)	.4796	.4733	.4764	.4720	.4634	.4512	.4388	.4223
ISP, SEC	.0	113.9	83.8	123.5	180.3	209.0	231.1	253.6
ISP(V), SEC	0	206.1	215.9	206.8	228.1	244.9	259.3	274.8
CSTAR, FT/SEC	.00	5318.85	5318.85	5318.85	5318.85	5318.85	5318.85	5318.85
CF	.00000	.68910	.50671	.74679	1.09078	1.26426	1.39786	1.53378
CF(V)	.00000	1.24663	1.30584	1.25066	1.37973	1.48167	1.56869	1.66225
EXPANSION COEFFICIENT	.000	1.233	1.232	1.234	1.237	1.240	1.243	1.248
EXIT VELOCITY, FT/SEC	.00	3665.23	2695.10	3972.08	5801.70	6724.41	7435.00	8157.93
GAS DENSITY, LB/CU IN	4.4202E-06	2.7524E-06	3.4429E-06	2.5203E-06	1.2036E-06	6.9005E-07	3.9713E-07	1.9251E-07
AREA, SQ IN	.0000	8.2658	8.9866	8.3297	11.9419	17.9707	28.2416	53.0977
EXPANSION RATIO	.0000	1.0000	1.0872	1.0077	1.4447	2.1741	3.4167	6.4238

ELEMENTS	GRAM-ATOM/100 GRAMS	INGRED NO.	PROPELLANT INGREDIENTS	PER CENT	DEL HF	SUM IS	1.000
HYDROGEN	3.09890	303	NYLON	31.8800	-72683.0		
CARBON	1.69031	268	OXYGEN (LIQUID @ 76.5 K)	68.1200	-10166.0		
NITROGEN	.28169						
OXYGEN	4.53919						

DENSITY 1.1269 GM/CC .04072 LB/CU IN

EQUILIBRIUM COMPOSITION

	CHAMBER	THROAT	EXIT	EXIT	EXIT	EXIT	EXIT	EXIT
PRESSURE LB/SQ IN	20.00000	11.21412	14.70069	10.00000	4.00000	2.00000	1.00000	.40000
TEMPERATURE (K)	3120.	2993.	3051.	2969.	2786.	2660.	2542.	2397.
TEMPERATURE (F)	5156.	4927.	5032.	4883.	4556.	4328.	4116.	3854.
ENTHALPY, KCAL/100 GM	-30.10	-44.12	-37.66	-46.80	-67.20	-81.49	-94.90	-111.40
HT CONT, CAL/GRAM	1116.94	1059.75	1085.88	1049.24	968.16	912.53	860.92	797.71
ENTROPY, CAL/100GM(K)	280.04	280.04	280.04	280.04	280.04	280.04	280.04	280.04
MOL WT P, GM/MOL	24.84	25.27	25.07	25.35	26.00	26.48	26.95	27.55
MOL WT G, GM/MOL	24.84	25.27	25.07	25.35	26.00	26.48	26.95	27.55
MOLES GAS	4.025	3.958	3.989	3.945	3.846	3.776	3.711	3.630
TOTAL MOLES	4.025	3.958	3.989	3.945	3.846	3.776	3.711	3.630
CPP, BTU/(MOL)(R)	11.0330	11.1791	11.1111	11.2081	11.4282	11.5863	11.7362	11.9197
CPG, BTU/(MOL)(R)	11.0330	11.1791	11.1111	11.2081	11.4282	11.5863	11.7362	11.9197
CPP, BTU/(LB)(R)	.4441	.4425	.4432	.4421	.4396	.4376	.4355	.4327
CPG, BTU/(LB)(R)	.4441	.4425	.4432	.4421	.4396	.4376	.4355	.4327
ISP, SEC	.0	110.5	81.1	120.6	179.7	211.5	237.5	266.0
ISP(V), SEC	.0	203.2	210.8	204.5	231.2	252.5	271.8	294.3
CSTAR, FT/SEC	.00	5318.99	5318.99	5318.99	5318.99	5318.99	5318.99	5318.99
CF	.00000	.66815	.49069	.72925	1.08684	1.27916	1.43638	1.60887
CF(V)	.00000	1.22885	1.27519	1.23711	1.39871	1.52755	1.64411	1.77992
EXPANSION COEFFICIENT	.000	1.078	1.078	1.077	1.076	1.074	1.073	1.072
EXIT VELOCITY, FT/SEC	.00	3553.86	2609.99	3878.85	5780.90	6803.84	7640.08	8557.55
GAS DENSITY, LB/CU IN	4.7750E-06	2.8386E-06	3.6214E-06	2.5605E-06	1.1191E-06	5.9691E-07	3.1782E-07	1.3784E-07
AREA, SQ IN	.0000	8.2660	8.8222	8.3960	12.8894	20.5321	34.3419	70.6939
EXPANSION RATIO	.0000	1.0000	1.0673	1.0157	1.5593	2.4839	4.1546	8.5524

MOLES PRODUCTS / 100 GRAMS PROPELLANT

C	2.1922E-10	7.1970E-11	1.2146E-10	5.7524E-11	9.4932E-12	2.3487E-12	5.6033E-13	7.8392E-14
CO	9.9253E-01	9.3855E-01	9.6403E-01	9.2754E-01	8.3942E-01	7.7161E-01	7.0356E-01	6.1434E-01
CO2	6.9778E-01	7.5176E-01	7.2628E-01	7.6277E-01	8.5089E-01	9.1870E-01	9.8675E-01	1.0760E+00
H	1.8662E-01	1.6320E-01	1.7389E-01	1.5873E-01	1.2689E-01	1.0600E-01	8.7546E-02	6.6413E-02
H2	2.3416E-01	2.1707E-01	2.2497E-01	2.1374E-01	1.8887E-01	1.7153E-01	1.5541E-01	1.3585E-01
H2O	1.2220E+00	1.2508E+00	1.2375E+00	1.2563E+00	1.2971E+00	1.3249E+00	1.3503E+00	1.3804E+00
N	1.7792E-05	1.0779E-05	1.3646E-05	9.7404E-06	4.2945E-06	2.2605E-06	1.1616E-06	4.5890E-07
NO	2.9979E-02	2.5208E-02	2.7368E-02	2.4325E-02	1.8109E-02	1.4244E-02	1.1010E-02	7.5694E-03
NO2	1.0760E-05	7.2391E-06	8.7280E-06	6.6810E-06	3.4573E-06	2.0478E-06	1.1812E-06	5.4162E-07
N2	1.2584E-01	1.2823E-01	1.2715E-01	1.2868E-01	1.3179E-01	1.3372E-01	1.3534E-01	1.3706E-01
O	1.7316E-01	1.4524E-01	1.5790E-01	1.4002E-01	1.0345E-01	8.0516E-02	6.1215E-02	4.0610E-02
O2	3.6298E-01	3.3794E-01	3.4989E-01	3.3271E-01	2.8965E-01	2.5525E-01	2.1982E-01	1.7217E-01
NO3(G)	3.6218E-11	1.6264E-11	2.3711E-11	1.3845E-11	3.7272E-12	1.3305E-12	4.5655E-13	1.0253E-13
H2O (L)	0.0000	0.0000	0.0000	0.0000	0.0000	0.0000	0.0000	0.0000
C (S)	0.0000	0.0000	0.0000	0.0000	0.0000	0.0000	0.0000	0.0000

FROZEN COMPOSITION								
PRESSURE LB/SQ IN	20.00000	11.19990	14.70069	10.00000	4.08000	2.00000	1.00000	.40000
TEMPERATURE (K)	3120.	2809	2951.	2751.	2323	2039.	1785.	1489.
TEMPERATURE (F)	5156.	4596	4852.	4493.	3722	3211	2753.	2219
ENTHALPY, KCAL/100 GM	30.10	43.83	37.57	-46.35	64 91	76.98	87.57	99.54
HT CONT, CAL/GRAM	1116 94	979.58	1042 22	954.38	768 81	648 06	542 19	422 51
ENTROPY, CAL/100GM(K)	280 04	280.04	280.04	280.04	280 01	280.04	280.04	280.04
MOL WT P, GM/MOL	24.84	24.84	24.84	24.84	24 84	24 84	24.84	24.84
MOL WT G, GM/MOL	24.84	24.84	24.84	24.84	24 84	24.84	24.84	24.84
MOLES GAS	4.025	4.025	4.025	4.025	4.025	4.025	4.025	4.025
TOTAL MOLES	4.025	4.025	4.025	4.025	4.025	4.025	4.025	4.025
CPP, BTU/(MOL)(R)	11.0330	10.9039	10.9663	10.8770	10.6390	10.4588	10.2077	9.8585
CPG, BTU/(MOL)(R)	11 0330	10.9039	10.9663	10.8770	10.6390	10 4588	10.2077	9.8585
CPP, BTU/(LB)(R)	.4441	.4389	.4414	.4378	.4282	.4210	.4109	.3968
CPG, BTU/(LB)(R)	.4441	.4389	.4414	.4378	.4282	.4210	.4109	.3968
ISP, SEC	.0	109.3	80.6	118.9	174.0	202.0	223.6	245.8
ISP(V), SEC	.0	198 7	208 0	199.4	220 5	237 1	251 4	266 9
CSTAR, FT/SEC	00	5135.65	5135.65	5135.65	5135 65	5135.65	5135.65	5135.65
CF	.00000	.68493	.50517	.74510	1.09038	1.26543	1.40103	1.54000
CF(V)	.00000	1.24493	1.30290	1.24934	1.38131	1.48548	1.57498	1.67200
EXPANSION COEFFICIENT	.000	1.221	1.221	1.222	1.221	1.227	1.229	1.233
EXIT VELOCITY, FT/SEC	.00	3517.56	2594.36	3826.59	5599.79	6498.79	7195.19	7908.92
GAS DENSITY, LB/CU IN	4.7750E-06	2.9703E-06	3.7107E-06	2.7075E-06	1.2827E-06	7.3061E-07	4.1739E-07	2.0017E-07
AREA, SQ IN	.0000	7.9811	8.6619	8.0487	11.6096	17.5624	27.7662	52.6713
EXPANSION RATIO	0000	1.0000	1.0853	1.0085	1 4546	2.2005	3.4790	6 5995

ELEMENTS	GRAM-ATOM/100 GRAMS	INGRED NO.	PROPELLANT INGREDIENTS	PER CENT	DEL HF	SUM IS	1.000
HYDROGEN	4.33877	73	BUTYL RUBBER	30.4300	-45056.0		
CARBON	2.16939	268	OXYGEN (LIQUID @ 76.5 K)	69.5700	-10166.0		
OXYGEN	4.34812						

DENSITY 1.0627 GM/CC .03839 LB/CU IN

EQUILIBRIUM COMPOSITION

	CHAMBER	THROAT	EXIT	EXIT	EXIT	EXIT	EXIT	EXIT
PRESSURE LB/SQ IN	20.00000	11.15736	14.70069	10.00000	4.00000	2.00000	1.00000	.40000
TEMPERATURE (K)	3086.	2943	3010.	2917.	2704.	2541.	2368.	2111.
TEMPERATURE (F)	5094.	4837.	4958.	4791.	4407.	4115.	3803.	3340.
ENTHALPY, KCAL/100 GM	-20.78	-37.15	-29.54	-40.11	-63.54	-79.77	-94.77	-112.66
HT CONT, CAL/GRAM	1226.46	1155.62	1188.03	1141.90	1035.01	954.79	870.71	748.12
ENTROPY, CAL/100GM(K)	313.45	313.45	313.45	313.45	313.45	313.45	313.45	313.45
MOL WT P, GM/MOL	21.19	21.53	21.37	21.59	22.09	22.42	22.69	22.93
MOL WT G, GM/MOL	21.19	21.53	21.37	21.59	22.09	22.42	22.69	22.93
MOLES GAS	4.720	4.644	4.680	4.631	4.528	4.461	4.407	4.361
TOTAL MOLES	4.720	4.644	4.680	4.631	4.528	4.461	4.407	4.361
CPP, BTU/(MOL)(R)	10.4577	10.5743	10.5197	10.5934	10.7378	10.8092	10.8302	10.7937
CPG, BTU/(MOL)(R)	10.4576	10.5742	10.5197	10.5933	10.7378	10.8092	10.8302	10.7937
CPP, BTU/(LB)(R)	.4936	.4911	.4923	.4906	.4862	.4822	.4773	.4707
CPG, BTU/(LB)(R)	.4936	.4911	.4923	.4906	.4862	.4822	.4773	.4707
ISP, SEC	.0	119.3	87.3	129.7	192.9	226.6	253.7	282.7
ISP(V), SEC	.0	218.3	226.8	219.7	247.7	269.8	289.3	310.9
CSTAR, FT/SEC	.00	5709.39	5709.39	5709.39	5709.39	5709.39	5709.39	5709.39
CF	.00000	.67248	.49202	.73073	1.08692	1.27672	1.42982	1.59332
CF(V)	.00000	1.23035	1.27782	1.23825	1.39610	1.52044	1.63018	1.75191
EXPANSION COEFFICIENT	.000	1.088	1.088	1.088	1.089	1.092	1.097	1.107
EXIT VELOCITY, FT/SEC	.00	3839.45	2809.12	4172.02	6205.64	7289.27	8163.39	9096.89
GAS DENSITY, LB/CU IN	4.1180E-06	2.4478E-06	3.1294E-06	2.2193E-06	9.7964E-07	5.2900E-07	2.8729E-07	1.3029E-07
AREA, SQ IN	.0000	8.8727	9.4855	9.0061	13.7166	21.6251	35.5555	70.3570
EXPANSION RATIO	.0000	1.0000	1.0691	1.0150	1.5459	2.4373	4.0073	7.9296

MOLES PRODUCTS / 100 GRAMS PROPELLANT

C	7.1557E-10	2.1953E-10	3.8717E-10	1.7579E-10	2.4030E-11	4.3802E-12	5.7895E-13	1.6353E-14
CH	1.3053E-10	3.7782E-11	6.8326E-11	2.9949E-11	3.8984E-12	7.2436E-13	1.0618E-13	4.2695E-15
CHO	1.0186E-05	5.5672E-06	7.4233E-06	4.9705E-06	1.8583E-06	8.3999E-07	3.4981E-07	8.6928E-08
CO	1.6862E+00	1.6504E+00	1.6674E+00	1.6440E+00	1.5920E+00	1.5571E+00	1.5267E+00	1.4879E+00
CO2	4.8320E-01	5.1899E-01	5.0200E-01	5.2533E-01	5.7736E-01	6.1228E-01	6.4265E-01	6.8152E-01
H	2.9635E-01	2.5293E-01	2.7356E-01	2.4543E-01	1.8111E-01	1.3305E-01	8.6086E-02	3.4137E-02
HO	2.2181E-01	1.7904E-01	1.9923E-01	1.7157E-01	1.1057E-01	6.9659E-02	3.6097E-02	9.1381E-03
H2	6.1426E-01	6.0435E-01	6.0870E-01	6.0296E-01	5.9691E-01	6.0202E-01	6.1866E-01	6.6066E-01
H2O	1.2960E+00	1.3490E+00	1.3243E+00	1.3579E+00	1.4266E+00	1.4660E+00	1.4896E+00	1.4871E+00
H2O2	3.3340E-06	1.8345E-06	2.4509E-06	1.6334E-06	5.5359E-07	2.0477E-07	5.8340E-08	5.7266E-09
O	6.5858E-02	4.6906E-02	5.5593E-02	4.3857E-02	2.1700E-02	1.0221E-02	3.4412E-03	3.4218E-04
O2	5.5896E-02	4.2373E-02	4.8802E-02	4.0019E-02	2.1235E-02	1.0287E-02	3.4645E-03	3.2899E-04
HO2	2.8345E-05	1.5622E-05	2.0919E-05	1.3899E-05	4.4747E-06	1.4856E-06	3.4215E-07	1.9365E-08
H2O (L)	0.0000	0.0000	0.0000	0.0000	0.0000	0.0000	0.0000	0.0000
C (S)	0.0000	0.0000	0.0000	0.0000	0.0000	0.0000	0.0000	0.0000

FROZEN COMPOSITION									
PRESSURE, LB/SQ IN	30.00000	14.14647	14.70069	10.00000	4.00000	2.00000	1.00000	.40000	
TEMPERATURE (K)	3086.	2758	2910.	2702.	2259	1968.	1708	1407	
TEMPERATURE (F)	5094	4506	4778	4404.	3607	3083.	2614	2073	
ENTHALPY, KCAL/100 GM	20.78	36.81	29.44	39.57	60 84	74.56	86.49	99.84	
HT CONT, CAL/GRAM	1226 46	1066 24	1139 94	1038.58	825 90	688 72	569 40	435 90	
ENTROPY, CAL/100GM(K)	313.45	313 45	313 45	313.45	313 45	313.45	313.45	313 45	
MOL WT P, GM/MOL	21 19	21.19	21.19	21.19	21 19	21.19	21.19	21 19	
MOL WT G, GM/MOL	21.19	21.19	21.19	21.19	21.19	21.19	21.19	21.19	
MOLES GAS	4 720	4.720	4.720	4.720	4 720	4.720	4.720	4.720	
TOTAL MOLES	4 720	4.720	4.720	4 720	4 720	4.720	4.720	4.720	
CPP, BTU/(MOL)(R)	10.4577	10.3207	10.3876	10.2937	10.0427	9 8495	9.5758	9 2137	
CPG, BTU/(MOL)(R)	10.4576	10.3207	10.3876	10.2937	10.0427	9 8495	9.5758	9 2137	
CPP, BTU/(LB)(R)	4936	.4871	.4903	.4858	.4740	.4649	4519	.4349	
CPG, BTU/(LB)(R)	4936	.4871	.4903	.4858	.4740	4649	4519	.4348	
ISP, SEC	.0	118 1	86 8	127.9	186 7	216 3	239.1	262.3	
ISP(V), SEC	0	213 4	223 6	214 1	236 1	253 4	268.2	284 2	
CSTAR, FT/SEC	00	5505.85	5505.85	5505.85	5505 85	5505.85	5505.85	5505.85	
CF	00000	.68998	.50704	.74715	1.09096	1.26404	1.39726	1.53265	
CF(V)	.00000	1.24700	1 30647	1.25095	1.37944	1.48093	1.56753	1 66053	
EXPANSION COEFFICIENT	000	1.236	1.235	1.237	1 240	1.243	1.246	1.251	
EXIT VELOCITY, FT/SEC	.00	3798.92	2791.66	4113.72	6006 64	6959.63	7693.11	8438.53	
GAS DENSITY, LB/CU IN	4 1180E-06	2.5654E-06	3 2097E-06	2.3512E-06	1.1248E 06	6 4563E-07	3.7200E-07	1 8062E-07	
AREA, SQ IN	0600	8.5564	9.3060	8.6214	12.3416	18.5580	29.1378	54.7089	
EXPANSION RATIO	0000	1 0000	1.0876	1.0076	1 4424	2.1689	3 4054	6 3939	

ELEMENTS	GRAM-ATOM/100 GRAMS	INGRED NO.	PROPELLANT INGREDIENTS	PER CENT	DEL HF	SUM IS	1.000
HYDROGEN	3.21950	73	BUTYL RUBBER	22.5800	-45056.0		
CARBON	1.60975	268	OXYGEN (LIQUID @ 76.5 K)	77.4200	-10166.0		
OXYGEN	4.83875						

DENSITY 1.0816 GM/CC .03908 LB/CU IN

EQUILIBRIUM COMPOSITION

	CHAMBER	THROAT	EXIT	EXIT	EXIT	EXIT	EXIT	EXIT
PRESSURE LB/SQ IN	20.00000	11.19952	14.70069	10.00000	4.00000	2.00000	1.00000	.40000
TEMPERATURE (K)	3123.	3000.	3057.	2977.	2802.	2681.	2569.	2432.
TEMPERATURE (F)	5162.	4939.	5042.	4898.	4583.	4366.	4164.	3917.
ENTHALPY, KCAL/100 GM	-18.04	-32.41	-25.77	-35.12	-56.01	-70.67	-84.46	101.47
HT CONT, CAL/GRAM	1125.91	1070.86	1095.41	1060.20	981.59	927.92	878.36	818.17
ENTROPY, CAL/100GM(K)	284.96	284.96	284.96	284.96	284.96	284.96	284.96	284.96
MOL WT P, GM/MOL	24.35	24.77	24.57	24.85	25.50	25.98	26.45	27.06
MOL WT G, GM/MOL	24.35	24.77	24.57	24.85	25.50	25.98	26.45	27.06
MOLES GAS	4.107	4.037	4.070	4.024	3.922	3.849	3.781	3.695
TOTAL MOLES	4.107	4.037	4.070	4.024	3.922	3.849	3.781	3.695
CPP, BTU/(MOL)(R)	10.8774	11.0290	10.9569	11.0573	11.2850	11.4505	11.6095	11.8088
CPG, BTU/(MOL)(R)	10.8774	11.0290	10.9569	11.0573	11.2850	11.4505	11.6095	11.8088
CPP, BTU/(LB)(R)	.4467	.4452	.4459	.4449	.4426	.4408	.4389	.4364
CPG, BTU/(LB)(R)	.4467	.4452	.4459	.4449	.4426	.4408	.4389	.4364
ISP, SEC	.0	111.8	82.0	121.9	181.7	214.0	240.4	269.4
ISP(V), SEC	.0	205.4	213.1	206.8	234.0	255.7	275.3	298.3
CSTAR, FT/SEC	.00	5379.81	5379.81	5379.81	5379.81	5379.81	5379.81	5379.81
CF	00000	.66854	.49037	.72893	1.08694	1.27980	1.43771	1.61132
CF(V)	00000	1.22852	1.27468	1.23696	1.39947	1.52909	1.64654	1.78371
EXPANSION COEFFICIENT	.000	1.075	1.075	1.074	1.072	1.071	1.070	1.068
EXIT VELOCITY, FT/SEC	.00	3596.63	2638.10	3921.49	5847.52	6885.09	7734.61	8668.58
GAS DENSITY, LB/CU IN	4.6756E-06	2.7731E-06	3.5432E-06	2.5032E-06	1.0915E-06	5.8109E-07	3.0875E-07	1.3348E-07
AREA, SQ IN	.0000	8.3605	8.9210	8.4948	13.0647	20.8422	34.9179	72.0644
EXPANSION RATIO	0000	1.0000	1.0670	1.0161	1.5627	2.4929	4.1765	8.6196

MOLES PRODUCTS / 100 GRAMS PROPELLANT

C	1.9592E-10	6.5978E-11	1.1045E-10	5.3404E-11	9.4119E-12	2.4761E-12	6.3586E-13	1.0043E-13
CH	2.0872E-11	6.2447E-12	1.1049E-11	4.9386E-12	7.2181E-13	1.6490E-13	3.6810E-14	4.8413E-15
CHO	3.7050E-06	1.9979E-06	2.6753E-06	1.7708E-06	6.5724E-07	3.0595E-07	1.4036E-07	4.8772E-08
CO	9.2162E-01	8.6904E-01	8.9420E-01	8.5890E-01	7.7485E-01	7.1060E-01	6.4625E-01	5.6169E-01
CO2	6.8812E-01	7.4071E-01	7.1554E-01	7.5084E-01	8.3489E-01	8.9915E-01	9.6349E-01	1.0481E+00
H	1.7787E-01	1.5830E-01	1.6747E-01	1.5480E-01	1.2815E-01	1.1034E-01	9.4303E-02	7.5498E-02
HO	3.5984E-01	3.2286E-01	3.4013E-01	3.1605E-01	2.6358E-01	2.2775E-01	1.9518E-01	1.5685E-01
H2	2.0483E-01	1.9169E-01	1.9792E-01	1.8923E-01	1.6961E-01	1.5540E-01	1.4173E-01	1.2440E-01
H2O	1.1360E+00	1.1774E+00	1.1580E+00	1.1850E+00	1.2442E+00	1.2853E+00	1.3233E+00	1.3692E+00
H2O2	9.1326E-06	5.8513E-06	7.2185E-06	5.3603E-06	2.6120E-06	1.4991E-06	8.5143E-07	3.9613E-07
O	1.9151E-01	1.6575E-01	1.7770E-01	1.6117E-01	1.2701E-01	1.0496E-01	8.5815E-02	6.4440E-02
O2	4.2663E-01	4.1103E-01	4.1871E-01	4.0786E-01	3.7959E-01	3.5590E-01	3.3061E-01	2.9523E-01
HO2	1.3483E-04	9.2739E-05	1.1070E-04	8.6148E-05	4.6868E-05	2.9177E-05	1.7931E-05	9.2156E-06
H2O (L)	0.0000	0.0000	0.0000	0.0000	0.0000	0.0000	0.0000	0.0000
C (S)	0.0000	0.0000	0.0000	0.0000	0.0000	0.0000	0.0000	0.0000

FROZEN COMPOSITION								
PRESSURE LB/SQ IN	20.00000	11.18486	14.70069	10.00000	4.00000	2.00000	1.00000	.40000
TEMPERATURE (K)	3123.	2807	2952.	2749.	2316	2029.	1772.	1473
TEMPERATURE (F)	5162.	4593	4854.	4489.	3708	3192	2729.	2192.
ENTHALPY, KCAL/100 GM	18.04	-32.10	25.67	-34.63	53.53	65.80	76.53	88.64
HT CONT, CAL/GRAM	1125.91	985.40	1049.62	960.02	771.05	648.37	541.02	419.98
ENTROPY, CAL/100GM(K)	284.96	284.96	284.96	284.96	284.96	284.96	284.96	284.96
MOL WT P, GM/MOL	24.35	24.35	24.35	24.35	24.35	24.35	24.35	24.35
MOL WT G, GM/MOL	24.35	24.35	24.35	24.35	24.35	24.35	24.35	24.35
MOLES GAS	4.107	4.107	4.107	4.107	4.107	4.107	4.107	4.107
TOTAL MOLES	4.107	4.107	4.107	4.107	4.107	4.107	4.107	4.107
CPP, BTU/(MOL)(R)	10.8774	10.7476	10.8105	10.7210	10.4821	10.2968	10.0437	9.6944
CPG, BTU/(MOL)(R)	10.8774	10.7476	10.8105	10.7209	10.4821	10.2968	10.0437	9.6944
CPP, BTU/(LB)(R)	.4467	.4414	.4439	.4403	.4305	.4228	.4125	.3981
CPG, BTU/(LB)(R)	.4467	.4414	.4439	.4403	.4305	.4228	.4125	.3981
ISP, SEC	.0	110.6	81.5	120.1	175.7	203.8	225.6	247.8
ISP(V), SEC	.0	200.7	210.1	201.4	222.5	239.2	253.5	268.9
CSTAR, FT/SEC	.00	5184.25	5184.25	5184.25	5184.25	5184.25	5184.25	5184.25
CF	.00000	.68622	.50565	.74563	1.09053	1.26508	1.40006	1.53813
CF(V)	.00000	1.24546	1.30382	1.24976	1.38084	1.48431	1.57307	1.66907
EXPANSION COEFFICIENT	.000	1.225	1.224	1.225	1.228	1.231	1.233	1.238
EXIT VELOCITY, FT/SEC	.00	3557.55	2621.42	3865.55	5653.58	6558.49	7258.28	7974.02
GAS DENSITY, LB/CU IN	4.6756E-06	2.9094E-06	3.6360E-06	2.6556E-06	1.2612E-06	7.1985E-07	4.1212E-07	1.9825E-07
AREA, SQ IN	.0000	8.0566	8.7486	8.1230	11.6543	17.6624	27.8764	52.7491
EXPANSION RATIO	.0000	1.0000	1.0859	1.0082	1.4515	2.1923	3.4601	6.5473

THEORETICAL ROCKET PERFORMANCE ASSUMING EQUILIBRIUM COMPOSITION DURING EXPANSION

PC = 10.0 PSIA

CHEMICAL FORMULA		WT FRACTION (SEE NOTE)	ENERGY CAL/MOL	STATE	TEMP DEG K
FUEL	AL 1.00000	0.200000	0.000	S	298.15
FUEL	H 2.00000	0.800000	-2154.000	L	20.27
OXIDANT	O 2.00000	1.000000	-3102.000	L	90.18

O/F= 9.8667 PERCENT FUEL= 9.2024 EQUIVALENCE RATIO= 0.6616 PHI= 0.6616

	CHAMBER	THROAT	EXIT	EXIT	EXIT	EXIT	EXIT	EXIT	EXIT	EXIT	EXIT
PC/P	1.0000	1.7147	2.0000	5.0000	10.000	20.000	50.000	100.00	200.00	500.00	1000.00
P, ATM	0.68046	0.39683	0.34023	0.13609	0.06805	0.03402	0.01361	0.00680	0.00340	0.00136	0.00068
T, DEG K	2938.8	2828.0	2797.4	2621.8	2495.2	2371.5	2212.9	2084.2	1945.0	1735.4	1559.4
RHO, G/CC	5.4336-5	3.3403-5	2.9068-5	1.2691-5	6.7752-6	3.6176-6	1.5767-6	8.4651-7	4.5756-7	2.0660-7	1.1520-7
H, CAL/G	-166.69	-325.98	-369.93	-618.58	-792.81	-955.99	-1156.17	-1296.08	-1425.98	-1581.70	-1686.59
U, CAL/G	-469.96	-613.69	-653.39	-878.28	-1036.04	-1183.75	-1365.20	-1490.75	-1606.06	-1741.23	-1829.63
G, CAL/G	-10559.9	-10327.4	-10262.9	-9890.68	-9617.15	-9342.93	-8982.02	-8666.94	-8304.69	-7718.89	-7201.36
S, CAL/(G)(K)	3.5365	3.5365	3.5365	3.5365	3.5365	3.5365	3.5365	3.5365	3.5365	3.5365	3.5365
M, MOL WT	19.256	19.533	19.611	20.062	20.386	20.692	21.038	21.276	21.465	21.617	21.663
(DLV/DLP)T	-1.05327	-1.04712	-1.04538	1.03526	-1.02795	-1.02106	-1.01333	1.00810	-1.00409	-1.00107	-1.00026
(DLV/DLT)P	2.1202	2.0306	2.0038	1.8344	1.6970	1.5551	1.3796	1.2474	1.1361	1.0414	1.0117
CP, CAL/(G)(K)	3.0550	2.9120	2.8671	2.5630	2.2934	1.9949	1.5938	1.2671	0.9673	0.6758	0.5600
GAMMA (S)	1.1093	1.1073	1.1068	1.1047	1.1043	1.1054	1.1105	1.1193	1.1356	1.1716	1.2011
SON VEL,M/SEC	1186.4	1154.5	1145.7	1095.6	1060.1	1026.3	985.5	954.8	925.0	884.3	847.8
MACH NUMBER	0.000	1.000	1.138	1.775	2.159	2.504	2.920	3.220	3.509	3.891	4.206

PERFORMANCE PARAMETERS

AE/AT	1.0000	1.0173	1.5627	2.4867	4.1480	8.5000	14.819	25.964	54.247	93.868
CSTAR, FT/SEC	5866	5866	5866	5866	5866	5866	5866	5866	5866	5866
CF	0.646	0.729	1.088	1.280	1.438	1.610	1.720	1.816	1.925	1.995
IVAC,LB-SEC/LB	224.1	225.7	255.3	278.7	299.9	324.4	340.5	354.7	370.7	380.8
ISP, LB-SEC/LB	117.7	133.0	198.3	233.4	262.1	293.4	313.5	331.0	350.9	363.7

MOLE FRACTIONS

ALO	0.00007	0.00004	0.00003	0.00001	0.00000	0.00000	0.00000	0.00000	0.00000	0.00000	0.00000
ALOH	0.00004	0.00002	0.00002	0.00001	0.00000	0.00000	0.00000	0.00000	0.00000	0.00000	0.00000
AL02	0.00001	0.00000	0.00000	0.00000	0.00000	0.00000	0.00000	0.00000	0.00000	0.00000	0.00000
AL02H	0.00113	0.00080	0.00072	0.00037	0.00021	0.00011	0.00003	0.00001	0.00000	0.00000	0.00000
H	0.03829	0.03293	0.03144	0.02301	0.01723	0.01207	0.00674	0.00350	0.00138	0.00020	0.00002
H02	0.00011	0.00008	0.00007	0.00004	0.00003	0.00002	0.00001	0.00001	0.00000	0.00000	0.00000
H2	0.05977	0.05383	0.05211	0.04179	0.03396	0.02627	0.01718	0.01067	0.00543	0.00133	0.00027
H20	0.56126	0.58537	0.59220	0.63219	0.66142	0.68936	0.72170	0.74451	0.76314	0.77889	0.78395
O	0.04546	0.03988	0.03833	0.02945	0.02320	0.01742	0.01100	0.00665	0.00330	0.00078	0.00015
OH	0.11660	0.10570	0.10260	0.08431	0.07072	0.05740	0.04118	0.02897	0.01790	0.00678	0.00227
02	0.17136	0.17516	0.17621	0.18220	0.18643	0.19040	0.19506	0.19848	0.20156	0.20470	0.20600
AL203(A)	0.00000	0.00000	0.00000	0.00000	0.00000	0.00000	0.00711	0.00720	0.00727	0.00732	0.00733
AL203(L)	0.00590	0.00619	0.00626	0.00660	0.00680	0.00695	0.00000	0.00000	0.00000	0.00000	0.00000

THEORETICAL ROCKET PERFORMANCE ASSUMING FROZEN COMPOSITION DURING EXPANSION

PC = 10.0 PSIA

CHEMICAL FORMULA

FUEL	AL	1.00000
FUEL	H	2.00000
OXIDANT	O	2.00000

WT FRACTION (SEE NOTE)	ENERGY CAL/MOL	STATE	TEMP DEG K
0.200000	0.000	S	298.15
0.800000	-2154.000	L	20.27
1.000000	3102.000	L	90.18

O/F = 5.8667 PERCENT FUEL= 91.2024 EQUIVALENCE RATIO 0.6616 PHI= 0.6616

	CHAMBER	THROAT	EXIT
PC/P	1.0000	1.7810	2.0000
P, ATM	0.68046	0.38206	0.34023
T, DEG K	2938.8	2655.7	2601.7
RHO, G/CC	5.4336-5	4.3761-5	3.0689-5
H, CAL/G	166.69	-333.18	-364.64
U, CAL/G	-469.96	-607.24	-633.12
G, CAL/G	10559.9	9725.11	9565.46
S, CAL/(G)(K)	3.5365	3.5365	3.5365
M, MOL WT	19.256	19.256	19.256
CP, CAL/(G)(K)	0.5927	0.5832	0.5811
GAMMA (S)	1.2108	1.2150	1.2159
SON VEL,M/SEC	1239.5	1180.3	1168.7
MACH NUMBER	0.000	1.000	1.101

PERFORMANCE PARAMETERS

AE/AT	1.0000	2.5223
CSTAR, FT/SEC	5676	5676
CF	0.682	0.744
IVAC, LB SEC/LB	219.4	220.2
ISP, LB-SEC/LB	120.4	131.2

MOLE FRACTIONS

AL	0.00007	ALOH	0.00004	AL02	0.00001	AL2O2(L)	0.00111
H	0.03829	H02	0.00011	H2	0.05977	H2O	0.56126
O	0.04546	OH	0.11660	O2	0.17136	AL2O3(L)	0.00590

THEORETICAL ROCKET PERFORMANCE ASSUMING EQUILIBRIUM COMPOSITION DURING EXPANSION

PC = 10.0 PSIA

	CHEMICAL FORMULA	WT FRACTION (SEE NOTE)	ENERGY CAL/MOL	STATE	TEMP DEG K
FUEL	AL 1.00000	0.200000	0.000	S	298.15
FUEL	H 2.00000	0.800000	-2154.000	L	20.27
OXIDANT	O 2.00000	1.000000	-3102.000	L	90.18

O/F= 6.5778 PERCENT FUEL= 13.1964 EQUIVALENCE RATIO= 0.9924 PHI= 0.9924

	CHAMBER	THROAT	EXIT	EXIT	EXIT	EXIT	EXIT	EXIT	EXIT	EXIT	EXIT
PC/P	1.0000	1.7132	2.0000	5.0000	10.000	20.000	50.000	100.00	200.00	500.00	1000.00
P, ATM	0.68046	0.39718	0.34023	0.13609	0.06805	0.03402	0.01361	0.00680	0.00340	0.00136	0.00068
T, DEG K	3012.9	2905.5	2875.8	2708.5	2591.0	2479.8	2340.7	2243.6	2145.1	2015.7	1915.6
RHO, G/CC	4.3270-5	2.6597-5	2.3120-5	1.0069-5	5.3594-6	2.8493-6	1.2343-6	6.5313-7	3.4669-7	1.5027-7	8.0031-8
H, CAL/G	-196.96	-396.76	-452.32	-765.30	-985.20	-1191.90	-1446.56	-1626.69	-1796.45	-2005.74	-2153.10
U, CAL/G	-577.80	-758.40	-808.70	-1092.62	-1292.68	-1481.08	-1713.58	-1878.99	-2034.11	-2225.07	-2359.01
G, CAL/G	-12848.6	-12597.5	-12528.1	-12138.8	-11865.1	-11605.0	-11275.4	-11047.8	-10804.0	-10470.0	-10197.1
S, CAL/(G)(K)	4.1991	4.1991	4.1991	4.1991	4.1991	4.1991	4.1991	4.1991	4.1991	4.1991	4.1991
M, MOL WT	15.721	15.966	16.035	16.443	16.746	17.041	17.420	17.671	17.936	18.264	18.488
(DLV/DLP)T	-1.07665	-1.07085	-1.06919	-1.05946	-1.05224	-1.04516	-1.03613	-1.03019	-1.02396	-1.01640	-1.01136
(DLV/DLT)P	2.5513	2.4858	2.4657	2.3365	2.2270	2.1083	1.9395	1.8193	1.6804	1.4964	1.3624
CP, CAL/(G)(K)	4.7338	4.6372	4.6053	4.3764	4.1576	3.8998	3.5025	3.2005	2.8299	2.3085	1.9039
GAMMA (S)	1.1076	1.1050	1.1043	1.1005	1.0981	1.0962	1.0946	1.0942	1.0948	1.0979	1.1031
SON VEL,M/SEC	1328.5	1293.0	1283.2	1227.6	1188.5	1151.7	1105.8	1074.8	1043.4	1003.7	974.8
MACH NUMBER	0.000	1.000	1.139	1.776	2.161	2.505	2.924	3.218	3.506	3.876	4.150

PERFORMANCE PARAMETERS

AE/AT	1.0000	1.0176	1.5662	2.4985	4.1831	8.6166	15.223	27.115	58.826	106.21
CSTAR, FT/SEC	6577	6577	6577	6577	6577	6577	6577	6577	6577	6577
CF	0.645	0.729	1.088	1.281	1.439	1.613	1.725	1.825	1.941	2.018
IVAC,LB-SEC/LB	251.2	253.1	286.4	313.0	337.0	365.0	383.8	400.8	420.8	434.3
ISP, LB-SEC/LB	131.9	149.1	222.4	261.9	294.2	329.7	352.7	373.1	396.7	412.6

MOLE FRACTIONS

AL	0.00001	0.00001	0.00001	0.00000	0.00000	0.00000	0.00000	0.00000	0.00000	0.00000	0.00000
ALO	0.00022	0.00014	0.00012	0.00005	0.00002	0.00001	0.00000	0.00000	0.00000	0.00000	0.00000
ALOH	0.00013	0.00009	0.00008	0.00004	0.00002	0.00001	0.00000	0.00000	0.00000	0.00000	0.00000
ALO2	0.00001	0.00001	0.00001	0.00000	0.00000	0.00000	0.00000	0.00000	0.00000	0.00000	0.00000
ALO2H	0.00170	0.00128	0.00117	0.00069	0.00044	0.00027	0.00014	0.00007	0.00003	0.00001	0.00000
H	0.07508	0.06835	0.06643	0.05535	0.04729	0.03957	0.03000	0.02397	0.01780	0.01077	0.00649
HO2	0.00005	0.00004	0.00003	0.00002	0.00001	0.00001	0.00000	0.00000	0.00000	0.00000	0.00000
H2	0.14484	0.13802	0.13600	0.12347	0.11340	0.10283	0.08815	0.07756	0.06556	0.04924	0.03681
H2O	0.58265	0.60977	0.61758	0.66381	0.69866	0.73326	0.77838	0.80895	0.84175	0.88326	0.91252
O	0.03251	0.02883	0.02780	0.02208	0.01815	0.01458	0.01042	0.00795	0.00561	0.00316	0.00180
OH	0.10389	0.09527	0.09282	0.07862	0.06830	0.05842	0.04611	0.03804	0.02994	0.02031	0.01397
O2	0.05230	0.05121	0.05085	0.04828	0.04582	0.04293	0.03842	0.03492	0.03063	0.02441	0.01944
AL2O3(A)	0.00000	0.00000	0.00000	0.00000	0.00000	0.00000	0.00000	0.00853	0.00868	0.00885	0.00896
AL2O3(L)	0.00660	0.00700	0.00710	0.00759	0.00788	0.00812	0.00838	0.00000	0.00000	0.00000	0.00000

THEORETICAL ROCKET PERFORMANCE ASSUMING EQUILIBRIUM COMPOSITION DURING EXPANSION

PC = 10.0 PSIA

CHEMICAL FORMULA

FUEL	AL	1.00000
FUEL	H	2.00000
OXIDANT	O	2.00000

WT FRACTION (SEE NOTE)	ENERGY CAL/MOL	STATE	TEMP DEG K
0.100000	0.000	S	298.15
0.900000	-2154.000	L	20.27
1.000000	-3102.000	L	90.18

O/F= 18.2224 PERCENT FUEL= 5.2023 EQUIVALENCE RATIO= 0.3969 PHI= 0.3969

	CHAMBER	THROAT	EXIT	EXIT	EXIT	EXIT	EXIT	EXIT	EXIT	EXIT	EXIT
PC/P	1.0000	1.7260	2.0000	5.0000	10.000	20.000	50.000	100.00	200.00	500.00	1000.00
P, ATM	0.68046	0.39424	0.34023	0.13609	0.06805	0.03402	0.01361	0.00680	0.00340	0.00136	0.00068
T, DEG K	2692.0	2562.2	2527.2	2308.2	2130.6	1939.5	1671.1	1470.7	1283.7	1062.9	915.7
RHO, G/CC	7.1669-5	4.4095-5	3.8685-5	1.7187-5	9.3859-6	5.1824-6	2.4132-6	1.3719-6	7.8595-7	3.7971-7	2.2037-7
H, CAL/G	-141.93	-263.74	-295.38	-480.67	-607.98	-723.96	-859.38	-948.29	-1026.17	-1113.77	-1169.69
U, CAL/G	-371.86	-480.26	-508.37	-672.42	-783.55	-882.95	-995.95	-1068.41	-1131.00	-1200.57	-1244.47
G, CAL/G	8092.89	7831.36	7759.53	7297.89	-6900.79	-6452.33	-5795.05	-5292.00	-4817.67	-4253.05	-3874.19
S, CAL/(G)(K)	2.9535	2.9535	2.9535	2.9535	2.9535	2.9535	2.9535	2.9535	2.9535	2.9535	2.9535
M, MOL WT	23.266	23.516	23.579	23.920	24.115	24.242	24.315	24.330	24.334	24.334	24.334
(DLV/DLP)T	-1.01842	-1.01384	-1.01269	-1.00664	-1.00331	-1.00129	-1.00024	-1.00005	-1.00001	-1.00000	-1.00000
(DLV/DLT)P	1.4394	1.3493	1.3254	1.1895	1.1044	1.0460	1.0103	1.0024	1.0004	1.0000	1.0000
CP, CAL/(G)(K)	1.3867	1.2297	1.1861	0.9193	0.7307	0.5822	0.4679	0.4285	0.4070	0.3867	0.3729
GAMMA (S)	1.1226	1.1252	1.1263	1.1379	1.1551	1.1803	1.2166	1.2368	1.2513	1.2677	1.2804
SON VEL,M/SEC	1039.2	1009.6	1001.8	955.5	921.1	886.1	833.8	788.4	740.8	678.5	632.9
MACH NUMBER	0.000	1.000	1.131	1.762	2.144	2.491	2.939	3.295	3.672	4.203	4.633

PERFORMANCE PARAMETERS

AE/AT	1.0000	1.0155	1.5385	2.4018	3.8925	7.5292	12.493	20.824	41.114	68.885
CSTAR, FT/SEC	5081	5081	5081	5081	5081	5081	5081	5081	5081	5081
CF	0.652	0.732	1.087	1.275	1.425	1.582	1.677	1.756	1.841	1.894
IVAC,LB-SEC/LB	194.4	195.7	220.3	239.3	255.8	273.6	284.6	293.8	303.8	309.9
ISP, LB-SEC/LB	103.0	115.6	171.7	201.4	225.0	249.9	264.9	277.4	290.8	299.0

MOLE FRACTIONS

ALOH	0.00024	0.00013	0.00011	0.00003	0.00000	0.00000	0.00000	0.00000	0.00000	0.00000	0.00000
H	0.00765	0.00521	0.00464	0.00189	0.00069	0.00016	0.00001	0.00000	0.00000	0.00000	0.00000
HO2	0.00012	0.00008	0.00007	0.00003	0.00002	0.00001	0.00000	0.00000	0.00000	0.00000	0.00000
H2	0.01327	0.01007	0.00926	0.00483	0.00233	0.00082	0.00011	0.00001	0.00000	0.00000	0.00000
H2O	0.48561	0.50266	0.50704	0.53120	0.54579	0.55579	0.56206	0.56347	0.56381	0.56388	0.56388
O	0.02631	0.01957	0.01789	0.00904	0.00425	0.00146	0.00018	0.00002	0.00000	0.00000	0.00000
OH	0.07273	0.05911	0.05550	0.03460	0.02070	0.01010	0.00253	0.00061	0.00011	0.00001	0.00000
O2	0.39195	0.40096	0.40328	0.41610	0.42390	0.42932	0.43276	0.43354	0.43374	0.43377	0.43378
AL2O3(A)	0.00000	0.00000	0.00000	0.00229	0.00232	0.00233	0.00234	0.00234	0.00234	0.00234	0.00234
AL2O3(L)	0.00212	0.00220	0.00221	0.00000	0.00000	0.00000	0.00000	0.00000	0.00000	0.00000	0.00000

THEORETICAL ROCKET PERFORMANCE ASSUMING FROZEN COMPOSITION DURING EXPANSION

PC - 10.0 PSIA

	CHEMICAL FORMULA	
FUEL	AL	1.00000
FUEL	H	2.00000
OXIDANT	O	2.00000

WT FRACTION (SEE NOTE)	ENERGY CAL/MOL	STATE	TEMP DEG K
0.100000	0.000	S	298.15
0.900000	2154.000	L	20.27
1.000000	-3102.000	L	90.18

O/F = 18.2224 PERCENT FUEL = 5.2023 EQUIVALENCE RATIO = 0.3967 PHI = 0.3969

	CHAMBER	THROAT	EXIT
PC/P	1.0000	1.7863	2.0000
P, ATM	0.68046	0.38093	0.34023
T, DEG K	2692.0	2423.5	2373.9
RHO, G/CC	7.1669-5	4.4566-5	4.0637-5
H, CAL/G	-141.93	-268.57	-291.72
U, CAL/G	-371.86	-475.57	-494.48
G, CAL/G	8092.89	7426.50	-7303.07
S, CAL/(G)(K)	2.9535	2.9535	2.9535
M, MOL WT	23.266	23.266	23.266
CP, CAL/(G)(K)	0.4758	0.4673	0.4656
GAMMA (S)	1.2188	1.2236	1.2247
SON VEL,M/SEC	1082.8	1029.4	1019.3
MACH NUMBER	0.000	1.000	1.098

PERFORMANCE PARAMETERS

AE/AT	1.0000	2.5210
CSTAR, FT/SEC	4930	4930
CF	0.685	0.745
IVAC, LB-SEC/LB	190.8	191.4
ISP, LB-SEC/LB	105.0	114.2

MOLE FRACTIONS

AL2O2I	0.00024	H	0.00765	HO2	0.00012	H2	0.01377
H2O	0.48561	O	0.02631	OH	0.07273	O2	0.35135
AL2O3(L)	0.00212						

THEORETICAL ROCKET PERFORMANCE ASSUMING EQUILIBRIUM COMPOSITION DURING EXPANSION

PC = 10.0 PSIA

CHEMICAL FORMULA		WT FRACTION (SEE NOTE)	ENERGY CAL/MOL	STATE	TEMP DEG K
FUEL	AL 1.00000	0.100000	0.000	S	298.15
FUEL	H 2.00000	0.900000	-2154.000	L	20.27
OXIDANT	O 2.00000	1.000000	-3102.000	L	90.18

O/F = 7.2889 PERCENT FUEL = 12.0643 EQUIVALENCE RATIO= 0.9922 PHI= 0.9922

	CHAMBER	THROAT	EXIT	EXIT	EXIT	EXIT	EXIT	EXIT	EXIT	EXIT	EXIT
PC/P	1.0000	1.7135	2.0000	5.0000	10.000	20.000	50.000	100.00	200.00	500.00	1000.00
P, ATM	0.68046	0.39712	0.34023	0.13609	0.06805	0.03402	0.01361	0.00680	0.00340	0.00136	0.00068
T, DEG K	2996.7	2889.2	2859.5	2691.9	2573.8	2461.9	2323.0	2220.5	2119.6	1985.6	1880.1
RHO, G/CC	4.2648-5	2.6215-5	2.2793-5	9.9300-6	5.2876-6	2.8123-6	1.2176-6	6.4682-7	3.4374-7	1.4934-7	7.9766-8
H, CAL/G	-201.27	-404.03	-460.33	-777.74	-1000.68	-1210.14	-1468.06	-1650.11	-1821.44	-2032.30	-2180.38
U, CAL/G	-587.66	-770.87	-821.83	-1109.64	-1312.33	-1503.12	-1738.74	-1904.88	-2061.14	-2252.99	-2386.97
G, CAL/G	-12988.3	-12732.5	-12661.7	-12264.0	-11983.1	-11715.0	-11380.2	-11124.9	-10866.0	-10504.9	-10203.0
S, CAL/(G)(K)	4.2670	4.2670	4.2670	4.2670	4.2670	4.2670	4.2670	4.2670	4.2670	4.2670	4.2670
M, MOL WT	15.412	15.651	15.719	16.117	16.411	16.698	17.054	17.320	17.572	17.880	18.085
(DLV/DLP)T	1.07332	-1.06749	-1.06583	1.05609	-1.04887	-1.04184	-1.03317	-1.02674	-1.02071	-1.01352	-1.00887
(DLV/DLT)P	2.4932	2.4247	2.4039	2.2698	2.1570	2.0354	1.8705	1.7344	1.5962	1.4163	1.2888
CP, CAL/(G)(K)	4.6929	4.5840	4.5484	4.2965	4.0593	3.7828	3.3797	3.0210	2.6366	2.1036	1.6993
GAMMA (S)	1.1080	1.1054	1.1047	1.1010	1.0988	1.0971	1.0958	1.0959	1.0972	1.1019	1.1093
SON VEL,M/SEC	1348.4	1302.6	1292.6	1236.5	1197.0	1159.7	1114.0	1080.8	1049.0	1008.7	979.2
MACH NUMBER	0.000	1.000	1.139	1.776	2.161	2.506	2.923	3.222	3.510	3.881	4.156

PERFORMANCE PARAMETERS

AE/AT	1.0000	1.0175	1.5657	2.4969	4.1789	8.6138	15.162	26.980	58.413	105.19
CSTAR, FT/SEC	6624	6624	6624	6624	6624	6624	6624	6624	6624	6624
CF	0.645	0.729	1.088	1.281	1.439	1.613	1.724	1.824	1.939	2.016
IVAC,LB-SEC/LB	253.0	254.9	288.4	315.1	339.3	367.5	386.3	403.2	423.2	436.6
ISP, LB-SEC/LB	132.8	150.1	224.0	263.7	296.3	332.0	355.1	375.5	399.2	415.0

MOLE FRACTIONS

AL	0.00001	0.00001	0.00001	0.00000	0.00000	0.00000	0.00000	0.00000	0.00000	0.00000
ALO	0.00019	0.00011	0.00010	0.00004	0.00002	0.00001	0.00000	0.00000	0.00000	0.00000
ALOH	0.00012	0.00008	0.00007	0.00003	0.00002	0.00001	0.00000	0.00000	0.00000	0.00000
ALO2	0.00001	0.00001	0.00000	0.00000	0.00000	0.00000	0.00000	0.00000	0.00000	0.00000
ALO2H	0.00159	0.00118	0.00109	0.00063	0.00040	0.00024	0.00012	0.00005	0.00002	0.00001	0.00000
H	0.07095	0.06424	0.06233	0.05134	0.04338	0.03580	0.02680	0.02035	0.01456	0.00818	0.00451
HO2	0.00005	0.00004	0.00003	0.00002	0.00001	0.00001	0.00000	0.00000	0.00000	0.00000	0.00000
H2	0.14224	0.13512	0.13301	0.11996	0.10947	0.09850	0.08373	0.07172	0.05934	0.04267	0.03022
H2O	0.59877	0.62643	0.63438	0.68145	0.71687	0.75199	0.79631	0.83010	0.86287	0.90386	0.93212
O	0.03060	0.02698	0.02597	0.02037	0.01655	0.01310	0.00924	0.00668	0.00454	0.00237	0.00123
OH	0.10145	0.09269	0.09020	0.07581	0.06537	0.05540	0.04332	0.03464	0.02663	0.01724	0.01122
O2	0.05155	0.05034	0.04994	0.04712	0.04446	0.04135	0.03674	0.03263	0.02812	0.02169	0.01666
AL2O3(A)	0.00000	0.00000	0.00000	0.00000	0.00000	0.00000	0.00374	0.00383	0.00390	0.00398	0.00403
AL2O3(L)	0.00248	0.00279	0.00287	0.00324	0.00344	0.00359	0.00000	0.00000	0.00000	0.00000	0.00000

THEORETICAL ROCKET PERFORMANCE ASSUMING FROZEN COMPOSITION DURING EXPANSION

PC = 10.0 PSIA

	CHEMICAL FORMULA	WT FRACTION (SEE NOTE)	ENERGY CAL/MOL	STATE	TEMP DEG K
FUEL	AL 1.00000	0.100000	0.000	S	298.15
FUEL	H 2.00000	0.900000	2154.000	L	20.27
OXIDANT	O 2.00000	1.000000	3102.000	L	90.18

O/F= 7.2689 PERCENT FUEL= 12.0643 EQUIVALENCE RATIO= 0.9922 PHI= 0.9922

	CHAMBER	THROAT	EXIT
PC/P	1.0000	1.7826	2.0000
P, ATM	0.68046	0.38171	0.34023
T, DEG K	2996.7	2704.9	2649.7
RHO, G/CC	4.2648-5	2.6505-5	2.4116-5
H, CAL/G	201.27	413.61	453.33
U, CAL/G	-587.66	762.38	794.98
G, CAL/G	12986.3	11955.4	11759.7
S, CAL/(G)(K)	4.2670	4.2670	4.2670
M, MOL WT	15.412	15.412	15.412
CP, CAL/(G)(K)	0.7336	0.7213	0.7187
GAMMA (S)	1.2133	1.2177	1.2186
SON VEL,M/SEC	1400.5	1333.0	1319.9
MACH NUMBER	0.000	1.000	1.100

PERFORMANCE PARAMETERS

AE/AT	1.0000	2.5219
CSTAR, FT/SEC	6402	6402
CF	0.683	0.744
IVAC, LB-SEC/LB	247.6	248.5
ISP, LB-SEC/LB	135.9	148.1

MOLE FRACTIONS

AL	0.00001	ALO	0.00019	ALOH	0.00012	AL02	0.00001
AL03(L)	0.00155	H	0.07095	HO2	0.00005	H2	0.14224
H20	0.59877	O	0.03060	OH	0.10145	O2	0.05155
AL2O3(L)	0.00248						

THEORETICAL ROCKET PERFORMANCE ASSUMING EQUILIBRIUM COMPOSITION DURING EXPANSION

PC = 10.0 PSIA

	CHEMICAL FORMULA	WT FRACTION (SEE NOTE)	ENERGY CAL/MOL	STATE	TEMP DEG K
FUEL	AL 1.00000	1.000000	0.000	S	298.15
OXIDANT	O 2.00000	1.000000	-3102.000	L	90.18

O/F= 1.3330 PERCENT FUEL= 42.8633 EQUIVALENCE RATIO= 0.6673 PHI= 0.6673

	CHAMBER	THROAT	EXIT	EXIT	EXIT	EXIT	EXIT	EXIT	EXIT	EXIT	EXIT
PC/P	1.0000	1.6991	2.0000	5.0000	10.000	20.000	50.000	100.00	200.00	500.00	1000.00
P, ATM	0.68046	0.40047	0.34023	0.13609	0.06805	0.03402	0.01361	0.00680	0.00340	0.00136	0.00068
T, DEG K	3881.2	3769.4	3736.3	3561.4	3440.1	3327.0	3188.8	3091.8	3000.6	2888.1	2808.6
RHO, G/CC	1.1657-4	7.1462-5	6.1464-5	2.6298-5	1.3809-5	7.2393-6	3.0761-6	1.6075-6	8.3900-7	3.5457-7	1.8458-7
H, CAL/G	-55.389	-128.81	-150.80	-269.56	-354.32	-435.10	-536.28	-608.92	-678.47	-766.01	-829.15
U, CAL/G	-196.75	-264.53	-284.85	-394.88	-473.66	-548.92	-643.42	-711.43	-776.67	-858.96	-918.42
G, CAL/G	-6683.28	-6565.78	-6531.37	-6351.45	-6228.96	-6116.62	-5981.74	-5888.74	-5802.62	-5698.12	-5625.38
S, CAL/(G)(K)	1.7077	1.7077	1.7077	1.7077	1.7077	1.7077	1.7077	1.7077	1.7077	1.7077	1.7077
M, MOL WT	54.561	55.193	55.387	56.471	57.284	58.089	59.144	59.934	60.718	61.745	62.516
(DLV/DLP)T	-3.56437	-3.46538	-3.43541	-3.27130	-3.15229	-3.03786	-2.89368	-2.78997	-2.69078	-2.56645	-2.47734
(DLV/DLT)P	47.1476	46.8427	46.7313	45.9675	45.2529	44.4393	43.2373	42.2492	41.2059	39.7586	38.6230
CP, CAL/(G)(K)	30.6401	31.0882	31.2081	31.7338	31.9747	32.0921	32.0748	31.9437	31.7208	31.2994	30.8945
GAMMA (S)	1.0846	1.0820	1.0813	1.0774	1.0747	1.0721	1.0691	1.0670	1.0650	1.0627	1.0610
SON VEL,M/SEC	800.9	783.8	778.8	751.6	732.5	714.5	692.3	676.5	661.5	642.9	629.5
MACH NUMBER	0.000	1.000	1.147	1.781	2.159	2.495	2.898	3.181	3.452	3.793	4.042

PERFORMANCE PARAMETERS

AE/AT	1.0000	1.0199	1.5911	2.5648	4.3408	9.0775	16.191	29.239	64.785	119.26
CSTAR, FT/SEC	4038	4038	4038	4038	4038	4038	4038	4038	4038	4038
CF	0.637	0.726	1.088	1.285	1.448	1.630	1.749	1.855	1.981	2.067
IVAC,LB-SEC/LB	153.8	155.1	176.5	193.5	209.0	227.3	239.8	251.2	264.9	274.4
ISP, LB-SEC/LB	79.9	91.1	136.5	161.3	181.8	204.6	219.5	232.8	248.7	259.5

MOLE FRACTIONS

AL	0.04868	0.04896	0.04904	0.04948	0.04976	0.04999	0.05019	0.05025	0.05021	0.05001	0.04974
ALO	0.13878	0.13343	0.13179	0.12267	0.11589	0.10924	0.10066	0.09436	0.08823	0.08042	0.07475
ALO2	0.00295	0.00248	0.00235	0.00173	0.00136	0.00107	0.00077	0.00060	0.00046	0.00033	0.00025
AL2O	0.02017	0.01918	0.01887	0.01712	0.01579	0.01447	0.01278	0.01155	0.01038	0.00893	0.00792
AL2O2	0.00363	0.00327	0.00317	0.00261	0.00224	0.00190	0.00152	0.00126	0.00105	0.00081	0.00066
O	0.44186	0.44663	0.44812	0.45656	0.46301	0.46948	0.47799	0.48435	0.49061	0.49868	0.50461
O2	0.12460	0.12113	0.12004	0.11381	0.10901	0.10417	0.09777	0.09298	0.08826	0.08215	0.07767
AL2O3(L)	0.21931	0.22491	0.22661	0.23602	0.24294	0.24968	0.25832	0.26465	0.27080	0.27866	0.28440

THEORETICAL ROCKET PERFORMANCE ASSUMING FROZEN COMPOSITION DURING EXPANSION

PC = 10.0 PSIA

	CHEMICAL FORMULA	WT FRACTION (SEE NOTE)	ENERGY CAL/MOL	STATE	TEMP DEG K
FUEL	AL 1.00000	1.000000	0.000	S	298.15
OXIDANT	O 2.00000	1.000000	-3102.000	L	90.18

O/F= 1.3330 PERCENT FUEL= 42.8633 EQUIVALENCE RATIO= 0.6673 PHI= 0.6673

	CHAMBER	THROAT	EXIT	EXIT	EXIT	EXIT	EXIT	EXIT	EXIT
PC/P	1.0000	1.7160	2.0000	5.0000	10.000	20.000	50.000	100.00	200.00
P, ATM	0.68046	0.39653	0.34023	0.13609	0.06805	0.03402	0.01361	0.00680	0.00340
T, DEG K	3881.2	3680.2	3625.1	3312.1	3093.2	2888.7	2638.5	2463.4	2299.7
RHO, G/CC	1.1657-4	7.1643-5	6.2405-5	2.7321-5	1.4627-5	7.8314-6	3.4296-6	1.8366-6	9.8369-7
H, CAL/G	-55.389	-129.73	-150.10	-265.78	-346.60	-422.08	-514.25	-578.63	-638.73
U, CAL/G	-196.75	-263.77	-282.13	-386.41	-459.26	-527.29	-610.35	-668.35	-722.49
G, CAL/G	6683.28	-6414.36	-6340.65	-5921.86	-5628.95	-5355.08	-5020.03	-4785.47	4566.00
S, CAL/(G)(K)	1.7077	1.7077	1.7077	1.7077	1.7077	1.7077	1.7077	1.7077	1.7077
M, MOL WT	54.561	54.561	54.561	54.561	54.561	54.561	54.561	54.561	54.561
CP, CAL/(G)(K)	0.3693	0.3698	0.3697	0.3695	0.3691	0.3687	0.3681	0.3674	0.3668
GAMMA (S)	1.1092	1.1093	1.1093	1.1094	1.1095	1.1096	1.1098	1.1100	1.1103
SON VEL,M/SEC	810.0	788.7	782.8	748.3	723.2	698.9	668.0	645.5	623.8
MACH NUMBER	0.000	1.000	1.137	1.773	2.159	2.506	2.933	3.241	3.542

PERFORMANCE PARAMETERS

AE/AT	1.0000	1.0171	1.5588	2.4748	4.1191	8.4084	14.703	65.000
CSTAR, FT/SEC	4003	4003	4003	4003	4003	4003	4003	4003
CF	0.646	0.730	1.087	1.279	1.436	1.606	1.715	1.811
IVAC, LB SEC/LB	152.9	154.1	174.1	190.0	204.3	220.7	231.7	241.5
ISP, LB SEC/LB	80.4	90.8	135.3	159.2	178.6	199.8	213.4	225.3

MOLE FRACTIONS

AL	0.04868	ALO	0.13878	ALO2	0.00295	AL2O	0.02017
AL2O2	0.00363	O	0.44186	O2	0.12460	AL2O3(L)	0.21931

THEORETICAL ROCKET PERFORMANCE ASSUMING EQUILIBRIUM COMPOSITION DURING EXPANSION

PC = 10.0 PSIA

	CHEMICAL FORMULA	WT FRACTION (SEE NOTE)	ENERGY CAL/MOL	STATE	TEMP DEG K
FUEL	AL 1.00000	1.000000	0.000	S	298.15
OXIDANT	O 2.00000	1.000000	-3102.000	L	90.18

O/F= 0.8890 PERCENT FUEL= 52.9381 EQUIVALENCE RATIO= 1.0005 PHI= 1.0005

	CHAMBER	THROAT	EXIT	EXIT	EXIT	EXIT	EXIT	EXIT	EXIT	EXIT	EXIT
PC/P	1.0000	1.6983	2.0000	5.0000	10.000	20.000	50.000	100.00	200.00	500.00	1000.00
P, ATM	0.68046	0.40066	0.34023	0.13609	0.06805	0.03402	0.01361	0.00680	0.00340	0.00136	0.00068
T, DEG K	3918.3	3805.5	3772.0	3595.6	3473.2	3359.3	3220.1	3122.4	3030.7	2917.7	2837.7
RHO, G/CC	1.2742-4	7.8096-5	6.7128-5	2.8691-5	1.5054-5	7.8859-6	3.3473-6	1.7478-6	9.1146-7	3.8476-7	2.0013-7
H, CAL/G	-45.622	-112.76	-132.95	-241.74	-319.47	-393.59	-486.52	-553.31	-617.30	-697.92	-756.13
U, CAL/G	-174.95	-237.00	-255.69	-356.61	-428.93	-498.07	-584.98	-647.59	-707.69	-783.58	-838.47
G, CAL/G	-6392.72	-6277.15	-6243.17	-6066.13	-5945.64	-5835.19	-5702.63	-5611.28	-5526.72	-5424.18	-5352.86
S, CAL/(G)(K)	1.6199	1.6199	1.6199	1.6199	1.6199	1.6199	1.6199	1.6199	1.6199	1.6199	1.6199
M, MOL WT	60.205	60.866	61.069	62.202	63.051	63.891	64.990	65.811	66.624	67.688	68.484
(DLV/DLP)T	**********	**********	**********	**********	**********	**********	**********	**********	**********	**********	**********
(DLV/DLT)P	**********	**********	**********	**********	**********	**********	**********	**********	**********	**********	**********
CP, CAL/(G)(K)	**********	**********	**********	**********	**********	**********	**********	**********	**********	**********	**********
GAMMA (S)	1.0832	1.0807	1.0800	1.0761	1.0733	1.0708	1.0678	1.0657	1.0637	1.0613	1.0596
SON VEL,M/SEC	765.6	749.5	744.7	719.1	701.1	684.2	663.2	648.4	634.3	616.7	604.2
MACH NUMBER	0.000	1.000	1.148	1.781	2.159	2.494	2.896	3.179	3.448	3.788	4.036

PERFORMANCE PARAMETERS

AE/AT	1.0000	1.0201	1.5926	2.5687	4.3500	9.1043	16.249	29.363	65.117	119.95
CSTAR, FT/SEC	3864	3864	3864	3864	3864	3864	3864	3864	3864	3864
CF	0.636	0.726	1.088	1.285	1.449	1.631	1.750	1.857	1.984	2.070
IVAC,LB-SEC/LB	147.2	148.4	168.9	185.2	200.1	217.7	229.7	240.7	253.9	263.1
ISP, LB-SEC/LB	76.4	87.2	130.6	154.4	174.0	195.9	210 2	223.0	238.2	248.6

MOLE FRACTIONS

AL	0.12136	0.12438	0.12534	0.13096	0.13543	0.14006	0.14638	0.15127	0.15620	0.16274	0.16765
ALO	0.21298	0.20698	0.20512	0.19473	0.18688	0.17906	0.16879	0.16109	0.15347	0.14355	0.13617
ALO2	0.00287	0.00242	0.00230	0.00170	0.00135	0.00106	0.00077	0.00060	0.00047	0.00034	0.00026
AL2	0.00002	0.00002	0.00002	0.00001	0.00001	0.00000	0.00000	0.00000	0.00000	0.00000	0.00000
AL2O	0.06567	0.06404	0.06351	0.06033	0.05773	0.05499	0.05121	0.04827	0.04529	0.04135	0.03839
AL2O2	0.00729	0.00669	0.00651	0.00554	0.00487	0.00424	0.00351	0.00301	0.00257	0.00207	0.00174
O	0.31569	0.31787	0.31854	0.32225	0.32498	0.32764	0.33100	0.33341	0.33571	0.33855	0.34055
O2	0.05469	0.05254	0.05187	0.04810	0.04527	0.04248	0.03889	0.03627	0.03375	0.03059	0.02833
AL2O3(L)	0.21943	0.22507	0.22680	0.23639	0.24349	0.25046	0.25945	0.26607	0.27253	0.28082	0.28691

THEORETICAL ROCKET PERFORMANCE ASSUMING FROZEN COMPOSITION DURING EXPANSION

PC = 10.0 PSIA

	CHEMICAL FORMULA	WT FRACTION (SEE NOTE)	ENERGY CAL/MOL	STATE	TEMP DEG K
FUEL	AL 1.00000	1.000000	0.000	S	298.15
OXIDANT	O 2.00000	1.000000	-3102.000	L	90.18

O/F = 0.8890 PERCENT FUEL = 52.9381 EQUIVALENCE RATIO= 1.0005 PHI = 1.0005

	CHAMBER	THROAT	EXIT	EXIT	EXIT	EXIT	EXIT	EXIT	EXIT
PC/P	1.0000	1.7132	2.0000	5.0000	10.000	20.000	50.000	100.00	200.00
P, ATM	0.68046	0.39718	0.34023	0.13609	0.06805	0.03402	0.01361	0.00680	0.00340
T, DEG K	3918.3	3723.4	3669.1	3364.1	3150.4	2950.2	2704.8	2532.5	2371.0
RHO, G/CC	1.2742-4	7.8267-5	6.8034-5	2.9681-5	1.5847-5	8.4613-6	3.6917-6	1.9714-6	1.0528-6
H, CAL/G	-45.622	-113.50	-132.39	-238.68	-313.17	-382.93	-468.40	-528.29	-584.36
U, CAL/G	-174.95	-236.40	-253.49	-349.72	-417.16	-480.31	-557.67	-611.88	-662.62
G, CAL/G	-6392.72	-6144.87	-6075.94	-5688.16	-5416.45	-5161.92	-4849.76	-4630.62	-4425.02
S, CAL/(G)(K)	1.6199	1.6199	1.6199	1.6199	1.6199	1.6199	1.6199	1.6199	1.6199
M, MOL WT	60.205	60.205	60.205	60.205	60.205	60.205	60.205	60.205	60.205
CP, CAL/(G)(K)	0.3482	0.3483	0.3484	0.3486	0.3485	0.3484	0.3479	0.3474	0.3468
GAMMA (S)	1.1047	1.1047	1.1047	1.1046	1.1046	1.1047	1.1048	1.1050	1.1052
SON VEL,M/SEC	773.2	753.7	748.2	716.4	693.2	670.9	642.4	621.7	601.6
MACH NUMBER	0.000	1.000	1.139	1.774	2.158	2.504	2.928	3.233	3.530

PERFORMANCE PARAMETERS

AE/AT	1.0000	1.0175	1.5636	2.4877	4.1495	8.4952	14.889	65.968
CSTAR, FT/SEC	3835	3835	3835	3835	3835	3835	3835	3835
CF	0.645	0.729	1.087	1.280	1.437	1.609	1.719	1.817
IVAC,LB-SEC/LB	146.4	147.5	166.9	182.2	196.0	212.0	222.7	232.2
ISP, LB-SEC/LB	76.9	86.9	129.6	152.6	171.3	191.8	204.9	216.5

MOLE FRACTIONS

AL	0.12136	ALO	0.21298	ALO2	0.00287	AL2	0.00002
AL2O	0.06567	AL2O2	0.00729	O	0.31569	O2	0.05469
AL2O3(L)	0.21943						

THEORETICAL ROCKET PERFORMANCE ASSUMING EQUILIBRIUM COMPOSITION DURING EXPANSION

PC = 10.0 PSIA

CHEMICAL FORMULA		WT FRACTION (SEE NOTE)	ENERGY CAL/MOL	STATE	TEMP DEG K
FUEL	SI 1.00000 H 4.00000	1.000000	7300.000	S	298.15
OXIDANT	O 2.00000	1.000000	-3102.000	L	90.18

O/F= 5.0000 PERCENT FUEL= 16.6667 EQUIVALENCE RATIO= 0.3985 PHI= 0.3985

	CHAMBER	THROAT	EXIT	EXIT	EXIT	EXIT	EXIT	EXIT	EXIT	EXIT	EXIT
PC/P	1.0000	1.7048	2.0000	5.0000	10.000	20.000	50.000	100.00	200.00	500.00	1000.00
P, ATM	0.68046	0.39914	0.34023	0.13609	0.06805	0.03402	0.01361	0.00680	0.00340	0.00136	0.00068
T, DEG K	2895.2	2814.3	2790.8	2662.5	2571.6	2485.1	2376.3	2296.9	2218.8	2114.9	2032.8
RHO, G/CC	8.8630-5	5.4390-5	4.6984-5	2.0250-5	1.0695-5	5.6406-6	2.4174-6	1.2724-6	6.6950-7	2.8666-7	1.5116-7
H, CAL/G	-42.902	-139.87	-168.06	-322.86	-432.63	-536.62	-665.93	-758.04	-845.56	-954.59	-1032.21
U, CAL/G	-228.83	-317.59	-343.43	-485.61	-586.71	-682.69	-802.27	-887.56	-968.63	-1069.56	-1141.23
G, CAL/G	-6873.22	-6779.38	-6752.27	-6604.30	-6499.60	-6399.59	-6272.07	-6176.87	-6080.17	-5944.09	-5828.11
S, CAL/(G)(K)	2.3592	2.3592	2.3592	2.3592	2.3592	2.3592	2.3592	2.3592	2.3592	2.3592	2.3592
M, MOL WT	30.943	31.469	31.625	32.509	33.165	33.808	34.636	35.243	35.827	36.555	37.056
(DLV/DLP)T	-1.25441	-1.22883	-1.22143	-1.18113	-1.15303	-1.12694	-1.09557	-1.07429	-1.05530	-1.03418	-1.02169
(DLV/DLT)P	6.3335	5.9479	5.8316	5.1595	4.6489	4.1408	3.4817	3.0012	2.5464	2.0071	1.6678
CP, CAL/(G)(K)	7.5736	7.1490	7.0178	6.2323	5.6067	4.9609	4.0897	3.4310	2.7886	2.0006	1.4874
GAMMA (S)	1.0938	1.0913	1.0906	1.0869	1.0845	1.0825	1.0805	1.0796	1.0795	1.0814	1.0853
SON VEL,M/SEC	922.4	900.8	894.5	860.3	836.2	813.4	785.1	764.9	745.8	721.2	703.6
MACH NUMBER	0.000	1.000	1.144	1.779	2.160	2.499	2.908	3.198	3.476	3.830	4.089

PERFORMANCE PARAMETERS

AE/AT	1.0000	1.0190	1.5807	2.5368	4.2734	8.8763	15.741	28.237	61.879	112.65
CSTAR, FT/SEC	4617	4617	4617	4617	4617	4617	4617	4617	4617	4617
CF	0.640	0.727	1.088	1.283	1.444	1.623	1.738	1.842	1.963	2.045
IVAC,LB-SEC/LB	176.0	177.5	201.4	220.6	237.9	258.3	272.0	284.5	299.4	309.6
ISP, LB-SEC/LB	91.9	104.4	156.1	184.1	207.3	232.8	249.5	264.3	281.7	293.4

MOLE FRACTIONS

H	0.01493	0.01458	0.01447	0.01378	0.01316	0.01245	0.01131	0.01027	0.00903	0.00705	0.00530
HO2	0.00013	0.00010	0.00010	0.00006	0.00004	0.00003	0.00002	0.00001	0.00001	0.00001	0.00000
H2	0.01291	0.01262	0.01253	0.01196	0.01147	0.01092	0.01006	0.00929	0.00839	0.00693	0.00560
H2O	0.23538	0.24002	0.24140	0.24928	0.25523	0.26123	0.26935	0.27573	0.28245	0.29205	0.29996
O	0.06025	0.05774	0.05699	0.05265	0.04930	0.04583	0.04098	0.03700	0.03266	0.02619	0.02067
OH	0.08515	0.08087	0.07961	0.07249	0.06723	0.06205	0.05522	0.04999	0.04461	0.03705	0.03080
O2	0.44204	0.44385	0.44439	0.44757	0.45009	0.45278	0.45673	0.46013	0.46403	0.47022	0.47586
SIO	0.06603	0.05930	0.05733	0.04643	0.03867	0.03137	0.02252	0.01653	0.01127	0.00568	0.00271
SIO2	0.01232	0.01075	0.01030	0.00799	0.00647	0.00514	0.00364	0.00268	0.00187	0.00102	0.00054
SIO2(L)	0.07084	0.08017	0.08288	0.09779	0.10832	0.11819	0.13018	0.13837	0.14570	0.15382	0.15855

THEORETICAL ROCKET PERFORMANCE ASSUMING FROZEN COMPOSITION DURING EXPANSION

PC = 10.0 PSIA

CHEMICAL FORMULA				WT FRACTION (SEE NOTE)	ENERGY CAL/MOL	STATE	TEMP DEG K
FUEL	SI 1.00000	H 4.00000		1.000000	7300.000	S	298.15
OXIDANT	O 2.00000			1.000000	-3102.000	L	90.18

O/F= 5.0000 PERCENT FUEL= 16.6667 EQUIVALENCE RATIO= 0.3985 PHI= 0.3985

	CHAMBER	THROAT	EXIT	EXIT
PC/P	1.0000	1.7777	2.0000	5.0000
P, ATM	0.68046	0.38277	0.34023	0.13609
T, DEG K	2895.2	2621.8	2568.7	2186.9
RHO, G/CC	8.8630-5	5.5054-5	4.9946-5	2.3466-5
H, CAL/G	-42.902	-144.75	-164.39	-304.05
U, CAL/G	-228.83	-313.12	-329.35	-444.49
G, CAL/G	6873.22	-6330.16	-6224.56	-5463.51
S, CAL/(G)(K)	2.3592	2.3592	2.3592	2.3592
M, MOL WT	30.943	30.943	30.943	30.943
CP, CAL/(G)(K)	0.3747	0.3704	0.3694	0.3619
GAMMA (S)	1.2068	1.2098	1.2104	1.2157
SON VEL,M/SEC	968.9	923.2	914.0	845.2
MACH NUMBER	0.000	1.000	1.103	1.749

PERFORMANCE PARAMETERS

AE/AT	1.0000	1.0093	2.9303
CSTAR, FT/SEC	4451	4451	4451
CF	0.681	0.743	1.090
IVAC, LB SEC/LB	172.0	172.6	191.3
ISP, LB SEC/LB	94.1	102.8	150.7

MOLE FRACTIONS

H	0.01493	HO2	0.00013	H2	0.01291	H2O	0.23538
O	0.06025	OH	0.08515	O2	0.44204	SIO	0.06603
SIO2	0.01232	SIO2(L)	0.07084				

THEORETICAL ROCKET PERFORMANCE ASSUMING EQUILIBRIUM COMPOSITION DURING EXPANSION

PC = 10.0 PSIA

	CHEMICAL FORMULA		WT FRACTION (SEE NOTE)	ENERGY CAL/MOL	STATE	TEMP DEG K
FUEL	SI 1.00000	H 4.00000	1.000000	7300.000	S	298.15
OXIDANT	O 2.00000		1.000000	-3102.000	L	90.18

O/F= 3.0000 PERCENT FUEL= 25.0000 EQUIVALENCE RATIO= 0.6642 PHI= 0.6642

	CHAMBER	THROAT	EXIT	EXIT	EXIT	EXIT	EXIT	EXIT	EXIT	EXIT	EXIT
PC/P	1.0000	1.7045	2.0000	5.0000	10.000	20.000	50.000	100.00	200.00	500.00	1000.00
P, ATM	0.68046	0.39922	0.34023	0.13609	0.06805	0.03402	0.01361	0.00680	0.00340	0.00136	0.00068
T, DEG K	2945.2	2866.6	2843.8	2720.1	2633.5	2552.1	2451.9	2381.1	2314.0	2230.8	2171.4
RHO, G/CC	7.7958-5	4.7841-5	4.1316-5	1.7796-5	9.3903-6	4.9468-6	2.1152-6	1.1105-6	5.8223-7	2.4752-7	1.2942-7
H, CAL/G	-15.883	-126.09	-158.19	-334.28	-459.23	-577.74	-725.34	-830.74	-931.19	-1056.96	-1147.22
U, CAL/G	-227.26	-328.18	-357.61	-519.48	-634.72	-744.29	-881.16	-979.14	-1072.70	-1190.12	-1274.54
G, CAL/G	-7603.28	-7510.86	-7484.33	-7341.70	-7243.44	-7152.43	-7041.88	-6964.75	-6892.54	-6803.73	-6740.96
S, CAL/(G)(K)	2.5762	2.5762	2.5762	2.5762	2.5762	2.5762	2.5762	2.5762	2.5762	2.5762	2.5762
M, MOL WT	27.688	28.189	28.338	29.186	29.821	30.449	31.271	31.885	32.495	33.292	33.889
(DLV/DLP)T	1.62507	1.59207	-1.58242	1.52913	1.49098	-1.45457	-1.40893	1.37618	-1.34486	-1.30557	-1.27736
(DLV/DLT)P	13.8043	13.4893	13.3920	12.8111	12.3471	11.8639	11.1987	10.6777	10.1433	9.4191	8.8600
CP, CAL/(G)(K)	19.2468	18.9956	18.9129	18.3760	17.9016	17.3720	16.5923	15.9461	15.2548	14.2769	13.4929
GAMMA (S)	1.0935	1.0908	1.0900	1.0858	1.0828	1.0801	1.0769	1.0746	1.0725	1.0699	1.0681
SON VEL,M/SEC	983.4	960.3	953.7	917.2	891.7	867.6	837.9	816.8	796.9	772.1	754.3
MACH NUMBER	0.000	1.000	1.144	1.780	2.160	2.499	2.908	3.197	3.473	3.823	4.079

PERFORMANCE PARAMETERS

AE/AT	1.0000	1.0190	1.5817	2.5402	4.2833	8.9147	15.844	28.513	62.889	115.38
CSTAR, FT/SEC	4923	4923	4923	4923	4923	4923	4923	4923	4923	4923
CF	0.640	0.727	1.088	1.284	1.445	1.624	1.740	1.844	1.967	2.050
IVAC,LB-SEC/LB	187.7	189.2	214.9	235.3	253.9	275.7	290.5	304.0	320.2	331.4
ISP, LB-SEC/LB	97.9	111.3	166.4	196.4	221.1	248.5	266.3	282.2	301.0	313.8

MOLE FRACTIONS

H	0.02663	0.02665	0.02666	0.02673	0.02680	0.02686	0.02694	0.02699	0.02701	0.02698	0.02691
HO2	0.00011	0.00009	0.00008	0.00005	0.00004	0.00003	0.00002	0.00001	0.00001	0.00001	0.00000
H2	0.02854	0.02838	0.02834	0.02804	0.02781	0.02756	0.02720	0.02690	0.02657	0.02610	0.02569
H2O	0.32513	0.33022	0.33171	0.34003	0.34605	0.35187	0.35928	0.36469	0.36998	0.37679	0.38184
O	0.05609	0.05456	0.05411	0.05165	0.04987	0.04817	0.04600	0.04441	0.04285	0.04082	0.03929
OH	0.09887	0.09465	0.09342	0.08661	0.08174	0.07709	0.07128	0.06713	0.06316	0.05819	0.05462
O2	0.25639	0.25579	0.25561	0.25450	0.25362	0.25272	0.25149	0.25055	0.24961	0.24839	0.24749
SIO	0.15552	0.14794	0.14570	0.13314	0.12394	0.11499	0.10355	0.09518	0.08706	0.07670	0.06915
SIO2	0.01891	0.01718	0.01669	0.01409	0.01236	0.01081	0.00902	0.00783	0.00677	0.00554	0.00474
SIO2(L)	0.03381	0.04453	0.04768	0.06515	0.07777	0.08990	0.10523	0.11632	0.12699	0.14050	0.15026

THEORETICAL ROCKET PERFORMANCE ASSUMING FROZEN COMPOSITION DURING EXPANSION

PC = 10.0 PSIA

	CHEMICAL FORMULA	WT FRACTION (SEE NOTE)	ENERGY CAL/MOL	STATE	TEMP DEG K
FUEL	SI 1.00000 H 4.00000	1.000000	7300.000	S	298.15
OXIDANT	O 2.00000	1.000000	3102.000	L	90.18

O/F= 3.0000 PERCENT FUEL= 25.0000 EQUIVALENCE RATIO= 0.6642 PHI= 0.6642

	CHAMBER	THROAT	EXIT	EXIT
PC/P	1.0000	1.7859	2.0000	5.0000
P, ATM	0.68046	0.38102	0.34023	0.13609
T, DEG K	2945.2	2651.5	2597.2	2192.3
RHO, G/CC	7.7958-5	4.8489-5	4.4202-5	2.0947-5
H, CAL/G	-15.883	-132.26	-153.58	-310.75
U, CAL/G	-227.26	-322.55	-339.99	-468.09
G, CAL/G	-7603.28	6962.91	6844.42	-5958.41
S, CAL/(G)(K)	2.5762	2.5762	2.5762	2.5762
M, MOL WT	27.688	27.688	27.688	27.688
CP, CAL/(G)(K)	0.3986	0.3935	0.3925	0.3833
GAMMA (S)	1.2196	1.2231	1.2238	1.2304
SON VEL,M/SEC	1038.6	986.8	977.0	900.0
MACH NUMBER	0.000	1.000	1.099	1.745

PERFORMANCE PARAMETERS

AE/AT	1.0000	1.0085	2.5085
CSTAR, FT/SEC	4727	4727	4727
CF	0.685	0.745	1.090
IVAC, LB-SEC/LB	182.9	183.5	202.9
ISP, LB-SEC/LB	100.6	109.5	160.2

MOLE FRACTIONS

H	0.02663	HO2	0.00011	H2	0.02854	H2O	0.32513
O	0.05609	OH	0.09887	O2	0.25639	SIO	0.15552
SIO2	0.01891	SIO2(L)	0.03381				

THEORETICAL ROCKET PERFORMANCE ASSUMING EQUILIBRIUM COMPOSITION DURING EXPANSION

PC = 10.0 PSIA

CHEMICAL FORMULA					WT FRACTION (SEE NOTE)	ENERGY CAL/MOL	STATE	TEMP DEG K
FUEL	C	1.00000	H	4.00000	1.000000	-21390.000	L	111.66
OXIDANT	O	2.00000			1.000000	-3102.000	L	90.18

O/F= 6.0000 PERCENT FUEL= 14.2857 EQUIVALENCE RATIO= 0.6649 PHI= 0.6649

	CHAMBER	THROAT	EXIT	EXIT	EXIT	EXIT	EXIT	EXIT	EXIT	EXIT	EXIT
PC/P	1.0000	1.7139	2.0000	5.0000	10.000	20.000	50.000	100.00	200.00	500.00	1000.00
P, ATM	0.68046	0.39703	0.34023	0.13609	0.06805	0.03402	0.01361	0.00680	0.00340	0.00136	0.00068
T, DEG K	2877.2	2769.6	2739.6	2569.8	2448.0	2329.4	2172.7	2049.0	1914.0	1707.7	1534.5
RHO, G/CC	7.1873-5	4.4181-5	3.8423-5	1.6755-5	8.9338-6	4.7635-6	2.0784-6	1.1141-6	6.0150-7	2.7146-7	1.5132-7
H, CAL/G	273.57	-393.92	-427.27	-615.48	-747.53	-871.37	-1023.22	-1129.44	-1228.20	-1346.70	-1426.53
U, CAL/G	-502.84	-611.54	-641.70	-812.19	-931.99	-1044.34	-1181.79	-1277.34	-1365.18	-1468.11	-1535.43
G, CAL/G	-8455.75	-8269.76	-8218.15	-7923.49	-7709.05	-7495.63	-7201.96	-6956.31	-6671.22	-6203.07	-5790.42
S, CAL/(G)(K)	2.8438	2.8438	2.8438	2.8438	2.8438	2.8438	2.8438	2.8438	2.8438	2.8438	2.8438
M, MOL WT	24.938	25.289	25.388	25.961	26.373	26.762	27.228	27.529	27.767	27.951	28.001
(DLV/DLP)T	-1.04646	-1.04164	-1.04026	-1.03204	-1.02590	-1.01991	-1.01251	-1.00763	-1.00379	-1.00091	-1.00020
(DLV/DLT)P	2.0218	1.9540	1.9331	1.7956	1.6776	1.5499	1.3730	1.2431	1.1307	1.0362	1.0092
CP, CAL/(G)(K)	2.2581	2.1821	2.1566	1.9707	1.7902	1.5770	1.2538	0.9945	0.7504	0.5179	0.4351
GAMMA (S)	1.1084	1.1060	1.1054	1.1028	1.1020	1.1028	1.1077	1.1167	1.1340	1.1716	1.1989
SON VEL,M/SEC	1031.2	1003.5	995.9	952.7	922.2	893.4	857.3	831.3	806.2	771.5	739.1
MACH NUMBER	0.000	1.000	1.139	1.775	2.159	2.504	2.922	3.219	3.506	3.884	4.202

PERFORMANCE PARAMETERS

AE/AT	1.0000	1.0175	1.5645	2.4920	4.1615	8.5173	14.870	26.080	54.504	94.333
CSTAR, FT/SEC	5102	5102	5102	5102	5102	5102	5102	5102	5102	5102
CF	0.645	0.729	1.088	1.281	1.438	1.611	1.721	1.818	1.927	1.997
IVAC,LB-SEC/LB	194.9	196.3	222.1	242.6	261.1	282.4	296.5	308.9	322.9	331.7
ISP, LB-SEC/LB	102.3	115.6	172.5	203.1	228.1	255.4	272.9	288.2	305.6	316.7

MOLE FRACTIONS

CO	0.07519	0.06744	0.06518	0.05158	0.04128	0.03124	0.01898	0.01110	0.00513	0.00100	0.00015
CO2	0.14688	0.15775	0.16089	0.17959	0.19357	0.20707	0.22348	0.23404	0.24213	0.24791	0.24919
H	0.02089	0.01786	0.01703	0.01242	0.00932	0.00658	0.00358	0.00187	0.00074	0.00010	0.00001
HO2	0.00010	0.00007	0.00007	0.00004	0.00002	0.00002	0.00001	0.00000	0.00000	0.00000	0.00000
H2	0.02645	0.02379	0.02302	0.01850	0.01511	0.01178	0.00760	0.00476	0.00243	0.00058	0.00011
H2O	0.36302	0.37791	0.38211	0.40636	0.42384	0.44045	0.46068	0.47417	0.48532	0.49480	0.49780
O	0.04277	0.03707	0.03551	0.02685	0.02098	0.01568	0.00960	0.00579	0.00285	0.00065	0.00012
OH	0.08833	0.07944	0.07694	0.06254	0.05215	0.04218	0.02968	0.02083	0.01280	0.00474	0.00156
O2	0.23637	0.23865	0.23923	0.24211	0.24373	0.24500	0.24639	0.24743	0.24860	0.25022	0.25105

THEORETICAL ROCKET PERFORMANCE ASSUMING FROZEN COMPOSITION DURING EXPANSION

PC = 10.0 PSIA

	CHEMICAL FORMULA	WT FRACTION (SEE NOTE)	ENERGY CAL/MOL	STATE	TEMP DEG K
FUEL	C 1.00000 H 4.00000	1.000000	-21390.000	L	111.66
OXIDANT	O 2.00000	1.000000	-3102.000	L	90.18

O/F= 0.0000 PERCENT FUEL= 14.2857 EQUIVALENCE RATIO= 0.6649 PHI= 0.6649

	CHAMBER	THROAT	EXIT	EXIT	EXIT	EXIT	EXIT	EXIT	EXIT	EXIT	EXIT
PC/P	1.0000	1.7834	2.0000	5.0000	10.000	20.000	50.000	100.00	200.00	500.00	1000.00
P, ATM	0.68046	0.38154	0.34023	0.13609	0.06805	0.03402	0.01361	0.00680	0.00340	0.00136	0.00068
T, DEG K	2877.2	2595.0	2542.1	2150.6	1889.2	1654.3	1380.4	1198.1	1035.2	847.1	723.7
RHO, G/CC	7.1873-5	4.4683-5	4.0675-5	1.9231-5	1.0946-5	6.2502-6	2.9962-6	1.7261-6	9.9879-7	4.8823-7	2.8576-7
H, CAL/G	-273.57	-399.61	-423.07	-594.05	-705.49	-803.24	-913.79	-984.90	-1046.49	-1115.03	-1158.34
U, CAL/G	-502.84	-606.40	-625.64	-765.43	-856.03	-935.06	-1023.78	-1080.37	-1128.99	-1182.54	-1216.01
G, CAL/G	8455.75	7779.32	7652.14	6709.95	6077.87	5507.69	4839.25	4391.94	3990.44	3524.04	3216.31
S, CAL/(G)(K)	2.8438	2.8438	2.8438	2.8438	2.8438	2.8438	2.8438	2.8438	2.8438	2.8438	2.8438
M, MOL WT	24.938	24.938	24.938	24.938	24.938	24.938	24.938	24.938	24.938	24.938	24.938
CP, CAL/(G)(K)	0.4497	0.4435	0.4422	0.4309	0.4212	0.4108	0.3959	0.3841	0.3721	0.3564	0.3452
GAMMA (S)	1.2154	1.2190	1.2198	1.2269	1.2333	1.2407	1.2520	1.2618	1.2725	1.2880	1.3002
SON VEL,M/SEC	1079.8	1027.0	1016.8	937.9	881.4	827.2	759.1	709.9	662.7	603.1	560.1
MACH NUMBER	0.000	1.000	1.100	1.746	2.157	2.545	3.049	3.437	3.837	4.400	4.858

PERFORMANCE PARAMETERS

AE/AT	1.0000	1.0087	1.0571	2.2051	3.4874	6.6170	10.897	18.066	35.421	59.018
CSTAR, FT/SEC	4929	4929	4929	4929	4929	4929	4929	4929	4929	4929
CF	0.684	0.744	1.090	1.265	1.401	1.541	1.624	1.693	1.766	1.811
IVAC, LB-SEC/LB	190.6	191.3	211.6	227.6	241.4	256.3	265.5	273.2	281.4	286.5
ISP, LB SEC/LB	104.7	114.1	167.0	193.9	214.7	236.0	248.8	259.3	270.6	277.5

MOLE FRACTIONS

CO	0.07519	CO2	0.14688	H	0.02089	HO2	0.00010	
H2	0.02645	H2O	0.36302	O	0.04277	OH	0.08833	
O2	0.23637							

THEORETICAL ROCKET PERFORMANCE ASSUMING EQUILIBRIUM COMPOSITION DURING EXPANSION

PC = 10.0 PSIA

	CHEMICAL FORMULA			WT FRACTION (SEE NOTE)	ENERGY CAL/MOL	STATE	TEMP DEG K
FUEL	C 1.00000	H 4.00000		1.000000	-21390.000	L	111.66
OXIDANT	O 2.00000			1.000000	-3102.000	L	90.18

O/F= 4.0000 PERCENT FUEL= 20.0000 EQUIVALENCE RATIO= 0.9973 PHI= 0.9973

	CHAMBER	THROAT	EXIT	EXIT	EXIT	EXIT	EXIT	EXIT	EXIT	EXIT	EXIT
PC/P	1.0000	1.7128	2.0000	5.0000	10.000	20.000	50.000	100.00	200.00	500.00	1000.00
P, ATM	0.68046	0.39728	0.34023	0.13609	0.06805	0.03402	0.01361	0.00680	0.00340	0.00136	0.00068
T, DEG K	2968.4	2862.4	2833.1	2669.5	2555.5	2448.5	2316.0	2221.2	2129.9	2012.6	1924.7
RHO, G/CC	6.0884-5	3.7427-5	3.2523-5	1.4151-5	7.5243-6	3.9944-6	1.7260-6	9.1388-7	4.8359-7	2.0847-7	1.1038-7
H, CAL/G	-344.22	-486.16	-525.72	-748.29	-904.84	-1052.17	-1234.03	-1362.66	-1484.17	-1634.59	-1741.10
U, CAL/G	-614.88	-743.22	-779.06	-981.19	-1123.85	-1258.44	-1424.98	-1542.98	-1654.54	-1792.68	-1890.39
G, CAL/G	9810.17	-9614.09	-9560.10	-9260.88	-9053.82	8860.00	-8619.41	-8445.75	-8276.13	-8052.58	-7878.68
S, CAL/(G)(K)	3.1889	3.1889	3.1889	3.1889	3.1889	3.1889	3.1889	3.1889	3.1889	3.1889	3.1889
M, MOL WT	21.795	22.128	22.223	22.777	23.187	23.588	24.103	24.479	24.842	25.298	25.620
(DLV/DLP)T	1.06574	-1.06148	-1.06025	-1.05305	1.04766	-1.04233	-1.03541	-1.03030	-1.02533	-1.01906	-1.01462
(DLV/DLT)P	2.3772	2.3385	2.3263	2.2438	2.1704	2.0878	1.9655	1.8638	1.7553	1.6038	1.4857
CP, CAL/(G)(K)	3.1647	3.1490	3.1416	3.0712	2.9868	2.8750	2.6846	2.5085	2.3055	1.9989	1.7419
GAMMA (S)	1.1075	1.1043	1.1035	1.0989	1.0959	1.0934	1.0908	1.0895	1.0888	1.0893	1.0913
SON VEL,M/SEC	1119.9	1089.9	1081.5	1034.8	1002.1	971.4	933.5	906.6	881.0	848.9	825.6
MACH NUMBER	0.000	1.000	1.140	1.777	2.161	2.506	2.923	3.220	3.506	3.871	4.141

PERFORMANCE PARAMETERS

AE/AT	1.0000	1.0177	1.5675	2.5029	4.1955	8.6605	15.289	27.309	59.545	108.08
CSTAR, FT/SEC	5546	5546	5546	5546	5546	5546	5546	5546	5546	5546
CF	0.645	0.729	1.088	1.281	1.440	1.614	1.727	1.827	1.944	2.023
IVAC,LB-SEC/LB	211.8	213.4	241.5	264.0	284.4	308.1	324.0	338.5	355.6	367.3
ISP, LB SEC/LB	111.1	125.7	187.5	220.9	248.2	278.3	297.7	314.9	335.1	348.6

MOLE FRACTIONS

CO	0.14983	0.14333	0.14137	0.12900	0.11883	0.10806	0.09308	0.08133	0.06936	0.05348	0.04170
CO2	0.12188	0.13253	0.13568	0.15496	0.17024	0.18600	0.20740	0.22385	0.24034	0.26190	0.27771
H	0.04545	0.04102	0.03979	0.03293	0.02817	0.02376	0.01845	0.01483	0.01154	0.00774	0.00531
HO2	0.00006	0.00004	0.00004	0.00002	0.00001	0.00001	0.00000	0.00000	0.00000	0.00000	0.00000
H2	0.06940	0.06574	0.06468	0.05840	0.05362	0.04883	0.04247	0.03763	0.03276	0.02627	0.02136
H2O	0.40700	0.42511	0.43026	0.46007	0.48188	0.50301	0.52988	0.54937	0.56808	0.59152	0.60811
O	0.03517	0.03093	0.02976	0.02343	0.01922	0.01548	0.01124	0.00854	0.00625	0.00382	0.00242
OH	0.08854	0.08069	0.07848	0.06595	0.05710	0.04882	0.03878	0.03188	0.02559	0.01821	0.01337
O2	0.08268	0.08061	0.07994	0.07524	0.07094	0.06602	0.05869	0.05259	0.04609	0.03705	0.03002

THEORETICAL ROCKET PERFORMANCE ASSUMING FROZEN COMPOSITION DURING EXPANSION

PC = 10.0 PSIA

	CHEMICAL FORMULA		WT FRACTION (SEE NOTE)	ENERGY CAL/MOL	STATE	TEMP DEG K
FUEL	C 1.00000	H 4.00000	1.000000	-21390.000	L	111.66
OXIDANT	O 2.00000		1.000000	-3102.000	L	90.18

O/F= 4.0000 PERCENT FUEL= 20.0000 EQUIVALENCE RATIO= 0.9973 PHI= 0.9973

	CHAMBER	THROAT	EXIT	EXIT	EXIT	EXIT	EXIT	EXIT	EXIT	EXIT	EXIT
PC/P	1.0000	1.7845	2.0000	5.0000	10.000	20.000	50.000	100.00	200.00	500.00	1000.00
P, ATM	0.68046	0.38132	0.34023	0.13609	0.06805	0.03402	0.01361	0.00680	0.00340	0.00136	0.00068
T, DEG K	2968.4	2675.2	2620.5	2214.6	1943.6	1700.2	1416.3	1227.3	1058.3	863.3	735.4
RHO, G/CC	6.0884 5	3.7858-5	3.4484-5	1.6322-5	9.2989-6	5.3151-6	2.5522-6	1.4727-6	8.5384-7	4.1872-7	2.4575-7
H, CAL/G	344.22	-493.11	-520.63	-722.21	-853.45	-968.45	-1098.35	-1181.78	-1253.90	-1333.96	-1384.39
U, CAL/G	-614.88	-737.03	-759.57	-924.13	-1030.66	-1123.47	-1227.49	-1293.68	-1350.40	-1412.67	-1451.45
G, CAL/G	9810.17	9023.95	-8877.12	-7784.17	-7051.25	-6390.08	-5614.62	-5095.31	-4628.81	-4086.74	-3729.59
S, CAL/(G)(K)	3.1889	3.1889	3.1889	3.1889	3.1889	3.1889	3.1889	3.1889	3.1889	3.1889	3.1889
M, MOL WT	21.795	21.795	21.795	21.795	21.795	21.795	21.795	21.795	21.795	21.795	21.795
CP, CAL/(G)(K)	0.5111	0.5041	0.5027	0.4897	0.4785	0.4661	0.4483	0.4341	0.4196	0.4009	0.3881
GAMMA (S)	1.2171	1.2208	1.2216	1.2288	1.2354	1.2432	1.2553	1.2659	1.2776	1.2944	1.3071
SON VEL,M/SEC	1174.0	1116.2	1105.1	1018.9	957.1	898.0	823.5	769.8	718.2	652.9	605.6
MACH NUMBER	0.000	1.000	1.099	1.746	2.157	2.545	3.050	3.439	3.841	4.408	4.872

PERFORMANCE PARAMETERS

AE/AT	1.0000	1.0086	1.4557	2.2014	3.4786	6.5910	10.839	17.938	35.068	58.284
CSTAR, FT/SEC	5353	5353	5353	5353	5353	5353	5353	5353	5353	5353
CF	0.684	0.745	1.090	1.265	1.401	1.540	1.623	1.691	1.764	1.808
IVAC,LB SEC/LB	207.1	207.8	279.8	247.1	262.0	278.1	288.0	296.3	305.1	310.5
ISP, LB SEC/LB	113.8	123.9	181.4	210.5	233.1	256.2	270.0	281.3	293.5	300.8

MOLE FRACTIONS

CO	0.14983	CO2	0.12188	H	0.04545	HO2	0.00006
H2	0.06940	H2O	0.40700	O	0.03517	OH	0.08854
O2	0.08268						

APPENDIX C

CARBONYL EXTRACTION OF LUNAR AND ASTEROIDAL METALS

538675 S24-90
N91-25247
p. 18

ENGINEERING, CONSTRUCTION, and OPERATIONS IN SPACE

Proceedings of Space 88

Sponsored by the
Aerospace Division of the American Society of Civil Engineers
American Institute of Aeronautics and Astronautics
NASA Johnson Space Center
Society of American Military Engineers
Space Studies Institute
U.S. Air Force Engineering and Services
U.S. Army Corps of Engineers

Corporate Sponsors
BDM International, Inc.
Bechtel National, Inc.
Lovelace Scientific Resources, Inc. of Albuquerque

Albuquerque, New Mexico
August 29-31, 1988

Edited by Stewart W. Johnson and John P. Wetzel

ASCE 1852

Published by the
American Society of Civil Engineers
345 East 47th Street
New York, New York 10017-2398

Carbonyl Extraction of Lunar and Asteroidal Metals

John S. Lewis[1], Thomas D. Jones[2], and William H. Farrand[2]

Abstract

The century-old Mond process for carbonyl extraction of metals from ore shows great promise as an efficient, low energy scheme for producing high-purity Fe, Ni, Cr, Mn, and Co from lunar or asteroidal feedstocks. Scenarios for winning oxygen from the lunar regolith can be enhanced by carbonyl processing of the metallic alloy by-products of such operations. The native metal content of asteroidal regoliths is even more suitable to carbonyl processing. High-purity, corrosion resistant Fe and Ni can be extracted from asteroidal feedstocks along with a Co-rich residue containing 0.5% platinum-group metals. The resulting gaseous metal carbonyls can produce a variety of end products using efficient vaporforming techniques.

Introduction

The exploitation of extraterrestrial natural resources will be essential to the successful economic development of the space frontier. In particular, the surfaces of the Moon and near-Earth asteroids offer materials -- structural materials, propellants, and life support fluids -- that we cannot afford to ignore if we are to sustain a growing human presence beyond low-Earth orbit. Confronted with the remote, low-g vacuum environment of the lunar or asteroid surface, we should emphasize the use, whenever possible, of simple, proven terrestrial refinement schemes in our initial exploitation of space resources. In the case of lunar and asteroidal mining, the Mond process for carbonyl extraction of iron and nickel (as well as other valuable siderophiles) shows great promise as a practical refining technique, capable of producing high purity metals from the local regolith or other feedstocks. In this paper we discuss the general traits of the carbonyl process, examine its advantages and drawbacks, show its application to lunar and asteroidal scenarios, and mention some potential uses for the metals produced.

The Carbonyl Process

The groundwork for the gaseous carbonyl process was

1 Professor, Department of Planetary Sciences, Univ. of Arizona, Tucson, AZ 85721
2 Space Sciences Bldg., Univ. of Arizona, Tucson, AZ 85721

laid near the turn of the century by the discovery of Fe and Ni carbonyls, culminating in the posthumous publication of a body of data on the synthesis, stability and reactions of a number of metal carbonyls by Mond et al. (1910). International Nickel adapted the process early in the century for use in its Sudbury, Ontario facility that alone produces nearly 60% of the global supply of nickel (Boldt, 1967).

The fundamental principle of the gaseous carbonyl process is simple. Metallic alloys of Fe, Ni, Co, etc. are exposed to carbon monoxide gas at modest pressures (about 10 bars) and temperatures on the order of 100 °C. Volatile carbonyls form spontaneously by reactions such as:

$$Fe + 5\ CO = Fe(CO)_5\ (g) \qquad (1)$$

$$Ni + 4\ CO = Ni(CO)_4\ (g) \qquad (2)$$

The conditions required for volatilization of iron and nickel are displayed in Figs. 1 and 2, respectively. These plots of the partial pressure of carbonyl gas at various values of $\log_{10}(P_{CO})$ and 1/T are derived from the equation for the gas equilibrium constant K_p. For example, using Eq. 1,

$$K_p = \frac{P_{Fe(CO)_5}}{a_{Fe}\,(P_{CO})^5} \qquad (3)$$

where P is the partial pressure of the particular gas and a is the activity of Fe, here assumed to be 1. Solving for P_{CO} and taking the log of both sides, we can write:

$$\log(P_{CO}) = 1/5\ [\ \log(P_{Fe(CO)_5}) - \log K_p\ ]. \qquad (4)$$

Since

$$\text{Log } K_p = -\Delta G^o/(2.303RT) \qquad (5)$$

substitution into (4) finally produces:

$$\log(P_{CO}) = \Delta G^o/(11.51)RT + (1/5)\log(P_{Fe(CO)_5}) \qquad (8)$$

This is the equation of a straight line, with variables $\log(P_{CO})$ and 1/T, and a slope of $\Delta G^o/(11.51R)$. Choosing different values of $P_{Fe(CO)_5}$ generates a family of parallel straight lines (Figs. 1,2).[5]

A close examination of these figures reveals the most favorable T,P environment for carbonyl formation. In Fig. 2, note that at 400 K (127°C), CO at a pressure of 1 bar (10^{-1} MPa) would be in equilibrium with nickel carbonyl gas with a partial pressure of 1 bar. As little as 0.02 bars of CO at room temperature would equilibrate to make 1 bar pressure of nickel carbonyl. High pressures are clearly unneeded; the equilibrium thermochemistry of the system

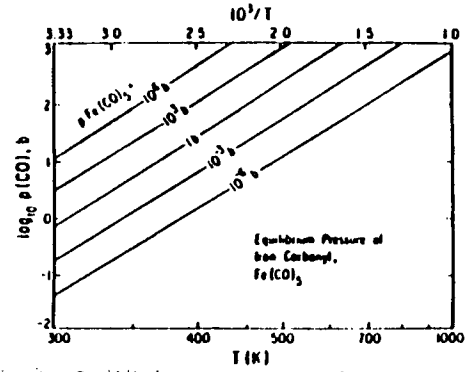

Fig. 1. Equilibrium pressure (p) and temperature (T) relations for iron carbonyl.

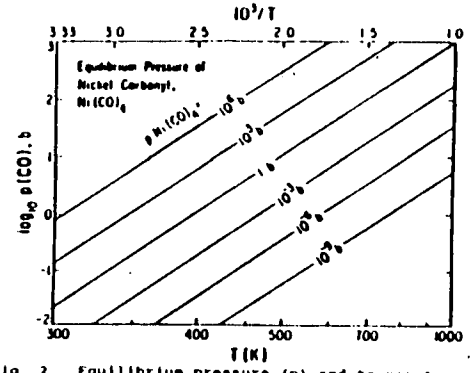

Fig. 2. Equilibrium pressure (p) and temperature (T) relations for nickel carbonyl.

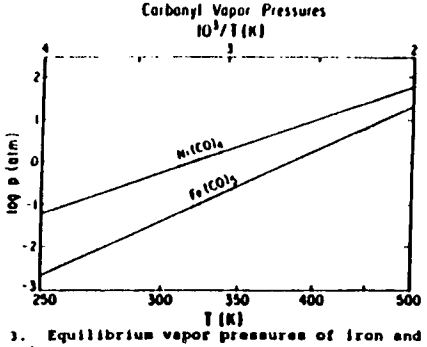

Fig. 3. Equilibrium vapor pressures of iron and nickel carbonyl.

favors the best yield of carbonyls at the lowest temperatures. If, for other reasons (kinetic factors, or limited reactor volume), it is found desirable to operate at much higher gas densities and pressures, higher temperatures can be tolerated: a pressure of 10 bars of CO is sufficient to keep nickel carbonyl stable and abundant (a partial pressure of 1 bar) at up to about 500 K. Note that the pressure of carbonyl gas in Eqn. 4 varies as the fifth power of the CO pressure, and that the iron and nickel carbonyls have different equilibrium stabilities. Therefore, passing the reaction product gas through a collecting bed with the same temperature but 10 times lower CO pressure than in the reactor could precipitate out up to 99.99% of the iron carbonyl as metallic Fe particles. The CO released can be recycled through the reaction chamber indefinitely.

The same principles apply to the formation of the gaseous carbonyls of many other elements (e.g. Os, Co, Ir, Ru, Rh, Pt, and Pd). Stability data for a number are available (See the JANAF Thermochemical Tables; Robie et al., 1978; Sykes and Townshend, 1955; Tripathi et al., 1976a,b.)

A further implication of the data given in Fig. 1 and 2 is that deposition conditions can easily be chosen so as to separate very pure Fe while retaining all the Ni in the gas phase. The commercial Mond process can produce Fe and Ni with purities of about 99.95% in a single step by taking advantage of this trait. Such ultra-high purity Fe and Ni, ideal for making tough, corrosion-resistant single crystals of very high tensile strength, cannot be made by either fractional distillation or zone refining, despite literature claims to the contrary, because of the very high mutual solubility of solid and liquid Fe and Ni. (The eutectic composition in the Fe-Ni is near 60% Ni, not near the pure end-member composition, and Ni and Fe have very similar vapor pressures.)

An entirely separate approach to carbonyl separation is available: the vapor pressures of the liquid carbonyls are large enough at and near room temperature to permit their fractional distillation. The vapor pressure data in Fig. 3 illustrate this alternative. By holding an Fe-Ni carbonyl liquid mixture at, say, 300 K, Ni carbonyl will have about 10 times the vapor pressure of Fe carbonyl, allowing preferential separation of the former. This process is even more effective at lower temperatures.

For process design, the kinetics of carbonyl formation and decomposition are just as important as thermodynamic stability. Literature data for Fe and Ni are available (Garratt and Thompson, 1934a,b; Carlton and Oxley, 1965, 1967; Kim et al., 1973; Oxley, 1966). The speed of volatilization of metallic feedstocks is striking, as is the temperature dependence of the formation rate of the

gaseous carbonyls. Rhee et al. (1973) have shown that the optimum temperature for Fe carbonyl formation is about 394 K (121°C). At lower temperatures the reaction rate is more sluggish, while at higher T the rate of decomposition of the carbonyls accelerates markedly. Above 400 K the rate of the net forward reaction varies as about $1/T^2$. As an example, an iron powder consisting of 100 μm grains, subjected to 21 bars of CO at 394 K for four hours, will be 50% converted into Fe carbonyl. Nickel, because of the greater stability of its carbonyl, reacts faster (Sykes and Townshend, 1955).

The advantages of the carbonyl process for space application are numerous. The only reactant required is CO, recoverable at the time of metal deposition and recyclable indefinitely. The basic process uses very little electric power, requires few moving parts, and can achieve the entire range of process temperatures by passive thermal control. The process is ideally suited for automatic operation. As the thermodynamics and kinetics of formation and decomposition are well-understood for the major carbonyls, process design can begin at once. For space applications, perhaps the most attractive of these is the low energy requirement. Passive solar heating and radiative cooling can provide the entire range of process temperatures.

The carbonyl process exhibits several obvious disadvantages. Nickel and iron carbonyls are extremely toxic, so contamination of any workers and their living facilities must be prevented. Another drawback for lunar applications is that CO will initially have to be delivered from Earth, but the gas is recyclable, and can be supplemented by combustion of organic wastes. In the asteroidal case, as we shall see, CO is easily derived from nearly every asteroid type suitable for metals extraction.

Lunar-specific Applications

Any scheme for producing oxygen from the lunar regolith could be enhanced by applying the Mond process to the solid by-products of such an operation. Among the suite of minerals in the lunar regolith, the one which seems most amenable to oxygen extraction would be ilmenite ($FeTiO_3$).

Ground and orbital studies from the Apollo missions indicate that ilmenite concentrations are highest in the lunar maria, particularly in Mare Tranquillitatis and southern Mare Serenitatis, where Apollo 11 and 17, respectively, found ilmenite making up to 10% of the mode of some soils. Studies of electrostatic techniques for beneficiation of lunar ilmenite from such soils indicate that grades and recoveries in the 90%+ level could be achieved (Agosto, 1984).

C-3

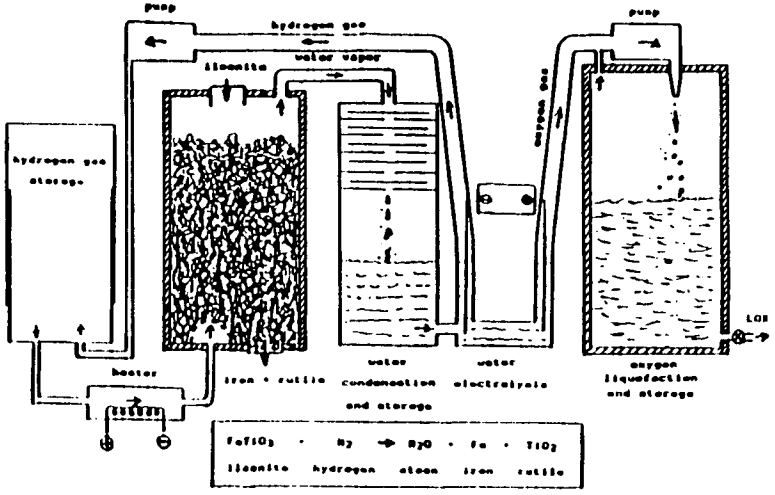

Fig. 4. The hydrogen-reduction of ilmenite produces oxygen with an Fe-TiO_2 residue.

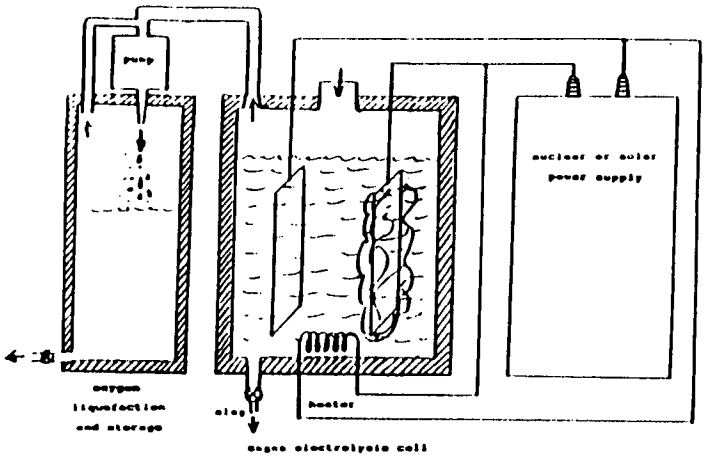

Fig. 5. Electrolysis of molten silicates produces oxygen at the anode while various metals plate out on the cathode.

A promising method for extracting oxygen from ilmenite is through the hydrogen-reduction process (Fig.4). The relevant reaction is:

$$FeTiO_3 + H_2 \rightarrow Fe + TiO_2 + H_2O \quad .$$

The H_2O can then be broken down to H_2 and $^1/_2$ O_2 via electrolysis with the hydrogen being recycled and the desired oxygen drawn off and liquified for storage and later shipment. Some hydrogen will be lost in this process, but some solar wind implanted hydrogen will also be released from the ilmenite feedstock.

The above reaction is endothermic, but not terribly so, with a ΔH of 9.7 Kcal/gm-mol at 900°C. At moderate temperatures of 700-1000°C, the per pass production of H_2O is 5% or less (Williams, 1984). The energy cost of the process is 5000 calories per gram of oxygen produced. Running the process at higher temperatures will produce higher yields, but that raises the associated problems of increased hydrogen loss rates through diffusion, sintering of solid reactants and products and, of course, higher energy usage.

Further tests of the hydrogen-reduction process are needed. Specifically, it must be determined how efficient the process is when the ilmenite feedstock contains no Fe^{3+}. Extraterrestrial ilmenites used in such tests could come from the lunar sample collection or from meteorites.

The solid residue of the hydrogen reduction process is a mass of native Fe and rutile (TiO_2). The Mond process could be effectively used to separate this residue into its components. Exposure to CO volatilizes Fe carbonyl which can then be thermally decomposed to yield high-purity iron for use in structural members. The left-over rutile can be used in products that require a refractory constituent or used as a feedstock for the production of pure Ti.

Another promising technique for winning oxygen from ilmenite is the carbothermal reduction process (Cutler and Krag, 1984). In this process, ilmenite feedstock is mixed with a carbon reductant and an anorthite fluxing agent and melted, causing the following endothermic reaction:

$$FeTiO_3 + C \rightarrow Fe + CO + TiO_2$$

The resulting iron is contaminated with carbon and can be subjected to the Mond process to purify the iron. When reacted with H_2, the CO (some of which could be removed for use as the Mond process reactant) can be converted to hydrocarbons and water through the Fischer-Tropsch process:

$$yCO + (2y+1)H_2 \rightarrow yH_2O + C_yH_{2y+2}$$

C-4

Oxygen can then be recovered via electrolysis and the original carbon reactant can be recovered via hydrocarbon cracking. The cost of carbothermal reduction is approximately 17,000 calories per gram of oxygen produced.

Although carbothermal reduction is an involved process, it does have some significant advantages over hydrogen reduction of ilmenite. Most notably, carbon removes more than 1.25 times its mass of oxygen per pass while hydrogen only removes 0.4 to 0.9 times its mass per pass. Also, carbon can be recovered from garbage and CO_2 waste gases and should be an easier reducing agent to handle than hydrogen. Disadvantages of the process are that it is more energy intensive than hydrogen-reduction and requires more processing steps.

While ilmenite makes up, at best, 10% of lunar soils, silicate minerals are as abundant as they are on Earth. While liberating oxygen from silicates is an energy intensive process, one proposed extraction scheme stands out because of its conceptual, if not practical, simplicity. Lindstrom and Haskin (1979) have experimented with a system of magma electrolysis (Fig. 5). A feedstock of silicates is melted and two electrodes are inserted into the melt; when an electric current is applied, oxygen is liberated at the anode while the cathode is plated with a mixture of Fe, Cr, Mn, Ti and possibly Si. The process requires 3000 calories of thermal and electrical energy per gram of feedstock. For reasonable oxygen yields (10% of the mass of solids) the cost per gram of oxygen is 30,000 calories. Note that instead of melting bulk lunar silicates, the feedstock could just as easily be ilmenite. In this case, the cathode deposit would consist dominantly of Fe and Ti. By exposing the cathode deposit to CO, the constituent metals can be volatilized and extracted.

Of the hydrogen reduction, carbothermal and magma electrolysis methods, the first appears more viable. It operates at lower temperatures, does not require massive sources of electrical power (all the process energy could be provided by a solar furnace), and is more energy-efficient than either the carbothermal process or electrolysis. Should future experimentation with magma electrolysis show that a free metal and a silica residue product are produced, then the additional expense of the latter process may be justified.

Application to Asteroidal Metals

The carbonyl process is especially suited to the extraction, separation, and refinement of the native metal alloys plentiful in the regoliths of certain types of asteroids, those corresponding to the unequilibrated ordinary chondrite meteorites. Metal content for the H and L (high and low iron) chondrites ranges up to 20%. (See

Table I.) The parent bodies of these meteorites have not undergone the melting and geochemical differentiation experienced on Earth and the Moon, and hence have not concentrated most of their metals in inaccessible cores. Because of the very low oxygen fugacity in metal-bearing meteorites, all the siderophile elements are readily available for direct extraction from the metal phase, not locked up in very dilute oxide solid solutions or microscopic inclusions in silicates. For example, after Fe/Ni carbonyl extraction, the remaining metallic residue contains mostly Co and small but significant amounts (0.5%) of the platinum-group siderophiles (Pd, Pt, Os, Ir, Au, Rh, Ru, Cu, etc.) which are worth roughly $10,000 per kg. Their recovery may be an attractive by-product of the process.

TABLE I: Fe and Ni Concentrations in Ordinary Chondrites

	CLASS		
	LL	L	H
meteorite total metal (%)	4±1	9±2	16±3
Ni concentration in metal	25±5	15±3	10±2
Co concentration in metal	1.2±0.2	0.7±0.1	0.5±0.1

The ordinary chondrites make up some 75% of the current terrestrial meteorite flux, implying that their parent bodies are well-represented in the near-Earth asteroid (NEA) population. Spectral analogs of ordinary chondrites are rare in the few dozen near-Earth asteroids classified so far; this situation is offset somewhat by the sheer numbers of NEA available. Shoemaker (1983) projects that there are some 1300 NEA > 1 km in diameter, and about 380,000 > 0.1 km across. Even more encouraging, about 1/5 of these objects should require less ΔV to reach from low Earth orbit (LEO) than does the lunar surface (for 1982 DB, 0.1 km s^{-1} vs. 6 km s^{-1}). Radar studies of NEA indicate that most objects are covered with a dusty regolith; metal grains may be easily beneficiated using a magnetic rake or separator. Where regolith is scarce or absent, the relatively low crushing strengths of the ordinary chondrites may permit grinding the surface rocks to an easily stored powder. The return vehicle would need bulk storage for the ore and a heat shield for an aerobraking return to LEO. We think the carbonyl processing facility is best located in LEO --asteroid operations should be limited to automated functions like bulk ore handling and perhaps magnetic separation.

The major advantage of asteroidal feedstocks for the carbonyl process is the low energy required to deliver mining equipment to the NEA and return useful ore to LEO.

Not only are many NEA more accessible from LEO than the lunar surface in terms of ΔV, but the return energy requirements are even lower (for a well-chosen asteroid like 1982 DB, the ΔV required is less than 100 m s^{-1}.) These asteroidal ores can be subjected immediately to the Mond process without any of the reduction or melting steps required for lunar feedstocks. Further, simple heating of any class of chondritic meteorite can supply all the necessary CO.

The major drawback to the exploitation of asteroid targets is the long flight-time associated with the low launch and return energies, typically on the order of 1 to 3 years. Moreover, the most energetically attractive asteroids have the longest synodic periods; launch windows occur for a given asteroid occur at typical intervals of about 5 years. As a result, dozens of energetically favorable asteroids would have to be discovered and characterized in order to support large scale mining.

Uses of Carbonyl-Derived Metals

Yet another attractive feature of carbonyl processing is that the separated metals are available as very pure powders, or in the gas phase as carbonyls. In the latter case the metal can be deposited directly onto a heated mold or mandrel that causes the carbonyl gas to decompose on contact. Nickel "vaporforming," as the process is called, is a successful commercial process that is today invading markets for precision nickel components previously supplied by machining, electroplating, casting, and other vapor deposition techniques (Meinel, 1985). Vaporformed nickel produced by a division of Formative Products Co. has a tensile strength of over 200,000 psi (> 1400 Mpa); surfaces of optical quality can be produced directly from the mold.

In perhaps the most demanding application tried to date, rhenium thrust chambers for advanced solar-powered rockets have been vaporformed in an analagous process from rhenium carbonyl. Carbonyl deposition is also widely used to apply thin films of Pt and Cr to mass-produced items like razor blades. Another technique for production of thin films is laser chemical vapor deposition, where metal is deposited on a surface heated by a focused laser. The beam dwell time and focus determine the film thickness. In space, this technique could produce lightweight films for solar collectors, solar power satellite structures, and electrical components.

With Fe the most plentiful metal in lunar and asteroidal ores, vaporforming of pure Fe as well as Fe-Ni alloys from a carbonyl gas mixture should be investigated as a high priority. Even if such processes prove unworkable, powder metallurgy may provide another means to use the high-purity iron produced by carbonyl extraction. Indeed, because of its corrosion resistance and strength, iron castings may be worth producing despite the high energy costs.

Conclusions

The gaseous carbonyl process offers significant advantages in lunar and asteroidal resource exploitation. To bring the method to a practical level of development for space application, we recommend: (1) Theoretical process design based on thermodynamic and kinetic data; (2) Construction of a boilerplate laboratory extraction system to test the process on synthetic metal alloys and on chondritic and iron meteorite samples; (3) Zero-g testing of the process on the shuttle or space station using actual meteorite samples; (4) evaluation of lunar and asteroidal ores through space-based geochemical observations and ground-based spectroscopy; and (5) deployment of an automated processor in the selected venue. Spacecraft observations could begin with lunar survey missions designed by Japan's NASDA for the mid-1990's. The Soviets have also announced an ambitious series of probes aimed at asteroid resource targets, beginning with the twin-spacecraft Phobos mission to the Martian moons in July 1988. If funded adequately under a revived U.S. space sciences program, the proposed Lunar Geosciences Observer and Near-Earth Asteroid Rendezvous missions can provide the specific compositional data needed to implement a space-based carbonyl extraction program.

References

Agosto, W.N. (1984) Electrostatic concentration of lunar soil minerals. In Lunar bases and space activities of the 21st century, (W.W. Mendell, ed.), pp.453-464. Lunar and Planetary Institute, Houston.

Boldt, J.R. (1967) The Winning of Nickel. Van Nostrand, Pittston, NJ.

Carlton, H.E., and Oxley, J.H. (1965). Kinetics of the heterogeneous decomposition of iron pentacarbonyl. Am. Inst. Chem. J. 11, 79-84.

Carlton, H.E., and Oxley, J.H. (1967). Kinetics of the heterogeneous decomposition of nickel tetracarbonyl. Am. Inst. Chem. J. 13, 86-91.

Cutler A.H. and Krag P. (1984) A carbothermal scheme for lunar oxygen production. In Lunar bases and space activities of the 21st century, (W.W. Mendell, ed.), pp.559-569. Lunar and Planetary Institute, Houston.

Garratt, A.P., and Thompson, H.W. (1934a). The thermal decomposition and oxidation of nickel carbonyl. J. Chem. Society, 1822-1825.

Garratt, A.P., and Thompson, H.W. (1934b). The spectra and photochemical decomposition of metallic carbonyls, Part II. Photochemical data. J. Chem. Society, 1817-1822.

JANAF Thermochemical Tables (1971). Second edition, National Standard Reference Service, U.S. National Bureau of Standards No. 37.

Kim, C.S., Rhee, C.S., Li, K., and Rothfus, R.R. (1973). Recovery of metallic iron from flotation tailings by pneumolytic transport I. Reduction by carbon monoxide in fluidized bed. Env. Sci. Tech. 7, 725-730.

Lindstrom D.J. and Haskin L.A. (1979) Electrochemical preparation of useful materials from ordinary silicate rocks. In Space Manufacturing Facilities 3, (J. Grey and C. Krop, eds.), pp.129-134. American Institute of Aeronautics and Astronautics, New York.

Meinel C.P. (1985) Metal carbonyl refining and vaporforming for asteroidal ores. In Space Manufacturing 5: Engineering with Lunar and Asteroidal Materials, (B. Faughnan and G. Maryniak, eds.), pp.150-159. American Institute of Aeronautics and Astronautics, New York.

Mond, L., Hirtz, H., and Cowap, M.D. (1910). LIV. Some new metallic carbonyls. J. Chem. Soc. 97, 798-810.

Oxley, J.H. (1966). High-purity metals. In Vapor Deposition. (C.F. Powell, J.H. Oxley, and J.M. Blocher, Jr., eds.) J. Wiley and Sons, Inc. New York, 452-483.

Rhee, C.S., Kim, C.S., Li, K., and Rothfus, R.R. (1973). Recovery of metallic iron from flotation tailings by pneumolytic transport, II. Formation of iron pentacarbonyl from partially reduced iron in fixed bed. Env. Sci. Tech. 7, 730-735.

Robie, R.A., Hemingway, B.S., and Fisher, J.R. (1978). Thermodynamic properties of minerals and related substances at 298.15K and 1 bar (10^5 pascals) pressure and at higher temperatures. U.S. Geological Survey Bulletin 1452. U.S. Government Printing Office, Washington, D.C.

Shoemaker, E.M. (1983). Asteroid and comet bombardment of the Earth. Ann. Rev. of Earth and Planet. Sci. 11, 461-494.

Sykes, K.W., and Townshend, S.C. (1955). The heat of formation of nickel carbonyl. J. Chem. Society, 2528-2529.

Tripathi, S.C., Shrivastava, S.C., Mani, R.P., and Shrimal, A.K. (1976a). Advances in platinum metal carbonyls and their substituted derivatives. I. Ruthenium and osmium. Inorg. Chim. Acta 15, 249-290.

Tripathi, S.C., Shrivastava, S.C., Mani, R.P., and Shrimal, A.K. (1976b). Advances in platinum metal carbonyls and their substituted derivatives. II. Rhodium, iridium, palladium and platinum carbonyls. Inorg. Chim. Acta 17, 257-290.

Williams R.J. (1984) Oxygen extraction from lunar materials: an experimental test of an ilmenite reduction process. In Lunar bases and space activities of the 21st century, (W.W. Mendell, ed.), pp.551-558. Lunar and Planetary Institute, Houston.

APPENDIX D

THEORETICAL PREDICTION OF VOLATILE-BEARING PHASES AND VOLATILE RESOURCES IN SOME CARBONACEOUS CHONDRITES

Space Manufacturing 7

Space Resources To Improve Life on Earth

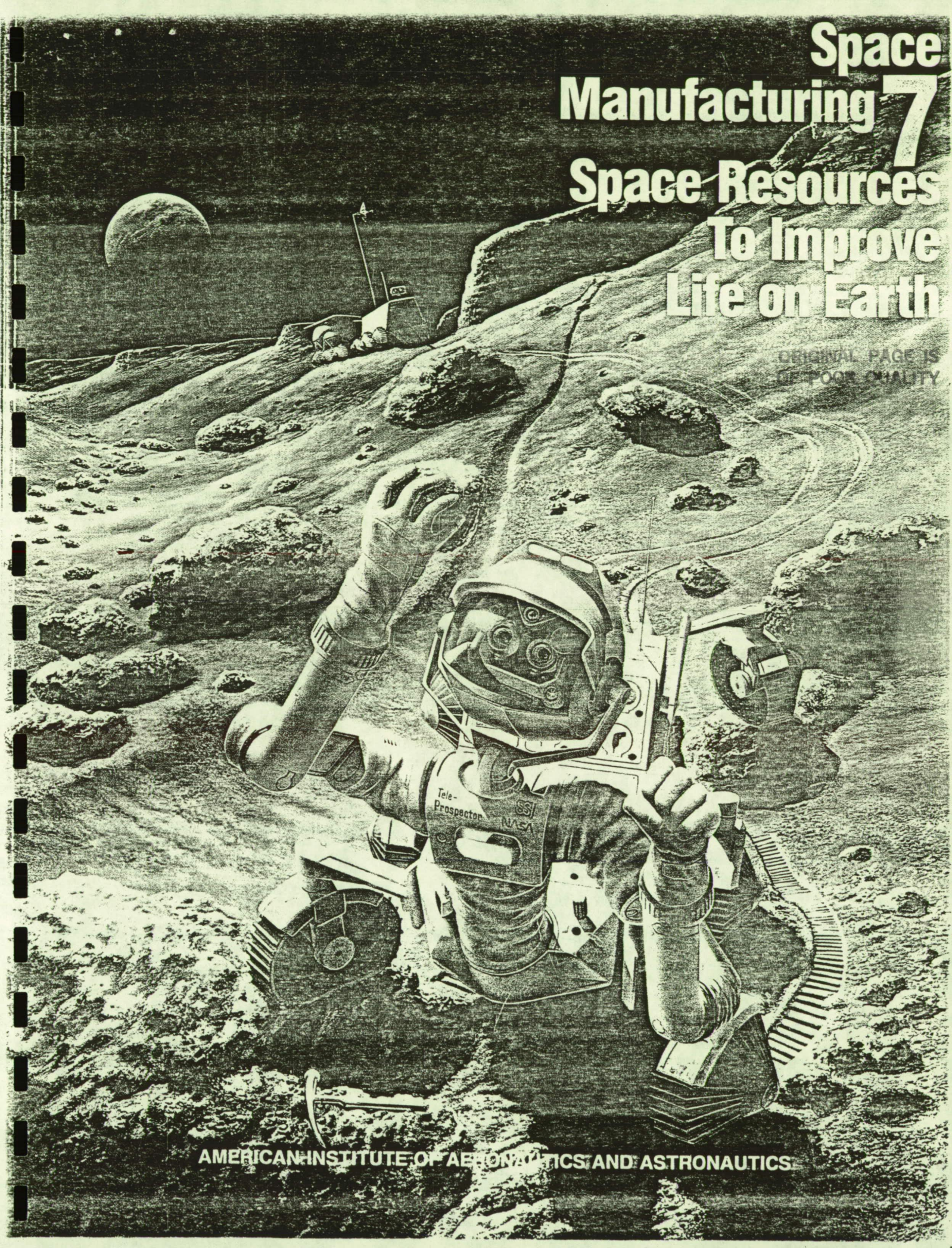

AMERICAN INSTITUTE OF AERONAUTICS AND ASTRONAUTICS

THEORETICAL PREDICTIONS OF VOLATILE BEARING PHASES AND VOLATILE RESOURCES IN SOME CARBONACEOUS CHONDRITES

Jibamitra Ganguly
Department of Geosciences
University of Arizona, Tucson, AZ 85721

Surendra K. Saxena
Department of Geology
Brooklyn College, Brooklyn, NY 11280

Abstract

Carbonaceous chondrites are usually believed to be the primary constituents of near-Earth asteroids and Phobos and Deimos, and are potential resources of fuels which may be exploited for future planetary missions. In this work we have calculated the nature and abundances of the major volatile bearing and other phases, including the vapor phase, that should form in C1 and C2 type carbonaceous chondrites as functions of pressure and temperature. The results suggest that talc, antigorite ± magnesite are the major volatile bearing phases and are stable below 400°C at 1 bar in these chondritic compositions. Simulated heating of a kilogram of C2 chondrite at fixed bulk composition between 400 and 800°C at 1 bar yields about 135 gm of volatile, which is made primarily of H_2O, H_2O, CH_4, CO_2 and CO. The relative abundances of these volatile species change as functions of temperature, and on a molar basis, H_2 becomes the most dominant species above 550°C. In contrast, C1 chondrites yield about 306 gm of volatile under the same condition, which consist almost completely of 60 wt% H_2O and 40 wt% CO_2. Preliminary kinetic considerations suggest that equilibrium dehydration of hydrous phyllosilicates should be attainable within a few hours at 600°C. These results provide the framework for further analyses of the volatile and economic resource potentials of carbonaceous chondrites.

Introduction

The near-Earth asteroids are potential resources of volatiles which can be used as propellants and life supporting purposes for planetary missions. As emphasized by Lewis and Lewis (1), these asteroids are at times the nearest bodies to Earth, and many of them can pass between Earth and Moon. These authors have also shown that within any arbitrary three-year period, there are roughly 300 and 90,000 launch opportunities to respectively kilometer and 100-meter sized asteroidal bodies as compared to 39 lunar launch windows. These facts and the potential volatile resources make the asteroids important candidates for detailed analyses for supporting future planetary missions.

Cost-effective or energy-efficient extraction of volatiles from the asteroids require knowledge of the nature and modal abundances of the constituent minerals in which the volatile components are structurally bound. There has been several studies on reflectance spectroscopy of near-Earth asteroids to characterize the nature of the volatile bearing minerals (2,3). While these studies report absorption band near 3 μm suggesting presence of hydrous phyllosilicates, more precise characterizations were equivocal. An obvious alternative approach to the resolution of the problem is to examine directly the asteroidal materials.

The spectral and density characteristics strongly suggest that a significant fraction of the near-Earth asteroids are made of carbonaceous chondrites (1,4). The most volatile rich of these meteorites are what are commonly known as C1 or (CI) and C2 (or CM) classes. However, the grain size of the volatile bearing phases are often too small (100 to 1000 Å) (5) to permit identification under optical microscope, and are best observed under high resolution transmission electron microscopy (HRTEM). Dolensky and McSween (5) have recently presented a summary of volatile bearing phases identified in the carbonaceous chondrites.

The primary objective of this work is to carry out theoretical calculations to predict modal abundances and compositions of the major mineral phases, along with the abundance and composition of the coexisting vapor phase, that could develop in the bulk compositions of C1 and C2 chondrites as functions of pressure and temperature. The results would provide the framework for engineering designs for the extraction of volatile components from asteroids as well as Phobos and Deimos, the two small natural satellites of Mars, which are also likely to be made of carbonaceous chondrites (1).

Theoretical Method

Principles

According to Duhem's theorem in classical thermodynamics (6,7), the equilibrium state of a closed system (i.e., a system of fixed composition and mass) is completely determined if any two variables are fixed regardless of whether these are intensive, extensive, or a combination of both. Ganguly and Saxena (7) have recently reviewed the various methods by which one may carry out the actual computation of the equilibrium assemblages. The

Table 1 Bulk chemical compositions of C1 and C2 carbonaceous chondrites

	C1	C2
Si	10.40	12.96
Ti	0.04	0.06
Al	0.84	1.17
Cr	0.23	0.29
Fe	18.67	21.56
Mn	0.17	0.16
Mg	9.60	11.72
Ca	1.01	1.32
Na	0.55	0.42
K	0.05	0.06
P	0.14	0.13
Ni	1.03	1.25
Co	0.05	0.06
S	5.92	3.38
H	2.08	1.42
C	3.61	2.30
O	45.61	41.74

method used in this study obtains the compositions and abundances of the equilibrium phase assemblages by minimizing the Gibbs Free Energy (G) of the system at fixed P-T conditions. The minimization is constrained to conserve the various elemental masses of the system through the method of Lagrangian multipliers (7). Because of the extremely small grain size of the phyllosilicates observed in carbonaceous chondrites, one should consider the effects of surface free energy on the formation of these phases. As a first approximation, we have, however, ignored this effect. Therefore, the actual equilibrium temperatures of volatile bearing phases could be lower than those predicted by our calculations.

System, Phases and Data Base

Table 1 shows the bulk compositions of C1 and C2 carbonaceous chondrites. These compositions are based on analyses of a number of fragments of Orgueil and

Table 2 Phases in the system Mg-Fe-Si-C-H-O-S considered in this work

The sources of thermochemical data are shown by reference numbers within parentheses. The Heat of Formation of the Fe-end members of the hydrous phyllosilicates are derived in this work.

Anhydrous Silicates and Oxides		
Olivine	$(Mg,Fe)_2SiO_4$	(8)
Orthopyroxene	$(Mg,Fe)SiO_3$	(8)
Periclase	(Mg,Fe)O	(23)
Quartz	SiO_2	(17)
Cristobalite	SiO_2	(17)
Hematite	Fe_2O_3	(23)
Magnetite	Fe_3O_4	(23)
Hydrous and Carbonate Phases		
Anthophyllite	$(Mg,Fe)_7Si_8O_{22}(OH)_2$	(8,27)
Talc	$(Mg,Fe)_3Si_4O_{10}(OH)$	(8)
Antigorite	$(Mg,Fe)_{48}Si_{34}O_{85}(OH)_{62}$	(8)
Chrysotile	$(Mg,Fe)_3Si_2O_5(OH)_4$	(8)
Brucite	$(Mg,Fe)(OH)_2$	(17,24)
Magnesite	$(Mg,Fe)CO_3$	(17,25)
Sulfides and Elements		
Troilite	FeS	(17)
Pyrite	FeS_2	(17)
Iron	Fe	(26)
Sulfur	S	(17)
Graphite	C	(17)
Vapor Phase	C-O-H-S	(15,16,17)

Species: H_2O, CO_2, CH_4, CO, O_2, H_2S, S_2, SO_2, COS

Murchison meteorites, respectively, and are summarized in Dodd (22). It can be easily seen from this table that the subsystem Mg-Fe-Si-C-H-O-S (MFCHOS) constitutes almost 96% by weight of the bulk compositions of C1 and C2 chondrites. In order to somewhat simplify the computational problem, we have confined the G minimization calculation to this subsystem, but evidently the phases whose compositions form outside of this subsystem cannot be major constituents of these chondrites.

Table 2 shows the list of phases that we have considered as possible crystallizing phases within the above subsystem along with the sources of the thermochemical data. The choice of these phases have been guided by the published reports of the mineralogy of carbonaceous chondrites whose compositions lie within the system MFCHOS (e.g., Zolensky and McSween (5)). The selection of thermochemical data in the system Mg-Si-O-H is based on the critical analysis of Chatterjee (8,11) for consistency with both calorimetric and experimentally determined phase equilibrium measurements. These data are similar to those of Berman (9). However, unlike those in Berman, the data are also consistent with high P-T experimental data involving distribution of Fe and Mg among coexisting silicates.

The heat capacities (C_p) and entropies (S^o) of the phases, if not available in any of the recent systematizations of self-consistent data set, are estimated by stoichiometric summation of the properties of oxides and structurally analogous compounds, as discussed in a number of publications (13,14).

There are no thermochemical data for the Fe-end members of the phyllosilicates listed in Table 2. The enthalpies of these phases are estimated according to the known relative properties of Fe- and Mg-end members of biotite, which is also a phyllosilicate. The data derived by Chatterjee (8) and Robie and Hemingway (10) for the Mg- and Fe^{2+}-end members (phlogopite and annite, respectively) yield an enthalpy difference of -359.566 KJ per mole of divalent cation at 1 bar, 298 K. We have used these values to estimate the enthalpies of formation from elements of Fe-end members of phyllosilicates at 1 bar, 298 K from the available data for the Mg-end members. The results are as follows (KJ/mol of Fe). Fe-talc: -1606.80; Fe-antigorite: -1127.53 and Fe-chrysotile: -1094.87. The corresponding values of the free energy of formation from elements (ΔG_f^o) for Fe-talc and Fe-antigorite at 1 bar, 298 K are -4477.18 and -4784.0 KJ/mol of Fe^{2+}, respectively.

The validity of the estimated thermochemical properties of the Fe-end members of the phyllosilicates may be tested as follows. The Fe-end members of talc and antigorite are unstable. Instead, the stable phases are closely analogous compounds, namely, minnesotite, which has a stoichiometry of $Fe_{27}Si_{36}O_{86}(OH)_{26}$ as compared to that of $Fe_{27}Si_{36}O_{90}(OH)_{18}$ for Fe-talc, and greenalite with a stoichiometry of $Fe_{48}Si_{32}O_{80}(OH)_{64}$ compared to $Fe_{48}Si_{34}O_{85}(OH)_{62}$ for Fe-antigorite. Anovitz et al. (12) have recently determined ΔG_f^o of minnesotite and greenalite from phase equilibrium data. Their results, ΔG_f^o (minnesotite) = -4577.78 KJ and ΔG_f^o (greenalite) = -4799.50 KJ, differ in the right direction from the corresponding values of Fe-talc and Fe-antigorite, considering the relative stabilities of the phases.

The stereochemical environments of divalent cations in biotite are quite similar to those in talc, both being 2:1 (TOT) layer silicates, and partly similar to those in antigorite, which is an 1:1 (TO) layer silicate (28). Thus, these phyllosilicates should have similar differences between the enthalpies of formation of the Fe- and Mg-end members. Further, since on the basis of observational data, the predicted compositions of the mineral phases in carbonaceous chondrites are expected to be Mg-rich, the effects of errors in the Fe-end member thermochemical properties and solid solution model will be relatively small. This can be easily understood by considering the form of G-X curve of a stable solution and evaluating the effects of errors in above properties near Mg-terminal segment.

The thermodynamic mixing properties of the Fe^{2+}- and Mg-end member components of the annydrous silicates are taken from the self-consistent summary of Chatterjee (8), while those of the phyllosilicates are assumed to be ideal for the lack of any data. The latter assumption is likely to be approximately valid at $T \geq 600^oC$, since at these conditions biotite solid solution is found to behave approximately ideally (7). At lower temperature, the phyllosilicates may deviate from ideal solution behavior, but perhaps not too dissimilarly to significantly affect their relative stabilities. Magnesite is also assumed to be an ideal solution of Fe-Mg components. As emphasized by Ganguly and Saxena (7), the computed dehydration conditions are not very sensitive to errors in activity-composition relations since the devolatilization equilibria are characterized by large enthalpy changes. The iron oxides and sulfides are considered to be stoichiometric phases since the solid solutions of Mg are around a few percent at the temperatures of interest.

The fluid properties are taken from Saxena and Fei (15,16) and Robie et al. (17). The "corresponding state method" of estimating P-V-T relation, as discussed by these authors, is extended to include the sulfur species. For mixing data, we have assumed that H_2S behave as H_2O, S_2 as

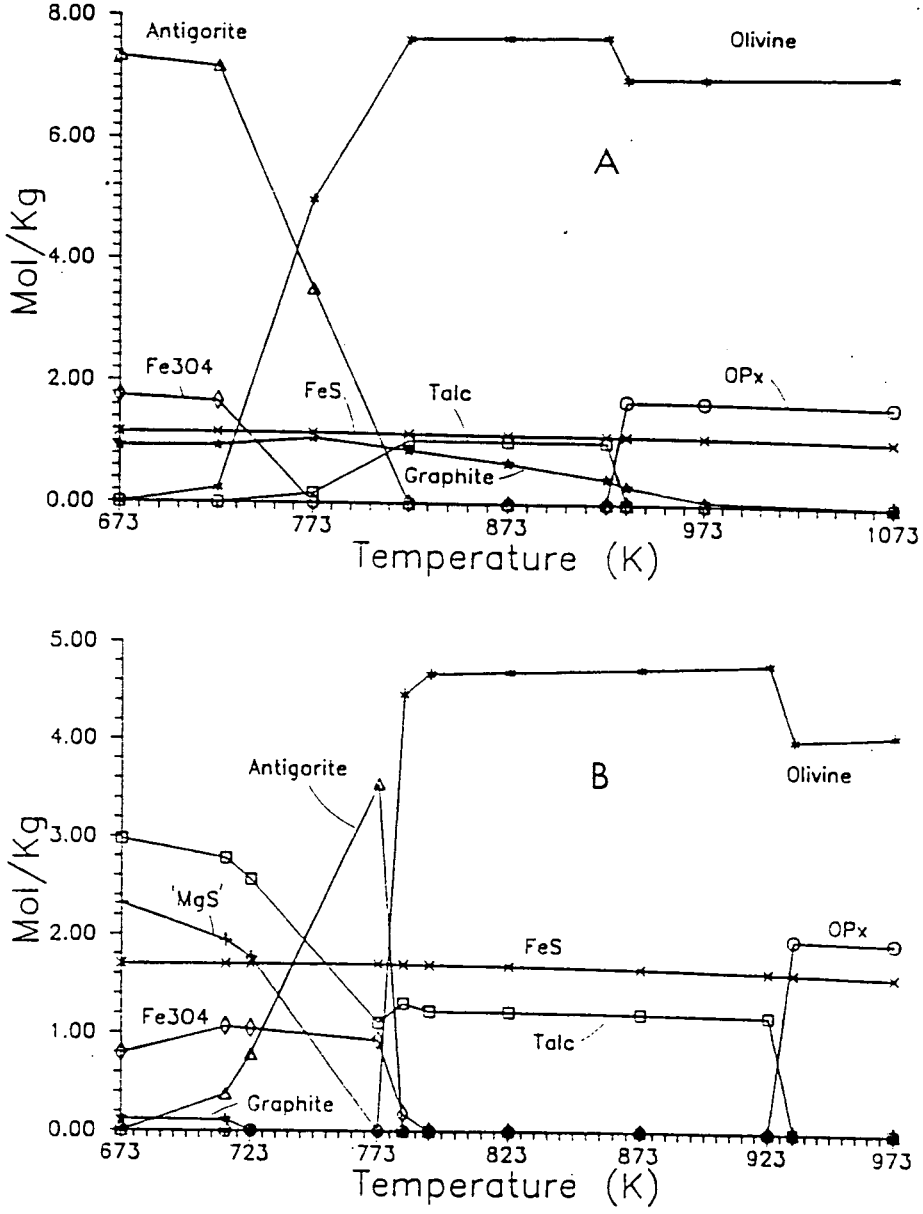

Fig. 1 Calculated modal abundances of minerals per kilogram of rock in (a) C1 and (b) C2 carbonaceous chondritic bulk compositions as functions of temperature at 2 Kb. The steps in the calculations are shown by symbols.

O_2, and SO_2 and COS as CO_2, and used the equivalent binary interaction parameters from Saxena and Fei (15).

Results

At 1 bar, the free energy minimization calculations do not yield any volatile bearing phase at $T \geq 400^{\circ}C$. At the present state of the thermochemical data, we do not believe that our calculations are reliable at lower temperatures. Indeed, we find results at lower temperatures which do not seem to follow the systematics of the results obtained at higher temperatures. Thus, we have calculated the equilibrium phase assemolages at a pressure of 2 Kb so that the volatile bearing phases appear at higher temperatures. This procedure at least permits recognition of the major volatile bearing phases. Some of these phases may be re-

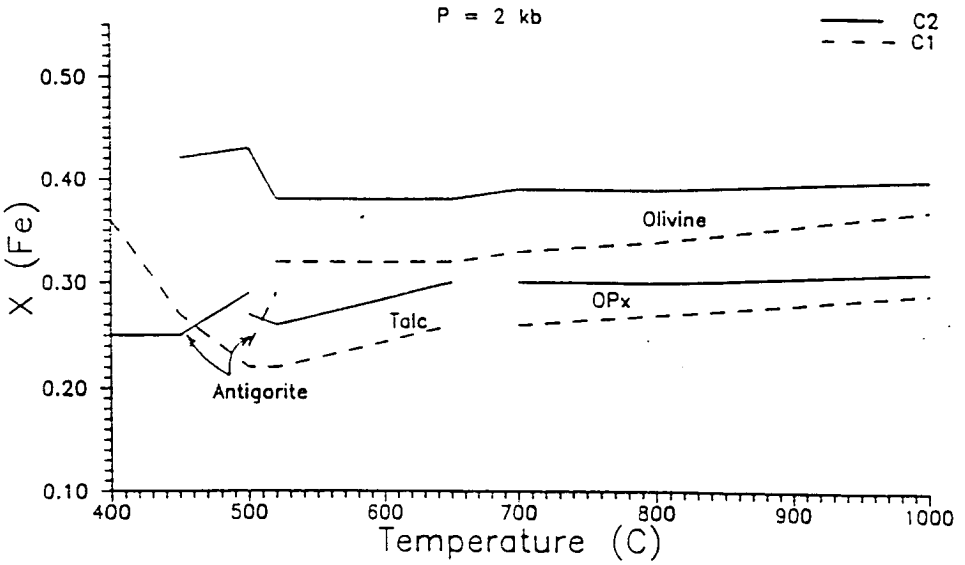

Fig. 2 Calculated compositions of the silicate phases in C1 and C2 carbonaceous chondrites as functions of temperature at 2 Kb.

placed by more stable assemblages at lower temperature, but should reappear during heating experiment. The results, which are illustrated in Figure 1, show that the primary volatile bearing phases in the C1 and C2 bulk compositions are talc, antigorite ± magnesite. Talc is stable to around 650°C at 2 Kb, and dehydrates to orthopyroxene (OPx) at higher temperature according to Tc + Ol = 5 OPx + H_2O. Antigorite and magnesite crystallize at T < 550°C, but magnesite is absent in C2 bulk composition at T ≥ 400°C. FeS is a stable phase at all temperatures investigated in this work. We, however, did not consider the formation of sulfate or pyrrhotite. Magnetite becomes a stable phase at T ≤ 500°C. Elemental sulfur found in C1 chondrite is invariably associated with pyrrhotite ($Fe_{1-x}S$) (5). This suggests decomposition of troilite (FeS) to pyrrhotite and sulfur.

Figure 2 shows the compositions of the ferromagnesian phases as function of temperature at 2 Kb for the C1 and C2 bulk compositions. Calculations at 1 bar also yield similar compositions. The observed compositions of these phases in the carbonaceous chondrites vary widely in Fe/Mg ratio. One way to achieve this diverse Fe/Mg ratio is by aqueous alteration which seems to be a characteristic of the carbonaceous chondrites. Fe^{++} fractionates very strongly into an aqueous phase relative to the silicates (18). Thus, varying degrees of equilibration with an aqueous phase could lead to a spectrum of Fe/Mg compositions of the ferromagnesian silicates. Aqueous alteration may not be the sole reason, but is likely to be an important contributing factor in the development of variable Fe/Mg ratio of the ferromagnesian silicates in carbonaceous chondrites.

The abundances of volatile species in equilibrium with the solids per kilogram of total mass of C2 chondrites are illustrated in Figure 3. Figures 3a and 3b illustrate the molar and mass abundances, respectively, as functions of temperature at 1 bar. It should be noted that the total mass of the volatiles do not change above 400°C, which means that under equilibrium condition C2 chondritic material will completely devolatize if heated above 400°C. The total yield of the volatile is about 14% of the initial mass of C2 chondrites. The change in the abundance of various species above 400°C is due to homogeneous reactions within the fluid phase. Above 550°C, hydrogen has the highest molar concentration in the vapor phase. Hydrogen is a very good propellant and reducing agent which may thus be preferentially extracted by heating the C2 chondritic material to T > 550°C.

In contrast to the C2 chondrites, the volatiles given off by C1 material above 400°C consist essentially of H_2O and CO_2 at 1 bar pressure. Per kilogram of material, the total yield of volatile is about 306 grams of which nearly 60 wt% is H_2O.

The above results are subject to considerable uncertainties owing to the

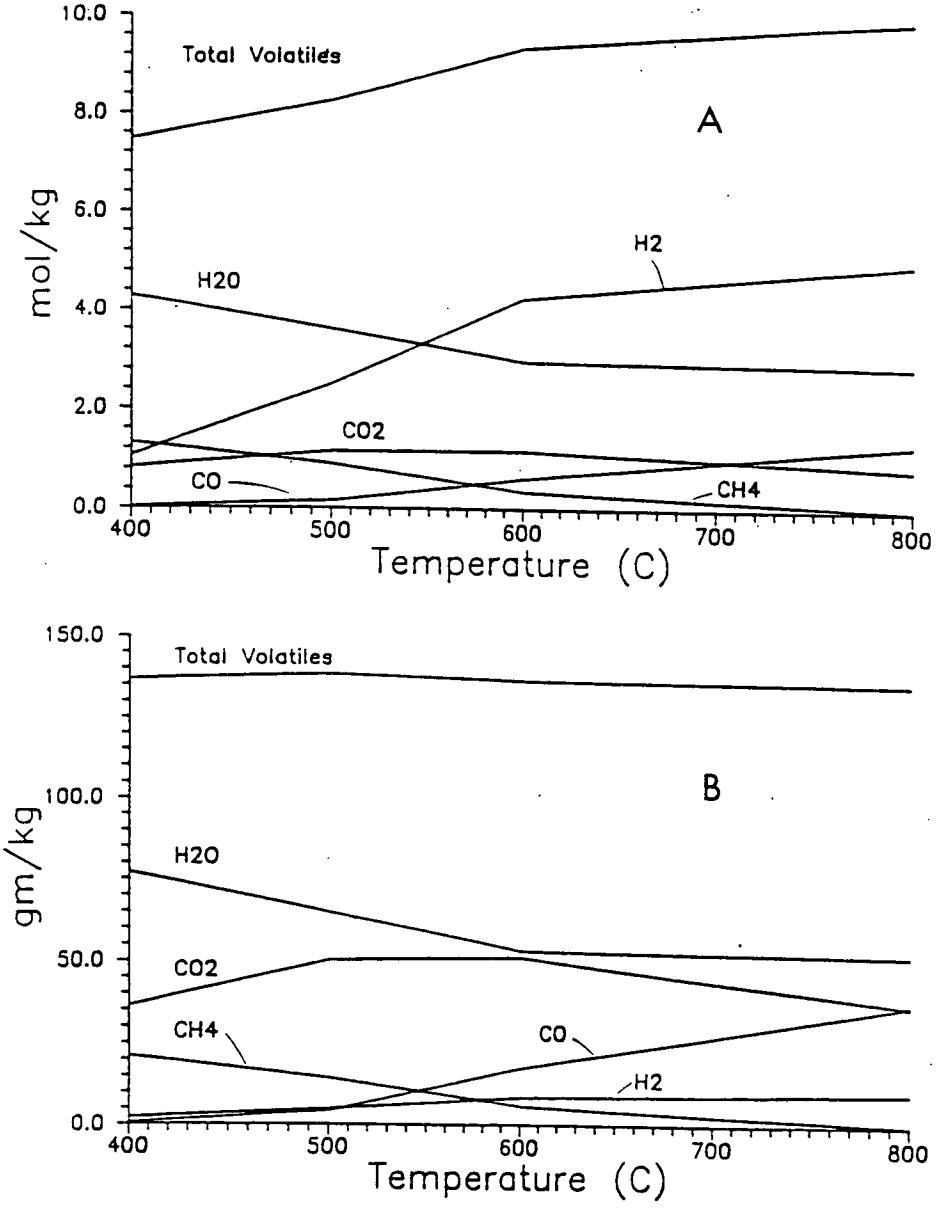

Fig. 3 Calculated equilibrium (a) molar and (b) mass abundances of the volatile species per kilogram of C2 chondritic material.

approximate nature of the thermochemical properties of the phyllosilicate solid solutions, and also since we have ignored the effects of surface free energy on the formation of extremely fine grained crystals. Further, carbonaceous chondrites of any given type do not have homogeneous compositions, but instead probably represent agglomeration of materials formed at different conditions at different parts of the solar system. However, these calculations are still useful in providing an idea of the relative stabilities, as well as upper stabilities of the volatile bearing phases and their average abundance. It is interesting to note that recent reflectance spectroscopic studies of carbonaceous chondrites seem to corroborate the predictions made above as to the nature of the most abundant hydrous phases (Gaffey, pers. comm.).

Kinetics of Devolatilization

The equilibrium calculations presented above provide a framework for the

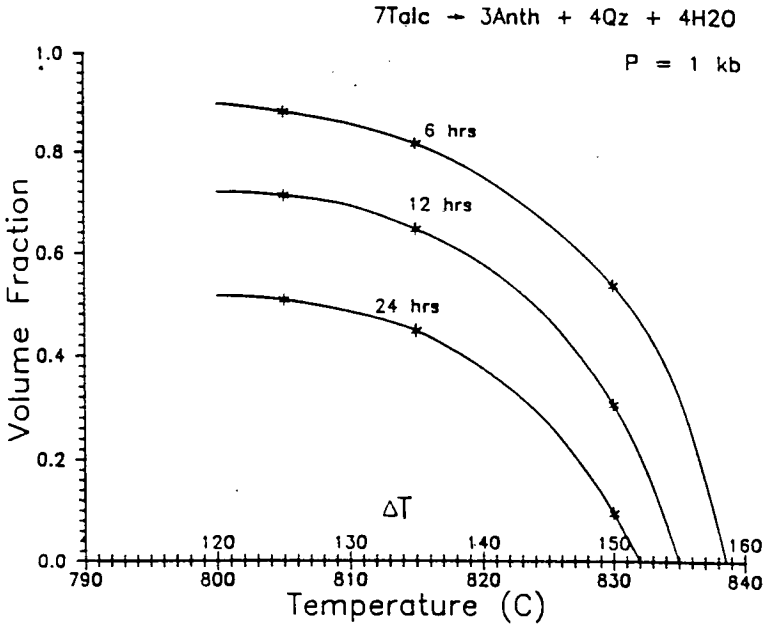

Fig. 4 Dehydration of talc as functions of time, temperature and extent of overstepping above the equilibrium dehydration boundary at 1 Kb. Volume fraction is that of talc remaining after reaction. Experimental data points, shown by asterisks, are from Greenwood (19).

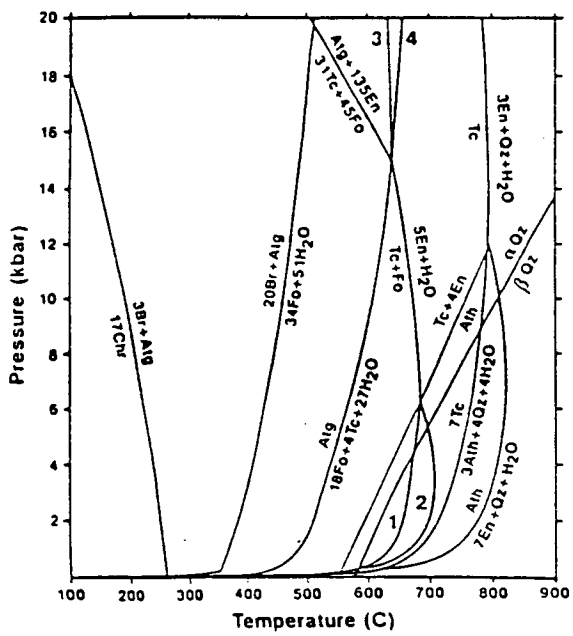

Fig. 5 Equilibrium relations of talc, antigorite and brucite along with other minerals in the system $MgO-SiO_2-H_2O$. Reproduced from Evans and Guggenheim (21).

evaluation of the volatile as well as some mineralogical resource potential of C1 and C2 carbonaceous chondrites. The actual extraction of volatiles as a function of temperature and heating rate, however, depends on the kinetics of the devolatilization process. For kinetic analysis, it is essential to identify the minerals in which the volatiles are most likely to be structurally bound. The above results suggest that talc, antigorite and magnesite are likely to be the major volatile bearing phases in carbonaceous chondrites.

Except for pure Mg-talc, there are no kinetic data for the other volatile bearing phases. The dehydration kinetics of talc was determined by Greenwood (19). At a given temperature, the rate of reaction depends on the rate constant, $K^{\ddagger}$, and the extent of departure from the equilibrium boundary. This is expressed in transition state theory (20) according to the relation Rate = $K^{\ddagger}(1-\exp(n\Delta G/RT))$, where n is a constant, commonly assumed to be unity, and ΔG is the Gibbs free energy of the reaction at the P,T condition of interest. Figure 4, which is constructed from Greenwood's experimental data, illustrates the dehydration kinetics of talc as functions of time, temperature and extent of overstepping (ΔT) above the equilibrium dehydration boundary at 1 Kb. It is evident from this figure that essentially complete dehydration of talc can be achieved within

6 hours at about 160°C above the equilibrium boundary.

The stability fields of the pure Mg-end members of various phyllosilicates of interest in this study are summarized for the condition of $P_{total} = P_{H2O}$ in Figure 5, which is reproduced from Evans and Guggenheim (21). According to our results, talc and other phyllosilicates completely dehydrate at $\geq$ 400°C at 1 bar in C1 and C2 bulk compositions. This is compatible with the phase relations shown in Figure 5. Thus, based on the results shown in Figure 4, one would anticipate that essentially complete dehydration of all phyllosilicates in C1 and C2 chondritic material is likely to be achieved in a matter of a few hours at $T \geq 600$°C. Detailed studies of the devolatilization kinetics of both phyllosilicates and carbonates as functions of temperature, fluid composition, and grain size are currently under way to evaluate the practical limitations of the extraction of volatiles from carbonaceous chondritic materials.

Acknowledgments

This research was supported by a NASA grant NAGW-1332 administered through the Center for Utilization of Local Planetary Resources at the University of Arizona. Thanks are due to Professor John Lewis for his invitation to join the NASA project and helpful discussions, to Dr. Larry Anovitz for making available his thermochemical data for minnesotite and greenalite before publication, and to Dr. Nilanjan Chatterjee and Kunal Bose for their help in the preparation of the manuscript. The skillful production of the manuscript in camera ready form by Jo Ann Overs is greatly appreciated.

References

1. Lewis, J.S., and Lewis, R.A. (1987) Space resources: Breaking the bonds of Earth. Columbia University Press, New York.

2. Jones, T., Lebofsky, L., and Lewis, J.S. (1989) Asteroidal H_2O and the hydration state of terrestrial raw materials. EOS Trans. Amer. Geophys. Union 70, 379.

3. Gaffey, M.J., and McCord, T.B. (1979) Mineralogical and petrological characterizations of asteroid surface materials, in Gehrels, T. (ed.) Asteroids, pp. 688-723, University of Arizona, Tucson.

4. Lewis, J.S., and Prinn, R.G. (1984) Planets and their atmospheres. Academic Press.

5. Zolensky, M., and McSween, H.S. (1988) Aqueous alteration, in Kerridge, J.F., and Mathews, M.S. (eds.) Meteorites and the early solar system, University of Arizona Press, Tucson.

6. Prigogine, I., and Defay, R. (1954) Chemical thermodynamics. Longman, London.

7. Ganguly, J., and Saxena, S.K. (1987) Mixtures and mineral reactions. Springer-Verlag.

8. Chatterjee, N. (1989) An internally consistent thermodynamic data base on minerals. Ph.D. thesis, City University of New York.

9. Berman, R.G. (1988) Internally consistent thermodynamic data for minerals in the system Na_2O-K_2O-CaO-MgO-FeO-Fe_2O_3-Al_2O_3-SiO_2-TiO_2-H_2O-CO_2. J. Petrology 29, 445-552.

10. Robie, R.A., and Hemingway, B.S. (1984) Heat capacities and entropies of phlogopite and paragonite between 5 and 900 K and estimates of enthalpies and Gibbs free energy of formation. Amer. Mineralogist 69, 858-868.

11. Chatterjee, N. (1987) Evaluaton of thermochemical data on Fe-Mg olivine, orthopyroxene, spinel and Ca-Fe-Mg-Al garnet. Geochim. Cosmochim. Acta 51, 2515-2525.

12. Anovitz, L.M., Essene, E., and Hemingway, B.S. (1989) Self-consistent thermodynamic data for the system Fe-Si-C-O-H: Applications to metamorphosed banded iron formations and iron-rich blueschists. Geochim. Cosmochim. Acta, in submission.

13. Lewis, G.N., and Randall, M. (1961) Thermodynamics. McGraw-Hill.

14. Helgeson, H.C., Delaney, J.M., Nesbitt, H.W., and Bird, D.K. (1978) Summary and critique of the thermodynamic properties of rock-forming minerals. Amer. J. Sci. 278A, 1-229.

15. Saxena, S.K., and Fei, Y. (1988) Fluid mixtures in the C-H-O system at high pressure and temperature. Geochim. Cosmochim. Acta 52, 505-512.

16. Saxena, S.K., and Fei, Y. (1987) High pressure and high temperature fluid fugacities. Geochim. Cosmochim. Acta 51, 783-791.

17. Robie, R.A., Hemingway, B.S., and Fisher, J.R. (1978) Thermodynamic properties of minerals and related substances at 298.15 K and 1 bar (10^5 pascals) pressure and higher temperatures. U.S. Geol. Survey Bull. 1452.

18. Eugster, H.P., and Ilton, E.S. (1983) Mg-Fe fractionation in metamorphic environments, in Saxena, S.K. (ed.)

Kinetics and equilibrium in mineral ractions, Springer-Verlag.

19. Greenwood, H.J. (1963) The synthesis and stability of anthophyllite. J. Petrology 4, 317-351.

20. Lasaga, A.C. (1981) Transition state theory, in Lasaga, A.C., and Kirkpatrick, R.J. (eds.) Kinetics of geochemical processes, Reviews in Mineralogy 8, 135-169.

21. Evans, B.W., and Guggenheim, S. (1988) Talc, pyrophyllite, and related minerals, in Bailey, S.W. (ed.) Hydrous phyllosilicates (exclusive of micas), Reviews in Mineralogy 19, 225-294.

22. Dodd, R.T. (1981) Meteorites: A petrological-chemical synthesis. Cambridge University Press.

23. Fei, Y., and Saxena, S.K. (1986) A thermochemical data base for phase equilibrium in the system Fe-Mg-Si-O at high pressure and temperature. Phys. Chem. Minerals 13, 311-324.

24. Babushkin, V.I., Matreyev, G.M., Mohedlov-Petrossyan, O.P. (1985) Thermodynamics of silicates. Springer-Verlag.

25. Barin, I., and Knacke, O. (1978) Thermochemical properties of inorganic substances. Springer-Verlag.

26. Gustafsson, P. (1984) A thermodynamic evaluation of Fe-C system. TRITA-MAC, Royal Inst. of Tech., Stockholm, Sweden.

27. Anovitz, L.M., Essene, E.J., Hemingway, B.S., Komada, N.L., and Westrum, E.F. (1988) The heat capacities of grunerite and deerite: Phase equilibria in the system Fe-Si-C-O-H and implications for the metamorphism of banded iron formations. EOS Trans. Amer. Geophys. Union 69, 515.

28. Bailey, S.W. (1988) Introduction, in Bailey, S.W. (ed.) Hydrous phyllosilicates (exclusive of micas), Reviews in Mineralogy 19, 1-8.

APPENDIX E

LUNAR OXYGEN AND METAL FOR USE IN NEAR-EARTH SPACE: MAGMA ELECTROLYSIS

LUNAR OXYGEN AND METAL FOR USE IN NEAR-EARTH SPACE: MAGMA ELECTROLYSIS

Russell O. Colson and Larry A. Haskin[1]

Abstract

Because it is energetically easier to get material from the Moon to earth orbit than from the Earth itself, the Moon is a potentially valuable source of materials for use in space. The unique conditions on the Moon, such as vacuum, absence of many reagents common on the earth, and presence of very non-traditional "ores" suggest that a unique and non-traditional process for extracting materials from the ores may prove the most practical. With this in mind, we have begun an investigation of unfluxed silicate electrolysis as a method for extracting oxygen, Fe, and Si from lunar regolith.

The advantages of the process include simplicity of concept, absence of need to supply reagents from Earth, and low power and mass requirements for the processing plant. Disadvantages include the need for uninterrupted high temperature and the highly corrosive nature of the high-temperature silicate melts which has made identifying suitable electrode and container materials difficult.

Introduction

One consequence of Earth's relatively high gravity is a relatively high energy cost for launching material from Earth into space, even near-Earth space. Because of this, as the need for propellants and constructional materials in near-Earth space grows, materials available from extraterrestrial sources should become economically attractive. The Moon is the closest potential source of such material. Its gravity is only about one-sixth that of Earth, low enough to improve greatly the payload/liftoff mass ratio for conventional rockets but still high enough to facilitate separation and manufacturing processes.

We know from the Apollo missions what the compositions and physical states of common materials on the lunar surface are (see Heiken et al., 1990, for extensive information about the nature of the Moon and its materials and conditions). We can thus begin to design and develop processes for providing, from lunar sources, the

1 Department of Earth and Planetary Sciences and McDonnell Center for the Space Sciences, Washington University, St. Louis, MO 63130

propellants and constructional materials we expect to need in near-Earth space. In our laboratory, we have chosen to investigate electrolysis of (simulated) molten lunar soil, a technique sometimes called "magma electrolysis", as a means of producing oxygen, iron, and silicon (Oppenheim, 1968; Kesterke, 1971; Lindstrom and Haskin, 1979; Haskin et al., 1990). We have chosen to investigate this uncommon technique because lunar surface conditions are very different from Earth's. On the Moon there is no water, air, or fossil fuel to serve as inexpensive solvents, oxidizing and reducing agents, fuels, or heat transfer agents. There are no suppliers of chemicals and no infrastructure for living or transportation. This suggests that it may not be economical to transfer well understood terrestrial technologies to the Moon's surface.

The Moon has sunlight (half the time), hard vacuum, and plentiful clinging dust (lunar "soil"). Production of useful materials from lunar resources is likely to prove economical to the extent that we learn how to take advantage of these conditions. Also, we must require that little material be brought from Earth to the lunar surface in relation to the quantities of product obtained. This is true because the principal anticipated cost of using lunar materials is that of lifting the necessary factories and equipment to process them from the Earth to the lunar surface. Therefore, reduced costs of transportation from the Earth to low-Earth orbit (which is the energy-expensive portion of the journey from the Earth to the Moon) will almost equally reduce the cost of using lunar materials in near-Earth space.

Because the Moon is largely unexplored, we do not know what specialized resources may be available. The only abundant resource we can presently count on is the common surface soils (regolith), whose average depth is unknown but probably exceeds three meters (Heiken et al., 1990). These soils are a good resource, containing some 45% (wt.) oxygen and 21% silicon, and up to 15% iron, 14% aluminum, 10% calcium, 6.6% magnesium, and 4.8% titanium, with the highest values for iron, magnesium, and titanium being in mare soils and those for aluminum and calcium in highlands soils (Heiken et al., 1990). The soils also contain minor proportions of sodium, chromium, manganese, metallic iron-nickel alloy (of meteoritic origin), and large quantities (at very low concentrations) of hydrogen, nitrogen, carbon, and noble gases (of solar wind origin; these can be extracted by heating the soil) (Haskin, 1990). All of the chemical elements are present in the soils, but most are present at very low concentrations.

We suggest that the earliest technologies for extraction and processing of extraterrestrial materials for early use in near-Earth space will have the following characteristics (Haskin, 1985; Haskin and Colson, 1990): They will come from a nearby source, most likely the Moon. They will have few and simple steps. They will require minimal material from the Earth. They will be reasonably automated, requiring only occasional tending. They will use an easily mined material as feedstock (probably lunar soil) and be able to accommodate a range of feedstock compositions.

We chose silicate electrolysis for study because of its apparent simplicity. The electrolytic cell could operate in batch mode, or may operate efficiently in continuous mode. We anticipate that it may need no moving parts. It can use lunar soil as feedstock, with no more preprocessing of the soil than sieving out of gravel and cobbles that might damage the cell before they could melt. (The bulk of the lunar soil is quite fine grained; gravel will be a scarce commodity on the Moon and we probably cannot afford to melt it.) We believe that silicate electrolysis can

convert the feedstock to oxygen and metal with high efficiency, some 40% oxygen and metal by weight. Our best current estimate is that its operation will require about twice as much energy as the theoretical minimum necessary to enable the chemical separation. In principle, the cell could operate on solar power during the lunar day, but for initial simplicity nuclear power seems preferable. The main problems are the high operating temperature (1,200 - 1,600°C) and the materials problems associated with corrosive, molten magma.

Review of Process Theory

The process theory is described in detail by Haskin et al., 1990, but we provide a brief review here. The cathode reactions that produce metal are the following:

$$Fe^{2+} + 2e^- = Fe^o \quad (1)$$

$$Si(IV) + 4e^- = Si^o \quad (2)$$

There is a competing reaction if the oxygen pressure is allowed to build up above the cell:

$$O_2 + 4e^- = 2O^{2-} \quad (3)$$

However, this reaction is not significant for oxygen fugacity less than about 10^{-3}. Other competing reactions include the reductions of trace and minor metals, such as Cr, Ti, Mn, and Ni, in the silicate melt.

At the anode, the principal desired reaction is the reverse of equation (3). However, this reaction is not significant because of low O^{2-} concentration and slow kinetics of formation of O^{2-} from silicate polymer chains. Therefore, the actual reaction during electrolysis involves oxidation of silicate polymer chains to form oxygen in the neutral state (Haskin et al., 1990). This process increases the extent of polymerization of the silicate. A serious competing reaction at the anode in melts with high iron concentrations is oxidation of Fe^{2+}.

$$Fe^{2+} = Fe^{3+} + e^- \quad (4)$$

Other competing reactions at the anode include oxidation of other multivalent cations such as Ti and Cr. Because reaction (4) is the primary competing reaction at the anode, the efficiency of oxygen production (defined as moles O_2 produced/4 · moles electrons passed through the melt) depends primarily on the concentration of Fe^{2+} cations. The dependence of oxygen production efficiency on Fe^{2+} concentration can be expressed as $\%O_2/(100-\%O_2) \approx 0.049/X_{FeO}$, where $\%O_2$ is the oxygen production efficiency in percent and X_{FeO} is molar fraction FeO in the melt. This has the consequence that electrolysis to produce oxygen as a main product is most efficiently carried out in melts with relatively low iron concentrations (<2%).

Power to drive the electrolysis equals E*I, where I is the current required to get oxygen at the desired rate and is proportional to oxygen production rate/oxygen production efficiency. This demonstrates the dependence of power requirements on oxygen production efficiency. E is the potential required to drive the electrolysis and is equal to $E_c-E_a - \eta_c-\eta_a - I(R_{cell})$, where E_c-E_a is the potential required to drive

the reaction(s) and is a function of the cation reduced. ($|E_c-E_a|$ increases in the order Fe < Si,Ti <Mg,Al < Ca) and the concentrations of the cations in the melt. The quantity $-\eta_c-\eta_a$ is the overpotential required because of slow reaction kinetics or, as we use it in this paper, because of cation mobility problems (inability of cations to migrate to the cathode fast enough to yield the desired production rate). R_{cell} is the resistance of the electrolysis cell and is equal to $L/\kappa A$ where L is the distance between electrodes, A is the electrode surface area, and κ is the melt conductivity. This expression illustrates the dependence of power on both cell configuration and resistivity of the molten feedstock. Not unexpectedly, κ is found to increase as the average ionic mobility of the melt increases. That is, κ increases systematically as mobile cations such as Fe, Mg, and Ca increase relative to Si and Al in the melt.

The electrolysis scenario for batch cell operation would be as follows: At low values for E_c-E_a (-0.7 to -1.3V), Fe is reduced at the cathode. As Fe is removed from the silicate melt, oxygen production efficiency increases and conductivity decreases, with a combined effect of increasing power requirements for oxygen production. Then, once Fe is nearly depleted, E_c-E_a is increased to more negative potentials (<-1.4V) and Si and Ti are reduced at the cathode. Because Fe has already been removed, oxygen production efficiency is high, and conductivity increases as SiO_2 is removed from the melt, resulting in a sharp drop in power required to produce oxygen. Theoretically, Mg, Al, and Ca could also be reduced at even more negative potentials.

Evaluation of the silicate electrolysis process and comparison with alternatives

The silicate electrolysis method for extracting oxygen from lunar regolith has several advantages over alternative processes. These include the absence of any need for reagents that must be brought from earth or recovered from the products; the wide range of feedstock compositions that are acceptable, and the lack of need for preprocessing of the feedstock; and the conceptual simplicity of the process. The primary disadvantages include the need to find durable materials for containers and electrodes in these high-temperature (1200-1600°C), highly corrosive silicate melts, high startup temperatures, and the need to keep the cell hot during the lunar nights.

In order to place what we know about the silicate electrolysis method into a context readily compared with other processes, we have identified several key questions to address. These are the following: How much power is required to produce a given amount of oxygen? What plant mass is required to produce oxygen at a given rate? What feedstock is required; is it a common lunar material or will it require location and ore-body verification? What preprocessing of lunar material is necessary to prepare it? What fraction of the feedstock is converted into products? What reagents are required for the process and at what rate must they be replenished? How complex is the process and how many steps does it involve? What is the product(s) of the process? What technology must be developed before the process is viable? What must yet be learned about the theory of the process before any or all of the questions above can be answered?

The complex dependence of the answer to one question on answers to others makes comparisons among proposed processes difficult. For example, if one process yields a more pure product than another, or more products, what is this worth in terms of

power required, plant mass, or process complexity? Also, how do we judge a promising but undeveloped technology, or technologies at different stages of development? If a problem in developing a technology cannot be solved quickly enough, then the process is not viable however promising its other aspects may be. Alternatively, once the problem is solved then the relative worth of the process is measured in terms of its other aspects. Despite these difficulties, the discussion below gives some grounds for evaluating the silicate electrolysis process and comparing it to alternative processes.

Power requirements:
Power requirements for any of several proposed processes for extracting oxygen can be divided into two categories, thermal and electrical, with electrical power supplied by a power plant, either nuclear or solar, while thermal power can be supplied, at least for some applications, by direct solar power and therefore is somewhat cheaper in terms of plant cost, mass required, and plant upkeep. The power required by silicate electrolysis is entirely electrical, with resistance heating in the magma supplying sufficient heat to melt new feedstock which might have otherwise been melted by direct solar energy. (If a batch mode is utilized, then initial melting could possibly be done by direct solar energy.)

The power required for silicate electrolysis is a function of electrode surface area, distance between electrodes, and composition of the magma (effecting the oxygen production efficiency and magma resistivity). Therefore, the power required can be decreased as we accept a greater plant mass, a greater possibility of shorting the electrodes (as the electrodes are moved closer together), and a more specialized feedstock. By choosing a reasonable trade-off among these variables we can derive a reasonable value for energy required per unit oxygen produced. The value reported by Eagle Engineering (1988) is about 15.6 MWh/MT oxygen. The value reported by Haskin et al (1990) is somewhat less at 13 MWh/MT oxygen (but does not included energy to compress oxygen, acquire and handle feedstock, etc.).

This value is about twice the theoretical minimum energy to extract oxygen and reduced Fe and Si in basaltic silicate melts. This value compares favorably with energy values reported for extracting oxygen by other processes, most of which require 2 to 4 times the theoretical minimum (e.g. Eagle Engineering, 1988). Some reports for very low energy requirements of 5 MWh/MT oxygen for hydrogen reduction of ilmenite have been made (Table 4.1, Eagle Engineering, 1988). This is almost identical to the theoretical minimum and probably can not be practically achieved. We point out that the theoretical minimum for getting oxygen from ilmenite is about 25-35% less than that for getting oxygen from basaltic melt (assuming both Fe and Si in melt are reduced), but this difference is not large compared to the uncertainties intrinsic in estimating the power that will be required for any particular process. Also, this estimate does not include the energy to preprocess the starting material to produce the ilmenite.

Plant mass:
Because of the few processing steps involved in silicate electrolysis and the simplicity of the process, the plant mass compares favorably with those for other processes. If we consider that accessory masses such as oxygen collecting facilities, material handling facilities, power plant mass, etc. are common to most processes, then we can reduce the comparison to one of the processing plant masses only. Most of the mass for the silicate electrolysis process is in the electrodes, magma containers,

electric busses, and the insulation/heat radiators. We have estimated this to be on the order of 3-10MT for 1000 MT oxygen/year. This is considerably less than the 20-80 MT expected for most other processes. However, if facilities are included to separate the components of the Fe-Si-Ti-Cr alloy product of silicate electrolysis, mass requirements might be increased to values comparable to other processes. Also, a considerable portion of the plant mass for silicate electrolysis may be in the form of Pt, an exceptionally expensive material, because Pt is the proposed anodic material. However, the cost of the Pt is small compared to the launching costs of greater masses of material.

Feedstock requirements:
In theory, the silicate electrolysis process can accept feedstock of nearly any composition with little or no preprocessing. The primary constraints are the efficiency of oxygen production, which decreases with increasing Fe in the melt, increasing power requirements, and the resistivity, which increases with increasing SiO_2 and Al_2O_3 in the melt, again increasing power requirements. Also, if the liquidus temperature of the melt were to rise above the temperature at which the electrolysis is done, the presence of crystals in the melt would further increase resistivity. However, a steady state residual melt may be achievable, which would act as a fluxing agent to buffer the efficiencies, resistivities, and liquidus temperature of the melt, thus making the process nearly independent of feedstock within the limits of lunar regolith compositions. Minimal monitoring of feedstock or product composition might be necessary so that temperatures and electrode potentials could be varied to maintain the composition of the residual flux within reasonable limits.

Reagents required:
The silicate electrolysis process requires no reagents that need to be supplied from Earth or recovered from the process.

Complexity of process:
Magma electrolysis is essentially a one step process taking place in one reaction pot. As such, it is one of the simplest processes proposed. Keeping the process simple is important for several reasons, including being easier to automate, fewer replaceable parts needed, and fewer things to go wrong with the operation, leading to less down time and fewer people needed to operate the plant. Simplicity can also decrease development time and cost. Fewer processing steps is also an advantage in that it generally results in lower mass requirements. We also note that because theoretical energy requirements to extract oxygen from a given composition are the same regardless of the process chosen, fewer steps give fewer opportunities for energy loss. The simplicity of the process is generally recognized as one of the main advantages of the silicate electrolysis method over other approaches. However, as already pointed out above, if pure metal products such as pure Fe or Si are desired, additional purification steps need to be added to the process necessarily adding to its complexity.

Products:
We have identified several basic products of silicate electrolysis. The main products are oxygen, produced at the anode, and a suite of metals and metal alloys produced at the cathode and consisting of Si, Fe, or Fe-Si alloys containing 0.2-1% Ti and Cr. The metal compositions vary as a function of imposed potential and magma composition. (Theoretically, but not yet observed in our experiments, Al, Mg, and

Ca could be reduced at increasingly negative potentials and at higher melt temperatures.) The mineral spinel precipitates from the residual melt at sufficiently low temperatures or with sufficient removal of SiO_2. This material varies in composition from Fe-Cr rich spinel to Mg-Al rich spinel depending on the composition of the magma and extent of electrolysis.

The remaining molten silicate would be an important byproduct; it can be cast into bars, sheets, beams, etc., or its CaO-MgO enriched composition may make it suitable for use in cements. So-called "waste heat" carried off with the products or radiated by the cell is another potentially useful byproduct.

Status of technology development:
We have determined that the products and efficiencies of silicate electrolysis are sufficient to justify engineering demonstration of technological feasibility. Here, we mention several problems that such experiments must address. The most critical is to test materials to serve as container, anode, and cathode, as nearly all metals and ceramics are corroded by these high-temperature silicate melts. We have in mind four general types of possible electrode or container materials.

One type of material is simply inert to the silicate and its products. As an example, Pt has been used extensively in experimental petrology as inert containers for silicate melts at high temperature. However, Pt combines with Si to form an alloy that melts below 1,000°C and is unsatisfactory as a cathode or container. Pt appears to be a suitable anode material, however (Haskin et al., 1990).

The second type of material involves a steady-state equilibrium. An "iron skull" container or cathode could be formed by balancing the heat generated by the electrolysis with heat lost to the surroundings to form a solid skin of product or feedstock enclosing the silicate melt and metal product. High melt resistivities (Haskin et al, 1990) coupled with the large distance between electrodes that would seem to be required to make the approach robust might make power requirements prohibitive for cathodes, but the cell container might be made in this fashion.

The third type of material would be in thermodynamic equilibrium with the silicate melt and electrolysis products and would therefore not react with them. Because the product is Si-Fe metal, Fe-Si alloys might serve as the cathode material (Haskin, et al., 1990). Similarly, the presence of spinel ($MgAl_2O_4$) on the liquidus of the residual silicate of the electrolysis process suggests the use of spinel as the containing material.

The fourth type of material would be destroyed by the process, but slowly. This option detracts from one of the intended advantages of unfluxed silicate electrolysis, the absence of any need to resupply reagents or other materials from Earth or to recover them from the products. Nevertheless, such an option may prove to be the most cost effective.

Theory:
We now understand in some detail the chemistry of the oxidation-reduction reactions involved in the electrolysis of silicate melts (Semkow and Haskin, 1985; Haskin et al., 1990). This includes identifying the reactions involved and studying their kinetics,

evaluating the dependence of oxygen production efficiency on melt composition, and determining the resistivities of melts as a function of composition.

We are now studying dynamic problems in the electrolysis and how they relate to overpotentials needed to drive reductions in the melt. We are studying whether material flow and thermal convection in a cell can keep fresh material at the electrodes or whether active mixing will be necessary. We are studying the effects of overpotential on product composition; preliminary experiments have yielded a metal with somewhat lower Si/Fe ratio than expected. Remaining uncertainties in activities of melt components still present a small but possibly significant uncertainty in estimating power requirements and product compositions.

Conclusions

Unfluxed silicate electrolysis offers several advantages over alternative processes. These include simplicity of the process and the absence of a need to supply reagents from earth. Power and mass requirements for the process are competitive. The main unsolved problems center around testing of materials to serve as cathode and container in high-temperature silicate melts. However, little work has been done in the way of engineering studies. This work needs to be done before we know whether the theoretical simplicity and efficiency of the silicate electrolysis process is also a practical simplicity.

Acknowledgements: We thank the National Aeronautics and Space Administration for partial support of this work through the UA/NASA Space Engineering Center for Utilization of Local Planetary Resources.

Appendix I: References

Eagle Engineering, Inc (1988). *Conceptual design of a lunar pilot plant lunar base systems study (LBSS).* EEI report No. 88-182.

Haskin, L. A. (1985). "Toward a Spartan scenario for use of lunar materials." In *Lunar Bases and Space Activities of the 21st Century*, (ed. W. W. Mendell), 435-443.

Haskin, L. A. (1990). "Water and cheese from the lunar desert: Abundances and accessibility of H, N, and C on the Moon. In *Lunar Bases and Space Activities of the 21st Century (II)*, (Ed. W.W. Mendell). (in press)

Haskin, L. A. and Colson, R. O. (1990). "Lunar resources: toward living off the lunar land." *Proceedings of the first annual invitational symposium of the UA/NASA Space Engineering Research Center for Utilization of Local Planetary Resources.* (Ed. T. Triffet) (in press).

Haskin, L. A., Colson, R. O., Lindstrom, D. J., Lewis, R. H., and Semkow, K. W. (1990). "Electrolytic smelting of lunar rock for oxygen and iron." In *Lunar Bases and Space Activities of the 21st Century (II)*, (Ed. W.W. Mendell). (in press)

Kesterke, D. G. (1971). *Electrowinning of oxygen from silicate rocks.* U.S. Bureau of Mines Report of Investigations 7587.

Lindstrom, D. J. and Haskin, L. A. (1979). "Electrochemical preparation of useful material from ordinary silicate rocks." In *Space Manufacturing Facilities*, (eds. J. Grey and C. Drop.) AIAA, 129-134.

Heiken G., Vaniman, D., and French, B (eds) (1990). *Lunar Sourcebook.* Oxford University Press. (Accepted for publication.)

Oppenheim, M. J. (1968). "On the electrolysis of molten basalt." *Mineral. Mag.* 36, 1104-1122.

Semkow, K. W. and Haskin, L. A. (1985). "Concentrations and behavior of oxygen and oxide ion in melts of composition $CaO \cdot MgO \cdot xSiO_2$." *Geochim. Cosmochim. Acta* 49, 1897-1908.

526-91

APPENDIX F

LUNAR RESOURCES—TOWARD LIVING OFF THE LUNAR LAND

LUNAR RESOURCES -- TOWARD LIVING OFF THE LUNAR LAND

Larry A. Haskin and Russell O. Colson, Department of Earth and Planetary Sciences and McDonnell Center for the Space Sciences, Washington University, St. Louis, MO 63130

Space is now an accessible part of the human environment, and it behooves us to learn in the broadest sense what's out there, how it got there, and how it works. In the narrower context of modes of exploration that place men and women in space, we should also learn how to keep ourselves healthy and safe, how to carry out activities in space, and how to use what we find there. Whatever the reasons may be for our activities in space, we should learn through those activities what the practical importance of space may be.

Why the Moon?

We can particularly improve our assessment of the value of space for human activities through the experience of living on the surface of another planetary body and learning how to use its indigenous materials. The nearest body appropriate for this is the Moon, which has properties and resources suitable for such exploration. The Moon, like low-Earth orbit, geostationary orbit, and lunar orbit, is part of near-Earth space, part of the Earth-orbit environment. Because it is close, in the near term it is the easiest and safest body outside of Earth to use. We know more about it than we know about any other planet except Earth. A Moonbase will build on the experience of the Apollo missions. Even with these advantages of proximity and our knowledge of its surface, the Moon still offers substantial technological challenge in engineering, mining, manufacturing, construction, and life support.

Economics will ultimately dictate where and what kinds of material we will use in space but, if we take a conservative approach, we might conclude that for near-term use in near-Earth space there are only two choices. One is the Earth and the other is the Moon. Because the Moon is the most likely object for testing and developing the first technologies for sustaining human presence on another planet, it is also the most likely economical near-term supplier of extraterrestrial material for use in near-Earth space. In the longer run, we may find it economical to use far more distant bodies such as near-Earth asteroids or Phobos to supply materials to near-Earth space (e.g., Lewis and Lewis, 1987). As we do not know what specific materials any of these bodies has to offer or what the physical states of their surfaces are, we cannot readily design technologies to use on them; we therefore assume that their use is decades in the future.

The Earth as a source for materials to use in space has the advantage of well developed technologies and manufacturing capabilities. It has the disadvantage of relatively high gravity and a consequent, unavoidable penalty in energy for lifting materials from its surface into orbit. The Moon has the advantage of intermediate gravity, low enough to enhance the payload/liftoff-energy ratio relative to lifting from Earth, but high enough to be of practical use in separating products from residues. Transport of lunar material to low-Earth orbit is particularly attractive if aerobraking supplants rocket energy for achieving that orbit. Whatever the actual cost of using a lunar materials may be, provided they do not require extensive crew time to produce, the largest part of that cost is for hauling the lunar factory from Earth to the Moon (e.g., Simon, 1985). Forseeable technologies that would reduce the cost of transporting materials from Earth, even to low-Earth orbit, would almost equally reduce the cost of operations on the lunar surface.

Technologically, the Moon is underdeveloped. Earth technologies cannot readily be transplanted to the lunar surface because conditions and starting materials there are not those found or used

on Earth. The Moon also remains largely underexplored. It is underexplored physically, so that we have no satisfactory assessment of the range of materials it has to offer. It is underexplored conceptually, in that we have not devoted enough effort or funds to learn how we might make use of what we already know is there. Many uses and technologies have been proposed, but few have been tested and none has been fully developed. The lead time for research and development is ten to fifteen years for the simplest proposed technologies, and we need serious laboratory work on them now if we are to test them, let alone hope to use them, at the proposed lunar outpost.

Lunar Resources and Surface Conditions

So, what is abundant on the Moon, and how might we use it? Here, we take a conservative view and accept as resources only those materials we know from Apollo experience to be common and present in such large quantities that we would not require further *on-surface* exploration to verify their existence as ore bodies. Abundant materials in the lunar highlands are breccias (rocks that consist of fragments of earlier rocks, produced on the Moon by the impacts of the meteoroids that made the heavily cratered lunar surface) and "soils" (the unconsolidated, pulverized products of the cratering impacts). In the lunar maria, prevalent materials are basaltic lavas and soils, and there may be substantial deposits of pyroclastic glasses (lunar volcanic ash). (The lavas and pyroclastic deposits would require on-surface verification as ore bodies because: thicknesses and continuity of lavas with specific characteristics, e.g., high proportions of ilmenite, would need to be demonstrated and thicknesses of pyroclastic deposits would need to be determined.)

In addition to these material resources, the lunar surface offers intermediate gravity, high vacuum, and dependable sunlight (half the time). It also offers extreme temperatures (120 °C in

the sun, -170 °C in the shade), no atmosphere to transfer heat or scatter light, clinging dust, and two-week-long days and nights.

The most likely material for initial use is lunar soil. The principal chemical constituents of the soils (e.g., Haskin and Warren, 1990) are oxygen (about 45% by wt.), silicon (about 21%), aluminum (about 13% in highland soils, 5% in mare soils), calcium (in most soils 8 - 10%), iron (some 15% in mare soils, 6% in highland soils), and magnesium (about 5%), plus some sodium and, in some mare soils, significant titanium (up to about 6%). Of course, all of the chemical elements are present in the soils, but most are present in minor or trace concentrations. There may be ores for some of the minor or trace elements; certainly, extensive amounts of chemical separation took place, as indicated by small, specialized fragments in the lunar sample collections. However, because the Moon lacks internal water, ores of most types we find on Earth are unlikely to be found there.

Guidelines for Early Lunar Technologies

Overall, simple transplantation of terrestrial technologies to the lunar surface seems inappropriate. Materials that are common on the lunar surface would be uncompetitive as starting materials for most terrestrial extraction processes. We especially would disdain them as sources of air and water, which we regard as free and abundant on Earth. Lunar surface conditions would also be unsuitable for most terrestrial technologies. Because of this, we tend to regard them (and conditions on the surfaces of other objects in the solar system) as impediments. However, with new ideas and proper understanding, we should be able to turn at least some of these conditions into advantages.

Initially, all operations on the lunar surface (as elsewhere in space) will be awkward and expensive. Thus, the simplest technologies that can produce crucial products will presumably be

the first technologies developed (e.g., Haskin, 1985). We can speculate that characteristics of desirable initial lunar technologies would include the following: Such technologies would have few and simple steps, including minimal preparation of feedstock and minimal effort to recycle reagents. They would require minimal material (reagents plus factory) to be brought from Earth. They would make efficient use of energy, or at least of power other than direct sunlight. They would be easy to install, have few moving parts, and be easy to maintain and operate, and thus require little astronaut time. They should be robust with respect to physical jarring during transport and installation. They should be robust with respect to feedstock composition: the ore body should be easy to mine and batches of feedstock should not require extensive compositional monitoring.

However unusual lunar soils may seem when compared with terrestrial ores, they are an excellent resource in terms of their chemical compositions and, for some purposes, their physical characteristics. It is convenient to illustrate this in the sort of everyday terms one might use if one were a pioneer settler on the Moon. Our pioneer settler must have the perspective of a chemist, however, to recognize much of the potential of the soil as a resource.

The Lunar Water Works: As pioneers, our first concern might be food and water, especially since the Moon has the reputation of being very dry and barren of carbon. It is proposed that there may (e.g., Arnold, 1979) or may not (e.g., Lanzerotti and Brown, 1981) be water at the lunar poles, but we ignore that possibility in our conservative scenario. Instead of water, let us consider the abundance of its chemical components, oxygen and hydrogen. The lunar supply of oxygen is enormous: oxygen is the most abundant chemical element (by weight, some 45%) in the lunar soils and rocks. It is chemically combined in those materials and must be extracted, as discussed below.

In contrast, concentrations of hydrogen are very low, but the total quantity available is nevertheless great. Lavas erupted from the Moon's interior contain such low amounts of hydrogen (and carbon and nitrogen) that we have been unable to observe them even with modern sensitive instruments, in contrast to terrestrial lavas, which typically contain at least 0.5% water. The lunar surface, however, has been bathed for billions of years in the solar wind, a flux of ionized atoms from the exterior of the sun. These ions embed themselves in the surfaces of the grains of soil that lie on the Moon's surface. The lunar surface is repeatedly "gardened" by infalling meteorites, so old, solar-wind-rich grains are buried and fresh grains exposed. In this way, large amounts of hydrogen have become buried in the soil, enough to produce (if combined with lunar oxygen) about one million U. S. gallons (about 3.8 million liters) of water per square mile (2.6 km^2) of soil to a depth of two yards (1.8 m) (Haskin, 1990). This hydrogen can be extracted by heating the soil to about 700 °C. Supplying the Lunar Water Works is a matter of technology and economics, but not a matter of availability of hydrogen and oxygen on the Moon.

The Lunar Farm: Like hydrogen, carbon and nitrogen are abundant in the lunar soil. Like hydrogen, they are derived from the solar wind and are present in very low concentrations. They are obtained along with hydrogen when lunar soil is heated. All the other nutrients necessary to life are likewise present in the soil. In principle, just as they do on Earth, plants should be able to extract these nutrients directly from the soil, once we have provided them with adequate lunar water, carbon dioxide, oxygen, and nitrogen. In practice, such soils would probably not be very fertile until their minerals had reacted with water, and hydroponic means of farming might be needed initially.

The Lunar Filling Station: At least initially, an important mode of transportation to and from the Moon base will be rockets. Hauling the fuel and oxidizer for these from Earth will be expensive. It may prove cheaper to provide them from lunar soil. The fuel of choice might be

hydrogen. For perspective, consider the production of 40 tonnes of hydrogen per year, a reasonable estimate of the amount needed for all transportation from low-Earth orbit in the early Moonbase era. That amount can be obtained from just 0.3 square kilometer of soil mined to a depth of one meter (Haskin, 1990).

Alternatively, lunar transport vehicles might burn a metal such as iron, aluminum, or silicon, even though these are less efficient rocket fuels than hydrogen. All three are major constituents of lunar soils, from which they can be extracted from chemical combination with oxygen. Each is a byproduct of one or more proposed processes for extraction of oxygen.

We need an oxidizer for the fuel, and oxygen is very abundant, although it is not trivial to extract it from the soils. Several techniques have been proposed, including extraction of oxygen from ilmenite by using hydrogen gas (e.g., Gibson and Knudsen, 1985; Williams, 1985), extraction by using carbon monoxide gas (e.g., Rosenberg et al., 1965; Cutler and Krag, 1985), extraction by processing with hydrofluoric acid or fluorine (e.g., Waldron, 1985; Burt, 1990), and extraction by electrolysis, either with a flux (Keller et al., 1989) or without a flux (e.g., Haskin et al., 1990, discussed below).

The Lunar Lumber Yard: Suppose we decide we need a new structure on the Moon or in space; what will the Lunar Lumber Yard have to offer? A case can be made that the "boards" of space construction will be made of glass. Molten lunar soil can be cast into silicate beams, rods, and sheets, be extruded as tubes, and be spun into fibers. These may have greater strength than similar products on Earth because in the space environment there is no water to react with their polymer bonds.

Iron, aluminum, and silicon are byproducts of oxygen extraction from lunar soils. Iron and aluminum can be fabricated into beams and rods for structural support. They can be drawn

into wires, both for structural use and for use as electrical and heat conductors. All three can be used as mirrors or mirror coatings to reflect sunlight.

The unprocessed soil itself can serve as thermal shielding to moderate habitats and other environments against the broad, diurnal temperature fluctuations at the lunar surface. It can also serve as radiation shielding against cosmic rays and solar flares. Partially distilled in a solar furnace, it seems possible that the residue from the soil might take on the composition of a good cement, and the water to turn it into concrete could be obtained from local sources, as mentioned above. Distilled further, the residue would be very refractory and could serve for heat shielding.

The Lunar Power Company: The Moon receives plentiful and predictable amounts of sunlight, and sunlight will surely be the eventual source of nearly all electrical power and heat used by the lunar pioneer. Except at very restricted locations at the lunar poles, sunlight is locally available only half the time, however, and for some purposes, the temporal distribution of sunlight is inconvenient. Storing energy derived from the sun over the two-week-long lunar night seems difficult, and might have to be done in the form of hydrogen, metals, and oxygen whose extraction was powered by solar energy. Thus, a strong case can be made that the power used initially on the Moon should be nuclear.

Initially, it may be economical to bring high yield solar panels to the Moon from Earth. Eventually, electrical power will probably be derived from lunar silicon, a byproduct of oxygen production, or from lunar ilmenite, recently shown to be photovoltaic. Conversion need not be efficient if a local material simply obtained is used as the photovoltaic.

Electrical power may be the first major import to the Earth from the Moon (once the souvenir market has been satisfied). Large arrays of relatively low-yield solar cells can be placed on the

Moon to supply large amounts of power for transmission to Earth (Criswell and Waldron, 1985). Also, lunar ^{3}He has been proposed for use as a fusion fuel superior to tritium (^{3}H) in that it is not radioactive, does not have to be made in nuclear fission reactors, and yields a proton instead of a more destructive neutron when it fuses with deuterium (^{2}H) (Wittenberg et al., 1987). The use of iron, aluminum, and silicon to coat mirrors to move sunlight around was indicated above.

"Magma Electrolysis," a Proposed Lunar Technology*

We are investigating electrolysis of molten silicate as a means of producing oxygen and metals for use on the Moon and in near-Earth space. (See also Oppenheim, 1968; Kesterke, 1971; Lindstrom and Haskin, 1979). Most of our effort so far has been to determine the nature and kinetics of the electrochemical reactions and the conductivities and other parameters necessary for design of a test cell. We have not yet designed a production-scale cell, but we have a rough idea of its characteristics (Haskin et al., 1990).

We envision a steady-state operation. The feedstock for the cell would be lunar soil that had been sieved to remove the small proportion of material larger than 0.3 cm. As the soil was fed into the cell, it would melt; the heat for melting would be furnished by "excess" electrical heat released into the melt owing to its resistance. The cell would have a volume of about one cubic meter and anode and cathode areas of about thirty meters each. Oxygen would be produced at the anode, and iron, silicon, or an alloy of the two would be produced at the cathode,

---

*The term "magma electrolysis" is catchy (e.g., du Fresne and Schroeder (1983); because to geoscientists the term "magma" indicates naturally occurring melts, we generally use the term "molten silicate electrolysis."

depending on the composition of the silicate melt in the cell. The operating temperature of the cell would be between 1,200 and 1,400 °C.

We estimate that the power required to produce one tonne of oxygen gas per 24 hours would be about 0.54 Mw, of which some 0.11 Mw would be used to melt and heat the feedstock, 0.19 Mw would be used to separate the oxygen and metal from chemical combination, and 0.24 Mw would be "excess" resistance heat, some of which would be needed to make up for radiation losses from the hot cell, and the rest of which would be available for other uses. In addition to the one tonne of oxygen gas, the cell would produce (for an average melt composition) some 0.64 tonne of iron and 0.62 tonne of silicon. About 4.8 tonnes of soil would pass through the cell per 24 hours, so some 2.5 tonnes of spent silicate melt would have to be removed along with the oxygen and metal. All products of the cell would be useful; nothing would need to be discarded. Potential uses are discussed above.

This process would satisfy many of the criteria set forth above for early lunar technologies. The cell proper would have no moving parts.although the equipment to mine, sieve, and introduce the lunar soil would and that to remove and store the oxygen might. Producing the oxygen, metals, and spent silicate would be a one-step process: we have not considered how to handle the products, an activity common to all proposed processes. The mass and size of the cell would be modest compared to the equipment for most proposed alternate processes (e.g., Eagle Engineering, 1988).

The power requirements would also be competitive with those of proposed alternate processes, if we include in the comparison the ancillary steps required by those processes such as ore refinement and reagent recycling that would not be needed for silicate electrolysis. The cell would need continuous electrical power, however, so that its contents would not freeze during the lunar night; initially, this requirement may best be met by use of nuclear power.

The process would use common lunar soil; any common soil found by the Apollo or Luna missions would be acceptable, although prior knowledge of the general type of soil might enable optimization of cell design or startup protocols. Different feedstocks would require somewhat different initial conditions of temperature and electrical potential but, once the bulk composition of the melt had been established in the cell, probable variations in feedstock composition would not greatly affect cell temperature or operating potential.

The main identified and unsolved problems of the process center around finding suitable materials for the electrodes and container. Iron and silicon form alloys with most metals. Molten silicate is very corrosive. Anodes can probably be made of platinum or coated with it, and cathodes can probably be made of high-temperature iron-silicon alloys. The container may have to be made of spinel, which would be brought into equilibrium with the silicate melt.

Conclusions

Lunar soils contain in abundance the materials required for life support, construction, and transportation. The high cost in energy of lifting material from the Earth's surface suggests that, in the near term, lunar material should be considered for use both on the Moon and in low-Earth orbit. However, most conventional technologies are not suited to efficient processing of lunar material, so new technologies need to be developed. Additional ideas are needed, but most crucial is investment in thorough testing of existing ideas on a laboratory bench scale. Development of those that prove promising in the laboratory should be begun immediately, because of the long lead time to prepare robust units for testing or use on the Moon.

Acknowledgements

We thank the National Aeronautics and Space Administration for partial support of this work through the UA/NASA Space Engineering Center for Utilization of Local Planetary Resources.

References

Arnold J. R. (1979) Ice in the lunar polar regions. J. Geophys. Res. 84, 5659-5668.

Burt, D. (1990) Lunar mining of oxygen using fluorine. In Lunar Bases and Space Activities of the 21st Century II, W. Mendell, ed. Lunar and Planetary Institute, Houston. (Accepted for publication).

Criswell, D. R. and Waldron R. D. (1985) Concept of the lunar power system. In Space Solar Power Review 5, 53-75.

Cutler A. H. and Krag P. (1985) A carbothermal scheme for lunar oxygen extraction. In Lunar Bases and Space Activities of the 21st Century, W. Mendell, ed. Lunar and Planetary Institute, Houston. pp. 559-569.

du Fresne, E. and Schroeder J. E. (1983) Magma electrolysis, in Research on the Use of Space Resources, W. F. Carroll, ed. JPL publication 83-86.

Eagle Engineering, Inc. (1988) Conceptual design of a lunar pilot plant lunar base systems study. EEI report No. 88-182.

Gibson M. A. and Knudsen C. W. (1985) Lunar oxygen production from ilmenite. In Lunar Bases and Space Activities of the 21st Century, W. Mendell, ed. Lunar and Planetary Institute, Houston. pp. 543-550.

Haskin, L. A. (1985) Toward a spartan scenario for use of lunar materials. In Lunar Bases and Space Activities of the 21st Century, W. Mendell, ed. Lunar and Planetary Institute, Houston. pp. 435-443.

Haskin, L. A. (1990) Water and cheese from the lunar desert: Abundances and accessibility of H, N, and C on the Moon. In Lunar Bases and Space Activities of the 21st Century II, W. Mendell, ed. Lunar and Planetary Institute, Houston. (Accepted for publication).

Haskin, L. A., Colson R. O., Lindstrom D. J., Lewis R. H., and Semkow K. W. (1990) Electrolytic smelting of lunar rock for oxygen, iron, and silicon. In Lunar Bases and Space Activities of the 21st Century II, W. Mendell, ed. Lunar and Planetary Institute, Houston. (Accepted for publication).

Haskin L. A. and Warren P. H. (1990) Chemistry. In Lunar Sourcebook, G. Heiken, D. Vaniman, and B. French, eds. Lunar and Planetary Science Institute, Houston. (Accepted for publication.)

Keller, R. (1989) Dry extraction of silicon and aluminum from lunar ores. EMEC Consultants final report to Johnson Space Center.

Kesterke D. G. (1971) Electrowinning of oxygen from silicate rocks. U.S. Bureau of Mines Report of Investigations 7587.

Lanzerotti L. J. and Brown W. L. (1981) Ice in the polar regions of the moon. J. Geophys. Res. 86, 3949-3950.

Lewis J. S. and Lewis R. A. (1987) Space Resources, Columbia U. Press, N.Y. 418 pp.

Lindstrom D. J. and Haskin L. A. (1979) Electrochemical preparation of useful material from ordinary silicate rocks. In Space Manufacturing Facilities, J. Grey and C. Drop, eds. AIAA, N.Y. pp. 129-134.

Oppenheim, M. J. (1968) On the electrolysis of molten basalt. Mineral. Mag. 36, 1104-1122.

Rosenberg S. D., Guter G. A., and Miller S. F. (1965) Manufacture of oxygen from lunar materials. Annals New York Acad. Sci. 123, 1106-1122.

Simon M. C. (1985) A parametric analysis of lunar oxygen production. In Lunar Bases and Space Activities of the 21st Century, W. Mendell, ed. Lunar and Planetary Institute, Houston. pp. 531-541.

Waldron R. W. (1985) Total separation and refinement of lunar soils by the HF leach process. Space Manufacturing 7, AIAA, New York. pp. 132-149.

Williams R. J. (1985) Oxygen extraction from lunar materials: An experimental test of an ilmenite reduction process. In Lunar Bases and Space Activities of the 21st Century, W. Mendell, ed. Lunar and Planetary Institute, Houston. pp. 551-558.

Wittenberg L. J., Santius J. F., and Kulcinski G. L. (1987) Lunar source of ^{3}He for commercial fusion. Fusion Technology 10, 167-178.

OMIT TO END

D-24

APPENDIX G

NEAR-EARTH ASTEROID DATA BASE

Number	Name	a	e	i	Omega	ω	M	H	Epoch	Diameter	Period	P(1.5)	Amplitudes	Class	Pv	References
	1937UB	Hermes						0.62								
	1950DA							0.84								
	1954XA							0.51								
	1959LM							0.72								
	1973HA							0.68								
	1974HA							0.42								
	1976CA							0.88		1.9	3.748			S(10)	0.06	8
	1979YA							1			3.6			CP(2)		
	1979XB							0.65								
	1981YA									1.3					0.07	4
	1982DB	1.4894422	0.3602384	1.42068	314.05543	157.87413	191.24669	0.95	10/27.0/84							
	1982YA	2.2993776	0.7724651	18.19278	9.627	119.10477	300.21486	0.52	12/01.0/85	1.7(S)		15.7			0.33(S)	4
										1.8(R)					0.28(R)	
	1983LC	2.631651	0.7091899	1.51856	159.07591	184.69196	8.8271	0.76	12/23.0/83							
	1983TF2	2.4389347	0.7363252	14.70372	8.32966	116.56936	328.90684	0.66	09/23.0/83							
	1983YA	2.6106835	0.6917034	16.22778	76.87026	11.68396	167.10796	0.81	12/01.0/85							
	1983YB							0.96								
	1984KB	2.2210346	0.762275	4.63662	170.56242	334.87816	61.62574	0.52	10/27.0/84	0.7				S(11)	0.1	9
	1986JK							0.9						C(12)		
	1986PA							0.59								
	1987KF							0.59								
	1987OA							0.61								
	1987QA							0.88								
	1987SB							0.75								
	1987ST							0.6								
	1988BG							0.64								
	1988TA							0.79						C(13)		
	5025P-L							0.45								
	6344P-L							0.97								
	6743P-L							0.8								
	1968VP4							0.72								
	1988XB							0.76								
	1989AC							1.9								
	1989AE							0.66								
433	Eros	1.4583663(2)	0.2229556	10.82623	303.74013	178.56784	122.06938	1.12		22	5.27			S(2)	0.13	13
719	Albert							1.13								
887	Alinda	2.4917002(2)	0.559008	9.35599	110.22592	349.66782	355.5394	1.1		4.2(S)	73.97	14.09		S(2)	0.22(S)	4
										5.9(R)					0.12(R)	
1036	Ganymed	2.6645933(2)	0.5365783	26.44737	215.62463	131.60167	343.73724	1.23		38.5(S)		9.6		S(2)	0.17(S)	4
										37.5(R)					0.03(R)	
1221	Amor	1.9192081	0.4354754	11.89801	170.86736	26.26689	208.44479	1.08								
1566	Icarus	1.0779852	0.8267816	22.89332	87.49949	31.17593	48.92903	0.19		0.9(S)	1.273	15.75			1.42	4
										0.9(R)					0.39(R)	
1580	Betulia	2.1948194(14)	0.4901462	52.11302	61.70256	159.31107	43.23522	1.12		7.4	5.13			C(14)	0.03	11
1620	Geographos	1.2448409(2)	0.3354856	13.31906	336.7	276.61221	212.33876	0.83		3.0(S)		15.31		S(2)	0.19(S)	4
										2.7(R)					.11(R)	
1627	Ivar	1.8626727(2)	0.3971427	8.44759	132.63002	167.37779	236.71615	1.12		8.1(S)	4.798	13.26		S(2)	0.12(S)	4
										10.2(R)					.08(R)	
1685	Toro	1.3670701(5)	0.4358524	9.37478	273.75616	126.87895	225.10126	0.77		5.2(R)	10.196	14.22		S(5)	0.14(R)	4
										3.4(S)					0.31(S)	
1862	Apollo	1.4712113(2)	0.5598442	6.34958	35.36775	285.46336	19.67048	0.65		1.4	3.065			Q(2)	0.21	6
1863	Antinous	2.2590375(2)	0.6068066	18.41804	346.92767	266.86822	60.3456	0.89		1.8	4.02			SQ(2)	0.18	4,5
1864	Daedalus	1.4609952(6)	0.6147112	22.1563	6.14702	325.36883	90.22275	0.56			8.57			SQ(6)		
1865	Cerberus	1.0802064(2)	0.4669061	16.0946	212.38757	325.10211	248.88903	0.58		1.0(S)	5.8	17.1		S(2)	0.26(S)	4
										13.2(R)					0.17(R)	
1866	Sisyphus	1.8933658	0.5392675	41.15075	63.008061	292.9462	187.6533	0.87		8.2(S)		12.9			0.18(S)	4
										13.2(R)					0.07(R)	
1915	Quetzalcoatl	2.5370847(2)	0.5740106	20.45079	162.38676	347.84106	49.77921	1.08		0.3(S)	4.9	19.37		SMO(2)	0.29(S)	4
										0.05(R)					0.15(R)	
1916	Boreas	2.2716716(3)	0.4504499	12.85017	340.23043	335.32466	198.80937	1.25						S(3)		

1977VA							1.13					IC(3)	
1979QB	2.3309568	0.4485951	3.35741	341.97948	11.762	320.32772	1.3	06/19.0/86					
1980AA							1.05			2.7			
1980WF	2.2307664	0.5140687	6.41179	241.18785	212.79919	59.38572	1.08	07/15.5/81	0.6			Q0(2)	0.18
1980YS	1.8152795	0.3211742	2.27866	58.67237	49.00677	9.54138	1.23	02/05.0/81					
1981QB	2.239072	0.5181123	37.1638	154.04232	248.10652	81.35838	1.08	08/19.0/82					
1982YA	1.7067344	0.6972531	34.5732	269.16224	143.63885	98.26809	1.12	10/27.0/84					
1983LB	2.909115	0.4786359	25.40049	80.93719	220.12593	14.79138	1.19	09/23.0/83					
1983RB	2.2233403	0.5070001	19.42719	168.88445	114.80819	141.71192	1.09	10/27.0/84					
1985D02							1.23					V(17)	
1985YB	2.574543	0.5673837	26.81631	23.39059	66.97072	40.05081	1.11	06/19.0/86					
1985WA	2.8520397	0.6024651	9.75528	43.177	250.85524	6.15787	1.13	12/01.0/85					
1986DA							1.17		2.3	3.58		N(4)	0.12
1986LA							1.06						
1986MA							1.17						
1986RA							1.23					C(12)	
1987PA							1.21						
1987QB							1.14						
1987SL							1.15						
1987SP3							1.05						
1987UA							1.22						
1987VC							1.04						
1988HE							1.21						

1917	Cuyo	2.149398	0.5048552	23.98337	187.83588	194.19571	353.61636	1.06					
1943	Anteros	1.430298(2)	0.255899	8.70519	245.76398	338.15616	214.90784	1.06	1.8(S)		16	S(2)	0.22(S) 4
									2.6(R)				0.10(R)
1951	Lick	1.3905249(15)	0.0616467	39.0961	130.13399	140.40717	209.94965	1.3				A(15)	
1980	Tezcatlipoca	1.7094184(3)	0.3652399	26.84838	246.0916	115.23865	151.37994	1.09	4.3(S)		14.15	SO(3)	0.21(S) 4
									6.8(R)				0.08(R)
1981	Midas	1.7762983	0.6501989	39.83437	356.51595	267.68185	329.10117	0.62					
2059	Baboquivari	2.6506663	0.5260623	10.3953	200.46254	191.28668	4.8118	1.26					
2061	Ansa(1960UA)	2.2639019(16)	0.5372786	3.74081	207.34161	155.8308	183.58042	1.05		11.5		TCO(16)	
2062	Atea	0.9664191(1)	0.1825996	18.93686	108.02875	147.89163	24.49963	0.79	0.9			S(1)	0.2 3
2063	Bacchus	1.0775353	0.3494244	9.41957	32.6831	55.01283	130.54814	0.7					
2100	Ra-Shalom	0.832089(2)	0.4363715	15.76003	170.27494	355.92296	27.17462	0.47	2.4(R)	19.79	16.43	C(2)	0.08(R) 4
									1.7(S)				0.16(S)
2101	Adonis	1.8747862	0.7639414	1.35996	350.57656	41.69714	355.02197	0.44					
2102	Tantalus	1.2900732	0.298486	64.01466	93.71879	61.61973	107.34471	0.9					
2135	Aristaeus	1.5999357	0.5032714	23.03911	190.77791	290.59957	86.95645	0.8					
2201	Oljato	2.1757492	0.7105624	2.51479	76.39765	95.72617	0.18775	0.63	1.2(S)	>24.	15.36		0.42(R) 4
									1.4(R)				0.52(S)
2202	Pele	2.2907682	0.5122192	8.78271	169.72649	217.25943	317.82989	1.12					
2212	Hephaistos	2.1672146(7)	0.8338571	11.80419	27.88999	208.27302	184.70232	0.36				SO(7)	
2329	Orthos	2.4024644	0.6587443	24.40612	168.86636	145.78333	182.99007	0.82					
2340	Hathor	0.8439709(3)	0.4499333	5.35547	210.99391	39.78085	340.8399	0.46				CSU(3)	
2368	Beltrovata	2.1051823(3)	0.4127799	5.25709	287.17567	41.94548	348.56612	1.24	2.3(S)	5.9	16	SO(3)	0.13(S) 4
									3.8(R)				0.05(R)
2608	Seneca	2.4912438(10)	0.5809893	15.33764	168.92256	33.86941	336.81479	1.04	0.9	5.9		S(10)	0.16 8
3102	1981QA	2.1507685(2)	0.4490919	8.41519	171.7379	154.24488	204.66523	1.19		148		SRS(2)	
3103	1982BB	1.4065476(3)	0.2545792	20.24209	129.26354	253.7046	289.45166	0.91	1.4(S)	5.71	15.46	P(8)	0.63(S) 4
									1.5(R)				0.53(R)
3122	1981ET3	1.7687402	0.4223896	22.18105	335.57423	27.48659	37.49196	1.02					
3199	Nefertiti	1.5745552(2)	0.2836854	32.37132	239.43884	53.28995	173.15009	1.13	2.2(R)	3	15.32	S(2)	0.26(R) 4
									1.3(S)				0.41(R)
3200	Phaethon	1.2712503(9)	0.3901732	22.08857	264.91074	321.30756	87.96383	0.14	6.9			P(9)	0.08 7
3271	1982BB	2.1029508	0.1947563	24.99761	158.3915	158.66861	124.88125	1.27					
3288	Seleucus	2.0320703(2)	0.457597	5.9352	218.152	349.20613	207.90714	1.1	2.8(R)	75	15.3	S(2)	0.17(R)
									1.3(S)				0.35(S)
3352	McAuliffe	1.8790539	0.3692907	4.77731	106.90168	15.56136	129.98022	1.19					
3360	1981VA	2.4604328	0.7438949	22.00617	245.9381	59.48132	34.17154	0.63	1.8(S)		16.85		0.10(S)
									2.9(R)				.04(R)
3361	Orpheus	1.209454	0.3225401	2.68776	189.17012	301.60438	261.12056	0.82					
3362	Khafu	0.3894954	0.4635945	9.92035	152.00408	54.35454	142.76245	0.53	0.7(S)		13.45		0.16(S) 4
									1.0(R)				0.07(R)
3551	1983RD	2.0918948(17)	0.4869563	3.51494	173.37374	193.03196	355.75832	1.07	0.3(S)	4.33	17.11	V(17)	.40(S) 4
									0.9(R)				0.28(R)
3552	1983SA	4.2363740(18)	0.7130884	30.74613	350.07178	316.57347	255.68374	1.21	18.7(S)		13.65	D(18)	0.02(S) 4
									29.6(R)				0.01(R)
3553	Hera	1.6447099	0.3203805	36.76134	231.97605	288.83803	67.77769	1.12					
3554	Amun	0.9737222(4)	0.2804185	23.25615	358.0276	359.3114	56.30461	0.7	2			K(4)	0.17 5
3671	Dionysus	2.1956644	0.5426289	13.62787	81.80421	203.50973	219.01058	1.01					
3691	1982FT	1.7743135	0.2940253	29.27319	348.25442	224.5422	47.50407	1.27					
3752	1985PA							0.99					
3753	1986TO							0.48					
3757	1982XB							1.02	0.5(S)	3.012	19.99	S(2)	0.15(S) 12
									0.7(R)				0.09(R)
3838	1986WA							0.45					
3908	1980PA							1.04				V(17)	
	1972RB							1.1					

Number	Name	a	e	i	omega	w	M	q	Epoch	Diameter	Period	T(1,0)	Amplitudes	Class	Pv	References
	1937UB	Hermes						0.62								
	1950DA							0.34								
	1954XA							0.51								
	1959LM							0.72								
	1973HA							0.88								
	1974HA							0.42								
	1978CA							0.88		1.9	3.748			S(10)	0.06	8
	1979VA							1			2.6			CP(2)		
	1979XB							0.55								
	1981VA									1.8					0.07	4
	1982DB	1.4894422	0.3602384	1.42068	314.05543	157.87413	191.24669	0.95	10/27.0/84							
	1982TA	2.2993774	0.7724651	12.19278	9.627	119.10477	300.21486	0.52	12/01.0/85	1.7(S)		15.7			0.33(S)	4
										1.8(R)					0.28(R)	
	1983LC	2.631651	0.7091899	1.51866	159.07591	184.69196	8.9271	0.76	12/23.0/83							
	1983TF2	2.4389347	0.7363252	14.70372	8.32964	116.56936	328.90684	0.66	09/23.0/83							
	1983VA	2.6106835	0.6917034	16.23778	76.87026	11.58396	167.10796	0.81	12/01.0/85							
	1983VB							0.96								
	1984KB	2.2210346	0.762275	4.63662	170.56242	334.87816	61.62574	0.52	10/27.0/84	0.7				S(11)	0.1	9
	1986JK							0.9						C(12)		
	1986PA							0.59								
	1987KF							0.59								
	1987OA							0.61								
	1987QA							0.88								
	1987SB							0.75								
	1987SY							0.6								
	1988BG							0.64								
	1988TA							0.79						C(13)		
	5025P-L							0.45								
	5344P-L							0.97								
	5743P-L							0.8								
	1986VP4							0.72								
	1988XB							0.76								
	1989AC							0.9								
	1989AZ							0.86								
433	Eros	1.4583663(2)	0.2228556	10.82623	303.71013	178.56734	122.06938	1.13		22	5.27			S(2)	0.18	10
719	Albert							1.13								
887	Alinda	2.4917002(2)	0.559008	9.25599	110.22582	349.66782	355.5394	1.1		4.2(S)	73.97	14.09		S(2)	0.23(R)	4
										5.3(R)					0.12(R)	
1036	Ganymed	2.6645933(2)	0.5365783	26.44737	215.62463	131.60167	343.73724	1.23		38.5(S)		9.6		S(2)	0.17(S)	4
										37.5(R)					0.03(R)	
1221	Amor	1.3192081	0.4354754	11.89801	170.86736	25.25639	208.44479	1.08								
1566	Icarus	1.0779852	0.8257816	22.99332	87.49949	31.17593	48.32903	0.19		0.9(S)	2.273	15.75			0.42	4
										0.9(R)					0.39(R)	
1580	Betulia	2.1948194(16)	0.4901462	52.11302	61.70256	159.31107	43.23522	1.12		7.4	6.13			C(14)	0.03	11
1620	Geographos	1.2448409(2)	0.3354856	13.31906	336.7	276.61221	212.33876	0.83		2.0(S)		15.91		S(2)	0.19(S)	4
										2.7(R)					.11(R)	
1627	Ivar	1.8626727(2)	0.3971427	8.44759	132.63002	167.37779	236.71615	1.12		8.1(S)	4.798	13.36		S(2)	0.12(S)	4
										10.2(R)					.08(R)	
1685	Toro	1.3670701(5)	0.4358524	9.37478	273.75616	126.87895	225.10126	0.77		5.2(R)	10.196	14.22		S(5)	0.14(R)	4
										3.4(S)					0.31(S)	
1862	Apollo	1.4712113(2)	0.5598442	6.34958	35.36775	285.46336	19.67048	0.65		1.4	2.065			Q(2)	0.21	6
1863	Antinous	2.2590375(2)	0.5068066	18.41804	346.92767	266.86822	60.3456	0.89		1.8	4.02			SQ(2)	0.18	4,5
1864	Daedalus	1.4609952(6)	0.6147112	22.1563	6.14702	325.36883	90.22275	0.56			8.57			SQ(6)		
1865	Cerberus	1.0802064(2)	0.4669061	16.0946	212.38757	325.10211	248.88903	0.58		1.0(S)	5.8	17.1		S(2)	0.26(S)	4
										13.2(R)					0.17(R)	
1866	Sisyphus	1.8933658	0.5332575	41.15075	63.008061	292.9462	187.5533	0.87		8.2(S)		12.9			0.18(S)	4
										13.2(R)					0.07(R)	
1915	Quetzalcoatl	2.5370847(2)	0.5740106	20.45079	162.38676	347.84106	49.77921	1.08		0.3(S)	4.9	19.27		SHO(2)	0.29(S)	4
										0.05(R)					0.15(R)	
1916	Boreas	2.2716716(3)	0.4504499	12.35017	340.23043	335.32466	198.80937	1.25						S(3)		

1917	Cayo	2.149398	0.5048552	23.98337	187.83588	194.19571	353.61636	1.06							
1943	Anteros	1.430298(2)	0.255899	8.70519	245.76398	338.15616	224.90784	1.06	1.8(S)		16		S(2)	0.22(S)	4
									2.6(B)					0.10(B)	
1951	Lick	1.3905249(15)	0.0616467	39.0961	130.13399	140.40717	209.34965	1.3					A(15)		
1980	Pascatlipoca	1.7096184(3)	0.2652389	26.34838	245.0916	115.22865	151.37994	1.09	4.3(S)		14.15		SO(3)	0.21(S)	4
									6.8(B)					0.08(B)	
1981	Midas	1.7762983	0.6501989	39.83437	356.51595	267.68185	329.10117	0.63							
1059	Bahequivari	1.6506663	0.5260823	10.3953	208.46254	191.28668	4.8118	1.26							
2061	Anna(1900A)	2.2639019(16)	0.5372786	3.74081	287.34161	155.8308	183.58042	1.05		11.5			TCO(16)		
2062	Aten	0.9664191(1)	0.1825996	18.93686	108.02875	147.89163	24.49963	0.79	0.9				S(1)	0.2	3
2063	Bacchus	1.0775353	0.3494244	9.41957	32.6831	55.01293	130.54814	0.7							
2100	Ra-Shalom	0.832089(2)	0.4363715	15.76003	170.27494	155.92296	27.17462	0.47	2.4(B)	19.79	16.43		C(2)	0.08(B)	4
									1.7(S)					0.16(S)	
2101	Adonis	1.8747862	0.7639414	1.35996	350.57656	41.69714	355.02197	0.44							
2102	Fantalus	1.2900732	0.2384486	64.01466	93.71879	61.61973	107.94471	0.9							
2135	Aristaeus	1.5999357	0.5032714	23.03911	190.77791	290.59957	16.95645	0.8							
2201	Oljato	1.1757492	0.7105624	2.51479	76.39765	95.72617	0.18775	0.63	1.2(S)	>24.	15.86			0.42(B)	4
									1.4(B)					0.52(S)	
2202	Pele	1.2907682	0.5122192	8.78271	169.72649	217.25943	317.82989	1.12							
2212	Hephaistos	2.1672146(7)	0.8338571	11.80419	27.68999	208.27302	184.70232	0.36					SG(7)		
2329	Orthos	2.4024644	0.6587443	24.40612	168.86636	145.78333	182.99007	0.82							
2340	Hathor	0.8439709(3)	0.4499333	5.85547	210.99391	39.78085	340.8399	0.46					CBD(3)		
2368	Beltrovata	2.1051823(3)	0.4127799	5.25709	287.17567	41.94548	348.56612	1.24	2.3(S)	5.3	16		SG(3)	0.13(S)	7
									3.8(B)					0.05(B)	
1608	Seneca	2.4912438(10)	0.5809893	15.33764	168.92256	33.56941	336.81479	1.04	0.9	5.9			S(10)	0.16	5
3102	1951QA	2.1507685(2)	0.4490919	9.41519	171.7379	154.24488	204.68523	1.19		148			SBS(2)		
3103	1992SB	1.4065476(9)	0.2545792	20.34209	129.26354	253.7046	299.45166	0.91	1.4(S)	5.71	15.46		S(9)	0.55(S)	4
									1.5(B)					0.53(B)	
3122	1981ST3	1.7687402	0.4223896	22.18105	335.57423	27.48659	37.49196	1.32							
3199	Nefertiti	1.5745552(2)	0.2836854	32.97132	239.43884	53.28995	173.15009	1.13	2.2(B)	3	15.32		S(2)	0.25(B)	4
									1.8(S)					0.41(B)	
3200	Phaethon	1.2712503(9)	0.8901732	22.08857	264.91074	321.80756	87.96383	0.14	6.3				P(9)	0.08	7
3271	1992KB	2.1029508	0.3947563	24.39761	158.3915	158.56861	124.88125	1.27							
3288	Seleucus	2.0320703(2)	0.457597	5.9352	218.152	349.20613	207.30714	1.1	2.8(B)	75	15.2		S(2)	0.17(B)	
									1.9(S)					0.15(S)	
3352	McAuliffe	1.8790539	0.3592907	4.77731	106.30168	15.56136	129.98022	1.19							
3360	1981VA	2.4604328	0.7438949	22.30617	245.3381	59.48132	34.17154	0.63	1.8(S)		16.85			0.10(S)	
									2.9(B)					.04(B)	
3361	Orpheus	1.209454	0.3225401	2.56776	199.17012	301.50438	251.12066	0.32							
3362	Khufu	0.3894954	0.4685945	9.82025	152.30408	54.85454	142.76245	0.53	0.7(S)		18.45			0.16(S)	4
									1.0(B)					0.07(B)	
3551	1983RD	2.0918948(17)	0.4869563	9.51494	173.37374	193.03196	355.75832	1.07	0.8(S)	4.93	17.11		P(17)	.10(S)	4
									0.9(B)					0.28(B)	
3552	1983SA	4.2363740(18)	0.7130884	30.74613	350.07178	316.57347	255.68374	1.21	18.7(S)		13.65		D(18)	0.02(S)	4
									29.6(B)					0.01(B)	
3553	Nera	1.6447099	0.3203805	36.76134	231.97605	288.83803	67.77769	1.12							
3554	Amun	0.9737222(4)	0.2304185	23.35615	358.0276	353.3114	56.30461	0.7	2				H(4)	0.17	5
3671	Dionysus	2.1956644	0.5426289	13.62787	81.30421	203.50973	219.01058	1.01							
3691	1982PT	1.7743135	0.2940253	20.27319	348.26442	224.5422	47.50407	1.27							
3732	1985PA							0.99							
3753	1986TO							0.48							
3757	1982XB							1.02	0.5(S)	9.012	18.99		S(2)	0.15(S)	12
									0.7(B)					0.09(B)	
3838	1986WA							0.45							
3908	1986PA							1.06					P(17)		
	1972RB							1.1							

1977YA							1.13			IC(3)	
1979QB	2.3309568	0.4405951	3.35741	341.37948	11.752	320.32772	1.3	06/19.0/86			
1980AA							1.35		2.7		
1980YP	2.2307664	0.5140687	6.41179	241.18785	212.79919	59.28572	1.38	07/15.5/81	0.6	X(2)	0.18
1980YS	1.8152795	0.3211742	2.27866	58.67237	49.00677	9.54138	1.23	12/05.0/81			
1981QB	2.239072	0.5181123	37.1638	154.04232	248.10652	81.35838	1.38	08/19.0/82			
1982YA	1.7067344	0.6972531	34.5732	269.16224	143.63885	98.26809	1.12	10/27.0/84			
1983LB	1.909115	0.4786359	25.40049	80.93719	220.12593	14.79138	1.19	09/22.0/83			
1983RB	2.2223403	0.5070001	19.42719	168.88445	114.80819	141.71192	1.39	10/27.0/84			
1985N02							1.23			Y(17)	
1985YB	2.574543	0.5673837	26.81631	23.29059	66.97072	40.05081	1.11	06/19.0/86			
1985YA	2.8520397	0.6024651	9.75528	43.177	350.85524	6.15787	1.13	12/01.0/85			
1986BA							1.17		2.3 3.58	K(4)	0.12
1986LA							1.86				
1986NA							1.17				
1986RA							1.23			C(12)	
1987PA							1.21				
1987QB							1.14				
1987SL							1.15				
1987SP3							1.35				
1987UA							1.22				
1987VC							1.34				
1988HE							1.21				

EARTART.DAT: Data obtained from the IRAS Asteroid and Comet Survey. These are observed near-earth asteroids (q .le. 1.3). See Table B-11, B-12 for data formats

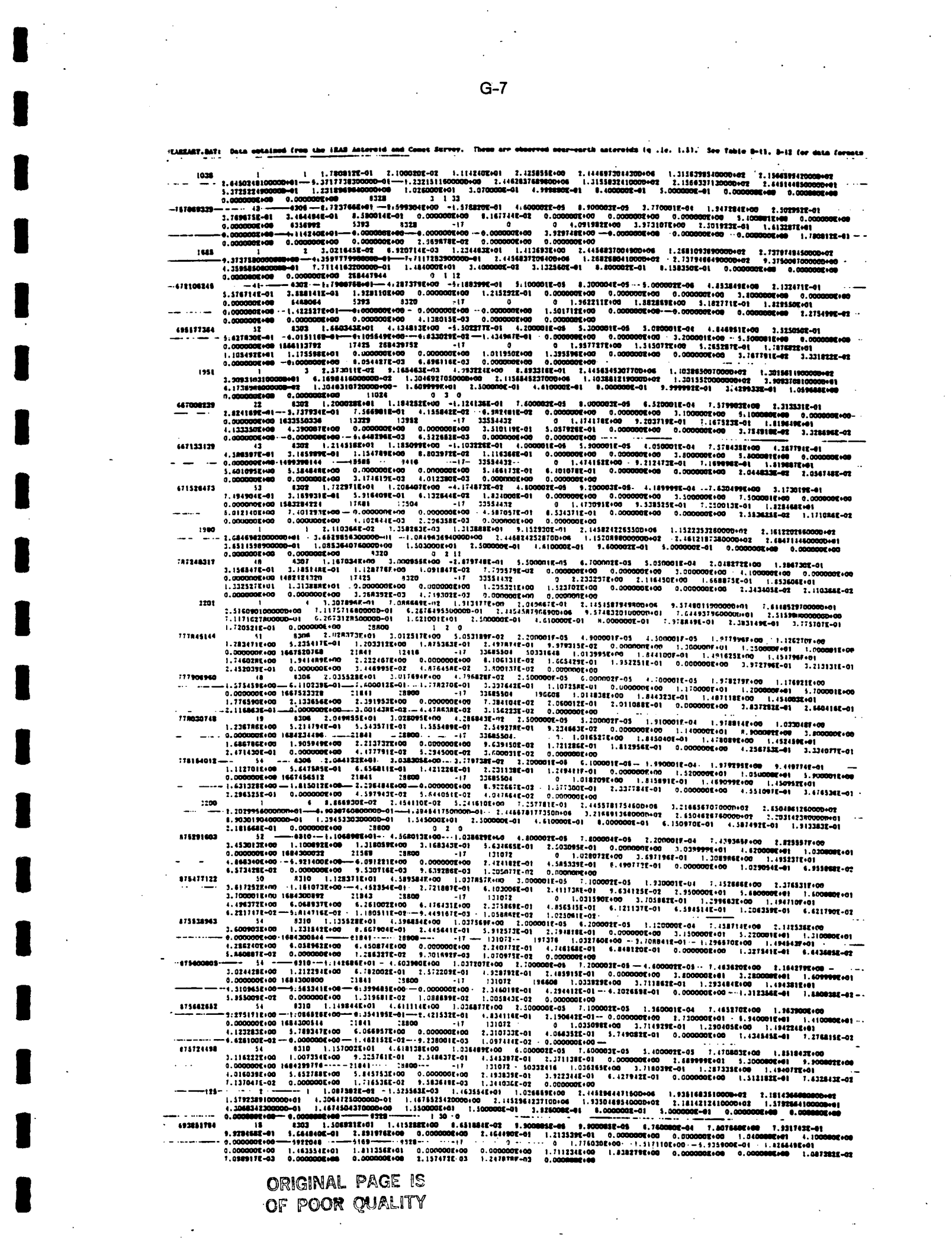

APPENDIX H

LIST OF ASTRONOMERS/OBSERVATORIES

John Africano
KPNO
P.O. Box 26732
Tucson, AZ 85726

Michael A'Hearn
Astronomy Dept
Bldg. 224, Rm 0206
University of Maryland
College Park, MD 20742

Eric Becklin
Institute for Astronomy
Univ. of Hawaii
2680 Woodlawn Drive
Honolulu, HI 96822

Reta Beebe
Astronomy Dept, New Mexico St.
Box 4500
Las Cruces, NM 88003

Jeffrey Bell
Planetary Geosciences Div.
HIG
2525 Correa Road
Honolulu, HI 96822

Michael Belton
KPNO
P.O. Box 26732
Tucson, AZ 85726

Richard Binzel
MIT
54-426
Cambridge, MA 02139

Victor Blanco
CTIO
Casilla 603
La Serena, Chile

Edward Bowell
Lowell Observatory
1400 Mars Hill Road
Flagstaff, AZ 86001

Andre Brahic
Observatoire de Paris
92190 Meudon, France

John Brandt
Lab for Astron. & Solar Phys
NASA-Goddard, Bldg. 21
Greenbelt, MD 20771

Robert A. Brown
Space Telescope Science Inst.
3700 San Martin Drive
Baltimore, MD 21218

Robert H. Brown
JPL, MS 183-501
4800 Oak Grove Drive
Pasadena, CA 91109

Donald E. Brownlee
Dept. of Astronomy
Univ. of Washington
Seattle, WA 98195

Marc Buie
Inst. for Astronomy
Univ. of Hawaii
2680 Woodlawn Dr.
Honolulu, HI 96822

Joseph Burns
Space Sciences Building
Cornell University
Ithaca, NY 14853

Ellen Bus
LPL
U of A
Tucson, AZ 85721

John J. Caldwell
Dept. of Phys.
York Univ.
4700 Keele St.
North York, ON M3J 1P3, Canada

Humberto Campins
Planetary Science Institute
2030 E. Speedway #201
Tucson, AZ 85719

Director
Cerro Tololo Inter-American Obs.
Casilla 603
La Serena, Chile

Anita Cochran
Astronomy Dept.
Univ. of Texas at Austin
Austin, TX 78712

Director
Crimean Astrophysical Observ.
USSR Academy of Sciences
p/o Nauchney
334413 Crimea

Dale Cruikshank
NASA-Ames
MS 245-6
Moffett Field, CA 94035

Catherine de Bergh
Obs. de Paris
92189 Meudon, France

Mario di Martino
Osservatorio Astron. di Torino
I-10025 Pino Torinese Italy

Jack Drummond
Steward Observatory
U of A
Tucson, AZ 85721

David Dunham
Computer Sci. Corp.
GreenTec II Bldg., 10110
Aerospace Road
Lanham-Seabrook, MD 20706

James L. Elliot
Phys. & Earth/Planetary Sci.
MIT, Bldg 54-422 A
Cambridge, MA 02139

Director
European Southern Observatory
Casilla 19001
Santiago 19 Chile

Linda French
Astronomy Dept.
MIT
Cambridge, MA 02139

Michael Gaffey
Geology Dept., West Hall
Rensselaer Polytechnic Inst.
Troy, NY 12180-3590

Tom Gehrels
LPL
U of A
Tucson, AZ 85721

Jonathan Gradie
Planetary Geosciences Div./HIG
Universtiy of Hawaii
2525 Correa Road
Honolulu, HI 96822

Daniel Green
Harvard-Smithsonian Astrophys.
60 Garden St.
Cambridge, MA 02138

Jay Goguen
Earth & Space Science Div.
JPL, MS 183-501
4800 Oak Grove Drive
Pasadena, CA 91109

G. Hahn
Astromiska Observatoriet
Box 515
75120 Uppsala, SWEDEN

Martha Hanner
JPL, MS 169-237
4800 Oak Grove Drive
Pasadena, CA 91109

Dr. Bruce Hapke
Dept. of Geol. & Planetary Sci.
Univ. of Pittsburgh
321 Old Engineering Hall
Pittsburgh, PA 15260

Alan Harris
JPL, MS 183-501
4800 Oak Grove Drive
Pasadena, CA 91109

Bill Hartmann
Planetary Science Institute
2030 E. Speedway #201
Tucson, AZ 85719

Eleanor Helin
Planetary & Oceanography
JPL
4800 Oak Grove Drive
Pasadena, CA 91109

Martin Hoffmann
University of Munster
Aussenstation, Hembrich 6
D-5569 Schalkenmehren, FDR

Ricardo Gil Hutton
Observatorio Municipal de Merc.
Calle 35 No. 876
6600 Mercedes Argentina

David Jewitt
U. of Hawaii
Dept. of Astronomy
2680 Woodlawn Drive
Honolulu, HI 96822

Charles Kowal
Computer Sci. Corp
Space Telescope Sci. Inst.
Homewood Campus
Baltimore, MD 21218

W. Landgraf
University Observatory
Geissmarlandstrasse 11
D-3400 Gottingen, FDR

Hal Larson
LPL
U of A
Tucson, AZ 85721

Steve Larson
LPL
U of A
Tucson, AZ 85721

Larry Lebofsky
U of A
LPL
Tucson, AZ 85721

David Levy
LPL
U of A
Tucson, AZ 85721

G. Wesley Lockwood
Lowell Observatory
1400 Mars Hill Road
Flagstaff, AZ 86001

Jane Luu
Institute for Astronomy
U. of Hawaii
2525 Correa Road
Honolulu, HI 96822

Brian Marsden
Center for Astrophysics
60 Garden Street
Cambridge, MA 02138

Dennis Matson
Earth & Space Sciences Division
MS 183-501, JPL
4800 Oak Grove Drive
Pasadena, CA 91109

Thomas McCord
Hawaii Institute of Geophysics
2525 Correa Road
Honolulu, HI 96822

Lucy-Ann McFadden
Cal. Space Inst. A-016
2265 Sverdrup Hall, UCSD
La Jolla, CA 92093-0216

Robert McMillan
LPL
U of A
Tucson, AZ 85721

R.H. McNaught
Siding Spring Observatory
Coonabaran, N.S.W. 2357
Australia

Karen Meech
Institute for Astronomy
2680 Woodlawn Drive
Honolulu, HI 96822

Robert Millis
Lowell Observatory
1400 Mars Hill Road
Flagstaff, AZ 86001

David Morrison
Space Science Division
NASA Ames N245-1
Moffett Field, CA 94035

Ray Newburn
Space Sci. Div, JPL
4800 Oak Grove Drive, T1166
Pasadena, CA 91109

Steve Ostro
JPL, MS 183-501
4800 Oak Grove Drive
Pasadena, CA 91109

Paolo Paolicchi
Instituto di Astronomia
Universita di Pisa
Piazza Torricelli 2
56100 Pisa ITALY

Carle Pieters
Dept. of Geological Sciences
Brown University
Providence, RI 02912

Frederick Pilcher
Illinois College
Jacksonville, IL 6265

Dr. Jurgen Rahe
Planetary Astron. Program
Code EL
NASA HQ
Washington, DC 20546

George Rieke
LPL
U of A
Tucson, AZ 85721

Gene Shoemaker
U.S. Geological Survey
2255 N. Gemini Drive
Flagstaff, AZ 86001

John Spencer
Inst. for Astron., U. of Hawaii
2680 Woodlawn Dr.
Honolulu, HI 96822

Alan Stern
Campus Box 392
U. of Colorado
Boulder, CO 80309

Mark Sykes
Steward Observatory
U of A
Tucson, AZ 85721

Laurence Taff
MIT, M-233 Lincoln Lab.
244 Wood Street
Lexington, MA 02173-0073

Ron Taylor
LPL
U of A
Tucson, AZ 85721

Ed Tedesco
JPL, 183-501
4800 Oak Grove Drive
Pasadena, CA 91109

Dave Tholen
Inst. for Astronomy, U. of Hawaii
2680 Woodlawn Drive
Honolulu, HI 96822

Alan Tokunaga
Inst. for Astron., U. of Hawaii
2680 Woodlawn Drive
Honolulu, HI 96822

Glenn Veeder
JPL, MS 183-501
4800 Oak Grove Drive
Pasadena, CA 91109

Joe Veverka
Astronomy Dept., 312 Space Sci.
Cornell University
Ithaca, NY 14853

Faith Vilas
Code SN3, Bldg 31, Rm 142
Johnson Space Center
Houston, TX 77058

Paul Weissman
JPL, 183-301
4800 Oak Grove Drive
Pasadena, CA 91109

George Wetherill
Dept. Terrestrial Magnetism
Carnegie Inst. of Washington
5241 Broad Brnach Road, NW
Washington, DC 20015

Wieslaw Wisniewski
LPL
U of A
Tucson, AZ 85721

Donald Yeomans
JPL, 301-150G
4800 Oak Grove Drive
Pasadena, CA 91109

V. Zappala
Osservatorio Astronomico de Torino
I-10025 Pino Torinese, ITALY

Ken Zeigler
P.O. Box 362
Claypool, AZ 85532

Ben Zellner
Space Telescope Science Inst.
Homewood Campus
Baltimore, MD 21218

United Kingdom Infrared Telescope
Flagstaff Station
P.O. Box 1149
Flagstaff, AZ 86002

Lick Observatory
University of California
Santa Cruz, CA 95064

Lowell Observatory
1400 Mars Hill Road
Flagstaff, AZ 86001

McDonald Observatory
University of Texas
P.O. Box 1337
Fort Davis, TX 79734

McGraw-Hill Observatory
University of Michigan
Ann Arbor, MI 48109-1090

Las Campanas Observatory
Casilla 601
La Serena, Chile

Table Mountain Observatory
JPL
Caltech
P.O. Box 367
Wrightwood, CA 92397

University of Wyoming
Dept of Phys. and Astronomy
Laramie, WY 82071

Anglo-Australian Observatory
Epping Laboratory
P.O. Box 296
Epping, NSW 2121

ESO
Casilla 19001
Santiago Chile 19

Osservatorio Astronomico di Torino
Strada Osservatorio 20
I-10025 Pino Torinese, Italy

Uppsala Astronomical Observatory
Box 515
S-751 20 Uppsala, Sweden

Allegheny Observatory
Obs. Station
Pittsburgh, PA 15213

Arecibo Observatory
P.O. box 995
Arecibo, PR 00612

U of A
Steward Observatory
Tucson, AZ 85721

Canada-France-Hawaii Telescope Corp.
P.O. Box 1597
Kamuela, HI 96743

The Observatories of the
Carnegie Institute of Washington
813 Santa Barbara Street
Pasadena, CA 91101

Cerro Tololo Inter-American Observatory
Casilla 603
La Serena, Chile 1353

University of Florida
Dept. of Astronomy
Gainesville, FL 32611

University of Hawaii
Mauna Kea Observatories
88-inch
2680 Woodlawn Drive
Honolulu, HI 96822

University of Hawaii
Mauna Kea Observatories
Infrared telescope
2680 Woodlawn Drive
Honolulu, HI 96822

Johns Hopkins University
Homewood Campus
Baltimore, MD 21218

KPNO
University of Arizona
Tucson, AZ 85721

United Kingdom Infrared Telescope
Joint Astronomy Centre
665 Komohana Street
Hilo, HI 96720

APPENDIX I

THE NUCLEUS OF COMET P/TEMPEL 2

THE ASTROPHYSICAL JOURNAL, 347:1155–1166, 1989 December 15

THE NUCLEUS OF COMET P/TEMPEL 2

MICHAEL F. A'HEARN[1,2]
Astronomy Program, University of Maryland
HUMBERTO CAMPINS[1,3]
Planetary Science Institute
DAVID G. SCHLEICHER[2] AND ROBERT L. MILLIS
Lowell Observatory
Received 1989 April 6; accepted 1989 June 17

ABSTRACT

We present the results of simultaneous optical photometry and infrared radiometry of comet P/Tempel 2. Periodic variations of brightness, previously detected in the optical by others, are present and in phase at all wavelengths in our data. Because the optical and thermal rotational light curves are in phase, we conclude that the variations are caused by the changing apparent cross section of an elongated nucleus rotating with a period near 8.9 hr. The variation of flux with aperture allows us to separate the contributions of the nucleus and the coma. In the apertures with which we monitored the light curve, the contribution by the coma is ~25% at maximum light in the optical and undetectable at the level of 10% at all times in the thermal infrared. By applying the standard thermal model for asteroids, we have determined the following nuclear properties: effective radius at maximum light, 5.9 km; visual geometric albedo, 0.022; and projected axial ratio near 2. The nucleus is very red but there is evidence that the reflectivity in the ultraviolet increases toward shorter wavelengths. Based on the observed rate of outgassing, ~1% of the surface is active. Properties common to all nuclei of periodic comets appear to include the very low albedo and the high axial ratio. The fraction of the surface which is active appears to vary significantly among nuclei, as does the character of the reflection spectrum.

Subject headings: comets — rotation

I. INTRODUCTION

Over the last 10 years or so, a resurgence of interest in measuring the properties of cometary nuclei has occurred. This resurgence is motivated by a desire to better understand the relationship between the nucleus and the more readily observed phenomena in the coma and to explore the relationship between cometary nuclei and Aten-Amor-Apollo (AAA) asteroids. The comae of comets have been conceptualized for many years as the product of outgassing from a dirty snowball (Whipple 1950) but the detailed nature of that snowball has remained elusive. Even the dramatic results from the *Vega* and *Giotto* spacecraft have left many questions unanswered concerning the nature of cometary nuclei, not the least of which is the degree to which P/Halley is typical of all comets. The possible relationship of comets to asteroids is based on the long-standing idea, originally suggested by Öpik (1963), that a significant fraction of the AAA asteroids are extinct cometary nuclei. Current estimates from dynamical arguments suggest, with very large error bars, that roughly half the AAA asteroids are derived from comets (Wetherill 1988).

Unfortunately, it is very difficult to observe cometary nuclei. The least ambiguous observations are those from spacecraft, but ground-based observations have been made which, with varying degrees of certainty, appear to refer to a cometary nucleus rather than to material of the coma. These results have been reviewed recently (A'Hearn 1988; Weissman *et al.* 1989) and will not be discussed in detail here. In general, there are two possible approaches to the problem of studying cometary nuclei from Earth. Jewitt and Meech (1988) have concentrated on observing comets optically at large heliocentric distances when the activity of the comet is expected to be small. We, on the other hand, have concentrated on observing comets which are relatively inactive even at small heliocentric distances which permits us to study the nuclei in the thermal infrared as well as in the optical (Campins *et al.* 1987, hereafter CAM87; Millis *et al.* 1988, hereafter MAC88). With both approaches there is always some uncertainty about the contamination of the measurements by coma although observers universally argue that their own measurements are relatively free from this problem.

Comet P/Tempel 2 is a particularly interesting object. It has been considered repeatedly as a potential target for a cometary mission, but none of these has yet come to fruition. Nevertheless, because of this possibility, the comet has been the object of ground-based study by numerous astronomers. It is known from the orbital lightcurve (Sekanina 1979)[4] that for much of the preperihelion arc the brightness of the coma is negligible. Similarly, the nongravitational acceleration is very small (Marsden 1985) suggesting low activity per unit mass of the nucleus (although a fortuitous geometry could also lead to a small nongravitational effect even with significant outgassing). P/Tempel 2 is, therefore, one of the few comets, the nuclei of which might be observable with Earth-based telescopes near

[1] Visiting Astronomer at the Infrared Telescope Facility which is operated by the University of Hawaii under contract from the National Aeronautics and Space Administration.
[2] Visiting Astronomer at the 88" (2.2 m) telescope of the University of Hawaii.
[3] Present address: Department of Astronomy, University of Florida.
[4] An updated version of the orbital light curve, including data from the apparition of 1983, was widely distributed by the International Halley Watch and is the version actually used.

perihelion. Accordingly, we planned an observational program of simultaneous optical and infrared photometry similar to those we carried out earlier on comets P/Neujmin 1 (CAM87) and P/Arend-Rigaux (MAC88). Other groups also observed P/Tempel 2 at this apparition. Jewitt and Luu (1988) determined a rotational period from CCD photometry in 1988 April, before the onset of outgassing, while Wisniewski (1988) confirmed their value for the period and determined the rotational light curve from conventional broad-band photometry in 1988 May. Wisniewski's rapid distribution of his light curve to other observers was invaluable in planning our observing strategy. In particular, after the first few observations we were able to predict the times of subsequent maxima and minima in order to optimize the observations.

II. OBSERVATIONS

The observations were scheduled for 1988 June near the time of the comet's closest approach to Earth. Although this time was somewhat after the predicted onset of activity, the light curve of Sekanina (1979) implied that activity would still be weak and the advantage to be gained by observing at minimum geocentric distance was significant. The infrared observations were carried out at the NASA Infrared Telescope Facility (IRTF) to measure the thermal emission from the comet on 1988 June 10 and 11 UT. The optical measurements were made with the University of Hawaii 2.2 m telescope during the same two nights and during a small portion of the night of June 9 UT. Subsequent nights were cloudy. The observing circumstances at the midpoint of the two full nights are as follows:

$$r_H = 1.72 \text{ AU}$$

$$\Delta = 0.79 \text{ AU}$$

$$\text{phase} = 20°$$

$$\dot{r}_H = -9.9 \text{ km s}^{-1}$$

In the infrared, the standard N filter (reference wavelength = 10.1 μm; Tokunaga 1986) and IRTF bolometer with a 4 mm aperture were used most frequently to define the light curve. On a few occasions, observations were made near maximum and minimum light (phases chosen to minimize the temporal variations) in four apertures, 3, 4, 5, and 6.5 mm, for which drift scans on stars yielded effective angular diameters of 5".3, 7".0, 7".8 and 8".7, respectively. The chopper throw was 30" north-south. Based on the photometry with different apertures, we estimate that the coma contribution to the reference beam was less than 0.5% of the comet's peak brightness. Measurements with the standard M (4.8 μm) and Q (20.0 μm) filters were also made to determine color temperatures. The star α Bootis was used as a primary standard with adopted magnitudes $M = -2.12$, $N = -3.17$, and $Q = -3.13$ (Tokunaga 1986). Two stars near the comet in the sky, α Serpentis and 110 Virginis, were observed frequently and used as local standards to monitor extinction and check for any instrumental variations. Neither of the local standards showed intrinsic variability although some changes in extinction were detected and corrected for. The observations were reduced and calibrated using the procedure and absolute fluxes discussed by Tokunaga (1986).

The optical observations were made with a photometer and pulse-counting electronics from Lowell Observatory and the standard International Halley Watch (IHW) filters which isolate various emission bands and portions of the reflected continuum. These filters are described in detail in an appendix to the *IHW Archive of Observations of P/Giacobini-Zinner* (Sekanina 1989). On June 9 an EMI 6256S photomultiplier was used completing the identical system to that which was used previously for comet P/Arend-Rigaux (MAC88). On June 10 and 11, we used an RCA 31034A photomultiplier which allowed use of filters at longer wavelengths than were used in the previous study. Since most of June 9 was devoted to another project, only ~1.5 hr were spent observing P/Tempel 2. Consequently, the data from that night were not well calibrated. The temporal variations were monitored using the two filters for the continuum at 4845 Å and 6840 Å and an aperture of 10".1 diameter. Sky was observed far from the comet (usually several tens of arcmin) after each set of observations of the comet (usually three 30 s integrations in each of the two continuum filters). The stars HD 149363 and HD 120086 were used for absolute calibration via the standard magnitudes defined by the IHW, while observations of two nearby comparison stars were interspersed between every set of cometary observations to monitor any variations in transparency or instrumental sensitivity or both. There was no indication of intrinsic variability in the brightness of the nearby comparison stars or in the extinction coefficients. Mean extinction coefficients for the two nights were used in reducing the data. Two or three times each night—usually near the times of maximum and minimum light when the brightness of the comet was changing most slowly—observations were made in apertures of 14".2, 20".0, and 28".5 in order to determine the radial brightness profile of the coma. An accurate measurement of this profile is required if the contributions of the nucleus and the coma to the observed signal are to be disentangled. The comet was also observed a few times through other filters of the IHW set in order to estimate production rates of various gases, gas-to-dust ratio, and so on.

a) Brightness Variations

The 4845 and 6840 Å observations taken through the 10".1 aperture and the N magnitudes measured through the 7" aperture are listed in Tables 1 and 2 for the nights of June 10 and 11, respectively. It was soon evident during our observing that both the reflected optical and the thermal infrared brightnesses of the comet were varying in phase. The peak-to-peak amplitude of the variation was 0.4 mag in the optical and 0.8 mag in the infrared. The existence of this variation was, in fact, no surprise. Jewitt and Luu (1988) had reported cyclic variations in April with an ~9 hour period and a peak-to-peak amplitude of 0.7 mag in the R passband, in good agreement with the amplitude we observed at N, while Wisniewski (1988), from V-filter observations in late May, had produced a convincing rotational light curve for Tempel 2 having a period of 8 hr. 58 minutes, and an amplitude of 0.5 mag. Wisniewski's observations were made through photometer apertures of 17" and 12" diameter; Jewitt and Luu observed with a CCD. The difference in optical amplitude reported by these investigators and our still smaller optical amplitude of ~0.4 mag very probably can be attributed to greater dilution by the coma of the signal from the nucleus as the comet became more active because, based on Sekanina's (1987) determination of the polar orientation, we all observed the comet at nearly identical projections. On the other hand, the observations of P/Tempel 2 in 1987 by Jewitt and Meech (1988), which exhibited a much smaller amplitude (<0.3 mag, given our present knowledge of the period), were

TABLE 1

OPTICAL LIGHT CURVE DATA

4845 Å				6840 Å			
U.T. (hour)	Observed Magnitude	Nuclear Magnitude	Phase (P=8.9 hr)	U.T. (hour)	Observed Magnitude	Nuclear Magnitude	Phase (P=8.9 hr)
1988 June 10							
–	–	–	–	7.134	14.800	15.074	0.627
7.207	15.879	16.220	0.636	7.256	14.761	15.024	0.641
7.833	15.903	16.253	0.706	7.788	14.818	15.097	0.701
8.084	15.978	16.358	0.734	8.048	14.836	15.120	0.730
8.400	16.042	16.450	0.770	8.345	14.877	15.174	0.763
8.950	16.128	16.578	0.831	8.915	15.051	15.409	0.828
9.060	16.186	16.667	0.844	9.103	15.082	15.452	0.849
9.399	16.162	16.630	0.882	9.433	15.128	15.518	0.886
9.708	16.216	16.714	0.917	9.746	15.116	15.500	0.921
9.931	16.199	16.687	0.942	9.895	15.095	15.471	0.938
10.116	16.132	16.584	0.962	10.082	14.993	15.329	0.959
10.284	16.047	16.457	0.981	10.245	14.920	15.231	0.977
10.775	15.910	16.263	0.037	10.741	14.784	15.053	0.033
11.022	15.852	16.183	0.064	11.056	14.726	14.979	0.068
11.353	15.891	16.237	0.101	11.321	14.704	14.952	0.098
11.532	15.809	16.125	0.122	11.498	14.660	14.897	0.118
11.890	15.797	16.109	0.162	11.867	14.658	14.894	0.159
12.066	15.869	16.206	0.182	12.032	14.715	14.966	0.178
12.220	15.902	16.252	0.199	12.186	14.738	14.995	0.195
12.398	15.853	16.185	0.219	12.330	14.779	15.047	0.211
12.844	16.058	16.473	0.269	12.388	14.942	15.260	0.274
13.196	16.126	16.575	0.309	13.163	14.971	15.299	0.305
1988 June 11							
6.278	15.856	16.189	0.228	6.221	14.714	14.964	0.221
6.726	16.025	16.425	0.278	6.687	14.872	15.167	0.274
6.844	16.053	16.466	0.291	6.308	14.905	15.211	0.287
7.078	16.091	16.522	0.318	7.126	15.001	15.340	0.323
7.350	16.231	16.738	0.348	7.314	15.079	15.448	0.344
7.840	16.267	16.796	0.403	7.798	15.107	15.488	0.399
7.983	16.220	16.720	0.419	7.949	15.077	15.445	0.416
8.142	16.187	16.668	0.437	8.109	15.058	15.419	0.434
8.287	16.188	16.670	0.454	8.254	15.020	15.366	0.450
8.429	16.185	16.665	0.470	8.396	15.010	15.352	0.466
8.723	16.046	16.456	0.503	8.689	14.897	15.200	0.499
8.920	15.988	16.372	0.525	8.954	14.905	15.211	0.529
9.093	15.988	16.372	0.544	9.127	14.829	15.111	0.548
9.544	15.844	16.173	0.595	9.506	14.762	15.025	0.591
9.751	15.818	16.137	0.618	9.679	14.737	14.993	0.610
9.895	15.816	16.135	0.634	9.862	14.689	14.933	0.631
10.046	15.774	16.079	0.651	10.013	14.695	14.940	0.648
11.050	16.075	16.499	0.764	11.009	14.832	15.115	0.759
11.326	15.965	16.340	0.795	11.290	14.859	15.150	0.791
11.554	15.976	16.355	0.821	11.587	14.954	15.276	0.824
11.874	16.109	16.549	0.857	11.837	15.029	15.379	0.852
12.274	16.057	16.472	0.902	12.238	15.101	15.479	0.898
12.455	16.075	16.499	0.922	12.488	15.013	15.357	0.926
12.535	16.050	16.462	0.931	12.575	15.013	15.357	0.935
12.838	16.018	16.415	0.965	12.795	14.959	15.283	0.960

obtained when the sub-Earth and subsolar points were at cometographic latitudes such that the variation of cross section should have been approximately half that for the later observations if the nucleus is basically prolate. Consequently, the smaller optical amplitude in 1987 is likely due to the different aspect.

Although our observations do not extend over a sufficient time interval to permit a precise period determination, we have estimated the period using the method of phase dispersion minimization (Stellingwerf 1978). This technique was previously applied to comet P/Arend-Rigaux by MAC88 and the reader is referred to that paper for details of the method. We performed separate period searches on the 4845 Å, 6840 Å, and 10 μm data for P/Tempel 2 from June 10 and 11. The statistic θ (see MAC88) for each of these sets of data is shown plotted against period in Figure 1. Possible periods in the data are those for which there is a local minimum in this plot. The increase in depth of the minima toward shorter periods is, to some degree, an artifact of the method. In computing θ, the data are divided into phase bins and the dispersion of the data points within each bin computed. The shorter the period, the narrower is each bin in time, and the less the intrinsic brightness variation of the comet will contribute to the dispersion within a bin. Note that the plots for all three data sets show a sharp minimum at a period of 4.45 days. The two adjacent minima, at 2.7 and 5.5 hr, are aliases of the strongest minimum with the 24 hr sampling interval between nights. The 4.45 hr period corresponds to a light curve having one maximum and one minimum per cycle but we believe, based on evidence which will be presented later in this paper, that the true rota-

TABLE 2

INFRARED LIGHT CURVE DATA (10.1 μm)

U.T. (hour)	Magnitude	Phase (P=8.9 hr)
1988 June 10		
7.200	3.630	0.635
7.317	3.663	0.648
7.400	3.607	0.657
7.600	3.658	0.680
7.783	3.710	0.700
8.150	3.733	0.742
8.450	3.862	0.775
8.550	3.884	0.787
8.717	4.016	0.805
8.800	4.031	0.815
9.133	4.230	0.852
9.217	4.403	0.861
9.383	4.361	0.880
9.600	4.320	0.904
9.767	4.299	0.923
9.933	4.106	0.942
10.200	4.039	0.972
10.550	3.884	0.011
10.617	3.820	0.019
10.767	3.743	0.036
10.867	3.743	0.047
11.083	3.568	0.071
11.233	3.614	0.088
11.383	3.604	0.105
11.600	3.584	0.129
11.700	3.562	0.140
11.817	3.470	0.154
12.550	3.750	0.236
12.717	3.890	0.255
12.950	3.929	0.281
13.117	3.961	0.300
13.167	4.220	0.305
13.433	4.359	0.335
1988 June 11		
5.733	3.562	0.167
5.783	3.582	0.172
5.950	3.650	0.191
6.167	3.638	0.215
6.300	3.725	0.230
6.483	3.790	0.251
6.550	3.779	0.258
6.883	4.048	0.296
6.933	4.063	0.301
7.117	4.107	0.322
7.367	4.244	0.350
7.517	4.377	0.367
7.667	4.312	0.384
7.767	4.357	0.395
7.883	4.367	0.408
7.983	4.378	0.419
8.083	4.288	0.431
8.217	4.254	0.446
8.383	4.099	0.464
8.533	4.075	0.481
8.883	3.838	0.521
9.050	3.825	0.539
9.350	3.768	0.573
9.433	3.748	0.582
9.533	3.743	0.594
9.700	3.785	0.612
9.850	3.801	0.629
9.900	3.807	0.635
10.017	3.745	0.648
10.117	3.696	0.659
10.200	3.736	0.669
10.300	3.721	0.680
10.417	3.712	0.693
10.617	3.699	0.715
10.783	3.735	0.734
10.917	3.766	0.749
11.167	3.946	0.777
11.200	3.897	0.781
11.283	4.042	0.790
11.400	3.939	0.803
11.467	3.958	0.811
11.633	3.996	0.830
11.750	3.996	0.843
12.000	4.246	0.871
12.200	4.209	0.893
12.317	4.112	0.906
12.433	4.177	0.919
12.533	4.272	0.931
12.650	4.125	0.944
12.900	4.119	0.972
12.950	4.014	0.978
13.267	3.893	0.013

tional light curve must have two maxima and two minima per cycle and thus a period of 8.9 hr corresponding to the broad minimum in Figure 1 centered at ~9 hr. This is in good agreement with the results of Jewitt and Luu (1988, 1989) and Wisniewski (1988). Light curves phased according to the periods corresponding with all the prominent minima in θ were plotted and confirm that a period of 8.9 hr yields the best light curve. We note that this is the shortest photometrically determined rotational period for a cometary nucleus except for the very first period so determined. Fay and Wisniewski (1978) determined a period of 5.2 hr for P/d'Arrest although the rather small amplitude of the variation yielded poor signal-to-noise ratio in the resultant power spectrum. All other rotational periods recently determined are substantially longer (Weissman *et al.* 1989).

Figure 2 shows the observations from June 10 and 11 phased according to a period of 8.9 hr and plotted as open circles and filled circles, respectively. In addition, the observations from June 9 have been included (*as filled triangles*) in the plot of the 4845 Å data. Zero phase arbitrarily has been set at 7.75 hr. UT. on June 9. Since the observations from June 9 are poorly calibrated, we have simply shifted those data arbitrarily to the same mean brightness as the data at the same phase from the other nights. Note that the apparent peak in the abbreviated light curve from June 9 at phase 0.1 is coincident with a maximum in the light curve from the other two nights, confirming the periodicity.

It is apparent in Figure 2 that the reflected optical and thermal infrared light curves are closely in phase as was also the case for P/Arend-Rigaux (MAC88). Now, as in the earlier paper, we interpret the alignment of the visible and infrared light curves to mean that the brightness variations result from the changing apparent cross section of an elongated, rotating nucleus. If the brightness variations were due to albedo features on the nucleus, the visible and IR light curves should be 180° out of phase. The large difference in amplitude between the visible and infrared light curves results at least in part from greater dilution of the optical observations by the signal from

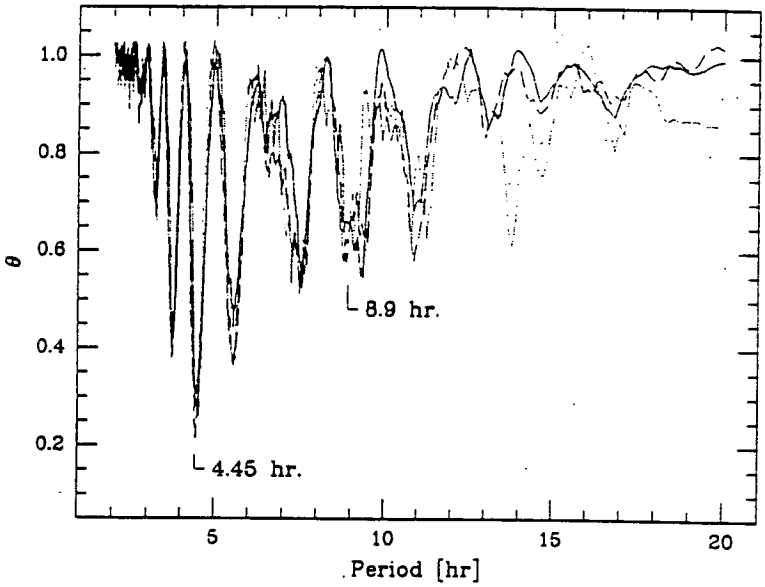

FIG. 1.—Phase-dispersion-measure for the light curve of comet P/Tempel 2 as a function of period. The statistic is shown for each of the three wavelengths at which light curves were obtained, 4845 Å (*dotted line*), 6840 Å (*dashed line*), and 10.1 μm (*solid line*). All show their deepest minimum at 4.45 hr which yields a single-peaked light curve. We believe that the correct rotational period is the one indicated by the broad but shallower minimum at twice that period, 8.9 hr.

the coma. In order to derive the size, shape, and albedo of P/Tempel 2's nucleus, it is necessary to first remove this contamination by the coma.

b) Removal of Coma

As noted above, observations were made of the aperture-dependence of the flux several times at the three monitoring wavelengths 4845 Å, 6840 Å and 10.1 μm. These observations were usually made near maximum or minimum light in order to minimize the temporal variation of the comet's brightness during the interval required to make measurements through all apertures. The sequence of these measurements was such that an observation with the monitoring aperture (10".1 and 7".0 diameter in the optical and infrared, respectively) was interspersed between each of the observations with the other apertures. This procedure took up to an hour, so it was necessary to use smooth curves through the data in Figure 2 to correct the observations to a common time assuming that the variation in flux was the same in all apertures (an assumption justified *a posteriori*). These corrections were as large as 6%.

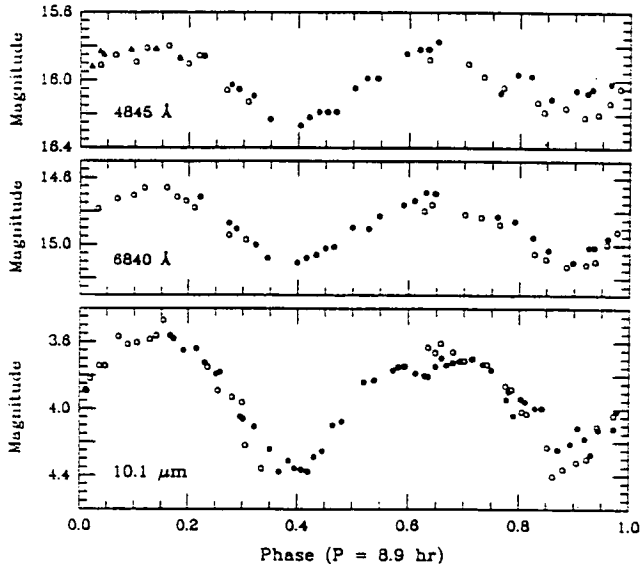

FIG. 2.—Phased light curves for comet P/Tempel 2 assuming a period of 8.9 hr including data from 1988 June 9 (4845 Å only; *filled triangles*), June 10 (*open circles*), and June 11 (*filled circles*). Zero phase is at 1988 June 9, 7.75 hr UT.

A simple radial outflow model for the dust predicts a surface brightness which varies as ρ^{-1}, where ρ is the projected distance from the nucleus, which in turn implies that the flux in a centered aperture varies linearly with the diameter. Although this is clearly an oversimplification since the coma may be varying, it provides a convenient reference point. In Figures 3 and 4 we have plotted the flux from P/Tempel 2 as a function of diameter of the aperture in the infrared and the optical, respectively. An examination of the variation with aperture size at 10.1 μm shows that on average a horizontal straight line adequately describes the data. Fitting straight lines by least squares and comparing the value of those lines at 7".0 and 0" shows that the contribution by the coma to the monitoring aperture is 10% ± 10% at maximum light. Thus, there is not a statistically significant detection of the coma at this wavelength, and we assume that the contribution is nil for our reductions, allowing for the possible contribution in our later discussion of uncertainties. There was not enough signal to even attempt to measure the variation with aperture size with the *M* and *Q* filters, and therefore we have assumed that the contribution by the coma at those wavelengths is also negligible. At least for *Q*, this assumption is supported *a posteriori* by the models discussed below.

At optical wavelengths, however, there is clearly a contribution by the coma. In Figure 4, the straight lines have been fitted by least squares to observations through the 10".1, 14".2, 20".0, and 28".5 apertures. The standard deviations of the slopes are ~ 10%, and the variation in slope from one set of observations

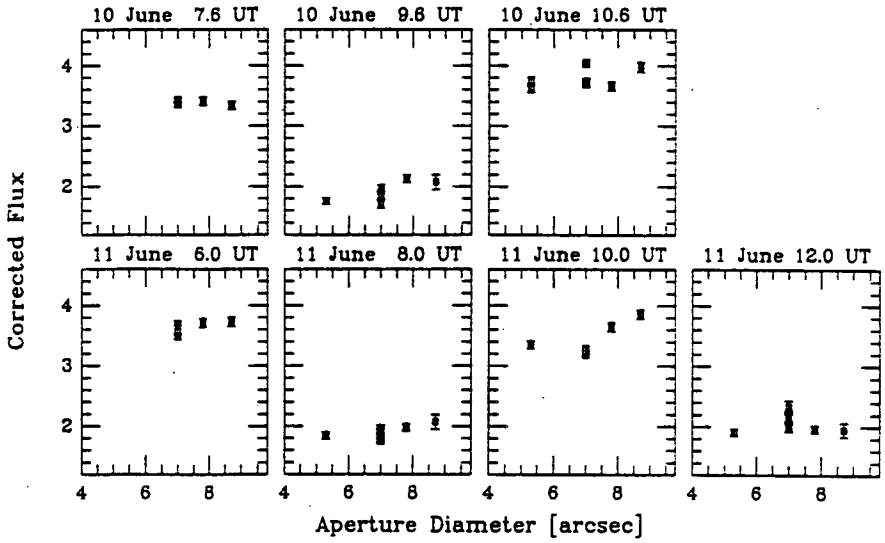

FIG. 3.—Variation of flux with aperture at 10.1 μm. The data are consistent with the absence of any coma.

to the next is not statistically significant. Based on the average slopes from Figure 4, the contribution by the coma to the flux in the 10".1 aperture at maximum light is 25% of the total flux at 4845 Å and 20% of the total flux at 6840 Å. At minimum light, the contributions are 35% and 28%, respectively.

The lack of significant temporal variation in the optical brightness profiles, it should be noted, argues strongly that the coma is not contributing significantly to the observed variations of brightness. For one thing, the amplitude of the observed variations is markedly greater than the variation in the coma contribution to the signal in the 10".1 aperture. Second, since the estimated time for dust to cross our apertures is comparable to the rotational period, any substantial variation in coma production would produce readily apparent distortions of the coma brightness profiles.

The coma contribution to the observations of the comet in the 10".1 aperture has been calculated on the basis of these values of the slope and subtracted from the observed signal to give the brightness of the nucleus alone. Columns (3) and (7) of Table 1 contain these nuclear magnitudes on the standard system defined by the IHW. These values are plotted as a function of light curve phase in Figure 5. The observed magnitudes at N, given in Table 2, are also plotted in Figure 5 since we have already argued that these 10.1 μm observations refer solely to the nucleus and do not require correction for coma.

A careful comparison of the panels in Figure 5 shows that the amplitude of the optical light curves is ~0.55 mag while that in the infrared is near 0.80 mag, a difference which is greater than the peak-to-peak scatter in the individual light curves. There are two possible explanations of this difference. One is that we have underestimated the amount of coma contamination of the optical measurements. In fact examination of Figure 4 does suggest a tendency for the observed variation with aperture to deviate from linearity in the sense of being

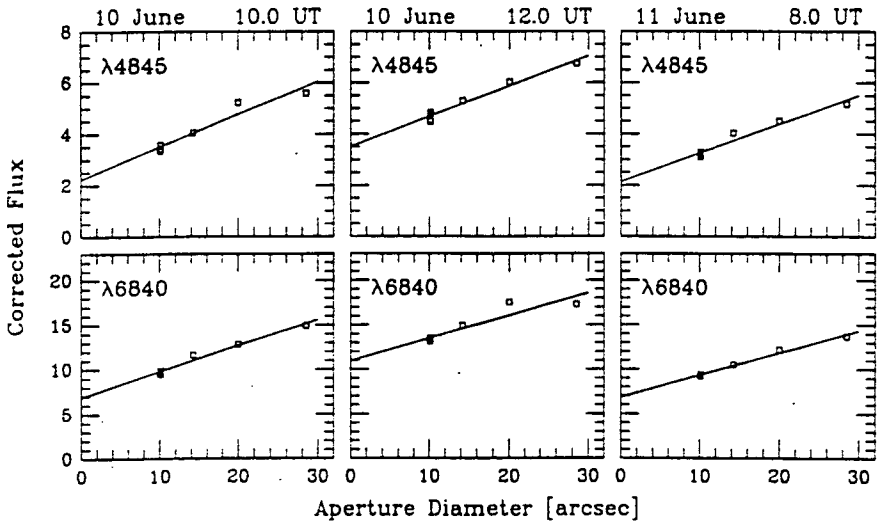

FIG. 4.—Variation of flux with aperture in the optical region. Straight lines have been fitted by least squares and indicate that a contribution from the coma is definitely present. The average slope for each filter was used for removal of coma from the data.

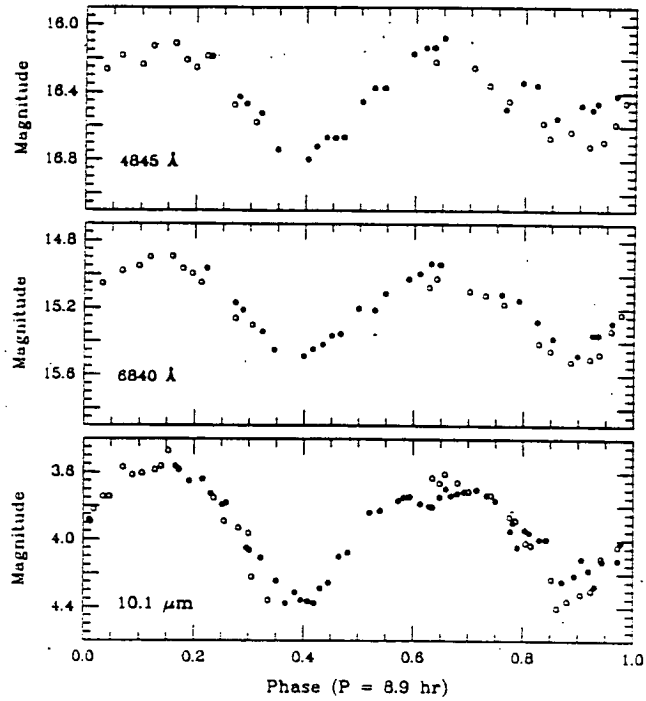

FIG. 5.—Rotational light curve of the nucleus of comet P/Tempel 2. The optical observations have been corrected for the contribution by the coma. The difference in amplitude between the optical and infrared could be due to incomplete correction for coma but could also be an effect due to the enhanced amplitude of a prolate spheroid in its thermal emission. Zero phase is 1988 June 9, 7.75 hr UT.

convex upward. Curvature of this type has been seen in some other comets and has been attributed to the effects of radiation pressure (Jewitt and Meech 1987) or evaporation of grains (Baum and Kreidl 1986). To explore the impact of possible curvature in the brightness profile of the coma, quadratic fits to the data in Figure 4 were performed. These fits yielded nuclear fluxes at maximum light 10%–50% smaller than deduced from the linear fits and, therefore, gave light curve amplitudes closer to that observed in the infrared. However, a reduced χ^2 analysis indicates that the improvement in the quality of the quadratic fits over that of the linear fits is not significant. Accordingly, we see no compelling justification for adopting the quadratic fits in computing the contribution by the coma but allow for that possibility in our later discussion of the uncertainties.

An alternative explanation of the difference in amplitude between the optical and IR light curves comes from the work of Brown (1985). Brown has shown that for elongated bodies, the amplitude of the thermal signal will be a function of wavelength as well as aspect. Because we have only the 10.1 μm light curve for P/Tempel 2, we are unable to confirm whether this effect is actually present in this comet. If it is, then it is by no means clear that the optical and IR light curves should have the same amplitude. In addition to the variation of the thermal amplitude with wavelength, there is also the possibility that the nucleus does not have uniform albedo. In any case, it is important to emphasize that if the coma contribution has been underestimated, the result will be an overestimate of the albedo of the nucleus but, because the albedo turns out to be so low, the determination of the nuclear effective radius, which varies as $(1 - A)^{-0.5}$, will be essentially unaffected.

c) *Emission by the Coma*

The observations of the coma, aimed at deriving rates of outgassing of the various molecular species, had to be interspersed among the observations of the light curve, just as with the observations to measure the dependence of flux on aperture size. These observations were, therefore, much less complete than would have been the case if determination of the outgassing had been our primary goal. The only species measured with large fields of view were OH and CN, the former because it is the best measure of the total gaseous outflow and the latter because it is usually the easiest species to measure in comets. C_2 and C_3 were measured only in the 10″.1 diameter aperture used for monitoring the variability. Of these, C_2 was measured numerous times because, if strong, it could contaminate the measurements of the continuum at 4845 Å. Fortunately, the emission by C_2 was weak enough that the contamination of the 4845 Å flux in the 10″.1 aperture was negligible, although still strong enough that we were able to detect the emission reliably with the filter centered on the emission band (5140 Å).

The observations of OH required special treatment because of the nonlinearity of atmospheric attenuation with airmass in the filter used to isolate this band. The IHW has calculated models of the atmospheric attenuation in this filter (U. Carsenty, private communication) using the actual transmission curve of this filter, stellar and cometary spectra, and atmospheric parameters suitable for Mauna Kea. The extinction can be linearized for these specific conditions by using an effective airmass:

$$X_{\text{eff}} = X - 0.07257 \times X^2 \ (B - \text{stars}) \ ;$$

$$X_{\text{eff}} = X - 0.0348 \times X^2 \ (\text{comets}) \ ;$$

$$k_{\text{comet}} = 0.9234 \times k_B \ .$$

Conversion to fluxes, both for OH and for the other species, was carried out using the transformations provided by the IHW (see appendices to the Giacobini-Zinner archive, Sekanina 1989). These formulae require continuum measurements which are used to remove the continuum that underlies the emission bands. In all cases the measurements of the continuum were sufficiently close in time that no correction was needed for the rotational variation. The resultant fluxes in the emission bands are given in Table 4 below.

The dust in the coma was measured as a byproduct of the removal of the brightness of the coma from the nuclear brightness as described above. This process is subject to all the uncertainties discussed in the previous section to an even higher degree since the desired component is now the smaller of the two components being separated. A single measurement at 4845 Å in an aperture of 56″.8 is less susceptible to these problems (only 28% of the light was due to the nucleus) but even in this case the result is somewhat uncertain.

III. MODELING AND INTERPRETATION

a) *Coma*

We interpret the observed emission-band fluxes in the coma in terms of molecular production rates as is common in cometary studies. The fluorescence efficiencies (g-factors) used to convert fluxes to column densities are given in Table 3. The column densities are then converted to production rates using a Haser model with the parameters given in Table 3. From the abundances of OH, we also calculate the production rate of

TABLE 3

A. HASER MODEL PARAMETERS[a]

Species	L/N (erg s^{-1})	Parent Scale (km)	Daughter Scale (km)
OH	8.23×10^{-16}	1.20×10^{5}	3.41×10^{5}
CN	1.16×10^{-13}	3.60×10^{4}	8.83×10^{5}
C_2	1.53×10^{-13}	4.71×10^{4}	3.24×10^{5}
C_3	3.39×10^{-13}	2.94×10^{3}	1.77×10^{5}

[a] At $r = 1.72$ AU.

B. VECTORIAL MODEL PARAMETERS[a]

$\tau(H_2O) = 82400$ s	$\tau(OH) = 200{,}000$ s
$v(OH) = 1.15$ km s^{-1}	fraction H_2O to OH = 0.93

[a] At $r = 1$ AU.

H_2O using a vectorial model (Festou 1981) with the parameters given in Table 3. For the species for which we have multiple measurements, there is no statistically significant variation with time so we have averaged all measurements to give an average production rate for June 10–11 for a given aperture. These results are given in Table 4. An examination of the relative abundances of the various gaseous species shows that the ratio of other species to H_2O is somewhat lower than typical of active comets but not by a large factor.

The production of dust is given by the quantity $Af\rho$ (A'Hearn *et al.* 1984), a directly observable (i.e., model independent) quantity which, for pure radial outflow at constant velocity and for constant scattering, is proportional to the production of those grains dominating the optical scattering. Since it was shown above that the coma was constant to within our precision, we quote only a single value for each aperture. A few measurements were made with a filter at 3650 Å (see Table 6 below) through the 10".1 diameter aperture but, as with M and Q, there was not sufficient signal-to-noise ratio to separate the coma from the nucleus directly. On the other hand, these data clearly show that the amplitude of the light curve at this wavelength is ~ 0.7 mag, noticably greater than that found at longer optical wavelengths. These data will be discusssed in more detail below but, since all evidence points to a constant coma, the amplitude suggests that the contribution by the coma is less than 20%, thereby allowing us to set an upper limit on the brightness of the coma at this wavelength.

We note that all our models assume spherical symmetry whereas it is well known that the coma of P/Tempel 2 is not circularly symmetric (e.g., Sekanina 1987). In many cases the lack of spherical symmetry will not materially affect the conclusions since, e.g., a set of jets in the plane of the sky can be approximated by fractions of the spherically symmetric case. Deviations from spherical symmetry become systematically less important as the field of view increases and in the limiting case in which one observes the entire comet the discrepancies vanish. For this reason we place much heavier weight on the observations with the large (56".8) aperture. Temporal variability is not included in any of our models and one must remember that any "production rates" represent an average rate over some appropriate interval depending on the transmit time of material in the field of view and the lifetimes of the relevant species and their parents.

The ratio of gas to dust is conveniently parameterized by the ratio $Q(H_2O)/Af\rho$. This ratio is independent of the effects due to the finite field of view of the instruments although it differs from the true ratio of gas to dust both by a conversion of units ($Af\rho$ has the units of cm) and by parameters of the dust and the gas which may vary from time to time and from comet to comet. In particular, it varies with the wavelength of the light used to determine $Af\rho$ due to the variation of reflectivity with wavelength. Nevertheless, we believe that this is the most observationally reasonable parameter for monitoring the ratio of gas to dust. Feldman and A'Hearn (1985) showed that the parameter did exhibit a correlation with heliocentric distance, which might indicate a variation of the parameters of the models but might also indicate real physical differences with heliocentric distance. At a given distance, the comets considered there showed rather little scatter. Comet P/Halley exhibited significant variation with heliocentric distance and closer than 1 AU did deviate noticeably from the usual relationship with distance (Feldman *et al.* 1987). Typical values of this ratio in P/Halley are in the range 10^{25} to 10^{26} (cm s^{-1}) using ultraviolet light and these numbers would be very roughly $\frac{1}{3}$ that value if the continuum were measured at 4845

TABLE 4

PRODUCTION OF THE COMA, JUNE 10–11

A. GAS

Species	Aperture Diameter	Radius (10^4 km)	Flux (ergs cm^{-2} s^{-1})	$\bar{N}$ (cm^{-2})	Q (s^{-1})
OH	56".8	1.62	3.3×10^{-12}	8.4×10^{11}	2.1×10^{27}
	10.1	0.29	1.5×10^{-13}	1.17×10^{12}	1.9×10^{27}
H_2O	56.8	1.62	...	...	3.2×10^{27}
	10.1	0.29	...	...	3.8×10^{27}
CN	56.8	1.62	1.6×10^{-12}	4×10^{9}	3×10^{24}
C_2	10.1	0.29	5×10^{-14}	8×10^{8}	2×10^{24}
C_3	10.1	0.29	3×10^{-14}	8×10^{8}	6×10^{22}

B. DUST

Wavelength (Å)	Aperture Diameter	Radius (10^4 km)	Flux (ergs cm^{-2} s^{-1} $Å^{-1}$)	$Af\rho$ (cm)
3650	10".1	0.29	$< 3 \times 10^{-16}$	< 18
4845	56.8	1.62	3.0×10^{-15}	15
	10.1	0.29	6.1×10^{-16}	18
6840	10.1	0.29	4.4×10^{-16}	17

Å. Comets generally considered to be dust-poor, like P/Encke and Bradfield 1979 X, have values near 2×10^{26} using the continuum at 4845 Å. The value for P/Tempel 2 is $\sim 1 \times 10^{26}$ (cm s)$^{-1}$, a very typical value for comets at this heliocentric distance. The only comet of which we are aware that exhibits a substantially higher value of this parameter is P/Neujmin 1 (CAM87) for which the dust was undetectable and for which we estimate a lower limit of 1×10^{27} (cm s)$^{-1}$.

b) Nucleus

The nucleus was modeled using the "standard" thermal modeling program described by Lebofsky *et al.* (1986) as in the previous modeling of comets P/Neujmin 1 (CAM87) and P/Arend-Rigaux (MAC88). The input parameters used were the following: thermal phase coefficient 0.01 mag degree^{-1}, visible phase coefficient 0.035 mag degree^{-1}, thermal emissivity 0.9, and thermal beaming factor 0.9. The visible phase coefficient is consistent with but not strongly constrained by the data at phases smaller than 30° presented by Sekanina (1987, Fig. 11). None of the other coefficients are known for this or for any comet but are taken from the standard model for asteroids. Because the observations were made at a relatively small phase angle (see § II), the results of the model are not very sensitive to assumptions about phase coefficients. This type of thermal modeling is appropriate for comets that are relatively inactive, such as P/Tempel 2, because the amount of energy that goes into sublimation is negligible compared to the total incident radiation (CAM87). The calculated effective radius at maximum light, which depends only on the infrared measurements as long as the optical albedo is low, is $5.90^{+0.24}_{-0.68}$ km. In this calculation a 10.1 μm mag at maximum light of 3.532 was used. This value includes the monochromatic correction of -0.043 mag for 270 K, given by Tokunaga (1986). The larger uncertainty toward smaller radii is due to the possibility that the coma contributes as much as 20% of the 10.1 μm flux at maximum light (see § II).

The axial ratios obtained from the amplitude of the visible light curve corrected for coma (0.55 mag) and from the 10.1 μm light curve amplitude (0.80 mag) were averaged to determine a minimum axial ratio for the nucleus of $1.9^{+0.6}_{-0.2}$; the larger uncertainty toward a more elongated nucleus is again due to the possiblity of a larger contribution by the coma. At the time of our observations, Earth was nearly in the equatorial plane of the comet according to the model of Sekanina (1987); if so, and assuming that the nucleus of this comet can be approximated by a prolate spheroid rotating about a minor axis, the observed light curve amplitude and effective radius are consistent with overall nuclear dimensions of $16.3 \times 8.6 \times 8.6$ km. The geometric albedo is 0.022 with an estimated uncertainty of $^{+0.004}_{-0.006}$. The effects of departures from sphericity on the results of the standard thermal model have been discussed by Brown (1985). We estimate the error in the calculated effective radius introduced by ignoring sphericity to be $\pm 5\%$. Brown's nonspherical thermal model predicts that the amplitude of the rotational light curve will be larger in the thermal infrared than in the visible. This effect could explain the different amplitudes observed in the visible and at 10.1 μm; on the other hand, this difference could also be due to an incomplete removal of the coma contribution in the visible (see § II). A more refined analysis of our observations and those of MAC88 aimed at improving our knowledge of the shape of the nuclei of comets P/Tempel 2 and P/Arend-Rigaux is in progress.

The observations at M (4.8 μm) and Q (20 μm), presented in Table 5, provide a check on the thermal modeling. Several measurements at Q were made at different points in the light curve in search of possible temperature variations predicted by the nonspherical thermal model. We detected only statistically marginal $N - Q$ color variations; a mean $N - Q = 1.85$ was observed, consistent with the brightness temperatures of 270 K at N and 256 K at Q, predicted by the standard thermal model. The comet was considerably fainter at M, hence the fluxes in this bandpass were not as well determined as those for Q. Only single values for M were obtained for each day near a maximum in the light curve; the resultant fluxes are slightly higher than predicted by the standard thermal model. This excess in the M flux is qualitatively similar to that observed in comet P/Arend-Rigaux (MAC88), where a significant contribution ($\sim 33\%$ of the flux) from the dust was observed in the M bandpass. In the case of comet P/Tempel 2, however, the signal was too weak to obtain reliable aperture photometry in the M filter to quantify the contribution by the dust coma at this wavelength.

TABLE 5

ADDITIONAL THERMAL DATA

UT (hr)	m (mag)	Q (mag)
June 10:		
12.48.....	8.56	...
13.05.....	...	1.98
June 11:		
07.60.....	...	2.34
08.98.....	...	1.99
09.63.....	...	1.73
10.25.....	8.28	...
10.72.....	...	1.94
11.58.....	...	2.13

The albedo of the nucleus derived here is an effective visual albedo but some additional information is available on the variation of albedo with wavelength. The narrow-band magnitudes given in Table 1 yield directly the color of the nucleus (averaging many values near maximum light), CI(48–68) = m(4845) − m(6840) = 1.20 with rms scatter of the individual points of 0.05 mag, whereas the solar color in this system is 0.87 based on observations of solar analogs. The nucleus of comet P/Tempel 2 is therefore rather red, with reflectivity gradient, $(ds/d\lambda)/s = 15\%$ per kÅ. There is some indication of a difference in color between the two maxima of the light curve; averaging several points near the separate maxima in Table 1, we find 1.226 ± 0.015 and 1.157 ± 0.014 (error of the mean based on scatter) but the true error bars are larger than the error bars based on scatter because of systematic effects due to the removal of coma. The differences between the two maxima could be due to either a true difference in color between the two observed faces of the nucleus or they could be due to differences in the contribution by the coma. Combining all sources of error, the uncertainty in the color is 0.06 mag.

Although we have data at 3650 Å, we cannot reliably remove the coma from those data because the signal-to-noise ratio is inadequate. Our data for the combined nucleus and coma at four different times are given in Table 6. Uncertainties are ~ 0.02 mag at the two longer wavelengths. At 3650 Å, the uncertainty due to photon statistics on the comet and on the sky amounts to 0.07 mag. Other errors, including extinction and the transfer to standard stars, combine quadratically with

TABLE 6

COLOR OF P/TEMPEL 2[a]

Date UT	*m*(3650) (mag)	*m*(4845) (mag)	CI(36–48) (mag)	CI(48–68) (mag)
Jun 10.475	16.97	15.90	1.07	1.20
Jun 11.333	17.56	16.23	1.33	1.15
Jun 11.404	16.73	15.82	0.91	1.08
Jun 11.471	17.36	15.97	1.39	1.11
Solar color	...	...	1.17	0.87

[a] 10".1 aperture.

this and imply a total error of no more than 0.09 mag. The color index between 3650 and 4845 Å, however, varies from bluer than the sun at maximum light to slightly redder at minimum light. Since all data at longer wavelengths imply that the coma is constant, and since the amplitude at 3650 Å is 0.7 mag (averaging the two maxima and comparing with the single minimum), significantly greater than at longer optical wavelengths, we conclude that the contribution by the coma at maximum light is less than 20%. We can therefore set a lower limit to the nuclear brightnesses at the two maxima: $m_{nuc}(3650) < 17.21$, 16.97. This yields colors CI(36–48) $= m(3650)-m(4845) < 1.01$, 0.82 compared to the corresponding solar color of 1.17, i.e., much bluer than the Sun. It should be noted that the bluer of the two colors occurs during the same maximum during which the other color index, CI(48–68), is less red than the average.

In Figure 6 we have plotted our data for the two maxima separately. The error bars on our data do not include all the uncertainty in the subtraction of coma because a portion of that uncertainty (the choice between linear and curved profiles) is coherent between the two filters at the longer wavelengths. Although the brightness at 4845 and 6840 Å might be significantly fainter than we have deduced if indeed the profile of the coma is curved, the effect is comparable in the two filters so that the uncertainty in the color is only marginally increased. On the other hand, we believe that we have removed the maximum possible amount of coma from the data at 3650 Å, suggesting that the error bars for those two points might be extended upward significantly. The error bars for the data from Spinrad, Stauffer, and Newburn (1979) are taken directly from their paper. The agreement between the observations of Jewitt and Luu (1989), of Spinrad *et al.*, and of ourselves at 4845 and 6840 Å is very good. Note that the data of Spinrad *et al.* show fine structure which results from combining data taken on two different observing runs at slightly different wavelengths. This is also easily understood if opposite faces of the nucleus have different colors as suggested by our data.

The very red color at visible wavelengths is characteristic of both S asteroids and the reddest D asteroids (although S asteroids have much higher albedos than does comet P/Tempel 2), and it is among the reddest cometary nuclei measured (Weissman *et al.* 1989). At our shortest wavelength, our results are consistent with those of Spinrad *et al.* in showing a significant increase of reflectivity giving some confidence that the result is not spurious. This result, if it truly refers to the nucleus and not to some very blue dust in the coma, makes the nucleus of comet P/Tempel 2 very unusual. The only other object in the solar system which shows this behavior is comet P/Schwassmann-Wachmann 1, for which the albedo clearly does not decrease at these wavelengths but which may be flat rather than increasing. Other objects do seem to have albedos which increase in the ultraviolet beyond 3000 Å but no others increase in this spectral range. We do not wish to discuss explanations for this effect in detail, however, because it is still possible that the blue color arises from a very large population of very blue, perhaps Rayleigh scattering, particles in the coma which vary with the rotation of the nucleus.

It is also significant that the color of the nucleus is quite different from the color of the grains in the coma. Examination of Table 4 shows that the grains in the coma have a very neutral color, whereas the nucleus is distinctly red except at the shortest wavelengths. Jewitt and Luu (1989) have reached a similar conclusion based on their long-slit spectra of the comet. There is no way of determining, from either our data or those of Jewitt and Luu, whether the difference is due to selective ejection of grains or to differences in scattering properties between the grains on the optically thick surface and grains in the optically thin coma.

We can combine the outgassing rate observed in the coma and the size of the nucleus to estimate the fraction of the surface of the nucleus which is active. Determination of that fraction of the surface of the nucleus which is active. Determination of that fraction depends, of course, on where the active area is on the nucleus since that determines the effective insolation. We have used the methods described by Cowan and A'Hearn (1979) to estimate the outgassing of water molecules per unit area for an isothermal nucleus (rapid rotation and high thermal conductivity), for a model which is everywhere in

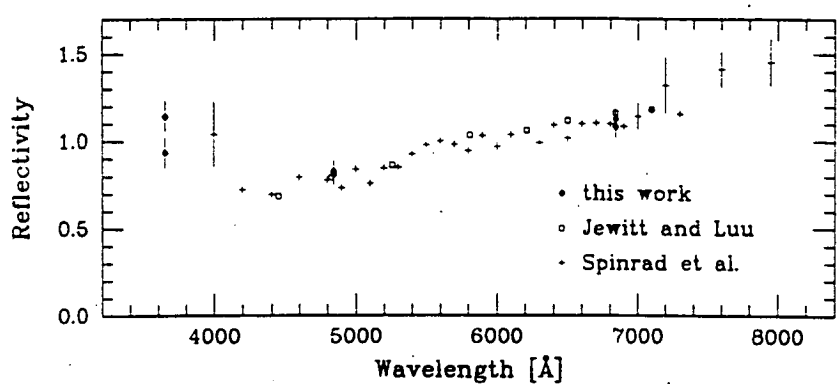

FIG. 6.—Spectral reflectivity of the nucleus of comet P/Tempel 2. Data from Spinrad *et al.* (1979) and from Jewitt and Luu (1989) as well as from the present work. See text for discussion of error bars and possible differences between the two faces of the nucleus.

local equilibrium (low thermal inertia), and for a model in which parallels of latitude are isotherms (rapid rotation). The range of rates of outgassing is from 2×10^{16} to 5×10^{17} cm^{-2} s^{-1}. According to the nuclear model of Sekanina (1987), the vent is at a high cometographic latitude. For this latitude and obliquity 90° and each latitude line being an isotherm, a typical rate of outgassing would be of order 3×10^{16} cm^{-2} s^{-1}. This is a lower limit to the outgassing per unit area since concentration of the heating to the daytime side nonlinearly increases the outgassing so that the average over the day is higher. Thus if the outgassing is from a single active vent vaporizing in equilibrium, its maximum area is 11 km^2 or 3% of the total surface. Much smaller areas are likely since the outgassing per unit area increases if the active area is more nearly normal to the direction to the Sun or if a latitude line is much hotter on the dayside than on the nightside as we would expect. It is clear from this discussion that comet P/Tempel 2, like comets P/Arend-Rigaux and P/Neujmin 1, has an almost totally inactive nucleus. The fraction of the surface which can be active in all three comets is at least an order of magnitude less than the fraction for P/Halley which itself has activity from no more than 30% of the surface (based on 15% in the sunlit hemisphere and an assumed comparable area on the dark hemisphere).

We also note that the geometry of Sekanina's model predicts that the vent should be alternating between daylight and darkness at the time of our observations so that some variability might be expected (Sekanina 1988). Because the lifetimes of H_2O and OH are both longer than the rotational period of the nucleus, the observed variation will be much less than the true variation in outgassing. A variation of the outgassing from one day to the next has been reported (A'Hearn *et al.* 1988) and will be discussed in more detail elsewhere. On the other hand, the constancy of the coma contributed by the dust argues against significant fluctuations in the outgassing unless the velocity of the dust leads to a transit time in our aperture much longer than the rotational period. If the velocity of the dust was less than 0.1 km s^{-1} this would be the case, and we should not see significant fluctuations.

The combination of the red slope of the reflectivity at long optical wavelengths with a possible increase in the near ultraviolet is unusual. The only similar curve of spectral reflectivity for a small body of which we are aware is that of comet P/Schwassmann-Wachmann 1 (S-W1). Although we cannot be sure that at quiescent phases the bare nucleus of this comet is visible, such a situation is often advocated and seems not unreasonable. Cochran, Cochran, and Barker (1982) measured the reflectivity of S-W1 in its quiescent phase (mag ~18.5) and found a reflectivity similar to that of P/Tempel 2, red at the longer optical wavelengths and gray or possibly bluish shortward of 4000 Å. Also as for P/Tempel 2, they found that the coma of S-W1 (measured during a subsequent outburst) was of a different color. The two comets are not, however, identical since the albedo of S-W1 was found by Cruikshank and Brown (1983) to be 0.13, very much higher than found here for P/Tempel 2.

TABLE 7

SUMMARY OF NUCLEAR PROPERTIES

Property	Value
R_{eff}	5.9 km
P	8.9 hr
p_v	0.022
T_B	270 K
Axial ratio	>1.9
Active fraction	<3%
Prolate spheroid	16.3 × 8.6 × 8.6 km

The reflectivities of these two comets appear unlike those of any standard types of asteroids. They are also significantly different from the reflectivities of other recently measured cometary nuclei: P/Neujmin 1 (CAM87) was very red even at the shortest wavelengths; P/Arend-Rigaux (MAC88) was almost neutral in color; P/Halley (Thomas and Keller 1989) was significantly less red at optical wavelengths. These other comets are similar in visual albedo and axial ratio and show a range of active surface fractions including the fraction found above for P/Tempel 2. The present results for P/Tempel 2 thus support the contention that cometary nuclei form a diverse group with no clear-cut match among the AAA asteroids.

We note finally that the results found here bear on models of cometary nuclei. Our results are generally consistent with the model of Sekanina (1987) in regard to the polar orientation and the general geometric description of the outgassing as being from a vent at high cometographic latitude. The combination of these results with similar results on the fraction of the surface which is active on other cometary nuclei qualitatively supports the widely discussed picture involving a mantle which gradually builds up on the surface of the nucleus, thereby choking off the vaporization.

IV. SUMMARY AND DISCUSSION

Simultaneous photometry at infrared and optical wavelength has allowed us to determine the albedo, size, and projected shape of the nucleus of comet P/Tempel 2. In gross size and shape it appears to be nearly identical to the nucleus of P/Halley, a prolate spheroid with axes $16 \times 8\frac{1}{2} \times 8\frac{1}{2}$ km. The nucleus of P/Tempel 2 differs from that of P/Halley in that the active portion of the surface is much less on P/Tempel 2, of order 1% as opposed to an estimated 15%–30% for P/Halley. The rotational period of P/Tempel 2's nucleus is near 9 hr, the second shortest of the photometrically determined rotational periods for comets. The outgassing and the changes around the orbit (1987–88) in the observed amplitude of the rotational modulation appear to be consistent with the nuclear model for this comet by Sekanina (1987) given that Sekanina (1988) has already pointed out that the nucleus is likely prolate rather than oblate. The spectral reflectivity of the nucleus is red in the optical, but there is a suggestion that in the ultraviolet the reflectivity increases toward shorter wavelengths. In the optical the redness is significantly greater than for P/Halley and comparable to the reddest of the other cometary nuclei measured and S as well as the reddest D asteroids. The increase at ultraviolet wavelengths, if real, is similar only to that seen for P/Schwassmann-Wachmann 1.

Observations of the nuclei of several periodic comets in recent years have shown that they are all dark and usually very aspherical. This is consistent with simple models for the growth of nuclei as fractal bodies by random accretion (Donn and Hughes 1986; Jewitt and Meech 1988). Furthermore, most of the surface is inactive on the nuclei of all periodic comets for which the relevant data exist. There is a selection effect in this conclusion because nuclei active over their entire surface are much harder to detect inside the coma. Nevertheless, a picture of gradual development of a mantle culminating in extinction of activity qualitatively fits all the available data on cometary

nuclei. It is still premature to make statements regarding the distribution of sizes or rotational periods because the sample of objects is too small and, at least as far as sizes are concerned, subject to very strong selection effects. Finally, it seems clear that nuclei differ significantly from one another in their spectral reflectivity. Although there are many spectral similarities to D and C asteroids, no pattern is yet clear in the reflectance spectra of cometary nuclei. For this reason, there is as yet no physical connection that can be directly established between cometary nuclei and Aten-Amor-Apollo asteroids.

We particularly thank Wieslaw Wisniewski for providing his light curve to us in the short interval between his and our observing runs and Uri Carsenty for carrying out the calculations for the extinction in the OH filter. We thank Larry Lebofsky and Mike Feierberg for providing the programs for the thermal models. We also thank Dave Jewitt for providing his results prior to publication and Bob Hawaii Brown for informative discussions of the effects of asphericity on the thermal models. The staff at the IRTF and the MKO 2.2 m provided excellent support for the observing. M. F. A'H. was supported by NASA grant NSG 7322, H. C. was supported by NSF grant AST 87-18071 and University of Arizona contract 113433 to PSI, and D. G. S. and R. L. M. were supported by NASA grant NGR-03-003-001. This is PSI contribution 269.

REFERENCES

A'Hearn, M. F. 1988, *Ann Rev. Earth Planet. Sci.*, **16**, 273.
A'Hearn, M. F., Feldman, P. D., Roettger, E., and Schleicher, D. 1988. *IAU Circ.*, No. 4622.
A'Hearn, M. F., Schleicher, D. G., Feldman, P. D., Millis, R. L., and Thompson, D. T. 1984, *A.J.*, **89**, 579.
Baum, W. A., and Kreidl, T. J. 1986, in *Asteroids, Comets, Meteors II*, ed. C.-I. Lagerkvist, B. A. Lindbald, H. Lundstedt, and H. Rickman (Uppsala: Uppsala Universitet), p. 397.
Brown, R. H. 1985, *Icarus*, **64**, 53.
Campins, N., A'Hearn, M. F., and McFadden, L.-A. 1987, *Ap. J.*, **316**, 847 (CAM87).
Cochran, A. L., Cochran, W. D., and Barker, E. S. 1982, *Ap. J.*, **254**, 816.
Cowan, J. J., and A'Hearn, M. F. 1979, *Moon and Planets*, **21**, 155.
Cruikshank, D. P., and Brown, R. H. 1983, *Icarus*, **56**, 377.
Donn, B., and Hughes, D. 1986, in *Exploration of Halley's Comet*, Vol. 3, ed. B. Battrick, E. J. Rolfe, and R. Reinhard (ESA SP-250), p. 523.
Fay, Jr., T. D., and Wisniewski, W. 1978, *Icarus*, **34**, 1.
Feldman, P. D., and A'Hearn, M. F. 1985, in *Ices in the Solar System*, ed. J. Klinger, D. Benest, A. Dollfus, and R. Smoluchowski (Dordrecht: Reidel), p. 453.
Feldman, P. D., *et al.* 1987, *Astr. Ap.*, **187**, 325.
Festou, M. C. 1981, *Astr. Ap.*, **95**, 69.
Jewitt, D., and Luu, J. 1989, *A.J.*, **97**, 1766.
Jewitt, D. C., and Luu, J. 1988, *IAU Circ.*, No. 4582.
Jewitt, D. C., and Meech, K. J. 1987, *Ap. J.*, **317**, 992.
———. 1988, *Ap. J.*, **328**, 974.
Lebofsky, L. A., *et al.* 1986, *Icarus*, **68**, 239.
Marsden, B. G. 1985, in *Dynamics of Comets: Thier Origin and Evolution*, ed. A. Carusi and G. B. Valsecchi (Dordrecht: Reidel), p. 343.
Millis, R. L., A'Hearn, M. F., and Campins, H. 1988, *Ap. J.*, **324**, 1194 (MAC88).
Öpik, E. J. 1963, *Adv. Astr. Ap.*, **2**, 219.
Sekanina, Z. 1979, *Icarus*, **37**, 420.
———. 1987, in *Symposium on the Diversity and Similarity of Comets*, ed. E. J. Rolfe and B. Battrick (ESA SP-278), p. 323.
———. 1988, *IAU Circ.* No. 4624.
———. 1989, Comet Giacobini-Zinner Test Disc, NASA Disc, NASA CD ROM # USA-NASA-IHW-GZ-0001.
Spinrad, H., Stauffer, J., and Newburn, Jr., R. L. 1979, *Pub. A.S.P.*, **91**, 707.
Stellingwerf, R. F. 1978, *Ap. J.*, **224**, 953.
Thomas, N., and Keller, H. U. 1989, *Astr. Ap.*, in press.
Tokunaga, A. T. 1986, *Photometry Manual*, NASA Infrared Telescope Facility.
Weissman, P., A'Hearn, M. F., McFadden, L.-A., and Rickman, H. 1989 in *Asteroids II*, ed. R. Binzel and M. S. Matthews (Tucson: University of Arizona Press), in press.
Wetherill, G. W. 1988, *Icarus*, **76**, 1.
Whipple, F. L. 1950, *Ap. J.*, **111**, 375.
Wisniewski, W. 1988, *IAU Circ.* No. 4603.

MICHAEL F. A'HEARN: Astronomy Program, University of Maryland, College Park, MD 20742

HUMBERTO CAMPINS: Department of Astronomy, University of Florida, SSRB 211, Gainesville, FL 32611

ROBERT L. MILLIS and DAVID G. SCHLEICHER: Lowell Observatory, 1400 Mars Hill Road West, Flagstaff, AZ 86001